



US Army Corps
of Engineers

AD A130977



DTIC FILE COPY

TECHNICAL REPORT GL-83-4

12

EVALUATION OF THE EROSION POTENTIAL OF EMBANKMENT CORE MATERIALS USING THE LABORATORY TRIAXIAL EROSION TEST PROCEDURE

by

Roberto L. Sanchez, Andrew I. Strutynsky,
Marshall L. Silver

Marshall L. Silver, Civil Engineer
151 Belle Avenue, Highland Park, Ill. 60035



April 1983

Final Report

Approved For Public Release, Distribution Unlimited

AUG 2 1983

A

Prepared for Office, Chief of Engineers, U. S. Army
Washington, D. C. 20314

Under Purchase Order No. DACW-39-80-M-4050;
CWIS Work Unit 31618

Monitored by Geotechnical Laboratory
U. S. Army Engineer Waterways Experiment Station
P. O. Box 631, Vicksburg, Miss. 39180

83 08 01 025

Destroy this report when no longer needed. Do not return
it to the originator.

The findings in this report are not to be construed as an official
Department of the Army position unless so designated
by other authorized documents.

The contents of this report are not to be used for
advertising, publication, or promotional purposes.
Citation of trade names does not constitute an
official endorsement or approval of the use of
such commercial products.

The covers of U. S. Army Engineer Waterways Experiment Station
(WES) engineering and scientific reports have been redesigned. Each
WES Laboratory and support organization will have its own distinctive
color imprinted on white coverstock. This standardizes WES publica-
tions and enhances their professional appearance.

Unclassified

SECURITY CLASSIFICATION OF THIS PAGE (When Data Entered)

REPORT DOCUMENTATION PAGE		READ INSTRUCTIONS BEFORE COMPLETING FORM
1. REPORT NUMBER Technical Report GL-83-4	2. GOVT ACCESSION NO. A130977	3. RECIPIENT'S CATALOG NUMBER
4. TITLE (and Subtitle) EVALUATION OF THE EROSION POTENTIAL OF EMBANKMENT CORE MATERIALS USING THE LABORATORY TRIAxIAL EROSION TEST PROCEDURE		5. TYPE OF REPORT & PERIOD COVERED Final report
7. AUTHOR(s) Roberto L. Sanchez Andrew I. Strutynsky Marshall L. Silver		6. PERFORMING ORG. REPORT NUMBER
9. PERFORMING ORGANIZATION NAME AND ADDRESS Marshall L. Silver, Civil Engineer 151 Belle Avenue Highland Park, Ill. 60035		6. CONTRACT OR GRANT NUMBER(s)
11. CONTROLLING OFFICE NAME AND ADDRESS Office, Chief of Engineers, U. S. Army Washington, D. C. 20314		10. PROGRAM ELEMENT, PROJECT, TASK AREA & WORK UNIT NUMBERS Purchase Order No. DACW 39-80-M-4050; CWIS Work Unit 31618
14. MONITORING AGENCY NAME & ADDRESS (if different from Controlling Office) U. S. Army Engineer Waterways Experiment Station Geotechnical Laboratory P. O. Box 631, Vicksburg, Miss. 39180		12. REPORT DATE April 1983
		13. NUMBER OF PAGES 335
		15. SECURITY CLASS. (of this report) Unclassified
		15a. DECLASSIFICATION/DOWNGRADING SCHEDULE
16. DISTRIBUTION STATEMENT (of this Report) Approved for public release; distribution unlimited.		
17. DISTRIBUTION STATEMENT (of the abstract entered in Block 20, if different from Report)		
18. SUPPLEMENTARY NOTES Available from National Technical Information Service, 5285 Port Royal Road, Springfield, Va. 22151.		
19. KEY WORDS (Continue on reverse side if necessary and identify by block number) Density Filter Water content Earth dams Hydraulic gradient Eroding fluid Piping Erosion Triaxial erosion test		
20. ABSTRACT (Continue on reverse side if necessary and identify by block number) -Triaxial erosion tests were used to study how the erosion rate in typical embankment dam core materials is influenced by soil compaction and by the chemistry of the eroding fluid. The tests were performed in a specially modi- fied triaxial cell which was able to apply confining pressure to compacted embankment dam materials and to direct the flow of the eroding fluid through a preformed erosion channel to model the conditions that exist in the core of an embankment dam. In addition, tests were performed to develop a method for testing the effectiveness of filters in preventing erosion from (Continued)		

DD FORM 1 JAN 73 1473 EDITION OF 1 NOV 68 IS OBSOLETE

Unclassified

SECURITY CLASSIFICATION OF THIS PAGE (When Data Entered)

Unclassified

SECURITY CLASSIFICATION OF THIS PAGE(When Data Entered)

20. ABSTRACT (Continued).

cracked embankment dam core materials. —

Five typical embankment dam core materials ranging from silty to clayey soils were studied. The results of the investigation may be summarized as follows:

- a. Varying the compacted density had little effect on erosion for silt materials compacted at the optimum molding water content. For clay materials, the erosion rate increased as the density decreased from 95 to 90 percent of standard Proctor maximum density.
- b. Varying the molding water content had a significant effect on the erodibility of silt core material, but this effect was less important for clay core material.
- c. The minimum erosion occurred when soil was compacted at or slightly above the optimum compaction water content. Significantly higher erosion occurred in specimens compacted dry of optimum.
- d. Erosion rates increased slightly with a decrease in eroding fluid ionic concentration. This increase was more significant for silt core materials than for clay core materials.
- e. Tests performed to study the effectiveness of using standard concrete sand (ASTM C 33) as a filter material for the downstream protection of cracked core materials showed that the filter sand was able to stop the erosion of even a highly erosive silt material under the action of hydraulic heads of up to 40 m, which was equivalent to a hydraulic gradient of 350.
- f. The soil erosion rate asymptotically approached a material and eroding fluid dependent constant defined as the Maximum Erosion Rate. This constant facilitates the incorporation of laboratory erosion test data into embankment dam design criteria.

Unclassified

SECURITY CLASSIFICATION OF THIS PAGE(When Data Entered)

PREFACE

The work described in this report was performed under Purchase Order No. DACW 39-80-M-4050, dated 31 July 1980, as part of work being performed at the U. S. Army Engineer Waterways Experiment Station (WES), Vicksburg, Mississippi, on "Design and Construction of Granular Filters for Embankment Dams," with funds provided by the Office, Chief of Engineers, U. S. Army, under Work Unit CWIS 31618.

This report was prepared by Mr. Roberto L. Sanchez, Mr. Andrew Strutynsky, and Dr. Marshall L. Silver. Ms. Meshkat S. Assian and Ms. Christyne Demos provided laboratory technical assistance; Ms. Mary Alice DeViney prepared all drawings and summary plots for the report and Ms. Charmagne Lawson provided typing assistance. Mr. Raul Valdes-Perez supervised the writing of the computer program to analyse and present erosion test data.

The work was monitored by Dr. Edward B. Perry, Soil Mechanics Division (SMD), Geotechnical Laboratory (GL), WES, under the general supervision of Mr. Clifford L. McAnear, Chief, SMD, and Dr. William F. Marcuson III, Chief, GL.

COL Nelson P. Conover, CE, and COL Tilford C. Creel, CE, were Commanders and Directors of WES during the period of study. Mr. F. R. Brown was Technical Director.



CONTENTS

	<u>Page</u>
PREFACE	1
CONVERSION FACTORS, U. S. CUSTOMARY TO METRIC (SI)	
UNITS OF MEASUREMENT	5
PART I: INTRODUCTION	6
Background	6
Current State of Knowledge	7
Requirements of a Successful Erosion Methodology	9
Limitations of Existing Test Methods	10
Purpose of the Triaxial Erosion Test	11
Model of the Physical Problem	11
PART II: TRIAXIAL EROSION TEST METHODOLOGY	13
Description of the Testing Equipment	13
Test Procedure	14
PART III: TEST PROGRAM	16
Objectives of the Study	16
Description of Materials Tested	17
PART IV: METHOD OF DATA COLLECTION	18
Specimen Characteristics	18
Erosion Test Parameters	18
PART V: METHOD OF DATA ANALYSIS	20
Computation of Hydraulic Gradient	20
Initial Crack Cross-Sectional Area	21
Variation of Cross-Sectional Area	21
Variation of Erosional Surface Area	23
Eroding Fluid Shear Stress	24
Erosion Rate	25
Solids Eroded as a Function of the Volume of Flow	26
Percent Weight Erosion Per Unit Time	26

	<u>Page</u>
PART VI: PRESENTATION OF DATA	28
PART VII: TEST RESULTS ON VARIABLES STUDIED	31
Molding Water Content	33
Dry Density	33
Eroding Fluid Concentration	34
Use of Standard Concrete Sand as Filter Material	34
PART VIII: DISCUSSION OF THE TEST RESULTS	36
Effect of Molding Water Content	36
Effect of Molding Water Content on Teton Dam Material	39
Effect of Dry Density on Erosion	39
Effect of Eroding Fluid Concentration	40
Effect of Using Standard Concrete Sands as Filter Material	41
Effect of Assumed Erosion Channel Shape	42
Effect of Assumed Hydraulic Behavior	42
PART IX: SUMMARY AND CONCLUSIONS	44
REFERENCES	47
TABLES 1-11 FIGURES 1-25	
APPENDIX A: DETAILS OF TEST RESULTS	A1
APPENDIX B: SUMMARY OF TEST RESULTS GIVEN IN APPENDIX A	B1
APPENDIX C: PROCEDURE FOR OBTAINING SOIL PORE WATER EXTRACTS	C1
APPENDIX D: NUMERICAL ANALYSIS OF THE EFFECT OF ASSUMED FLOW CHANNEL SHAPE ON TRIAXIAL EROSION TEST RESULTS	D1
APPENDIX E: EXPERIMENTAL STUDY OF TRIAXIAL EROSION TEST HYDRAULIC BEHAVIOR	E1

APPENDIX F: ESTIMATES OF FIELD EROSION RATES FOR THE TETON DAM FAILURE AND POSSIBLE DESIGN APPLICATIONS	F1
APPENDIX G: NOTATION	G1

CONVERSION FACTORS, U. S. CUSTOMARY TO METRIC (SI)
UNITS OF MEASUREMENT

U. S. customary units of measurement used in this report can be converted to metric (SI) units as follows:

<u>Multiply</u>	<u>By</u>	<u>To Obtain</u>
cubic feet	0.02831685	cubic metres
cubic inches	16.38706	cubic centimetres
feet	0.3048	metres
gallons (U. S. liquid)	3.785412	cubic decimetres
inches	2.54	centimetres
pounds (force)	4.448222	newtons
pounds (force) per square foot	47.88026	pascals
pounds (force) per square inch	6894.757	pascals
pounds (mass)	0.4535924	kilograms
square feet	0.09290304	square metres
square inches	6.4516	square centimetres
tons (2000 pounds, mass)	907.1847	kilograms

EVALUATION OF THE EROSION POTENTIAL OF EMBANKMENT

CORE MATERIALS USING THE LABORATORY TRIAXIAL

EROSION TEST PROCEDURE

PART I: INTRODUCTION

Background

1. The erosion of impervious core materials is an important problem in Geotechnical Engineering. One early description of a sudden and catastrophic failure due to cracking and erosion occurred in 1864, when nearly a quarter of the Dale Dyke Dam in England was breached. The waters flooded parts of the city of Sheffield to a depth of three meters and killed 250 people in the most devastating dam failure ever to have occurred in Great Britain (Smith, 1971). A recent reminder of this problem was the failure of the Teton Dam in Idaho which caused the loss of 11 lives, the loss of an 85 million dollar project and the lodging of over 400 million dollars in claims for loss of private property (U. S. Bureau of Interior, 1977).

2. Hsu (1981) in Table 1 provides a list of 49 more dams which have experienced erosion problems in the last 100 years; in 33 of those dams, erosion occurred through the embankment while in the remaining dams erosion occurred through the foundation. Fortunately, for most of these dams, there was adequate warning and catastrophic damage was avoided by lowering the reservoir water level and by performing remedial repairs.

Current State of Knowledge

3. Available field data: In the last decade, an increasing number of case histories have been presented in the literature describing embankment dam seepage and erosion (Bertram, 1967; Sherard, 1973; USCOLD, 1975). Table 2 summarizes these and other field observations of dams which have experienced erosion problems and provides useful quantitative design values.

4. As may be seen in Table 2, measurements of the volume of leakage flow as a function of time are usually available. In many cases, erosion problems are first detected by noticing rapid increases in leakage flows and/or the appearance of longitudinal cracks or crater like depressions at the crest of a dam. In most cases, these observations provided adequate warning time to perform remedial work to prevent breaching of the dam.

5. However, there is almost a complete lack of data describing the rate at which solids are removed from an eroding dam. As may be seen in Table 2, it is common to find expressions such as "dirty leakage", or "from clear to chocolate milk" as the only available data describing the

amount of solids being washed out from the core of a dam. Also, there is very little information on the size of the erosion channel.

6. The authors recognize that there is great difficulty in (1) obtaining measurements of the amount of solids being eroded from a dam and (2) obtaining the size of an erosion channel. However, the availability of this type of quantitative information is critical if we are to improve our present design criteria to prevent erosion from occurring. The following paragraphs summarize the current design philosophy on cracking, erosion, and the protection of embankment dam core materials.

7. Cracking and erosion: Based upon the field observations mentioned above, investigators have concluded that it is possible that core materials will crack regardless of design provisions. In general, cracks are caused by differential settlement between the compressible core and the stiffer shell material (load transfer) and/or the opening of a crack due to the fluid pressure of the reservoir water (hydraulic fracture).

8. It is also currently assumed that for cohesionless materials (such as filter materials) cracks will collapse upon saturation. In cohesive materials, however, the cracks may remain open due to the undrained strength of the material (Vaughan, 1976). Pressurized water from the reservoir may flow through these cracks and cause concentrated leaks to appear downstream. It is this concentrated flow which has led to the erosion of core and transition materials in a number of dams. At present, the "safe" assumptions to make in the design of an embankment

dam are: "Regardless of the design considerations involved, it is possible that the embankment dam material will crack" (Sherard, 1973), and "... some erosion will occur from the walls of a crack with water flowing through it..." (Vaughan, 1976). Therefore, a filter is assumed to be necessary to protect core material. Presently, filter design criteria are based on the grain-size characteristics of core, filter and shell materials. Table 3 presents a list of design criteria as summarized by Hsu (1981). Filters, however, are costly to install and maintain which makes their use oftentimes unfeasible, especially for small dams such as those associated with small agricultural projects.

Requirements of a Successful Erosion Test Methodology

9. Based upon field observations and the present state of knowledge of erosion in dams, investigators have concluded that the following factors correlate with the incidence of erosion failures (Aitchison and Woods, 1965; Sherard, 1976; Parkin, 1976):

- Rapid reservoir filling
- The presence of cracks and discontinuities
- Compaction on the dry side of optimum
- Low ion concentration of the eroding fluid
- A high concentration of sodium ions in the soil pore water

10. Any laboratory test must take into account these factors as well as model 1) the state of stress, and 2) the hydraulic conditions under which embankment dam erosion occurs.

11. Further, an erosion test should be able to model the behavior of flow through cracked core material into soil filters. Such tests are important because filters designed using the criteria presented in Table 3 for intact core material have sometimes failed to prevent erosion damage when cracks have developed. These filter criteria presented in Table 3 were generally developed from tests on uncracked base materials. Therefore, the need to develop filter criteria based on laboratory tests which use soils with open cracks has been recognized (Sherard, 1977; Vaughan, 1978; Gori bello and Lei Lam, 1979; Ofegbu, 1981).

Limitations of Existing Test Methods

12. The previous discussion suggests that the following two characteristics must be combined to properly model the erosion behavior of cracked embankment core materials in the laboratory:

- The physical and chemical characteristics of the soil and of the eroding fluid.
- The insitu state of stress and hydraulic conditions acting on the cracked soil.

13. An indepth review of equipment and procedures available to study the erosion potential of clays, prepared by Perry (1975), provided information that showed that few if any current testing procedures successfully combine both of these testing requirements. In general, this review showed that there are basically four classes of test equipment and methodologies used to measure the erosion potential of soil materials. These include: 1) the pinhole test and the similar, physical ero-

sion test (PET), 2) the rotating cylinder test, 3) the flume test, and 4) the hollow cylinder test. These existing procedures do not adequately model the insitu state of stress, the effectiveness of filters, or the mechanisms of flow through a crack as described in Table 4.

Purpose of the Triaxial Erosion Test

14. To minimize the limitations discussed previously, a triaxial erosion test was developed by the authors (Sanchez and Silver, 1982) based on the physical model presented below. Subsequent sections describe this laboratory triaxial erosion test methodology and present the results of tests performed on typical embankment dam materials using this test method.

Model of the Physical Problem

15. The physical conditions in an embankment dam during first filling are presented diagrammatically in Figure 1a. If a transverse crack exists in the core, it will be under a state of stress as shown in Figure 1b. The total vertical stress, σ_v , will tend to close the crack while the total horizontal stress, σ_h , will tend to keep the crack open. The magnitude of both the vertical and horizontal stress is influenced by load transfer (arching) caused by differential settlement between the shell and the core. The compacted soil element is initially in a partially saturated state under these total stress conditions.

16. As the reservoir is filled, a water force, u , will act on the upstream side of the crack. The water pressure acting on the downstream

side of the crack will be zero. The resulting pressure head, h , along the length of the crack, l_e , and the gradient, h/l_e , will tend to keep the crack open and cause water to flow through the crack. It is this flow that can erode material from the surface of the crack.

17. Based on the physical characteristics described above, the main parameter required for the study of erosion from a cracked core material is the erosion rate, \dot{e} (defined as the weight lost per unit area of crack per unit time) as a function of the fluid shearing stress, τ , applied to the surface of the crack. Further, to better understand why soils erode and to be able to quantitatively determine the amount of material that will be eroded from a dam, it is important to understand how the erosion rate, \dot{e} , is affected by changes in the following variables:

- soil compaction water content and dry density
- crack dimensions, surface roughness, and tortuosity
- confining pressure,
- eroding fluid gradients, and
- the chemistry both of the pore and eroding fluid

18. Two of these factors were investigated using the test equipment and procedures described in detail elsewhere (Sanchez and Silver, 1982) and summarized in the following sections.

PART II: TRIAXIAL EROSION TEST METHODOLOGY

Description of the Testing Equipment

19. The components of the testing equipment are pictured and schematically represented in Figures 2 and 3. The following paragraphs briefly describe the triaxial erosion test equipment:

20. Triaxial Cell: The test is performed in a standard triaxial cell with an enlarged drainage system and modified top and bottom platens. Pictures of the top and bottom platens are provided in Figure 4.

21. Water Supply System: Three 8 liter (2 gal.)*capacity cylindrical pressure tanks were independently controlled to provide a continuous high rate of flow to the triaxial specimen at a desired constant pressure head.

22. Effluent Beakers: Effluent containing eroded particles flowing out of the specimen was collected and volumetrically measured in 2000 ml and 4000 ml capacity graduated beakers. The weight of the solids eroded was determined by decanting the fluid from the beakers and then drying and weighing the solid residue. A screen equivalent in size to a No.10 sieve was mounted on the bottom platen of the triaxial cell to help support the specimen. The maximum particle size of all specimens tested was smaller than the No.10 sieve, so therefore the bottom platen screen did not interfere with the erosion of particles.

23. Compaction Mold: A split compaction mold 7.1 cm in diameter and 15.5 cm in height was used to form specimens. A forming nozzle, having

* A table of factors for converting U. S. customary units of measurement to metric (SI) units is presented on page 5.

the exact same shape as the injecting flow nozzle in the top platen (Fig.4), was attached to the bottom plate of the mold. This bottom plate and the forming nozzle were both slotted to permit insertion of a thin blade (2.3 cm wide by 0.2 cm thick) to form the crack. This forming blade was mounted on the head of a specimen extruding jack as shown in Figure 5: the blade was jacked up slowly in increments, to avoid splitting the specimen, through the slotted bottom plate of the mold and through the specimen. By this process an erosion channel having known dimensions was formed in the specimen.

Test Procedure

24. The tests were performed using standard triaxial specimens which were compacted in the special mold described above. A triangular orifice was molded into one end of the specimen by the forming nozzle. This orifice directed the flow of water through the specimen and prevented the flow of water around the circumference of the specimen or between the specimen and the confining membrane. The compaction procedure, described in detail by Silver (1976), was used to minimize specimen preparation effects on soil behavior; the method consists of tamping moist soil in layers (3 layers for this investigation) with each layer compacted to a prescribed dry density. The procedure makes corrections for the fact that in compacting a material in layers, each succeeding layer densifies the material in the layers below.

25. After all the layers were compacted, the forming blade was jacked-up through the specimen to preform a flow channel for the eroding fluid. The specimen was then placed inside the triaxial cell and the specimen was surrounded by a triaxial membrane so that both axial and

lateral confining pressures could be applied to simulate an insitu stress condition (Fig. 1). Hydraulic flow was modeled by allowing water to flow from the top to the bottom of the specimen. Distilled water was used for all erosion tests except for a limited number of tests conducted to study the effect of eroding fluid concentration (see paragraphs 70-71). The hydraulic pressure was held constant at the top of the specimen using the large volume, pressurized reservoirs described previously; the hydraulic pressure at the end of the outflow line was maintained at atmospheric pressure (Fig. 3). This laboratory test therefore modeled both the stress and flow conditions presented in Figure 1.

PART III: TEST PROGRAM

Objectives of this Study

26. The need to understand how various factors contribute to internal erosion or piping failure of a cracked core in an embankment dam has long been recognized. However, many independent and related factors influence erosion test results. Therefore, the scope of this report was limited to an evaluation of the influence of the following important factors within the range of values given in Table 5:

- Compaction water content and dry density
- Ionic concentration of the eroding fluid

27. To minimize the number of variables, the initial slot dimensions of 2.3 cm wide by 0.2 cm thick, a confining cell pressure of 98 kPa (14.2 psi), and a hydraulic head of 12 kPa (1.75 psi) equal to a hydraulic gradient of 10, were all kept constant for this investigation. The effect of hydraulic gradient on erosion values measured in the test was described in detail by Sanchez and Silver (1982). Varying the hydraulic gradient over the range 17 to 75 was found to have little effect on the erosion rate of materials of the type studied in this test program.

28. In addition, this investigation studied the validity of assumptions made to model the physical processes occurring in the triaxial erosion test. The investigation also determined the possibility of using this test method in evaluating the performance of filters for the protection of cracked fine-grained soils.

Description of the Materials Tested

29. The study consisted of a series of triaxial erosion tests performed on five embankment dam core materials, designated A,B,C,D, and E. These materials represent a wide range of soil types, from a moderately plastic clay to a silt, as may be seen from their index properties listed in Table 6. Material E is a slightly clayey silt from the core of the Teton Dam. Figures 6 through 10 show the grain size and compaction characteristics for these materials.

30. Recent research (Arulanandan et.al., 1976) suggests that mechanical index properties, such as those given in Table 6, seem to have little or no relation to the erosion behavior of soils. However, it has been extensively reported in both the Soil Science and Geotechnical Engineering literature that the chemistry of the soil pore water may give a better indication of the soil erosion characteristics. Table 7 presents the results of pore water chemistry tests for Materials A through E. These results can be used to compare the qualitative erosion behavior predicted by identification charts given in the literature (e.g. Sherard et.al., 1976) to the quantitative values obtained in this investigation. Appendix C describes the procedure for obtaining soil pore water extracts.

PART IV: METHOD OF DATA COLLECTION

31. Data obtained for each test included 1) a description of the physical characteristics of the erosion test specimen both before and after the test, 2) the hydraulic parameters of the test system, 3) the quantity of fluid flowing through the specimen as a function of time, and 4) the amount of solid material eroded from the specimen as a function of time. Methods used to obtain and calculate these values are described in more detail in the following paragraphs.

Specimen Characteristics

32. Atterberg Limit tests, hydrometer tests and compaction tests were performed on all materials tested. Initial specimen density was determined using measurements taken with a Pi-tape and a scale, and by weighing the specimen. Specimen height changes were monitored during each erosion test using a dial gage attached to the loading rod of the triaxial cell. After the test, the shape of the eroded crack was qualitatively described. The dimensions of the specimen were again measured and the specimen was oven dried and weighed to determine its final weight.

Erosion Test Parameters

33. Test parameters measured and monitored during the erosion test included: 1) fluid pressure at the top of the specimen; 2) volume of eroded fluid and solids as functions of time; and 3) height change of the specimen. Both cell pressure and head water pressure were measured to an accuracy of 5 kPa (0.7 psi). The volume of the eroded fluid was

recorded to an accuracy of 50 ml. Time was measured to the nearest 0.01 min and dry weight of the eroded solids was recorded to the nearest 0.01 gram.

34. Prior to the test, the confining cell pressure and water supply head pressure were read with a calibrated gage or pressure transducer. During the test, flow into the effluent receiving beakers was continuously timed at flow intervals of between 400 and 500 ml. The time was recorded when a beaker was filled to capacity with fluid and eroded material, and the next beaker began to fill.

35. The test parameters described above were used to determine the relationship between material properties, hydraulic parameters, and the time rate of material erosion. Typical data showing these relationships is presented in subsequent sections.

PART V: METHOD OF DATA ANALYSIS

36. Data from each erosion test was analyzed to obtain values of the erosion rate, \dot{e} (defined as the weight lost per unit cross-sectional area of the crack per unit time) as a function of the eroding fluid shear stress, τ . To obtain these parameters, calculations were first made to determine the variations of erosion weight loss versus time (g/min) and the quantity of flow passing through the crack versus time (cm³/min).

37. Computation of Hydraulic Gradient: The hydraulic pressure at the end of the outflow line was maintained at atmospheric pressure. Therefore, the hydraulic gradient was:

$$i = \frac{h - h_b}{l_e} \quad (1)$$

where:

i = hydraulic gradient;

h = head of water applied to the top of the specimen in meters;

h_b = head of water applied at the end of the outflow line (equal to zero in this study) ;

l_e = eroded crack length in meters (obtained by subtracting the nozzle height from the final height of the specimen).

38. Initial Crack Cross-Section: It was assumed that 1) the initial cross-sectional area of the crack, A_x , and 2) the cross-sectional area of the crack after confining pressure was applied to the specimen, but before initiating the flow, $A_x(0)$, were equivalent and equal to the cross-sectional area of the blade forming the crack (Fig. 1b):

$$A_x = A_x(0) = d \cdot w \quad (2)$$

where:

A_x = initial cross-sectional area of the crack, equal to the cross-sectional area of the forming blade;

$A_x(0)$ = crack cross-sectional area at time equal to zero, after application of confining pressure;

d = thickness of the forming blade and of the crack;

w = width of the forming blade and of the crack.

This assumption implies that there was little if any closure of the crack as a result of applying the confining pressure.

39. Variation of Cross-Sectional Area with Time: To compute erosion rates and fluid shear stresses, numerical values for the surface area and cross-sectional area of the crack were required as a function of time. Assumptions were required to compute these areas as no direct measurement could be made during the test. One of these assumptions was made based on the observation that after the completion of a test, the

erosion surface did not vary significantly along the length of the crack. For this condition, the variation of the cross-sectional area of the crack, $A_x(t)$, with time can be shown to be (Sanchez and Silver, 1982):

$$A_x(t) = \frac{P \cdot t}{\rho \cdot l_e} + A_x(0) \quad (3)$$

where:

$A_x(t)$ = cross-sectional area of crack as a function of time in cm^2 :

P = slope of cumulative dry weight eroded versus time plot in g/min ;

t = time in minutes;

ρ = dry density of specimen in g/cm^3 ;

l_e = eroded length of the specimen at the end of the test in cm ; and

$A_x(0)$ = cross-sectional area at $t = 0$ in cm^2 .

40. The eroded length of the specimen, l_e (equal to the initial height of the specimen minus the nozzle length and the final vertical dial gauge reading) was regarded as a constant since it varied less than about 0.2 cm during any test.

41. Variation of Erosional Surface Area: After the cross-sectional area was computed, the wetted perimeter of the erosion channel, and hence the erosional surface area was calculated. Observations made at the end of a test indicated that in almost all cases the final eroded shape was roughly elliptical. However, for this report it was assumed that the crack enlarged in a rectangular fashion, as shown in Figure 1. The rectangle was assumed to have a constant width equal to the width of the slot-forming blade; only the thickness was assumed to vary with time to account for the soil volume being eroded. Using this assumption, the erosional surface area as a function of time, $A_s(t)$, can be shown to be equal to:

$$A_s(t) = 2 \cdot [A_x(t)/w + w] \cdot l_e \quad (4)$$

where:

$A_s(t)$ = erosional surface area of crack as a function of time in cm^2 ;

w = width of the forming blade and of the crack in cm; and

l_e = eroded length of the specimen at the end of test in cm.

42. In Appendix D, other assumptions were made for the time rate of change of the shape of the erosion channel. Results of analyses assuming a constant width elliptical erosion channel and a variable width elliptical erosion channel were compared to the constant width rectangular shape assumption presented in Equation 4. These analyses indicated that

using the simple rectangular assumption resulted in erosion channel size parameters within $\pm 15\%$ of the possibly more accurate elliptical erosion channel size parameters. This small difference was felt to be insignificant for the purposes of this study.

43. Eroding Fluid Shear Stress: The flow through the crack was analyzed as a closed channel pipe flow. Reynold's numbers were calculated and in all cases they were less than about 2000 indicating laminar flow. Assuming that laminar flow did indeed occur, the fluid shear stress, τ , was derived as (John and Haberman, 1971):

$$\tau = \frac{\psi V \mu}{D_h \xi} \quad (5)$$

where:

τ = fluid shear stress in N/m^2 ;

V = average fluid velocity [equal to $Q/A_x(t)$] in cm/min ;

μ = viscosity of water in $N \cdot \text{sec}/m^2$;

D_h = hydraulic diameter of the crack in cm ; equal to

$$D_h = \frac{4 A_x(t)}{A_s(t)/l_e} \quad (6)$$

ξ = conversion factor equal to 60 sec/min ; and

ψ = flow parameter (equal to 12 for this study).

44. Appendix E presents detailed results of a series of hydraulic experiments performed to check the validity of the assumption that flow through the erosion channel was laminar. These experiments showed that some flow separation could be introduced into the flow at the abrupt transition between the narrow injecting flow nozzle and the rapidly enlarging flow channel.

45. An analysis of this flow separation indicated that the equations for laminar shear stress were still applicable if the value of the shear stress was increased (Olson, 1980). Thus, the value of the flow parameter, ψ , in Equation 5 was increased by 30% over its average laminar value of 9.3 to an adjusted value of 12 to account for this possible flow separation. Appendix E presents more details of this analysis.

46. Erosion Rate: The erosion rate, $\dot{\epsilon}$, was computed as:

$$\dot{\epsilon} = \frac{P}{A_s(t)} \quad (7)$$

where:

$\dot{\epsilon}$ = erosion rate g/(cm² • min) ;

P = slope of cumulative weight eroded versus time curve (g/min) :

$A_s(t)$ = erosional surface area of crack in cm².

47. Solids Eroded as a Function of Volume of Flow: The literature suggests that estimates of the amount of erosion occurring through the core of a dam may be obtained from field measurements of the weight of solids and the volume of water flowing from the dam (Bertram, 1967; Kjaernsli and Torblaa, 1968). For comparison with these published values, an erosion factor, S, was defined and calculated as the dry weight of solids eroded divided by the volume of water collected.

48. Percent of Weight Erosion per Unit Time: Another useful value that may be used to compare the results of this investigation to the results obtained by others is the percent erosion per unit time, α . This value is defined as follows:

$$\alpha = \frac{P \cdot 100\%}{W_i} \quad (8)$$

where:

α = the percent erosion per unit time in percent/min ;

P = slope of cumulative dry weight eroded versus time plot in g/min; and

W_i = Dry weight of the specimen at the beginning of a test in grams.

It should be noted that a similar erosion quantity is often given in the literature. That quantity is simply called "Percent Erosion" and is defined as the cumulative weight of material eroded divided by the initial

weight of the specimen, W_i (e.g. Lewis and Schmidt, 1977). It may be seen that "Percent Erosion" does not include the effect of test duration. It therefore has limited use in quantifying erosion, unless all specimens are tested for the same amount of time.

PART VI: PRESENTATION OF DATA

49. The results of typical triaxial erosion tests for specimens of different embankment core material types are shown in Figures 11 through 15. These figures correlate specimen characteristics and experimental values measured in the erosion test. These experimental values include the cumulative volume of flow and the cumulative weight of solids eroded from the walls of the crack, both as functions of time. Plotted in each figure are typical results for a silt (high erodibility) and for a clay (low erodibility) to indicate the range of values measured in the testing program.

50. For example, Figure 11 gives the form of test results showing the volume of fluid flowing through a crack as a function of time. This straight line relationship, with a small range of variation in all tests, indicates that the flow rate is constant under any applied constant gradient. The slope of this line which is the flow rate, Q (cm^3/min), has been computed by linear regression for each test and is given in Table 8.

51. Figure 12 shows typical results giving the cumulative dry weight of solids eroded from the walls of the crack as a function of time. This relationship in all tests was also found to be linear. The slope, denoted by P (g/min), for each test was computed and is also shown in Table 8. Values for P were high for the silt core materials and lower for the clay core materials.

52. Typical plots of the cumulative dry weight of solids eroded as a function of volume of flow are shown in Figure 13. The slopes of these lines, the erosion factor, S (ppm), presents a useful quantity that has been cited in dam literature to provide a quantitative value for the amount of erosion measured in the field. It is thus useful to relate field measurements, in terms of embankment material characteristics and estimates of the crack dimensions, to results of laboratory tests to provide criteria for the evaluation of cracking and erosion in existing and future dams. These test results found high values of S for the silt core materials and lower values of S for clay core materials.

53. Figure 14 presents typical plots of cumulative weight of solids eroded per unit area of crack surface as a function of time. This data may be used with Equation 7 to calculate the erosion rate, \dot{e} . Higher erosion values were measured for silt core materials than for clay core materials.

54. Figure 15 plots typical curves of erosion rate, \dot{e} , as a function of the fluid shear stress, τ . Typical computations for these quantities are shown in Table 9. Note that both the fluid shear stress and the erosion rate were highest at the beginning of a test and decreased with time which on these plots increases towards the left of the figure.

55. Detailed test results of the form presented above for all specimens tested are given in Appendix A. Note that the plots presented in Appendix A that involve measurements of the volume of flow are drawn to two different scales because flow quantities before failure (when the specimen caved in at a severely eroded point on the sample surface) were about ten times smaller for silt specimens than for clay specimens.

56. Table 8 summarizes the results in Appendix A by presenting specimen measurements and test values for the flow rate, Q , the rate of weight erosion, P , and the ratio of solids eroded to the volume of flow, S , at any time t . It may be noted that these values of Q , P , and S were obtained without making any assumption about the shape of the erosion channel. Therefore, these values provide comparative data with which to relate results obtained from this test method with results obtained from other laboratory and field test methods that do not include measurements of the erosional surface area.

57. An interesting hypothesis may be made based upon the results given in Appendix A by noting that the erosion rate asymptotically approached a constant value as the fluid shear stress increased. Therefore, the erosion rate at which the slope of the erosion rate versus fluid shear stress curve was a minimum, was defined as "the maximum erosion rate" for each specimen. It should be noted that the maximum erosion rate will vary from one specimen to another depending on the compaction and eroding fluid used to test the material. Typical values of the maximum erosion rate, \dot{e}_{\max} , are shown in Figure 15 and given in Table 8. It should also be noted that this maximum erosion rate value is a simple constant which takes into account the erosional surface area. Therefore, the maximum erosion rate provides a better method of quantifying erosion than other parameters which do not include the erosional surface area such as percent erosion, percent erosion per unit time (α), and the ratio of solids to volume of fluid factor (S). Appendix F presents a possible method in which the maximum erosion rate parameter may be used for design.

PART VII: TEST RESULTS ON VARIABLES STUDIED

58. The effect of material and fluid parameters (including molding water content, dry density, and eroding fluid ionic concentration) on the erosion potential of a wide range of embankment core material types was investigated. Detailed test results are reported for Material B which was a slightly silty clay, and for materials D and E which were slightly clayey silts.

59. Two more materials, A and C, were also tested in this experimental program. The results of tests performed on Materials A and C are presented in Table 10. Material A was a clay, while Material C was a sandy clay. When tested, Material A exhibited extremely high resistance to erosion. For example, after 5 hours in the triaxial erosion test apparatus, less than 7 grams of solids were eroded from Material A specimens. On the other hand, for materials B, D, and E, between 35 and 133 grams of solids were eroded from the specimens within 30 minutes after the beginning of a test. This large difference in the erosion characteristics of Material A as compared to the other materials tested may be also observed by comparing the maximum erosion rate values measured for each material. The maximum erosion rate for Material A was only $0.0004 \text{ g/min-cm}^2$, whereas the maximum erosion rate values ranged from a minimum of 0.01 g/min-cm^2 for Material B to a maximum value of about 0.35 g/min-cm^2 for Material D or E. Thus, further tests with Material A were not performed.

60. Tests were also performed on a sandy clay, Material C, but the flow rate during a typical test decreased rapidly from the usual average

of about 500 cm³/min to a low value of only 100 cm³/min. Almost no weight erosion took place at this very low flow rate. It was observed that the high percentage of sand particles (32% coarser than the No.200 sieve) in this material was causing the crack to clog up. Therefore, additional tests were performed on Material C to study the effect of removing some sand from the material. It was found that the flow rate and thus erosion increased when material greater than the No.50 sieve (23% retained) was removed.

61. Further tests are needed to determine whether the sand particles in Material C actually caused the crack to seal internally, or whether the sand particles were being lodged on dead areas of the bottom platen of the apparatus, as described in Appendix E.

62. The use of an upstream sandy filter has been recommended by dam consultants for many years (Wilson and Marsal, 1979). Test results on Material C suggests that such filters might have been effective in preventing total failure in dams which had cracking problems. The behavior of Material C suggests that if enough sand particles are washed into a crack, the crack will clog resulting in reduced seepage and erosion.

63. The erosion rate versus shear stress curves presented in Appendix A have been summarized in Appendix B for each material tested to show the effects of molding water content, dry density, and eroding fluid ionic concentration on erosion. A listing of the specimens tested and additional computations performed to observe these effects have also been provided in Appendix B.

64. Molding Water Content: From the data in Appendix B the effect of specimen molding water content on the erosion characteristics of typical embankment core materials was investigated.

65. Figure 16 shows the effect of molding water content on the maximum erosion rate, \dot{e}_{\max} , for Materials B, D, and E. Figure 17 shows the effect of molding water content on another erosion parameter, percent erosion per unit time (α). This quantity provides comparative data between the triaxial erosion test and other laboratory test methods that do not take into account the erosional surface area.

66. A comparison of the data presented in Figures 16 and 17 shows that the molding water content has a large influence on the erosion of silt materials (Materials D and E). This effect, however, is less pronounced for clay materials (Material B). These results suggest that close control of the compaction water content during construction (if feasible from a practical viewpoint) may minimize the erosion potential of silt but not clay.

67. Dry Density: The effect of specimen dry density on the erodibility of typical embankment core materials was also investigated using the data in Appendix B.

68. Figure 18 shows the effect of specimen dry density on the maximum erosion rate, \dot{e}_{\max} , for Materials B, D, and E compacted at the optimum moisture content. Another indication of the effect of specimen dry density on erosion for these materials is presented on Figure 19 which plots percent erosion per unit time, α .

69. Both of these figures show that there is little effect of dry density on erosion for silt specimens compacted at the optimum molding water content. However, the clay material (Material B) was more erodible as the density decreased.

70. Eroding Fluid Concentration: The effect of the ionic concentration of the eroding fluid on the erodibility of a clay, Material B, and of a silt, Material E, was also investigated. Two ion concentrations were used (3 meq/l and 6 meq/l). These concentrations values are within the range of typical reservoir waters. The 3 meq/l solution used in the study was tap water with 2/3 calcium ions, 1/3 magnesium ions and a trace of sodium. The 6 meq/l concentration was prepared on the basis of one third equal parts of sodium, magnesium and calcium ions.

71. Figure 20 shows that the maximum erosion rate, \dot{e}_{max} , decreased slightly (as expected) when the eroding fluid ionic concentration was increased from 3 meq/l to 6 meq/l. This effect was slightly more pronounced for silt than for clay.

72. Use of Standard Concrete Sand as Filter Material: The possibilities of applying the triaxial erosion test methodology to test the effectiveness of filter materials for the protection of cracked fine-grained soils was investigated.

73. Figure 21 shows the grain size limits for a standard concrete sand material (ASTM C-33). This figure also shows the grain size distribution of the standard concrete sand used as the filter for this investigation, and the grain size distribution of a typical base soil (Material E).

74. The filter material was compacted in three layers to a dry density of 1.763 Mg/m^3 (110 lb/ft^3) at a water content of 12% and then frozen. Base specimens were prepared in the same manner as for the other erosion test specimens. The base specimen was then placed on top of the filter specimen in the triaxial erosion cell and the filter was allowed to thaw for about two hours prior to testing. The direction of flow in the test was downward through the cracked base material and into the intact sand filter.

75. The results of these tests, summarized in Table 11, showed that the standard concrete sand was effective in eliminating the loss of base material of even the highly erosive Material E (Teton Dam material) at hydraulic heads of up to 40 meters which was equivalent to a gradient of 350.

PART VIII: DISCUSSION OF THE TEST RESULTS

76. Results of this study were compared to results obtained by other researchers. The following paragraphs describe these comparisons and discuss the test results in more detail.

77. Effect of Molding Water Content: Figures 16 and 17, summarizing the effect of molding water content on erosion, show an initial decrease, an inflection point, and then an increase in both the maximum erosion rate, \dot{e}_{\max} , and percent erosion per unit time, α , as the water content increases. Similar behavior was observed and reported by Lewis and Schmidt (1977) for tests performed on an Oklahoma silty clay using the pinhole test. The plastic and liquid limits for their material were given as 15% and 31%, respectively. Their results are presented in Figure 22. The results of their investigation and the results obtained in this report for a similar material (Material B) have also been replotted in terms of percent erosion per unit time, α , as shown in Figure 23.

78. Another similar study, conducted by Grissinger (1962), used the flume test to study the effect of compaction water content on the erosion potential of a Grenada silt loam (Perry, 1975). The plastic and liquid limits for this material were given as 20 and 31 percent, respectively. The optimum water content was not provided, but an estimated value of 21% was calculated from the Atterberg Limits (Bowles, 1970). The results of Grissinger's investigation have been replotted in terms of the maximum erosion rate and are shown in Figure 24. This figure shows that the erosion behavior of the Grenada silt loam was similar to the behavior measured for Materials B, D, and E.

79. Lewis and Schmidt noted that the initial decrease in erosion with increasing water content was contrary to expectations from a consideration of the theory of structure-stability of clay particles. This theory suggests that there are two principal forces which act between adjacent particles: attractive (or Van der Waal) forces between the atoms of different particles, and repulsive (or Osmotic) forces between the electrical double layer surrounding each particle. Higher compaction water content results in a larger distance between the clay particles. Therefore, since the attractive Van der Waal forces are inversely proportional to some high power of the interparticle distance, the attractive forces decrease with increasing water content due to the increased particle distance. Thus, the erosion should have increased as the water content increased.

80. In addition, higher compaction water content should yield a lower ionic concentration. This lower ionic concentration has been reported to produce a stronger repulsion, or an increase in osmotic forces, between particles (Resendiz, 1977). Therefore, this lower ionic concentration should have also resulted in an increase in erosion. This discussion may explain the behavior shown in Figures 16, 17, 22, 23, and 24 for water contents above optimum, but it does not explain the decrease in erosion observed for water contents below optimum.

81. The initial decrease in erosion for water contents below optimum was attributed by Lewis and Schmidt to slaking. Slaking is the breakdown of soil upon immersion in a fluid. One of the mechanisms that contributes to this soil breakdown is the action of capillary absorption of the fluid and its subsequent compression of the air within the voids of

the soil. This compression may become higher than the forces keeping the soil particles together, causing slaking. A reduction in slaking and therefore in erosion should occur as the amount of entrapped air available for compression decreases as the water content increases.

82. The inflection point, shown in Figures 16, 17, and 22, is of particular interest since it corresponded to the point of minimal erosion. For the tests performed by Lewis and Schmidt on the Oklahoma silty clay, this inflection point coincided with the water content at both the plastic limit (15%) and the standard Proctor optimum moisture content (14%). Therefore, the change from decreasing erosion to increasing erosion was attributed to the amount of water within the voids at or above the plastic limit.

83. It may be seen that Grissinger's results are of the same form, and that the inflection point also coincides with the water content at both the plastic limit (20%) and at the standard Proctor optimum moisture content (21%). However, Lewis and Schmidt's results for specimens compacted by the modified Proctor method, as shown in curve B of Figure 23, showed the inflection point being somewhat shifted towards the modified Proctor optimum water content of 10%.

84. For the materials tested for this report, however, the inflection point did not coincide with the plastic limit; the inflection point was 1 or 2 percentage points above the optimum water content of each material while the plastic limit was about 6 percentage points above the optimum water content for all three materials. Thus, it appears that the optimum compaction moisture content is a better indicator of the mechanism affecting erosion than the plastic limit.

85. Effect of Molding Water Content on Teton Dam Material: It is interesting to note that the core of the Teton dam embankment was compacted at an average water content of 18.5%, or 1% dry of the core's average optimum water content of 19.6%. (U.S Department of the Interior, 1977). It may be seen in Figure 16, that compacting Teton Dam specimens (Material E) at a molding water content 1% dry of optimum, gave an erosion rate of 0.3 g/min-cm^2 which was twice as high as the minimum measured erosion rate obtained at +1.5 % wet of optimum of 0.16 g/min-cm^2 . Both of these erosion rates are high. Erosion tests which provide quantitative data could be useful to the dam designer faced with making a choice between two nondispersive borrow materials for the core of a dam or a choice of compaction water contents on a given core material.

86. Effect of Density on Erosion: Figures 18 and 19 summarize the effect of variation in specimen density on erosion. Limited data shows that there was little effect of specimen density on erosion from 95% to 99% of standard Proctor maximum density for the silt materials D and E. However, there was some decrease in erosion when the density of clay (Material B) was increased from 90% to 98% of standard Proctor density.

87. Figure 25 further evaluates the effect of density on erosion by plotting percent erosion per unit time versus percent standard Proctor density for the clay material B and an Oklahoma silty clay studied by Lewis and Schmidt (1977). Data from Lewis and Schmidt were replotted using only specimens which were at about the same moisture content of either 13% to 15% or 7% to 8%. The higher moisture content corresponded with both the plastic limit and the standard Proctor optimum moisture content of 15%.

88. No effect of density on erosion was noted for specimens at a water content of 13% to 15% which was at about the standard optimum and the plastic limit. However, at a water content of 7% to 8%, decreasing density had an effect of increasing erosion by over 1.5 times. This water content was below both the modified optimum of 10% and the plastic limit of 15%.

89. Data from Material B was obtained from tests performed on material compacted at its optimum water content of 15%, which was 6% below the plastic limit of 21%. The density varied from 90% to 98% of standard Proctor density (97 PCF to 106 PCF). For Material B the percent erosion per unit time decreased from 0.33 %/min to 0.08 %/min for this increase in density.

90. In evaluating this data it should be noted that specimens used for Lewis and Schmidt's study were compacted by both the standard and modified Proctor methods. Therefore, the compaction energy may also influence erosion for fabric sensitive materials such as clays.

91. Effect of Eroding Fluid Concentration: Figure 20 shows that increasing the ionic concentration of the eroding fluid had little effect on the erodibility of the clay core material (Material B), but decreased the erodibility of the silt core materials (Materials D and E).

92. Field observations and other laboratory investigations have also indicated that a marked decrease in the amount of erosion is expected for an increase in the ionic concentration of the eroding fluid. Arulnandan, et. al. (1975) provided an explanation for this behavior. They

noted that when the ionic concentration of the fluid is lower than the ionic concentration of the pore fluid, water may move into the surface of the soil by osmosis. This increase in water content would increase the interparticle distance at the surface, and thus reduce bonding between particles such that the erodibility of the material would be increased. This explanation is in accord with the explanation offered previously for the increase in erosion observed when the molding water content is above the optimum water content of the material.

93. On the other hand, similar investigations by Arulanandan, et. al. (1973) have shown that although two eroding fluids may have the same ionic concentration, calcium cations have a larger effect on reducing the amount of erosion than sodium cations. Moreover, it is interesting to note that although the total concentrations of the two eroding fluids used in this study were different (3 and 6 meq/l), the amount of calcium cations present in each eroding fluid was the same (2 meq/l). Therefore, it is possible that the relative erosion insensitivity of the materials tested to different ionic concentrations was due to the equivalent amount of calcium cations present in the eroding fluids.

94. Effect of Using Standard Concrete Sands as Filter Material: In 1977, Sherman proposed the use of standard concrete sand (ASTM C-33) as a filter for all fine-grained materials (Wilson and Marsal, 1979). Results of the limited amount of data from the filter tests performed for this report suggested that standard concrete sand filters are effective in preventing erosion of a highly erosive silt (Material E) at pressure heads of up to 40 meters. Therefore, Sherman's proposition may repre-

sent a simple and more economical alternative for the protection of cracked embankment dam core materials than present filter design criteria based solely upon the grain size distribution of intact core and transition materials (Table 3).

95. Effect of Assumed Erosion Channel Shape: Appendix D presents the results of a numerical analysis to investigate the validity of assuming that the triaxial erosion test flow channel eroded as a constant width rectangle. It may be remembered that it was assumed that only the thickness of the rectangular flow channel varied with time to account for the soil volume being eroded. The results of calculations performed using this simple model were numerically compared to results obtained using two different flow channel shape models: 1) a constant width elliptical shape, and 2) a variable width elliptical shape having both the width and thickness varying with time to account for the soil volume being eroded.

96. The results of the numerical comparison showed that parameters calculated using the simple constant width rectangle shape model varied by less than $\pm 15\%$ from the parameters calculated using either of the two more sophisticated shape models. This variation was felt to be insignificant for the results presented in this report. Therefore, the simple rectangular channel was used.

97. Effect of Assumed Hydraulic Behavior: Appendix E presents the results of an experimental study to observe and characterize the flow occurring through a plexiglas model of the triaxial erosion test flow channel. Observations of these hydraulic experiments indicated that

flow separation could be introduced during an erosion test at the top of the erosional channel at the abrupt transition between the narrow injecting flow nozzle and the rapidly enlarging erosional channel. This flow separation was not severe at gradients below approximately 35 and for crack thicknesses less than about 0.7 cm.

98. An equation for duct entrance effects on fluid wall shear stress was used to estimate a 30% increase over laminar wall shear due to flow separation effects (Olson, 1980). This 30% increase in shear was accounted for in the flow parameter ψ in Eq.5 of PART V.

99. Some additional experiments were performed to investigate optimization of the triaxial erosion test hydraulic design so that flow separation would be lessened. Replacing the top platen and injecting flow nozzle with a top platen having a gradual transition conical flow entrance resulted in a marked suppression of flow separation. Some additional study is recommended to optimize the hydraulic design of the triaxial erosion test apparatus.

PART IX: SUMMARY AND CONCLUSIONS

A triaxial erosion test was used to study the influence of the engineering properties of soils and chemistry of the eroding fluid on the erodibility of typical embankment dam core materials. The test modeled the flow of water through a cracked element of soil under a state of stress and hydraulic conditions similar to those existing in the core of a dam. The following conclusions were reached based on the results of the investigation:

1) High erosion took place in silt soils, moderate erosion took place in clayey silt soils and effectively no erosion took place in clay soils. These results are in agreement with results obtained by others using the pinhole test, and other similar test procedures.

2) The erodibility of silt materials is greatly influenced by variation in the molding water content. However, the effect of molding water content on erodibility is less pronounced for clayey materials. These results suggest that control of the compaction water content during construction may reduce the erosion potential of embankments with silt cores, but not for embankments with clay cores.

3) The water content at the plastic limit has been suggested in the literature as an indicator of the moisture content at which minimum erosion will occur. In contrast, the results of this investigation indicate that the optimum compaction water content is a better indicator than the plastic limit of the moisture content at which minimal erosion will occur. This inconsistency can be explained when it is noted that

for some of the materials cited in the literature, the water content at the plastic limit was very close to the optimum compaction moisture content.

4) Limited data obtained indicated that density has little effect on the erosion potential of silt embankment dam core material compacted at the optimum molding water content. However, clayey materials were somewhat sensitive to variations in density; for clays erodibility increased as density decreased.

5) Tests also showed that the ionic concentration measurably influenced the erodibility of silt core materials but had less effect on the erodibility of clay core materials. The higher the ionic concentration of the eroding fluid, the lower the erosion.

6) Tests indicated that standard concrete sand material (ASTM C-33) as a downstream filter, clogs core cracks by collecting core material particles downstream. Such downstream filters effectively prevented erosion even for highly erosive materials under hydraulic heads of up to 40 meters. Such sand filter materials may provide more economical protection of cracked embankment dam core materials than filters designed using criteria based upon the grain-size distribution of core and transition materials.

7) It was found that the erosion rate, \dot{e} , asymptotically approached a maximum value for increasing values of fluid shear stress. If a maximum value of erosion rate does in fact exist as a material constant under known compaction and environmental conditions, it would be a useful material parameter for embankment dam design.

8) It is recommended that more research be conducted to:

- a) Optimize the hydraulic characteristics of the triaxial erosion test apparatus.
- b) Further study the inter-relationship between moisture content, density and the erosion rate.
- c) Further study the possibility that a maximum erosion rate exists, and how this concept may be used in embankment dam design.

REFERENCES

1. Aitchison, G.D., and Wood, C.C. (1965), "Some interactions of Compaction, Permeability, and Post-Construction Deflocculation Affecting the Probability of Piping Failure in Small Earth Dams," Sixth International Conference on Soil Mechanics and Foundation Engineering, Montreal, Vol.1, pp.442-446.
2. Arulanandan, K., Loganathan, P., and Krone, R.B. (1975), "Pore and Eroding Fluid Influences on Surface Erosion of Soil," Journal of the Geotechnical Engineering Division, American Society of Civil Engineers, Vol. 100, No. GT1, January, pp.51-65.
3. Arulanandan, K., Loganathan, P. and Krone, R.B. (1976), Closure to the Paper: "Pore and Eroding Fluid Influences on Surface Erosion of Soil," Journal of the Geotechnical Engineering Division, American Society of Civil Engineers, Vol.102, No.GT8, August, pp.883-884.
4. Arulanandan, K. (1978), "Erosion in Relation to Filter Design Criteria for Earth Dams," Presented for Conference on New Perspective on Dam Safety, Stanford University, August.
5. Arulanandan, K., Gillogley, E., and Tully, R. (1980), "Development of a Quantitative Method to Predict Critical Shear Stress and Rate of Erosion of Natural Undisturbed Cohesive Soils," Technical Report No. GL-80-5, U.S. Army Engineer Waterways Experiment Station, CE, Vicksburg, Mississippi, July.
6. Bertram, G.E. (1967), "Experiences with Seepage Control Measures in Earth and Rockfill Dams," Ninth International Congress On Large Dams, Istanbul, Turkey, Vol.3, pp.91-110.
7. Bowles, J.E. (1970). Engineering Properties of Soils and their Measurement, 2nd Edition, McGraw Hill Book Company, New York.
8. Brater, E.F., and King, H.W. (1976), Handbook of Hydraulics, 6th Edition, McGraw Hill Book Company, New York.
9. Gori Bello, J.I., Lei Lam, S.F.A. (1979), "Filtros Protectores En Presas De Tierra," Trabajo Presentado Ante La Universidad Catolica Andres Bello Como Parte De Los Requisitos Para Optar Al Titulo De Ingeniero Civil, Caracas, Venezuela, November.

10. Grisinger, E.H. (1966), "Resistance of Selected Clay Systems to Erosion by Water," Water Resources Research, Vol.2, no.1, pp.131-138.
11. Hjeldnes, E.I., and Lavania, B.V.K. (1980), "Cracking Leakage and Erosion of Earth Dam Materials," Journal of the Geotechnical Engineering Division, American Society of Civil Engineers, Vol.105, No.GT2, February, pp.117-135.
12. Hsu, S.J.C. (1981), "Aspects of Piping Resistance to Seepage in Clayey Soils," Tenth International Conference on Soil Mechanics and Foundation Engineering, Stockholm, Vol.1, pp.421-428.
13. Iwai, K. (1976), Fundamental Studies of Fluid Flow Through a Single Fracture, Ph.D. thesis, University of California, Berkeley.
14. Jaworski, G.W., Duncan J.M., and Seed H.B. (1981), "Laboratory Study of Hydraulic Fracturing," Journal of the Geotechnical Engineering Division, American Society of Civil Engineers, Vol.107, No.GT6, June, pp.713-732.
15. John, J.E.A., and Haberman, W.L. (1971). Introduction to Fluid Mechanics, Prentice-Hall, Inc., Englewood Cliffs, New Jersey.
16. Kjaernsli, B., and Torblaa, I. (1968). "Leakage Through Horizontal Cracks in the Core of Hyttejuvet Dam," Publication No.80, Norwegian Geotechnical Institute, Oslo, pp.39-47.
17. Lewis, D. A. and Schmidt, N. O. (1977), "Erosion of Unsaturated Clay in a Pinhole Test," Dispersive Clays. Related Piping, and Erosion in Geotechnical Projects, ASTM STP 623, Edited by J.L. Sherard and R.S. Decker, American Society for Testing and Materials, Philadelphia, pp.260-273.
18. Lu, P.C. (1979), Fluid Mechanics, Iowa State University Press, Ames, pp.468.
19. Olson, R.M. (1980). Essentials of Engineering Fluid Mechanics, Harper and Row Publishers, New York.

20. Ofoegbu Iroanya, G. (1981), "Design Procedures for the Protection of Earth Dam Cores Against Piping Damage," a thesis submitted in conformity with the requirements for the Degree of Master of Applied Science at the University of Toronto, Ontario.
21. Parkin, A.K. (1976), "A Review of Hydraulic Fracturing in Dams," Internal Report 53103-1, Norwegian Geotechnical Institute, November.
22. Perry, E.B. (1975), "Piping in Earth Dams Constructed of Dispersive Clay; Literature Review and Design of Laboratory Tests," Technical Report No. S-75-15, U.S. Army Engineer Waterways Experiment Station, CE, Vicksburg, Mississippi, November.
23. Perry, E.B., and Postol, G.J. (1977), "Dispersion Characteristics of Clay from Mushroom Cave, Meramec Park Lake Project, Meramec River Missouri," Dispersive Clays, Related Piping and Erosion in Geotechnical Projects, ASTM STP 623, Edited by J.L. Sherard and R.S. Decker, American Society for Testing and Materials, Philadelphia, pp.313-329.
24. Perry, E.B. (1979), "Susceptibility of Dispersive Clay at Grenada Dam, Mississippi, to Piping and Rainfall Erosion," Technical Report No. GL-79-14, U.S. Army Engineer Waterways Experiment Station, CE, Vicksburg, Mississippi, September.
25. Petry, T.M., and Haliburton T.A. (1975), "Determination of Dispersive Clay Soil Erodibility by Using a Physical Test," Transportation Research Record Publication 532, Washington, D.C., pp.95-104.
26. Resendiz, D. (1977), "Relevance of Atterberg Limits in Evaluating Piping and Breaching Potential," Dispersive Clays, Related Piping and Erosion in Geotechnical Projects, ASTM STP 623, Edited by J.L. Sherard and R.S. Decker, American Society for Testing and Materials, Philadelphia, pp.341-353.
27. Richards, L.A., Ed. (1954), Diagnosis and Improvement of Saline and Alkali Soils, Agriculture Handbook No.60, U.S. Department of Agriculture, Washington, D.C.
28. Sanchez, R.L., and Silver, M.L. (1982), "Laboratory Triaxial Erosion Test Procedure for the Evaluation of the Erosion Potential of Embankment Dam Materials," U.S. Army Engineer Waterways Experiment Station, CE, Vicksburg, Mississippi (unpublished).

29. Sherard, J.L. (1973), "Embankment Dam Cracking," Embankment Dam Engineering, Casagrande Volume, edited by R.C. Hirschfeld and S.J. Poulos, Wiley, N.Y., pp.272-353.
30. Sherard, J.L., Dunnigan, L.P., Decker, R.S., and Steele, E.F. (1976), "Pinhole Test For Identifying Dispersive Soils," Journal of the Geotechnical Engineering Division, American Society of Civil Engineers, Vol.102, No.GT1, January, pp.69-85.
31. Sherard, J.L., Decker, R.S., and Ryker, N.L. (1972), "Piping Damage in Earth Dams of Dispersive Clay," Performance of Earth and Earth-Supported Structures, American Society of Civil Engineers, Vol.1, pp.589-626.
32. Silver, M.L. (1976), "Laboratory Triaxial Testing Procedures to Determine the Cyclic Strength of Soils," Report No. NUREG-31, U.S. Nuclear Regulatory Commission, Washington, D.C.
33. Swanberg, N.E. (1966), "An Experimental Study of the Relation of Soil Strength Properties to Erodibility of Soil," a thesis submitted in conformity with the requirements for the Degree of Master of Science at the University of Minnesota. Minneapolis, Minnesota.
34. U.S. Department of the Interior (1976), "Failure of Teton Dam," Independent Panel to Review Cause of Teton Dam Failure, Denver, Colorado, December.
35. U.S. Department of the Interior, (1977), "Failure of Teton Dam: A Report of Findings," Teton Dam Failure Review Group, Denver, Colorado, April.
36. USCOLD (1975), Lessons from Dam Incidents, USA, American Society of Civil Engineers, New York.
37. Vaughan, P.R., and Soares, H.F. (1982), "Design of Filters for Clay Cores of Dams," Journal of the Geotechnical Engineering Division, American Society of Civil Engineers, Vol.108, No.GT1, January, pp. 17-31.
38. Vaughan, P.K. (1976), "Cracking of Embankment Dam Cores and the Design of Filters for their Protection," Sociedad Espanola De Mecanica De Suelo y Cimentaciones, Numero 23, Madrid, Sept.-Oct.

39. Wilson, S.D., and Marsal, R.J. (1979), Current Trends in Design and Construction of Embankment Dams, American Society of Civil Engineers, New York.

TABLE 1

LIST OF DAMS WHICH HAVE
EXPERIENCED EROSION PROBLEMS

NO	YEAR		NAME OF THE DAM	TYPE OF DAM	HEIGHT m	OCCURRENCE OR DEFECT	CAUSE
	CONSTRUCTION	OCCURRENCE					
1	-	1890	Garrison, Calif., USA	Homogeneous dam	6.60	Piping through dam	
2	1895	1895	Angels, USA	Homogeneous dam	17.40	Piping through dam	
3	-	1896	Bradford, England	Homogeneous dam	29.70	Piping through dam	
4	1899	1899	Lake Francis, Calif.	Homogeneous dam	25.40	Piping through dam	
5	1893	1904	Avalon, USA	Stone dam	19.40	Piping through dam	
6	1901	1904	Greenlick, USA	Homogeneous dam	20.40	Piping through dam	
7	1907	1909	Blackrock, USA	Stone dam	23.10	Piping through dam foundation	
8	1905	1910	Jalesbury, USA	Homogeneous dam	19.80	Piping through foundation	
9	1911	1913	Blackfoot, USA	Stone dam	16.20	Piping through foundation	
10	1912	1914	Horse Creek, Cal. USA	Homogeneous dam	18.20	Piping through foundation	
11	1913	1914	Habron, USA	Homogeneous dam	18.20	Piping through foundation	
12	1913	1915	Lyman, USA	Homogeneous dam	21.50	Piping through foundation	
13	1902	1916	Lake Tommy, USA	Homogeneous dam	20.50	Piping through dam	
14	1920	1921	Forayt, USA	Homogeneous dam	21.50	Piping through foundation	
15	1920	1923	Apishapa, Cal., USA	Homogeneous dam	37.00	Piping through dam	Cracking due to differential settlement
16	1927	1928	Lake Almarour, USA	Homogeneous dam	42.90	Piping through foundation	
17	1929	1929	Little Field, USA	Homogeneous dam	41.30	Piping through dam	
18	1930	1930	Corpus Christi, USA	Homogeneous dam	20.20	Piping through foundation	
19	1903	1932	Deschutes Forebay, Cal USA	Homogeneous dam	17.50	Piping through dam	
20	1899	1935	Lake Francis, USA	Homogeneous dam	25.40	Piping through dam	
21	1938	1939	Dry Creek, Mont. USA	Homogeneous dam	15.20	Piping through dam and foundation	
22	1946	1948	Wister, Oklahoma, USA	Homogeneous dam	16.00	Piping through dam	
23	1947	1948	Fred Barr, USA	Homogeneous dam	19.80	Piping through dam	
24	1949	1949	Wister, USA	Homogeneous dam	29.70	Piping through foundation	
25	1949	1950	Stockton, Calif., USA	Homogeneous dam	26.70	Piping through dam	Cracking due to differential settlements
26	1940	1954	Pampulha, Brazil	Homogeneous dam with concrete slab on upstream face	11.50	Piping through dam (complete failure)	High gradients due to rupture of concrete plate and inadequate internal drainage
27	1899	1957	Mill Creek, USA	Homogeneous dam	22.10	Piping through foundation	
28	1959	1960	Parr Forest, USA	Homogeneous dam	49.50	Piping through dam	
29	1960	1960	Alamo Arroyo, Site 2	Homogeneous dam	22.50	Piping through foundation	
30	1959	1962	Cobb Creek #1	Homogeneous dam	24.80	Piping through foundation	
31	1951	1963	Baldwin Mills, USA	Homogeneous dam	86.50	Piping through dam	
32	1962	1963	Little Bear Creek, USA	Homogeneous dam	28.00	Piping through dam	
33	-	1963	Chaparral, Oregon, USA	Rockfill dam with clay core	174	Piping through dam	Cracks due to differential settlement
34	1962	1963	Jewell Creek Watershed 3, USA	Homogeneous dam	22.80	Piping through foundation	
35	1960	1964	Jewell Creek Watershed 16, USA	Homogeneous dam	18.2	Piping through foundation	
36	1964	1964	Bunder Wala, India	Homogeneous dam	6.6	Piping through dam	
37	-	1964	Boudart, Oregon USA	Rockfill dam with impervious core	147	Piping through dam	Transverse cracks due to irregular placement of rockfill

From Hsu (1981)

TABLE 1 (continued)

NO	YEAR		NAME OF THE DAM	TYPE OF DAM	HEIGHT m	OCCURRENCE OR DEFECT	CAUSE
	CONSTRUCTION	OCCURRENCE					
38	1961	1965	Balderhead, England	Rockfill dam with impervious core	52.4	Piping through dam	Poor filter grading and segregation
39	-	1965	Djetiluhur, Indonesia	Rockfill dam with clay core	126	Piping through dam	Horizontal fissures due to core consolidation
40	1964	1965	Hyttejuvet, Norway	Rockfill dam with impervious core	100	Piping through core of the dam	Hydraulic fissuring in core, segregation of filter
41	1963	1963	Yard's Creek Upper Reservoir, N. Y., USA	Rockfill dam with impervious core	26.70	Piping through dam	Cracking in core and filter due to excessive fines in filter
42	1965	1966	Matuhina, New Zealand	Rockfill dam with impervious core	66.80	Piping through dam	Cracking in core and filter due to excessive fines in filter
43	1970	1971	Viddalsvatn, Norway	Rockfill dam with impervious core	76.80	Piping through dam	Cracking in core and filter due to excessive fines in filter
44	1970	1971	Seitavare, Sweden	Rockfill dam	116.90	Piping through foundation	Concentration of high gradients due to discontinuities in foundation permeability
45	1970	1971	Bastusel, Sweden	Rockfill dam with impervious core	44.00	Piping through foundation	Discontinuity in foundation leading to seepage concentration
46	1970	1971	Flagstaff Gully, Tasmania, Australia	Rockfill dam with impervious core	44.00	Piping through dam	Open cracks in rock, cracking in filter, erodible clay in core
47	1975	1976	Teton, Idaho, USA	Rockfill dam with impervious core	100	Piping through contact between core and foundation leading to total failure	Erodible material, open joints in rock. Inadequate filter gradation and low permeability
48	1975 - 1977	1978	Cofferdam in Amazon Region, Brazil	Rockfill dike and compacted clay	15	Piping and failure of a section through compacted clay core	High gradients, poor transition and filter leading to failure of a section
49	1970	1973	Tarbela, West Pakistan	Rockfill dam with clay core	147	Piping in upstream clay blanket	Piping of sand, clay through openwork boulder-gravel foundation

From Hsu (1981)

TABLE 2
SUMMARY OF FIELD
OBSERVATIONS FOR DAMS
WHICH HAVE EXPERIENCED
EROSION PROBLEMS

EMBANKMENT DAM			CORE MATERIAL			FIELD OBSERVATIONS			References		
NAME (Location)	TYPE	HEIGHT (m)	Description of Core Material	Atterberg Limits LL PL (%)	Compacted Water Content (%)	Compacted Density (g/cm ³)	Estimated Crack Dimensions (m)	Leakage Range (l/sec) (m/sec) ^a		WARNING OF PIPING PROBLEM In Solids Leakage Field	POSSIBLE CAUSE OF PIPING Problem
Soldershead (England) (1965)	Backfill with clay core	45	1000	Gravelly, Sandy Clay	30-40 IS Standard ASTM Optimum	N.A.	20	N.A.	5 to 55	Small depression at downstream toe of dam. Another crack (3 meters in diam. and 25 meter deep) developed. - Concentrated leakage developed at downstream toe of dam. - Grading of core - Leakage through zonel cracks due to differential settlement. - Core material settling after grading.	Sherard, 1973
Pytojuvet (Norway) (1965)	Backfill with impermeable core	90	600	Gravelly, Clayey Silt (glacial moraine)	1.5% below to 2% above Std. ASTM OPT.	97% to 100% Std. ASTM Max.	24	longitudinal cracks 5mm wide and length of 11m along crest of dam	2 to 53	"7.1 gram Concentrated leakage of clay water emerged at downstream toe of dam. - Very fine, gray silt." - Concentrated leakage of clay water emerged at downstream toe of dam. - First filling observed.	Kjornali and Torbia, 1967; Sherard, 1973
Teton Dam (Idaho, U.S.A.) (1976)	Backfill with impermeable core	93	976	Slightly Clayey/ Silt	1.4% below Std. ASTM Optimum	98% of Std. ASTM Max.	30	Seepage path developed from downstream toe of dam to embankment to a tunnel 12 meters long by downstream toe 2 meter in diam.	60 to 570	"Clear to slightly cloudy water." - Small leaks noted down- stream 10 to 15 days before failure - Wet spot on embankment 2 meters before failure	U.S. Dept. of Interior, 1976 end 1977
Witaco (Chihuahua, U.S.A.) (1949)	Heterogeneous	27	1740	Silty Clay	At about Std. ASTM Optimum	97% of Std. ASTM Maximum	15	6 mm cracks at crest observed erosion tunnel 9.6 meters wide observed	142 to 570 over length of 150 m	"Muddy and carrying suspended solids." - Concentrated leakage during first filling observed about 1 meter above toe - Dispersive Material Caused by tunnels	Bertram, 1967; Sherard, 1973
Yard's Dam (New Jersey U.S.A.) (1943)	Backfill with impermeable core	26	2743	Gravelly Clayey Sandy Silt (glacial moraine)	25-33 6-10 "Near Std. ASTM Optimum"	N.A.	8.0	N.A.	19 to 90 over a length of 91 m	"Clean to chocolate milk." - Dirty leakage at downstream toe of dam during first filling - Seven individual areas of leakage appeared through "Microcracks"	Sherard, 1973

• liters/second.

TABLE 3

SUMMARY OF FILTER
DESIGN CRITERIA

AUTHOR	CRITERIA DEVELOPED	REMARKS		
Stearns (1) (1900)	Ideas to provide filter protection to prevent washing out of fines by seepage	(1) Trans. ASCE, Vol. 48 P. 267.		
Bligh (1910)	$C_c = \frac{L}{hcr}$ C_c = creep ratio L = percolation path hcr = maximum permissible head i = hydraulic gradient	(1) Recommended C_c Values: Type of material C_c 1 - Silt & sand (slightly comp.) 18 0,06 - Fine micaceous sand 15 0,07 - Coarse sand 12 0,08 - Boulders, gravel, sand mixtures 5-9 0,2 to 0,11		
Lars (1935)	$C_v = \frac{\frac{1}{i} S + t}{hcr}$ C_v = weighted creep ratio S = length of percolation in horizontal direction t = length of percolation in vertical direction i = hydraulic gradient	(2) Recommended C_v Values: Type of material C_v 1 Very fine sand or silt 8,5 0,12 Fine sand 7,0 0,14 Medium sand 6,0 0,17 Coarse sand 5,0 0,20 Gravel, fine 4,0 0,25 Medium gravel 3,5 0,285 Coarse gravel 3,0 0,33 Boulders, stone, gravel 2,5 0,40		
Marsa (1935)	$i_g = \frac{h}{L} (1 - P) (S - 1)$ i_g = flotation gradient h = difference in head L = length of path P = porosity S = specific gravity	(3) For $S = 2,65$ Porosity (P) Critical if 0,30 1,15 0,35 1,07 0,40 0,99 0,50 0,825		
Cresser, Justin Hinds (1945)	$\frac{h}{L} > 8 \text{ or } 10$ h = difference in head L = length of path	(3A) for highly pervious foundations, without cutoff provisions or filter protection		
Cedargren (1973)	$G_s = \frac{\sigma_v}{u}$ G_s = factor of safety with respect to "blowup" or "bulk heave" σ_v = the total vertical stress at any point u = corresponding pore pressure	(4) if weighted filter is provided, $G_s \geq 1,5$		
B - Filter Design Criteria Based on Laboratory Testing				
AUTHOR	BASE MATERIAL (B)	FILTER MATERIAL (F)	CRITERIA DEVELOPED	REMARKS
Terraghi (1922)	Criteria probably based on experience and reasoning		$\frac{D_{15} F}{D_{85} B} \leq 4$	(5) Subscripts 15 and 85 refer to the percentage finer by weight than grain size D. F and B indicate Filter and Base material respectively
			$\frac{D_{15} F}{D_{15} B} \geq 4$	(6) $C_u = \frac{D_{60}}{D_{10}}$ = (coefficient of uniformity)

From Hsu (1981)

TABLE 3 (continued)

SUMMARY OF FILTER
DESIGN CRITERIA

AUTHOR	BASE MATERIAL (B)	FILTER MATERIAL (F)	CRITERIA DEVELOPED		REMARKS
Bartram (1939)	Silt, fine sand (quartz, Ottawa Sand)	Uniform quartz & Ottawa Sand	$\frac{D_{15} F}{D_{85} B} \leq 6$	(7)	
			$\frac{D_{15} F}{D_{15} B} \leq 9$	(8)	
Newton & Harley (1940)	Well graded gravelly sand	Natural bank gravels, fairly uniform fines screened out	$\frac{D_{15} F}{D_{15} B} \leq 32$	(9)	- do not agree with Terzaghi's and Bartram's criteria.
			$\frac{D_{15} F}{D_{30} B} \leq 15$	(10)	
U.S. Army Corps of Engineers Waterways Experiment Station (USACE - WES) (1941/42/48/53)	Random material all types, fine to coarse uniform sand	Random type natural pit-run gravels	$\frac{D_{15} F}{D_{15} B} \geq 4$	(11)	- gradation of filters should be approximately parallel to base. Filter should be well graded
			$\frac{D_{15} F}{D_{15} B} \leq 20$	(12)	- To avoid movement of filter into drain pipe perforations or joints see equations (20) and (21)
			$\frac{D_{30} F}{D_{30} B} \leq 25$	(13)	
			$\frac{D_{15} F}{D_{85} B} \leq 5$	(14)	
			$\frac{D_{15} F}{D_{85} B} < 6$ (15); $CuB < 1,5$		
			$\frac{D_{15} F}{D_{15} B} < 40$ (16); $CuB < 4,0$		
1955	cohesive soils (all types)	concrete sand, coarse aggregate recommended	$\frac{D_{15} F}{D_{15} B} > 5$	(17)	For medium to high plastic clays disregard equation (17) and use, $D_{15} F = 0,4$ mm, provided
			$\frac{D_{30} F}{D_{30} B} \leq 25$	(18)	$CuF \leq 20,0$
			$\frac{D_{15} F}{D_{85} B} \leq 5$	(19)	
			$\frac{D_{85} F}{\text{slot width}} \geq 1,2$	(20)	
			$\frac{D_{85} F}{\text{hole diam.}} > 1,0$	(21)	

From Hsu (1981)

TABLE 3 (continued)

SUMMARY OF FILTER
DESIGN CRITERIA

AUTHOR	BASE MATERIAL (B)	FILTER MATERIAL (F)	CRITERIA DEVELOPED		REMARKS
USSR 1947/55/74	Artificial Blended materials of various ranges including uniform material	Artificial uniform filters	$5 < \frac{D_{50} F}{D_{50} B} < 10$	(22)	Other requirements: 1. 100% passing 3 in. sieve 2. percent passing sieve # 200 < 5% 3. finer section of base and filter material should be approximately parallel 4. use eq. 22 for natural subrounded uniform material 5. for natural graded filters use eq. 23 and 24 6. for crushed rock filters use eq. 25 and 26 7. To avoid movement of filter into drain pipe opening use equation (27)
			$12 < \frac{D_{50} F}{D_{50} B} < 50$	(23)	
			$12 < \frac{D_{15} F}{D_{15} B} < 40$	(24)	
			$9 < \frac{D_{50} F}{D_{50} B} < 30$	(25)	
			$6 < \frac{D_{15} F}{D_{15} B} < 18$	(26)	
			$\frac{D_{85} F}{\text{max. opening of pipe drain}} \geq 2$	(27)	
Sherard et al (1963)			$\frac{D_{15} F}{D_{15} B} \geq 5$	(28)	Other requirements: 1. 100% passing 3 inch sieve 2. percent passing sieve # 200 < 5% 3. grain curves approximately parallel 4. use base material passing 1 in. sieve
			$\frac{D_{15} F}{D_{85} B} \leq 5$	(29)	
Vaughan (1978)	cohesive soils	non plastic silt, sand	"perfect filter" retaining clay in suspension or clay flocks		Testing recommended to establish criteria

From Hsu (1981)

TABLE 4
SUMMARY OF THE CHARACTERISTICS OF
SEMIOTEST PROCEDURES

Test Procedure	Ability to provide desired flow and rate range of specimens	Ability to apply desired conditions to specimens	Ability to properly measure the flow path	Ability to measure specimen rates and directions during testing	Ability to do filter tests	Comments	Reference
Isotonic Test	<ul style="list-style-type: none"> - typical range of flow up to 1 ml/min - low flow rates from 0.1-100 ml/min - gradient 0-100 	No	Yes, but expensive equipment due to size of the circularly shaped chamber	Possible, but flow rates may be small because of small specimen diameter	Yes, but at low gradients	<ul style="list-style-type: none"> - Simple and economical, but provides only qualitative results 	- Sherrard et. al. (1966); Perry (1975)
Flow Test	<ul style="list-style-type: none"> - low flow rates from 0.1-100 ml/min - gradient 0-100 	No	Yes, flow path is along the perimeter of the specimen	Specimen measurement of flow rates during testing	Yes	<ul style="list-style-type: none"> - One of the advantages of this test is the availability of the pin hole test 	- Perry and Millerton (1975); Perry (1975)
Flow Test	<ul style="list-style-type: none"> - large range of flow rates (velocity of up to 1.25 ml/min) - gradient may not be measured 	No	No, flow path is the center of the specimen	Specimen measurement of flow rates during testing	No	<ul style="list-style-type: none"> - Applicable to streambed erosion - Only estimated specimen may be tested - Good operators with high level of competence 	- Arslanoglu et. al. (1966); Perry (1975)
Flow Test	<ul style="list-style-type: none"> - low flow rates from 0.1-100 ml/min - gradient 0-100 	No	Yes, flow path is the center of the specimen	Specimen measurement of flow rates during testing	No	<ul style="list-style-type: none"> - Applicable to streambed erosion - Best expensive equipment - Uninterrupted specimens may be tested - Best expensive equipment - Best expensive 	- Arslanoglu et. al. (1966); Perry (1975)
Flow Test	<ul style="list-style-type: none"> - high flow rates from 0.1-100 ml/min - gradient 0-100 	No	Yes, flow path is the center of the specimen	Specimen measurement of flow rates during testing	No	<ul style="list-style-type: none"> - Standard terminal equipment may be modified to obtain results in streambed erosion - Best expensive equipment - Best expensive equipment - Best expensive equipment 	- This report

TABLE 5
EROSION TEST PROGRAM PARAMETERS

A) CONSTANT PARAMETERS

FACTOR	VALUE
Specimen Size	71.1 cm diameter 15.5 cm high
Initial Slot Dimensions	2.3 cm wide 0.2 cm thick
Triaxial Cell Confining Pressure	98 Kn/m ² (14.2 psi)
Hydraulic Head	1.3 meters
Eroded Length	11.5 cm
Hydraulic Gradient	10

B) VARIABLE PARAMETERS

FACTOR	LOWER LIMIT	UPPER LIMIT
Percent of Optimum Compaction Water Content (95% of Maximum Std. Proctor)	-4%	+4%
Percent of Maximum Standard Proctor Density (At Optimum Molding W/C)	90%	99%
Ion Concentration of Eroding Water	0 meq/l	6 meq/l
Standard Concrete Sand Filter	No Filter	Filter Present

TABLE 6
SUMMARY OF INDEX PROPERTIES OF ALL MATERIALS TESTED

Material Reference Letter	Description of Material	Atterberg Limits		Specific Gravity of Solids G_s	Maximum Dry Density (Std. Proctor) (Mg/m ³) (lb/ft ³)	Optimum Moisture Content (%)
		W_L	W_P			
A	Grey Clay	44	20	2.64	1.579	19.0
B	Tan Silty Clay	35	21	2.65	1.731	15.0
C	Reddish Sandy Lean Clay	63	45	2.72	1.611	22.0
D	Tan Clayey Silt	24	21	2.68	1.761	15.3
E	Tan Clayey Silt	27	25	2.67	1.615	19.0

TABLE 7

SOIL CHEMISTRY TEST RESULTS FROM PORE WATER EXTRACTS

Material	Sodium Na (meq/l)	Calcium Ca (meq/l)	Magnesium Mg (meq/l)	Potassium K. (meq/l)	Total Dissolved Solts TDS	Percent Sodium (%)	Sodium Adsorption Ratio SAR
A	1.17	10.28	0.30	0.20	12.03	9.7	0.51
B	4.12	32.04	17.93	0.95	55.04	7.5	0.82
C	0.68	0.14	0.05	0.05	0.92	73.9	2.21
D	2.60	8.28	2.27	0.54	13.69	19.0	1.13
E	1.55	1.70	1.82	0.17	5.24	29.6	1.17

$$TDS = Na + Ca + Mg + K$$

$$SAR = \frac{Na}{\sqrt{0.5(Ca + Mg)}} \quad (\text{from Richards, 1954})$$

TABLE 8
SUMMARY OF EROSION TEST RESULTS
MATERIAL: B (silty clay)

CONFINING PRESSURE = 99.0 kPa
HEAD OF WATER = 1.3 m

ERODED LENGTH = 0.12 m
HYDRAULIC GRADIENT = 10. m/m

Specimen Number	Specimen Dry Density (Mg/m ³)	Percent of Max Density (%)	Percent of Opt. w/c (%)	Initial Specimen Dry Mass W _i (g)	Final Specimen Dry Mass W _f (g)	Average Flow Rate (cm ³ /min)	Rate of Weight Erosion P (g/min)	Soils to Volume Ratio S (ppm)	Max Erosion Rate (g/cm ² -min)
B110	1.648	95	+2.0	995	959	515	0.5	976	0.01
B111	1.656	95	0.0	1004	936	458	1.0	2300	0.02
B112	1.609	93	-4.0	977	857	474	2.7	5700	0.04
B113	1.646	95	-2.0	998	896	541	2.5	4500	0.04
B114	1.702	98	0.0	1042	971	440	0.8	1800	0.01
B115	1.617	94	+4.0	987	934	486	1.2	2400	0.02
B117	1.645	95	+3.0	1002	956	515	1.2	2300	0.03
B119	1.641	95	+3.0	1002	929	519	1.1	2100	0.02
B120	1.640	95	+4.0	998	879	551	1.7	3100	0.03
B121	1.638	95	+1.5	989	929	495	0.5	1100	0.01
B123	1.551	90	0.0	943	875	337	3.2	6500	0.05
B701	1.642	95	+1.5	995	908	568	0.8	1400	0.01

* Optimum molding water content = 15.0 %

ERODED LENGTH $\approx 0.12m$
HYDRAULIC GRADIENT $\approx 10. m/m$

***Optimum molding water content = 15.0%**

TABLE 9
EXAMPLE OF ANALYSIS OF
TEST RESULTS FOR IRIAXIAL EROSION TEST

MATERIAL TYPE: SPECIMEN NUMBER:		B 117		R. L. SANCHEZ		AVERAGE FLOW RATE (Q):		515. CC/MIN	
TESTED BY:		3 26 82		1.645 G/CC		RATE OF WEIGH EROSION (P):		1.2 G/MIN	
DAIL ILSIED:		3.0 PERCENT		2.30 CM		DENSITY OF ERODING FLUID:		1.000 G/CC	
SPECIMEN DRY DENSITY:		0.23 CM		11.50 CM		VISCOSITY OF ERODING FLUID:		0.001 M*SEC/SQ.M	
% OF OPTIMUM WATER CONTENT:		INITIAL SLOT WIDTH:		INITIAL SLOT THICKNESS:		CONFINING PRESSURE:		98.00 KN/SQ.M	
INITIAL SLOT WIDTH:		INITIAL SLOT THICKNESS:		ERODED LENGTH:		HEAD OF WATER:		1.30 M	
INITIAL SLOT THICKNESS:		ERODED LENGTH:				HYDRAULIC GRADIENT:		10. M/M	
VOLUME OF FLOW (LITERS CC)	TIME (MIN)	CUM. WEIGHT ERODED (G)	CROSS SECTION AREA (SQ.CM)	VELOCITY OF FLOW (CM/MIN)	ERODED SURFACE AREA (SQ.CM)	CUM. WEIGHT ERODED PER AREA (G/SQ.CM)	EROSION RATE (GRAMS/ MIN * SQ.CM)	FLUID SHEAR STRESS (N/SQ.M)	REYNOLDS NUMBER
3.5	6.51	1.2	0.9	547.	62.	0.12	0.02	0.157	633.
7.0	12.43	12.2	1.3	391.	66.	0.18	0.02	0.085	597.
10.5	19.12	20.7	1.8	290.	71.	0.29	0.02	0.050	558.
14.0	25.80	29.4	2.2	230.	75.	0.39	0.02	0.036	530.
15.0	27.70	32.3	2.3	226.	76.	0.43	0.02	0.033	521.
16.0	30.40	35.1	2.5	210.	77.	0.45	0.02	0.029	510.
17.0	33.10	37.5	2.6	196.	79.	0.47	0.02	0.026	499.

TABLE 10
SUMMARY SHOWING THE ERODIBILITY OF MATERIALS

Material	Specimen No.	Description of Material Erodibility	Rate of Weight Erosion (g/min) P	Maximum Erosion Rate (g/cm ² -min) c_{max}	Test Duration (min)
A	A-110	Extremely low erosion rate	0.022	0.0004	303.45
B	B-113	Low erosion rate	0.25	0.04	32.5
C	C-110 (Sandy)*	Very low erosion rate	0.9	0.01	76.71
	C-120 (Coarse particles)**	Erosion rate increased	16.4	0.18	4.78
D	D-173 removed	High erosion rate	3.60	0.36	4.26
E	E-102	High erosion rate	2.86	0.35	3.65

*Bottom platen design may have contributed to blockage

**Passed through No. 50 Sieve

TABLE 11

SUMMARY OF FILTER TEST RESULTS

Specimen Number	Maximum Pressure Head Applied (m)	Maximum Rate of Flow Measured (cm ³ /min) Q	Rate of Weight Erosion (g/min) P	Maximum Erosion Rate (g/cm ² -min) \dot{e}_{max}	Test Duration (min)
E - 107 (without filter)	1.3	600	11.1	0.18	9
E - 800 (with filter)	40.0	10	0.0	0.0	410
E - 801 (with filter)	40.0	13	0.0	0.0	560

* For the filter specimens (E800, and E801) the hydraulic pressure was applied in 5 meters per 10 minute intervals and allowed flow overnite.

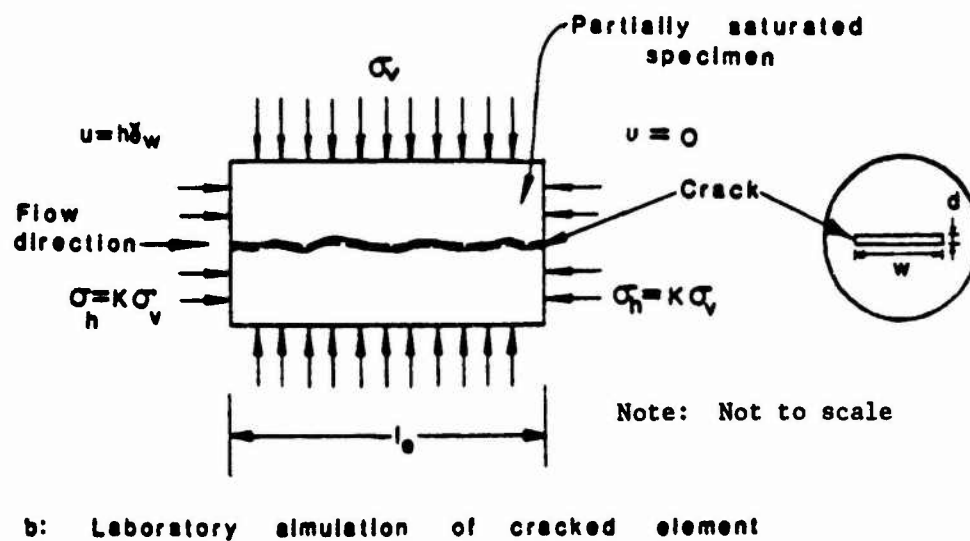
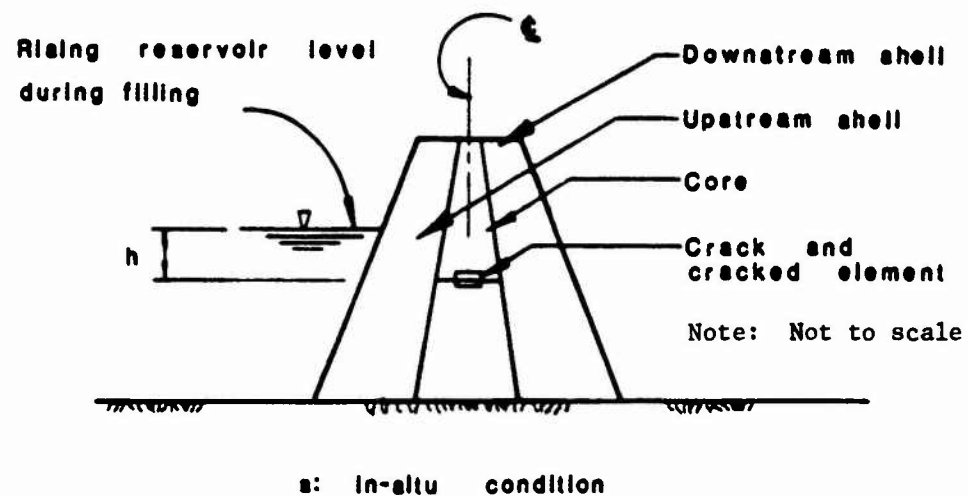


Fig. 1 Physical conditions modeled in cracked earth dam core material erosion studies.

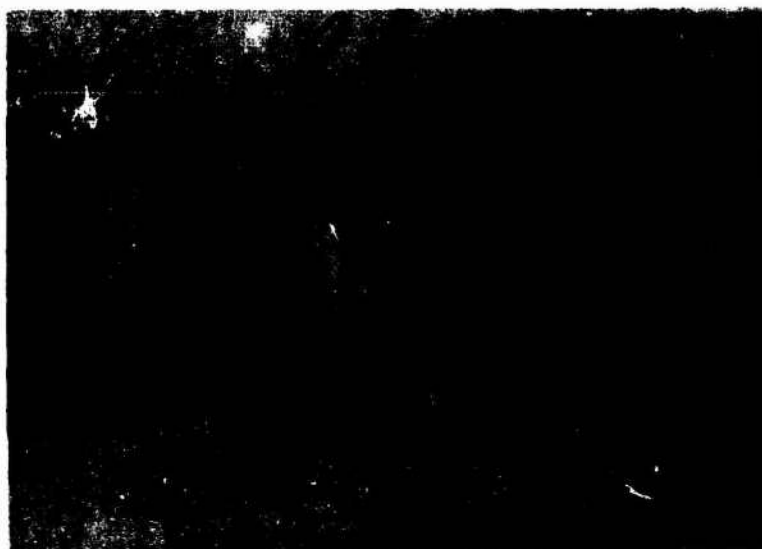


Fig. 2 Photographs of Erosion Test Equipment and Erosion
Test Cell.

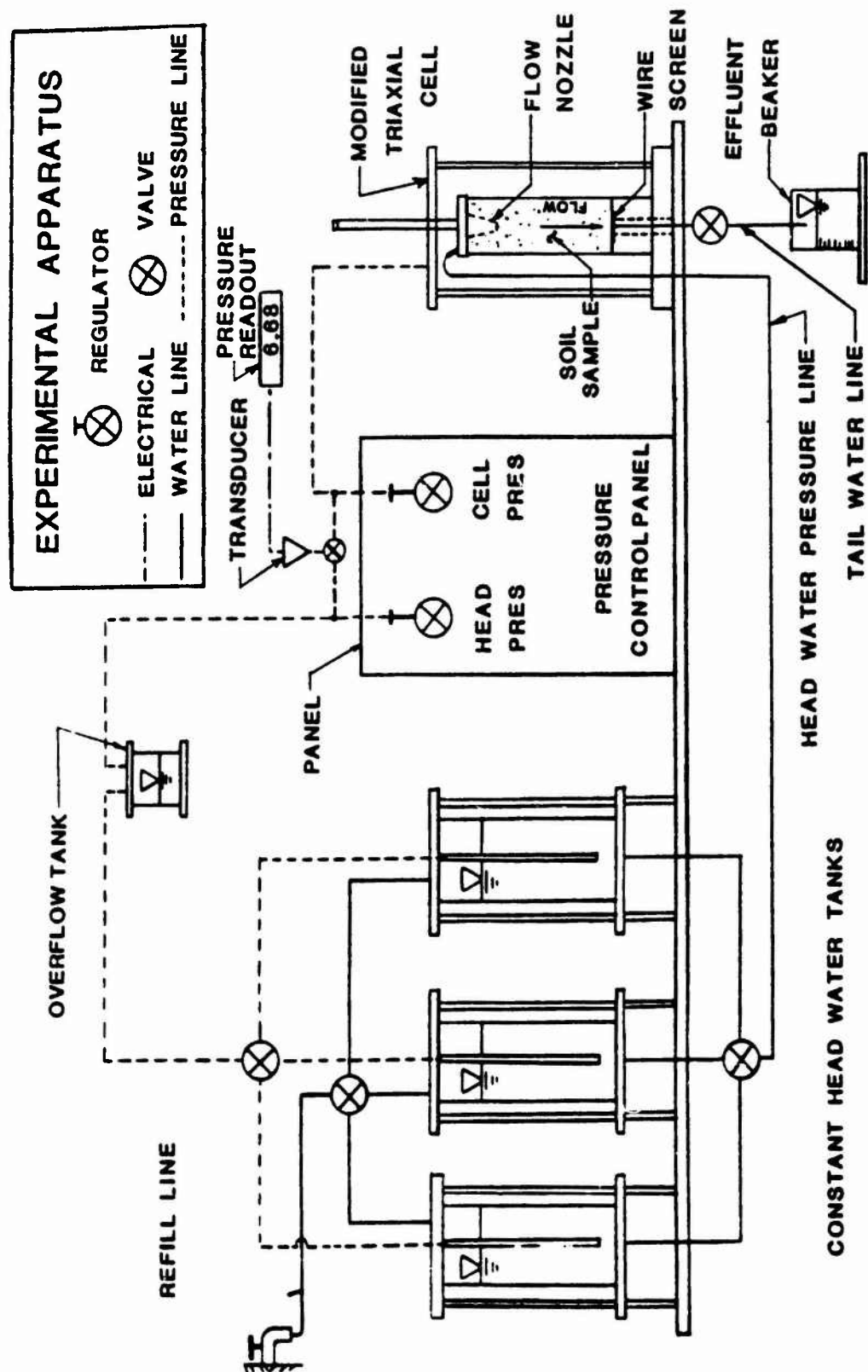
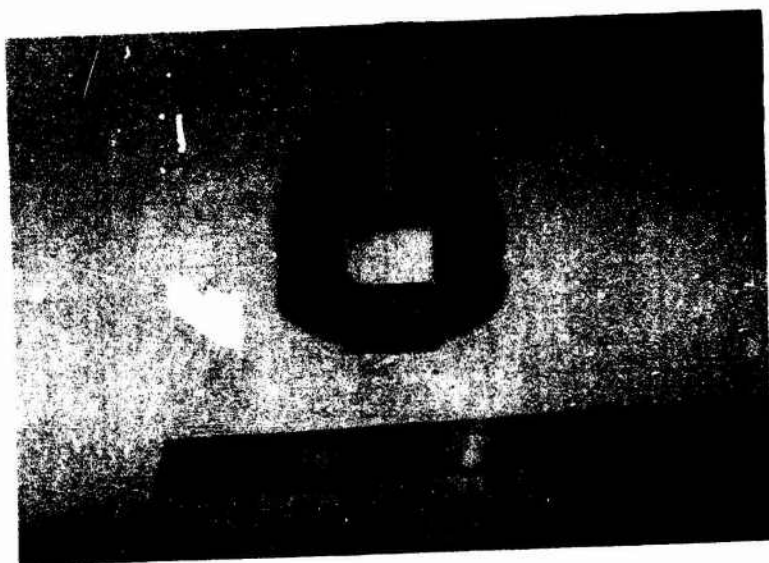


Fig. 3 Schematic Representation of Triaxial Erosion Test Apparatus

(a)

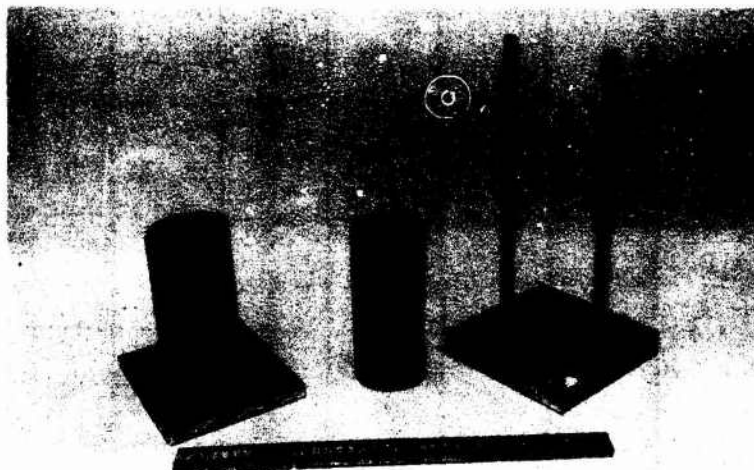


(b)



Fig. 4 Photographs of top (a) and bottom (b) erosion test platens.

(a)



(b)

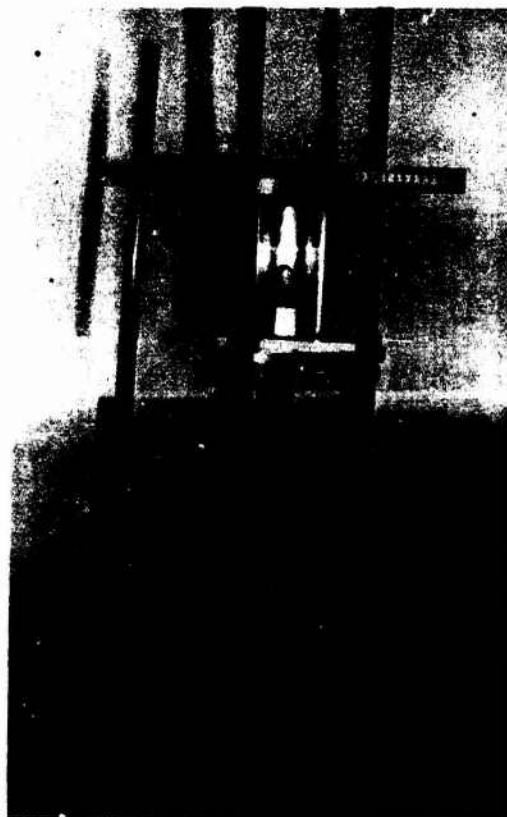


Fig. 5 Photographs of a) mold used to prepare reconstituted specimens showing the nozzle insert and b) specimen extruder modified to form a crack in the erosion specimen.

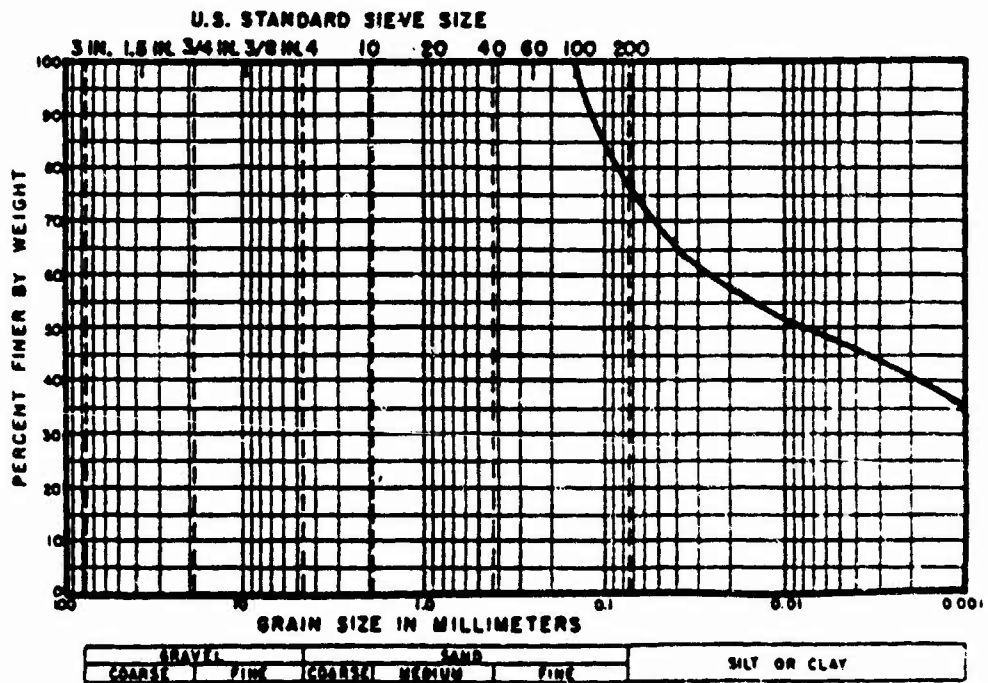
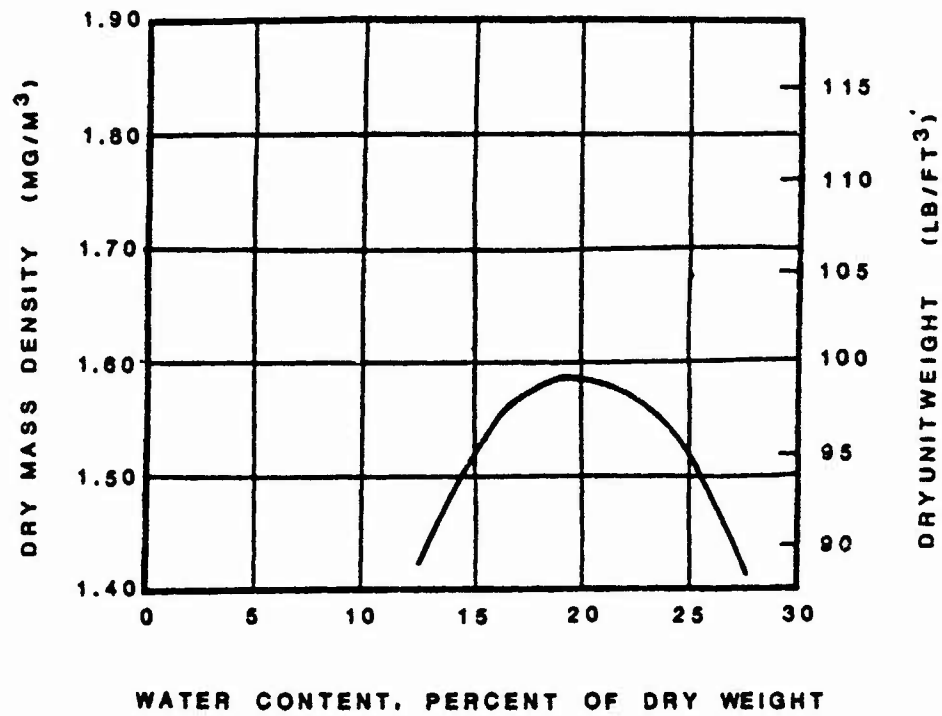


Fig. 6 Standard Proctor compaction curve and grain size distribution for Material A.

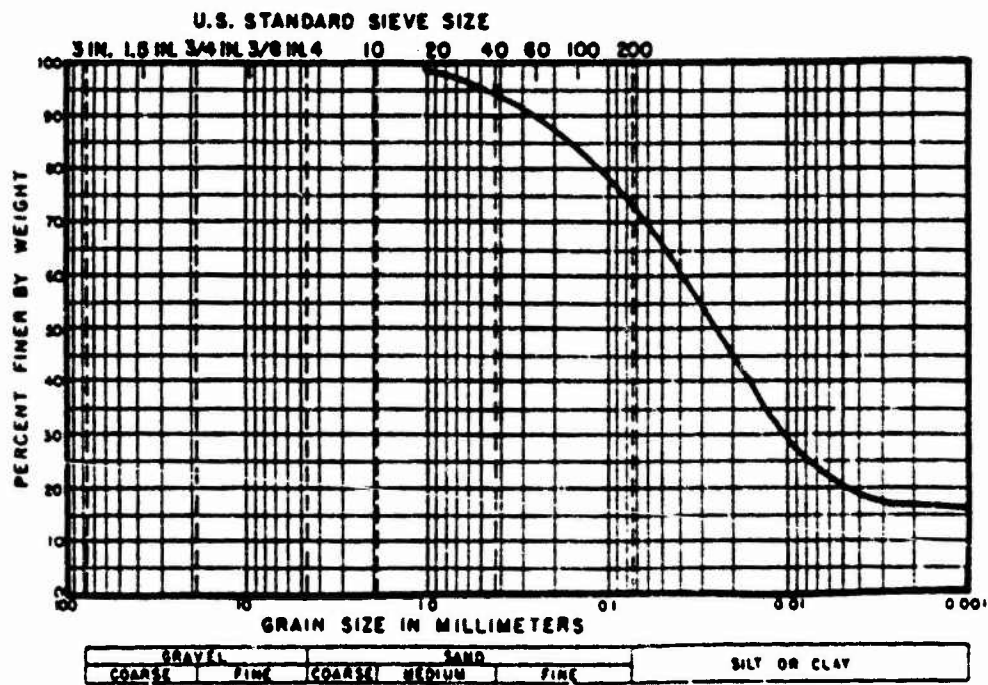
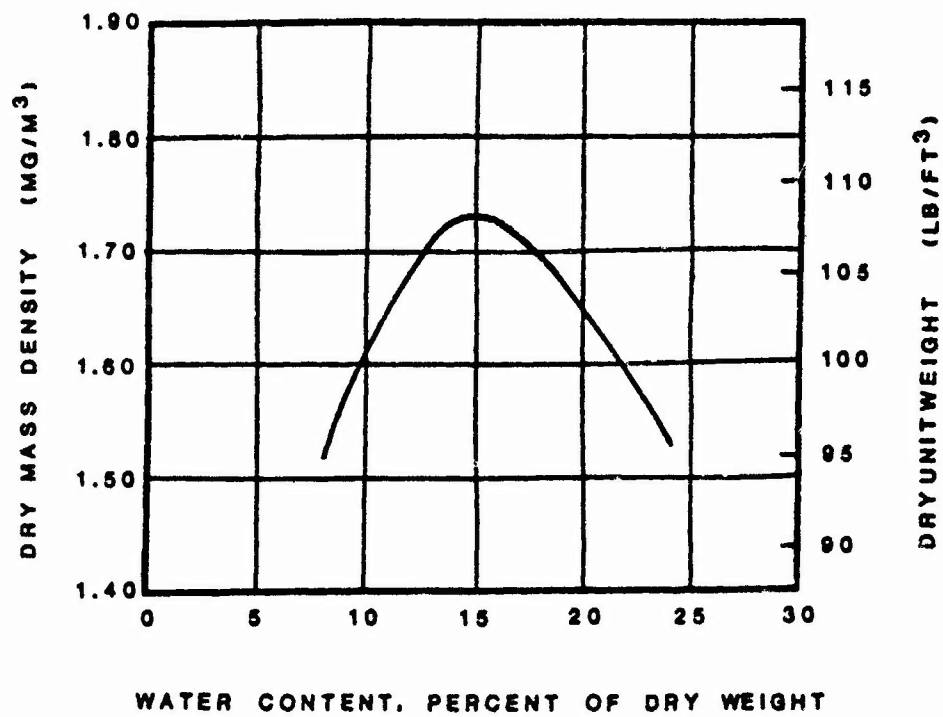


Fig. 7 Standard Proctor compaction curve and grain size distribution for Material B.

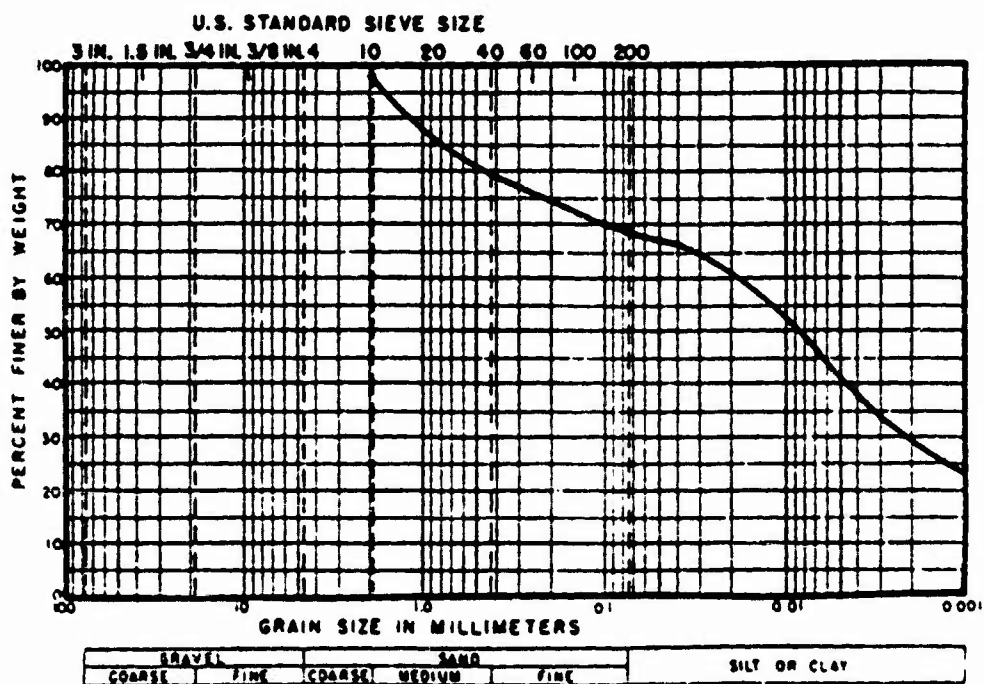
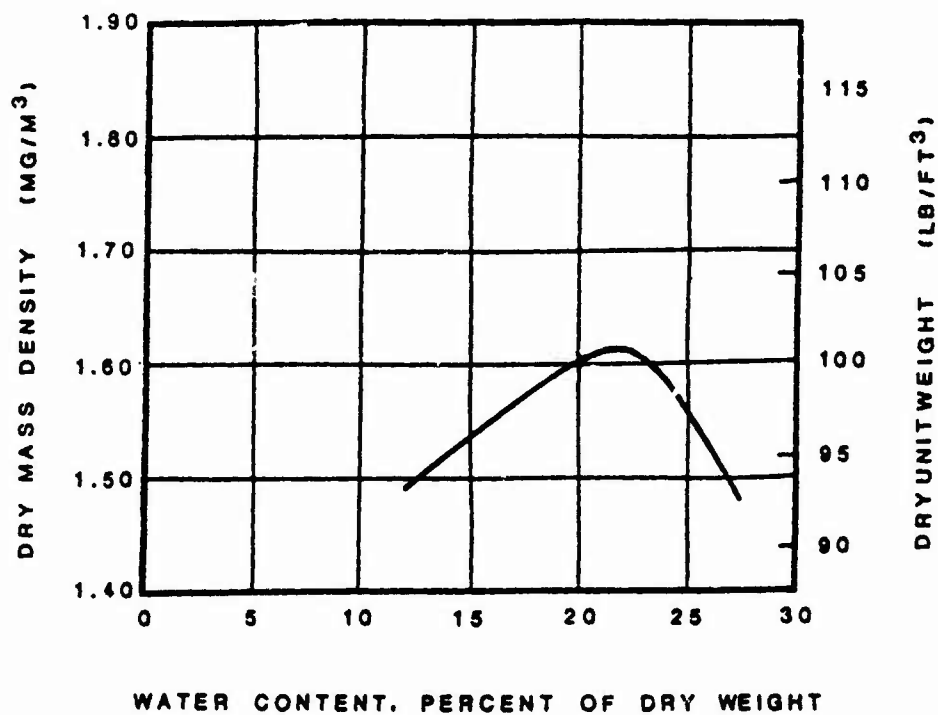


Fig. 8 Standard Proctor compaction curve and grain size distribution for Material C.

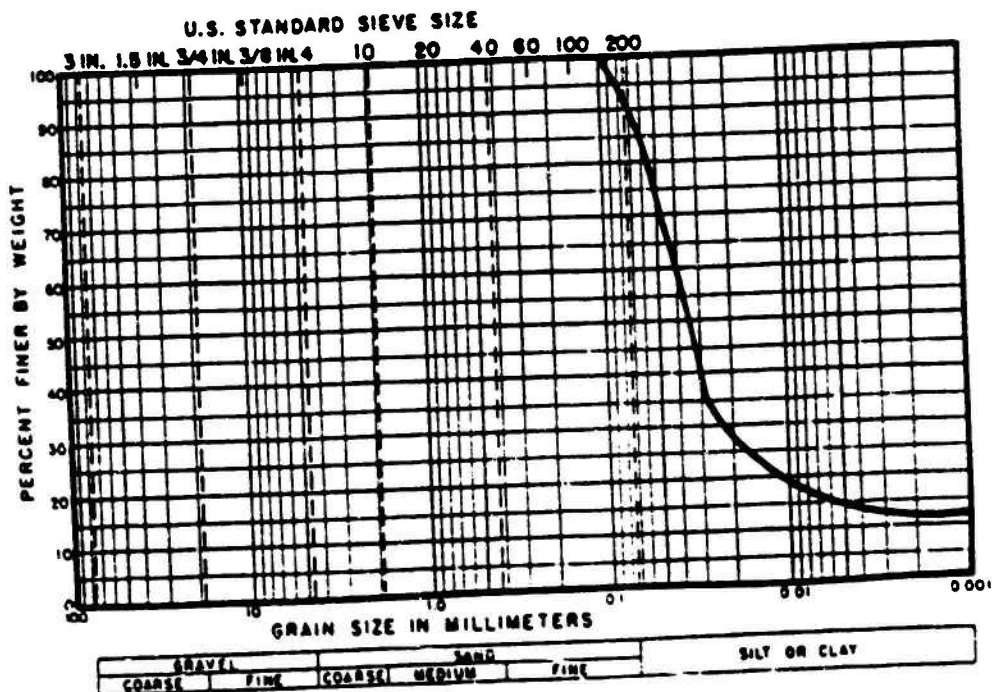
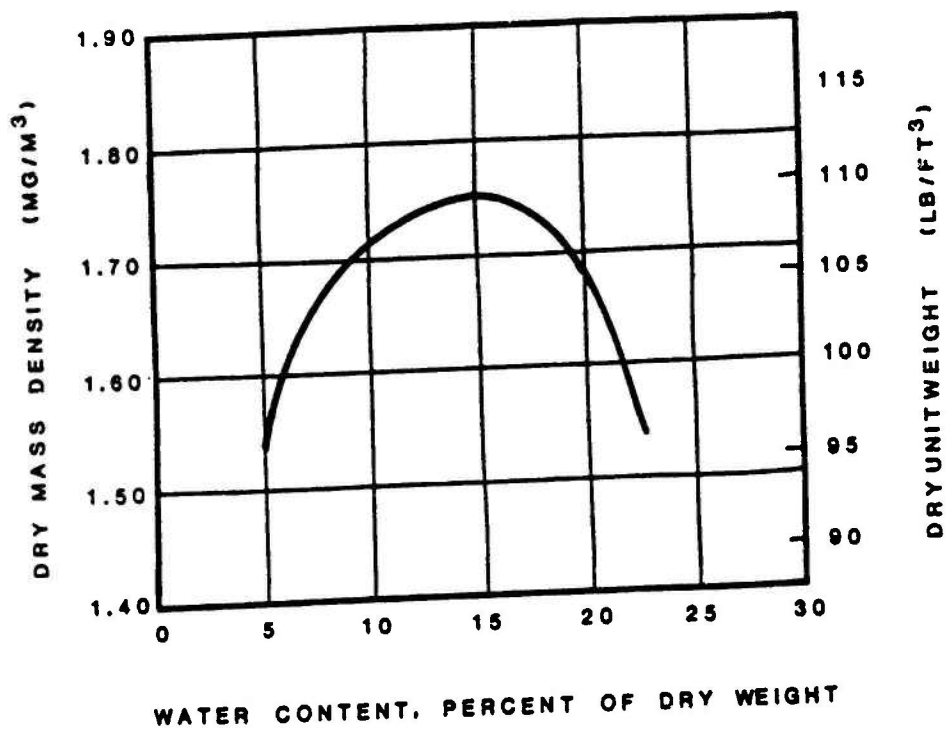
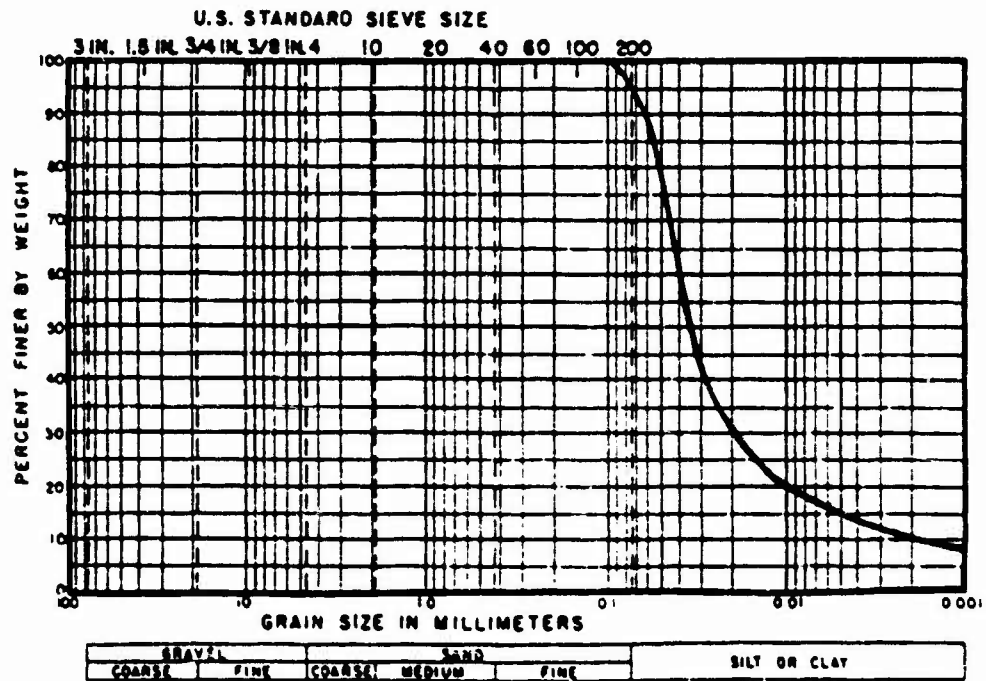
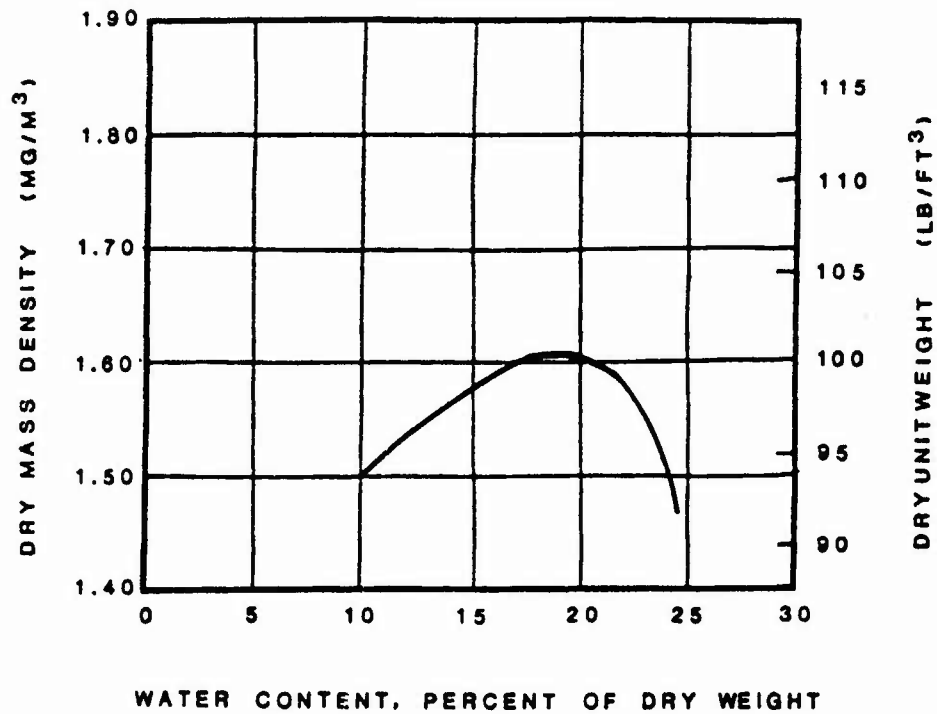


Fig. 9 Standard Proctor compaction curve and grain size distribution for Material D.



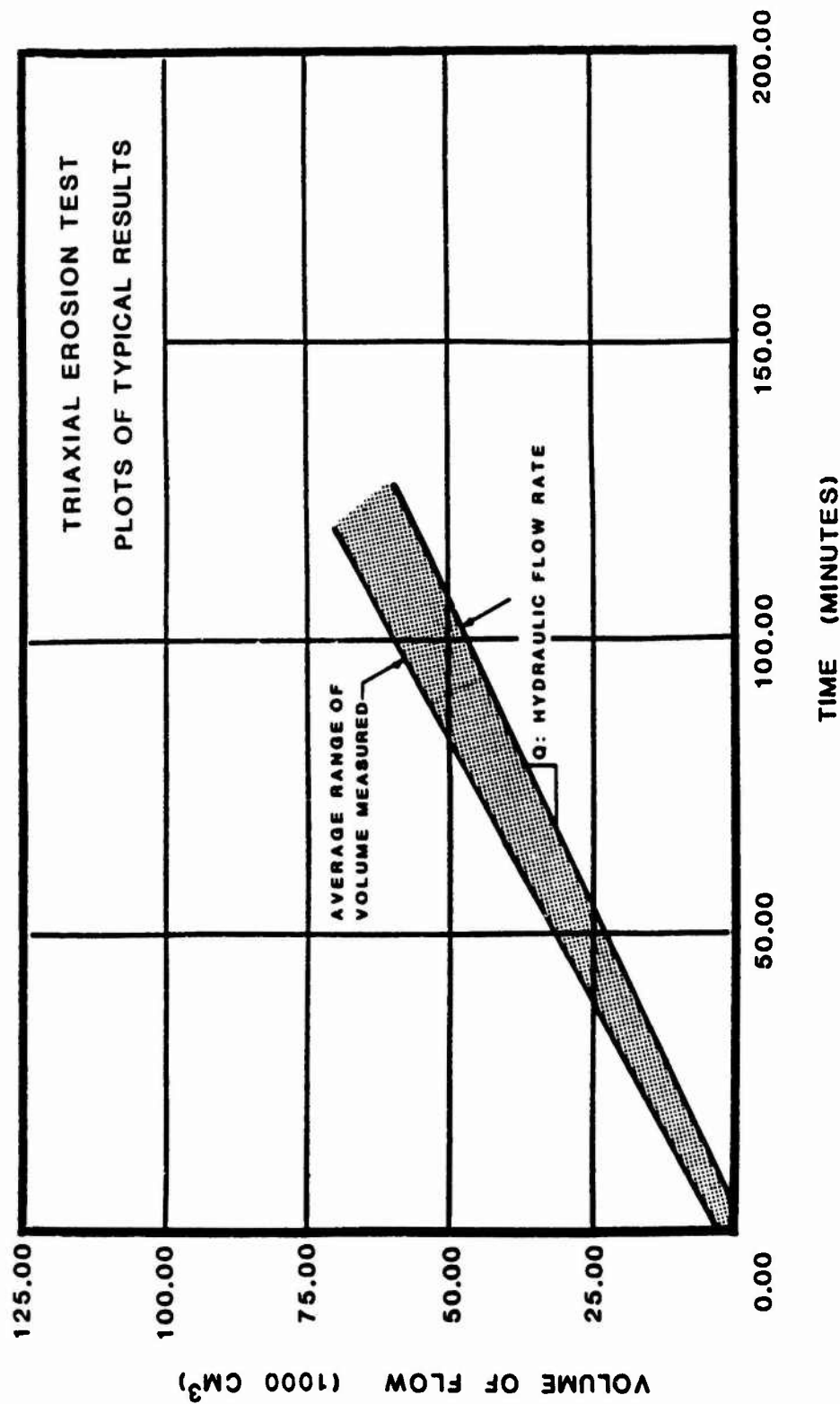


Fig. 11 Summary plot showing the cumulative volume of flow through a crack as a function of time for all specimens. All specimens were tested at hydraulic gradient of 10. The slope of these lines equals the flow rate Q .

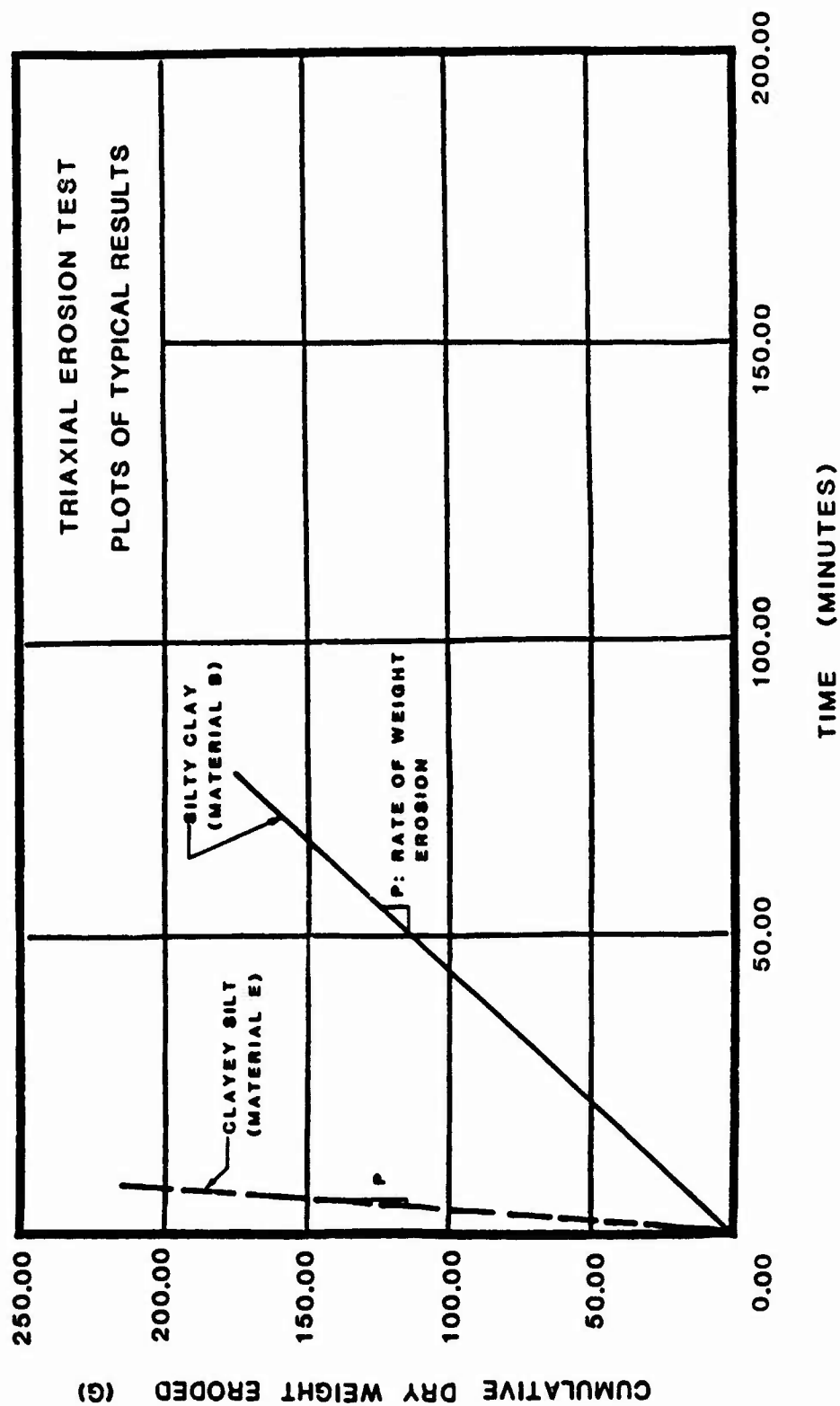


Fig. 12 Typical plot of cumulative dry weight eroded from the surface of a crack as a function of time for a hydraulic gradient of 10. The slope of these lines is the rate of weight erosion factor, P .

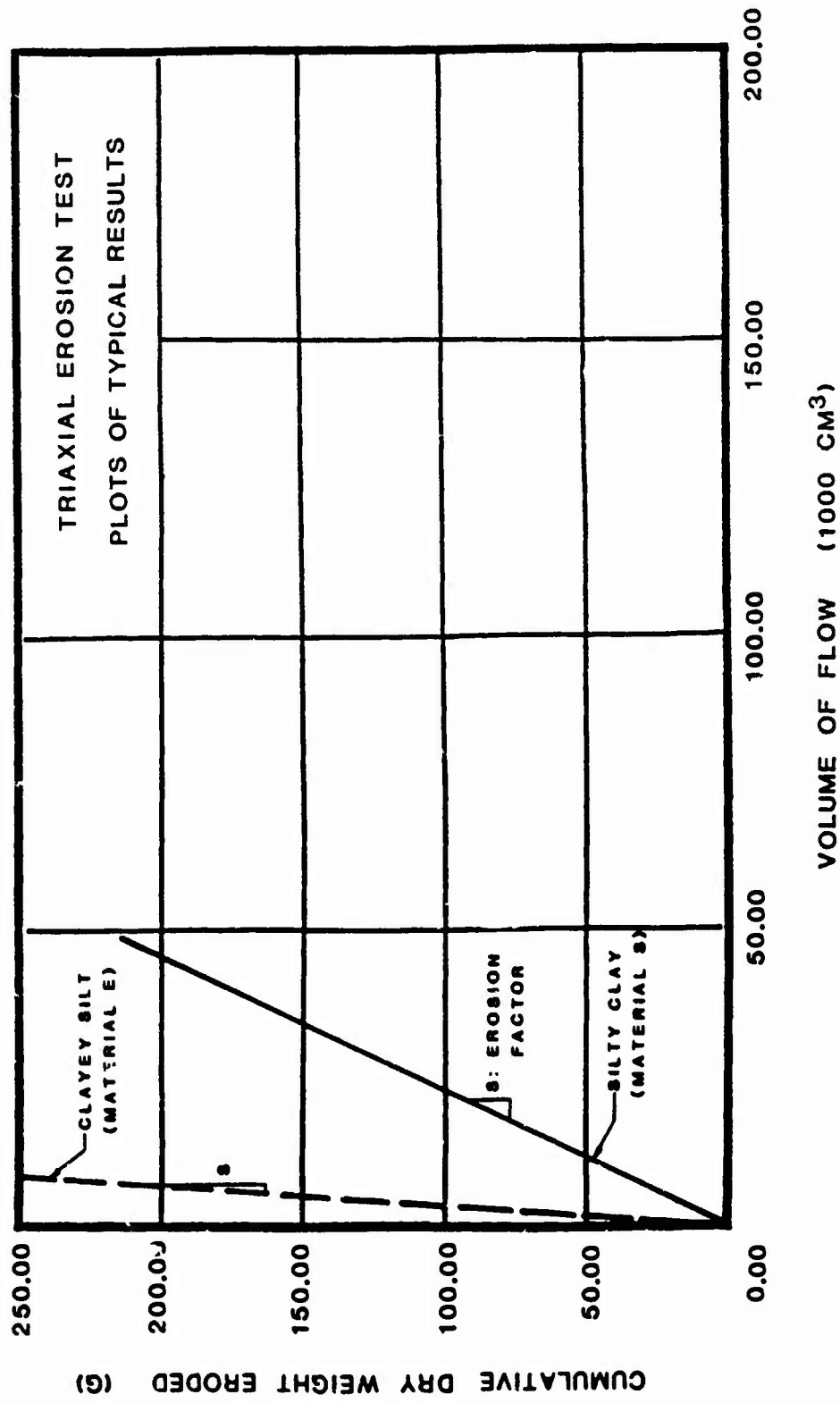


Fig. 13 Typical plot of the cumulative dry weight of solids eroded from the surface of a crack as a function of the volume of flow for a hydraulic gradient of 10. The slope of these lines is equal to the erosion factor S.

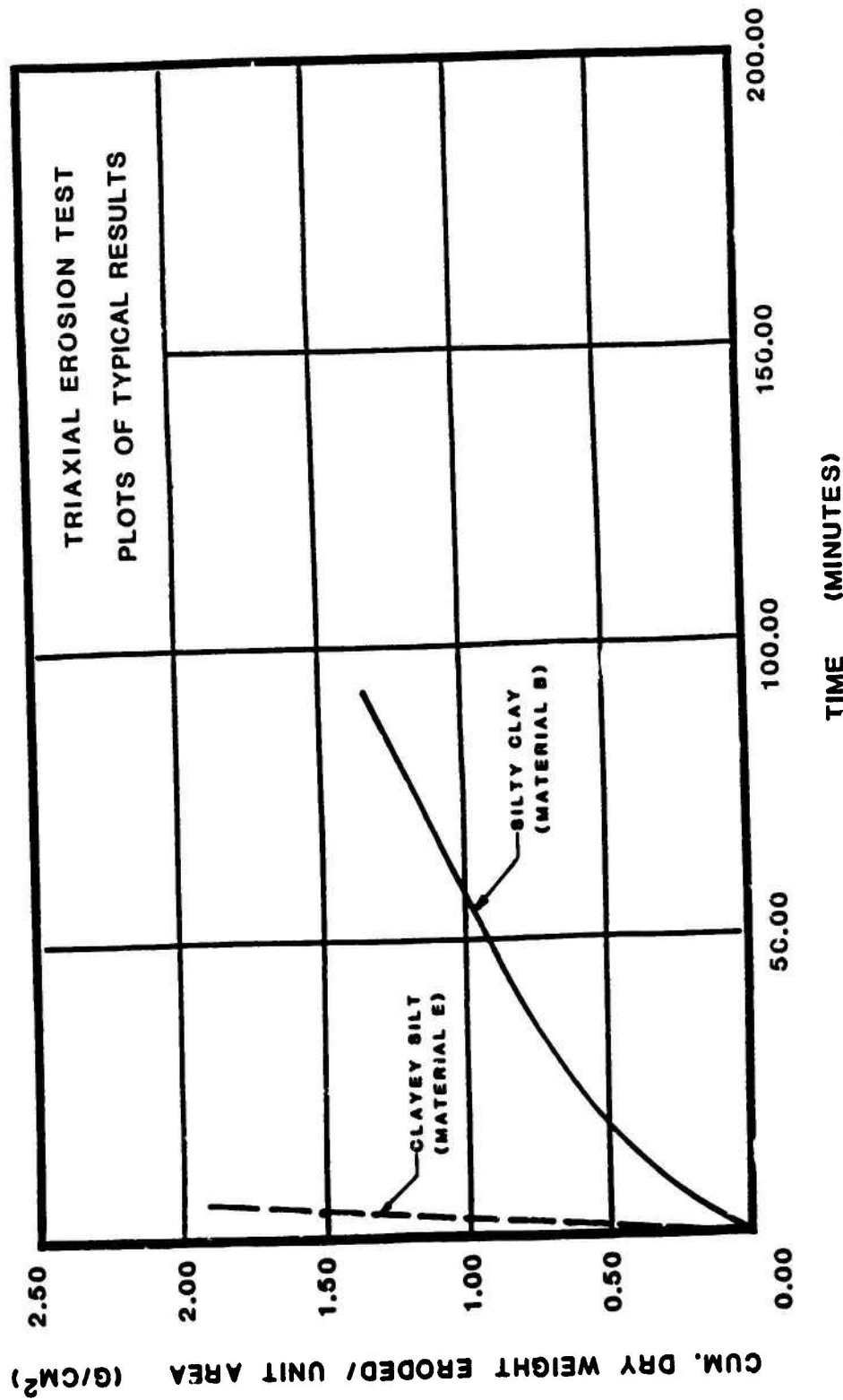


Fig. 14 Typical plot of the cumulative dry weight of solids eroded per unit area of crack as a function of time for a hydraulic gradient of 10.

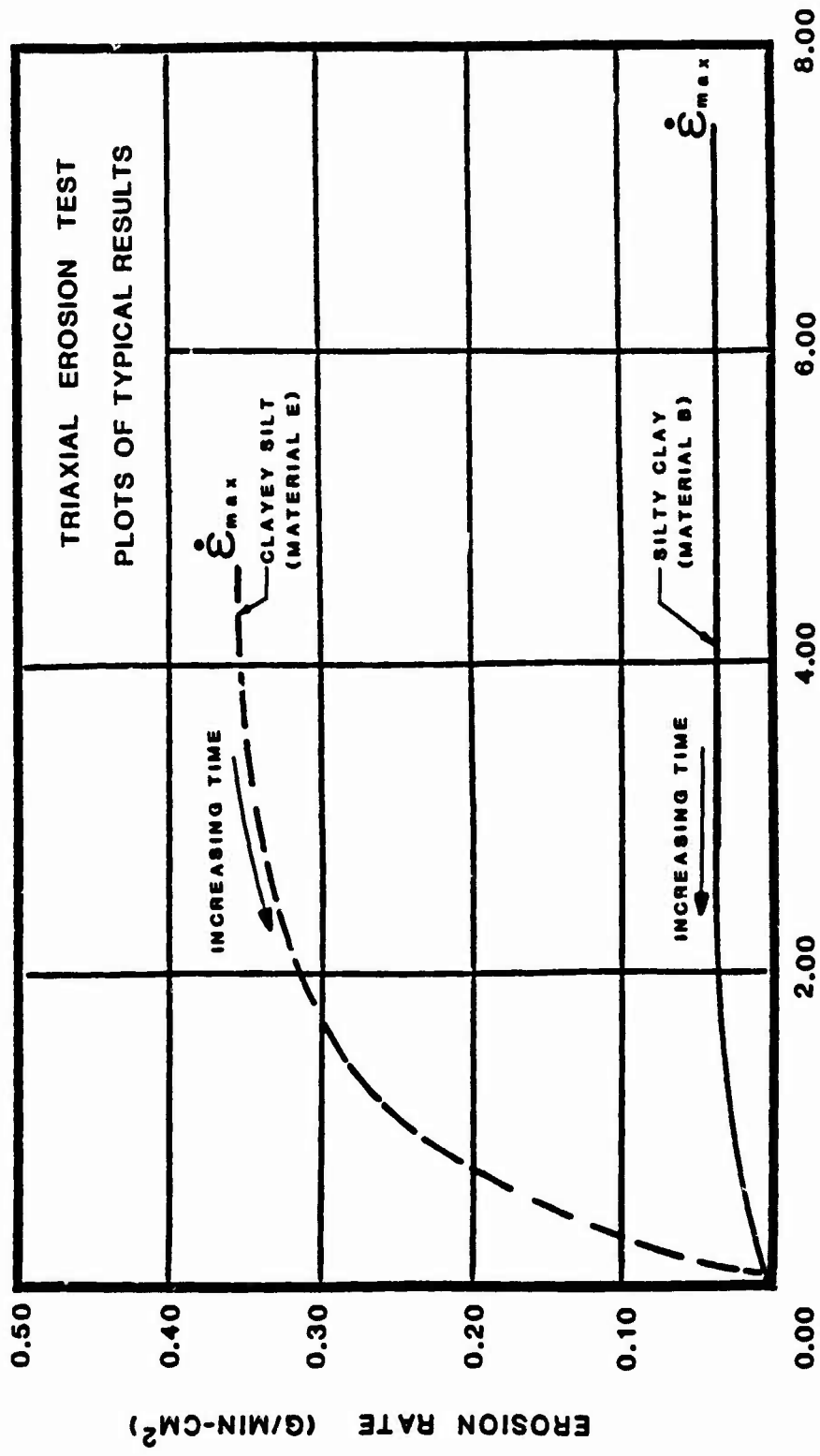


Fig. 15 Typical plot showing the erosion rate, $\dot{\epsilon}$, as a function of fluid shear stress, τ , for a hydraulic gradient of 10.

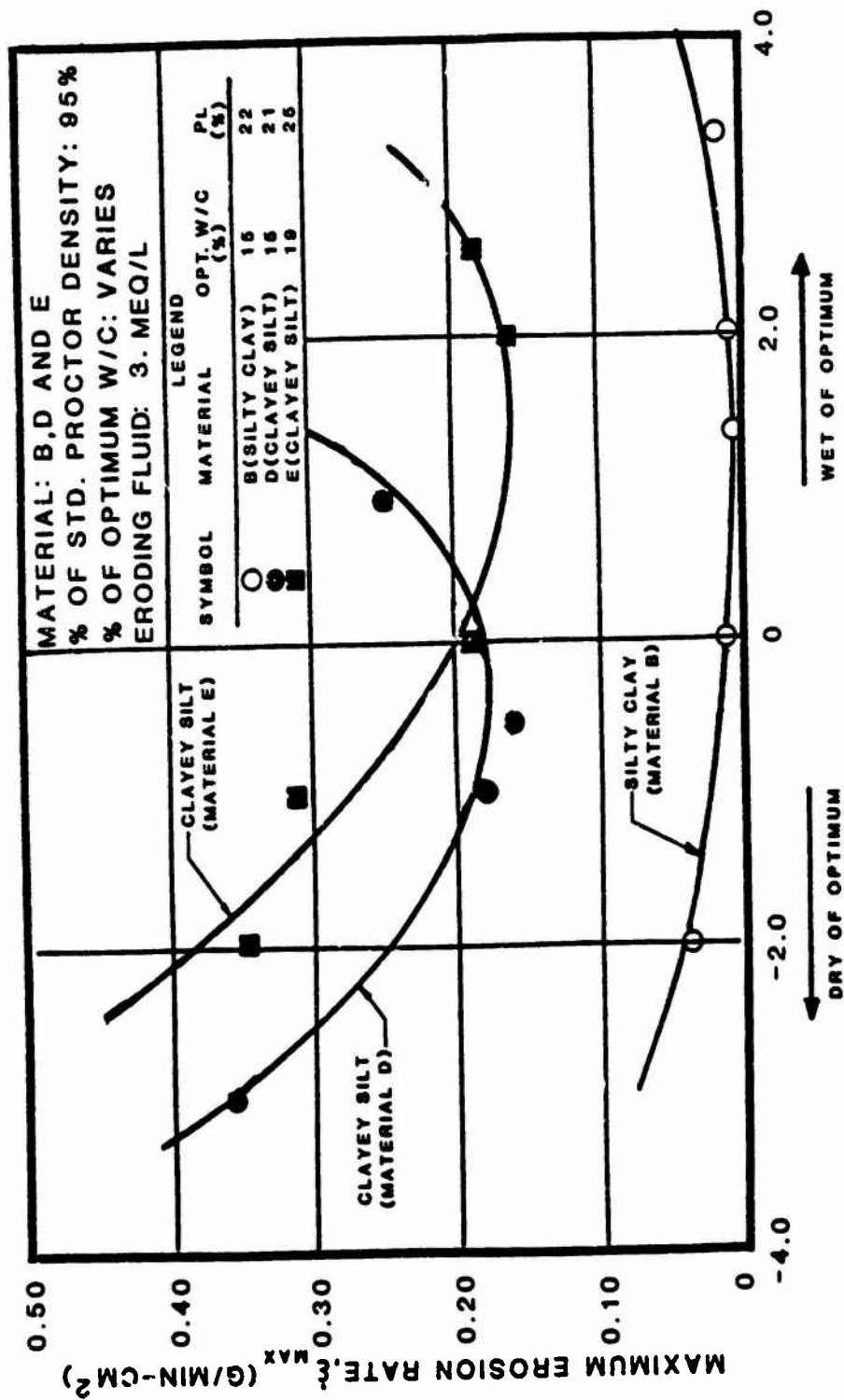


Fig. 16 Summary curve showing the effect of percent of optimum molding water content on maximum erosion rate, \dot{e}_{max} , for materials B, D, and E specimens.

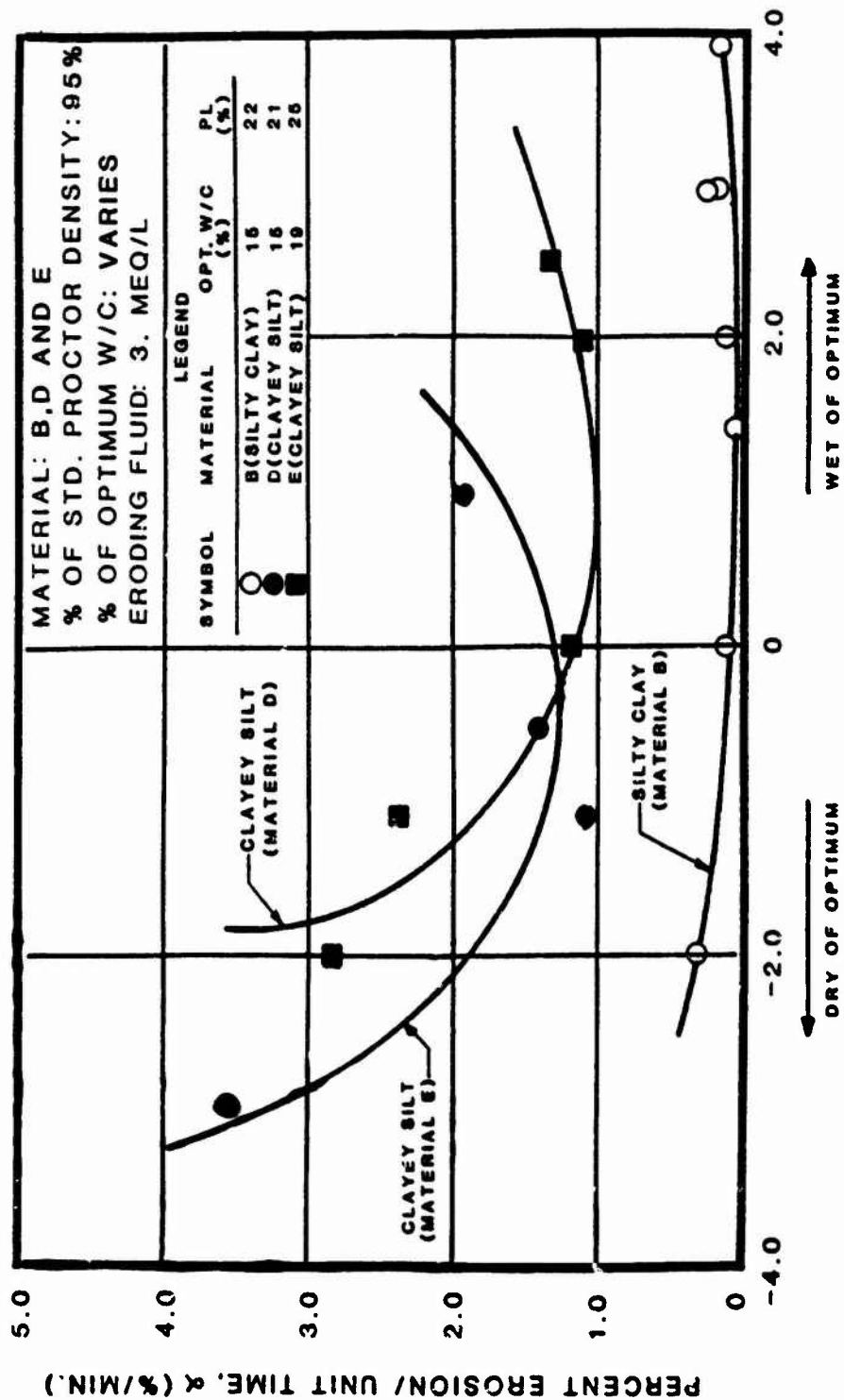


Fig.17 Summary curve showing the effect of percent of optimum molding water content on percent erosion per unit time, α , for materials B, D, and E specimens.

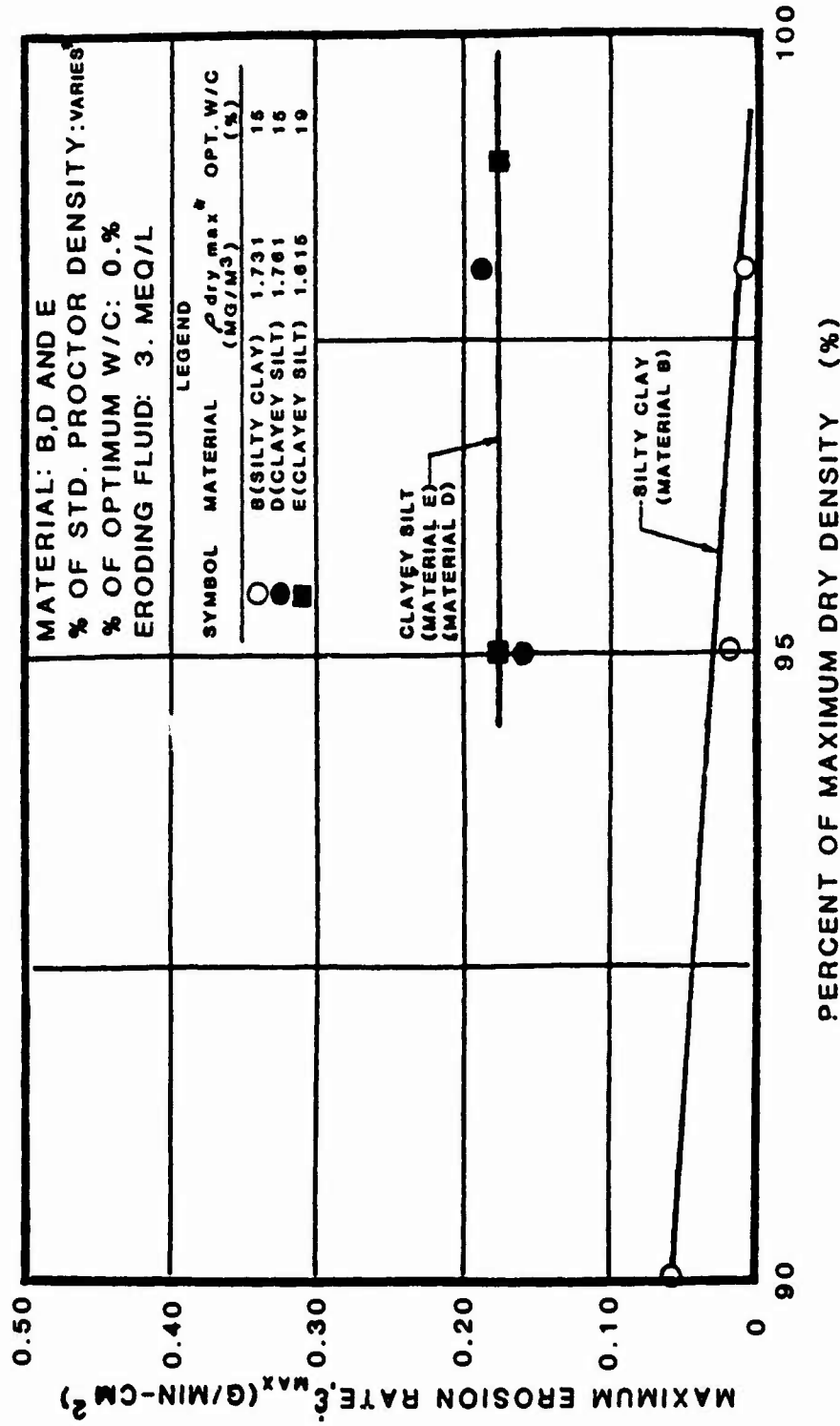


Fig. 18 Summary curve showing the effect of specimen dry density on the maximum erosion rate, E_{max} , for materials B, D, and E specimens.

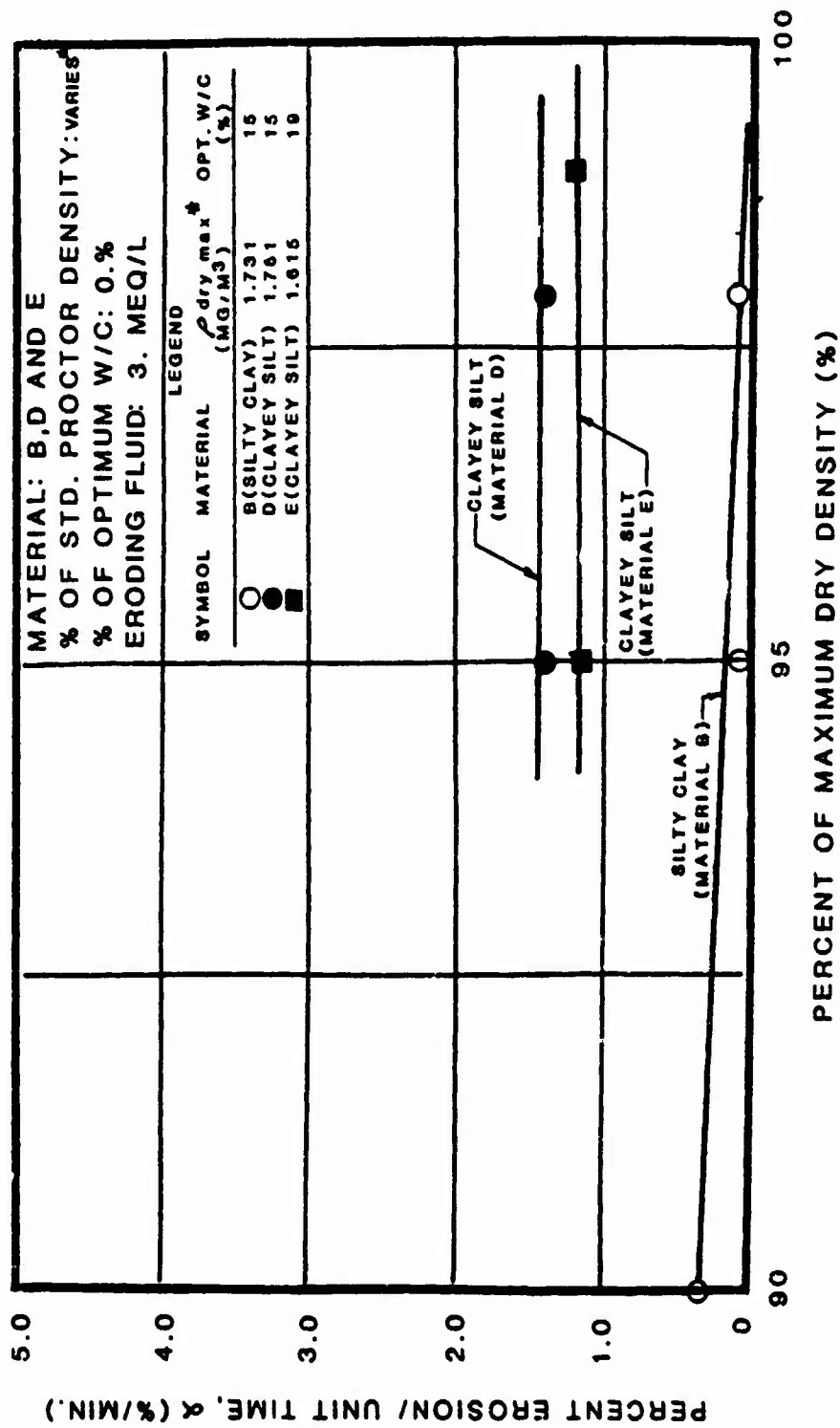


Fig. 19 Summary curve showing the effect of specimen dry density on the percent erosion per unit time, α , for materials B, D, and E specimens.

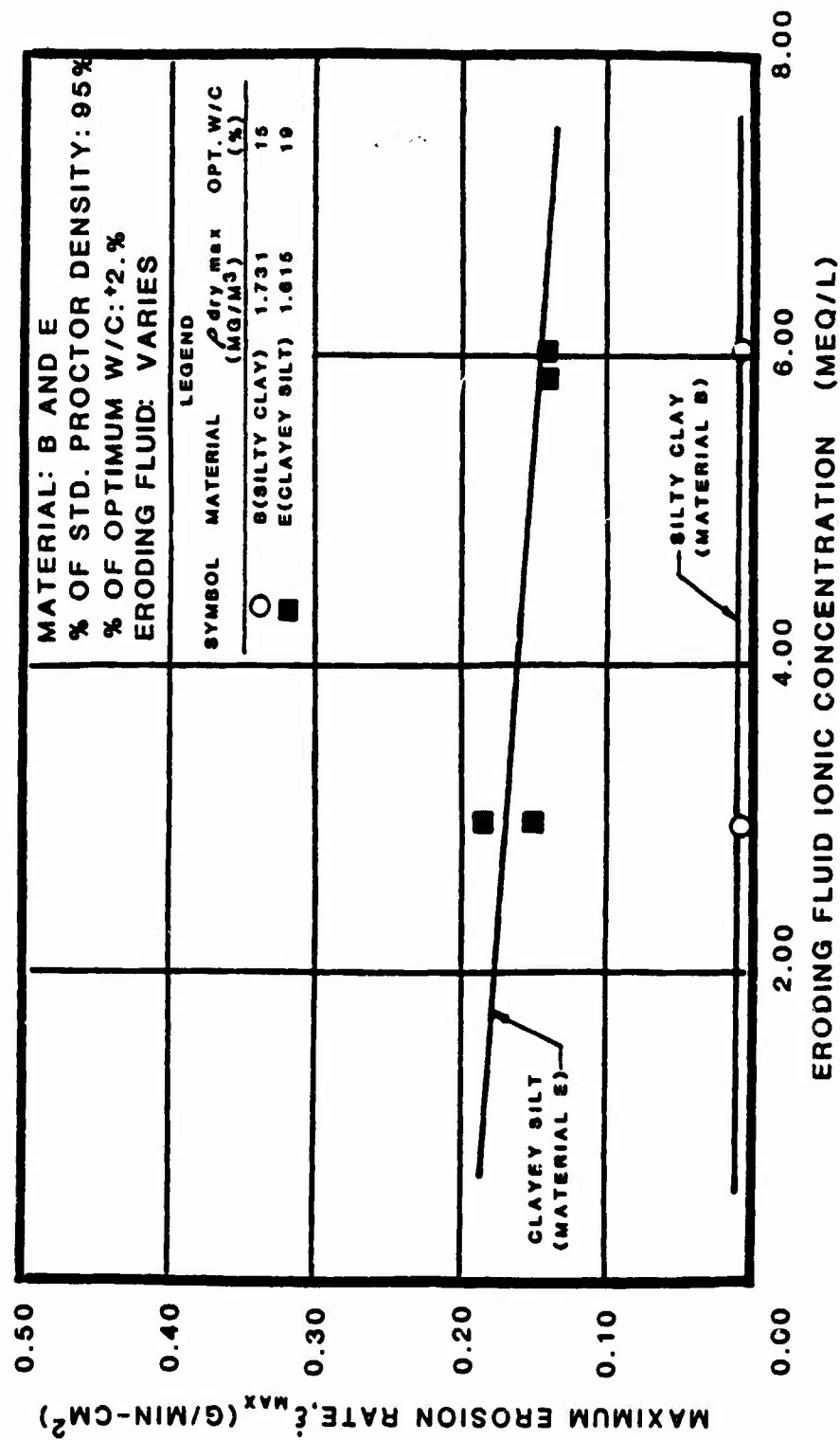


Fig. 20 Summary curve showing the effect of eroding fluid ionic concentration on the maximum erosion rate, \dot{e}_{max} , for materials B and E specimens.

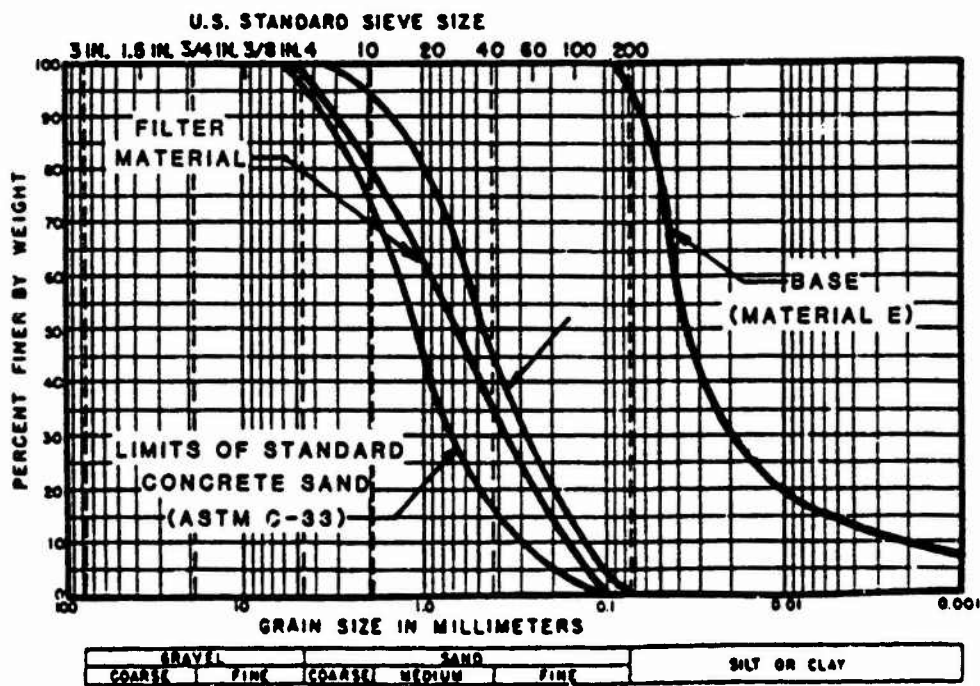
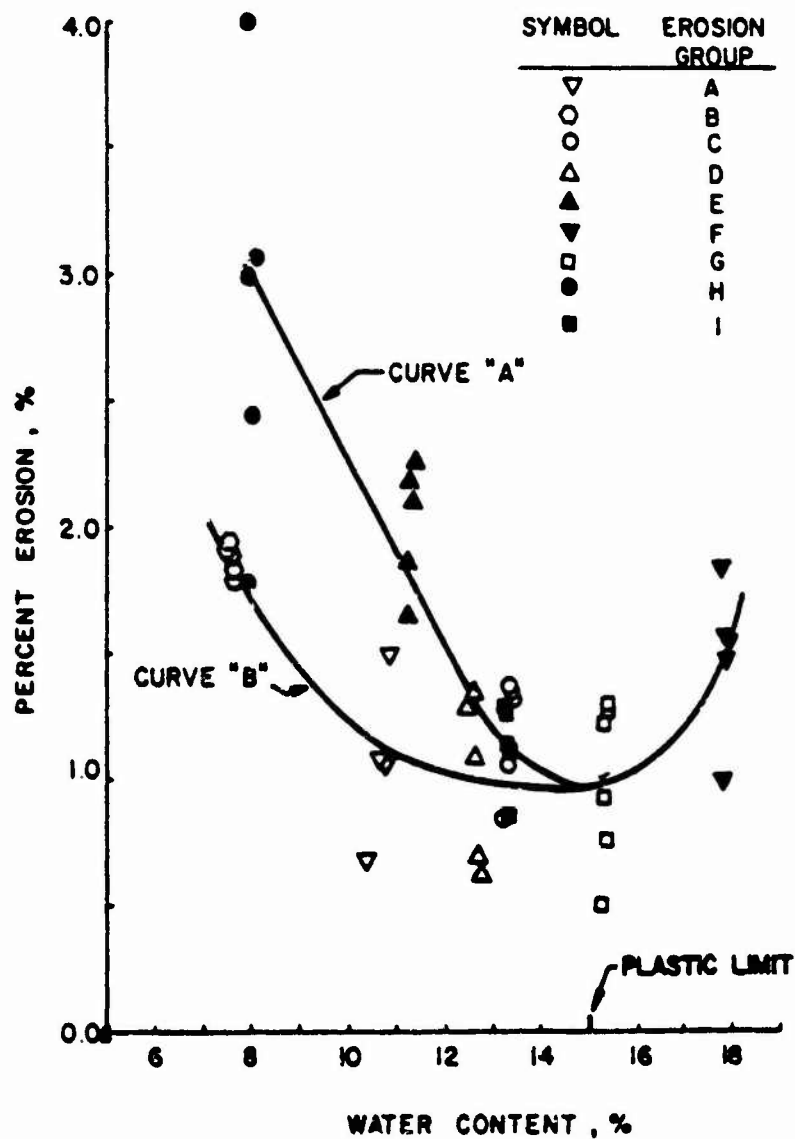


Fig. 21 Grain size distribution for concrete sand filter and base (Material E), used in filter tests.



CURVE A - Pinhole specimens compacted by standard Proctor energy.

CURVE B - Pinhole specimen compacted by modified Proctor energy.

Fig. 22 Percent erosion versus molding water content for pinhole erosion test investigation by Lewis and Schmidt (1977).

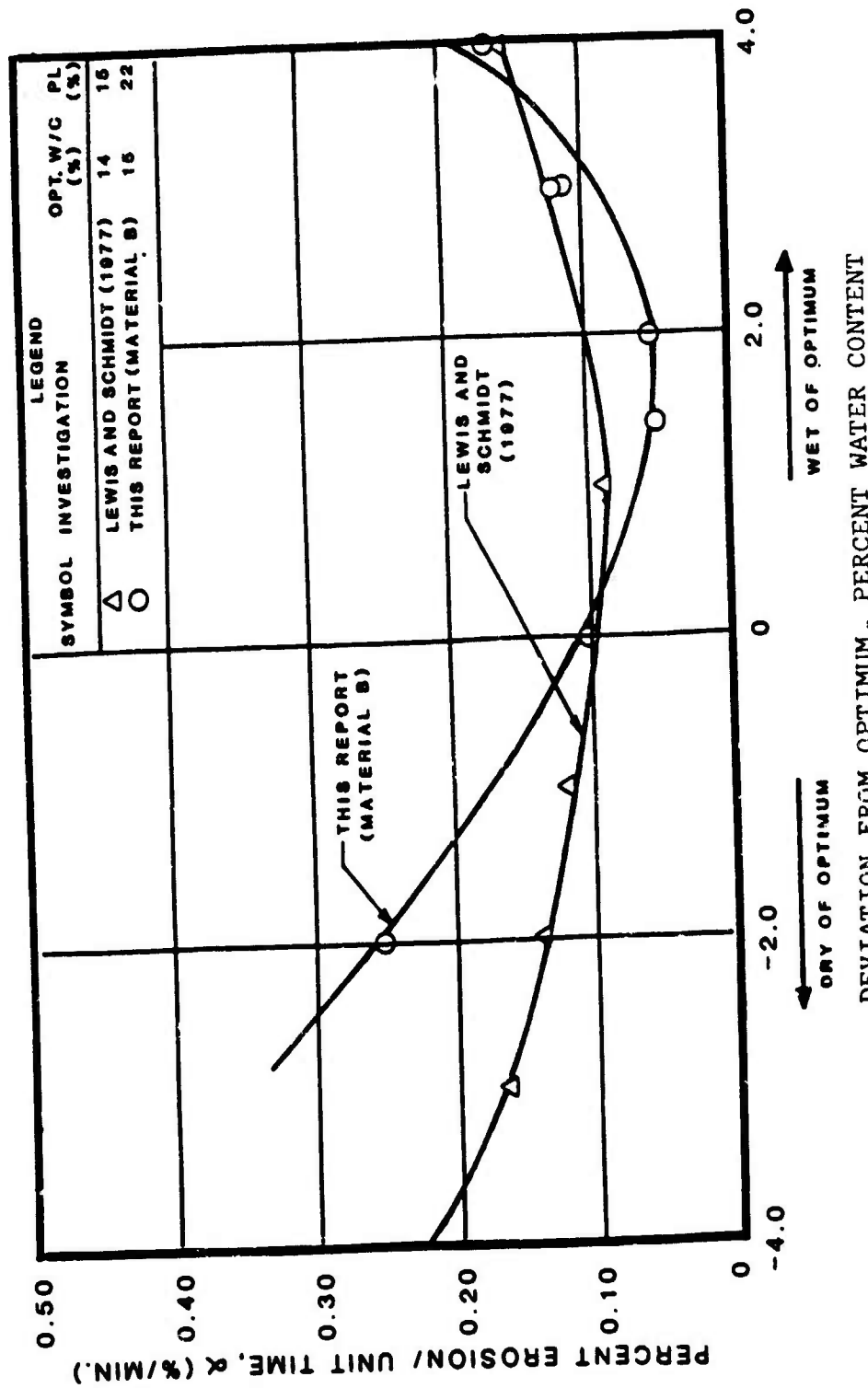


Fig. 23 Comparative plots of percent erosion per unit time, α , as a function of percent of optimum molding water content for Material B specimens and for the pinhole test investigation conducted by Lewis and Schmidt (1977).

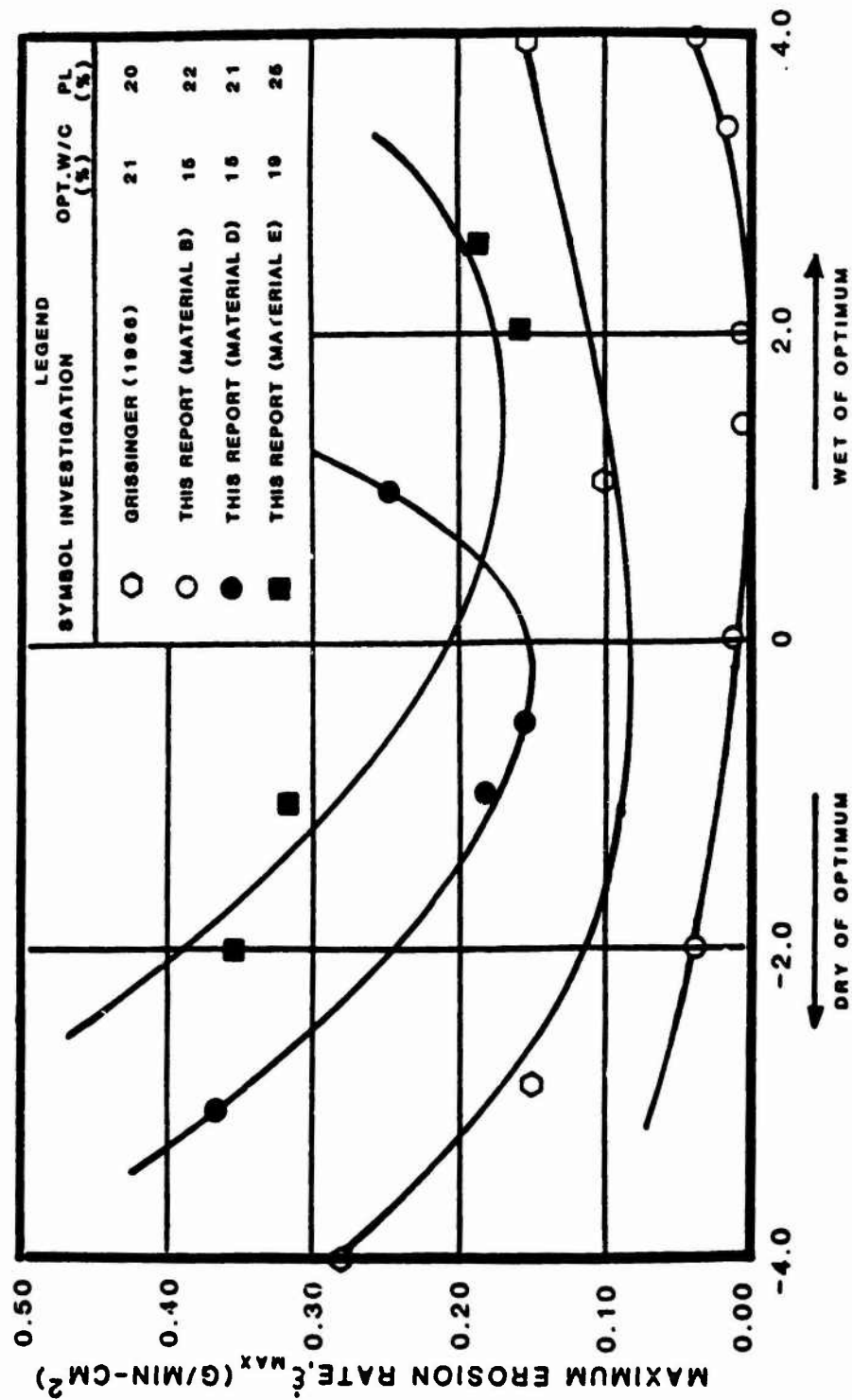


Fig. 24 Comparative plots of maximum erosion rate as a function of percent of optimum molding water content for materials B, D, and E specimens and for the investigation conducted by Grissinger (1962).

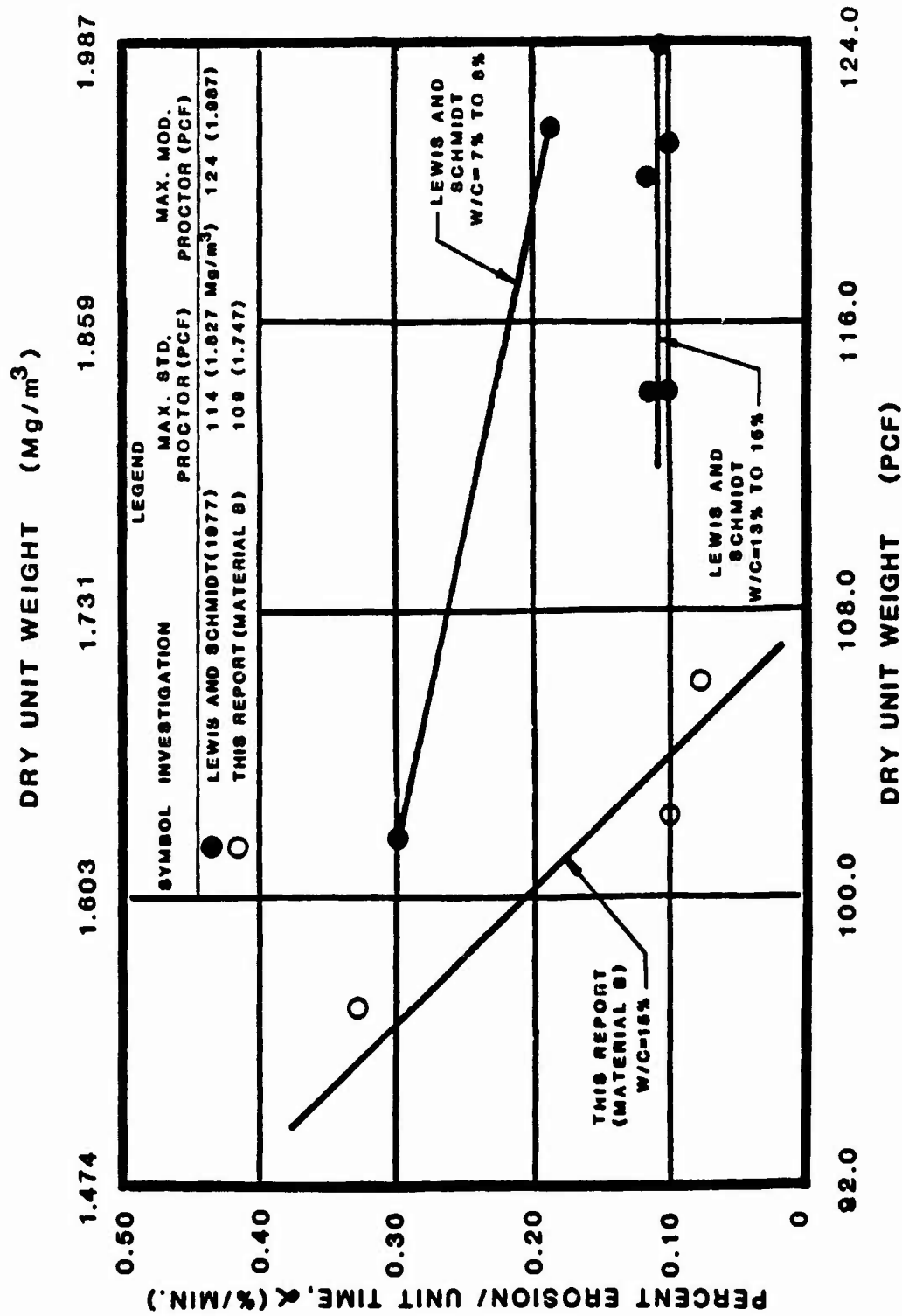


Fig. 25 Comparative plots of percent erosion per unit time, α , as a function of density, ρ , for Material B specimens and for the pinhole test investigation conducted by Lewis and Schmidt (1977).

APPENDIX A
DETAILS OF TEST RESULTS

TABLE A1

TEST RESULTS FOR TRIAXIAL EROSION TEST

MATERIAL TYPE: SPECIMEN NUMBER :		A 110		AVERAGE FLOW RATE (Q):		317. CC/MIN		
TESTED BY:		R. L. SANCHEZ		RATE OF WEIGHT EROSION (P):		0.8 G/MIN		
DATE TESTED:		4 12 82		DENSITY OF ERODING FLUID:		1.000 G/CC		
SPECIMEN DRY DENSITY:		1.406 G/CC		VISCOSITY OF ERODING FLUID:		0.001 H*SEC/50.0		
% OF OPTIMUM WATER CONTENT:		1.0 PERCENT		CONFINING PRESSURE:		90.00 LB/50.0		
INITIAL SLOT WIDTH:		2.30 CM		HEAD OF WATER:		1.30 M		
INITIAL SLOT THICKNESS:		0.23 CM		HYDRAULIC GRADIENT:		10. M/H		
ERODED LENGTH:		11.50 CM						

VOLUME OF FLOW (LITERS CC)	TIME (MIN)	CUM. WEIGHT ERODED (G)	CROSS SECTION AREA (SQ. CM)	VELOCITY IN FLOW (CM/HR)	ERODED SURFACE AREA (SQ. CM)	CUM. WEIGHT ERODED PER AREA (G/SQ. CM)	EROSION RATE (G/HR) (CM/HR) STRESS (LB/50.0)	REYNOLDS NUMBER
35.6	03.30	2.6	0.6	512.	59.	0.04	0.00	412.
70.0	104.36	5.4	0.7	435.	60.	0.29	0.00	404.
105.0	303.45	6.8	0.9	370.	61.	0.11	0.00	396.

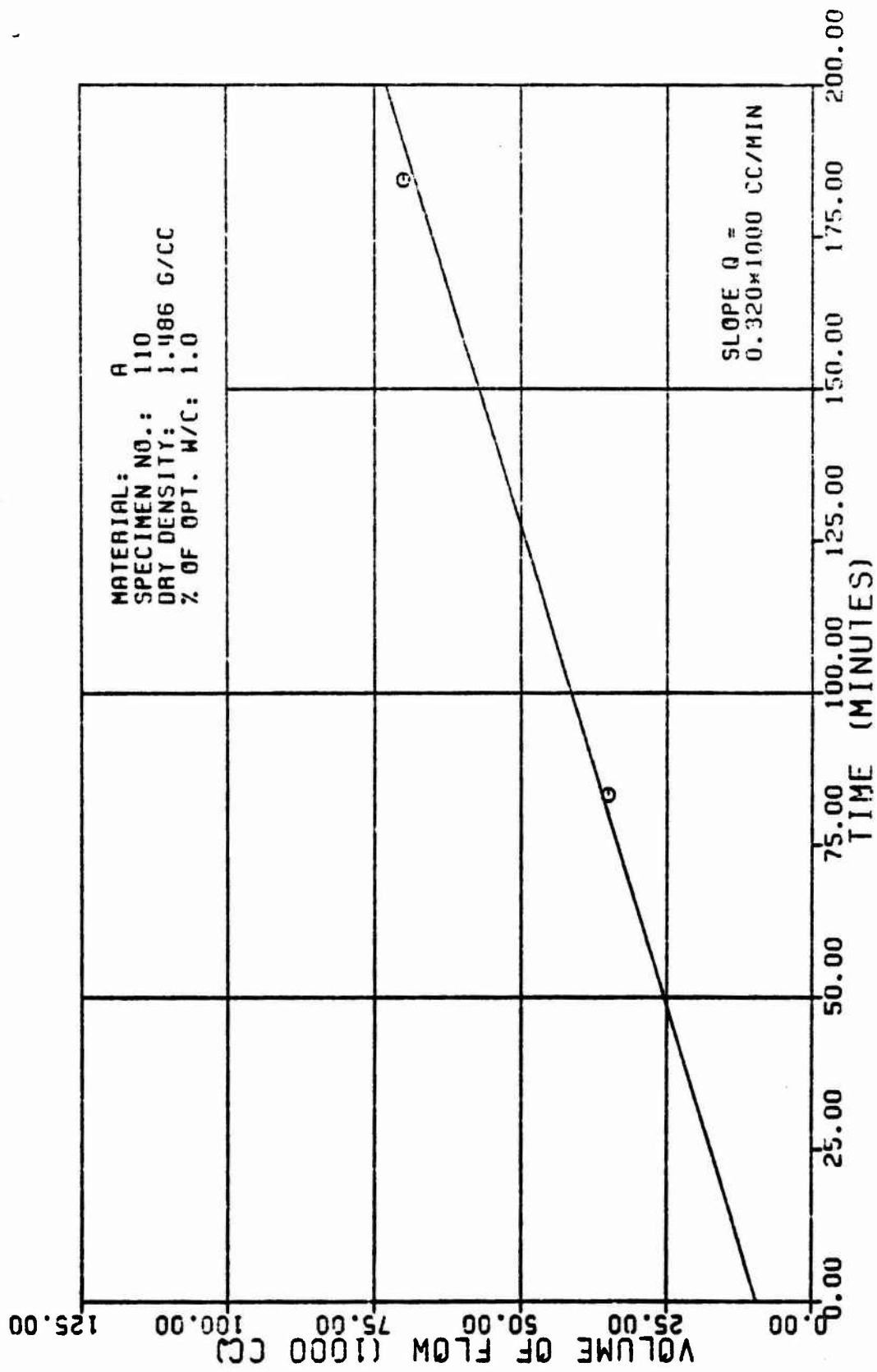


Figure A1a

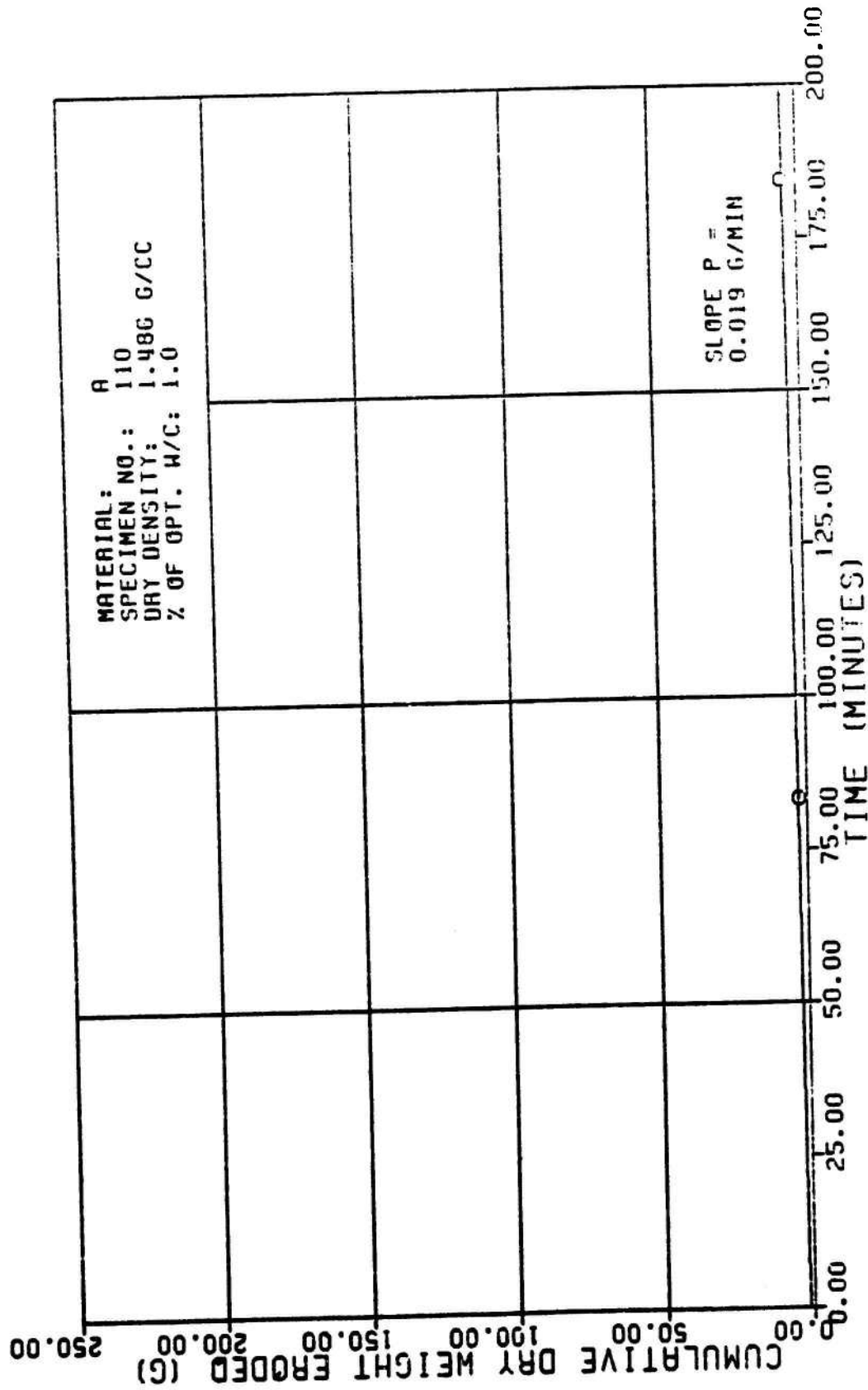


Figure Alb

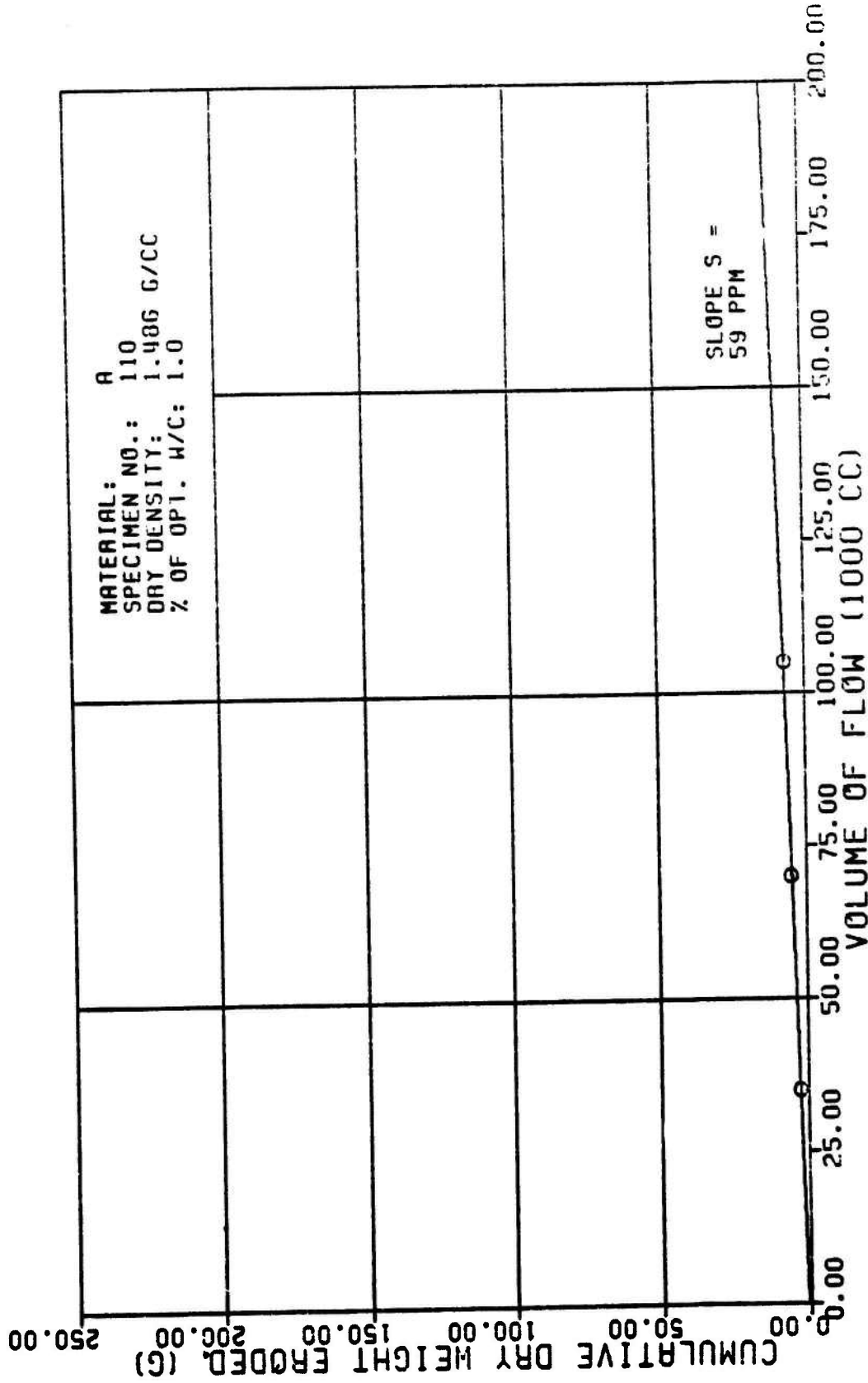


Figure Alc

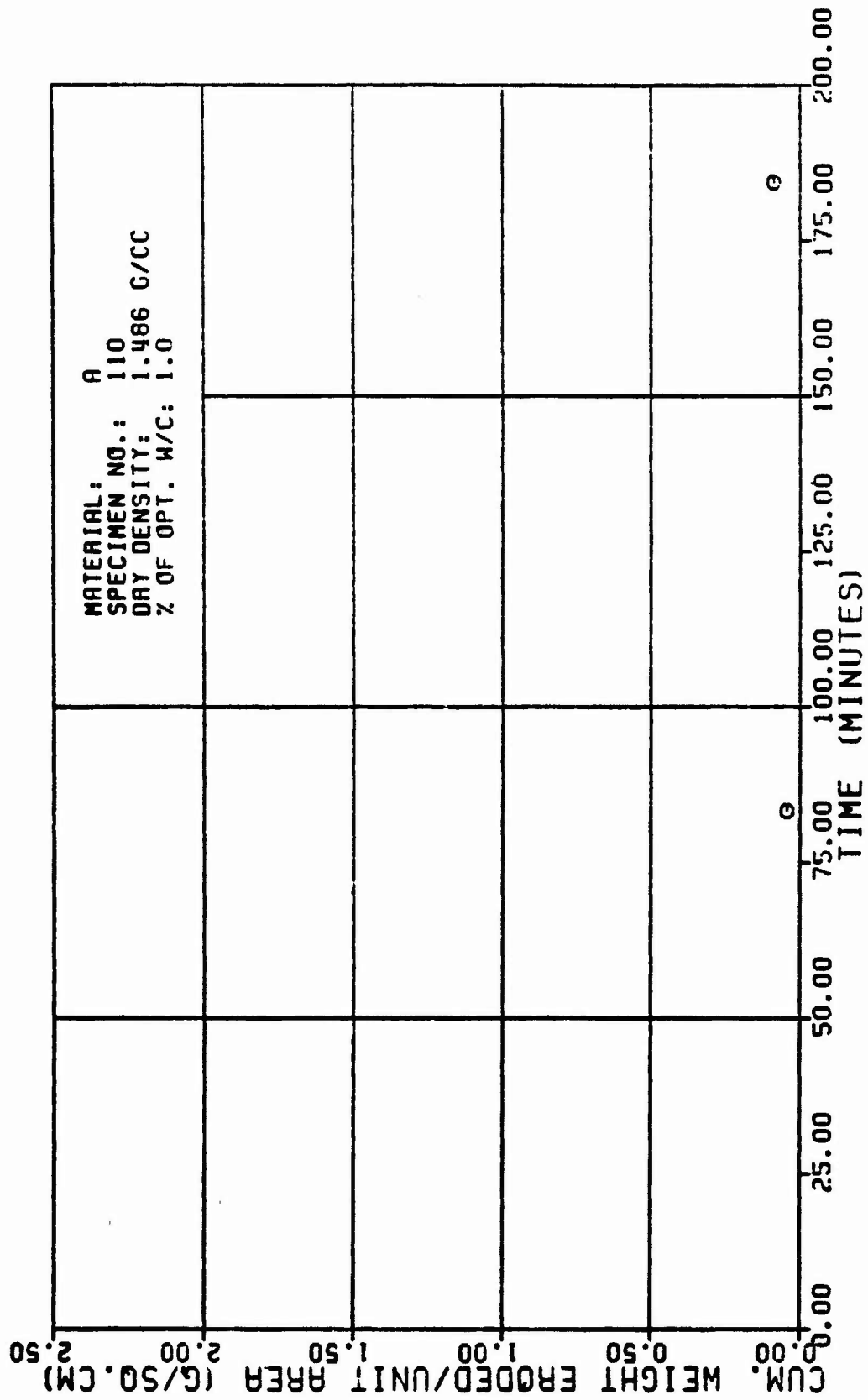


Figure A1d

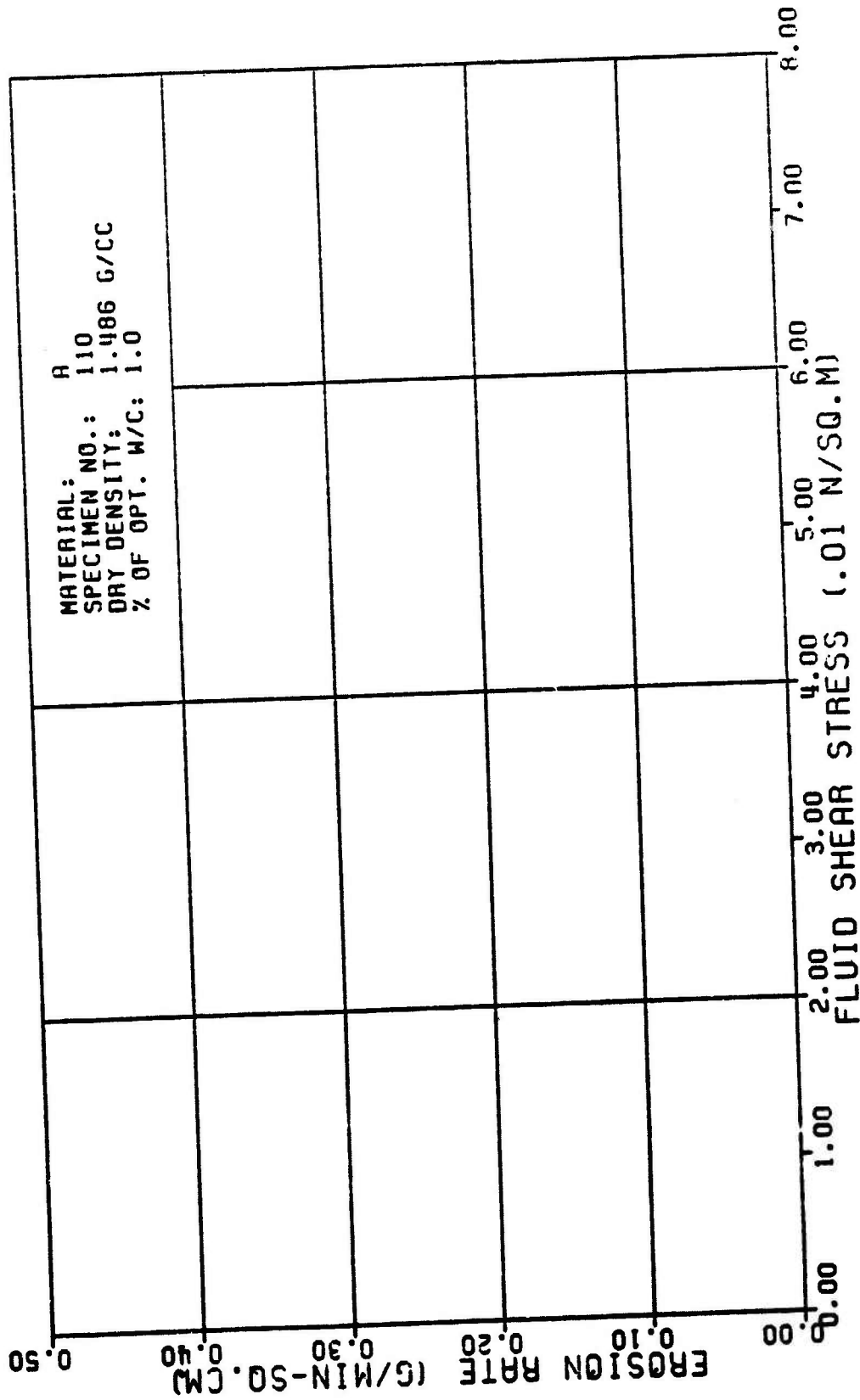


Figure Ale

TABLE A2

TEST RESULTS FOR TRIAXIAL EROSION TEST

MATERIAL TYPE: SPECIMEN NUMBER : TESTED BY:		C 118 N. L. SANCHEZ		AVERAGE FLOW RATE (Q): 142. CC/MIN					
DATE TESTED:		3 28 82		RATE OF WEIGHT EROSION (P): 8.9 G/MIN					
SPECIMEN DRY DENSITY:		1.607 G/CC		DENSITY OF ERODING FLUID: 1.000 G/CC					
% OF OPTIMUM WATER CONTENT:		-2.8 PERCENT		VISCOSITY OF ERODING FLUID: 0.001 M ² SEC/50.M					
INITIAL SLOT WIDTH:		2.38 CM		CONFINING PRESSURE: 98.00 KN/SQ.M					
INITIAL SLOT THICKNESS:		8.23 CM		HEAD OF WATER: 1.38 M					
ERODED LENGTH:		11.68 CM		HYDRAULIC GRADIENT: 18. 11/M					

VOLUME OF FLOW (LBS/ CC)	TIME (MIN)	CUM. WEIGHT ERODED (G)	CROSS SECTION AREA (SQ.CH)	VELOCITY OF FLOW (CM/MIN)	ERODED SURFACE AREA (SQ.CH)	CUM. WEIGHT ERODED PER AREA (G/SQ.CH)	EROSION RATE (GRAMS/ MIN * SQ.CH)	FLUID SHEAR STRESS (N/SQ.M)	REYNOLDS NUMBER
2.8	18.17	7.4	1.8	136.	64.	8.12	8.81	0.036	172.
4.8	21.08	14.4	1.6	89.	69.	8.21	8.81	0.017	150.
6.8	32.88	24.2	2.1	66.	75.	8.37	8.81	0.010	140.
8.8	44.63	39.4	2.8	51.	81.	8.48	8.81	0.006	135.
10.8	59.21	59.2	3.5	48.	89.	8.67	8.81	0.004	122.
11.3	76.71	84.6	4.4	32.	98.	8.86	8.81	0.003	112.

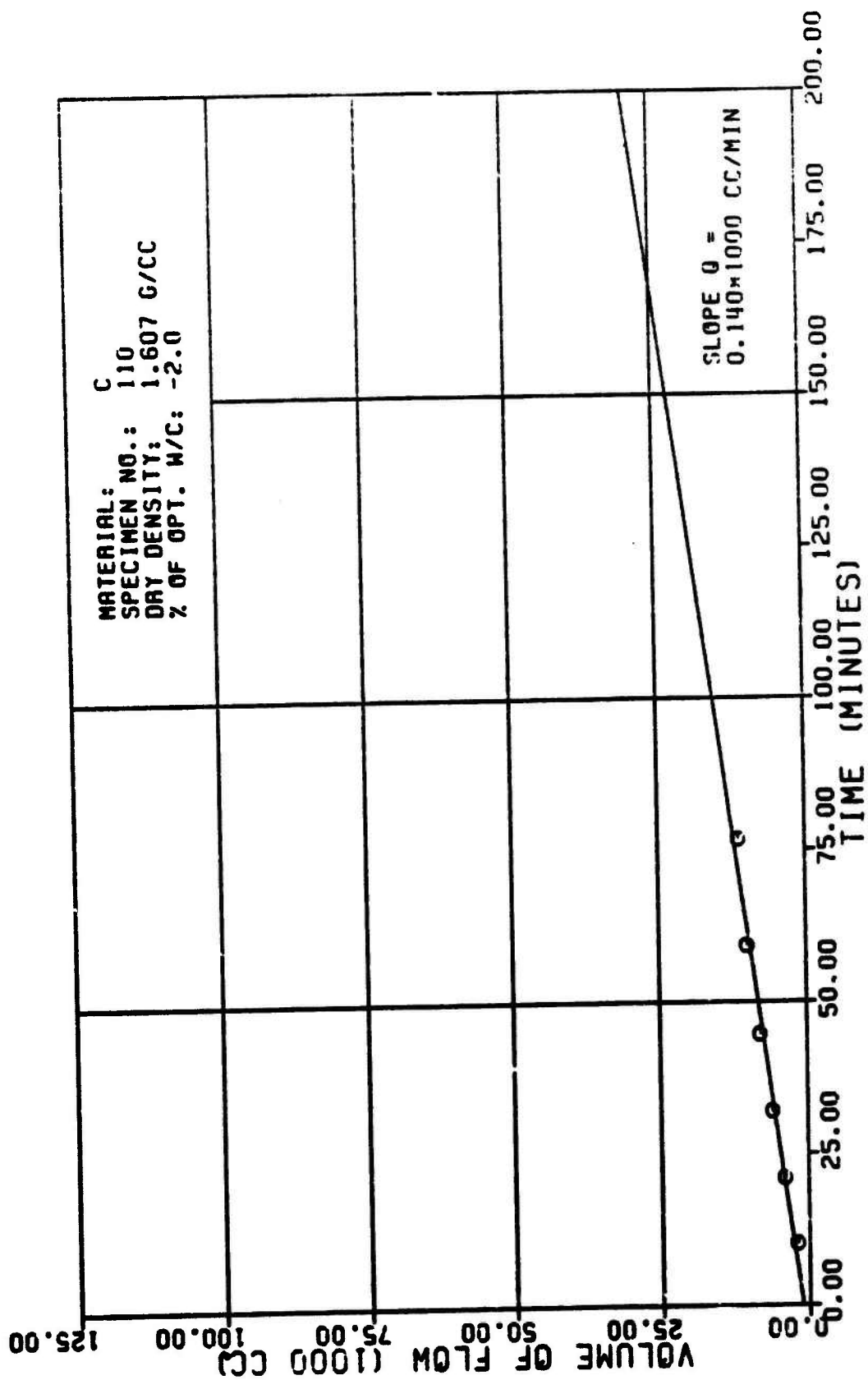


Figure A2a

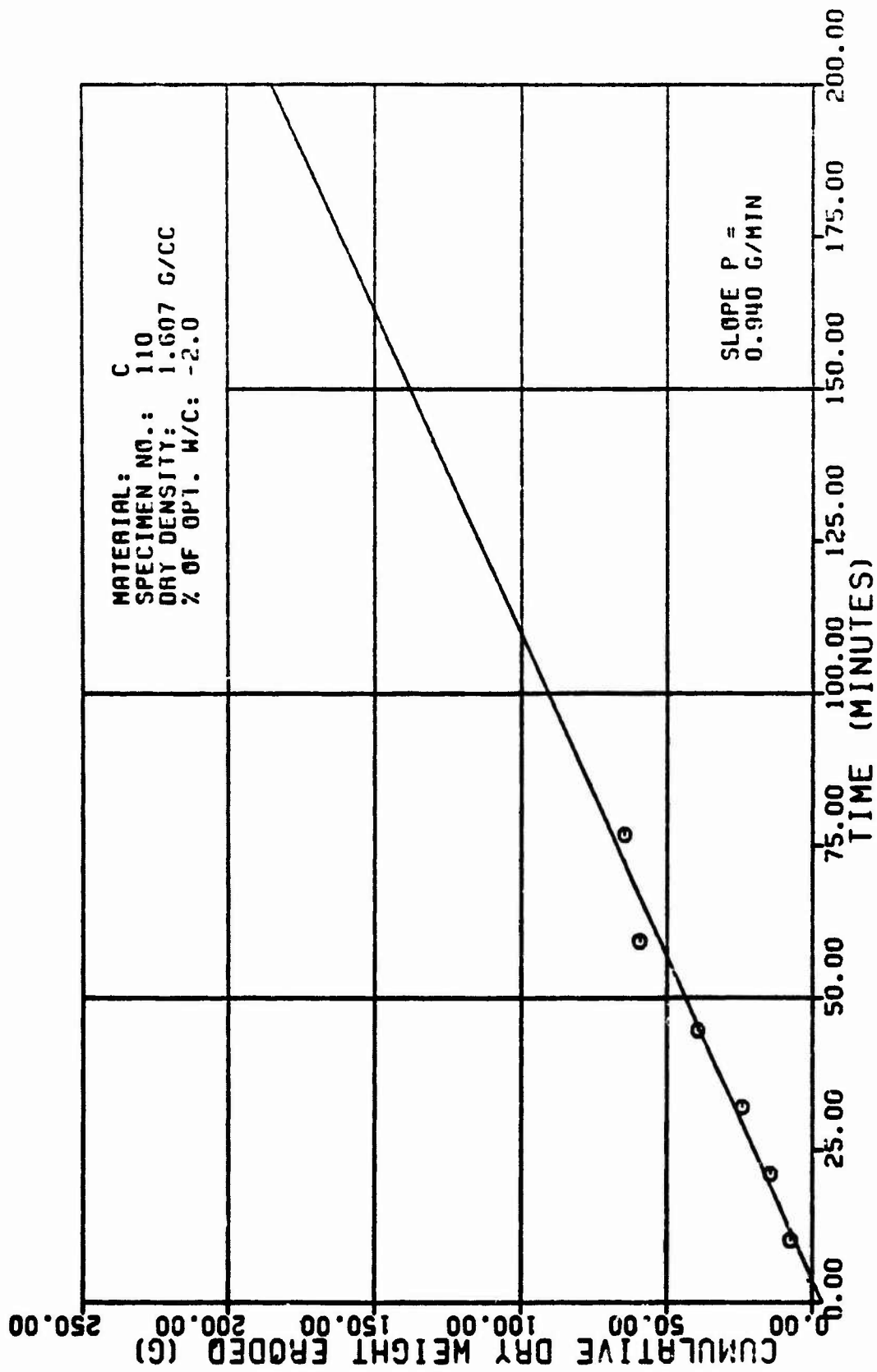


Figure A2b

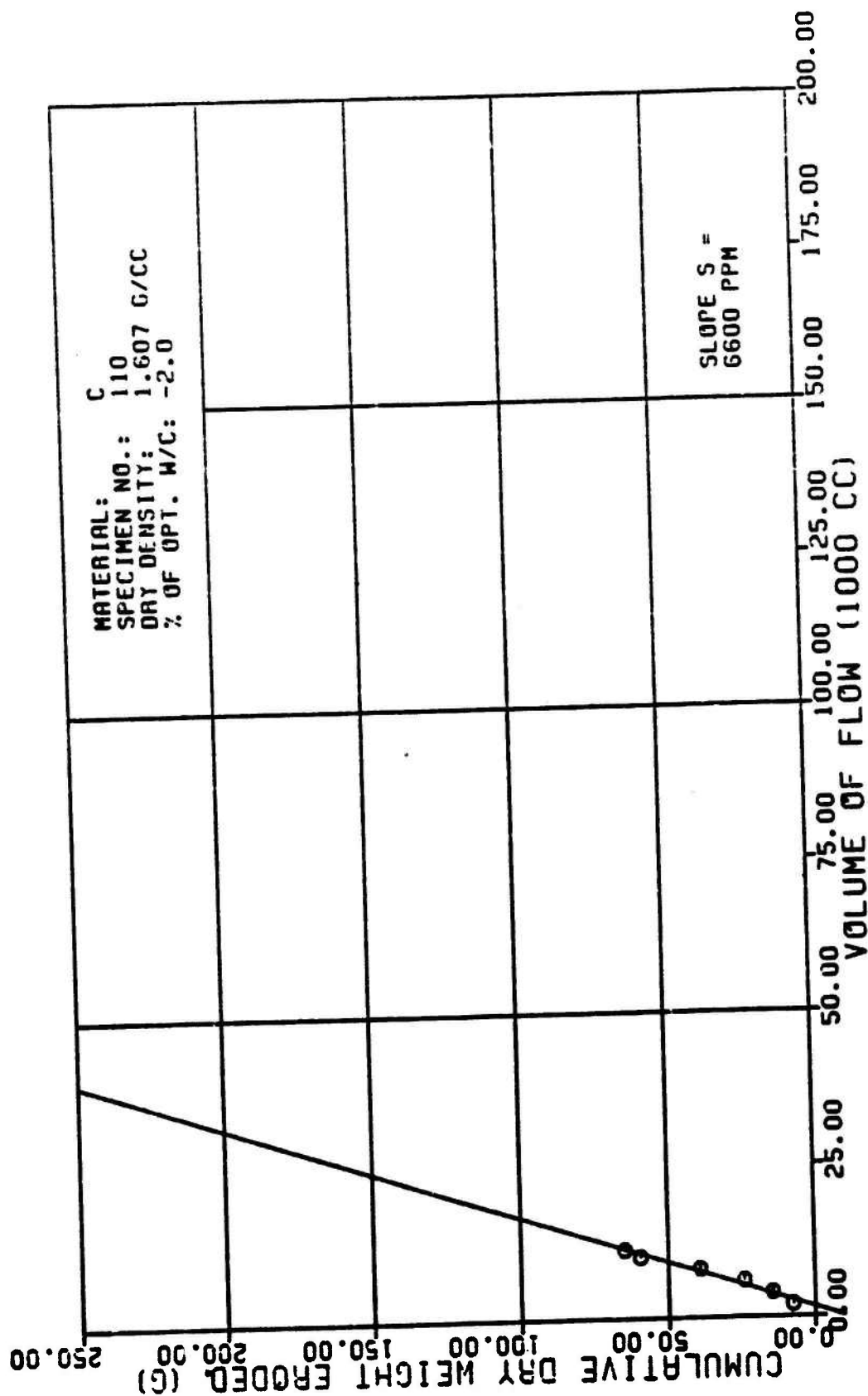


Figure A2c

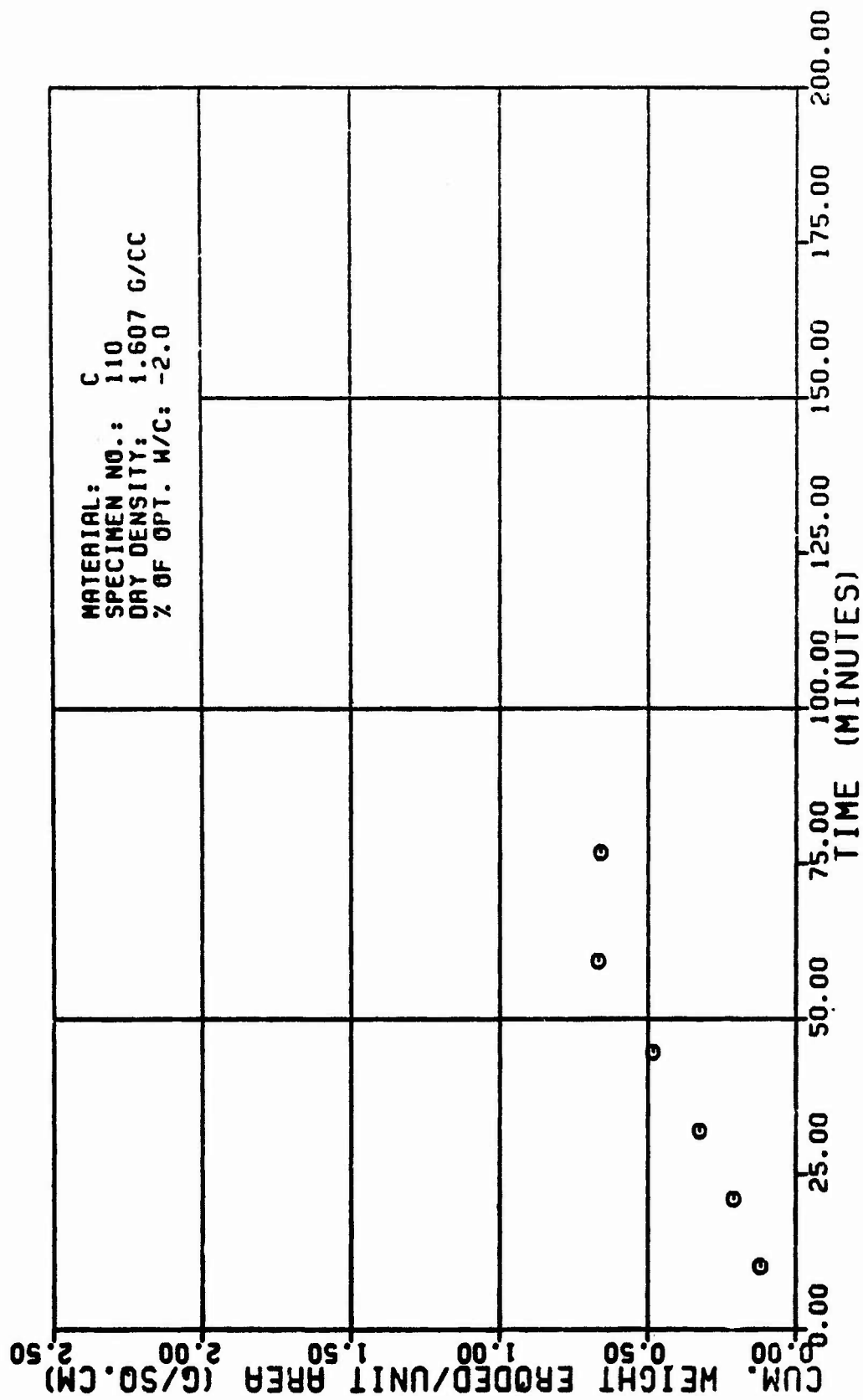


Figure A2d

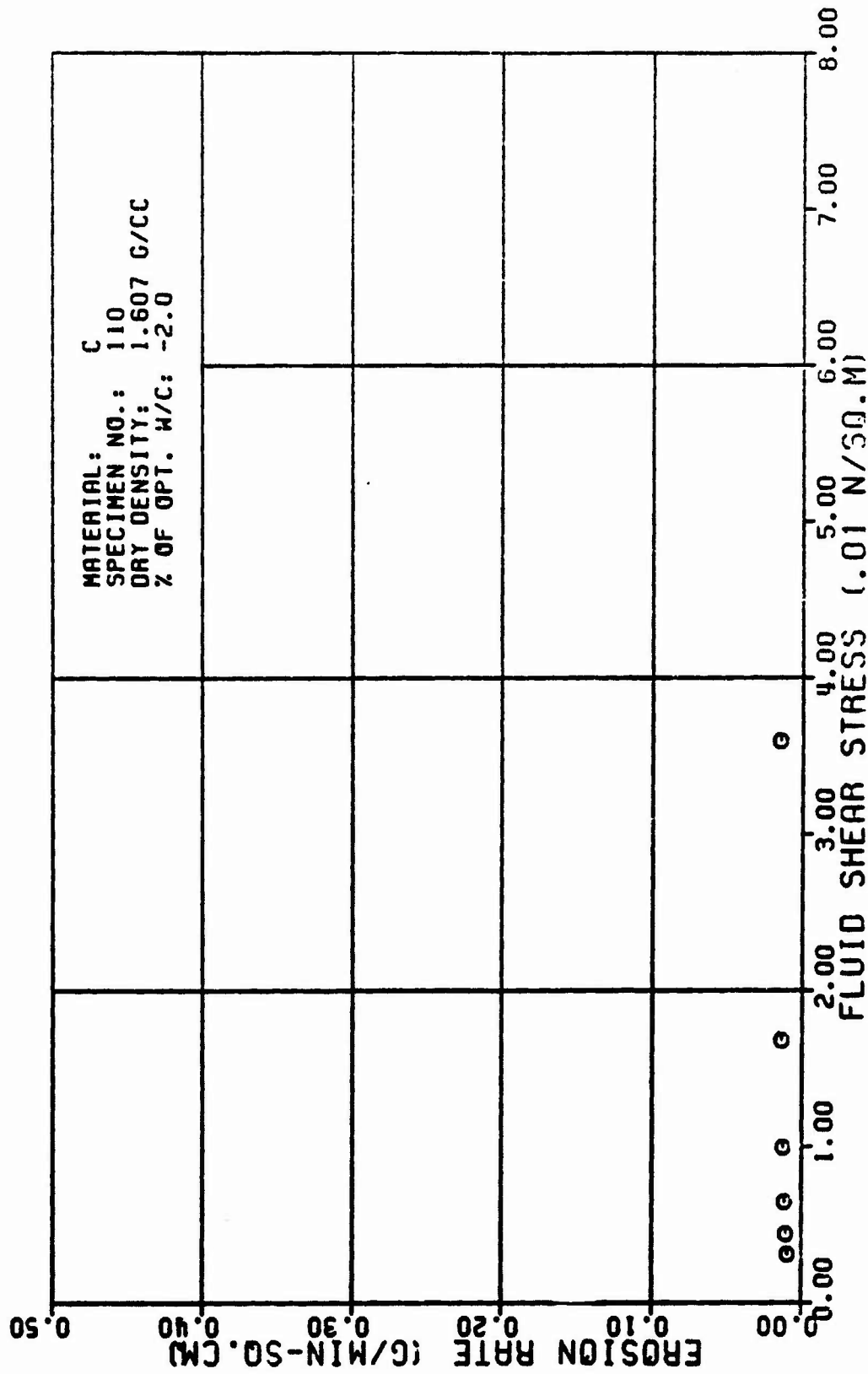


Figure A2e

TABLE A3

TEST RESULTS FOR TRIAXIAL EROSION TEST

MATERIAL TYPE:		C		104. CC/MIN	
SPECIMEN NUMBER :		111		1.7 G/MIN	
TESTED BY:		R. L. SANCHEZ			
DATE TESTED:		3 30 82			
SPECIMEN DRY DENSITY:		1.570 G/CC		1.0000 G/CC	
% OF OPTIMUM WATER CONTENT:		-4.5 PERCENT		0.001 W*SEC/SQ.M	
INITIAL SLOT WIDTH:		2.30 CM		90.00 KN/SQ.M	
INITIAL SLOT THICKNESS:		0.23 CM		1.30 M	
ERODED LENGTH:		11.60 CM		10. H/M	
AVERAGE FLOW RATE (Q):					
RATE OF WEIGHT EROSION (P):					
DENSITY OF ERODING FLUID:					
VISCOSITY OF ERODING FLUID:					
CONFINING PRESSURE:					
HEAD OF WATER:					
HYDRAULIC GRADIENT:					
CUM. WEIGHT ERODED (G)		CROSS SECTION AREA (SQ.CH)		VELOCITY OF FLOW (CM/MIN)	
TIME (MIN)		ERODED SURFACE AREA (SQ.CH)		CUM. WEIGHT ERODED PER AREA (G/SQ.CH)	
EROSION RATE (GRAMS/ (MIN " SQ.CH))		FLUID SHEAR STRESS (N/SQ.M)		REYNOLDS NUMBER	
VOLUME OF FLOW (1000 CC)					
2.0		11.04		10.6	
3.3		23.57		39.8	

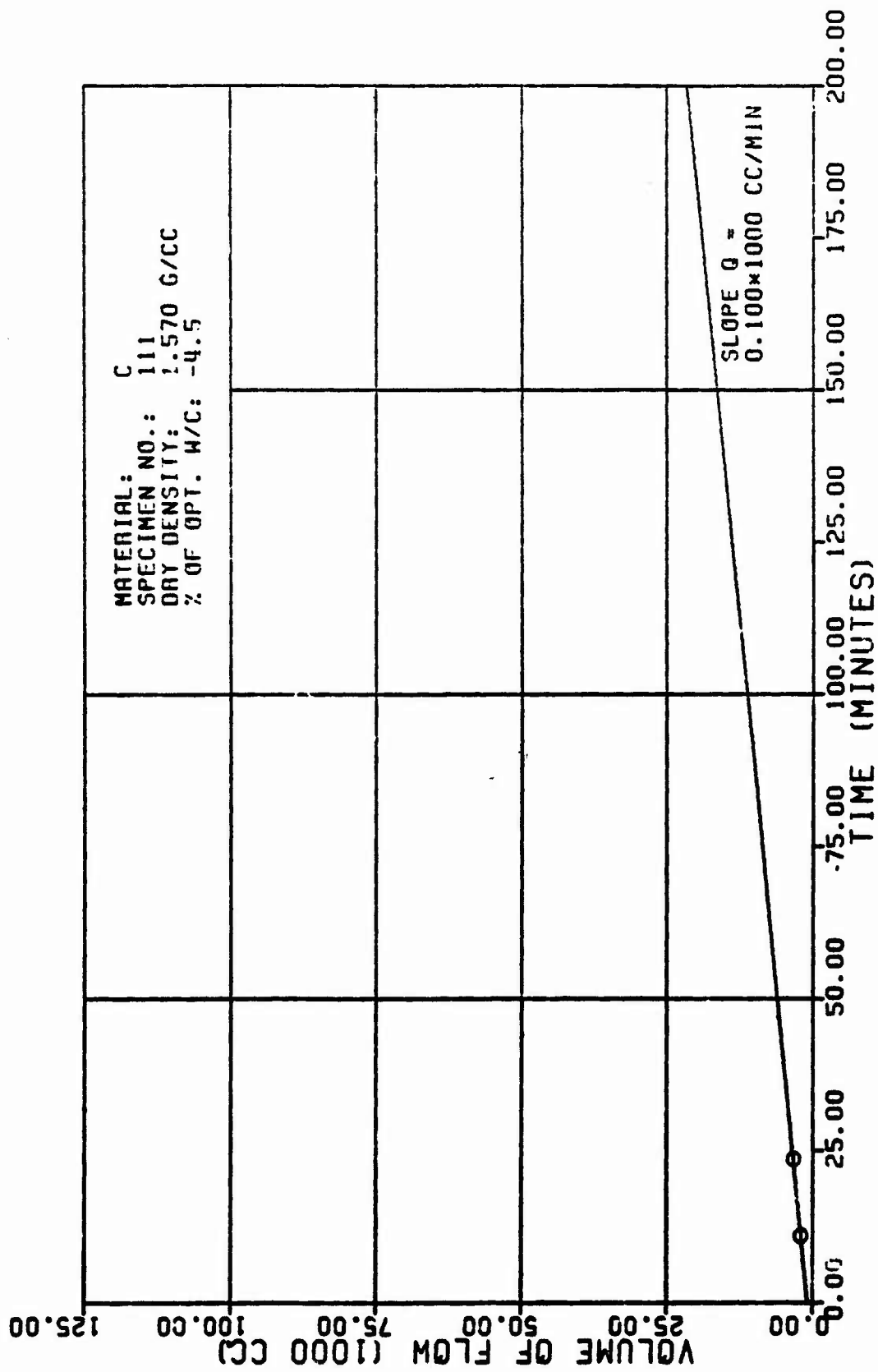


Figure A3a

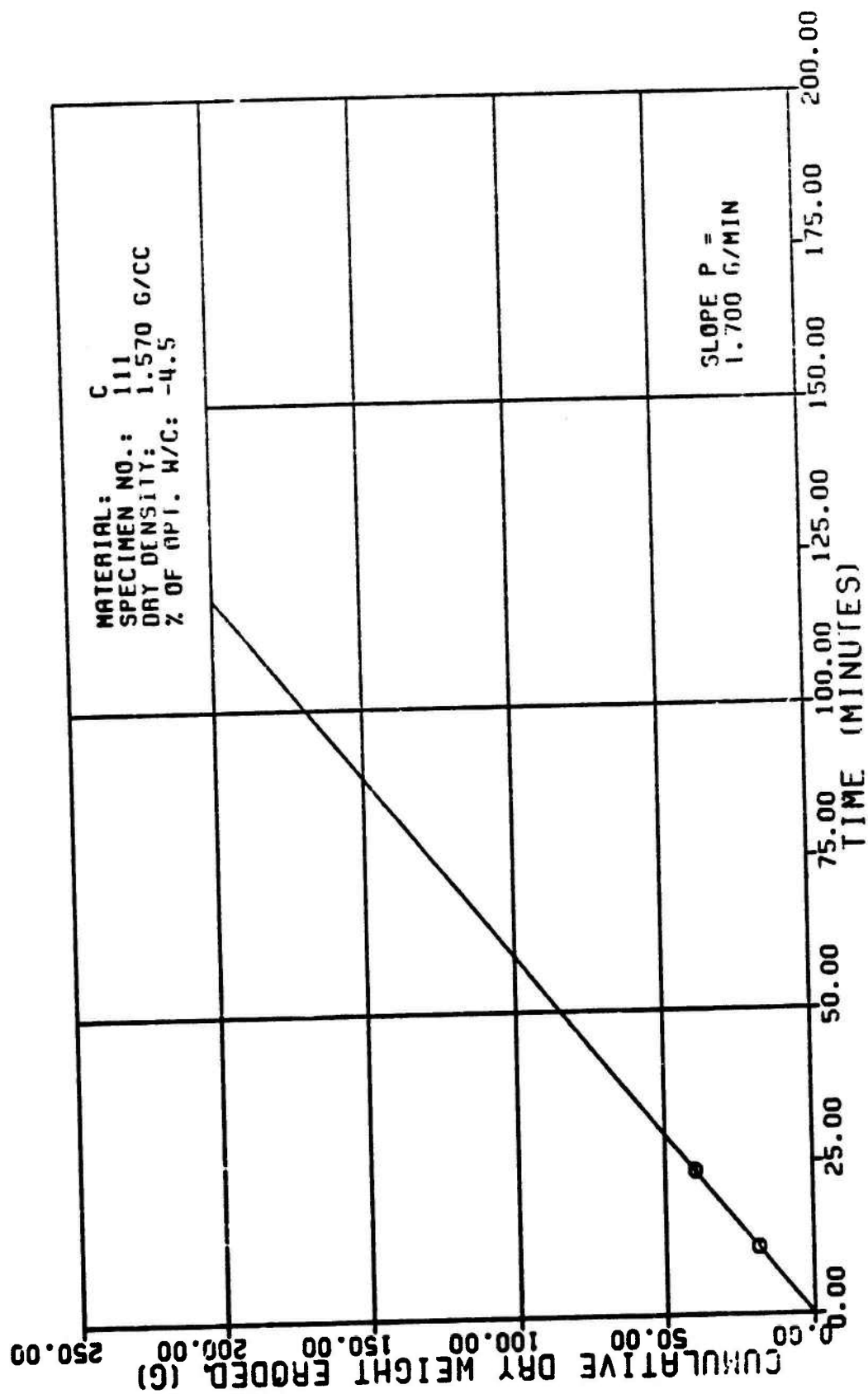


Figure A3b

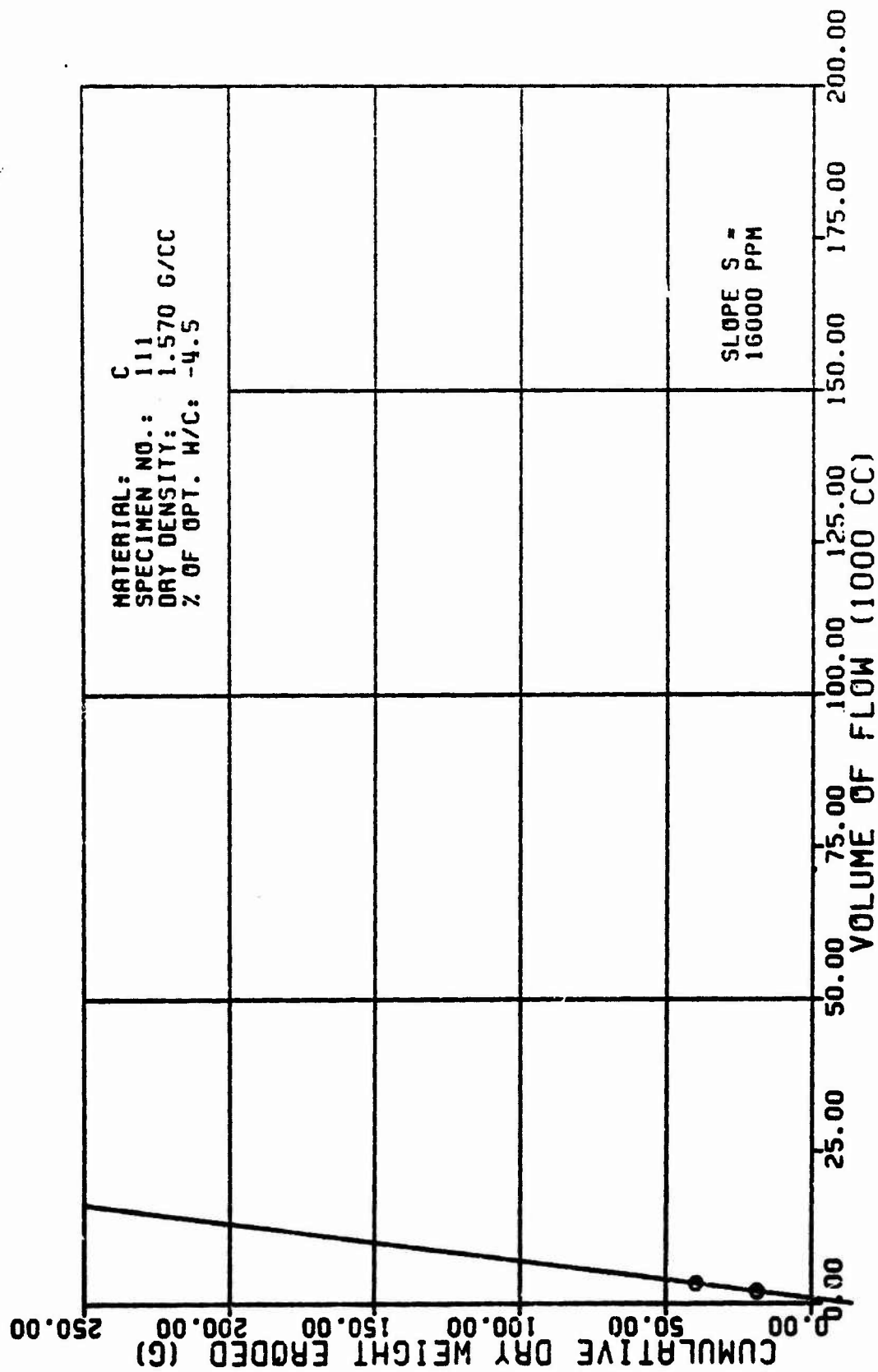


Figure A3c

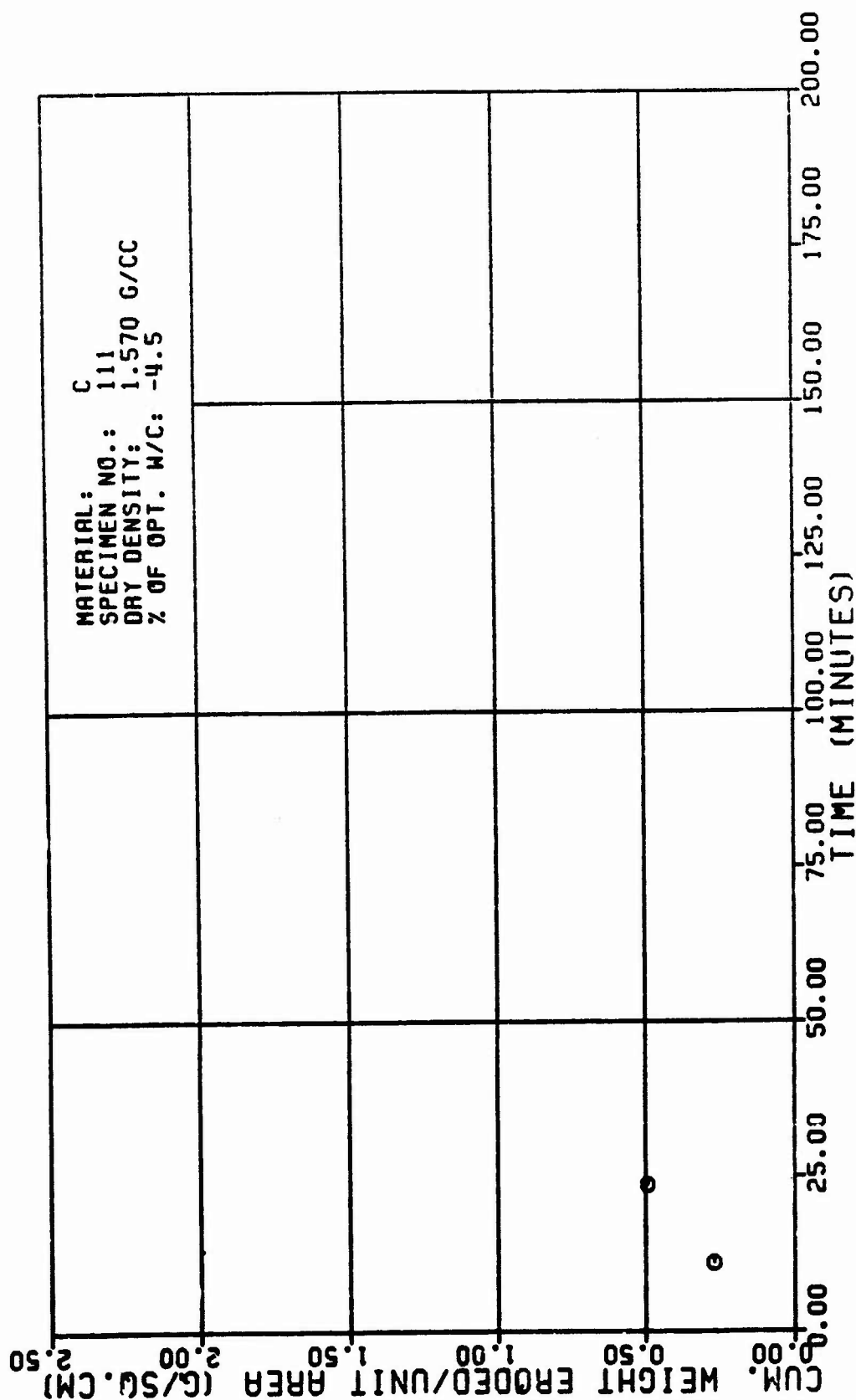


Figure A3d

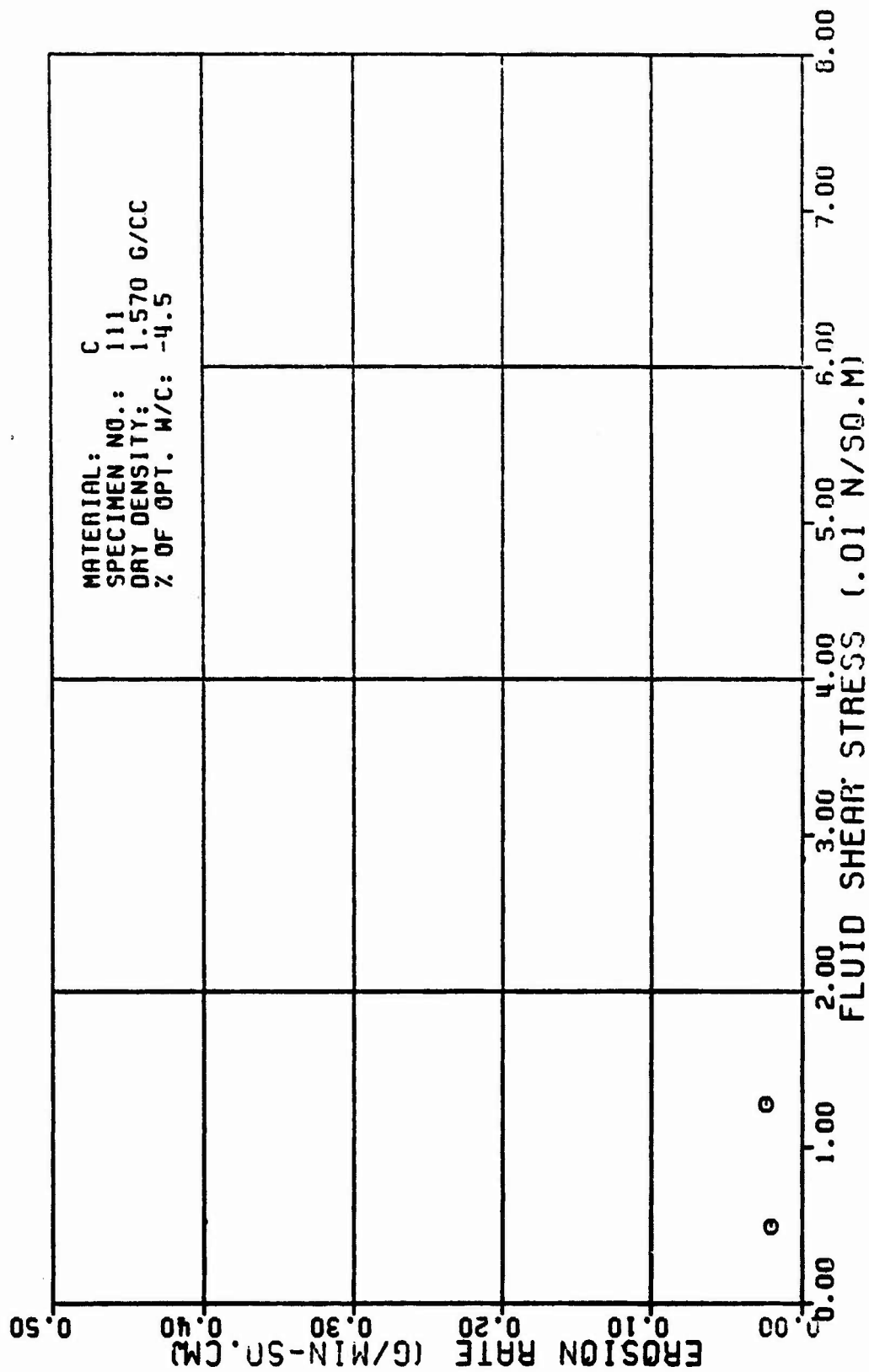


Figure A3e

TABLE A4

TEST RESULTS FOR TRIAXIAL EROSION TEST

MATERIAL TYPE: SPECIMEN NUMBER : TESTED BY:		C 12B K. L. SANCHEZ		704. CC/MIN					
DATE TESTED:		5 20 82		16.4 G/MIN					
SPECIMEN DRY DENSITY:		1.423 G/CC		1.000 G/CC					
% OF OPTIMUM WATER CONTENT:		-1.0 PERCENT		0.001 M*SEC/SQ.M					
INITIAL SLOT WIDTH:		2.30 CM		90.00 KG/SQ.M					
INITIAL SLOT THICKNESS:		0.23 CM		1.30 H					
ERODED LENGTH:		11.40 CM		10. M/N					

VOLUME OF FLOW (1000 CC)	TIME (MIN)	CUM. WEIGHT ERODED (G)	CROSS SECTION AREA (SQ.CH)	VELOCITY OF FLOW (CM/MIN)	ERODED SURFACE AREA (SQ.CH)	CUM. WEIGHT ERODED PER AREA (G/SQ.CH)	EROSION RATE (GRAMS/ MIN * SQ.CH)	FLUID SHEAR STRESS (H/SQ.H)	REYNOLDS NUMBER
2.0	3.36	30.5	3.9	120.	91.	0.33	0.10	0.010	506.
3.0	4.70	53.8	5.4	131.	106.	0.51	0.16	0.011	507.

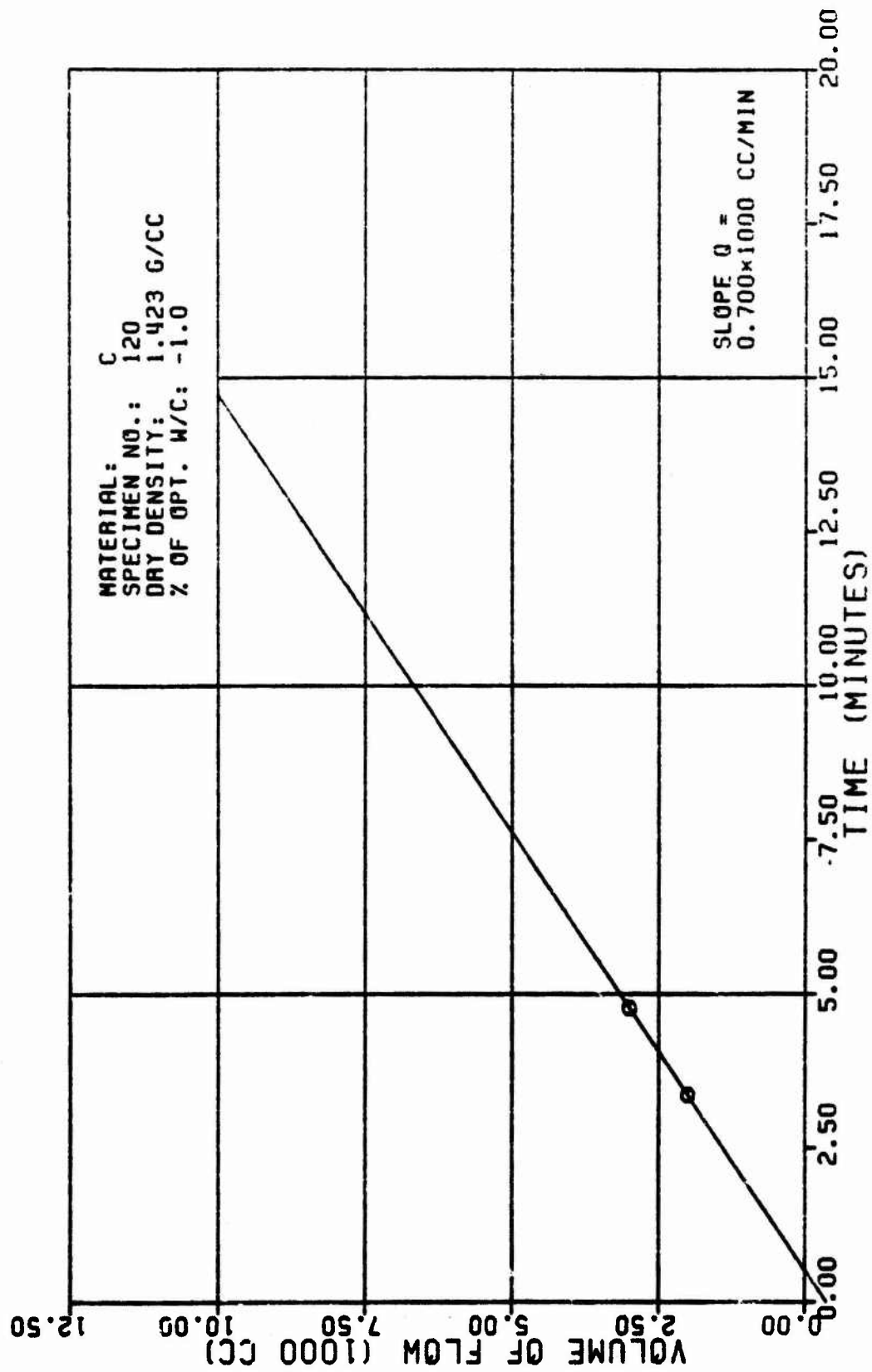


Figure A4a

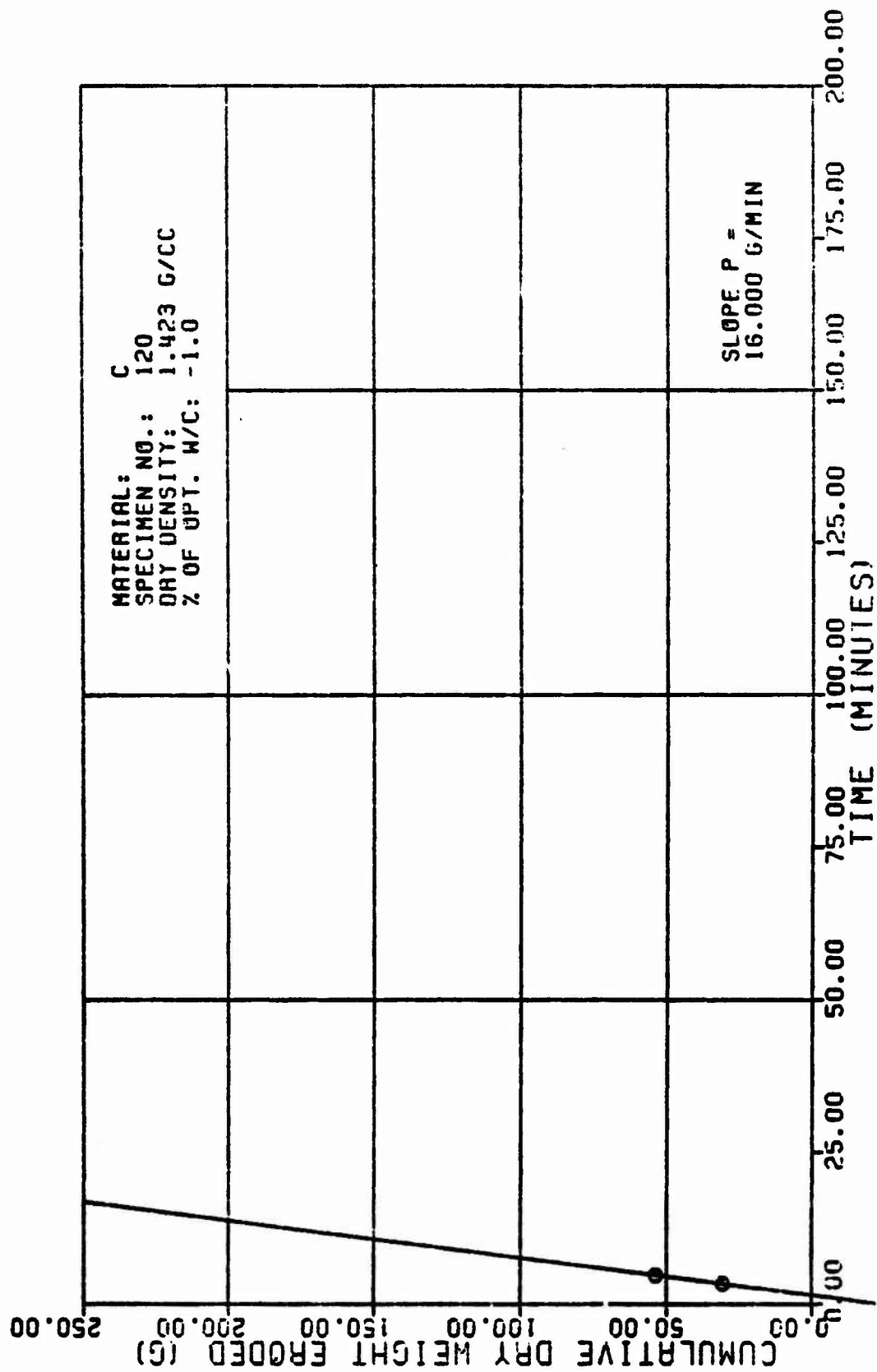


Figure A4b

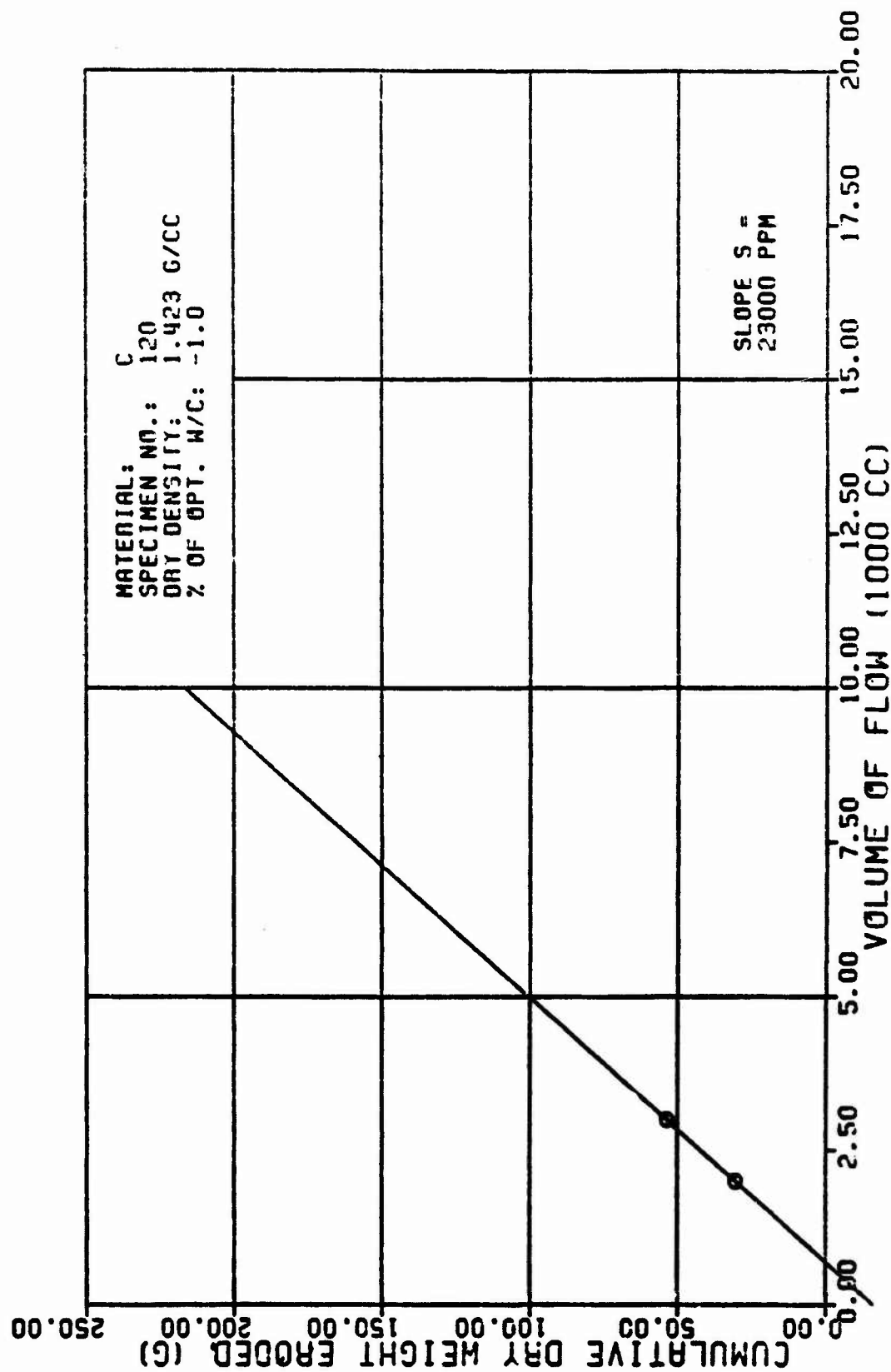


Figure A4c

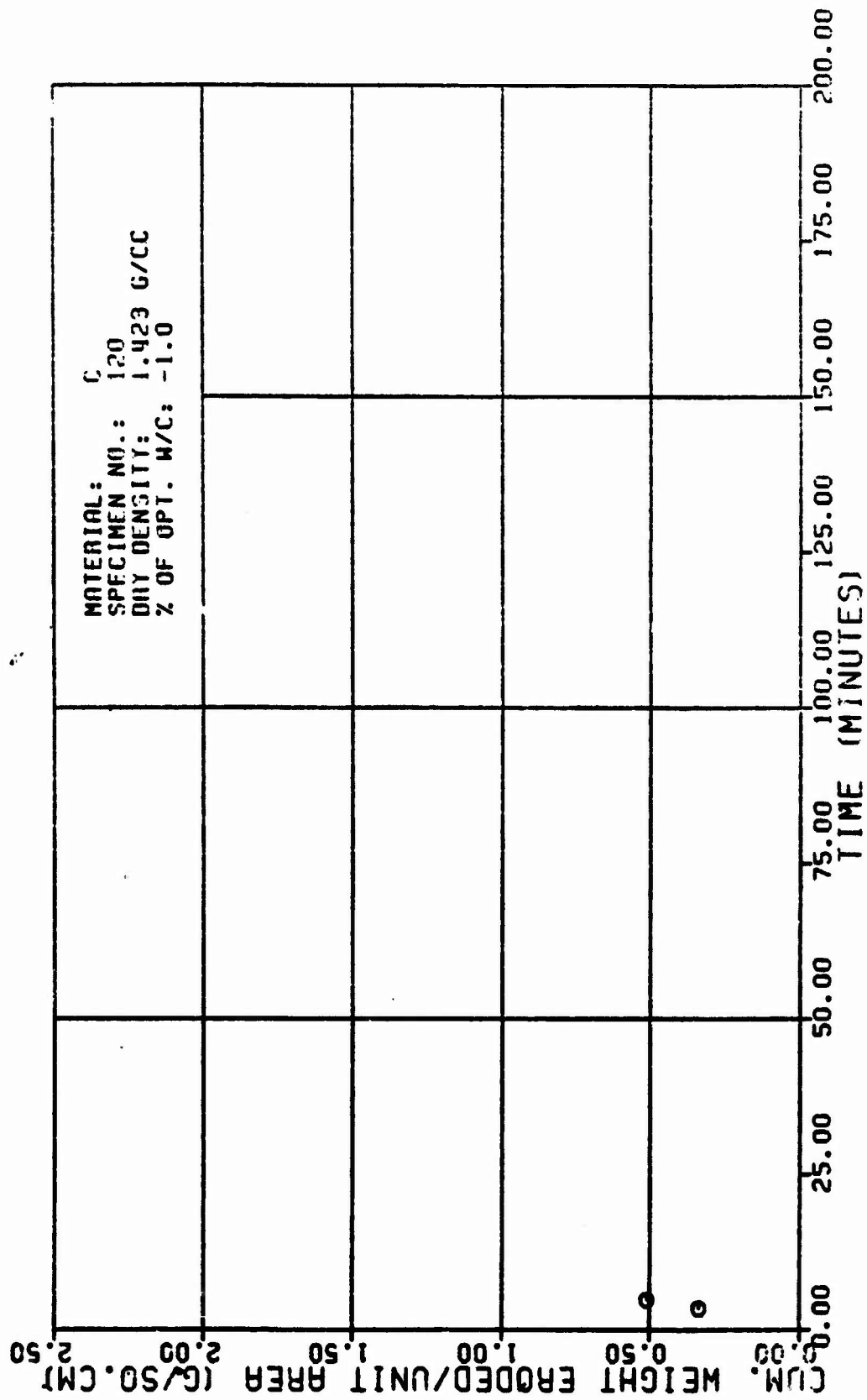


Figure A4d

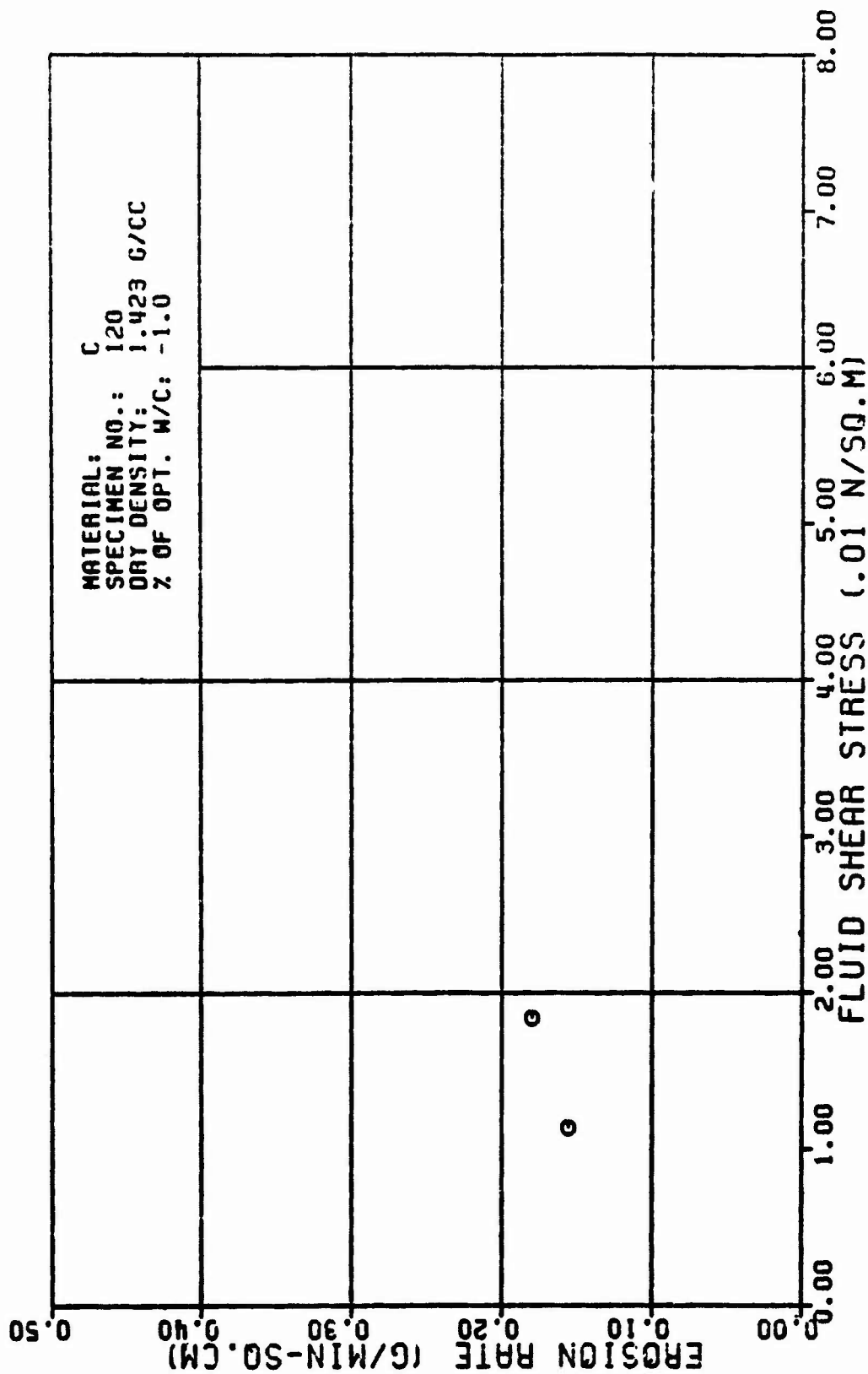


Figure A4c

TABLE A5

TEST RESULTS FOR TRIAXIAL EROSION TEST

MATERIAL TYPE: SPECIMEN NUMBER : TESTED BY:		D 118 R. L. SANCHEZ		AVERAGE FLOW RATE (Q): RATE OF WEIGHT EROSION (P):		515. CC/MIN 8.5 G/MIN			
DATE TESTED:		3 10 92		DENSITY OF ERODING FLUID: VISCOSITY OF ERODING FLUID:		1.000 G/CC 8.001 M*SEC/SQ.M			
SPECIMEN DRY DENSITY:		1.640 G/CC		CONFINING PRESSURE:		98.10 KN/SQ.M			
% OF OPTIMUM WATER CONTENT:		2.8 PERCENT		HEAD OF WATER:		13.88 M			
INITIAL SLOT WIDTH:		2.32 CM		HYDRAULIC GRADIENT:		15. M/M			
INITIAL SLOT THICKNESS:		8.23 CM							
ERODED LENGTH:		11.50 CM							
VOLUME OF FLOW (L/1000 CC)	TIME (MIN)	CUM. WEIGHT ERODED (G)	CROSS SECTION AREA (SQ.CM)	VELOCITY OF FLOW (CM/MIN)	ERODED SURFACE AREA (SQ.CM)	CUM. WEIGHT ERODED PER AREA (G/SQ.CM)	EROSION RATE (GRAMS/ MIN " " SQ.CM)	FLUID SHEAR STRESS (N/SQ.M)	REYNOLDS NUMBER
3.0	4.90	2.7	8.7	775.	60.	8.95	8.01	8.384	658.
7.0	9.90	8.8	8.8	844.	61.	8.89	8.01	8.218	644.
10.0	15.23	7.5	8.9	940.	63.	8.12	8.01	8.159	630.
14.0	20.71	10.4	1.1	474.	64.	8.16	8.01	8.122	615.
17.0	26.61	13.0	1.2	414.	66.	8.21	8.01	8.095	601.
21.0	32.61	17.6	1.4	367.	67.	8.26	8.01	8.077	587.
24.0	38.91	21.0	1.6	328.	69.	8.30	8.01	8.063	573.
28.0	46.46	24.3	1.7	295.	71.	8.34	8.01	8.052	559.
31.0	52.20	27.9	1.9	267.	72.	8.39	8.01	8.044	548.

TABLE FOR SPECIMEN NUMBER: 8118 (CONTINUES)

VOLUME OF FLOW (1000 CC)	TIME (MIN)	CUM. WEIGHT ERODED (G)	CROSS SECTION AREA (SQ. CM)	VELOCITY OF FLOW (CM/MIN)	ERODED SURFACE AREA (SQ. CM)	CUM. WEIGHT ERODED PER AREA (G/SQ. CM)	EROSION RATE (GRAMS/ MIN. X SQ. CM)	FLUID SHEAR STRESS (N/30.0 N)	REYNOLDS NUMBER
36.8	59.85	31.2	2.1	243.	74.	8.42	8.81	8.837	531.
36.8	66.87	34.8	2.3	222.	76.	8.48	8.81	8.832	517.
42.8	74.38	37.8	2.6	206.	78.	8.46	8.81	8.828	504.
48.8	82.82	41.8	2.7	189.	80.	8.51	8.81	8.824	491.
49.8	90.18	44.8	2.9	176.	82.	8.54	8.81	8.821	479.
52.8	98.16	50.3	3.1	164.	85.	8.68	8.81	8.819	467.
53.1	107.88	51.8	3.2	161.	85.	8.61	8.81	8.819	464.

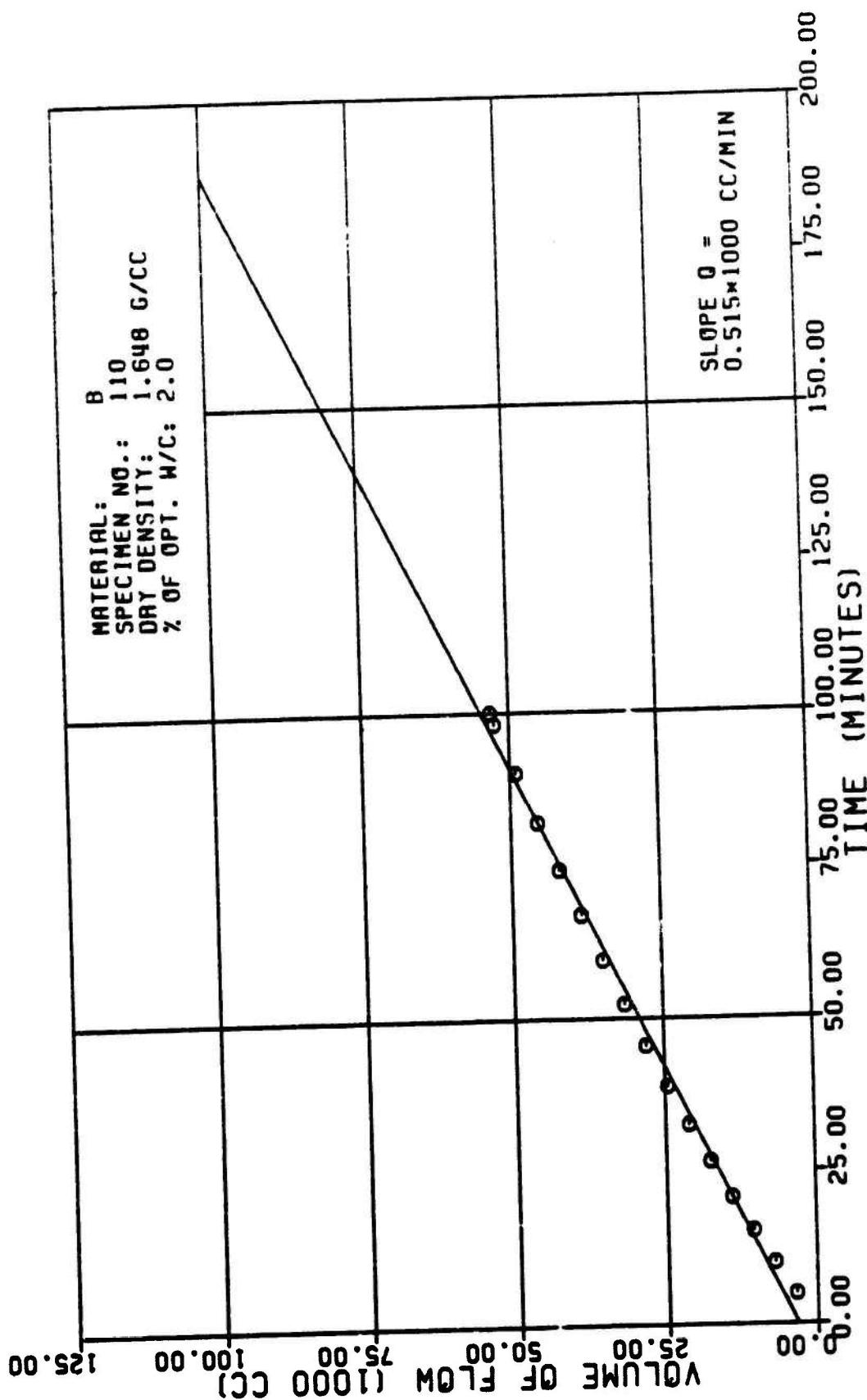


Figure A5a

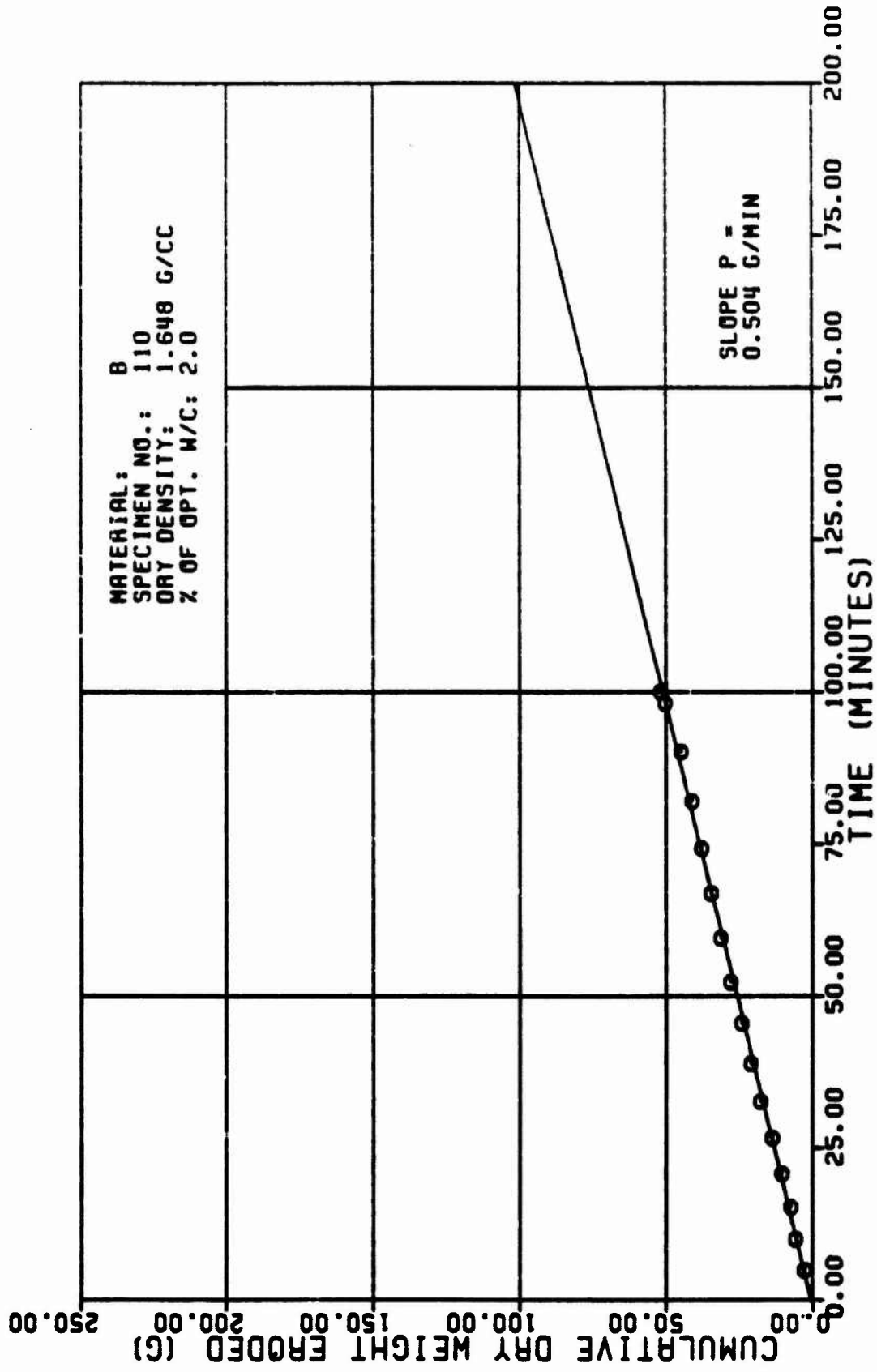


Figure A5b

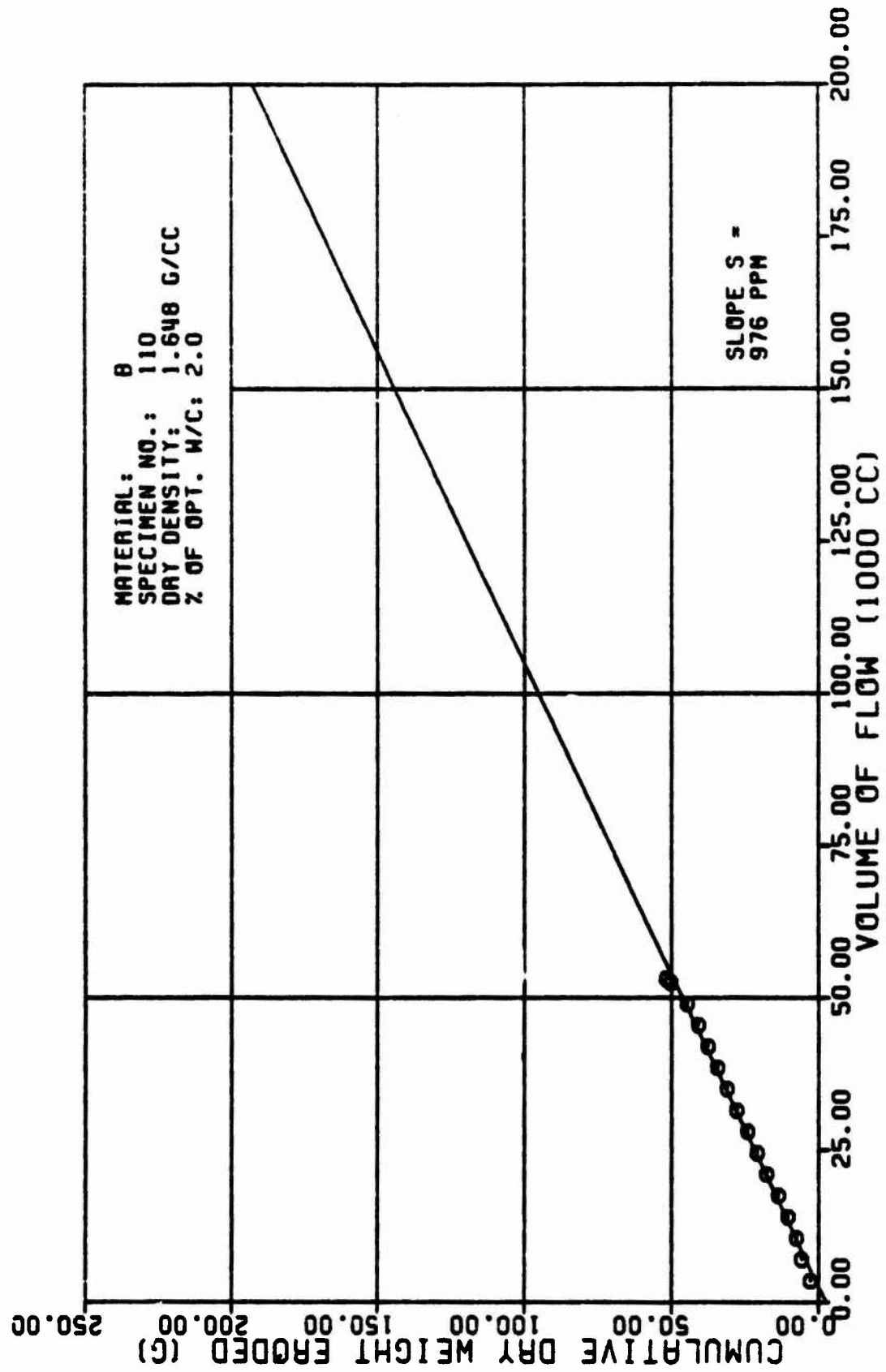


Figure A5c

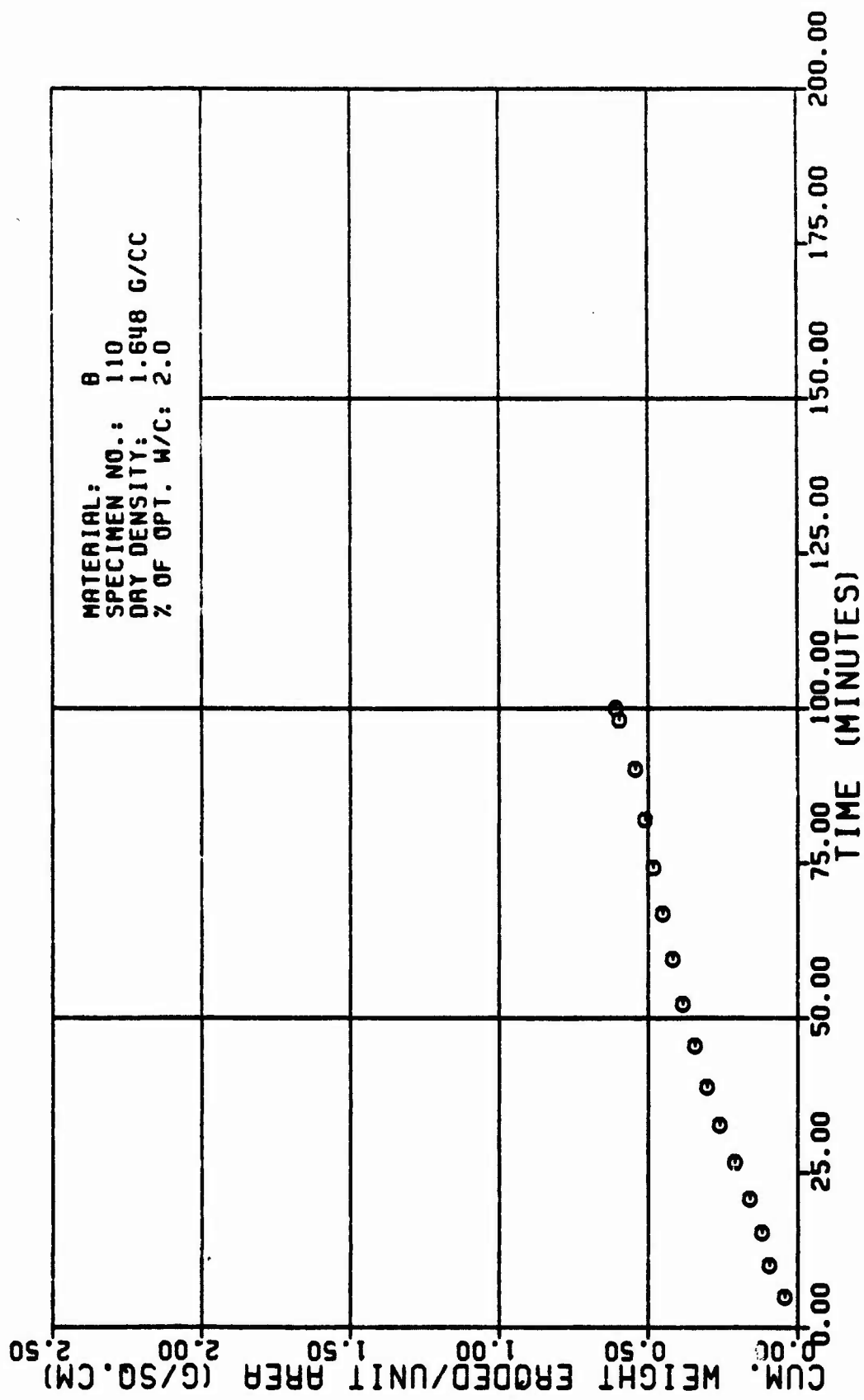


Figure A5d

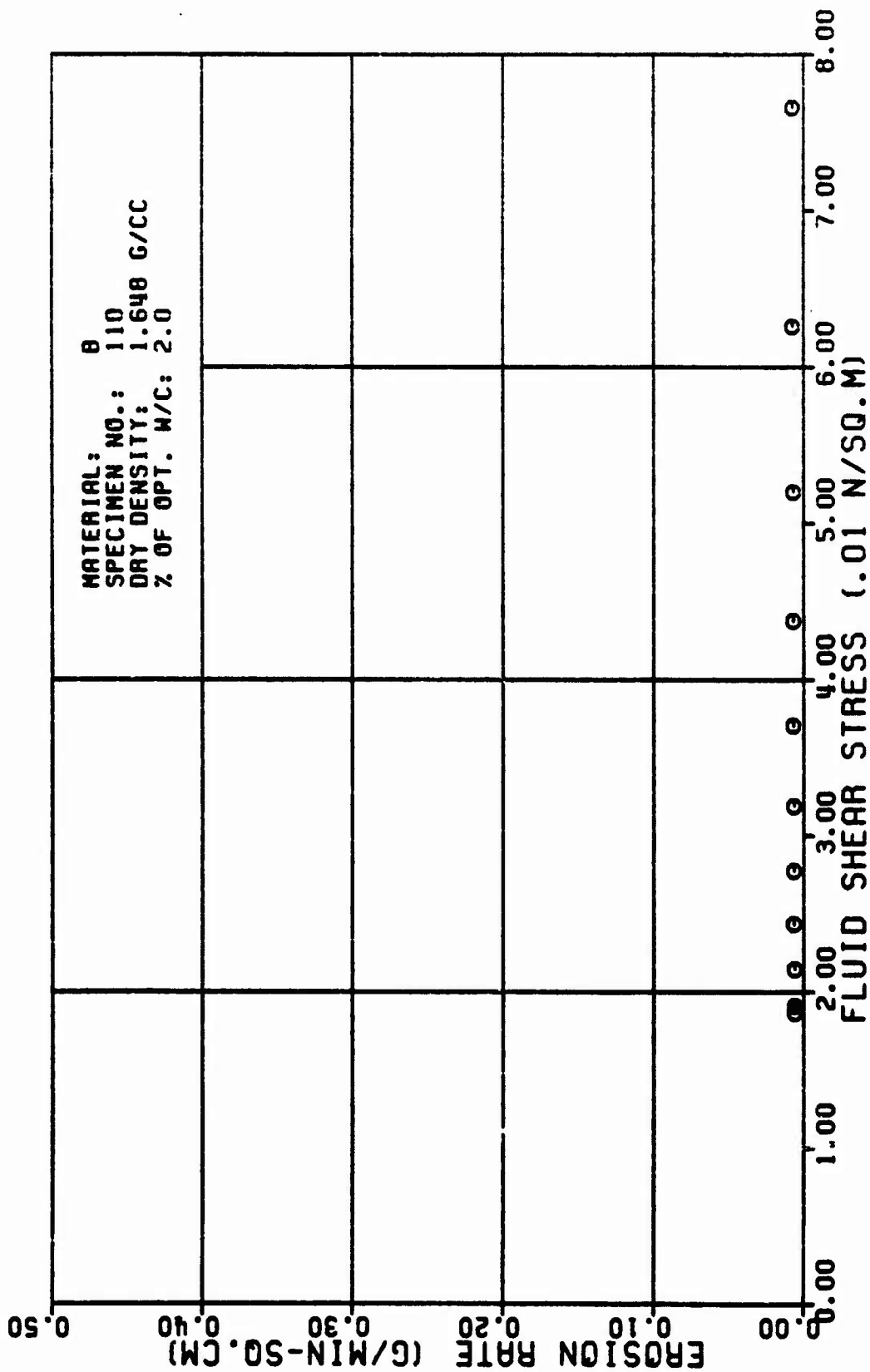


Figure A5e

TABLE A6

TEST RESULTS FOR TRIAXIAL EROSION TEST

MATERIAL TYPE: SPECIMEN NUMBER : TESTED BY.		0 111 R. L. SANCHEZ		AVERAGE FLOW RATE (Q): RATE OF WEIGHT EROSION (P): DENSITY OF ERODING FLUID: VISCOSITY OF ERODING FLUID: CONFINING PRESSURE: HEAD OF WATER: HYDRAULIC GRADIENT:		459. CC/MIN 1.5 G/MIN 1.556 G/CC 5.551 M*SEC/SQ.M 98.15 KN/SQ.M 1.3 MM 15. M/M			
DATE TESTED:		3 19 62							
SPECIMEN DRY DENSITY:		1.656 G/CC							
% OF OPTIMUM WATER CONTENT:		5.5 PERCENT							
INITIAL SLOT WIDTH:		2.32 CM							
INITIAL SLOT THICKNESS:		5.23 CM							
ERODED LENGTH:		11.65 CM							

VOLUME OF FLOW (1000 CC)	TIME (MIN)	CUM. WEIGHT ERODED (G)	CROSS SECTION AREA (SQ.CM)	VELOCITY OF FLOW (CM/MIN)	ERODED SURFACE AREA (SQ.CM)	CUM. WEIGHT ERODED PER AREA (G/SQ.CM)	EROSION RATE (GRAMS/ MIN IN. SQ.CM)	FLUID SHEAR STRESS (N/SQ.M)	REYNOLDS NUMBER
3.5	6.02	6.1	5.9	595.	63.	5.15	5.52	5.151	563.
7.5	13.49	12.5	1.3	365.	67.	5.10	5.52	5.501	532.
15.5	25.65	17.7	1.7	276.	75.	5.25	5.51	5.555	503.
14.5	28.57	24.2	2.1	222.	74.	5.32	5.51	5.534	475.
17.5	35.83	35.5	2.5	184.	79.	5.39	5.51	5.525	455.
21.5	43.81	38.7	2.9	156.	83.	5.47	5.51	5.519	425.
24.5	51.72	48.9	3.4	136.	97.	5.56	5.51	5.515	405.
27.5	59.85	54.5	3.8	122.	91.	5.71	5.51	5.513	385.

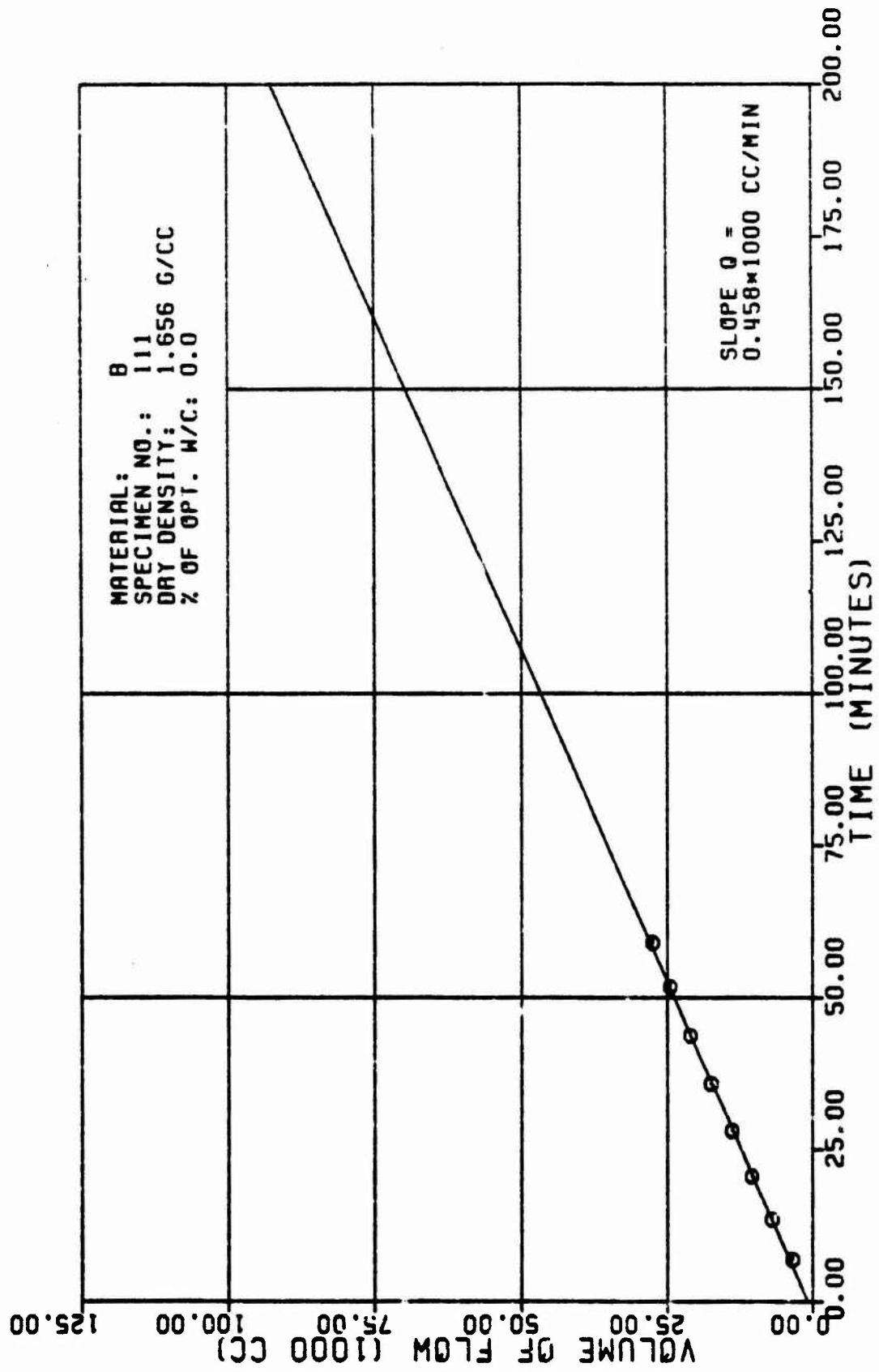


Figure A6a

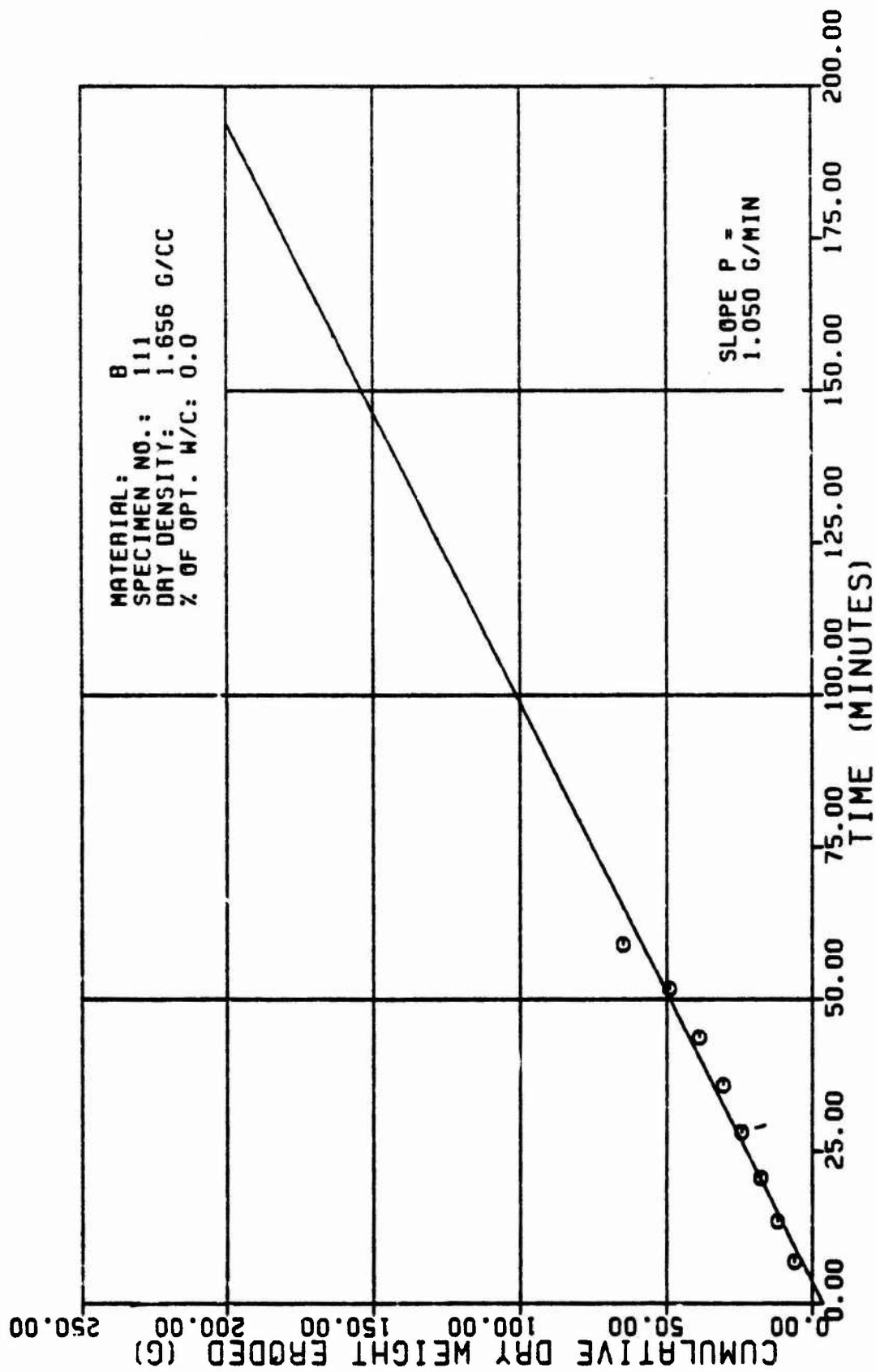


Figure A6b

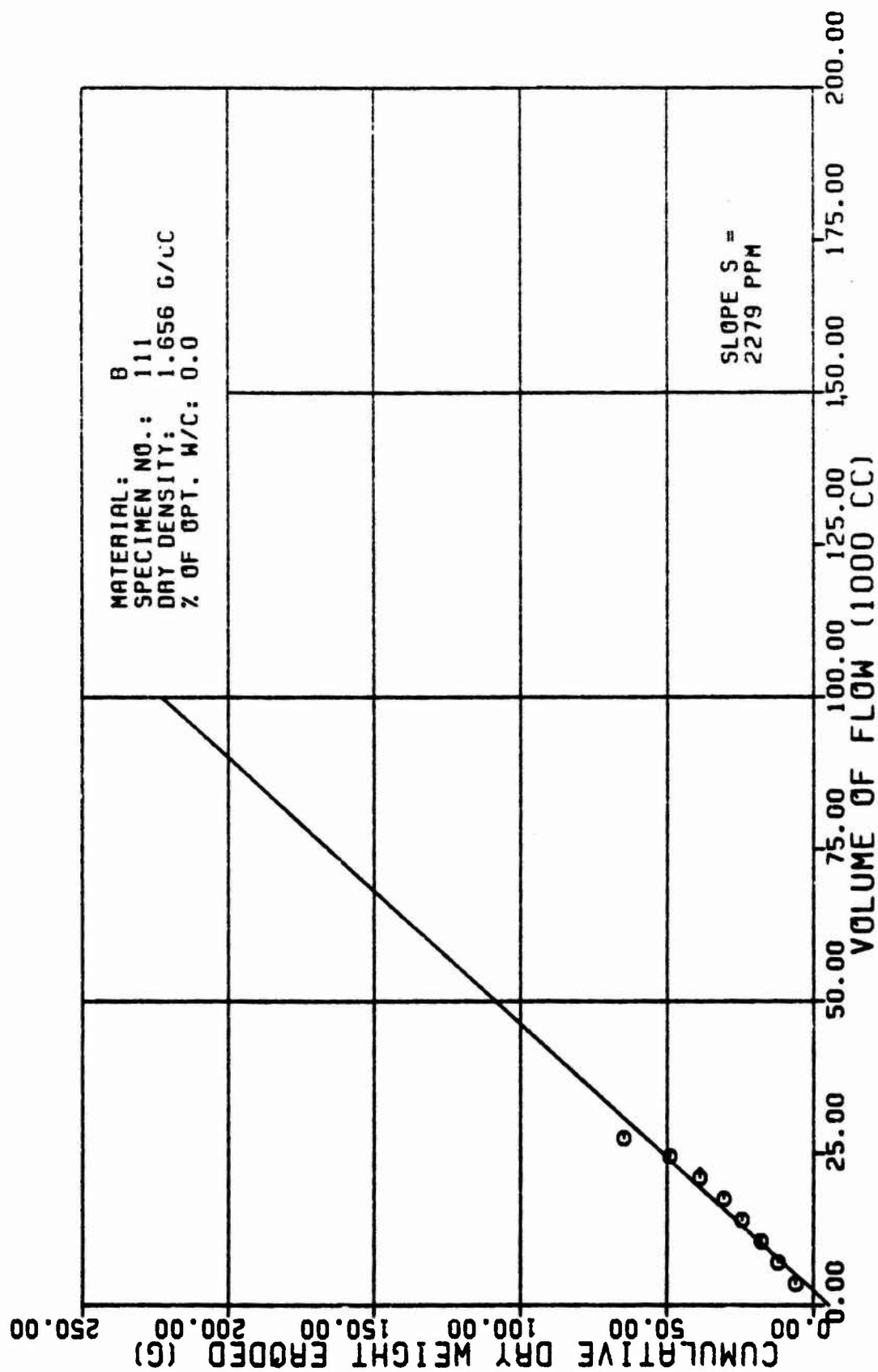


Figure A6c

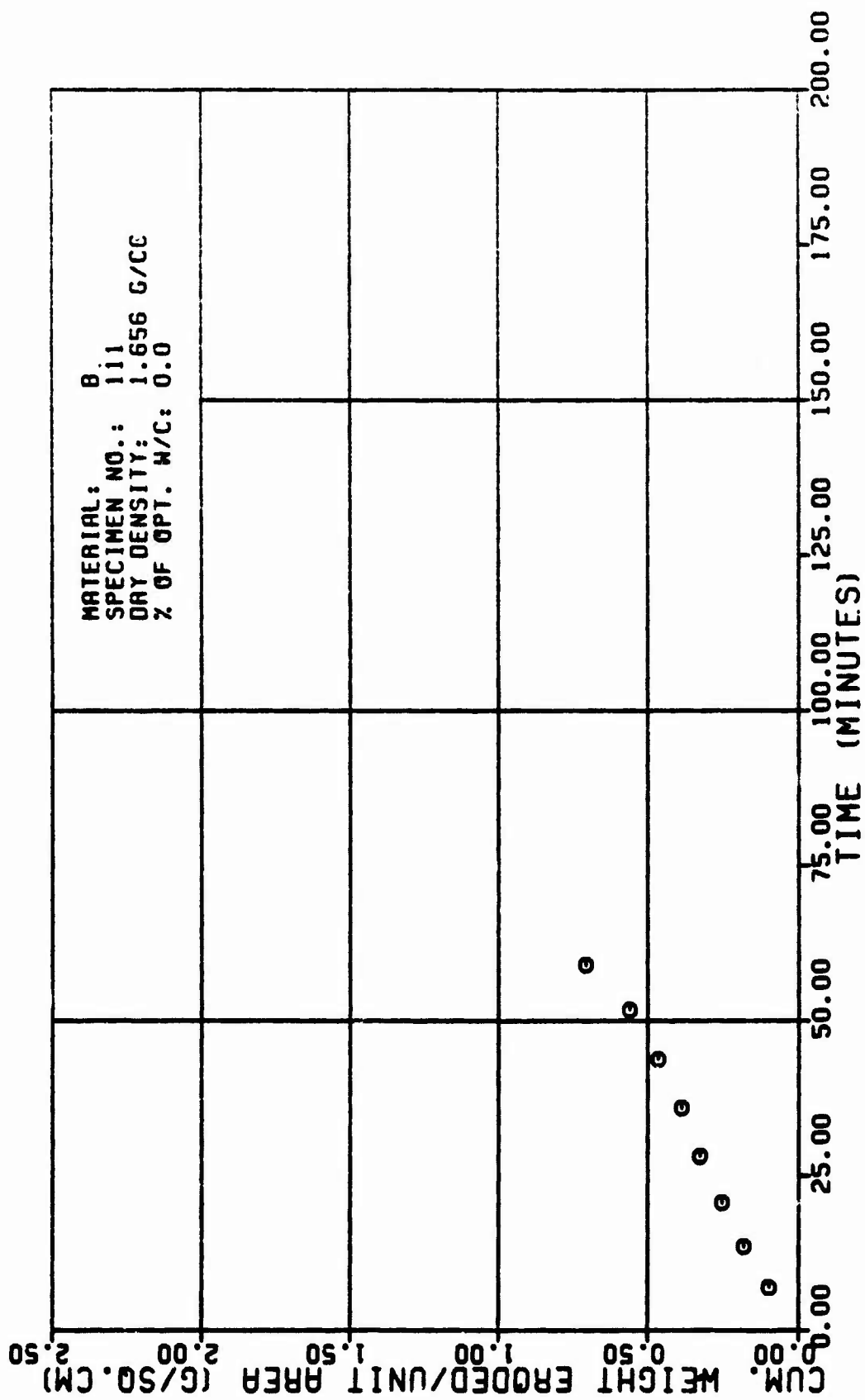


Figure A6d

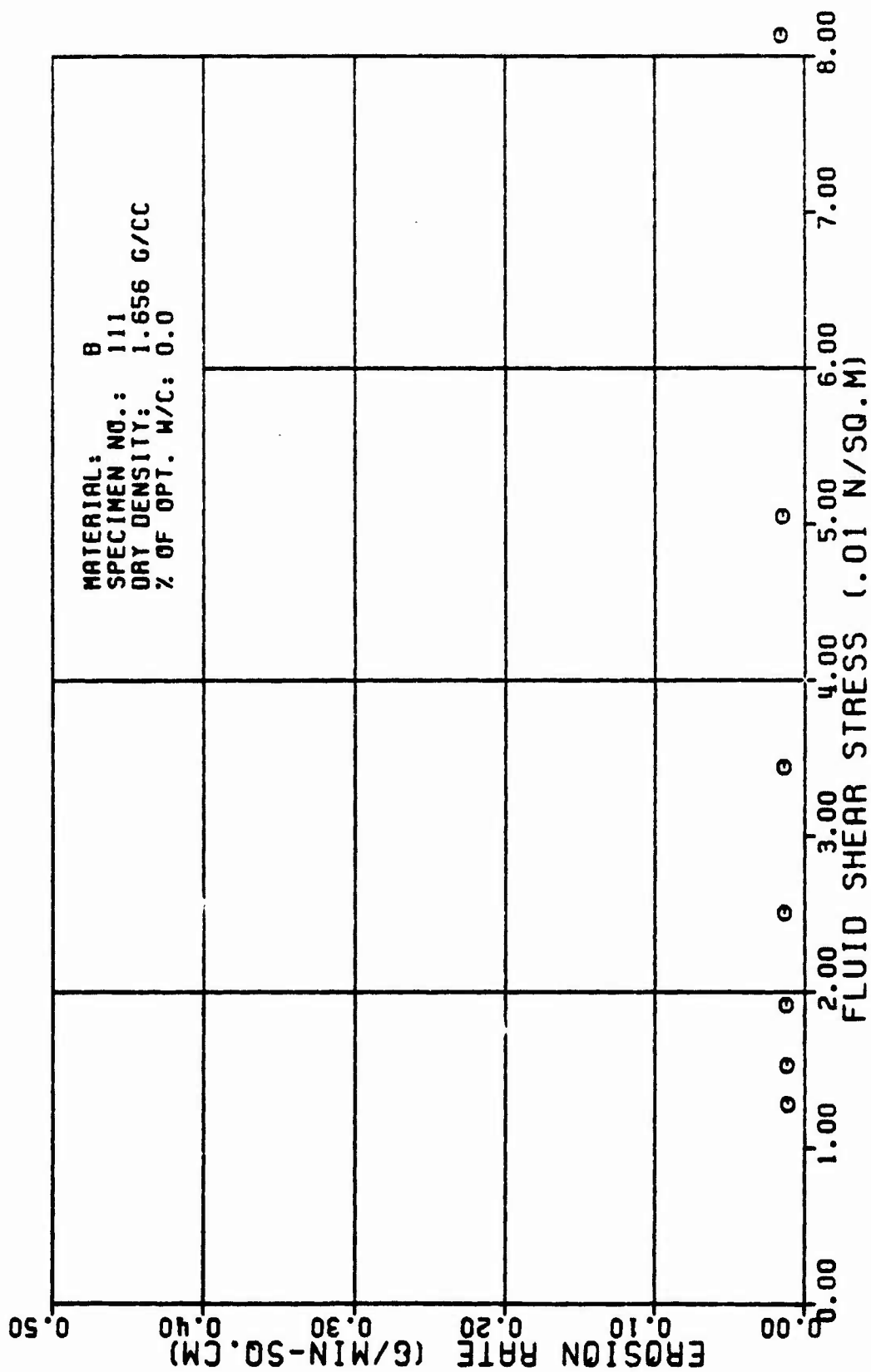


Figure A6e

TABLE A7

TEST RESULTS FOR TRIAXIAL EROSION TEST

MATERIAL TYPE: SPECIMEN NUMBER : TESTED BY:		D 112 R. L. SANCHEZ		AVERAGE FLOW RATE (Q): 474. CC/MIN					
DATE TESTED:		3 29 82		RATE OF WEIGHT EROSION (P): 2.7 G/MIN					
SPECIMEN DRY DENSITY:		1.009 G/CC		DENSITY OF ERODING FLUID: 1.000 G/CC					
% OF OPTIMUM WATER CONTENT:		-4.8 PERCENT		VISCOSITY OF ERODING FLUID: 0.001 N*SEC/SQ.M					
INITIAL SLOT WIDTH:		2.32 CM		CONFINING PRESSURE: 98.10 KN/SQ.M					
INITIAL SLOT THICKNESS:		0.23 CM		HEAD OF WATER: 1.3 M					
ERODED LENGTH:		11.05 CM		HYDRAULIC GRADIENT: 10 N/M					

VOLUME OF FLOW (1000 CC)	TIME (MIN)	CUM. WEIGHT ERODED (G)	CROSS SECTION AREA (SQ.CH)	VELOCITY OF FLOW (CM/MIN)	ERODED SURFACE AREA (SQ.CH)	CUM. WEIGHT ERODED PER AREA (G/SQ.CH)	EROSION RATE (GRAMS/ MIN * SQ.CH))	FLUID SHEAR STRESS (N/SQ.M)	REYNOLDS NUMBER
3.5	5.99	16.3	1.5	206.	69.	0.23	0.04	0.009	529.
7.0	13.73	26.4	2.5	100.	79.	0.33	0.03	0.025	464.
10.5	20.59	45.7	3.5	136.	89.	0.53	0.03	0.015	412.
14.0	27.99	55.8	4.6	103.	100.	0.55	0.03	0.010	367.
17.5	35.07	97.4	5.7	63.	111.	0.79	0.02	0.007	330.
19.5	40.05	107.0	5.4	74.	110.	0.91	0.02	0.006	310.

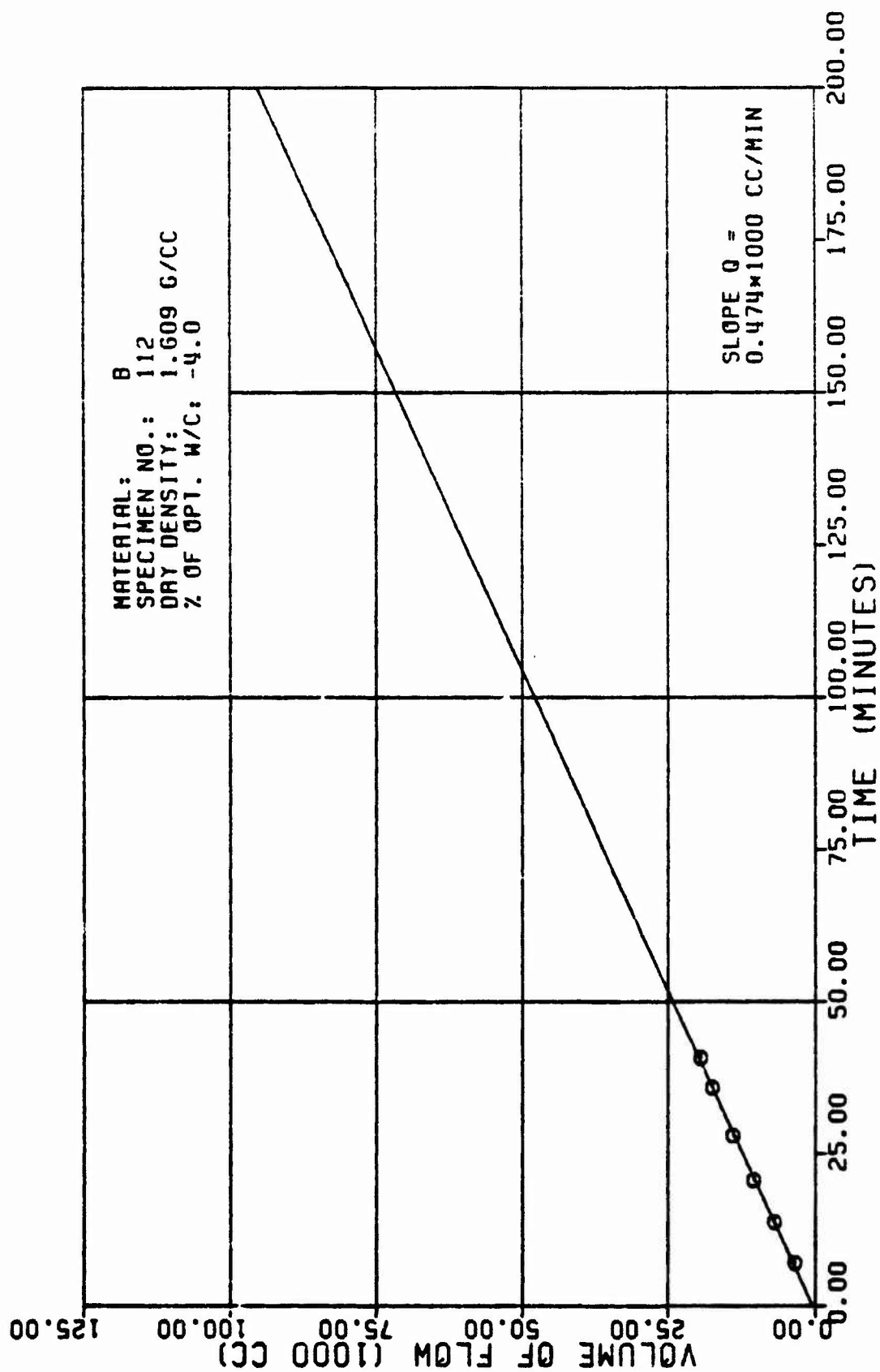


Figure A7a

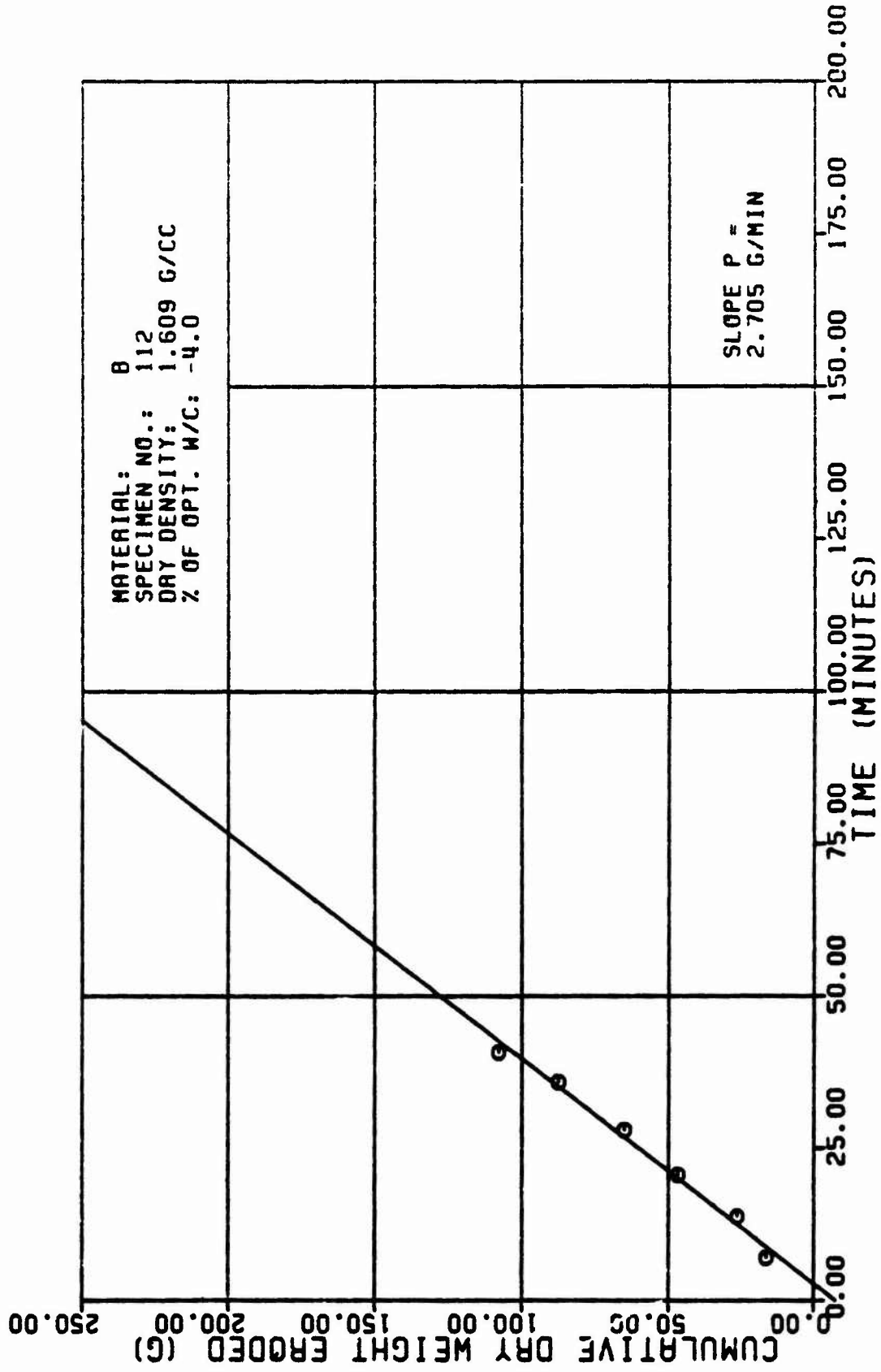


Figure A7b

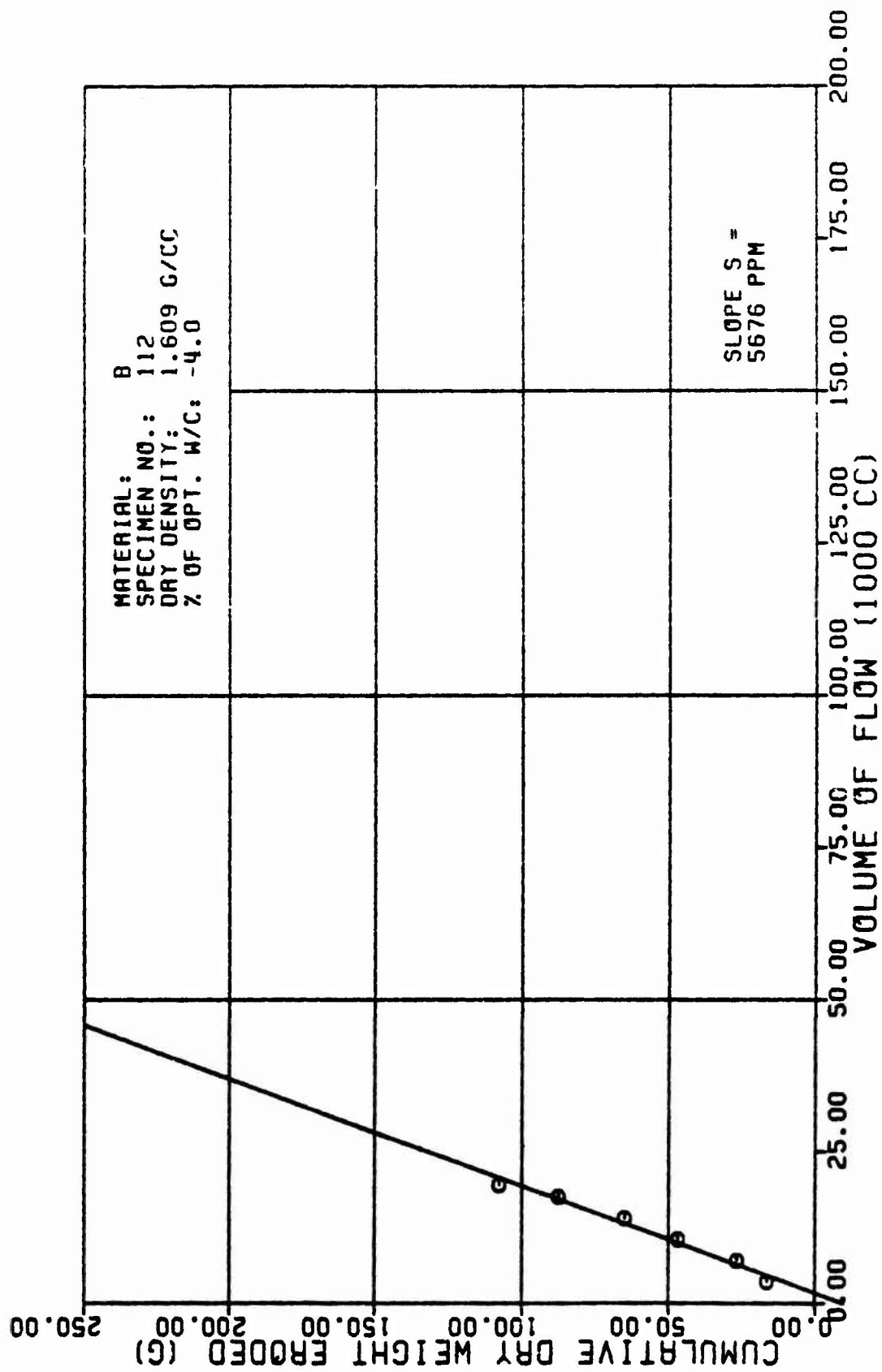


Figure A7c

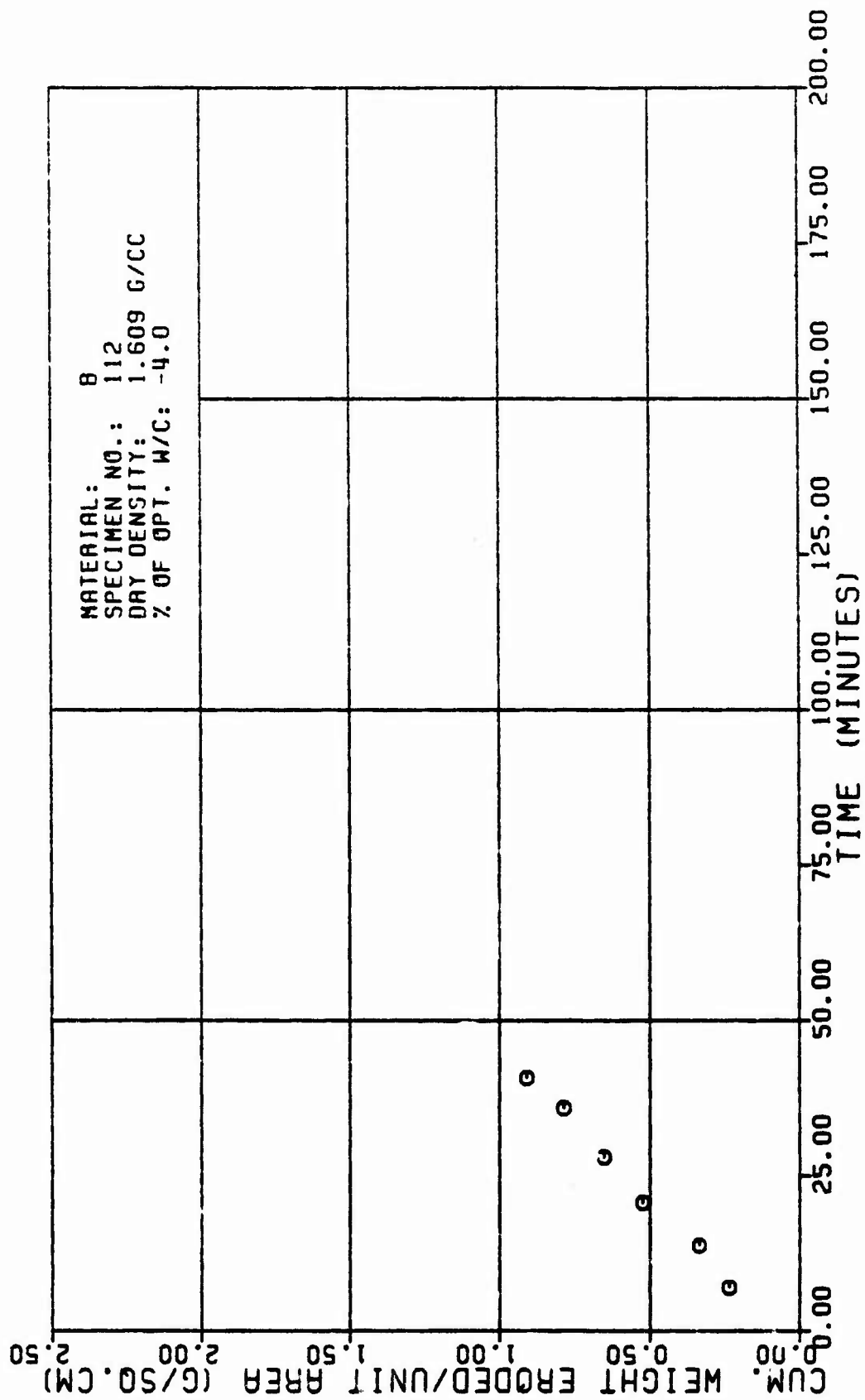


Figure A7d

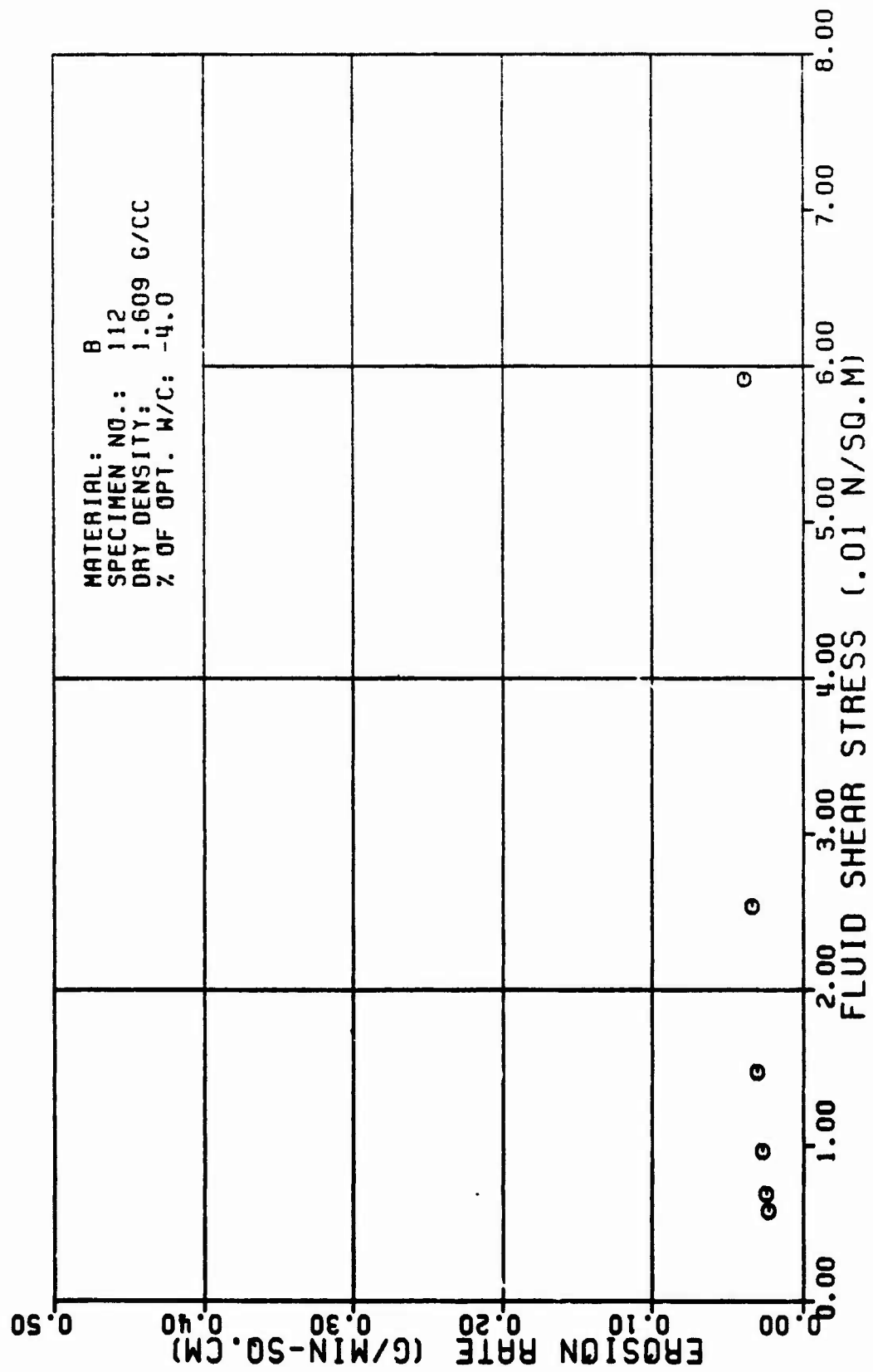


Figure A7e

TABLE A8

TEST RESULTS FOR TRIAXIAL EROSION TEST

MATERIAL TYPE: SPECIMEN NUMBER : TESTED BY:		B 113 R. L. SANCHEZ		AVERAGE FLOW RATE (Q): 644 CC/MIN					
DATE TESTED:		2-28-82		RATE OF WEIGHT EROSION (P): 2.5 G/MIN					
SPECIMEN DRY DENSITY:		1.646 G/CC		DENSITY OF ERODING FLUID: 1.000 G/CC					
% OF OPTIMUM WATER CONTENT:		-2.8 PERCENT		VISCOSITY OF ERODING FLUID: 0.001 N*SEC/CM.M					
INITIAL SLOT WIDTH:		2.32 CM		CONFINING PRESSURE: 98.10 KN/CM.M					
INITIAL SLOT THICKNESS:		0.23 CM		HEAD OF WATER: 1.30 M					
ERODED LENGTH:		11.60 CM		HYDRAULIC GRADIENT: 10% M/M					

VOLUME OF FLOW (1000 CC)	TIME (MIN)	CUM. WEIGHT ERODED (G.)	CROSS SECTION AREA (SQ.CM)	VELOCITY OF FLOW (CM/MIN)	ERODED SURFACE AREA (SQ.CM)	CUM. WEIGHT ERODED PER AREA (G/SQ.CM)	EROSION RATE (GRAMS/ (MIN/CM) SQ.CM)	FLUID SHEAR STRESS (N/CM.M)	REYNOLDS NUMBER
3.5	6:57	18.25	1.4	393.	60.1	0.23	0.003	0.003	619.
7.0	12:37	29.14	2.3	248.	76.1	0.30	0.003	0.003	548.
10.5	19:06	42.02	3.1	176.	85.1	0.56	0.003	0.003	494.
14.0	25:28	60.10	3.9	139.	93.0	0.65	0.003	0.003	451.
17.5	32:50	75.16	4.7	115.	101.1	0.79	0.003	0.003	415.

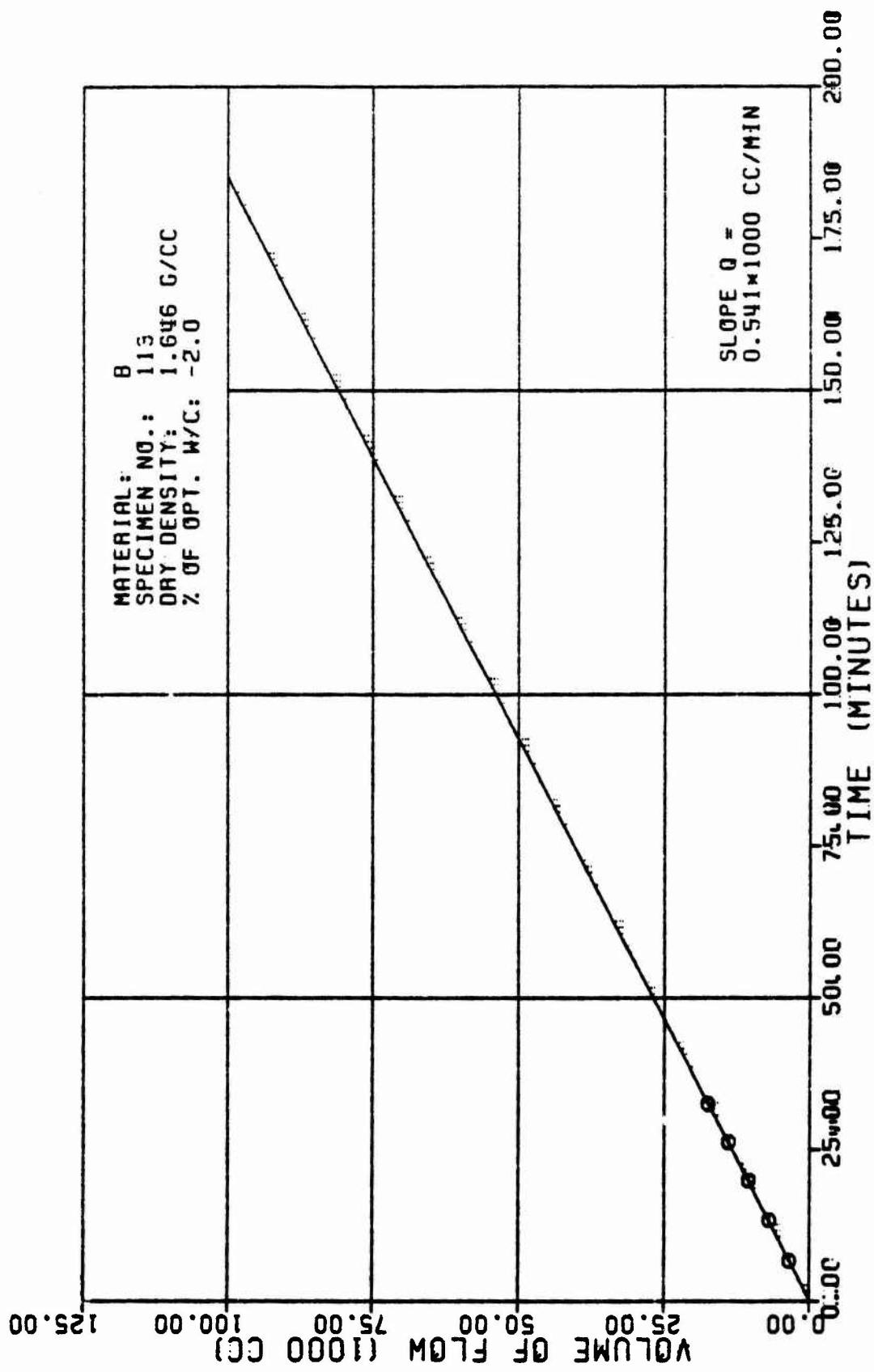


Figure A8a

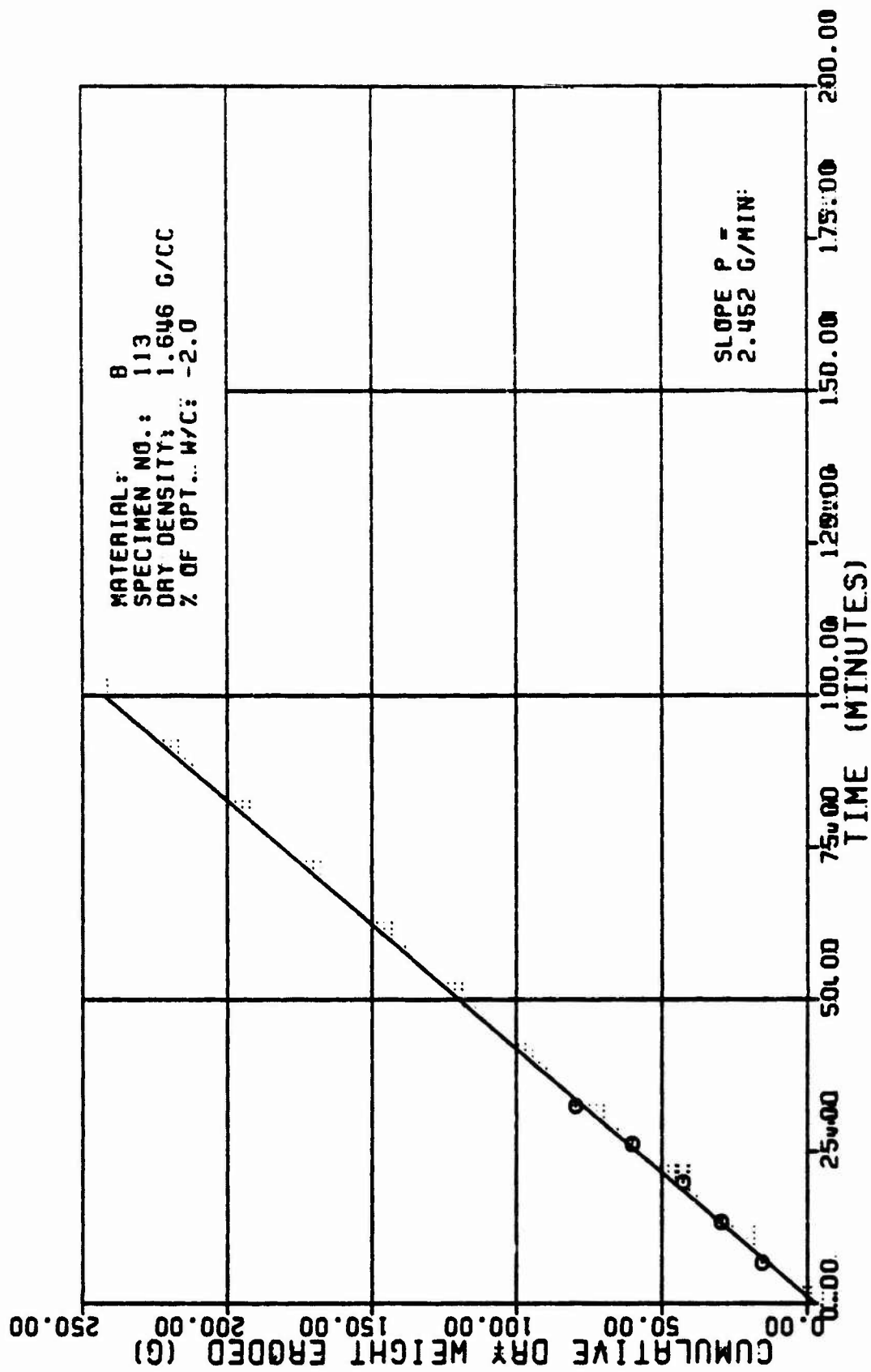


Figure A8b

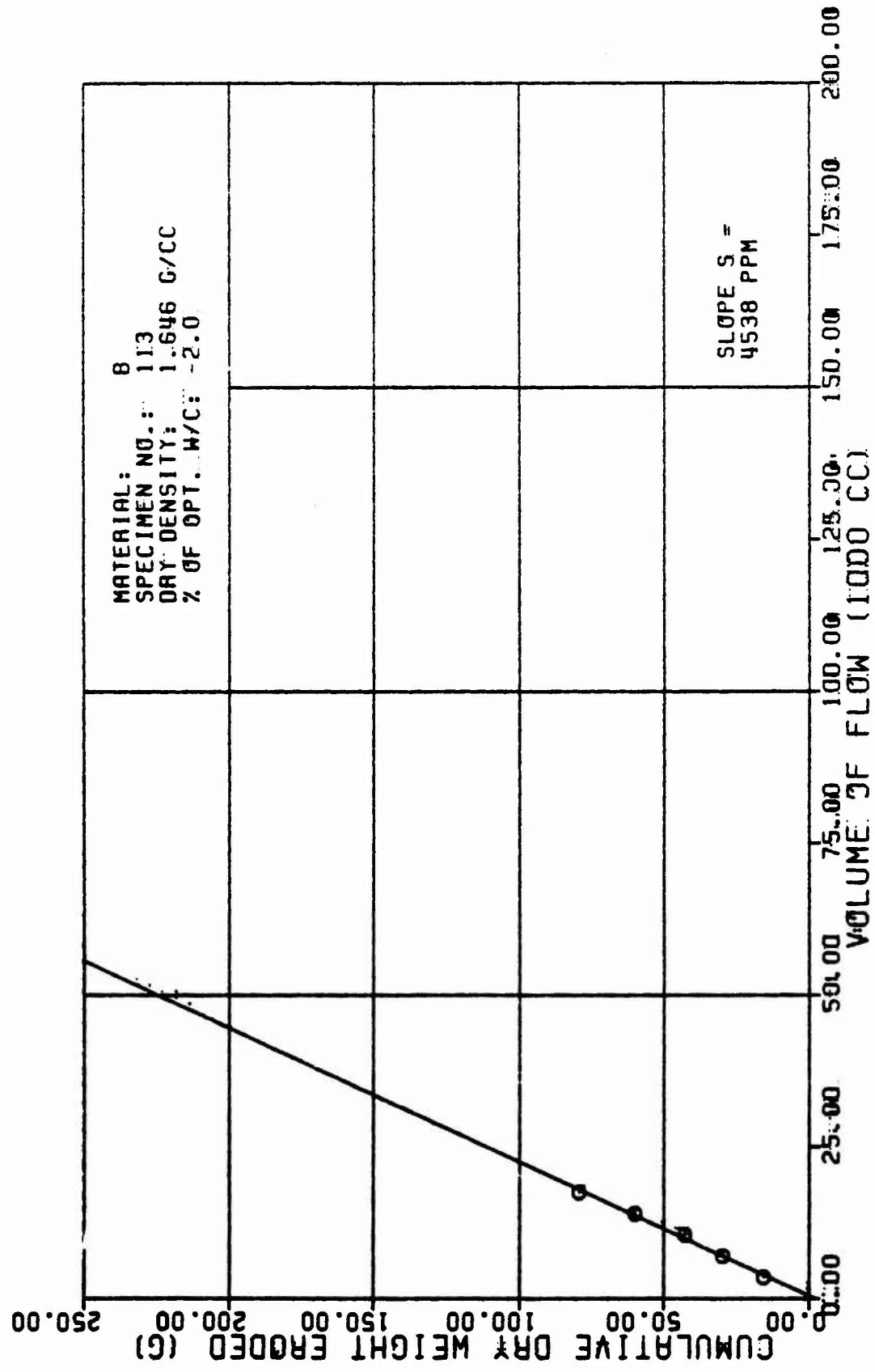


Figure A8c

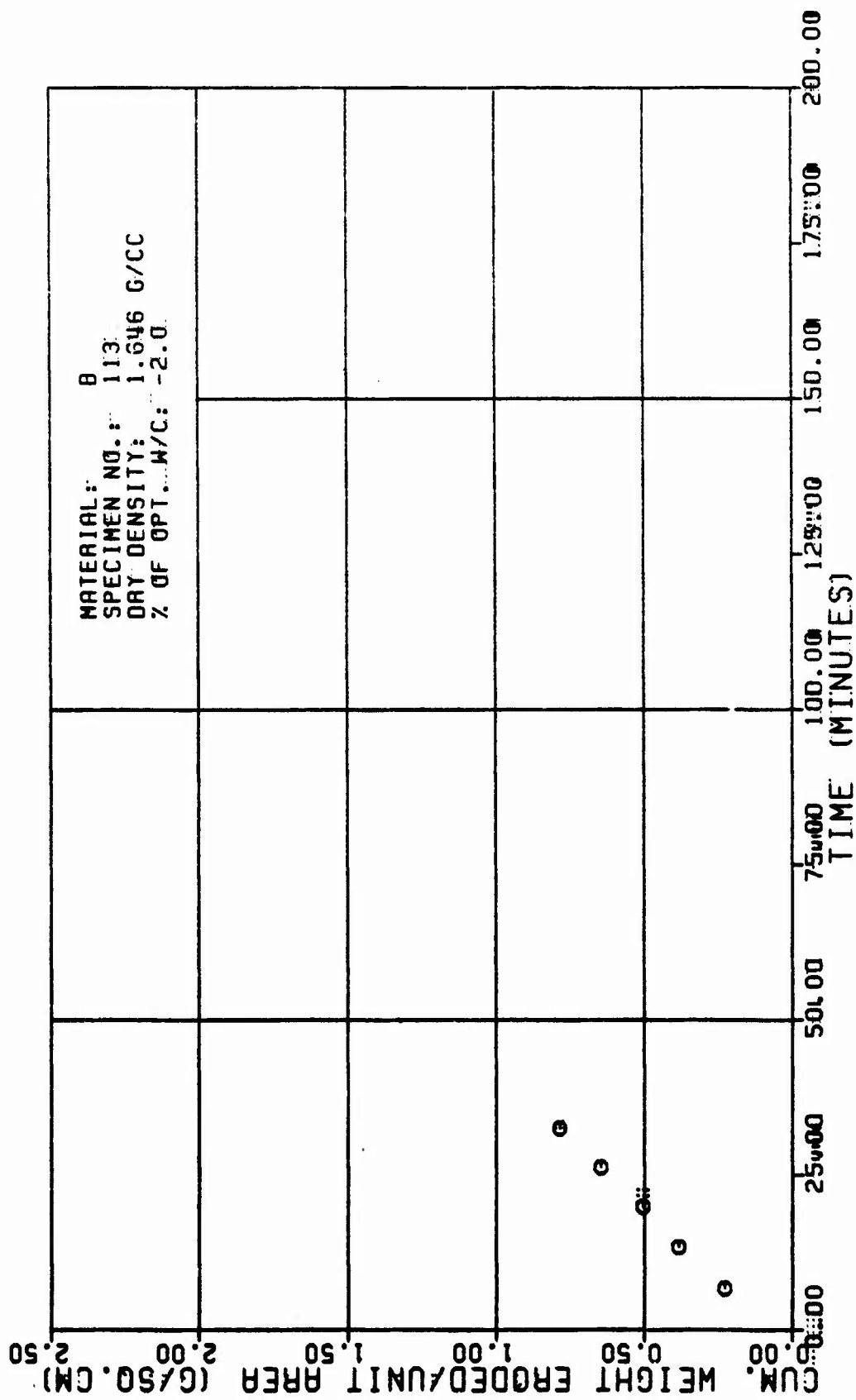


Figure A8d

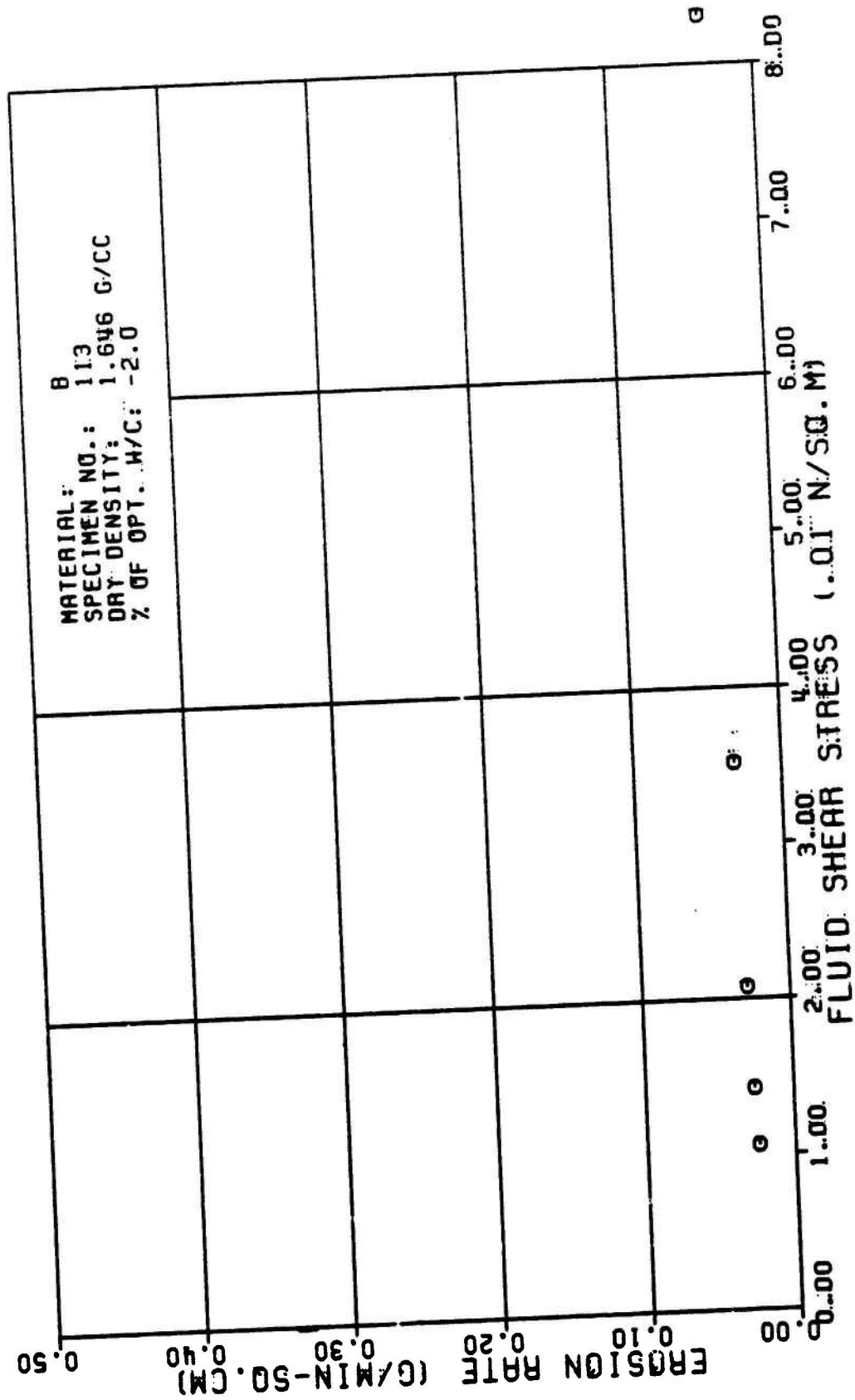


Figure A8e

TABLE A9

TEST RESULTS FOR TRIAXIAL EROSION TEST

MATERIAL TYPE: SPECIMEN NUMBER : TESTED BY:		B 114 R. L. SANCHEZ		AVERAGE FLOW RATE (Q):		448. CC/MIN			
DATE TESTED:		3 21 82		RATE OF WEIGHT EROSION (P):		8.8 G/MIN			
SPECIMEN DRY DENSITY:		1.782 G/CC		DENSITY OF ERODING FLUID:		1.888 G/CC			
% OF OPTIMUM WATER CONTENT:		8.8 PERCENT		VISCOSITY OF ERODING FLUID:		8.881 M*SEC/SQ.M			
INITIAL SLOT WIDTH:		2.32 CM		CONFINING PRESSURE:		98.18 KN/SQ.M			
INITIAL SLOT THICKNESS:		8.23 CM		HEAD OF WATER:		1.3 88 M			
ERODED LENGTH:		11.88 CM		HYDRAULIC GRADIENT:		18. M/M			

VOLUME OF FLOW (1000 CC)	TIME (MIN)	CUM. WEIGHT ERODED (G)	CROSS SECTION AREA (SQ.CM)	VELOCITY OF FLOW (CM/MIN)	ERODED SURFACE AREA (SQ.CM)	CUM. WEIGHT ERODED PER AREA (G/SQ.CM)	EROSION RATE (GRAMS/ (MIN * SQ.CM))	FLUID SHEAR STRESS (N/SQ.M)	REYNOLDS NUMBER
3.8	7.18	4.1	8.8	535.	63.	8.86	8.81	8.174	549.
7.8	14.21	9.8	1.1	398.	66.	8.14	8.81	8.181	525.
18.8	21.82	16.4	1.4	314.	69.	8.24	8.81	8.866	582.
14.8	29.18	23.6	1.7	288.	72.	8.33	8.81	8.846	488.
17.8	36.82	29.8	2.8	218.	78.	8.38	8.81	8.834	468.
21.8	44.88	34.6	2.3	189.	78.	8.44	8.81	8.827	441.
24.8	52.64	48.1	2.7	166.	82.	8.49	8.81	8.822	424.
28.8	61.14	47.8	3.8	147.	85.	8.55	8.81	8.818	486.
31.8	69.68	84.2	3.3	132.	89.	8.61	8.81	8.815	398.

TABLE FOR SPECIMEN NUMBER: B114 (CONTINUES)

VOLUME OF FLOW (1000 CC)	TIME (MIN)	CUM. WEIGHT ERODED (G)	CROSS SECTION AREA (SQ. CM)	VELOCITY OF FLOW (CM/MIN)	ERODED SURFACE AREA (SQ. CM)	CUM. WEIGHT ERODED PER AREA (G/SQ. CM)	EROSION RATE (GRAMS/ MIN " " SQ. CM)	FLUID SHEAR STRESS (N/SQ. CM)	REYNOLDS NUMBER
35.5	70.23	51.0	3.7	119.	92.	5.67	5.51	5.513	375.
36.3	95.02	66.1	3.0	116.	93.	5.75	5.51	5.512	371.

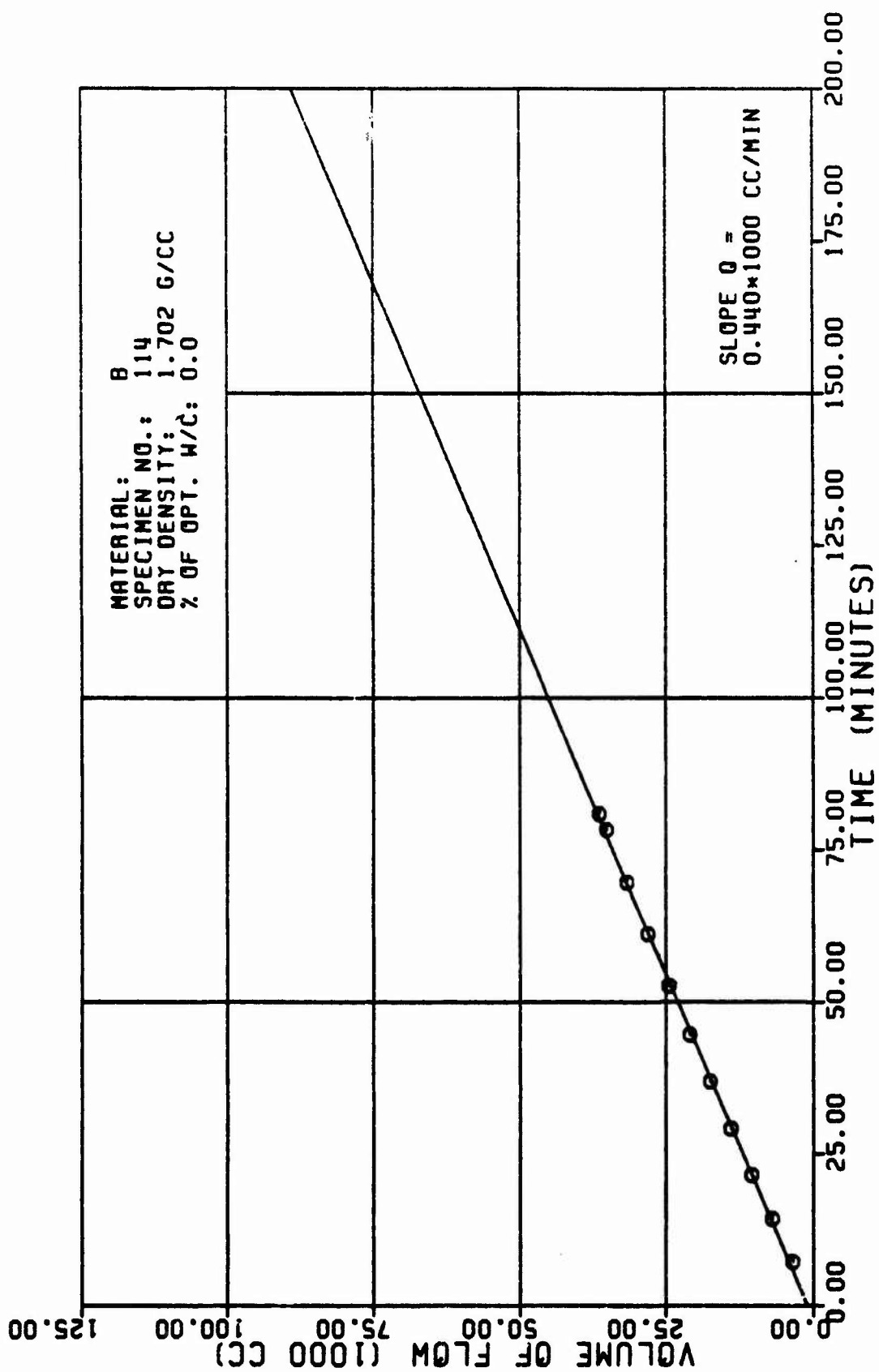


Figure A9a

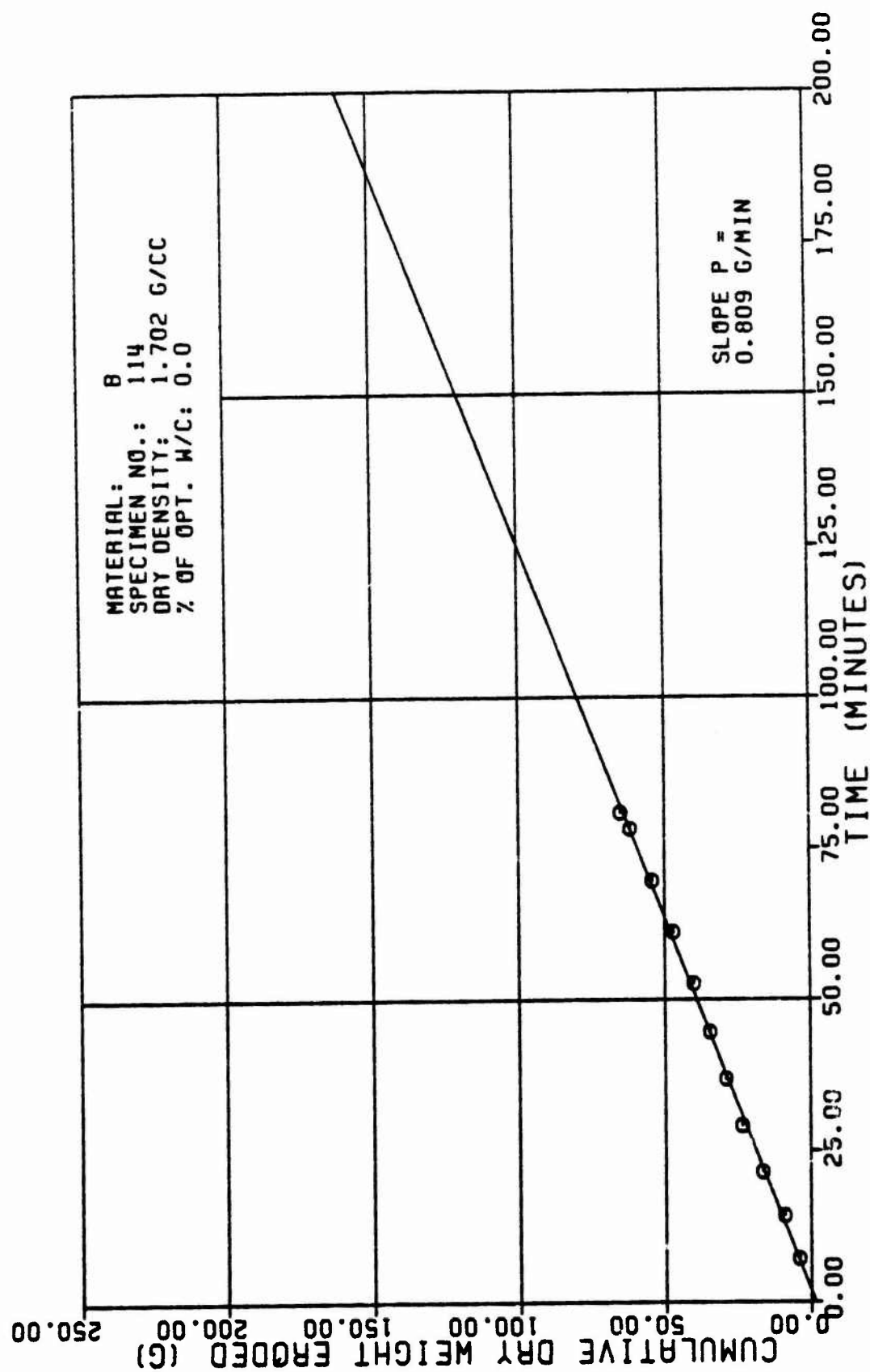


Figure A9b

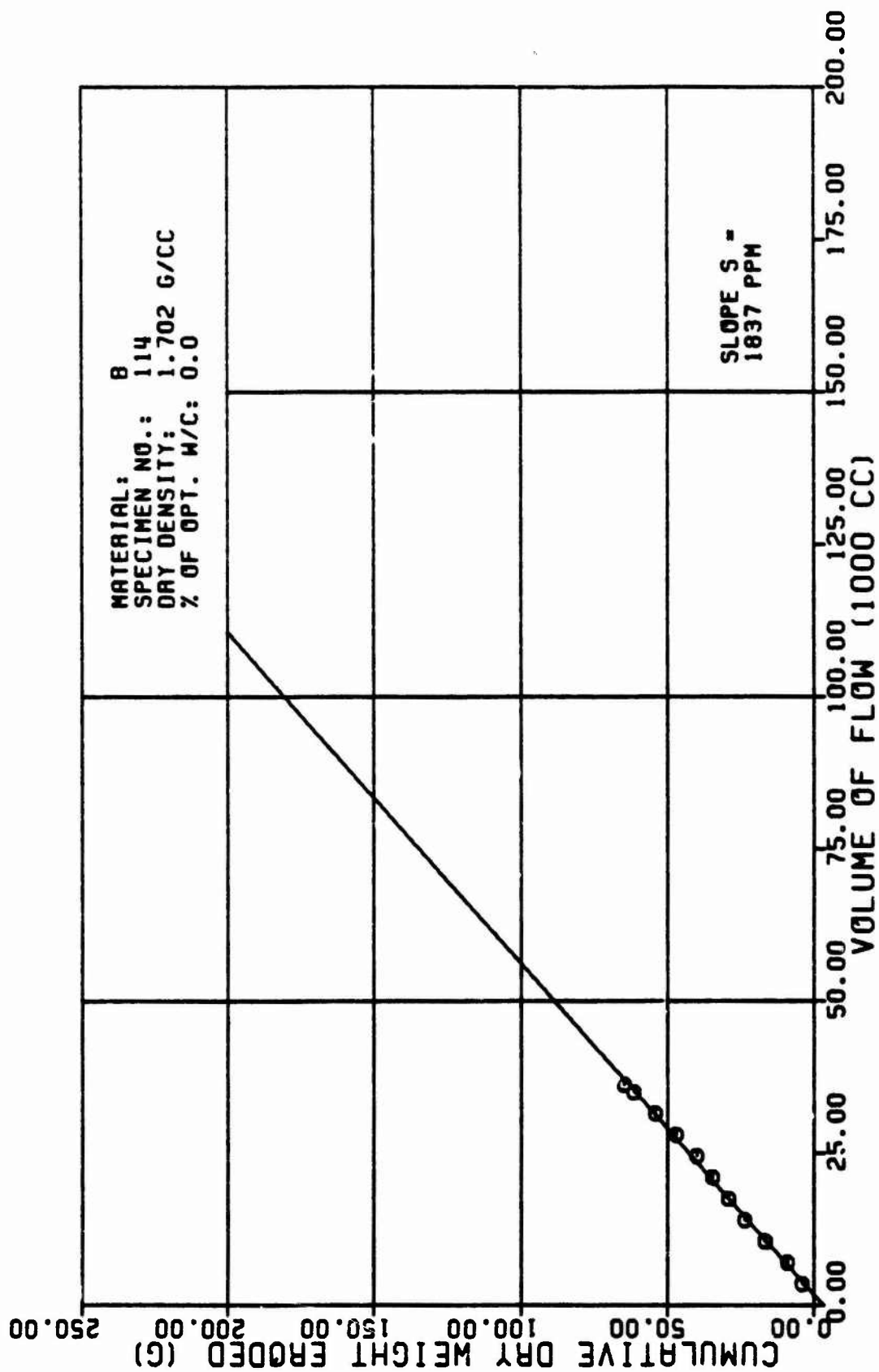


Figure A9c

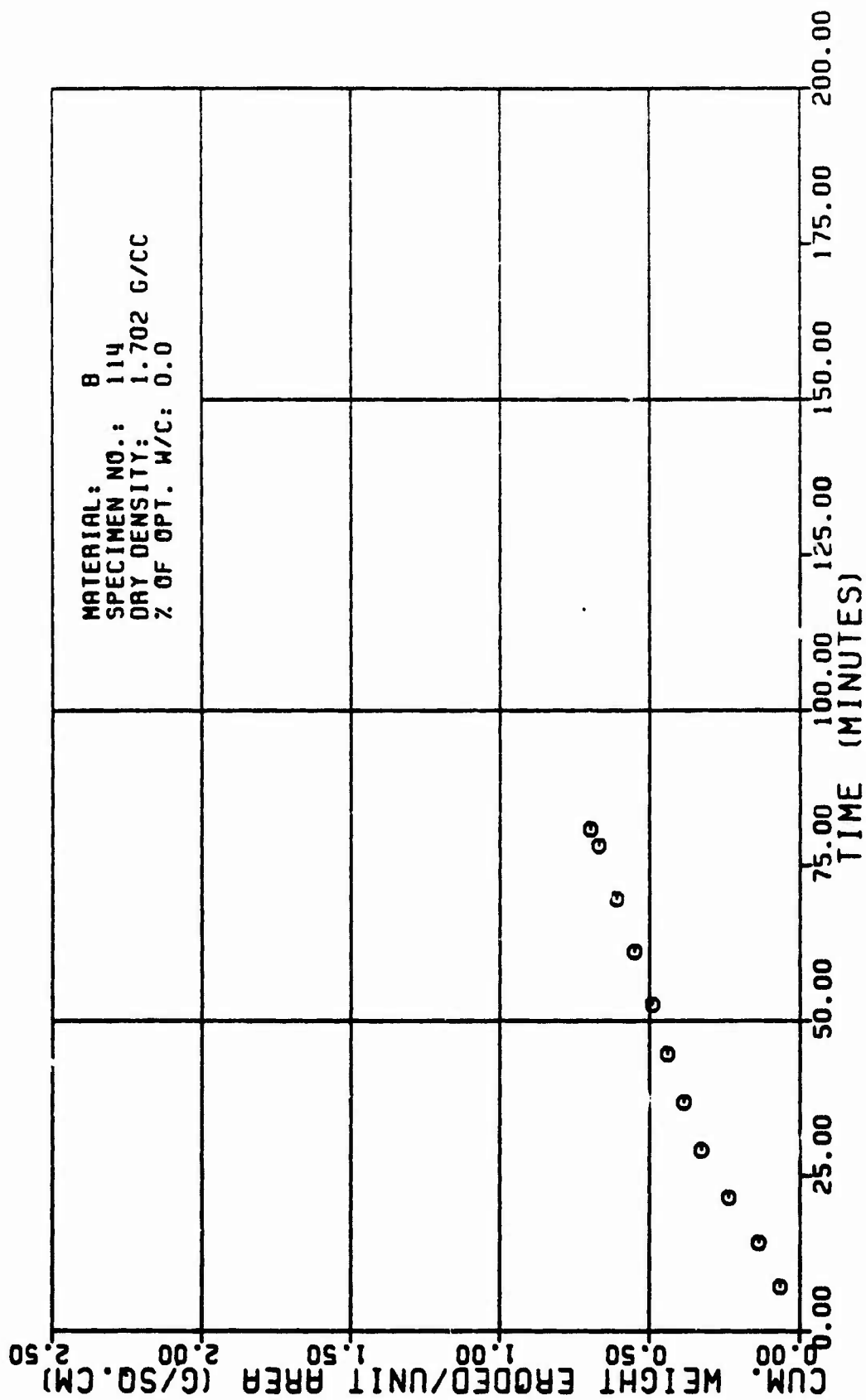


Figure A9d

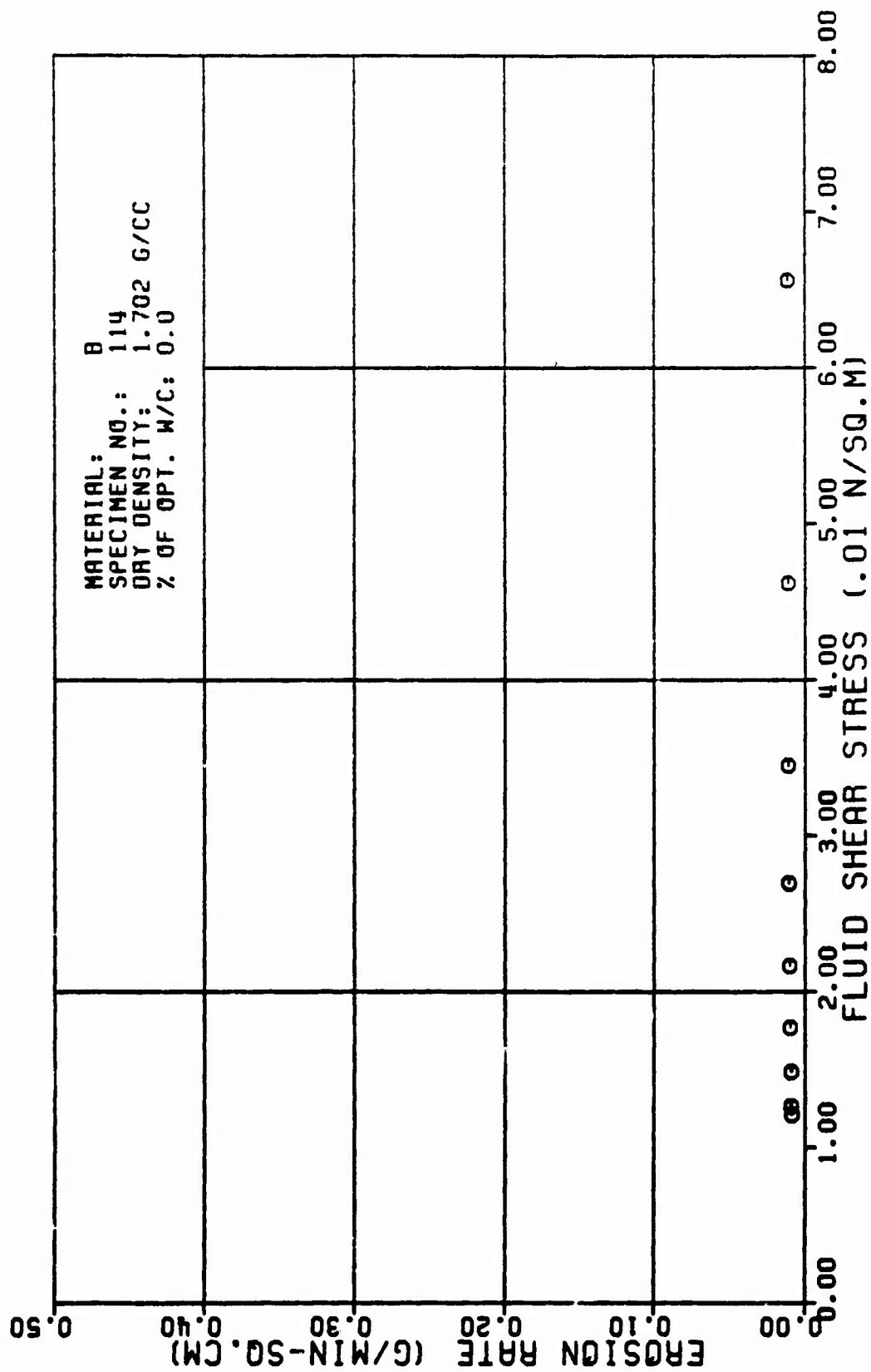


Figure A9e

TABLE A10

TEST RESULTS FOR TRIAXIAL EROSION TEST

MATERIAL TYPE: SPECIMEN NUMBER :		B 116		AVERAGE FLOW RATE (Q):		485. CC/MIN			
TESTED BY:		R. L. SANCHEZ		RATE OF WEIGHT EROSION (P):		1.2 G/MIN			
DATE TESTED:		3 29 82		DENSITY OF ERODING FLUID:		1.888 G/CC			
SPECIMEN DRY DENSITY:		1.617 G/CC		VISCOSITY OF ERODING FLUID:		9.991 M*SEC/SQ.M			
% OF OPTIMUM WATER CONTENT:		4.8 PERCENT		CONFINING PRESSURE:		98.15 KN/SQ.M			
INITIAL SLOT WIDTH:		2.32 CM		HEAD OF WATER:		13.88 M			
INITIAL SLOT THICKNESS:		8.23 CM		HYDRAULIC GRADIENT:		18. M/M			
ERODED LENGTH:		11.68 CM							
VOLUME OF FLOW (1000 CC)	TIME (MIN)	CUM. WEIGHT ERODED (G)	CROSS SECTION AREA (SQ.CM)	VELOCITY OF FLOW (CM/MIN)	ERODED SURFACE AREA (SQ.CM)	CUM. WEIGHT ERODED PER AREA (G/SQ.CM)	EROSION RATE (GRAMS/ MIN * SQ.CM)	FLUID SHEAR STRESS (N/SQ.M)	REYNOLDS NUMBER
3.5	6.86	7.1	8.9	534.	53.	8.11	8.82	8.168	597.
7.8	12.84	14.4	1.3	308.	67.	8.22	8.82	8.895	564.
15.5	19.19	23.8	1.7	293.	78.	8.33	8.82	8.854	533.
14.8	25.14	32.3	2.1	232.	76.	8.43	8.82	8.836	583.
17.5	31.94	41.0	2.5	193.	79.	8.53	8.81	8.826	476.
21.8	39.88	49.3	2.9	165.	83.	8.89	8.81	8.828	451.
22.5	45.43	58.9	3.4	143.	88.	8.80	8.81	8.816	427.

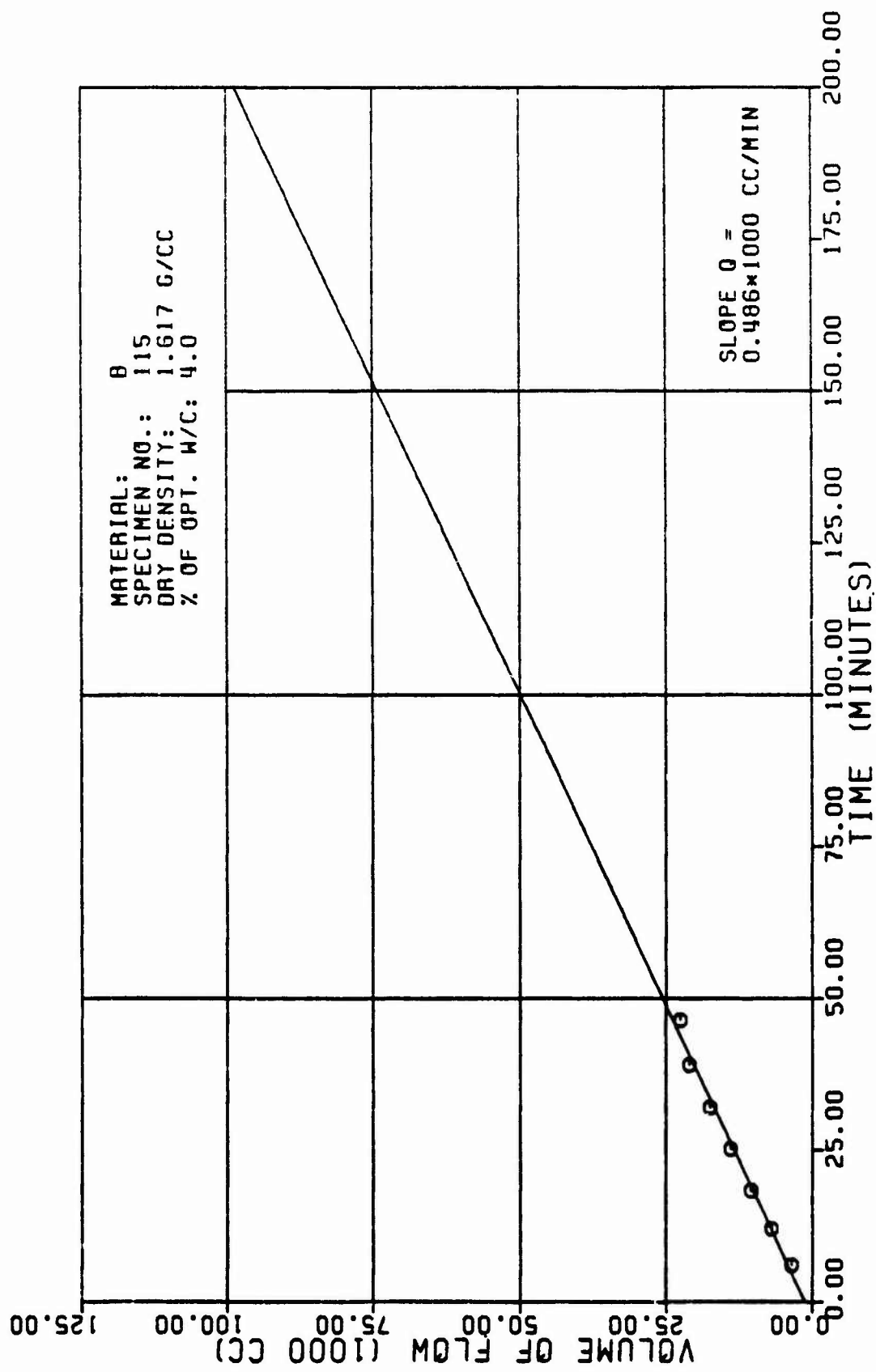


Figure A10a

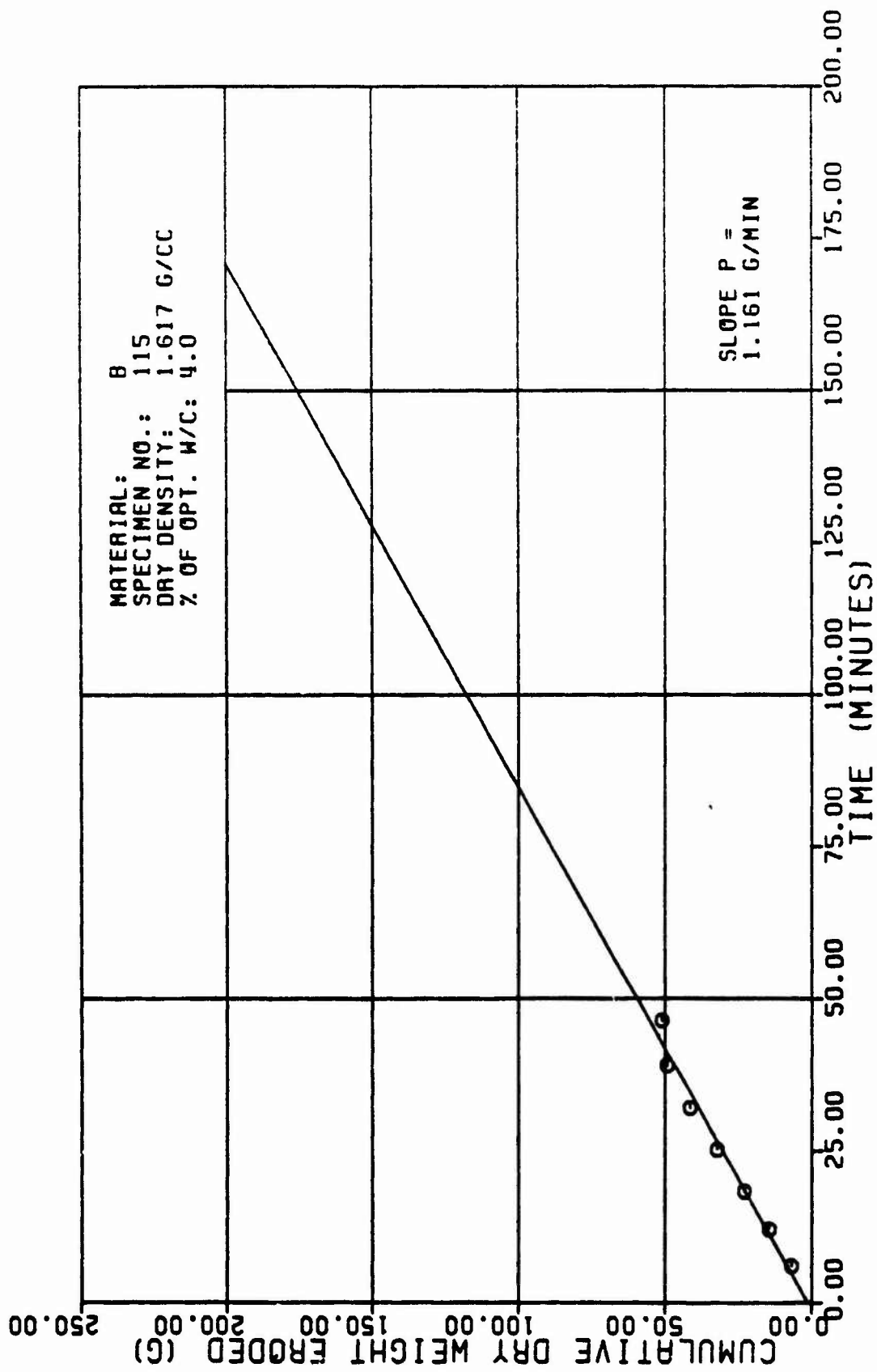


Figure A10b

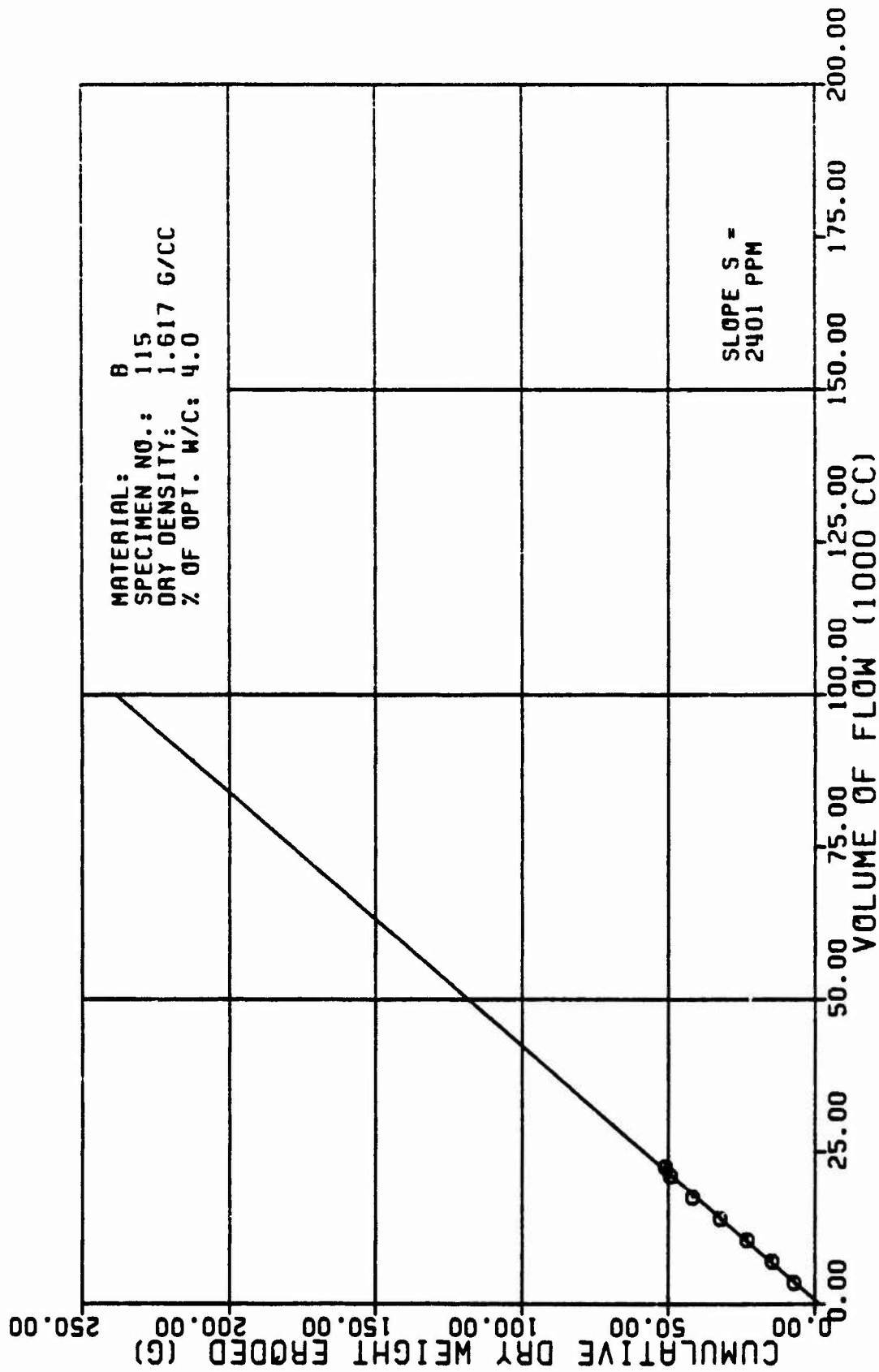


Figure A10c

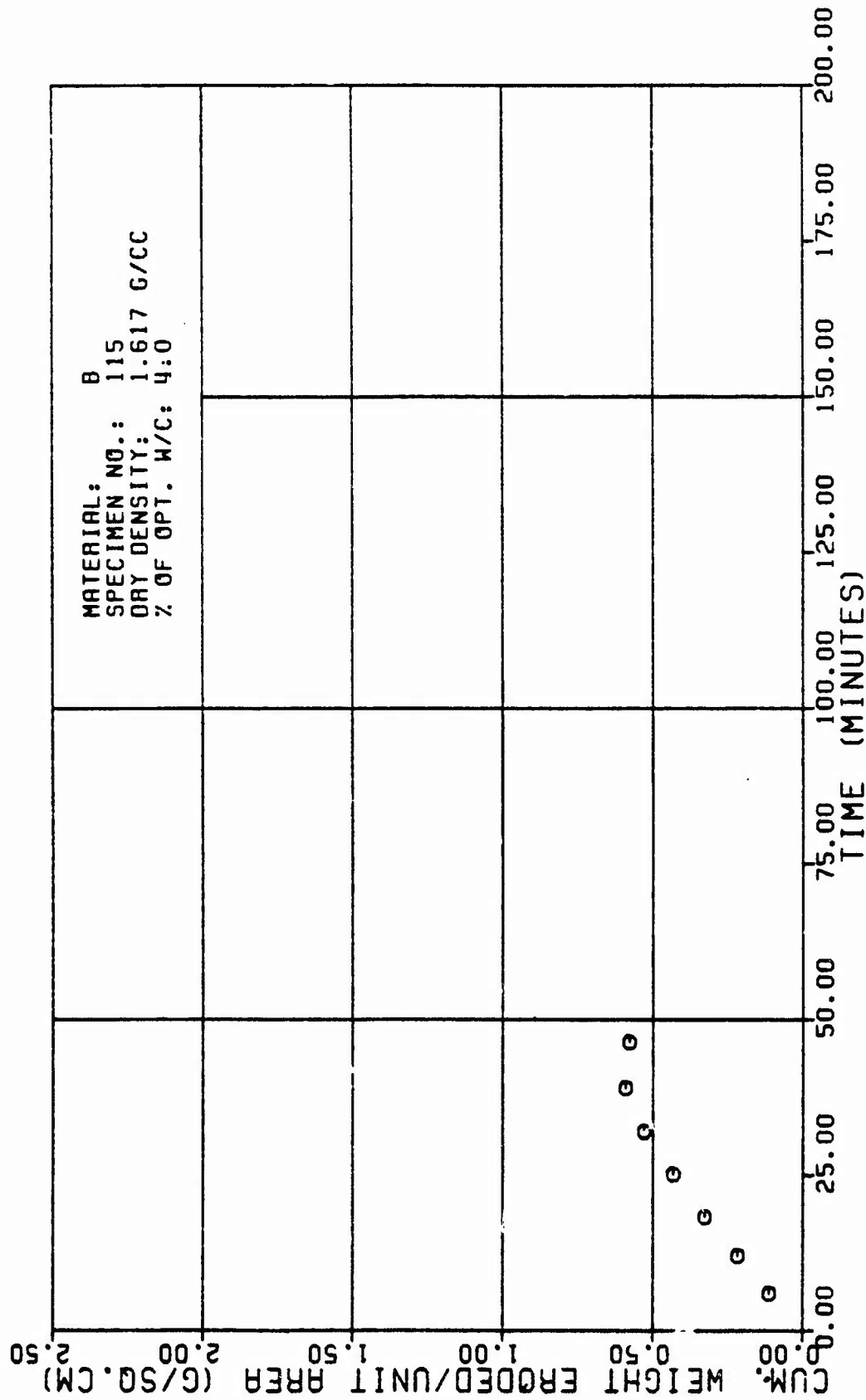


Figure A10d

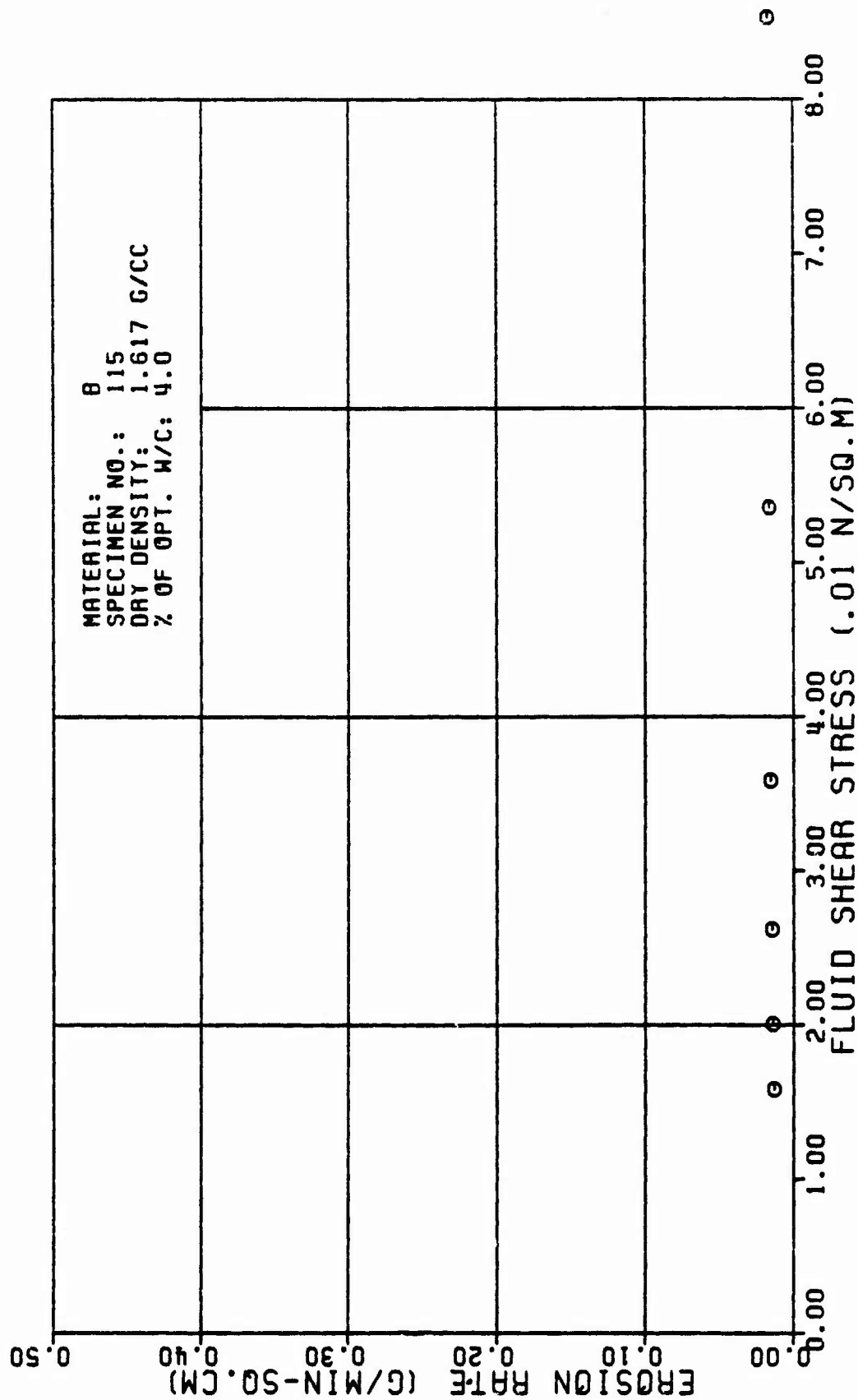


Figure A10e

TABLE A11

TEST RESULTS FOR TRIAXIAL EROSION TEST

MATERIAL TYPE: SPECIMEN NUMBER : TESTED BY:		B 117 R. L. SANCHEZ		AVERAGE FLOW RATE (Q): RATE OF WEIGHT EROSION (P):		515. CC/MIN 1.2 G/HIN			
DATE TESTED:		3 26 82		DENSITY OF ERODING FLUID: VISCOSITY OF ERODING FLUID:		1.000 G/CC 0.091 N*SEC/SQ.M			
SPECIMEN DRY DENSITY:		1.645 G/CC		CONFINING PRESSURE:		90.00 KH/SQ.M			
% OF OPTIMUM WATER CONTENT:		3.0 PERCENT		HEAD OF WATER:		1.30 M			
INITIAL SLOT WIDTH:		0.32 CM		HYDRAULIC GRADIENT:		10. H/M			
INITIAL SLOT THICKNESS:		0.23 CM							
ERODED LENGTH:		11.50 CM							
ERODED SHAPE:		CONSTANT WIDTH RECTANGLE							

VOLUME OF FLOW (1000 CC)	TIME (MIN)	CUM. WEIGHT ERODED (G)	CROSS SECTION AREA (SQ.CH)	VELOCITY OF FLOW (CM/HIN)	ERODED SURFACE AREA (SQ.CH)	CUM. WEIGHT ERODED PER AREA (G/SQ.CH)	EROSION RATE (GRAMS/ (MIN * SQ.CH))	FLUID SHEAR STRESS (N/SQ.M)	REYNOLDS NUMBER
3.5	6.51	7.2	0.5	1000.	42.	0.17	0.03	0.401	934.
7.0	12.43	12.2	0.9	598.	69.	0.10	0.02	0.209	570.
10.5	19.72	20.7	1.3	390.	102.	0.20	0.01	0.131	306.
14.0	25.00	29.4	1.7	302.	130.	0.23	0.01	0.100	304.
15.0	27.70	32.3	1.0	202.	139.	0.23	0.01	0.093	285.
16.0	30.10	35.1	2.0	250.	151.	0.23	0.01	0.005	261.
17.0	33.10	37.5	2.2	237.	163.	0.23	0.01	0.070	242.

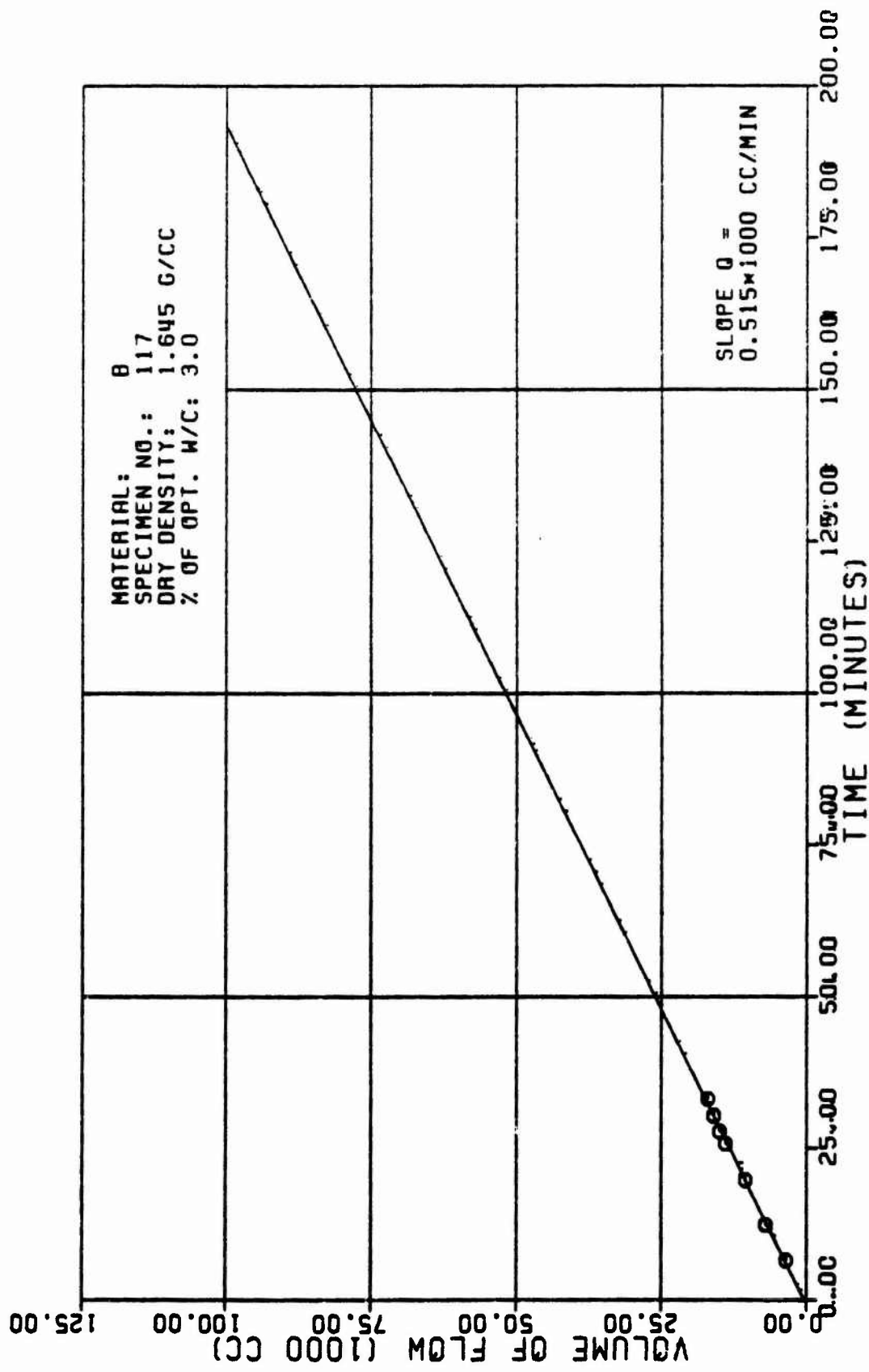


Figure Alla

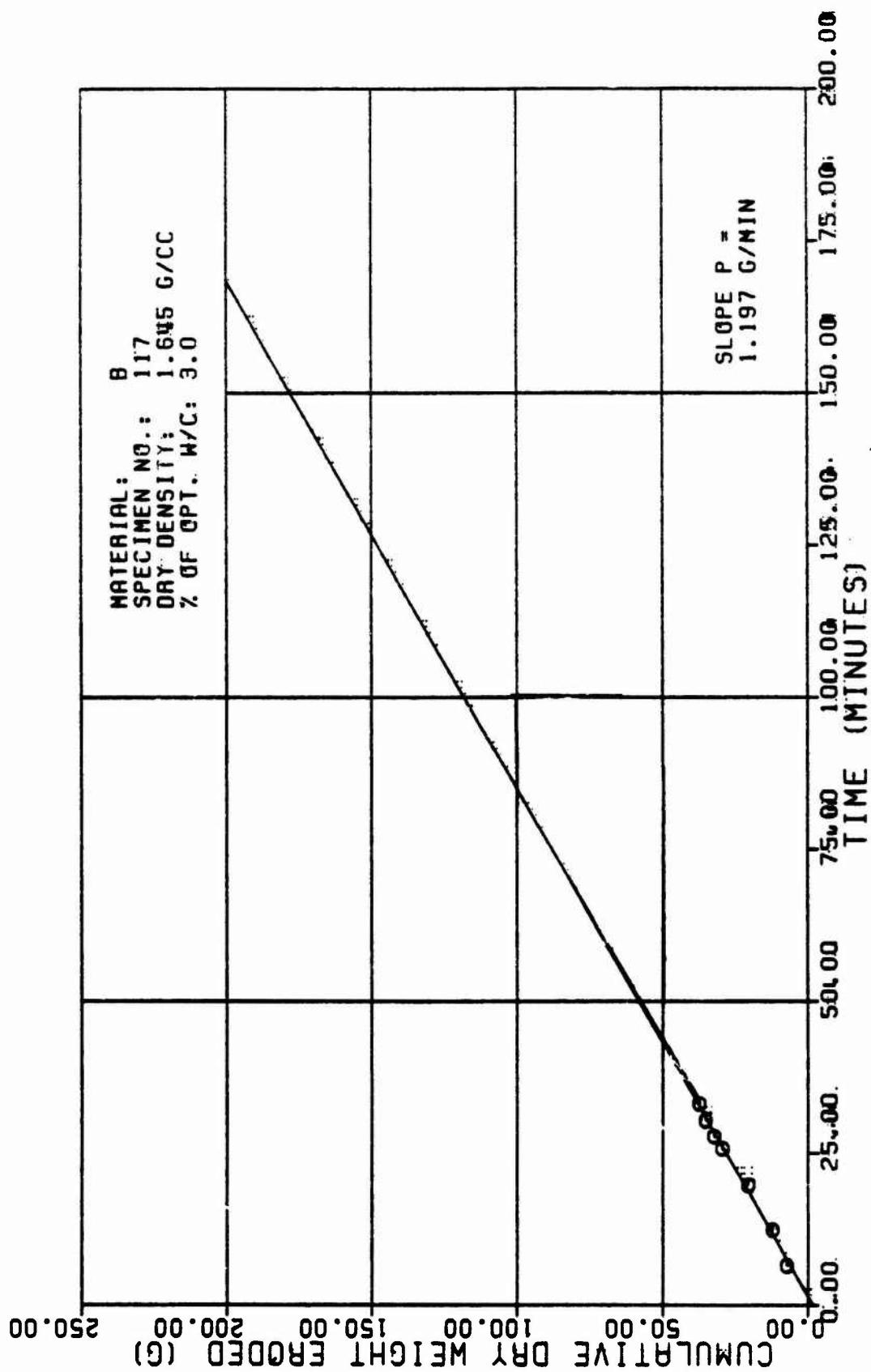


Figure A11b

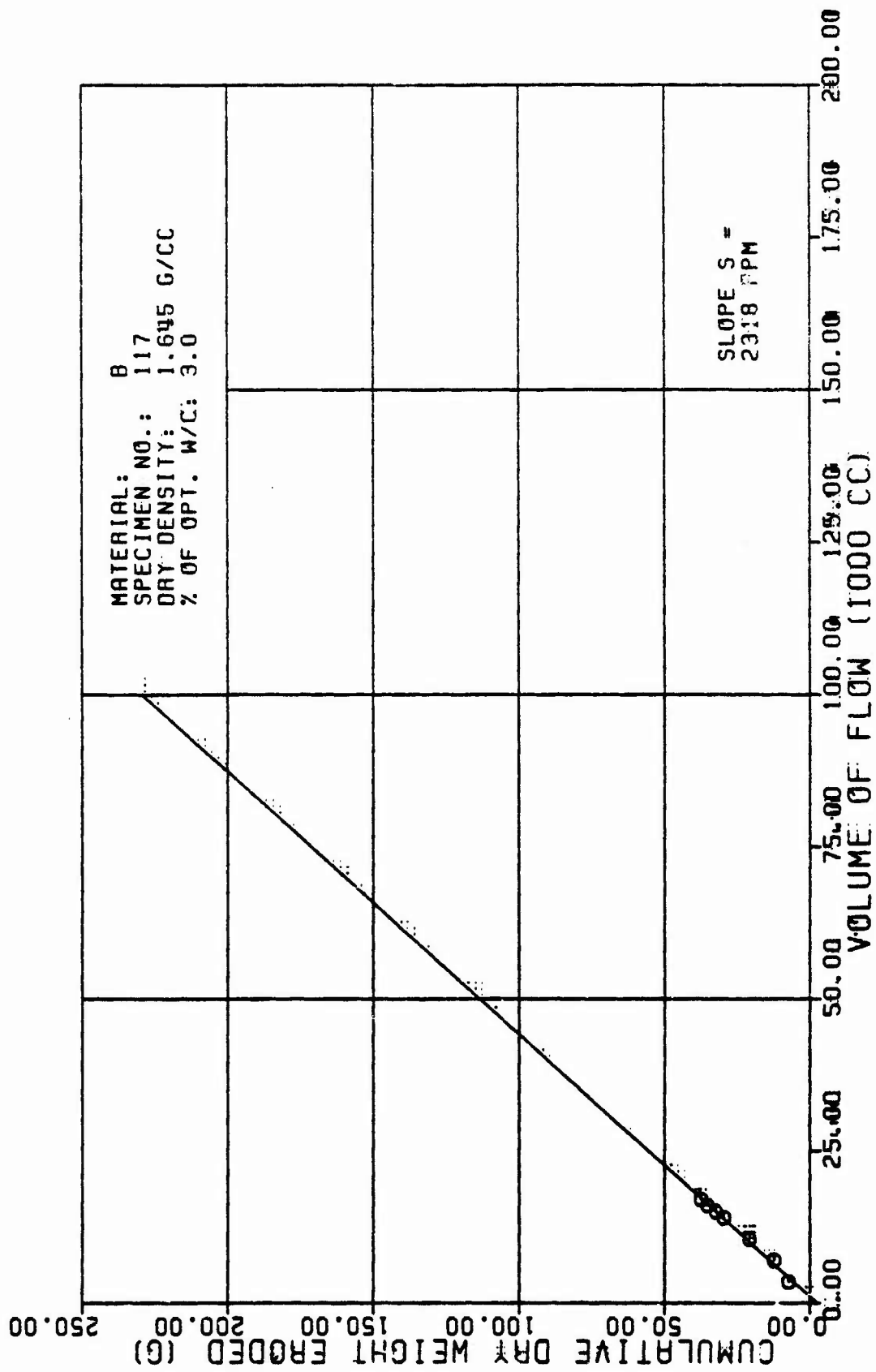


Figure Allc

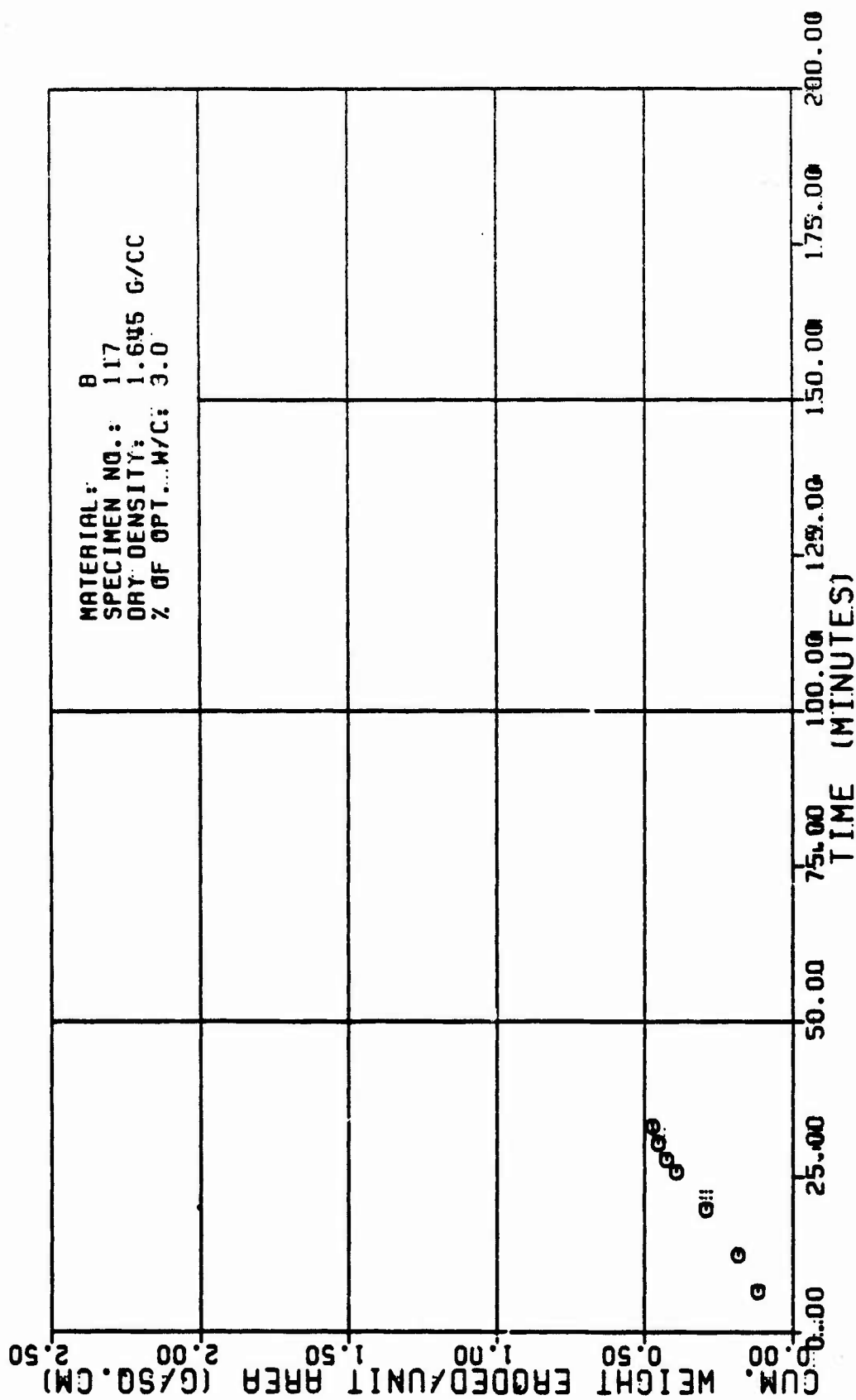


Figure A11d

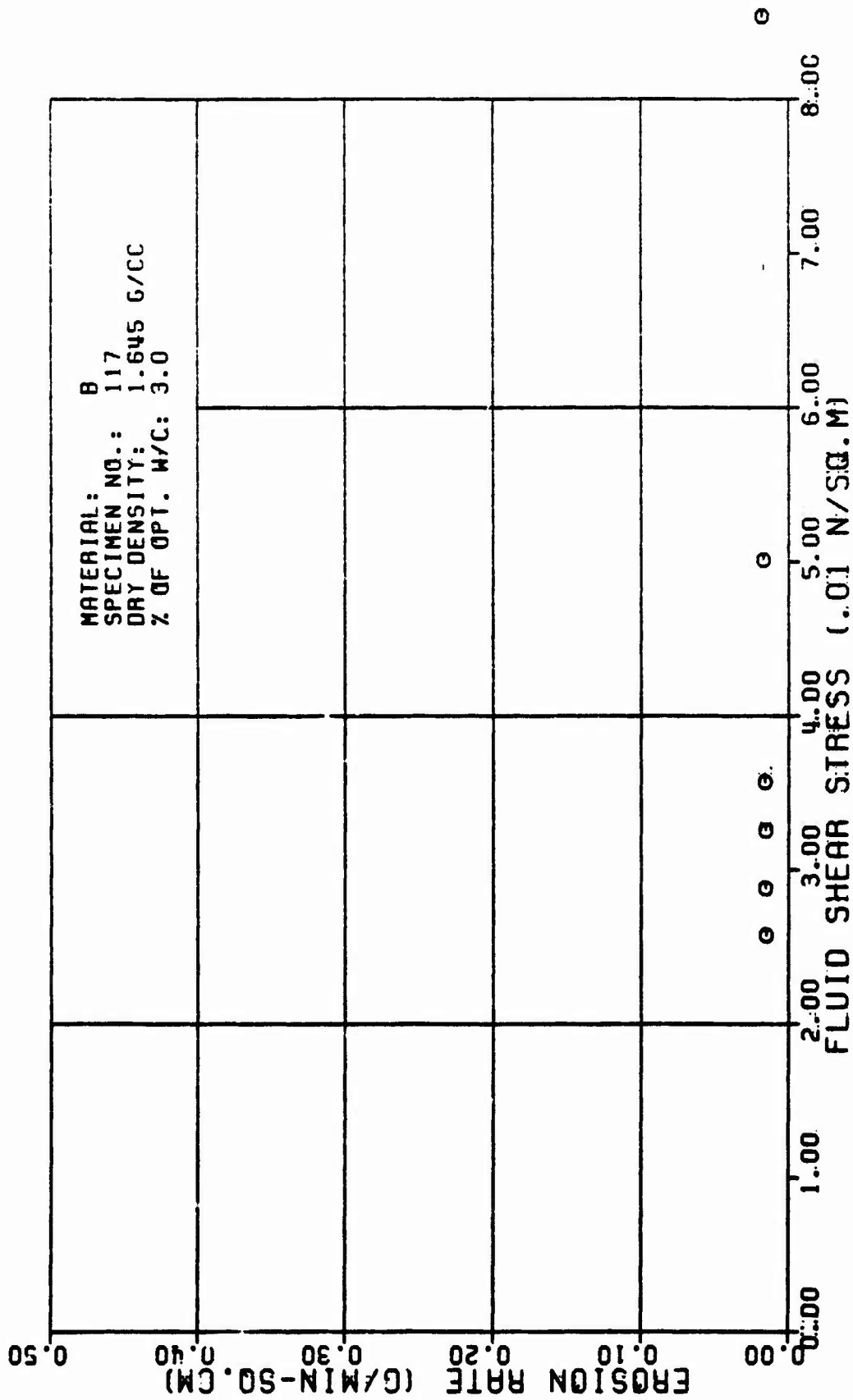


Figure A11e

TABLE A12

TEST RESULTS FOR TRIAXIAL EROSION TEST

MATERIAL TYPE: SPECIMEN NUMBER : TESTED BY:		8 119 R. L. SANCHEZ		AVERAGE FLOW RATE (Q): RATE OF WEIGHT EROSION (P):		519. CC/MIN 1.1 G/MIN			
DATE TESTED:		4 8 82		DENSITY OF ERODING FLUID: VISCOSITY OF ERODING FLUID:		1.000 G/CC 0.001 M*SEC/SQ.M			
SPECIMEN DRY DENSITY:		1.641 G/CC		CONFINING PRESSURE:		98.10 KN/SQ.M			
X OF OPTIMUM WATER CONTENT:		3.8 PERCENT		HEAD OF WATER:		13.00 M			
INITIAL SLOT WIDTH:		2.32 CM		HYDRAULIC GRADIENT:		10. M/M			
INITIAL SLOT THICKNESS:		0.23 CM							
ERODED LENGTH:		11.60 CM							

VOLUME OF FLOW (1000 CC)	TIME (MIN)	CUM. WEIGHT ERODED (G)	CROSS SECTION AREA (SQ.CM)	VELOCITY OF FLOW (CM/MIN)	ERODED SURFACE AREA (SQ.CM)	CUM. WEIGHT ERODED PER AREA (G/SQ.CM)	EROSION RATE (GRAMS/ MIN * SQ.CM)	FLUID SHEAR STRESS (N/SQ.M)	REYNOLDS NUMBER
3.5	6.69	11.7	8.9	567.	63.	0.19	0.02	0.168	638.
7.0	12.67	18.8	1.3	413.	66.	0.28	0.02	0.094	605.
10.5	19.90	26.9	1.7	311.	71.	0.38	0.02	0.057	578.
14.0	26.89	34.3	2.0	257.	74.	0.46	0.01	0.041	542.
17.5	32.64	40.9	2.4	217.	78.	0.53	0.01	0.030	516.
21.0	39.34	47.1	2.8	187.	82.	0.58	0.01	0.024	492.
24.5	45.80	55.1	3.1	165.	85.	0.65	0.01	0.019	471.
28.0	52.46	61.7	3.5	147.	89.	0.69	0.01	0.016	451.
30.0	58.80	68.9	3.9	134.	93.	0.74	0.01	0.014	433.

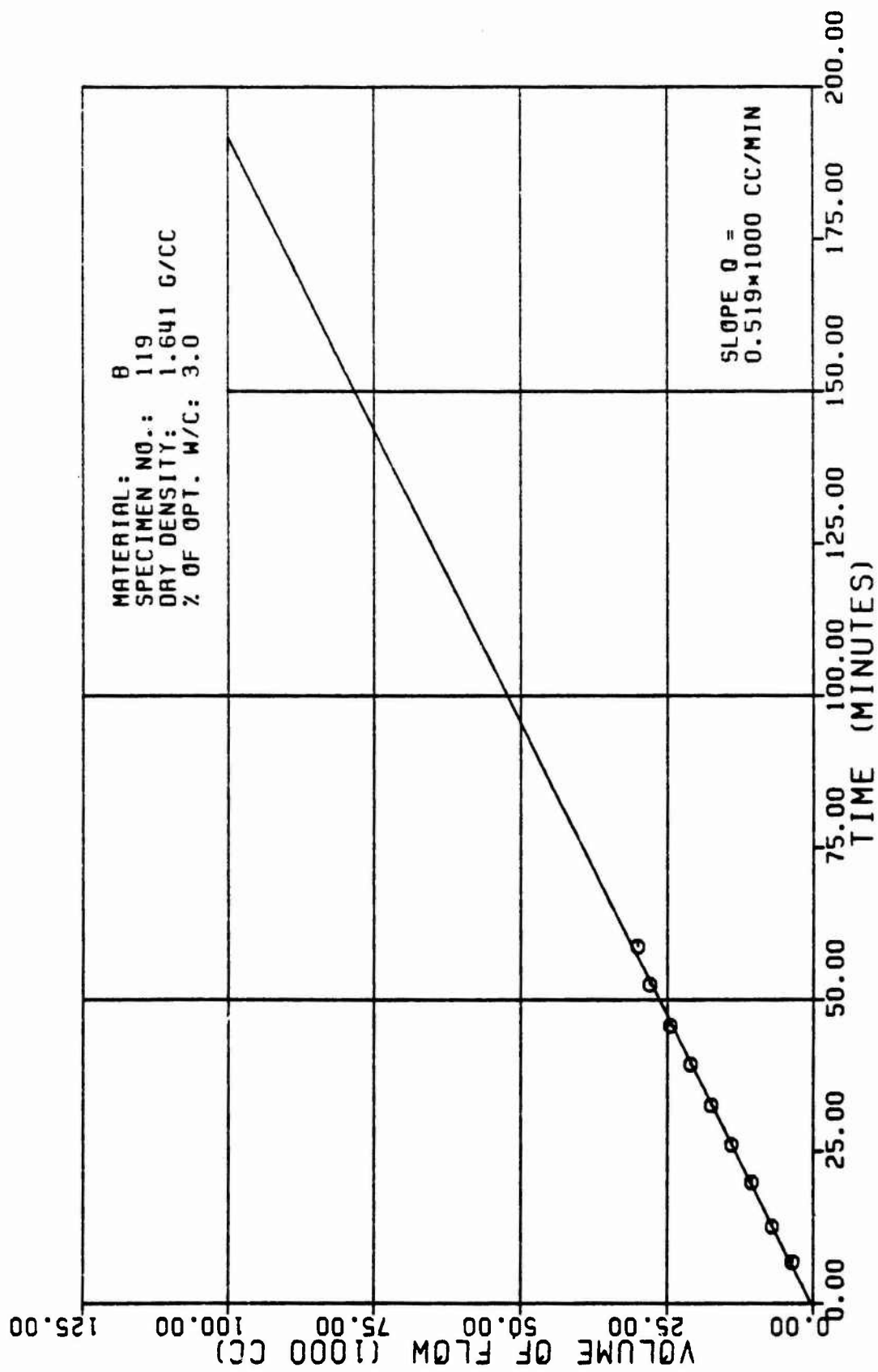


Figure A12a

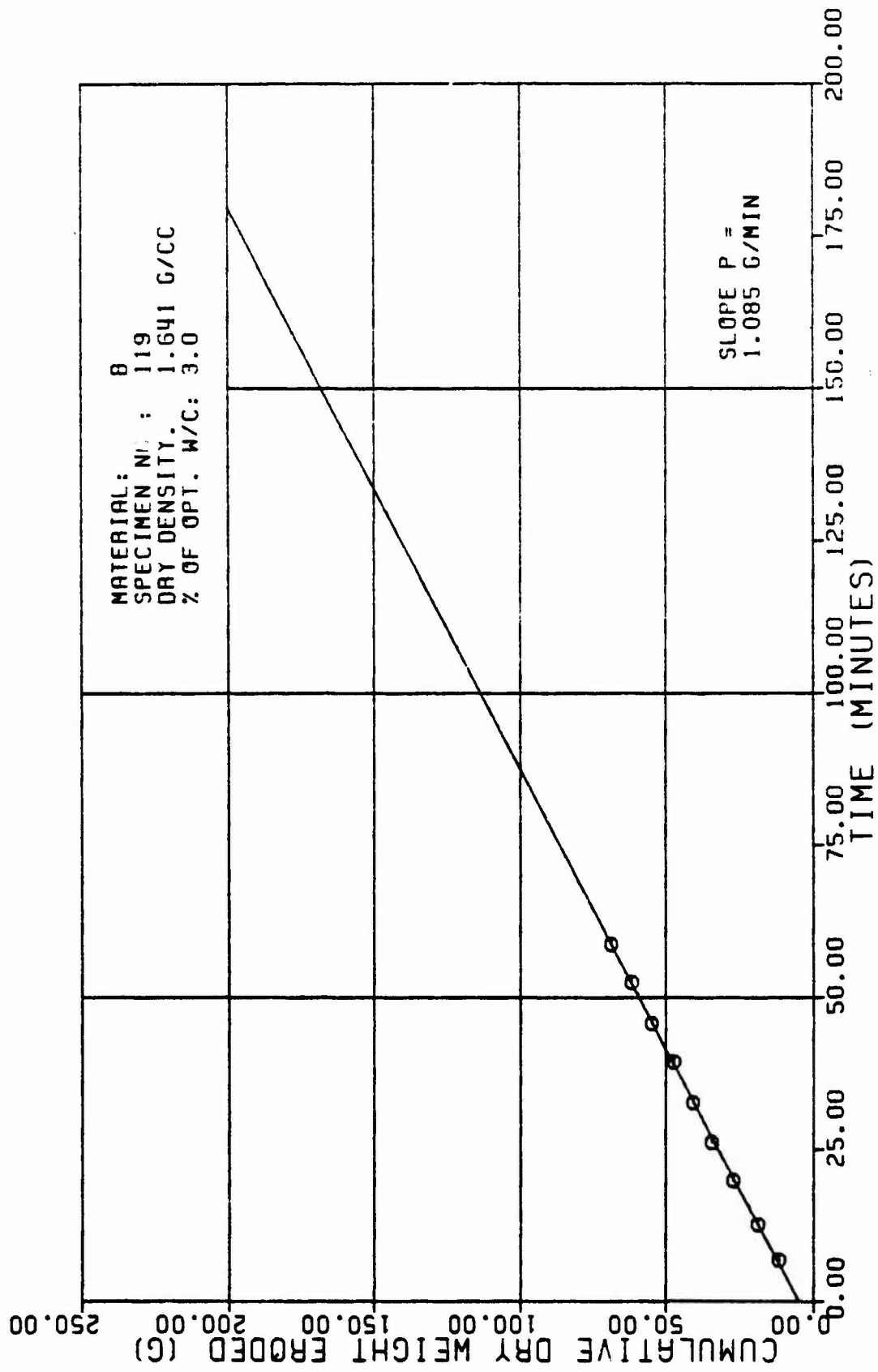


Figure A12b

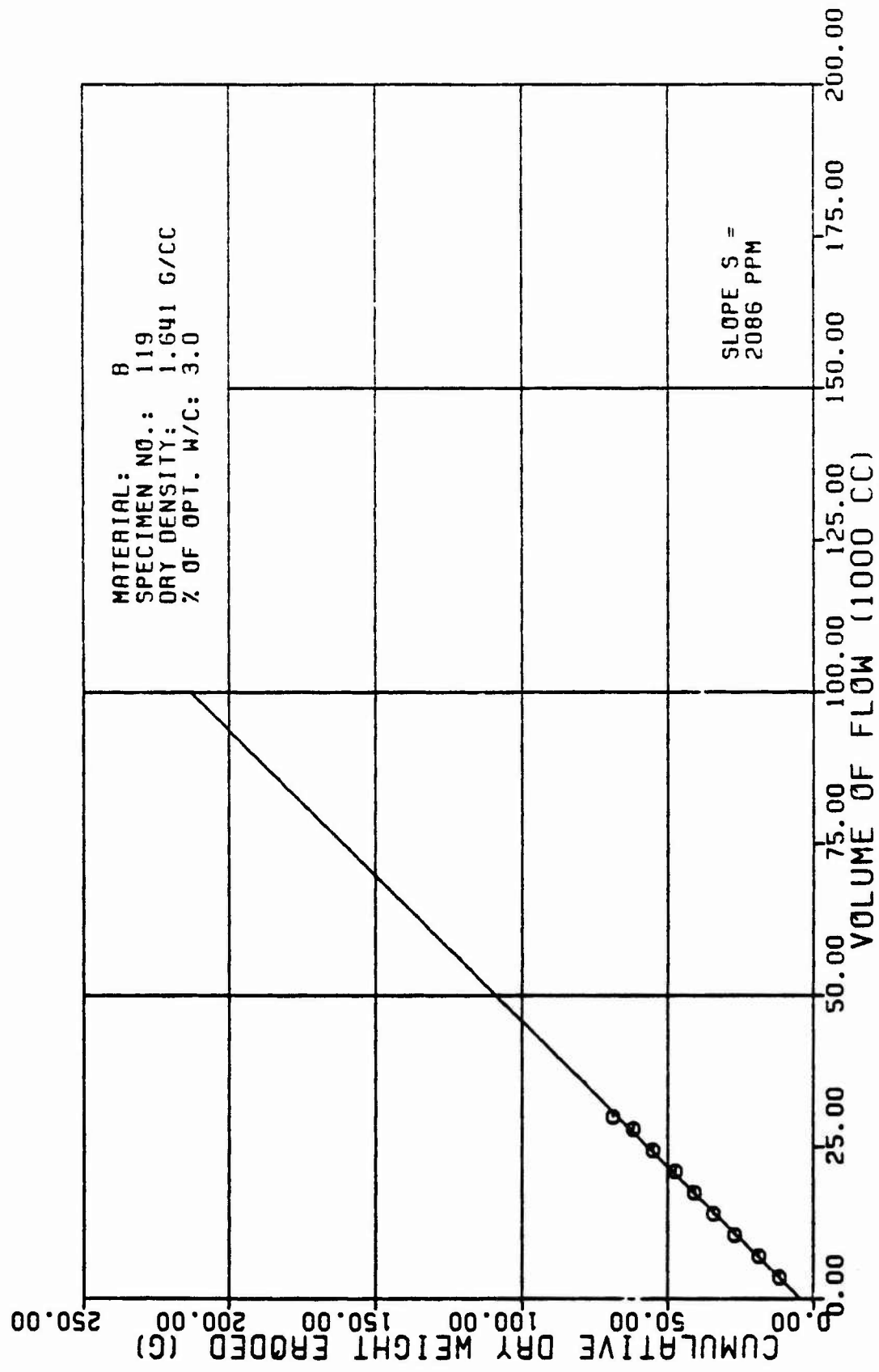


Figure A12c

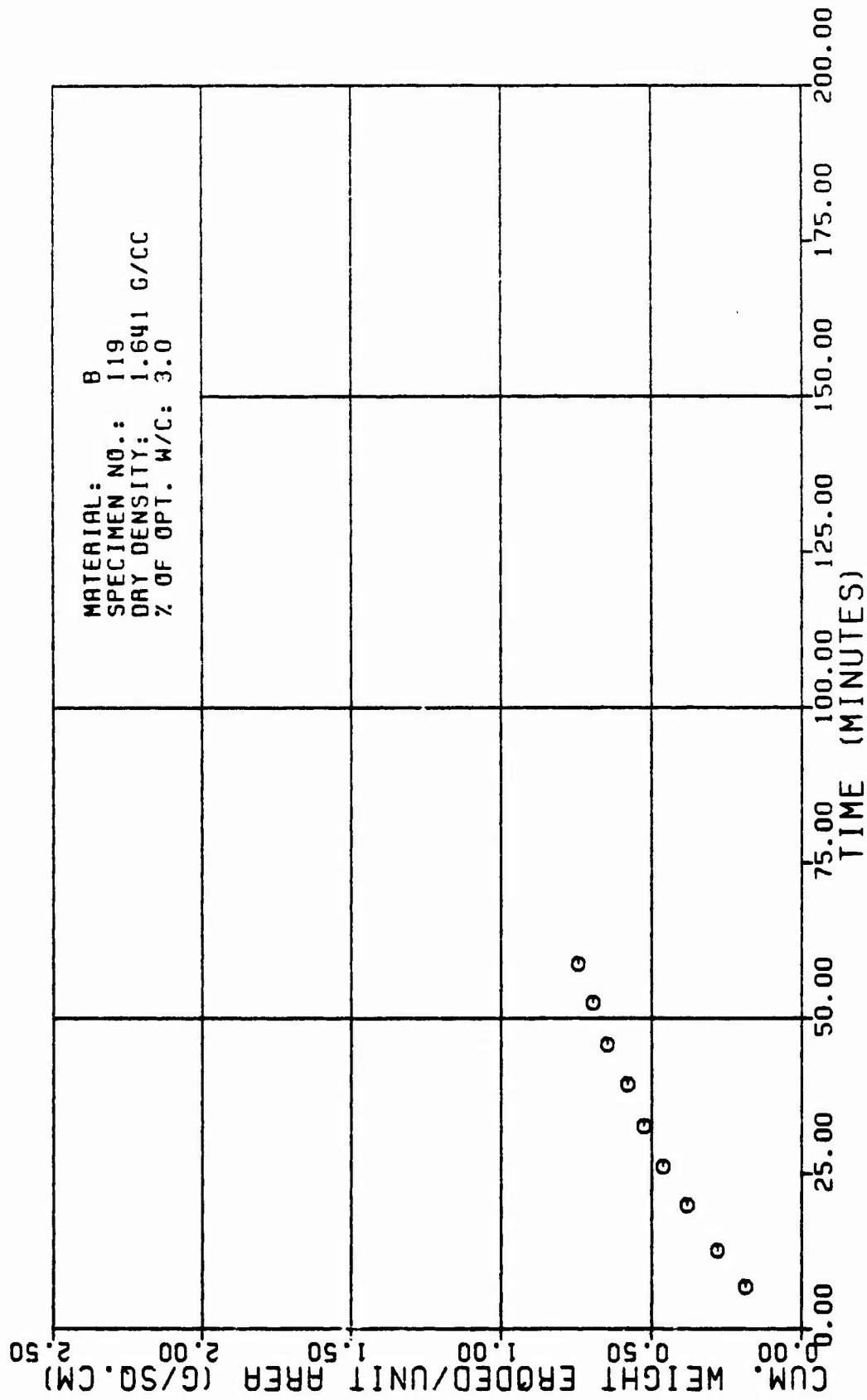


Figure A12d

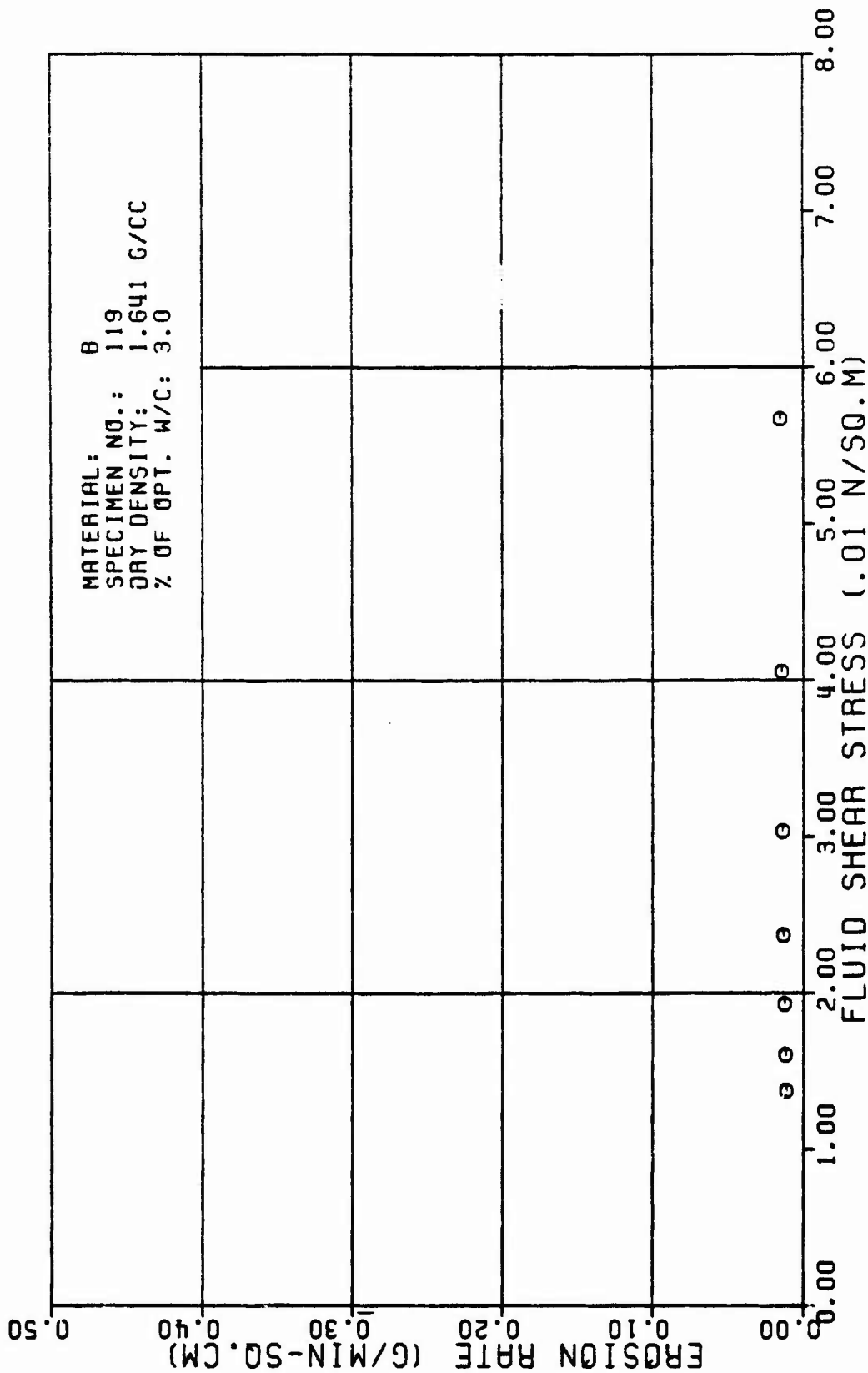


Figure A12e

TABLE A13

TEST RESULTS FOR TRIAXIAL EROSION TEST

MATERIAL TYPE: SPECIMEN NUMBER :		B 12#		R. L. SANCHEZ		551. CC/MIN	
TESTED BY:		4		8 82		1.7 G/MIN	
DATE TESTED:		1.648		G/CC		1.888 G/CC	
SPECIMEN DRY DENSITY:		4.8		PERCENT		8.881 N*SEC/SQ.M	
% OF OPTIMUM WATER CONTENT:		2.32		CM		98.18 KN/SQ.M	
INITIAL SLOT WIDTH:		8.23		CM		13.88 M	
INITIAL SLOT THICKNESS:		11.58		CM		18. M/M	
ERODED LENGTH:							

TABLE FOR SPECIMEN NUMBER: 812B (CONTINUES)

VOLUME OF FLOW (1000 CC)	TIME (MIN)	CUM. WEIGHT ERODED (G)	CROSS SECTION AREA (SQ.CM)	VELOCITY OF FLOW (CM/MIN)	ERODED SURFACE AREA (SQ.CM)	CUM. WEIGHT ERODED PER AREA (G/SQ.CM)	EROSION RATE (GRAMS/ MIN * SQ.CM)	FLUID SHEAR STRESS (N/SQ.M)	REYNOLDS NUMBER
35.8	63.13	182.5	6.3	88.	116.	8.89	8.81	8.887	366.
37.8	66.58	113.8	6.6	84.	119.	8.95	8.81	8.887	356.

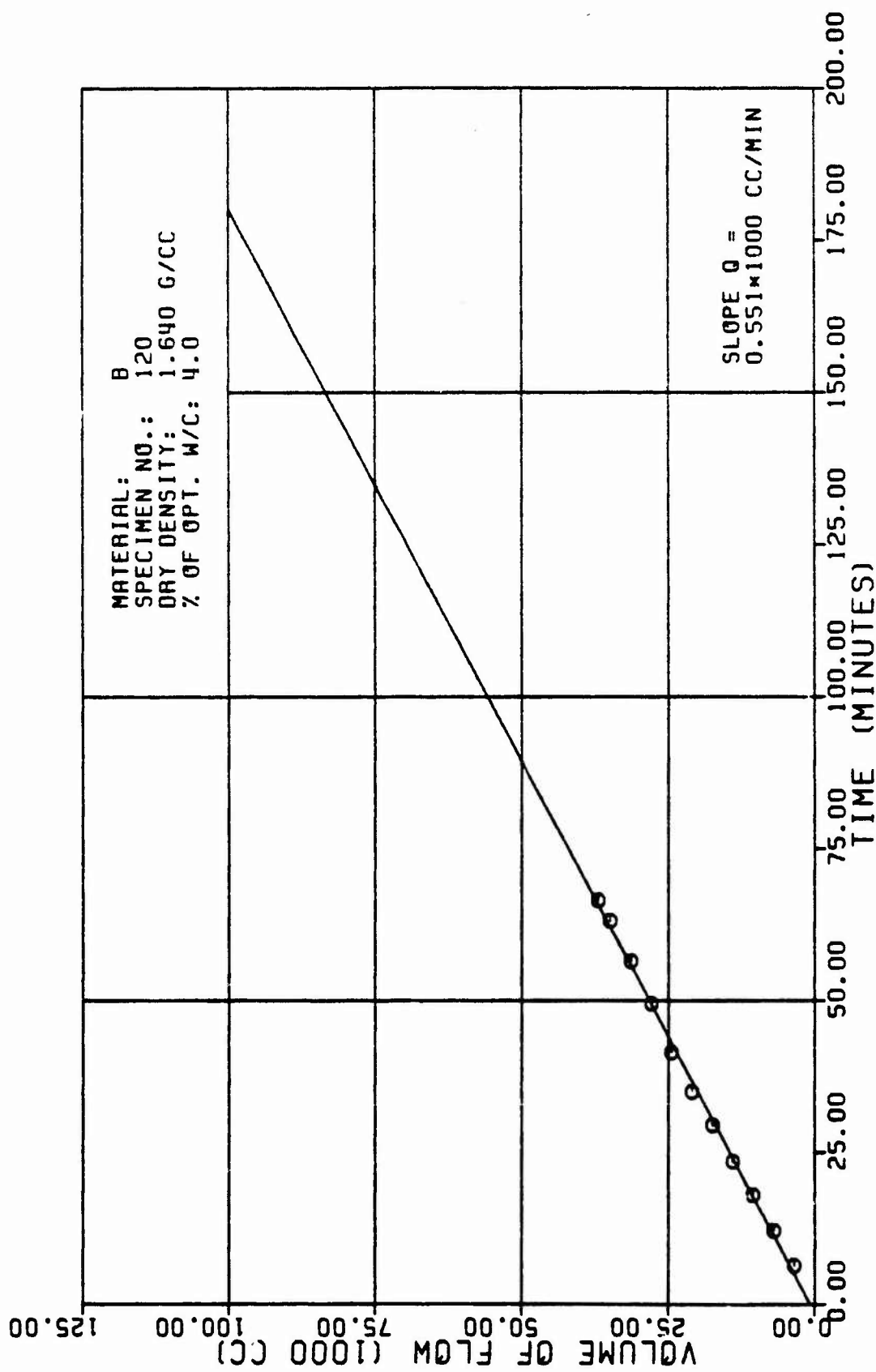


Figure A13a

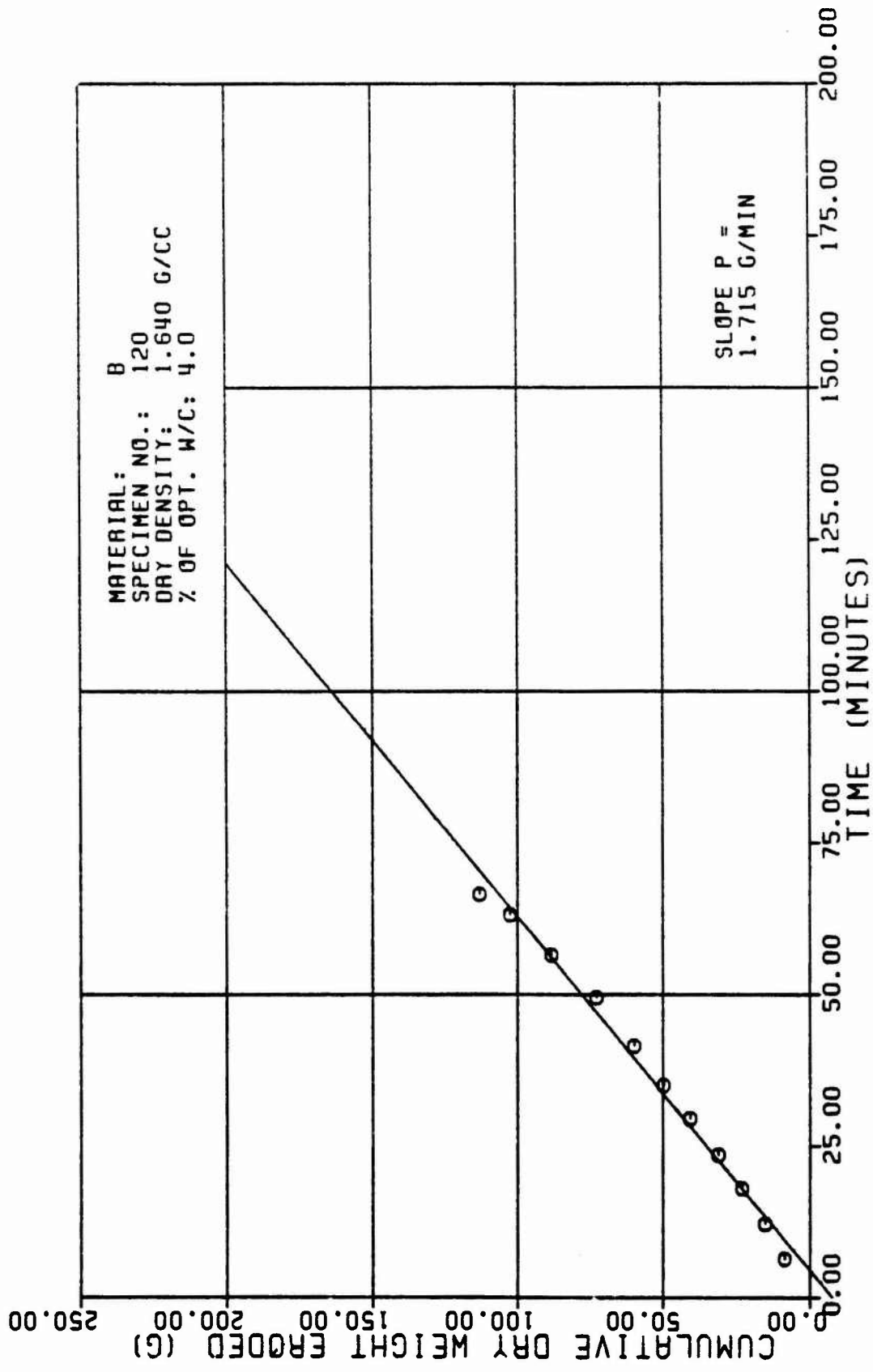


Figure A13b

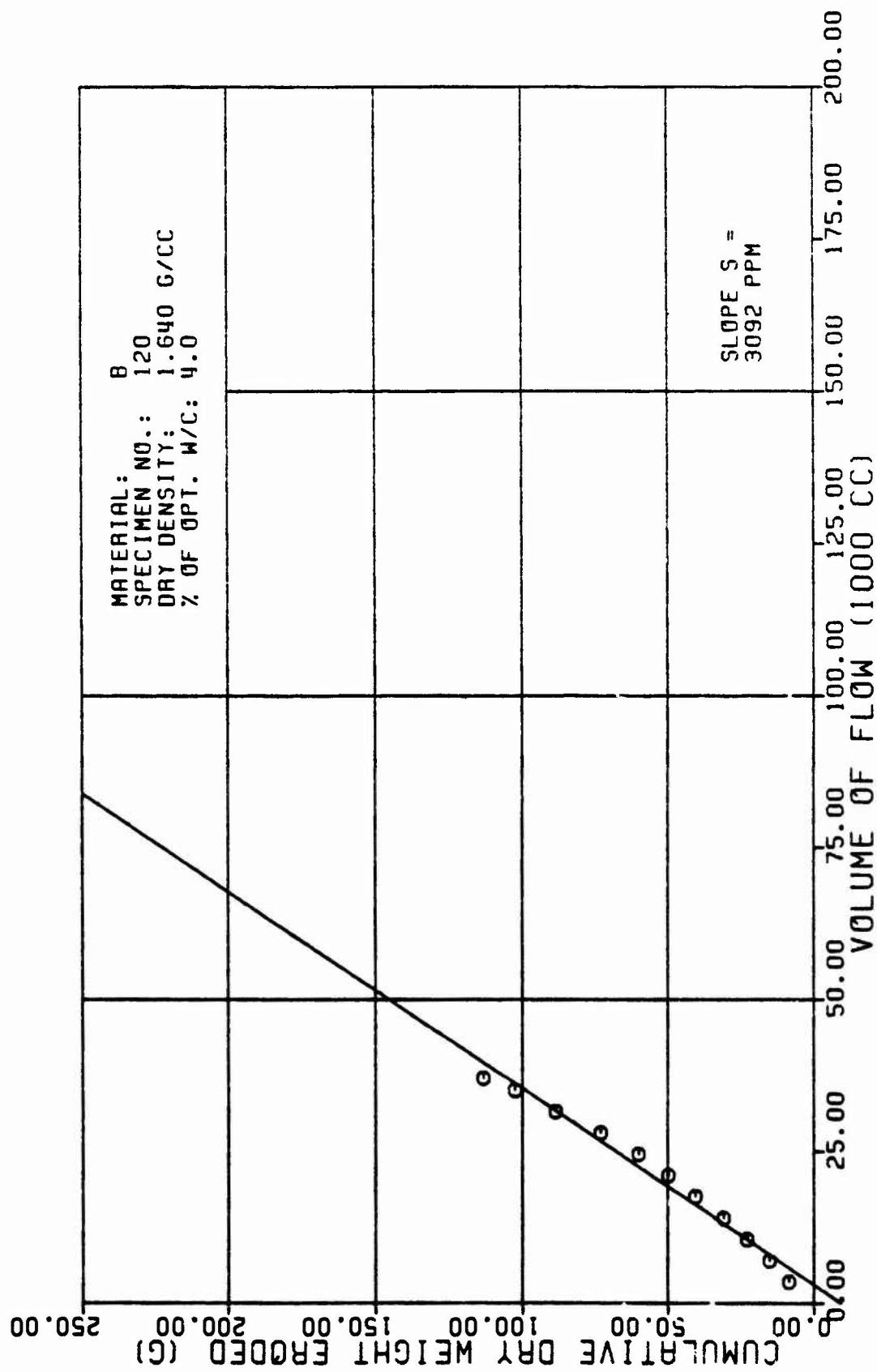


Figure A13c

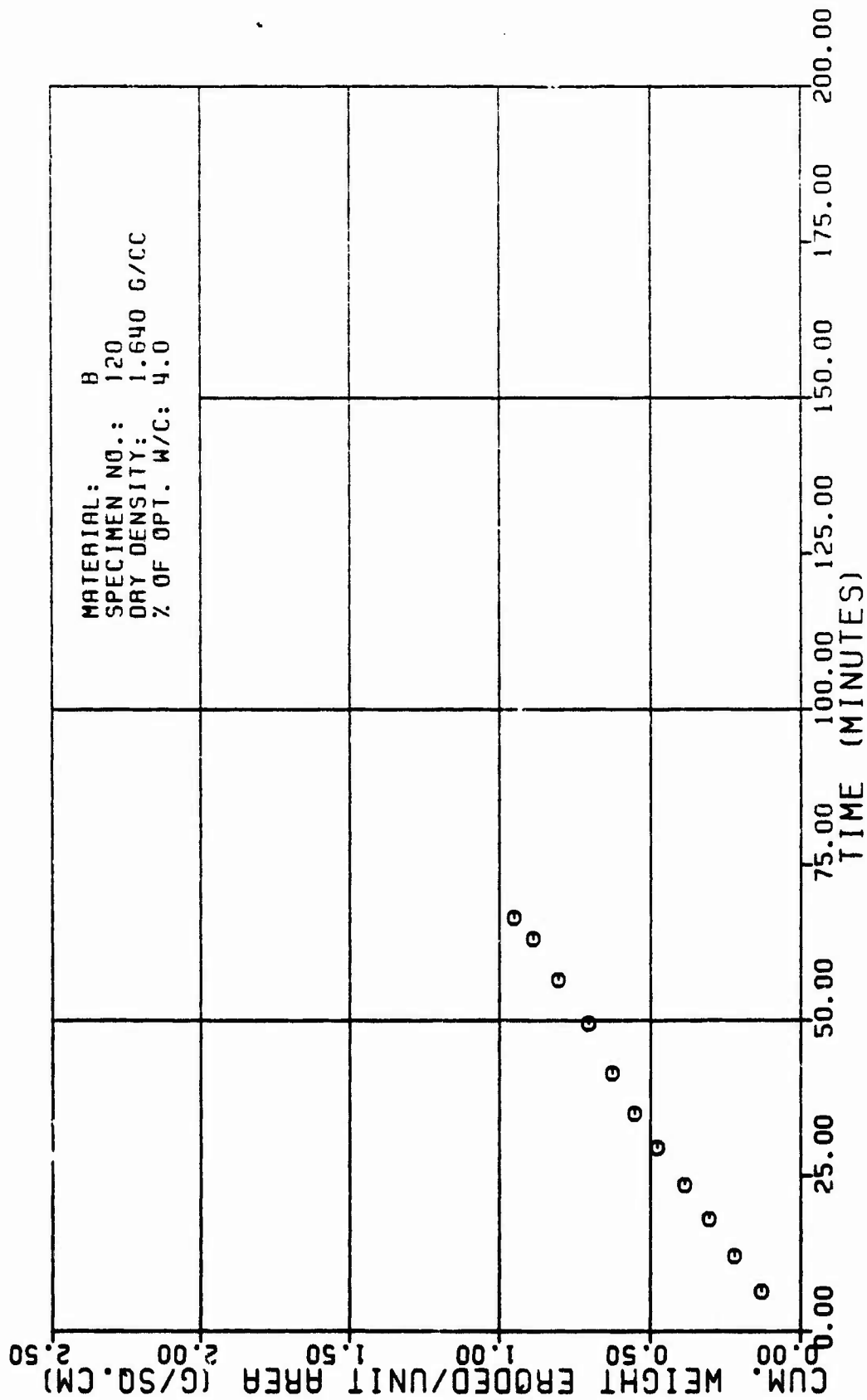


Figure A13d

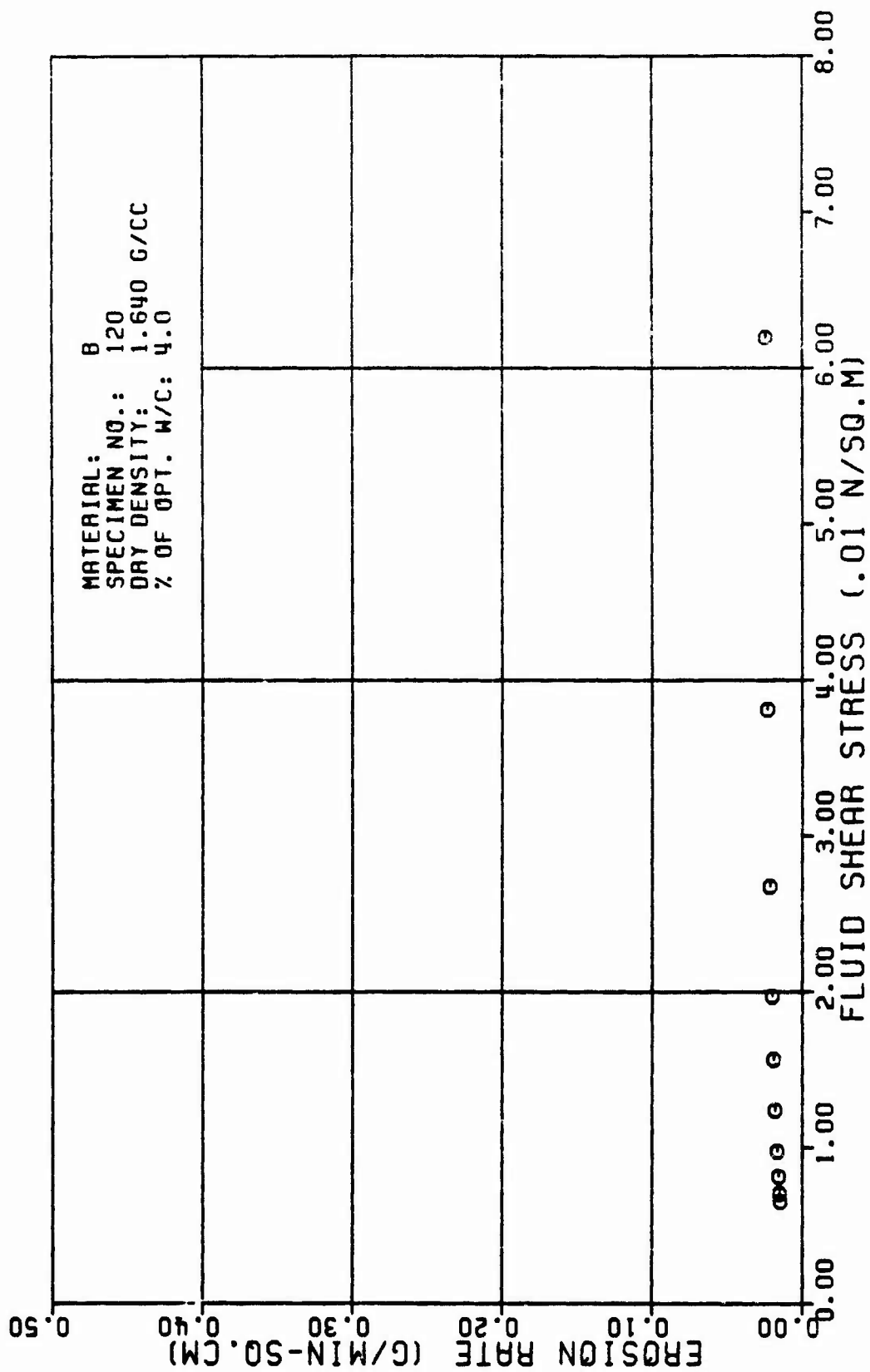


Figure A13e

TABLE A14

TEST RESULTS FOR TRIAXIAL EROSION TEST

MATERIAL TYPE: SPECIMEN NUMBER : TESTED BY:		B 121 R. L. SANCHEZ		AVERAGE FLOW RATE (Q): RATE OF WEIGHT EROSION (P):		495. CC/MIN 8.5 G/MIN			
DATE TESTED:		4 11 82		DENSITY OF ERODING FLUID: VISCOSITY OF ERODING FLUID:		1.000 G/CC 8.881 N*SEC/SQ.M			
SPECIMEN DRY DENSITY:		1.638 G/CC		CONFINING PRESSURE:		98.18 KN/SQ.M			
X OF OPTIMUM WATER CONTENT:		1.5 PERCENT		HEAD OF WATER:		13.88 M			
INITIAL SLOT WIDTH:		2.32 CM		HYDRAULIC GRADIENT:		18. M/M			
INITIAL SLOT THICKNESS:		8.23 CM							
ERODED LENGTH:		11.68 CM							

VOLUME OF FLOW (1000 CC)	TIME (MIN)	CUM. WEIGHT ERODED (G)	CROSS SECTION AREA (SQ.CH)	VELOCITY OF FLOW (CM/MIN)	ERODED SURFACE AREA (SQ.CH)	CUM. WEIGHT ERODED PER AREA (G/SQ.CH)	EROSION RATE (GRAMS/ (MIN * SQ.CH))	FLUID SHEAR STRESS (N/SQ.M)	REYNOLDS NUMBER
3.5	6.44	8.9	8.7	695.	61.	8.15	8.81	8.257	628.
7.5	12.13	14.8	8.9	569.	63.	8.22	8.81	8.176	612.
18.5	19.88	17.1	1.1	467.	64.	8.27	8.81	8.122	594.
14.8	28.74	28.8	1.2	397.	66.	8.31	8.81	8.891	578.
17.5	31.89	24.8	1.4	349.	68.	8.37	8.81	8.872	563.
21.8	38.48	27.9	1.6	318.	78.	8.48	8.81	8.858	549.
24.5	48.38	31.4	1.8	277.	72.	8.44	8.81	8.848	534.
28.8	56.47	38.2	2.1	236.	75.	8.47	8.81	8.836	512.
31.5	62.88	38.6	2.3	228.	76.	8.51	8.81	8.832	502.

TABLE FOR SPECIMEN NUMBER: B121 (CONTINUES)

VOLUME OF FLOW (1000 CC)	TIME (MIN)	CUM. WEIGHT ERODED (G)	CROSS SECTION AREA (SQ.CM)	VELOCITY OF FLOW (CM/MIN)	ERODED SURFACE AREA (SQ.CM)	CUM. WEIGHT ERODED PER AREA (G/SQ.CM)	EROSION RATE (GRAMS/ (MIN * SQ.CM))	FLUID SHEAR STRESS (N/SQ.M)	REYNOLDS NUMBER
36.8	68.51	42.4	2.4	283.	78.	8.54	8.81	8.828	498.
38.5	74.92	46.2	2.6	198.	88.	8.58	8.81	8.825	479.
42.8	81.46	49.8	2.8	177.	92.	8.61	8.81	8.822	468.
45.5	88.23	54.4	3.8	166.	94.	8.65	8.81	8.828	458.
48.7	98.25	58.8	3.3	152.	86.	8.68	8.81	8.817	443.

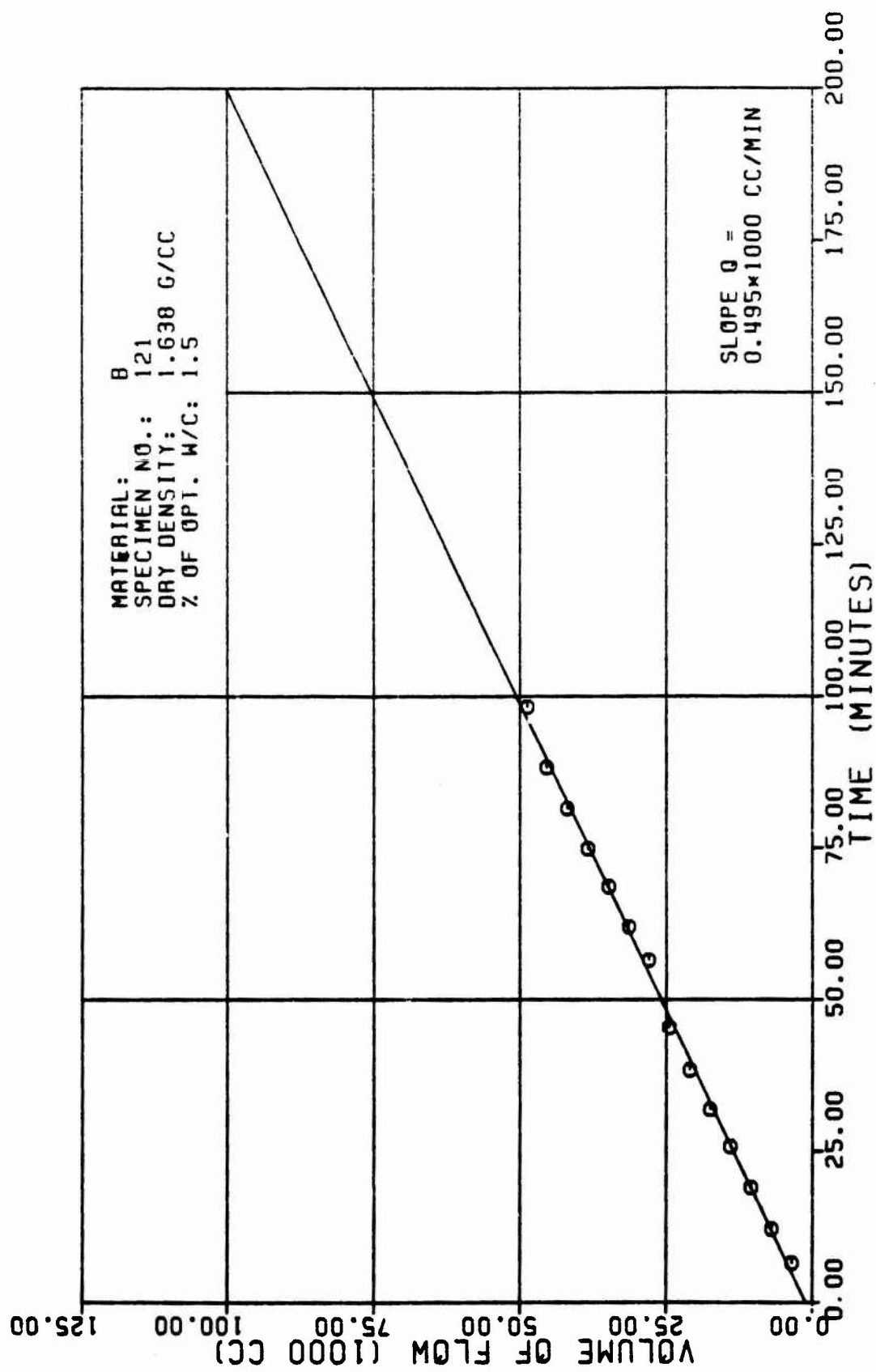


Figure A14a

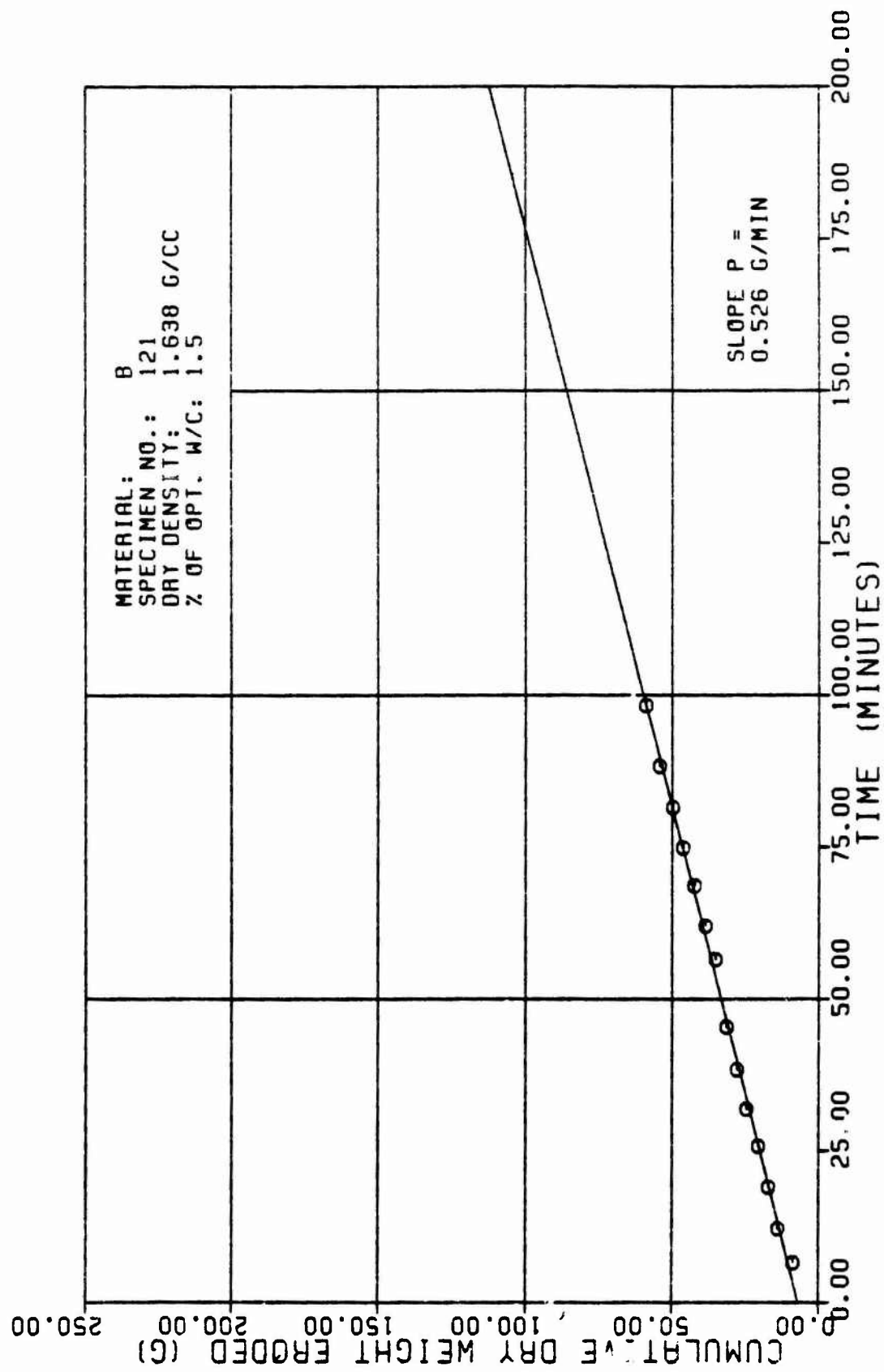


Figure A14b

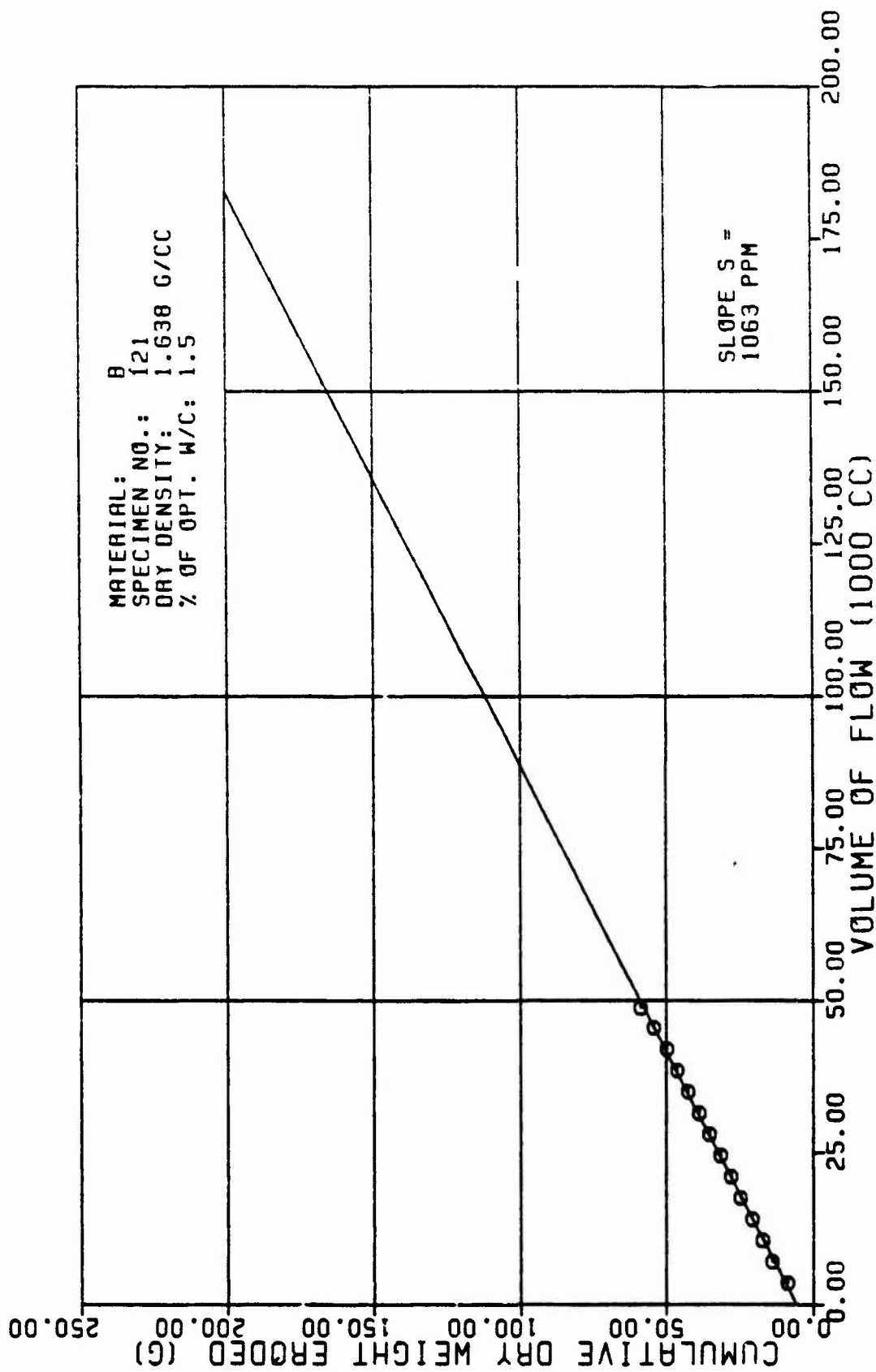


Figure A14c

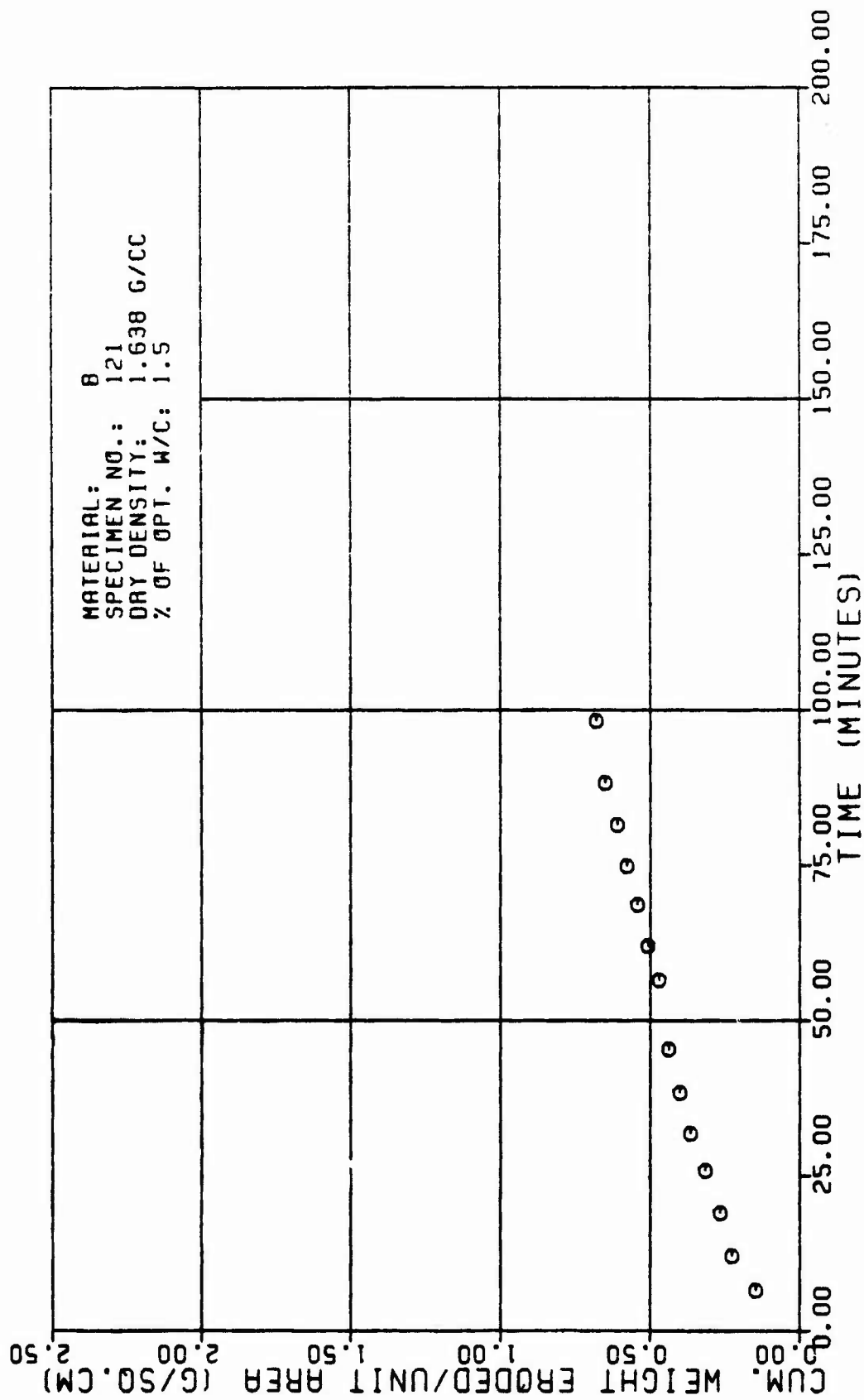


Figure A14d

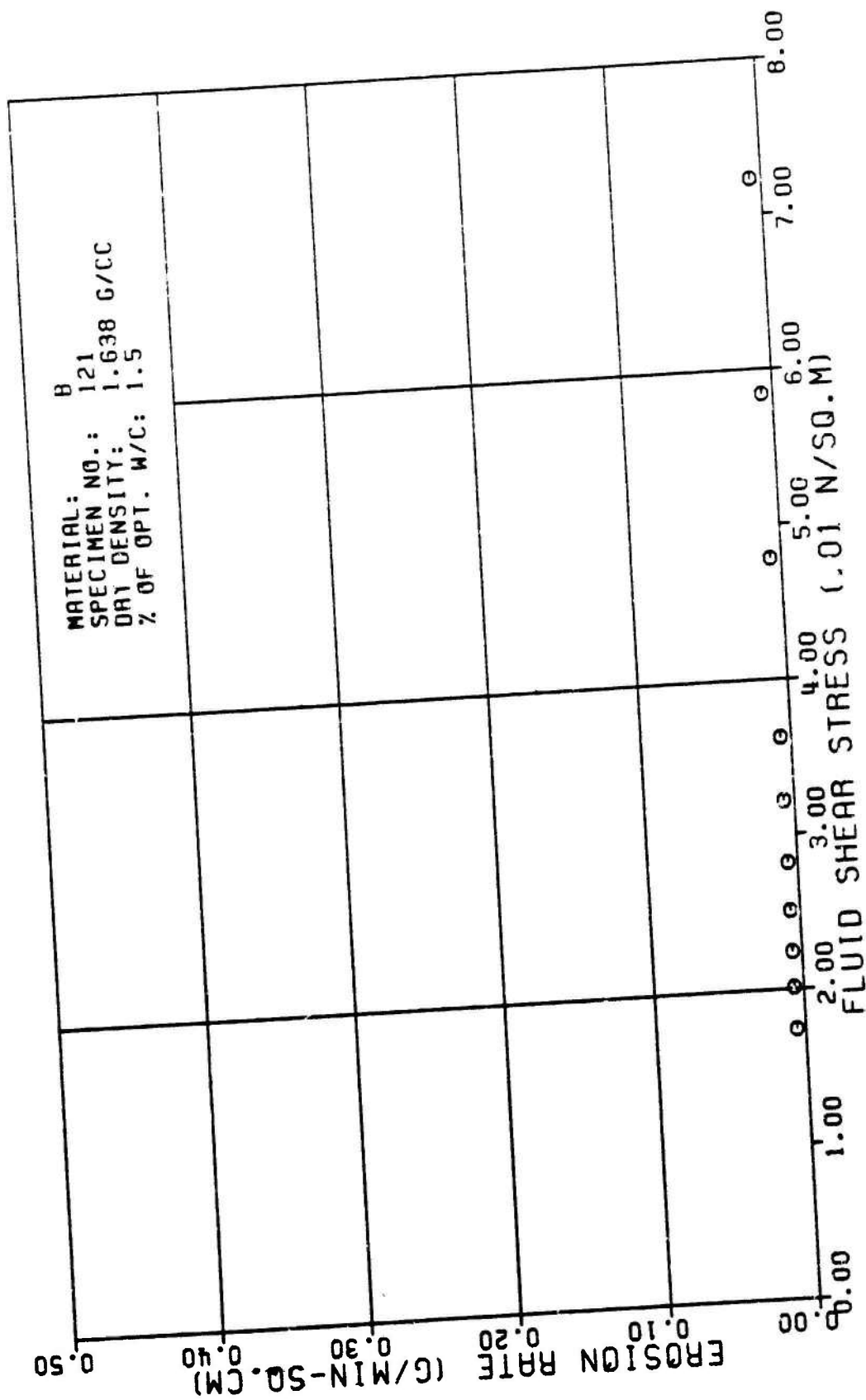


Figure A14e

TABLE A15

TEST RESULTS FOR TRIAXIAL EROSION TEST

MATERIAL TYPE: SPECIMEN NUMBER : TESTED BY:		B 123 R. L. SANCHEZ		AVERAGE FLOW RATE (Q): RATE OF WEIGHT EROSION (P):		487. CC/MIN 3.2 G/MIN			
DATE TESTED:		5 25 82		DENSITY OF ERODING FLUID: VISCOSITY OF ERODING FLUID:		1.000 G/CC 0.001 N*SEC/SQ.M			
SPECIMEN DRY DENSITY:		1.551 G/CC		CONFINING PRESSURE:		98.00 KN/SQ.M			
X OF OPTIMUM WATER CONTENT:		0.0 PERCENT		HEAD OF WATER:		1.30 M			
INITIAL SLOT WIDTH:		2.35 CM		HYDRAULIC GRADIENT:		10. M/M			
INITIAL SLOT THICKNESS:		0.23 CM							
ERODED LENGTH:		11.40 CM							
VOLUME OF FLOW (1000 CC)	TIME (MIN)	CUM. WEIGHT ERODED (G)	CROSS SECTION AREA (SQ.CM)	VELOCITY OF FLOW (CM/MIN)	ERODED SURFACE AREA (SQ.CM)	CUM WEIGHT ERODED PER AREA (G/SQ.CM)	EROSION RATE (GRAMS/ (MIN * SQ.CM))	FLUID SHEAR STRESS (N/SQ.M)	REYNOLDS NUMBER
1.2	1.91	12.1	0.9	560.	61.	0.20	0.05	0.172	607.
4.5	9.17	30.1	2.2	225.	74.	0.41	0.04	0.034	591.
8.0	16.23	54.3	3.4	142.	86.	0.63	0.04	0.016	728.
9.3	10.89	66.2	3.9	125.	91.	0.73	0.03	0.013	496.

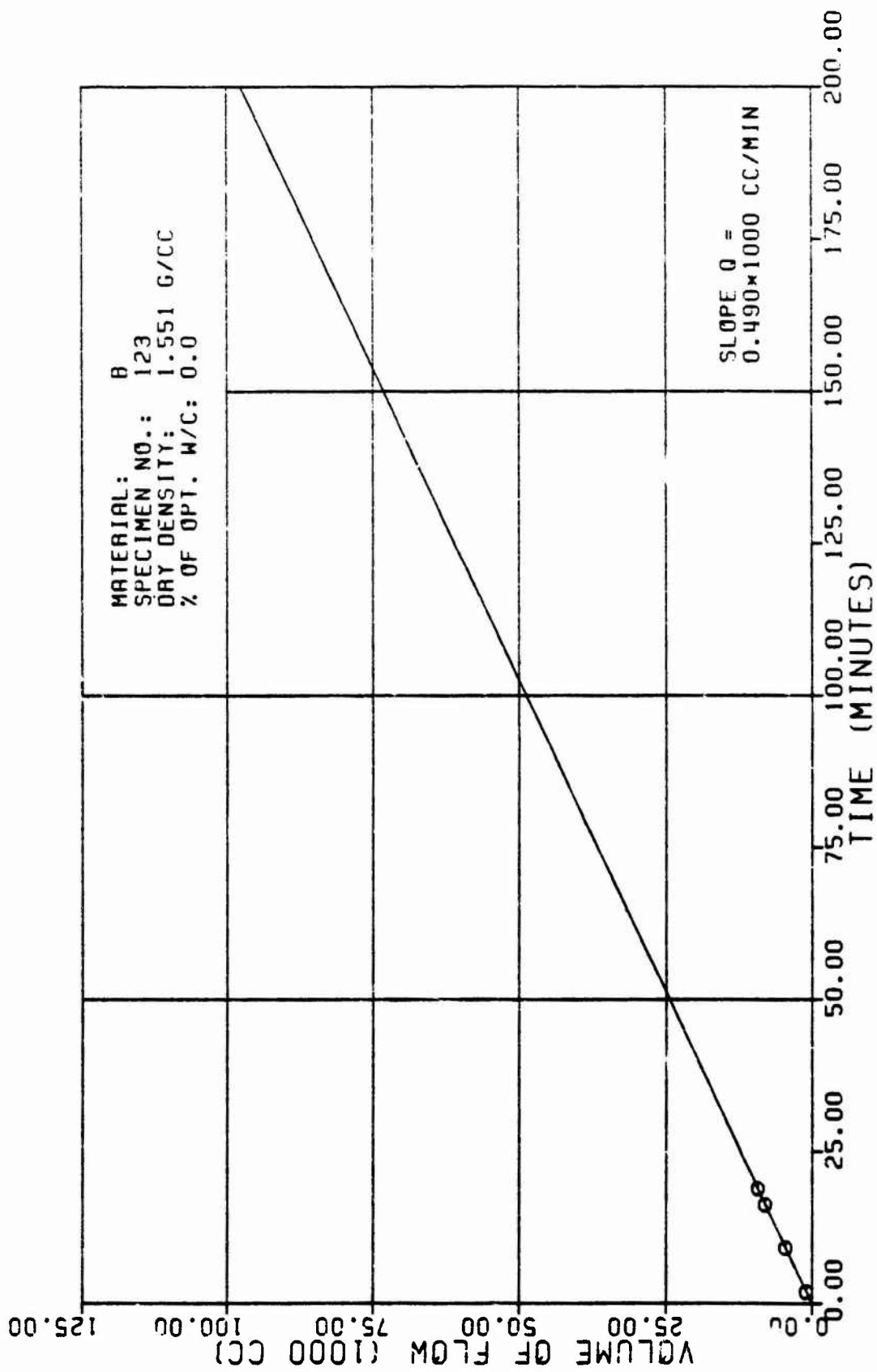


Figure A15a

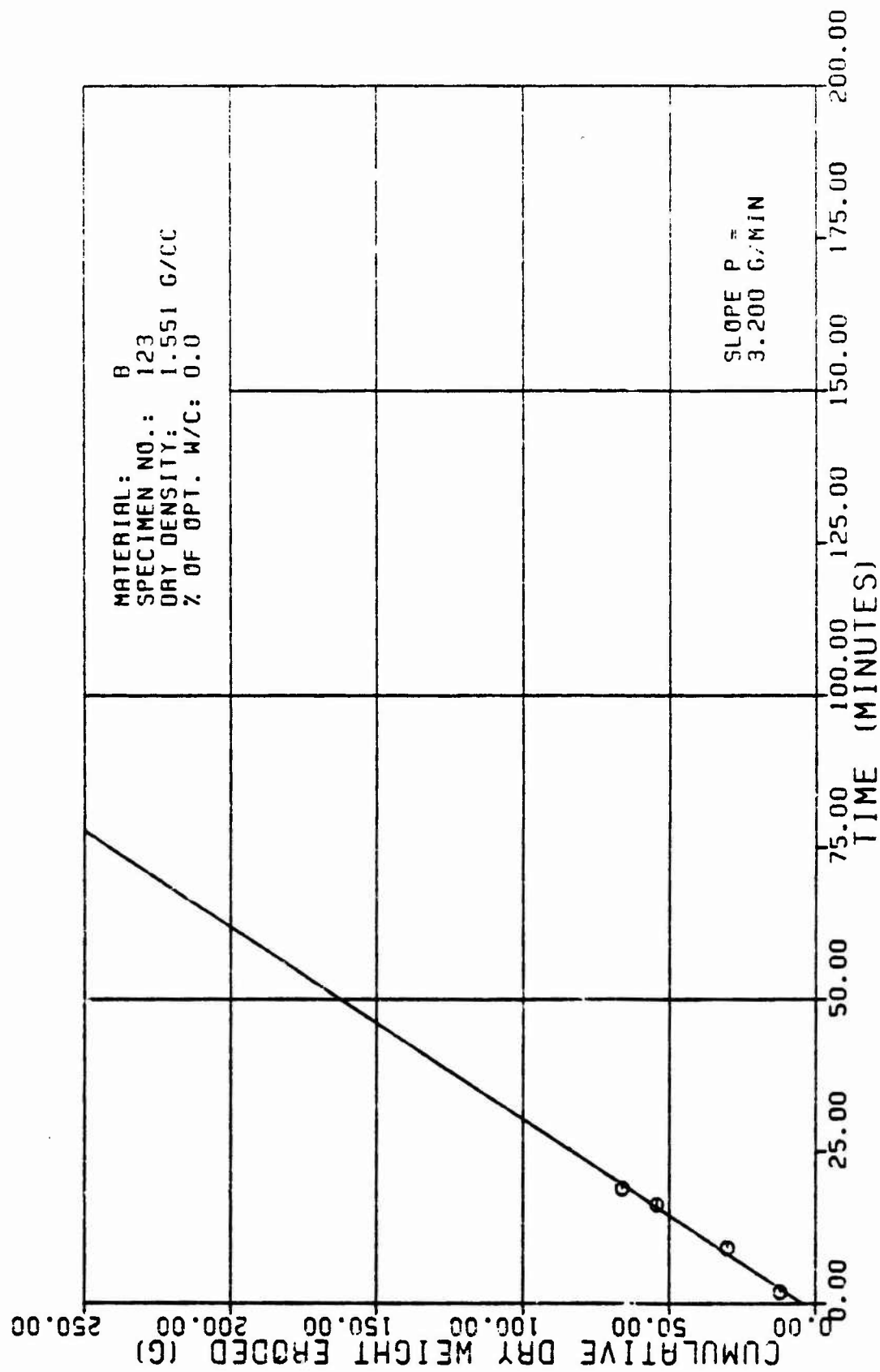


Figure A15b

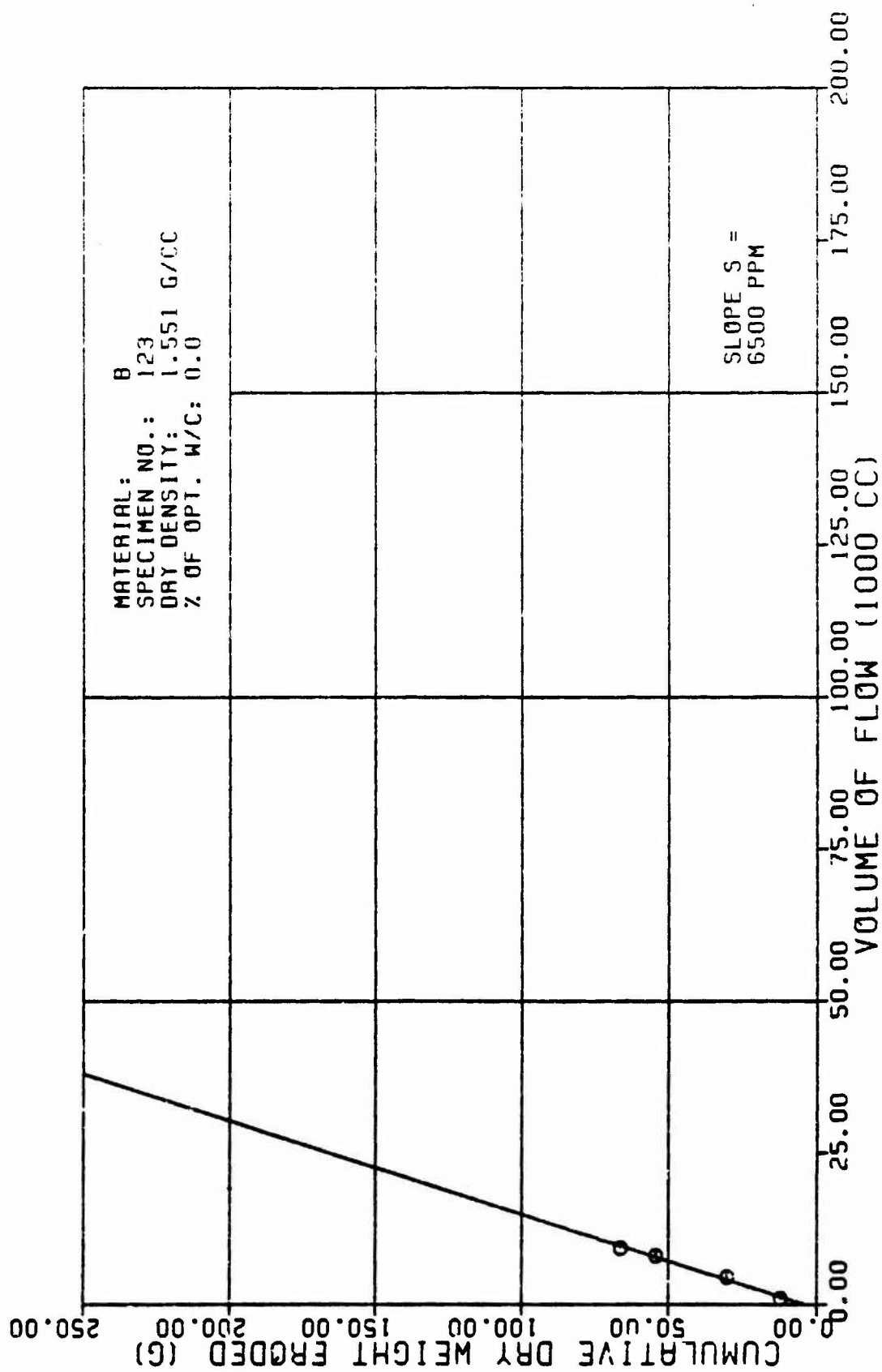


Figure A15c

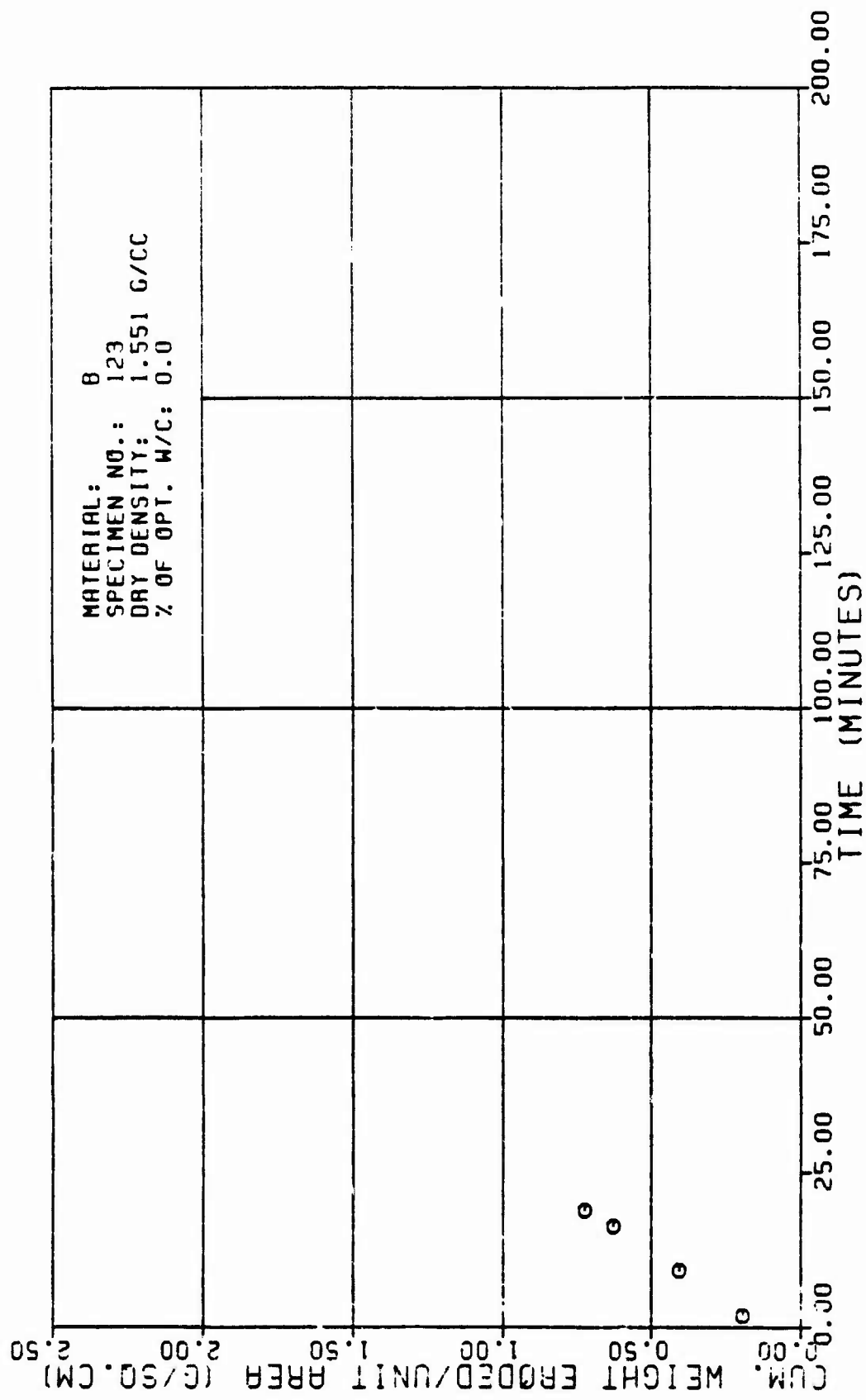


Figure A15d

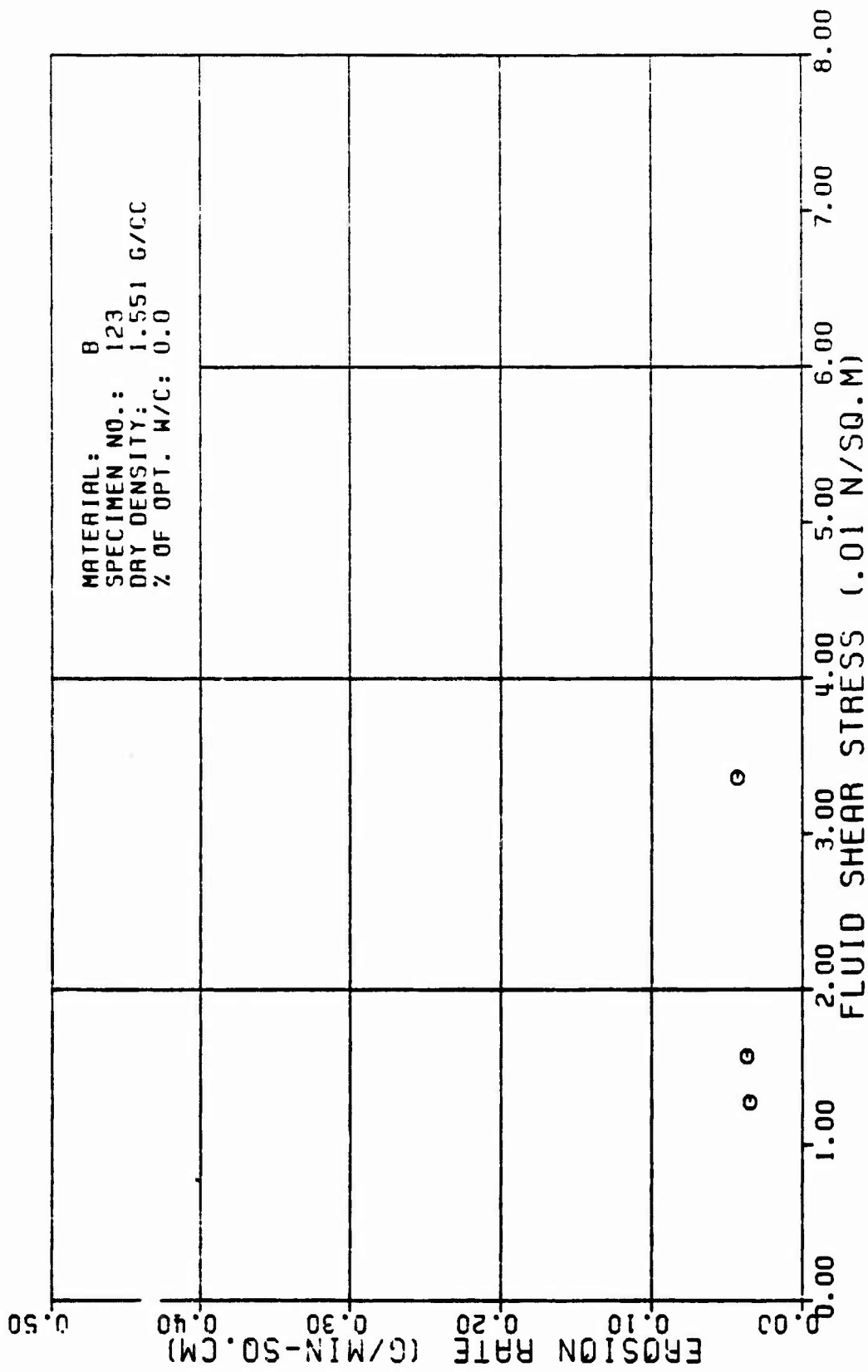


Figure A15e

TABLE A16

TEST RESULTS FOR TRIAXIAL EROSION TEST

MATERIAL TYPE: SPECIMEN NUMBER : TESTED BY:		6 781 R. L. SANCHEZ		AVERAGE FLOW RATE (Q): RATE OF VEIGHT EROSION (P):		558. CC/MIN 8.8 G/MIN			
DATE TESTED:		4 11 82		DENSITY OF ERODING FLUID: VISCOSITY OF ERODING FLUID:		1.888 G/CC 8.881 N*SEC/SO.M			
SPECIMEN DRY DENSITY:		1.642 G/CC		CONFINING PRESSURE:		98.18 KN/SO.M			
% OF OPTIMUM WATER CONTENT:		1.5 PERCENT		HEAD OF WATER:		13.88 M			
INITIAL SLOT WIDTH:		2.32 CM		HYDRAULIC GRADIENT:		18. M/M			
INITIAL SLOT THICKNESS:		8.23 CM							
ERODER LENGTH:		11.68 CM							

VOLUME OF FLOW (1000 CC)	TIME (MIN)	CUM. WEIGHT ERODER (G)	CROSS SECTION AREA (SQ.CM)	VELOCITY OF FLOW (CM/MIN)	ERODED SURFACE AREA (SQ.CM)	CUM. WEIGHT ERODED PER AREA (G/SQ.CM)	EROSION RATE (GRAMS/ (MIN * SQ.CM))	FLUID SHEAR STRESS (N/SQ.M)	REYNOLDS NUMBER
3.5	6.32	8.5	8.8	717.	62.	8.14	8.81	8.241	711.
7.8	11.88	14.4	1.8	559.	64.	8.22	8.81	8.152	687.
18.6	17.62	18.8	1.3	453.	66.	8.27	8.81	8.183	662.
14.8	23.92	28.9	1.6	376.	69.	8.38	8.81	8.874	637.
17.8	29.68	26.1	1.7	327.	71.	8.37	8.81	8.858	617.
21.8	35.42	29.6	2.8	287.	74.	8.48	8.81	8.846	597.
24.6	41.86	32.6	2.2	253.	76.	8.43	8.81	8.837	576.
28.8	47.68	36.7	2.5	229.	79.	8.47	8.81	8.831	559.
31.8	63.77	48.6	2.7	288.	81.	8.58	8.81	8.827	541.

TABLE FOR SPECIMEN NUMBER: 87B1 (CONTINUES)

VOLUME OF FLOW (1000 CC)	TIME (MIN)	CUM. WEIGHT ERODED (G)	CROSS SECTION AREA (SQ. CM)	VELOCITY OF FLOW (CM/MIN)	ERODED SURFACE AREA (SQ. CM)	CUM. WEIGHT ERODED PER AREA (G/SQ. CM)	EROSION RATE (GRAMS/ MIN - SQ. CM)	FLUID SHEAR STRESS (N/SQ. M)	REYNOLDS NUMBER
36.8	68.16	44.6	3.8	198.	84.	8.53	8.81	8.823	525.
38.6	68.78	49.1	3.2	176.	86.	8.57	8.81	8.828	518.
42.8	71.88	54.6	3.6	164.	89.	8.62	8.81	8.818	496.
43.8	76.28	67.8	3.6	157.	98.	8.64	8.81	8.817	489.
48.6	79.88	61.8	3.8	151.	91.	8.67	8.81	8.816	488.
47.4	81.54	64.9	3.9	147.	92.	8.78	8.81	8.816	475.
49.2	84.95	69.2	4.8	142.	94.	8.74	8.81	8.814	468.
61.8	91.13	79.6	4.3	133.	96.	8.83	8.81	8.813	456.
61.2	91.36	88.6	4.3	133.	97.	8.84	8.81	8.813	455.

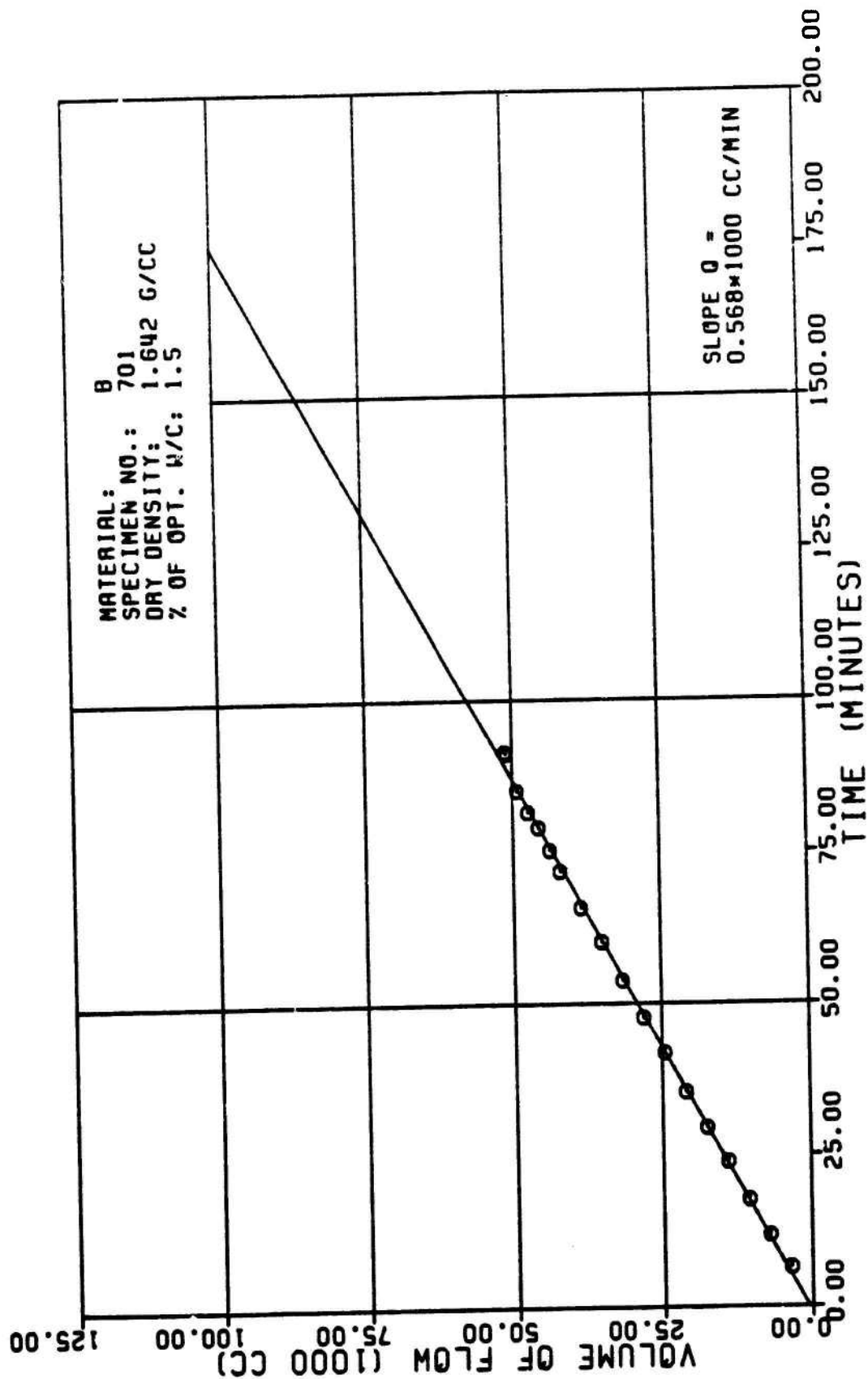


Figure A16a

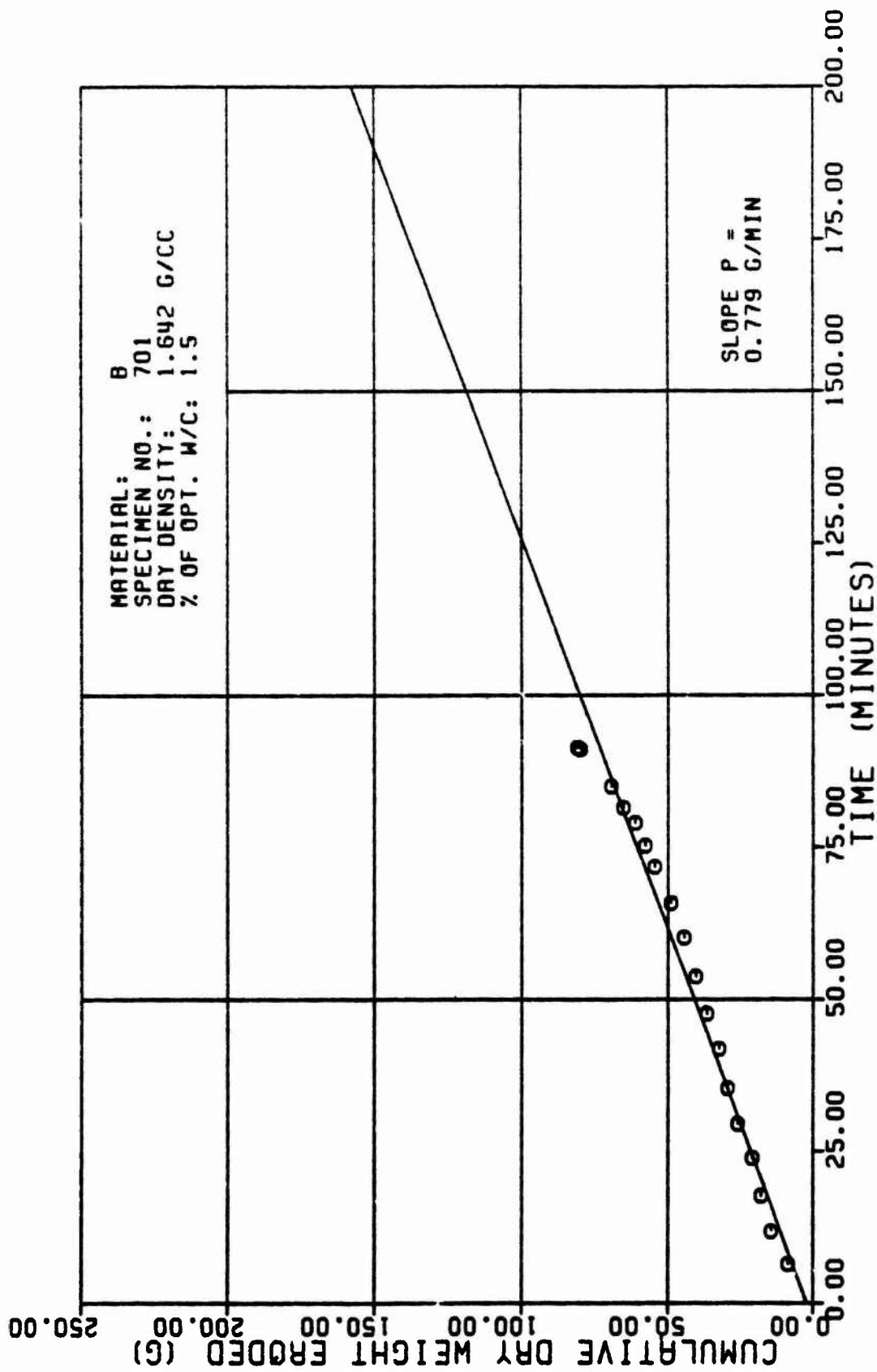


Figure A16b

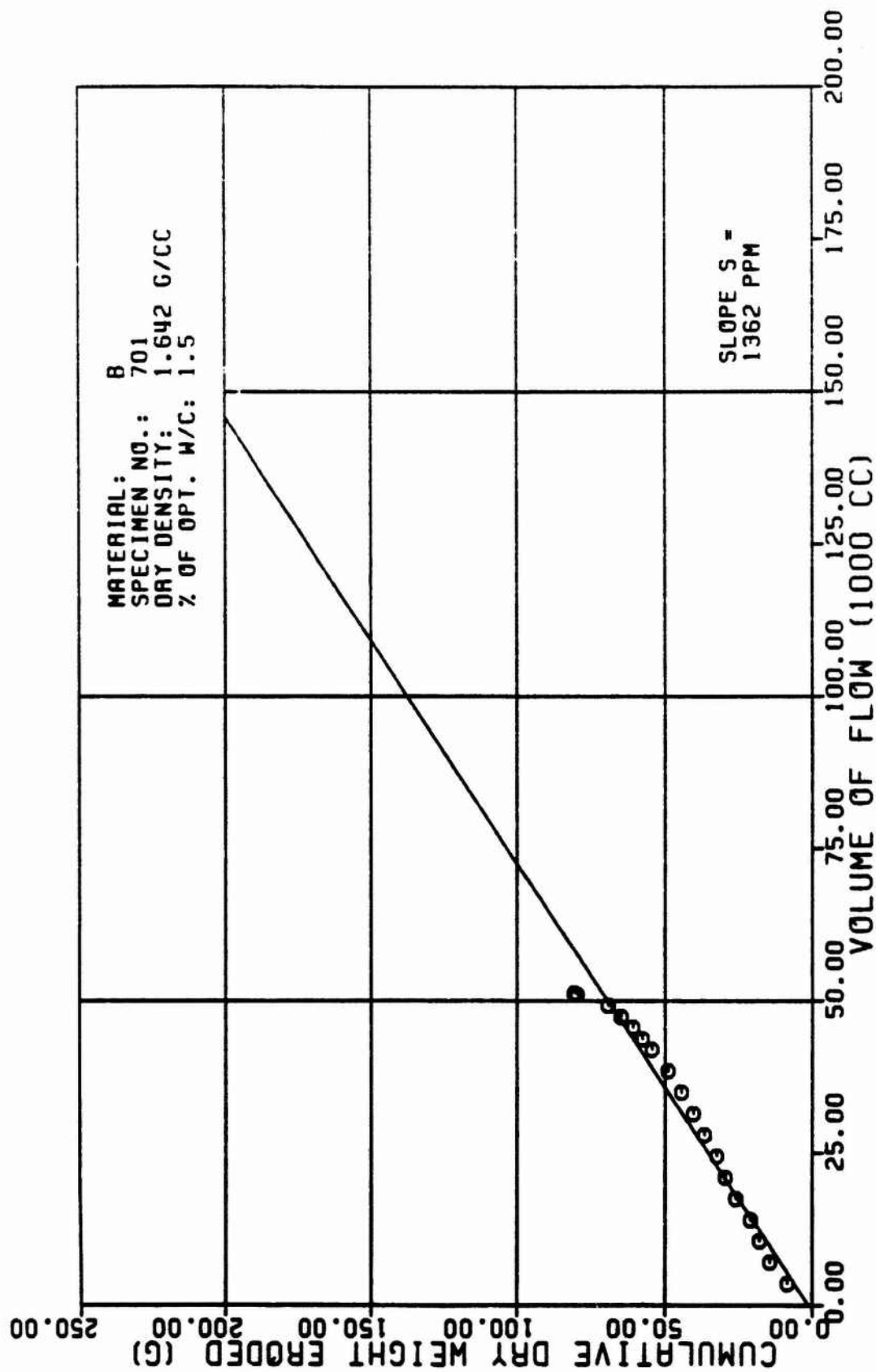


Figure A16c

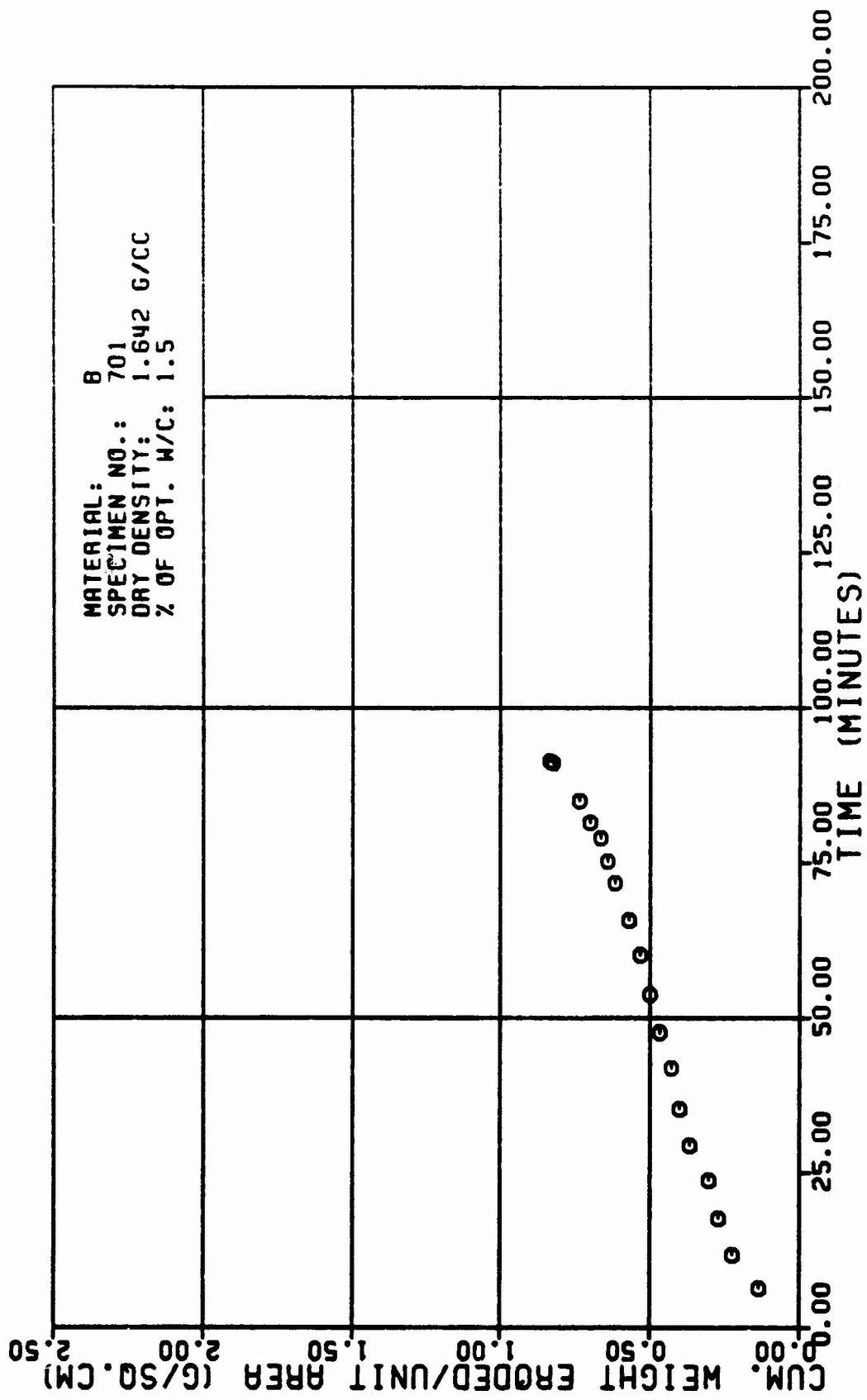


Figure A16d

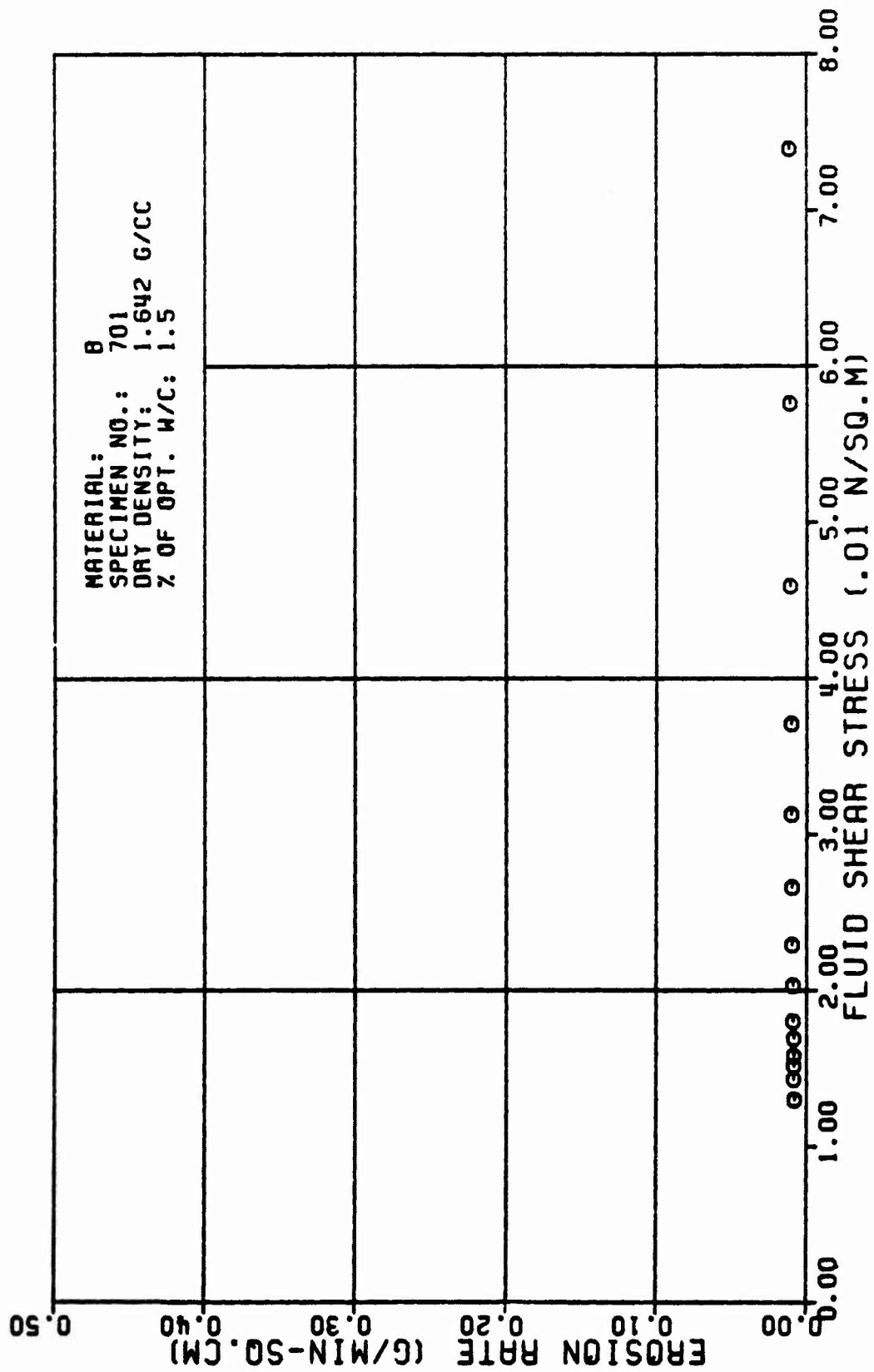


Figure A16e

TABLE A17

TEST RESULTS FOR TRIAXIAL EROSION TEST

MATERIAL TYPE: SPECIMEN NUMBER : TESTED BY:		D 178 R. L. SANCHEZ		568. CC/MIN					
DATE TESTED:		4 7 82		13.9 G/MIN					
SPECIMEN DRY DENSITY:		1.676 G/CC		1.888 G/CC					
% OF OPTIMUM WATER CONTENT:		-5.6 PERCENT		8.881 N*SEC/SO.M					
INITIAL SLOT WIDTH:		2.32 CM		98.18 KN/SQ.M					
INITIAL SLOT THICKNESS:		8.23 CM		13.88 M					
ERODED LENGTH:		11.58 CM		18. M/M					
VOLUME OF FLOW (1000 CC)	TIME (MIN)	CUM. WEIGHT ERODED (G)	CROSS SECTION AREA (SQ.CM)	VELOCITY OF FLOW (CM/MIN)	ERODED SURFACE AREA (SQ.CM)	CUM. WEIGHT ERODED PER AREA (G/SQ.CM)	EROSION RATE (GRAMS/ (MIN * SQ.CM))	FLUID SHEAR STRESS (N/SQ.M)	REYNOLDS NUMBER
2.5	4.88	82.4	3.8	164.	66.	8.68	8.16	8.818	496.
4.5	7.68	181.3	6.8	98.	113.	8.98	8.12	8.888	386.

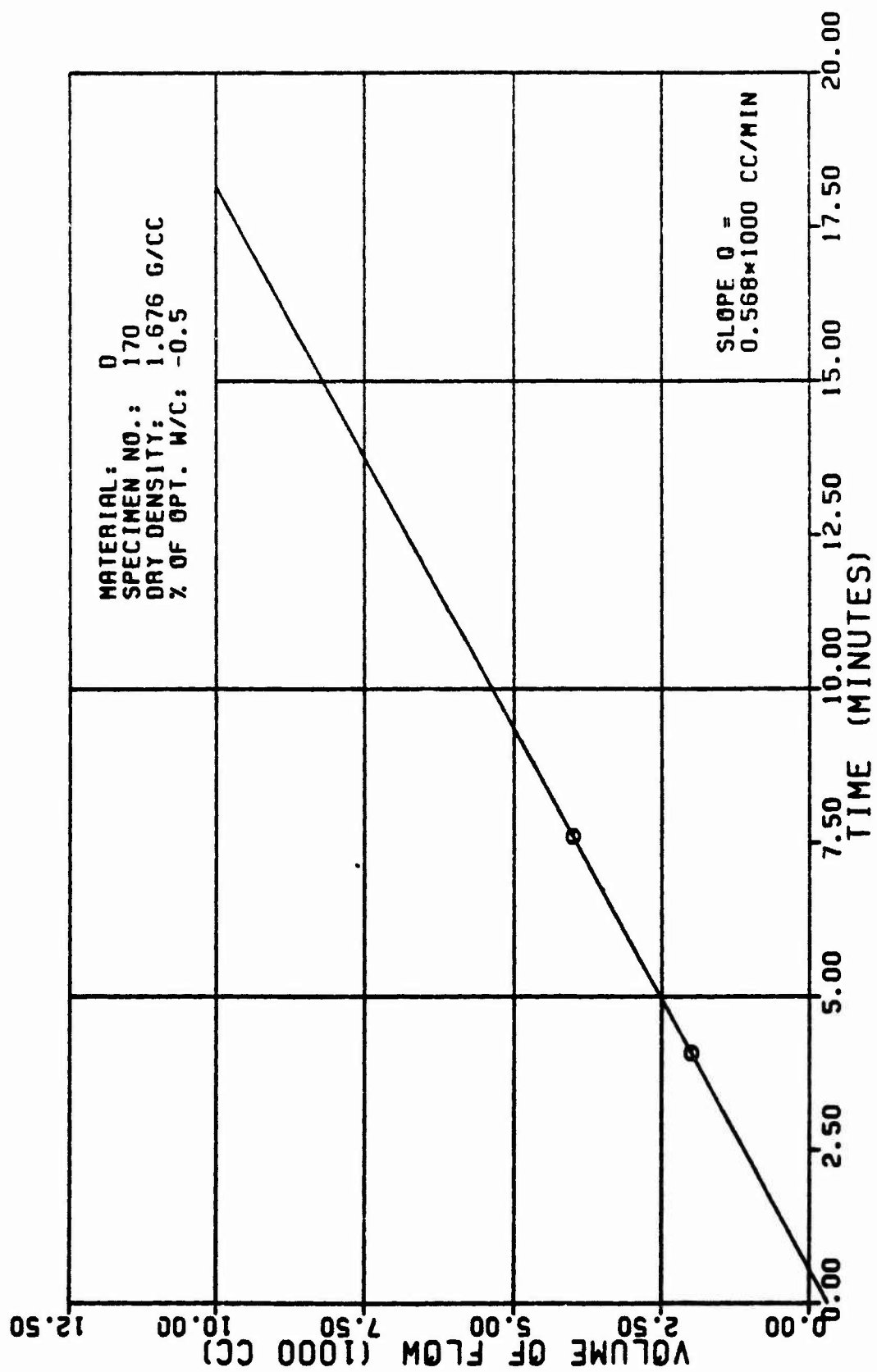


Figure A17a

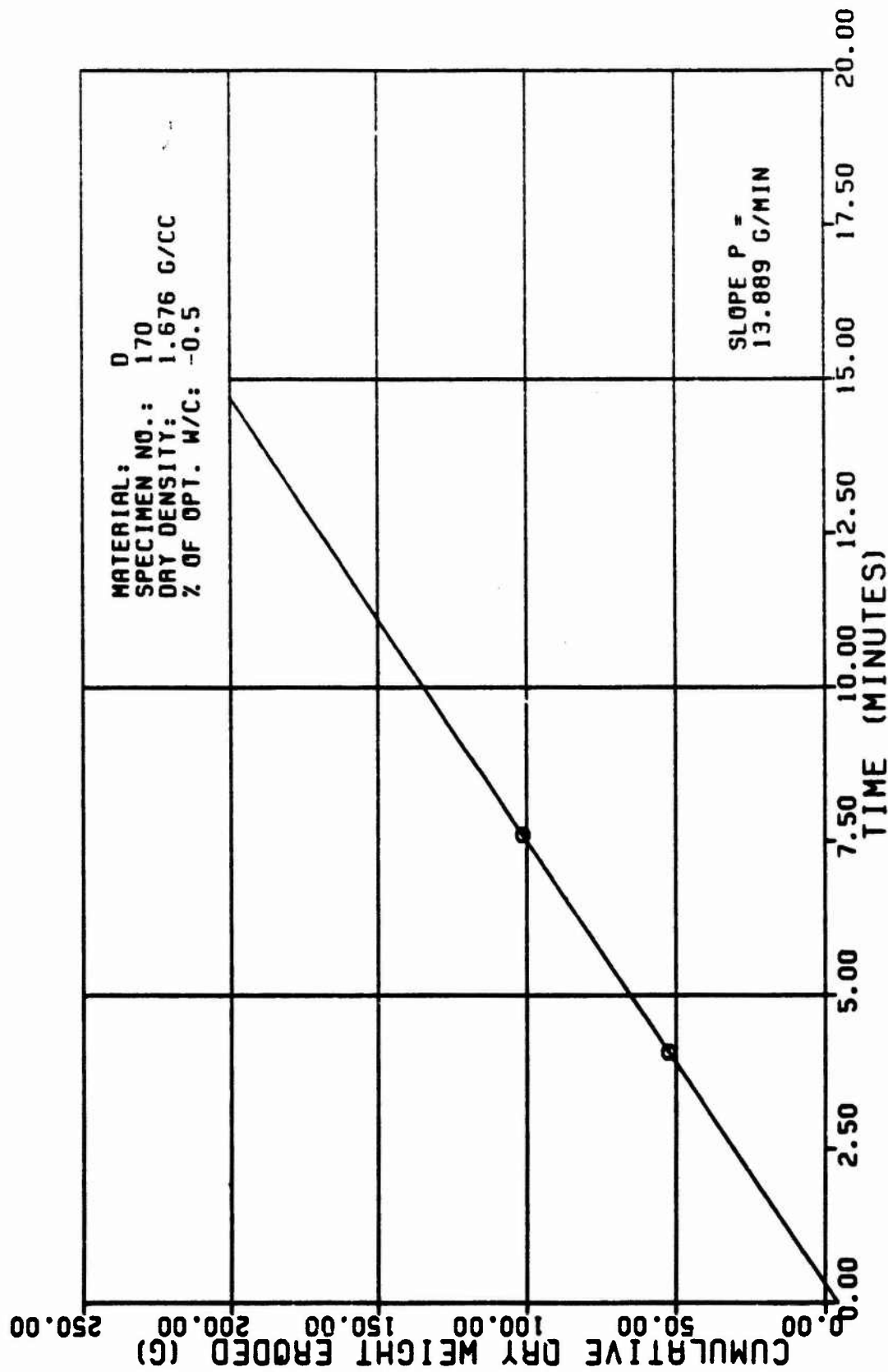


Figure A17b

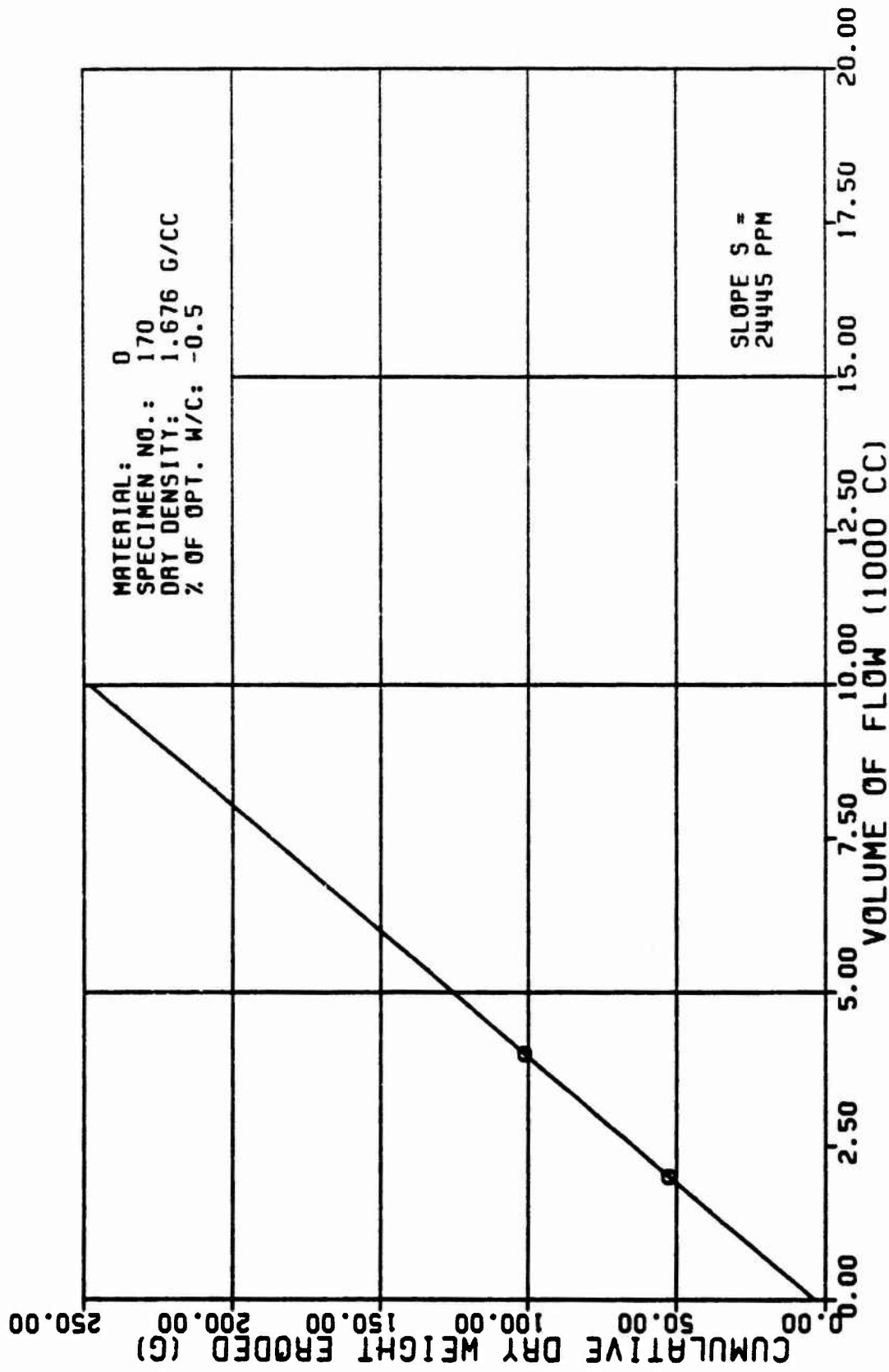


Figure A17c

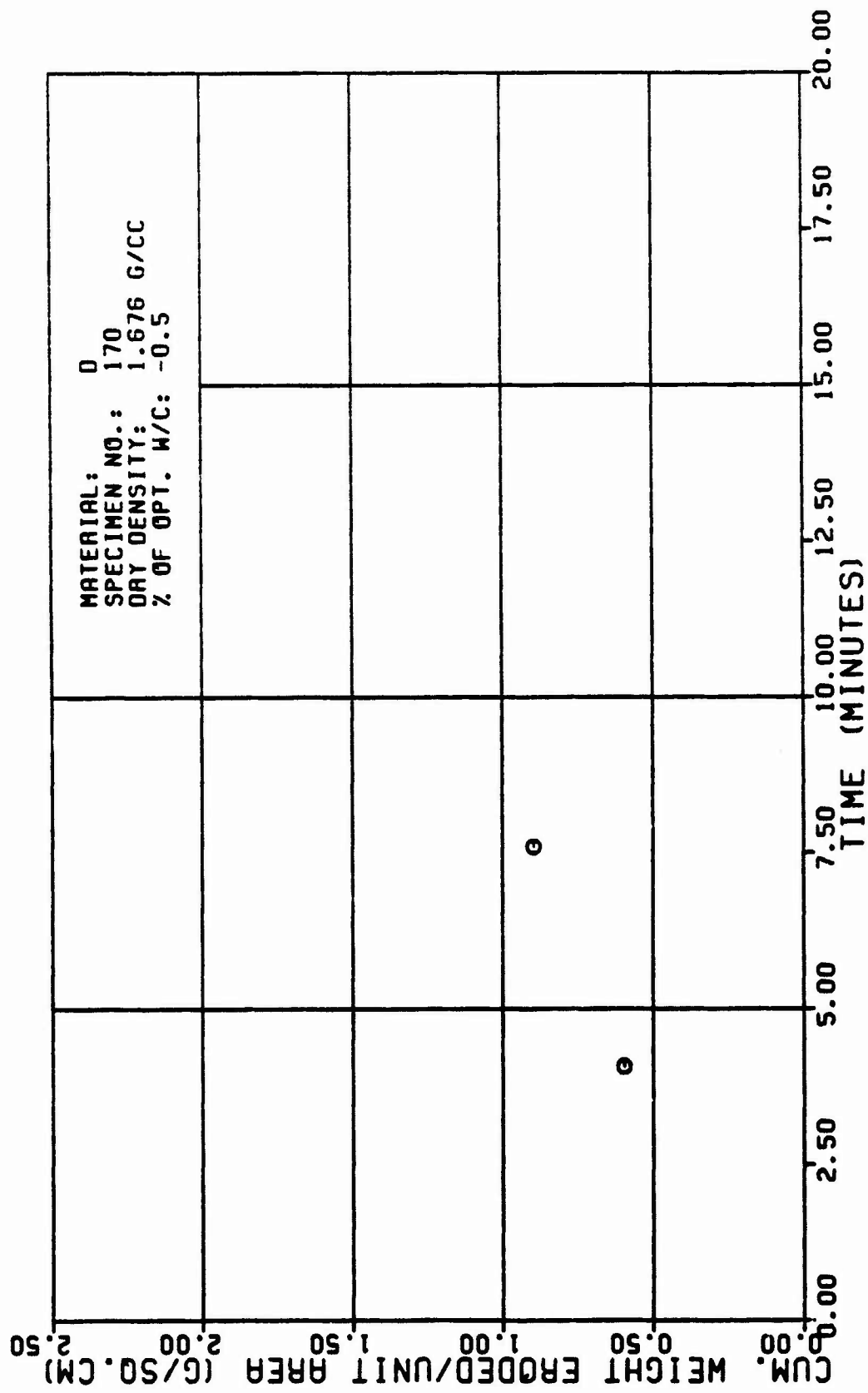


Figure A17d

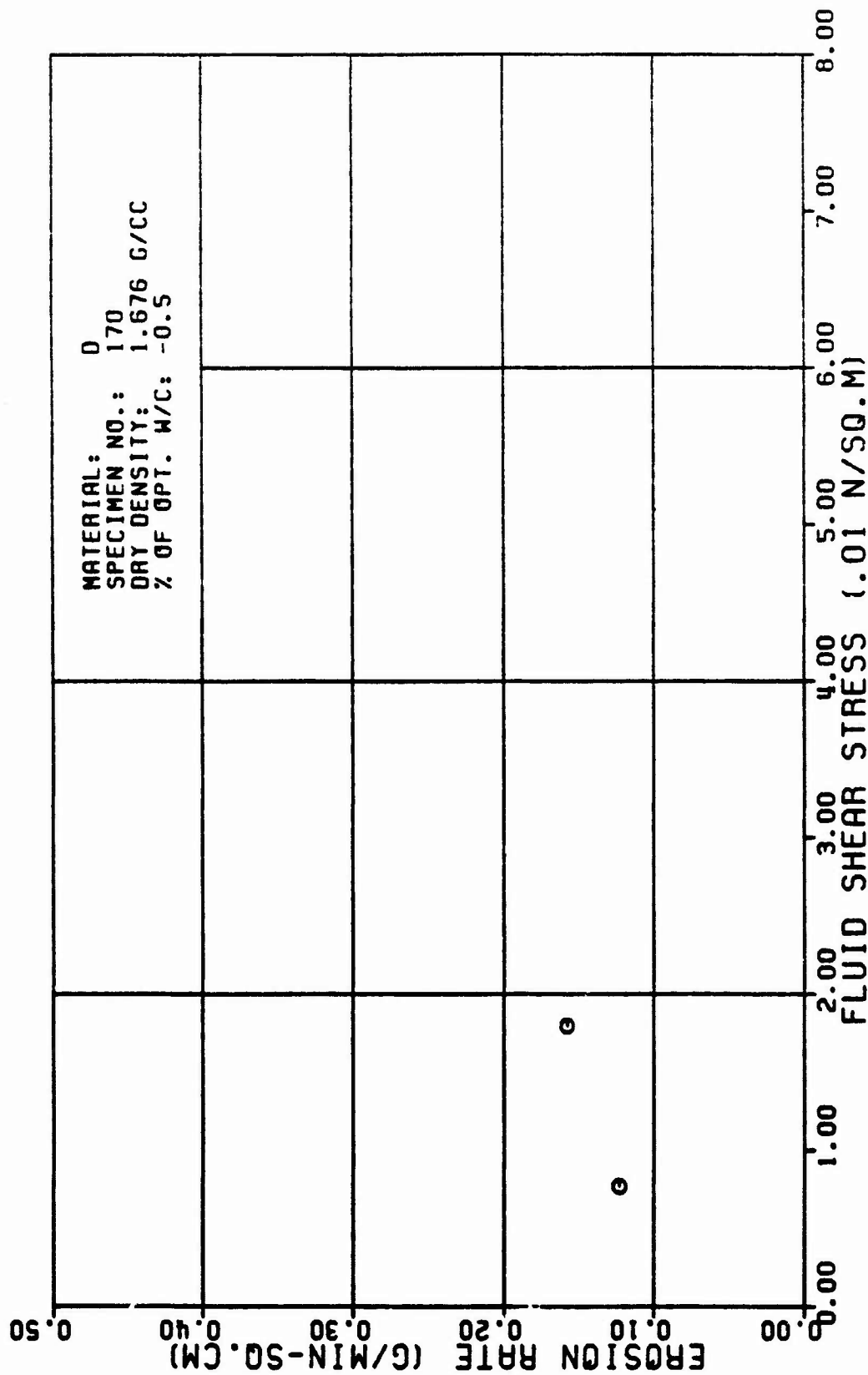


Figure A17e

TABLE A18

TEST RESULTS FOR TRIAXIAL EROSION TEST

MATERIAL TYPE: SPECIMEN NUMBER : TESTED BY:		D 171 R. L. SANCHEZ		585. CC/MIN					
DATE TESTED:		4 7 82		RATE OF WEIGHT EROSION (P):					
SPECIMEN DRY DENSITY:		1.659 G/CC		1.888 G/CC					
% OF OPTIMUM WATER CONTENT:		1.8 PERCENT		8.881 N-SEC/SQ.M					
INITIAL SLOT WIDTH:		2.32 CM		98.18 KN/SQ.M					
INITIAL SLOT THICKNESS:		8.23 CM		13.88 M					
ERODED LENGTH:		11.68 CM		18. M/M					
AVERAGE FLOW RATE (Q):									
DENSITY OF ERODING FLUID:									
VISCOSITY OF ERODING FLUID:									
CONFINING PRESSURE:									
HEAD OF WATER:									
HYDRAULIC GRADIENT:									
EROSION RATE (GRAMS/ (MIN * SQ.CM))		CUM. WEIGHT ERODED PER AREA (G/SQ.CM)		FLUID SHEAR STRESS (N/SQ.M)					
ERODED SURFACE AREA (SQ.CM)		VELOCITY OF FLOW (CM/MIN)		REYNOLDS NUMBER					
CROSS SECTION AREA (SQ.CM)		CUM. WEIGHT ERODED (G)							
TIME (MIN)		VOLUME OF FLOW (1000 CC)							
1.8	1.77	43.9	2.3	259.	76.	8.57	8.25	8.838	592.
2.8	3.57	75.8	4.8	146.	94.	8.81	8.28	8.815	481.
3.8	5.29	189.1	5.7	183.	111.	8.98	8.17	8.889	488.
3.8	6.48	131.7	6.8	86.	122.	1.88	8.15	8.887	378.

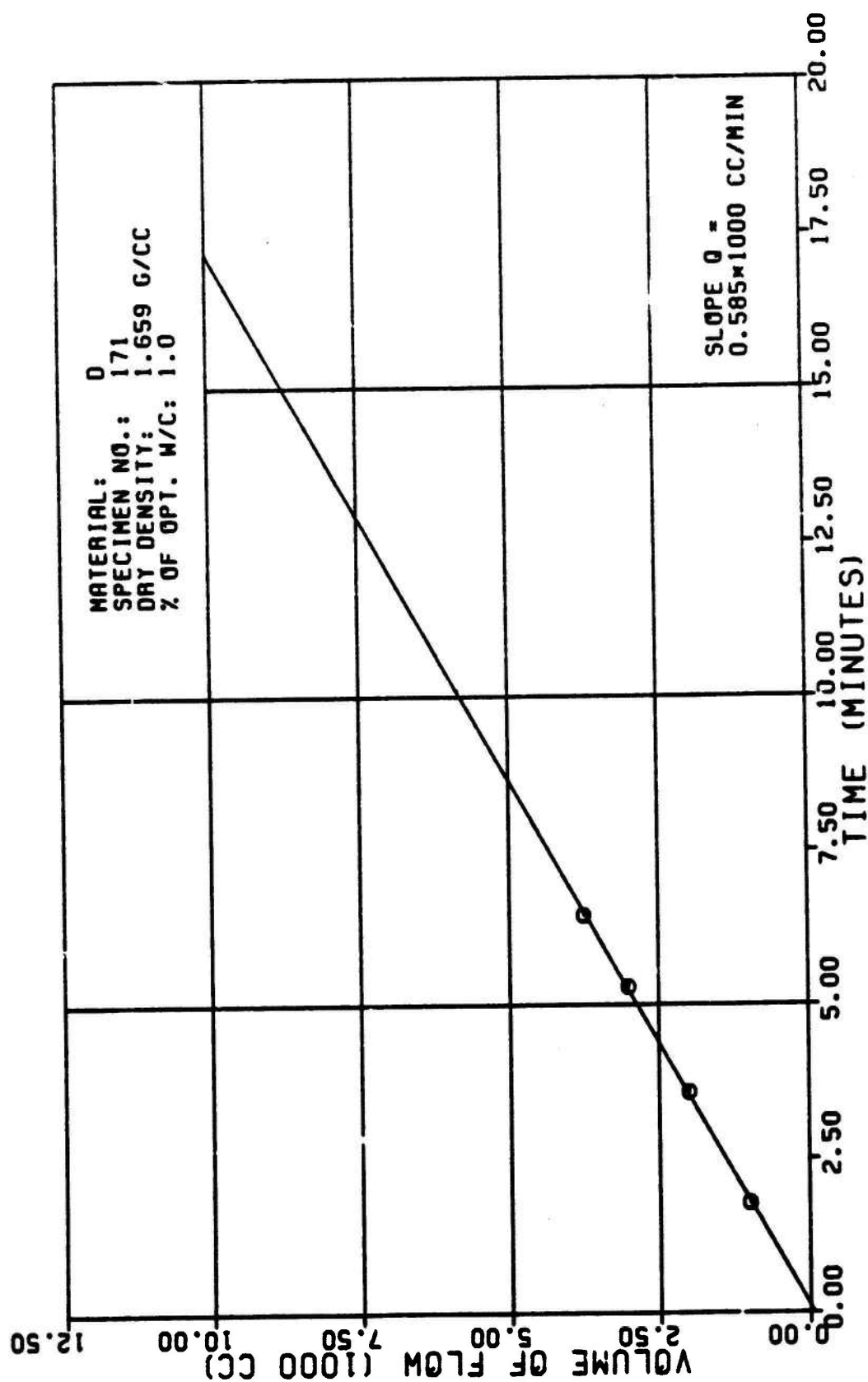


Figure A18a

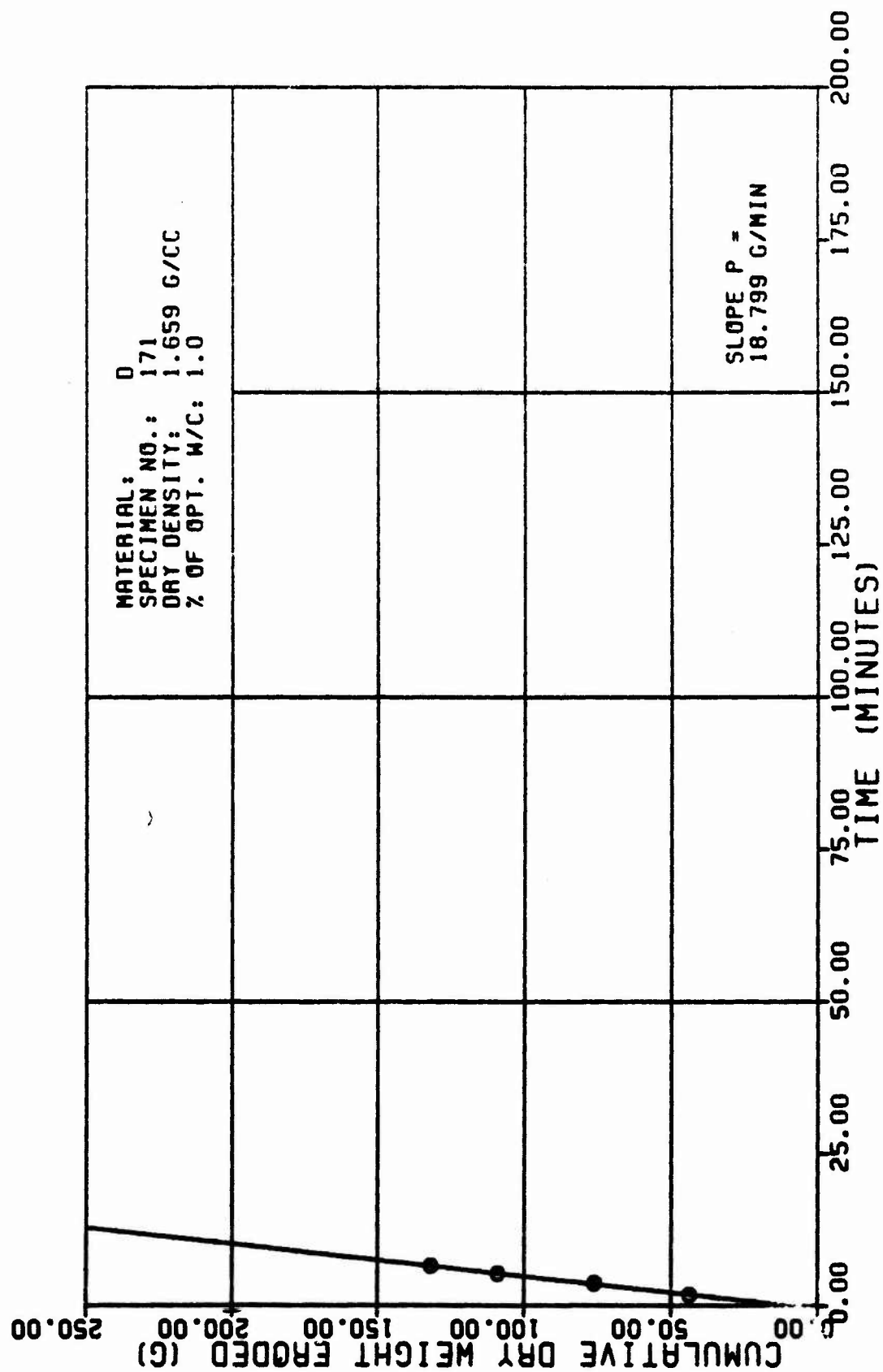


Figure A18b

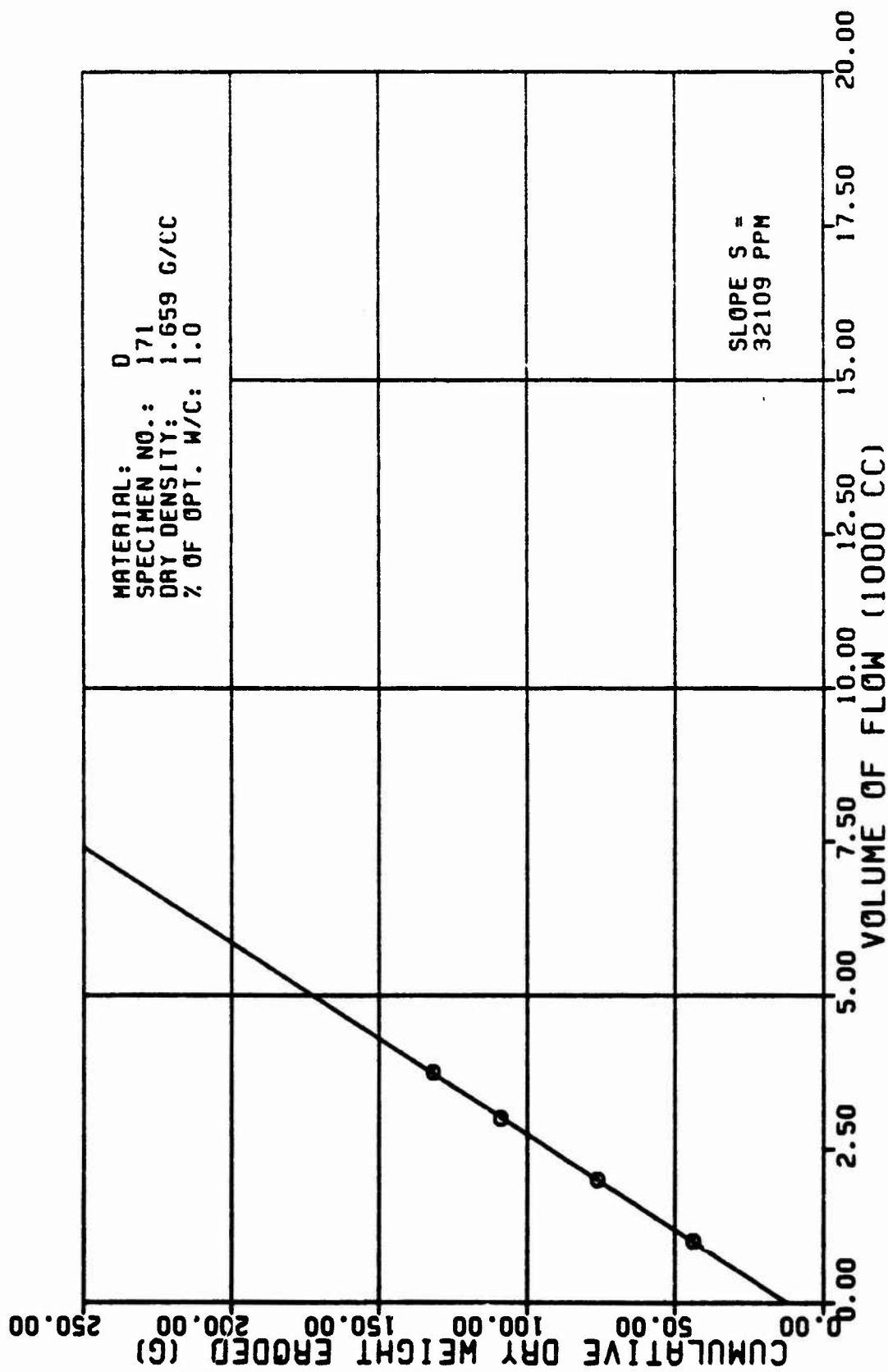


Figure A18c

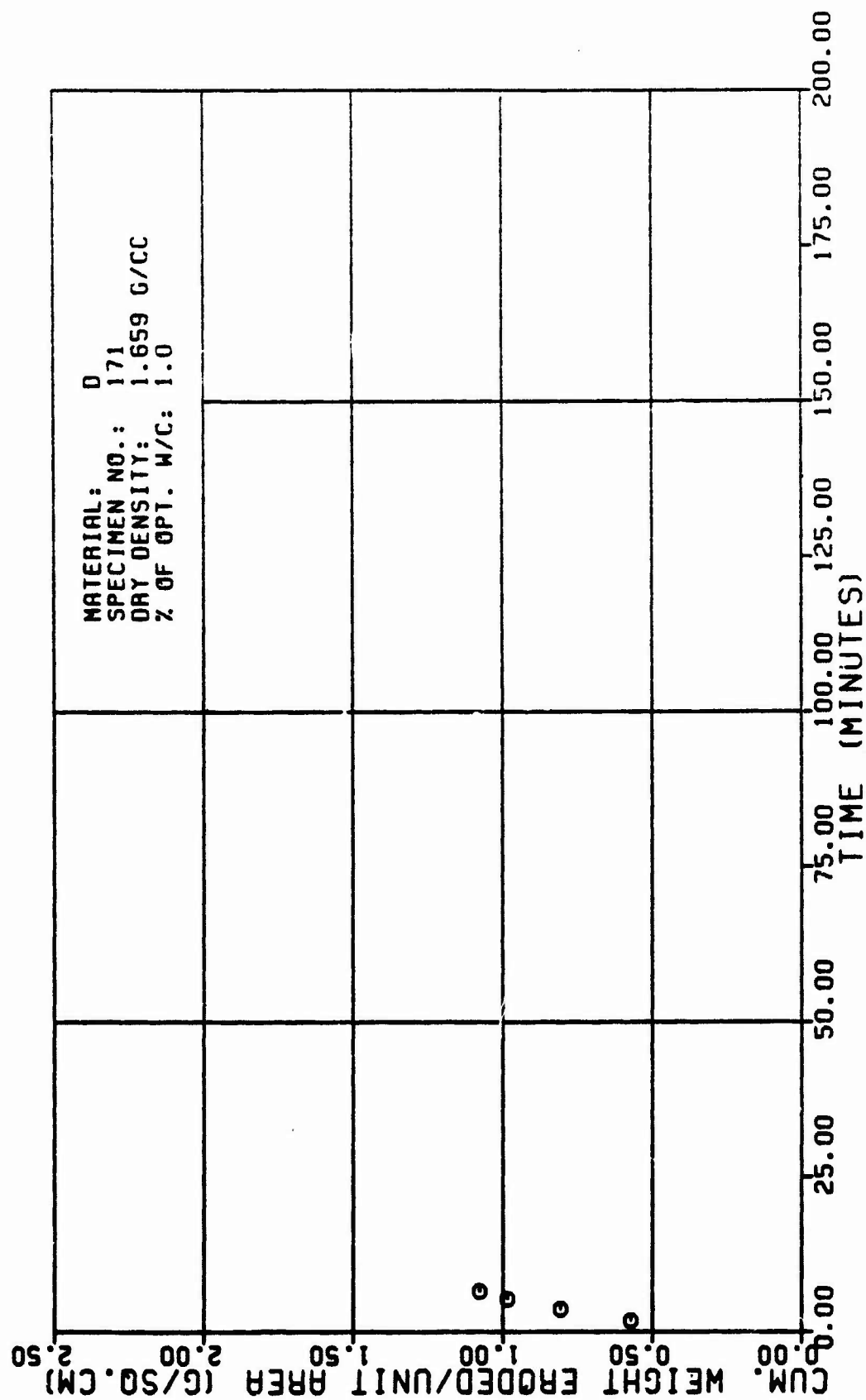


Figure A18d

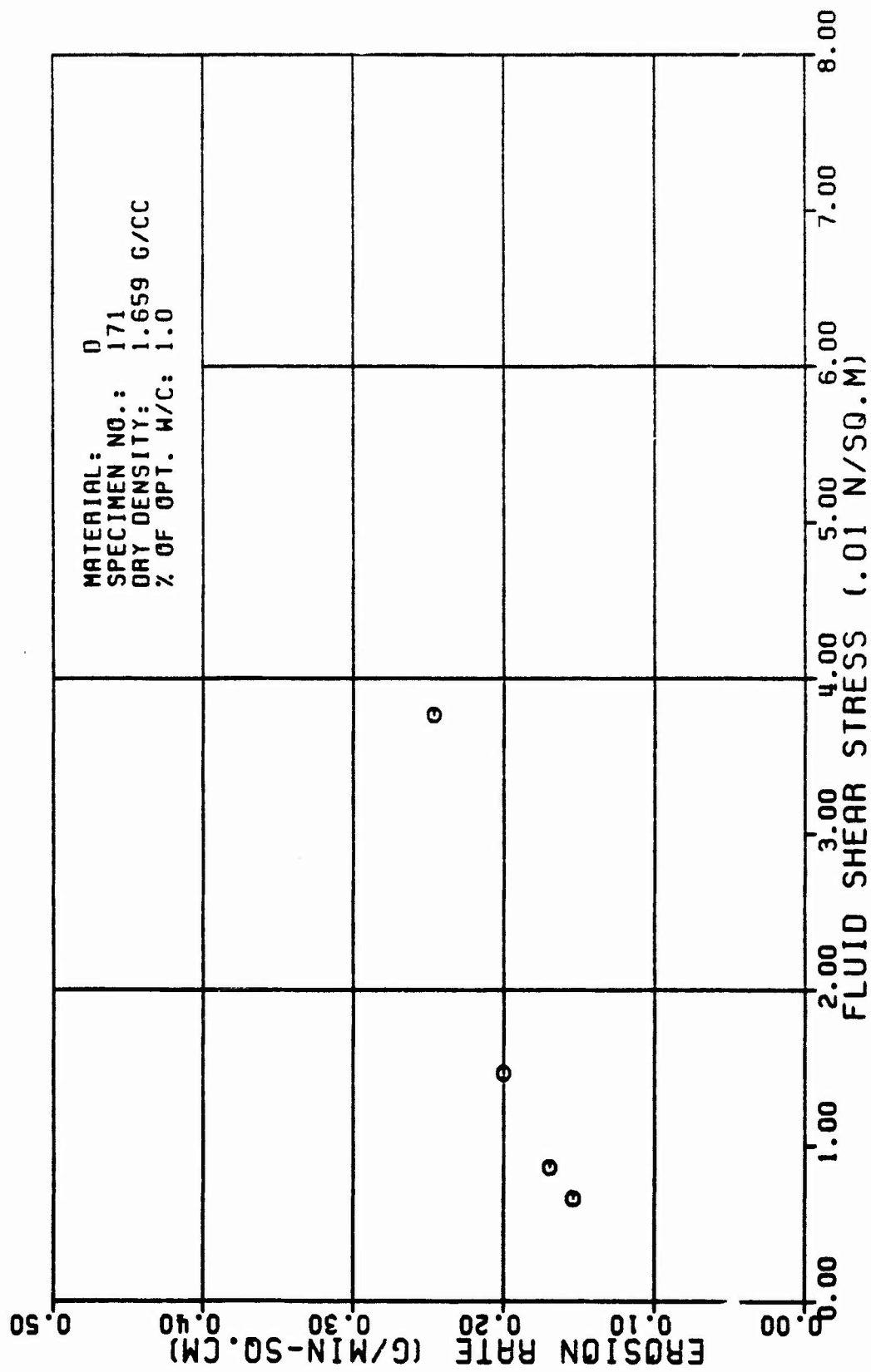


Figure A18e

TABLE A19

TEST RESULTS FOR TRIAXIAL EROSION TEST

MATERIAL TYPE: SPECIMEN NUMBER : TESTED BY:		B 172 R. L. SANCHEZ		555. CC/MIN					
DATE TESTED:		4 11 82		14.2 G/MIN					
SPECIMEN DRY DENSITY:		1.722 G/CC		1.555 G/CC					
X OF OPTIMUM WATER CONTENT:		1.0 percent		5.551 N*SEC/SQ.M					
INITIAL SLOT WIDTH:		2.32 CM		98.15 KN/SQ.M					
INITIAL SLOT THICKNESS:		5.23 CM		13.55 M					
ERODED LENGTH:		11.65 CM		15. M/M					
VOLUME OF FLOW (1000 CC)	TIME (MIN)	CUM. WEIGHT ERODED (G)	CROSS SECTION AREA (SQ.CM)	VELOCITY OF FLOW (CM/MIN)	ERODED SURFACE AREA (SQ.CM)	CUM. WEIGHT ERODED PER AREA (G/SQ.CM)	EROSION RATE (GRAMS/ (MIN * SQ.CM))	FLUID SHEAR STRESS (N/SQ.M)	REYNOLDS NUMBER
1.5	2.15	21.8	2.5	247.	74.	8.29	8.19	8.539	522.
2.5	4.11	45.1	3.5	145.	88.	8.51	8.16	8.516	438.
3.5	6.15	78.6	4.9	103.	152.	8.77	8.14	8.559	377.

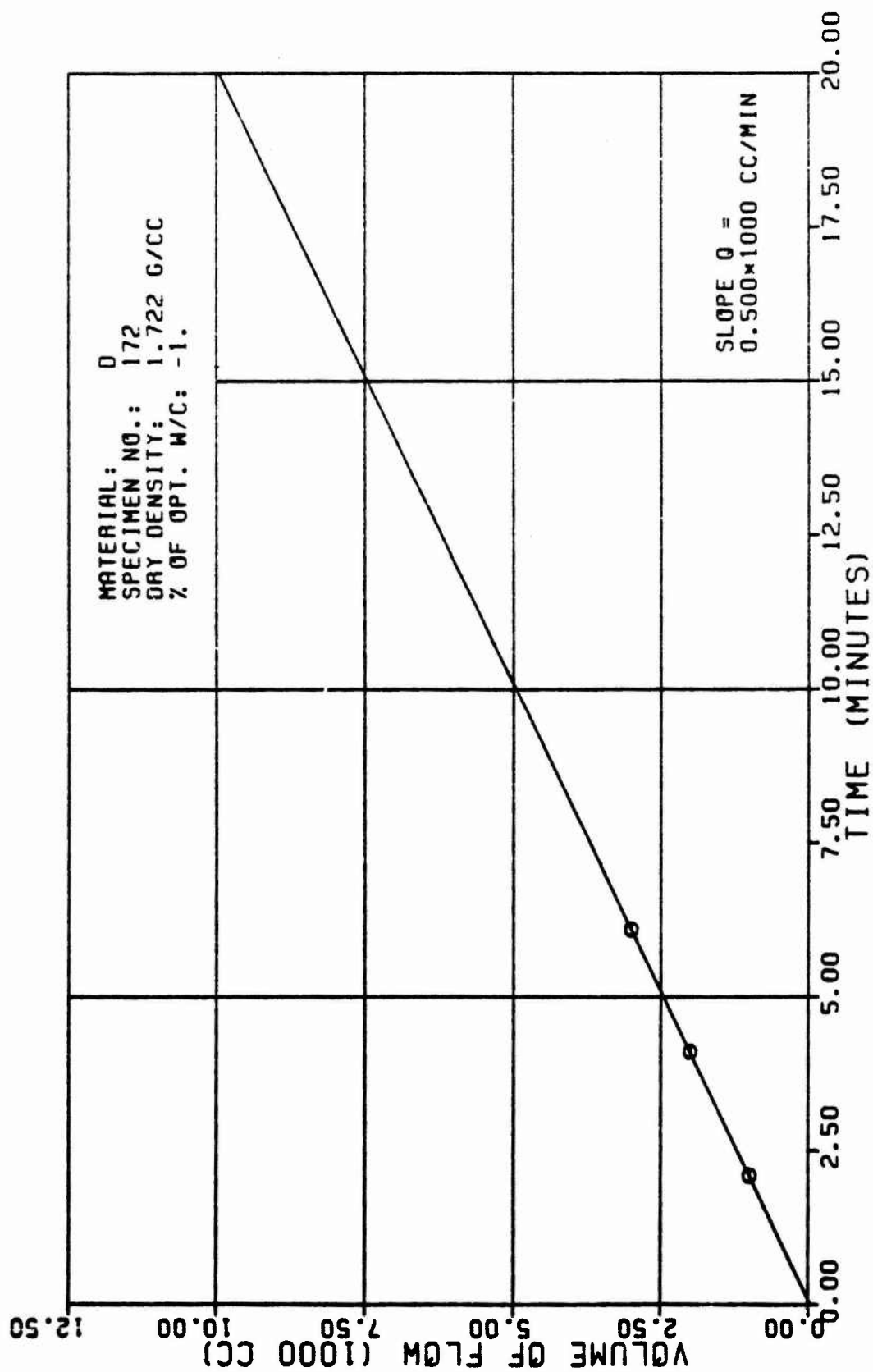


Figure A19a

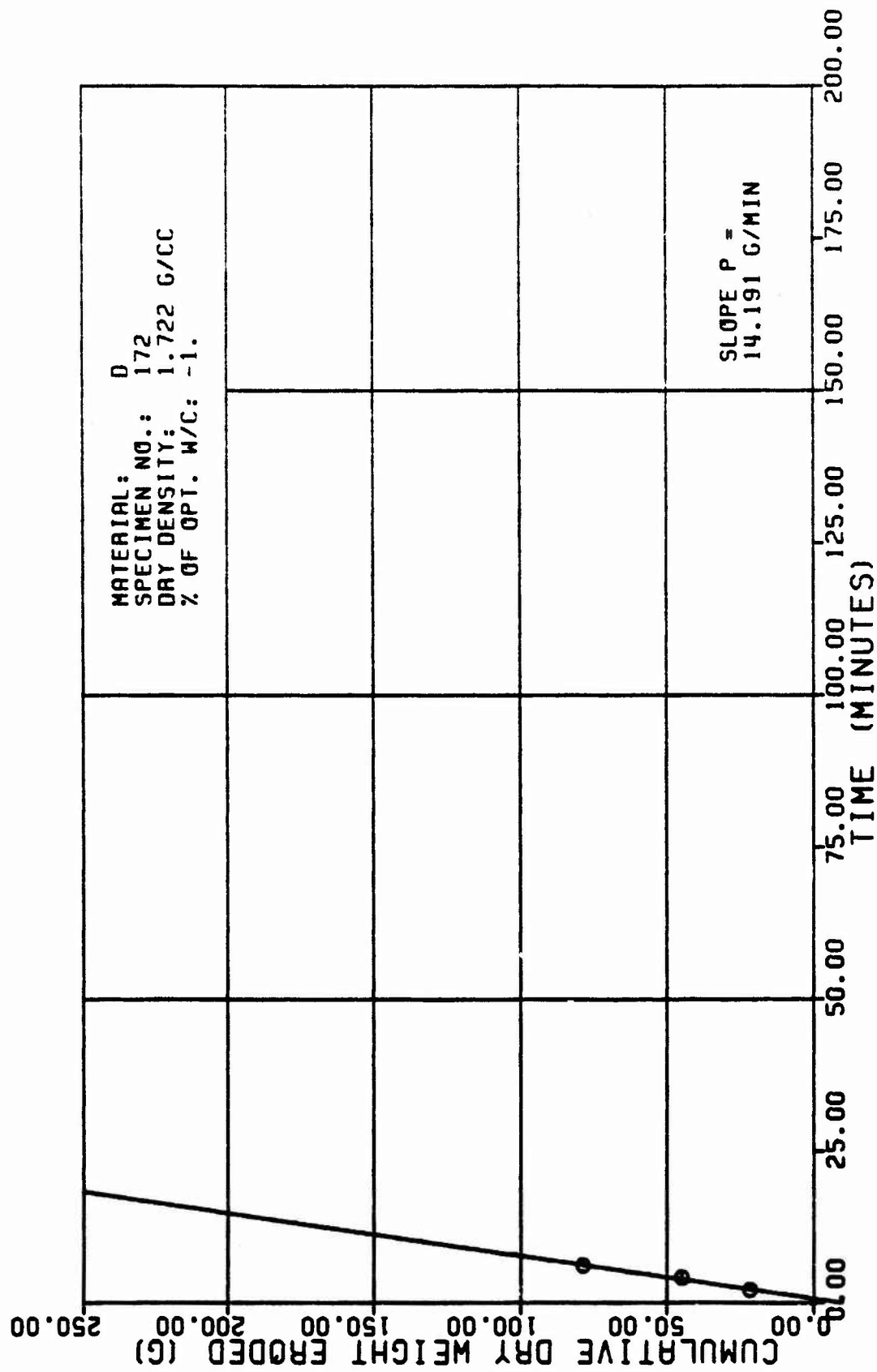


Figure A19b

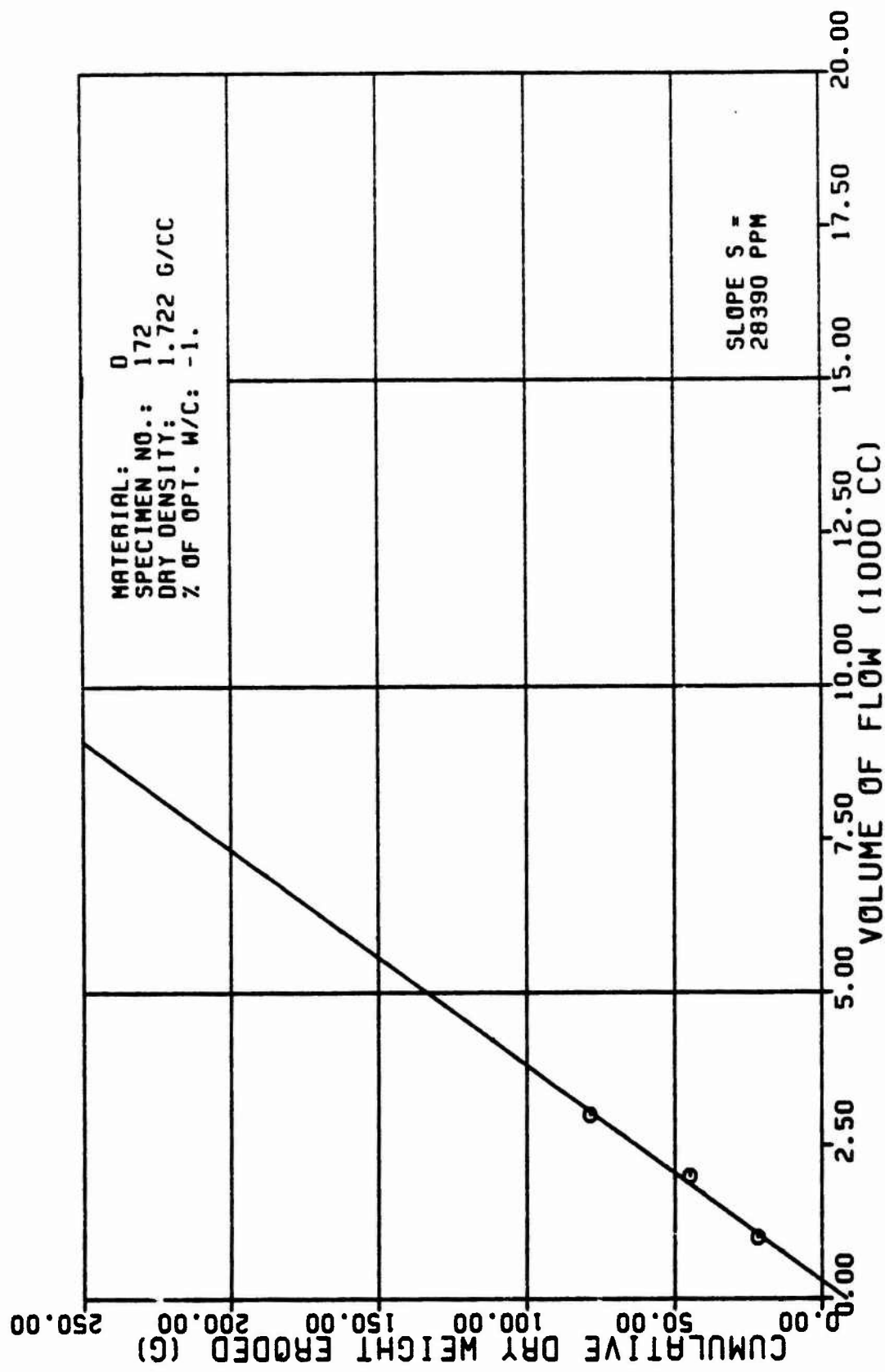


Figure A19c

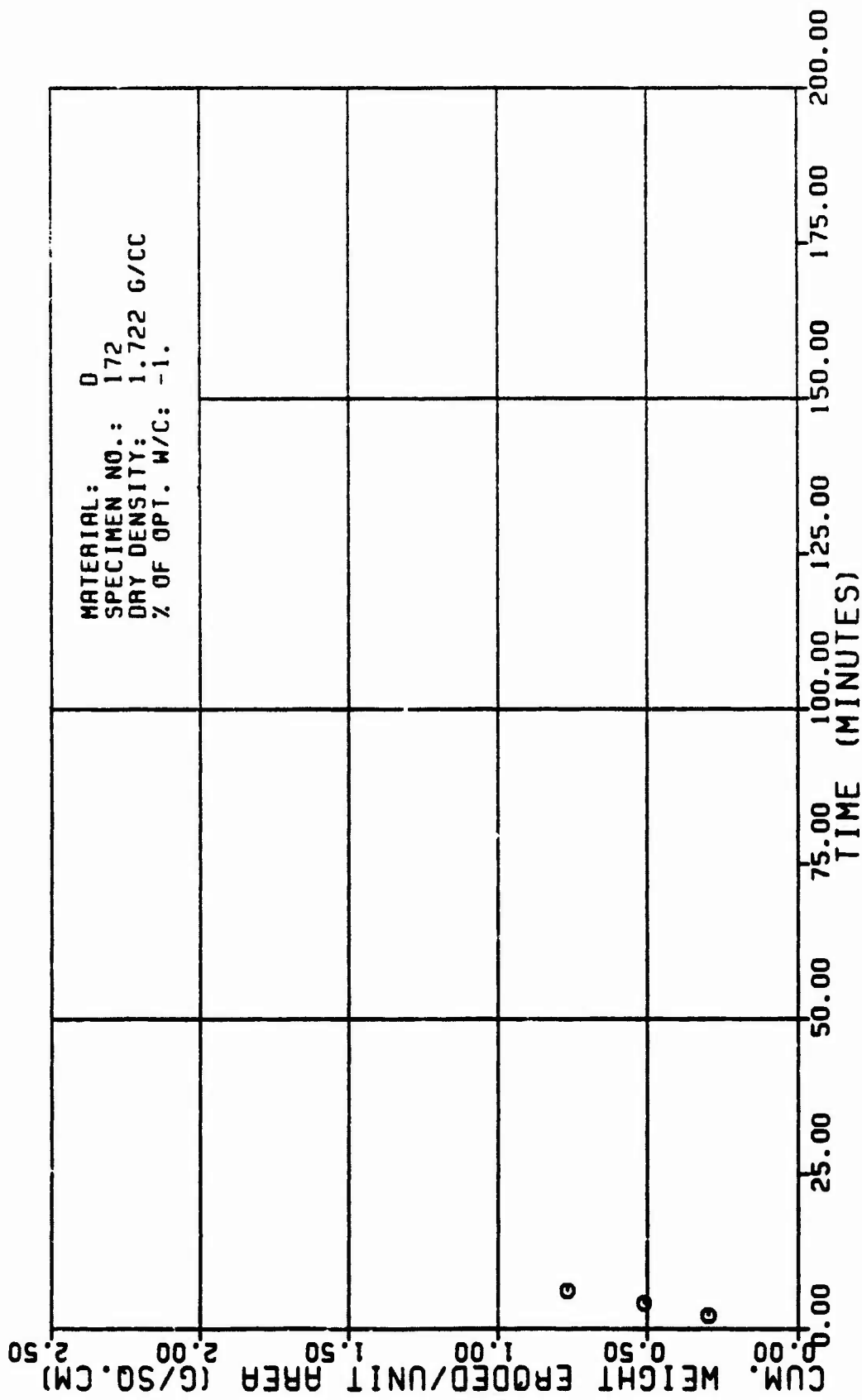


Figure A19d

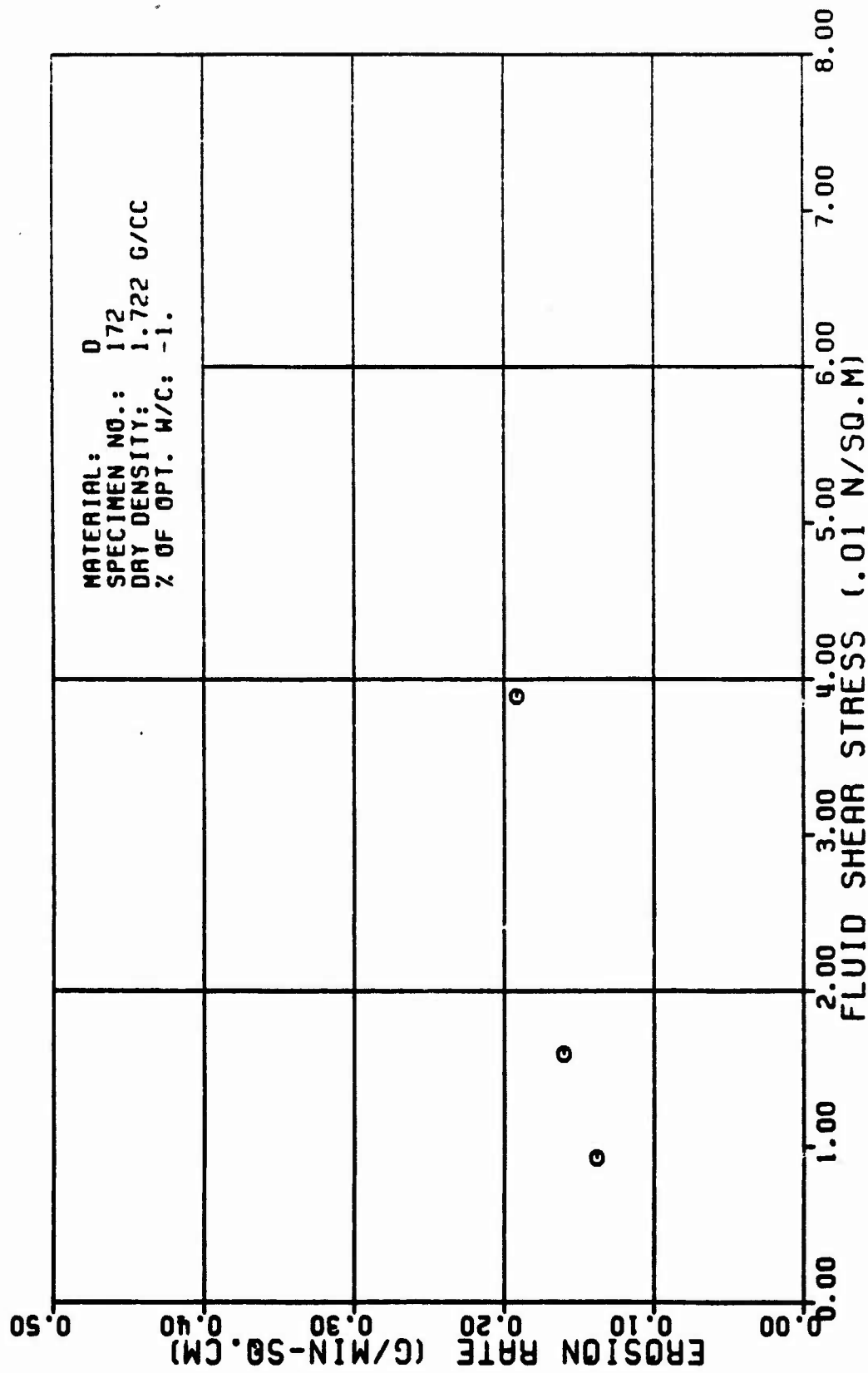


Figure A19e

TEST RESULTS FOR TRIAXIAL EROSION TEST

MATERIAL TYPE: D 173		SPECIMEN NUMBER : R. L. SANCHEZ		AVERAGE FLOW RATE (Q): 616. CC/MIN					
TESTED BY:		DATE TESTED: 4 14 82		RATE OF WEIGHT EROSION (P): 35.6 G/MIN					
SPECIMEN DRY DENSITY: 1.682 G/CC		DENSITY OF ERODING FLUID: 1.888 G/CC		G/CC					
% OF OPTIMUM WATER CONTENT: -3.8 PERCENT		VISCOSITY OF ERODING FLUID: 8.881 N*SEC/SQ.M		N*SEC/SQ.M					
INITIAL SLOT WIDTH: 2.32 CM		CONFINING PRESSURE: 98.18 KN/SQ.M		KN/SQ.M					
INITIAL SLOT THICKNESS: 8.23 CM		HEAD OF WATER: 13.88 M		M					
ERODED LENGTH: 11.88 CM		HYDRAULIC GRADIENT: 18. M/M		M/M					

VOLUME OF FLOW (1000 CC)	TIME (MIN)	CUM. WEIGHT ERODED (G)	CROSS SECTION AREA (SQ.CM)	VELOCITY OF FLOW (CM/MIN)	ERODED SURFACE AREA (SQ.CM)	CUM. WEIGHT ERODED PER AREA (G/SQ.CM)	EROSION RATE (GRAMS/ (MIN * SQ.CM))	FLUID SHEAR STRESS (N/SQ.M)	REYNOLDS NUMBER
1.8	2.38	47.4	4.9	126.	182.	8.47	8.36	8.811	464.
2.8	3.98	99.6	7.9	78.	132.	8.76	8.28	8.886	358.
2.2	4.26	122.4	8.6	72.	139.	8.88	8.26	8.885	341.
-----						-----			

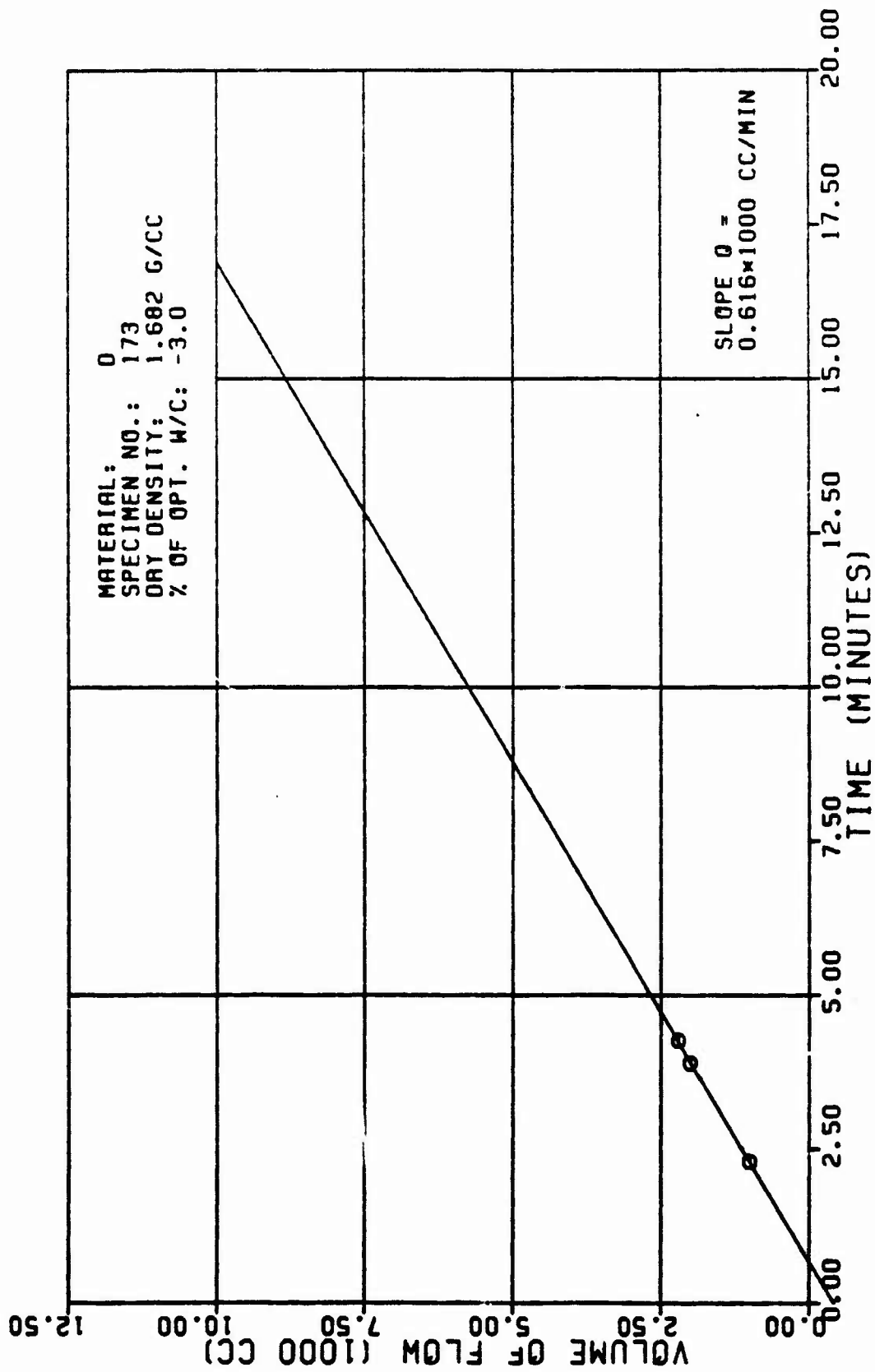


Figure A20a

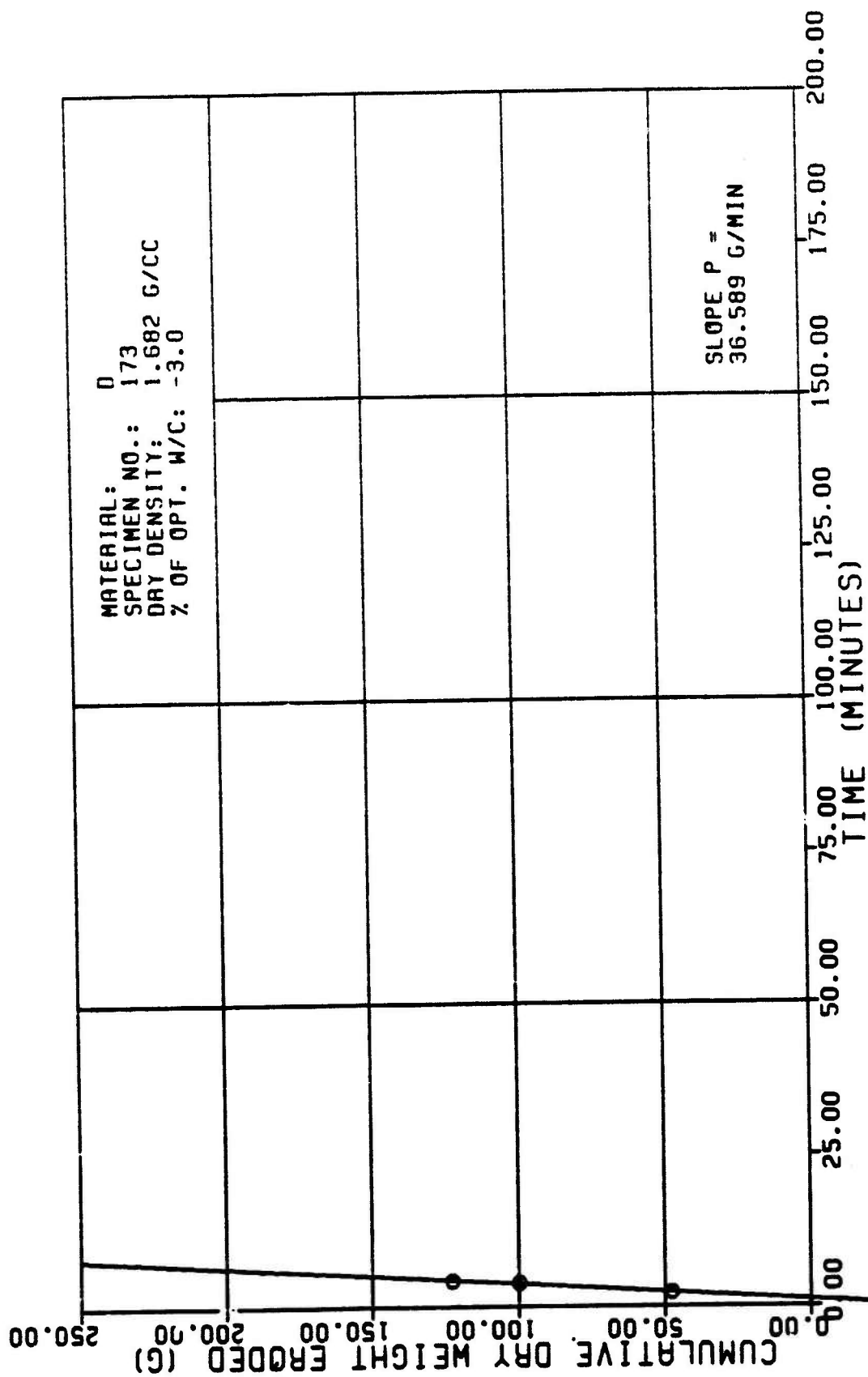


Figure A20b

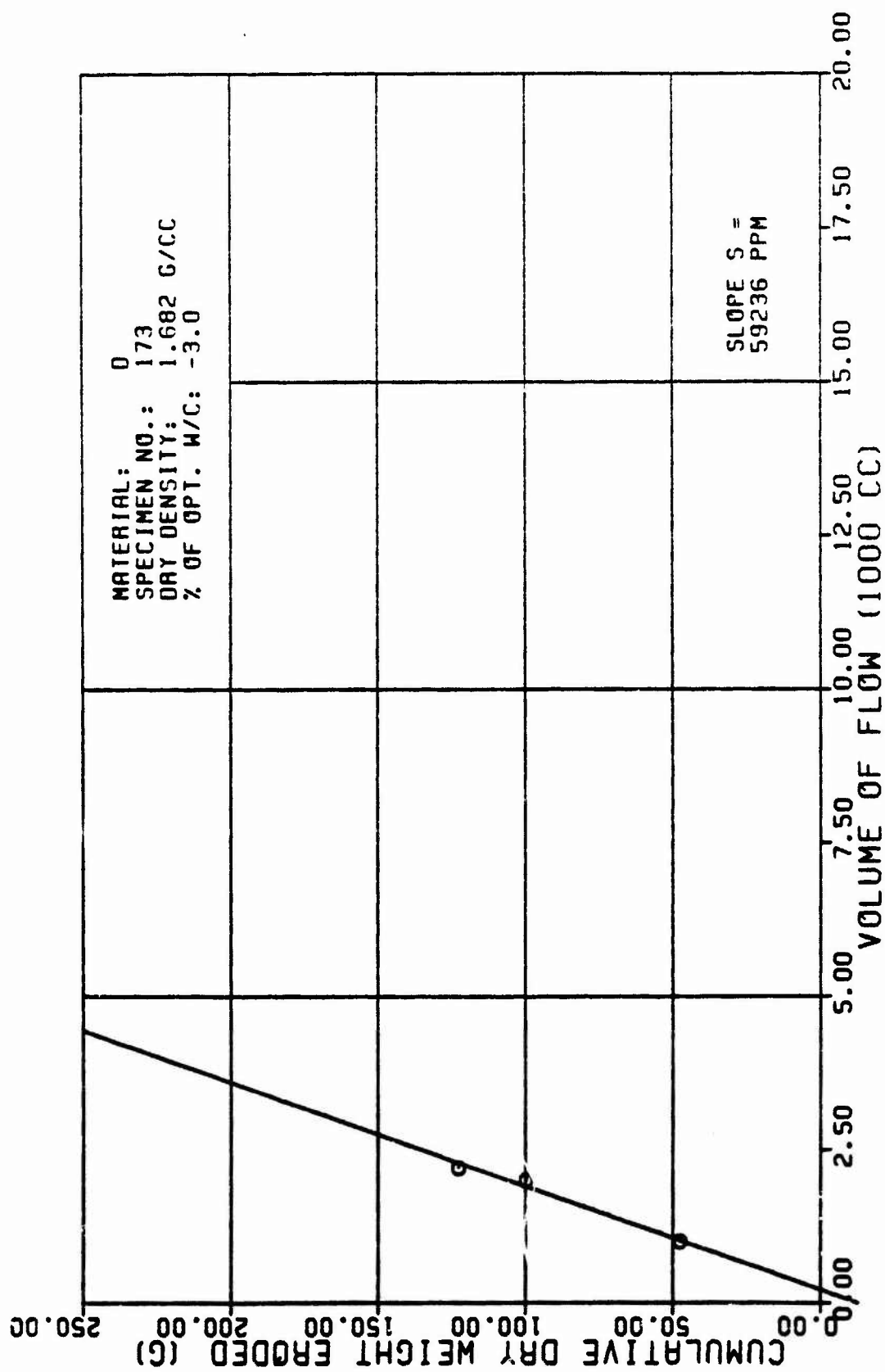


Figure A20c

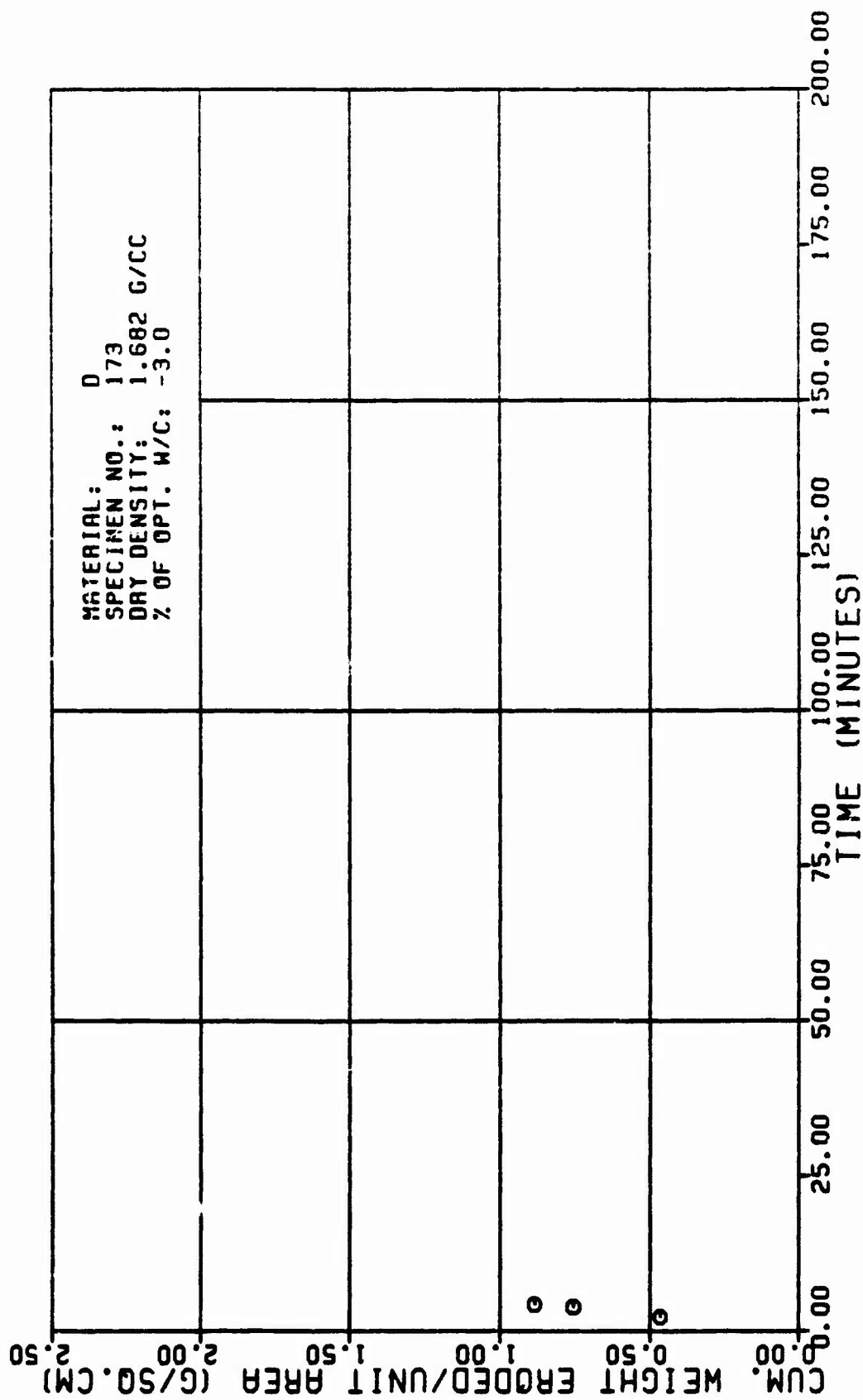


Figure A20d

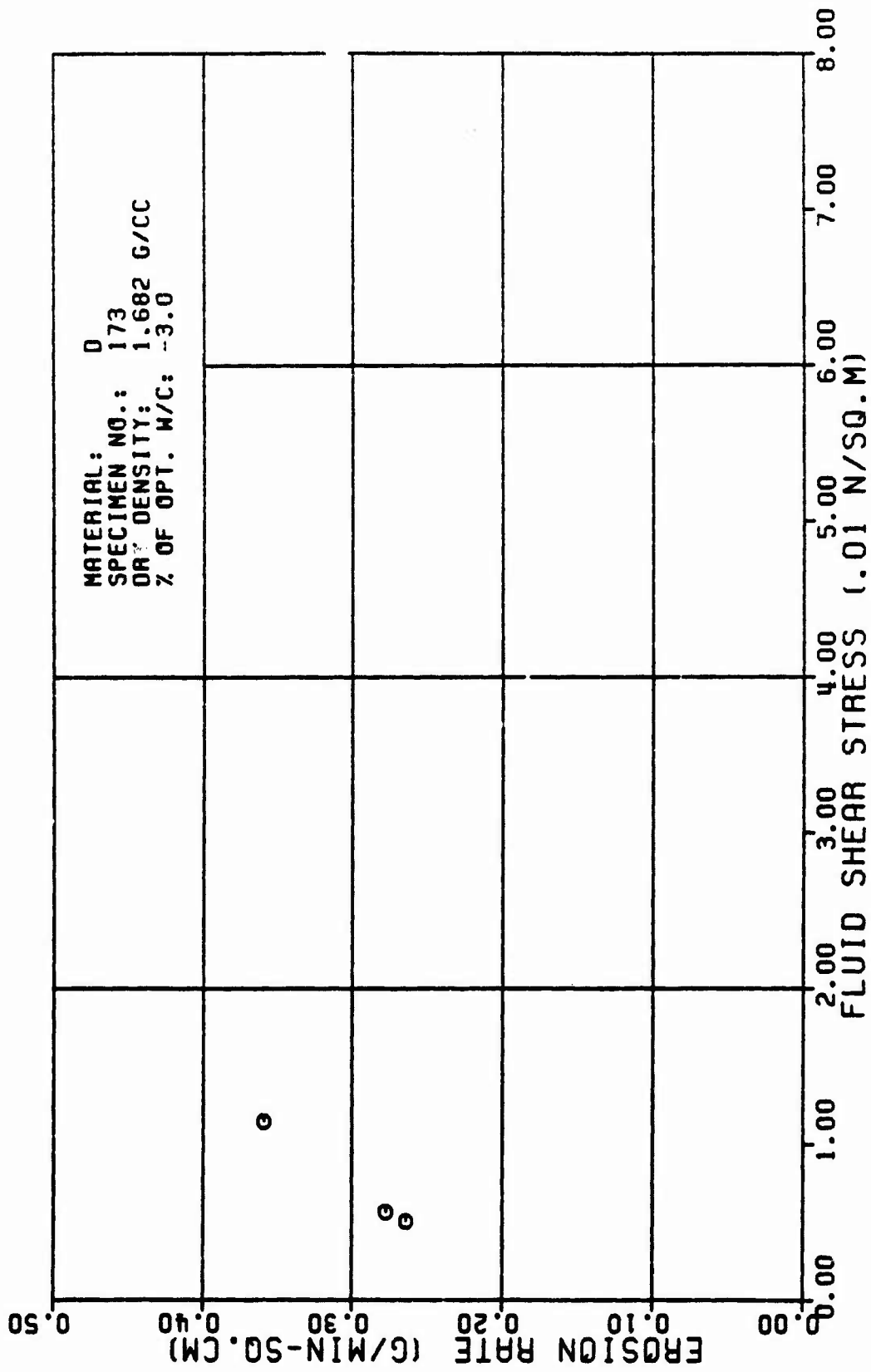


Figure A20e

TABLE A21

TEST RESULTS FOR TRIAXIAL EROSION TEST

MATERIAL TYPE: SPECIMEN NUMBER : TESTED BY:		D 175 R. L. SANCHEZ		AVERAGE FLOW RATE (Q):		552. CC/MIN													
DATE TESTED:		5 28 82		RATE OF WEIGHT EROSION (P):		11.1 G/MIN													
SPECIMEN DRY DENSITY:		1.680 G/CC		DENSITY OF ERODING FLUID:		1.000 G/CC													
% OF OPTIMUM WATER CONTENT:		-1.0 PERCENT		VISCOSITY OF ERODING FLUID:		0.001 M*SEC/SO.M													
INITIAL SLOT WIDTH:		2.30 CM		CONFINING PRESSURE:		90.00 KN/SO.M													
INITIAL SLOT THICKNESS:		0.23 CM		HEAD OF WATER:		1.30 M													
ERODED LENGTH:		11.50 CM		HYDRAULIC GRADIENT:		1.0 M/M													
VOLUME OF FLOW (1000 CC)		CUM. WEIGHT ERODED (G)		CROSS SECTION AREA (SQ.CH)		VELOCITY OF FLOW (CM/MIN)		ERODED SURFACE AREA (SQ.CH)		CUM. WEIGHT ERODED PER AREA (G/SQ.CH)		EROSION RATE (GRAMS/ (MIN * SQ.CH))		FLUID SHEAR STRESS (N/SO.M)		REYNOLDS NUMBER			
0.5		0.05		6.9		1.0		544.		63.		0.11		0.18		0.147		671.	
1.0		1.70		16.3		1.5		368.		68.		0.23		0.16		0.073		623.	
1.5		2.53		24.4		2.0		208.		73.		0.34		0.15		0.045		502.	
2.0		3.49		35.9		2.5		219.		78.		0.46		0.14		0.030		542.	
2.5		4.44		46.5		3.0		102.		83.		0.56		0.13		0.022		508.	
3.0		5.36		57.4		3.6		154.		89.		0.65		0.12		0.017		477.	
3.5		6.22		67.6		4.1		135.		94.		0.72		0.12		0.014		452.	
4.0		7.22		77.6		4.6		119.		99.		0.70		0.11		0.011		426.	

TABLE FOR SPECIMEN NUMBER: D175 (CONTINUES)

VOLUME OF FLOW (1000 CC)	TIME (MIN)	CUM. WEIGHT ERODED (G)	CROSS SECTION AREA (SQ. CM)	VELOCITY OF FLOW (CM/MIN)	ERODED SURFACE AREA (SQ. CM)	CUM. WEIGHT ERODED PER AREA (G/SQ. CM)	EROSION RATE (GRAMS/ (MIN * SQ. CM))	FLUID SHEAR STRESS (N/SQ. M)	REYNOLDS NUMBER
4.5	9.16	87.3	5.2	106.	105.	8.03	8.11	8.809	404.
5.5	9.73	106.2	6.1	91.	114.	8.93	8.18	8.807	372.
6.5	10.78	114.6	6.7	83.	128.	8.96	8.89	8.886	353.

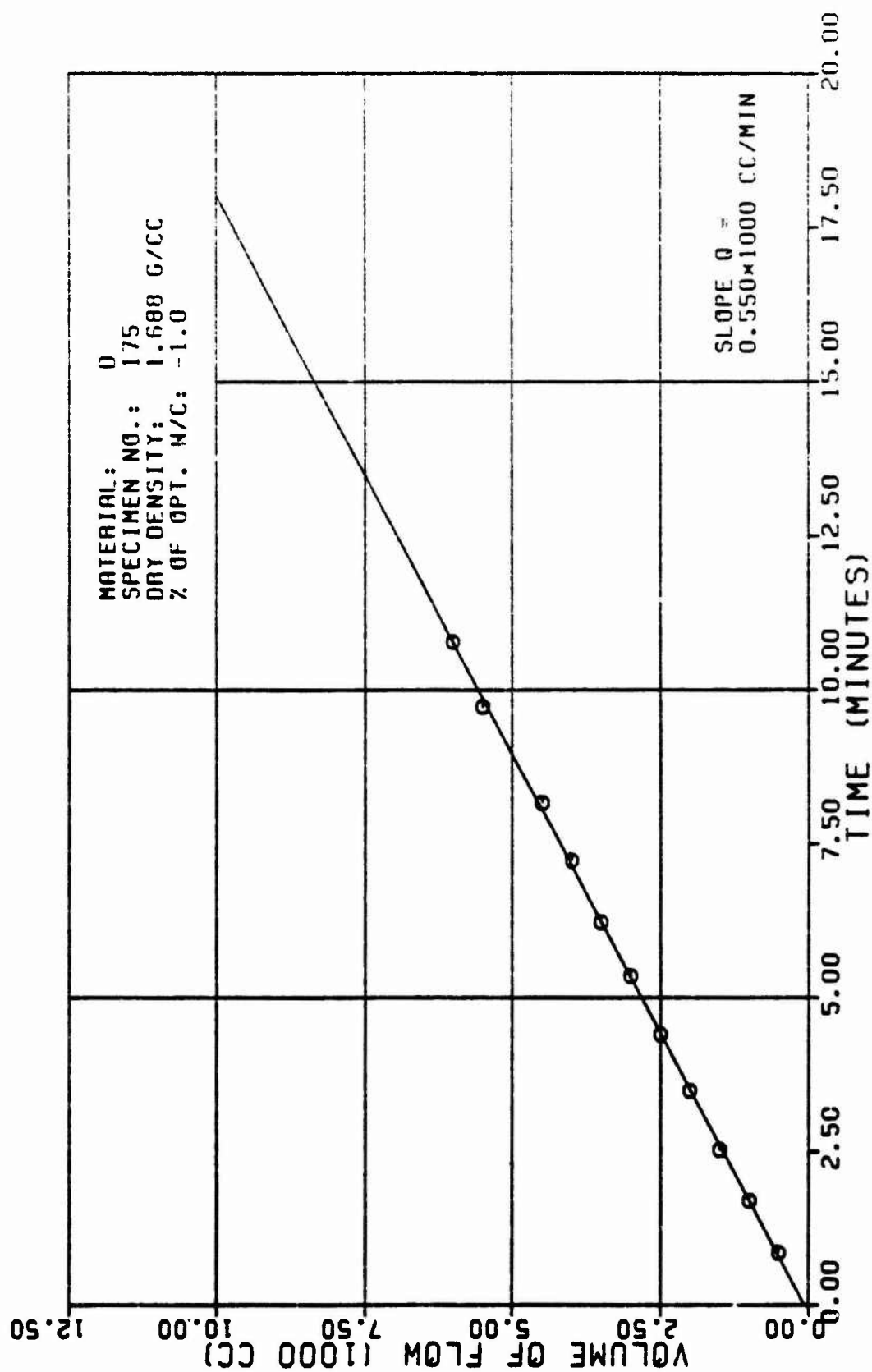


Figure A21a

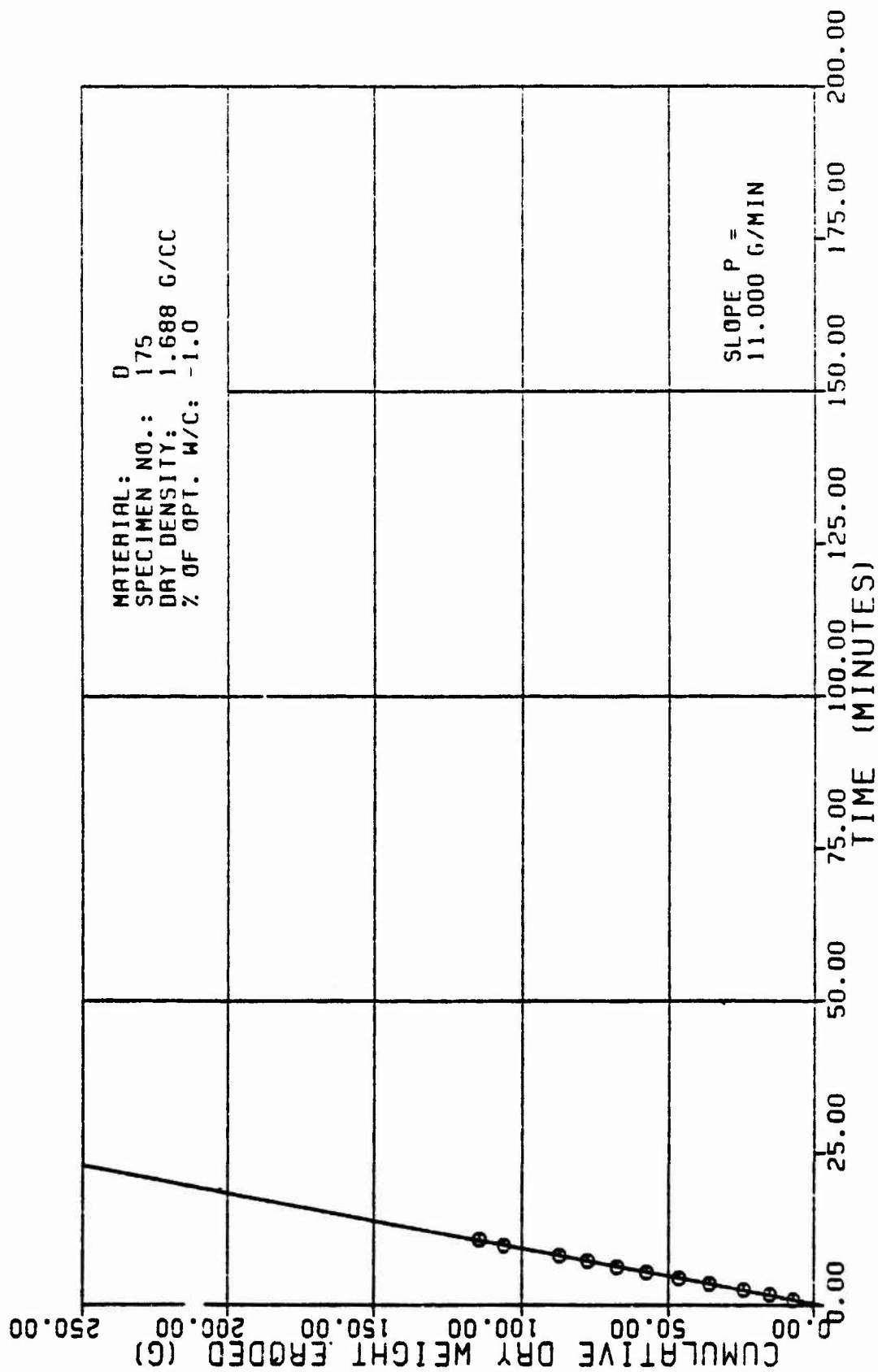


Figure A21b

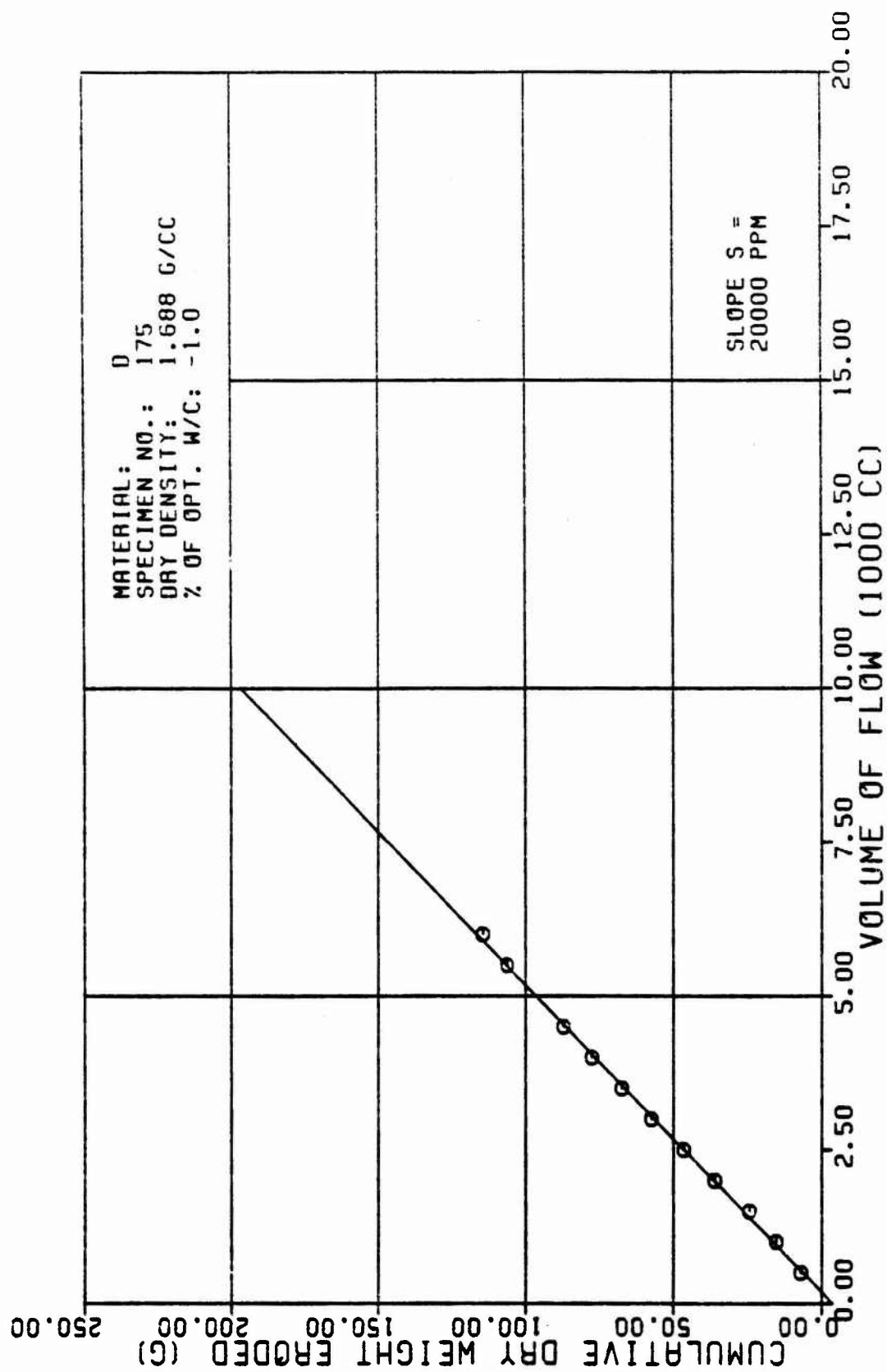


Figure A21c

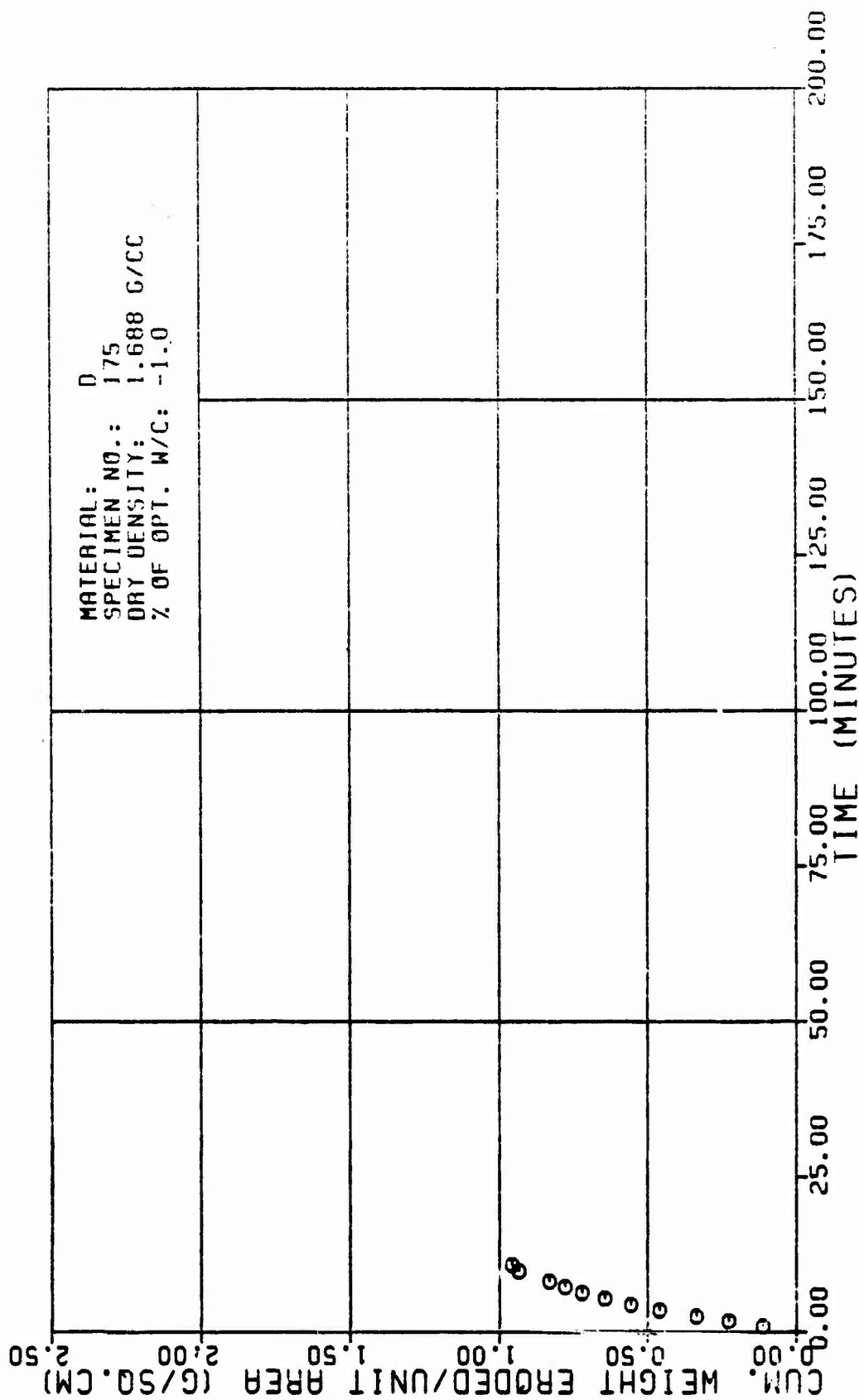


Figure A21d

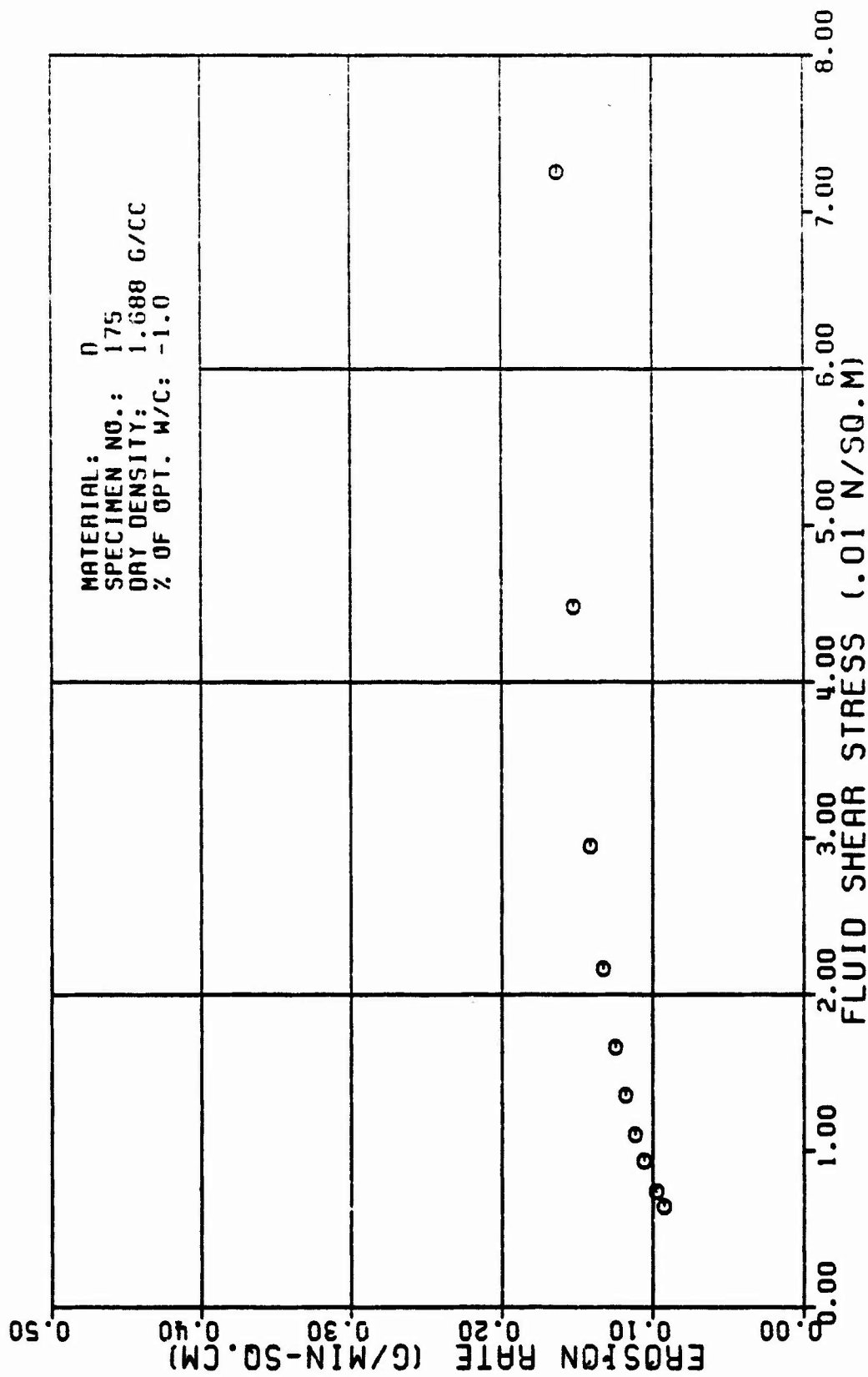


Figure A21e

TABLE A22

TEST RESULTS FOR TRIAXIAL EROSION TEST

MATERIAL TYPE: SPECIMEN NUMBER : TESTED BY:		E 102 SANCHEZ & ASSIAN		AVERAGE FLOW RATE (Q):		542. CC/MIN			
DATE TESTED:		3 24 82		RATE OF WEIGHT EROSION (P):		26.5 G/MIN			
SPECIMEN DRY DENSITY:		1.531 G/CC		DENSITY OF ERODING FLUID:		1.000 G/CC			
% OF OPTIMUM WATER CONTENT:		-2.0 PERCENT		VISCOSITY OF ERODING FLUID:		0.001 N-SEC/SQ.M			
INITIAL SLOT WIDTH:		2.32 CM		CONFINING PRESSURE:		98.10 KN/SQ.M			
INITIAL SLOT THICKNESS:		0.23 CM		HEAD OF WATER:		13.00 M			
ERODED LENGTH:		11.60 CM		HYDRAULIC GRADIENT:		10. M/M			

VOLUME OF FLOW (1000 CC)	TIME (MIN)	CUM. WEIGHT ERODED (G)	CROSS SECTION AREA (SQ.CM)	VELOCITY OF FLOW (CM/MIN)	ERODED SURFACE AREA (SQ.CM)	CUM. WEIGHT ERODED PER AREA (G/SQ.CM)	EROSION RATE (GRAMS/ (MIN * SQ.CM))	FLUID SHEAR STRESS (N/SQ.M)	REYNOLDS NUMBER
0.6	1.10	53.6	2.2	249.	76.	0.71	0.35	0.037	555.
1.2	2.25	76.4	3.9	139.	93.	0.82	0.29	0.014	452.
1.4	2.65	97.7	4.5	121.	99.	0.99	0.27	0.011	425.

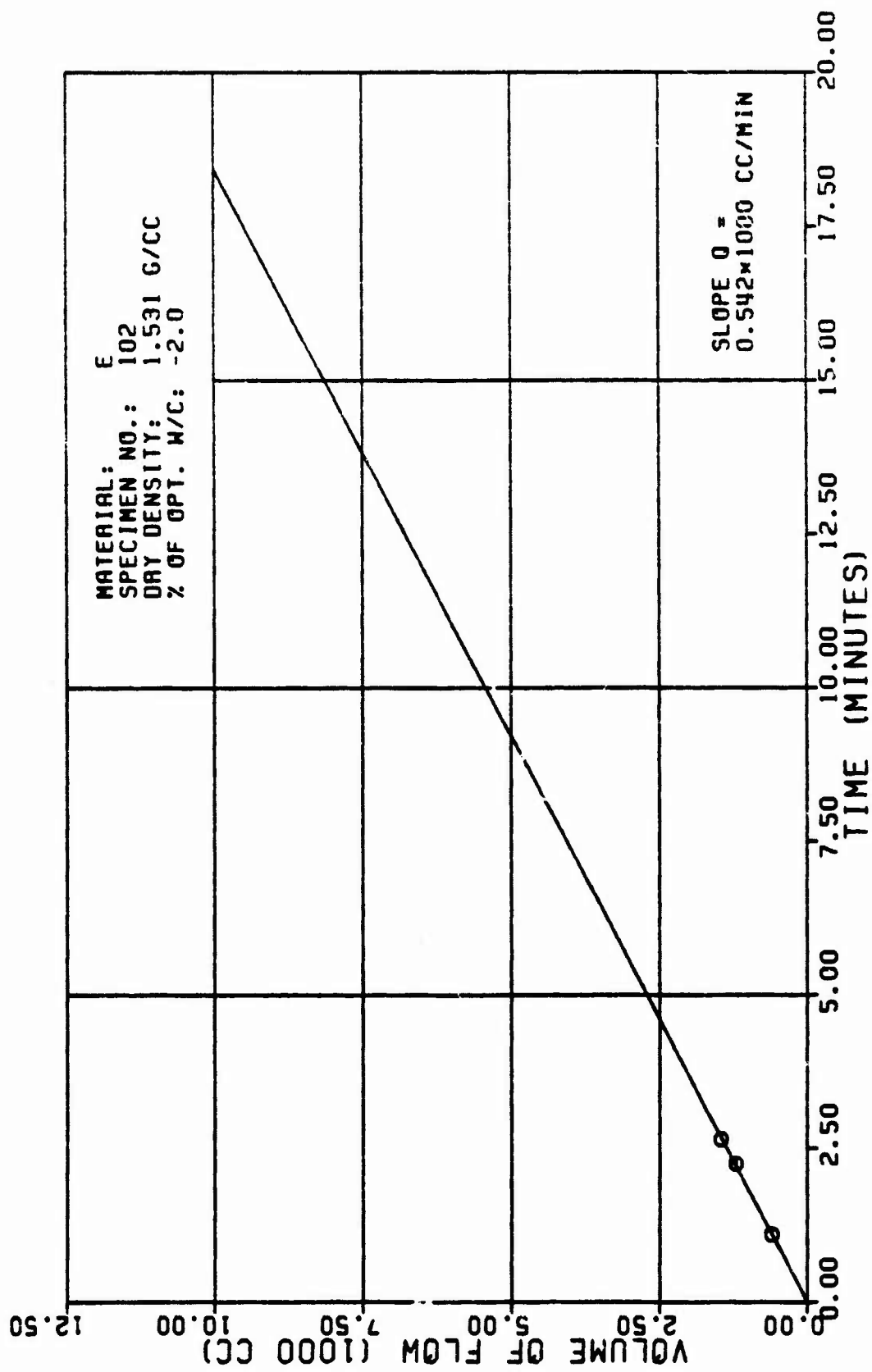


Figure A22a

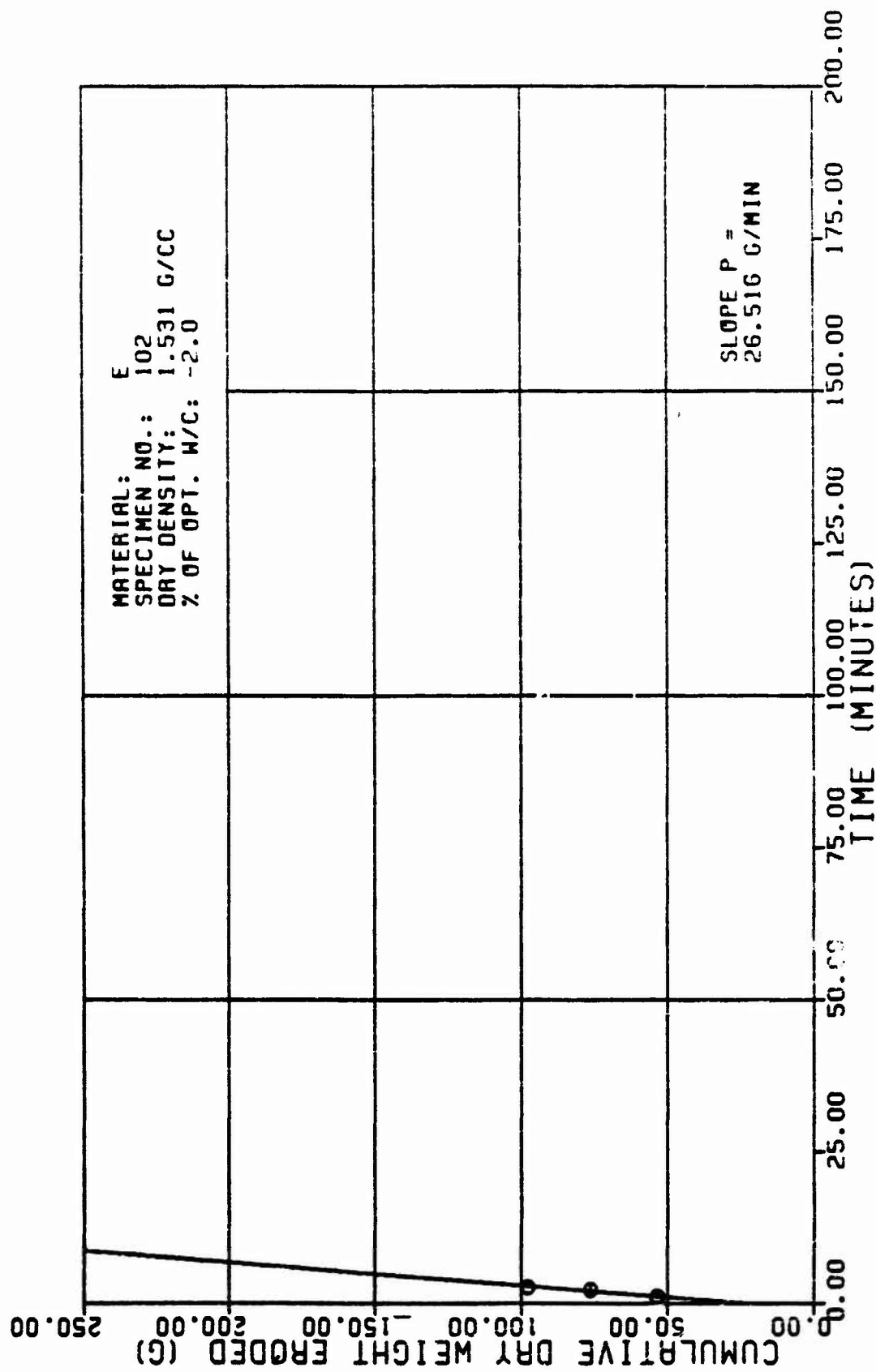


Figure A22b

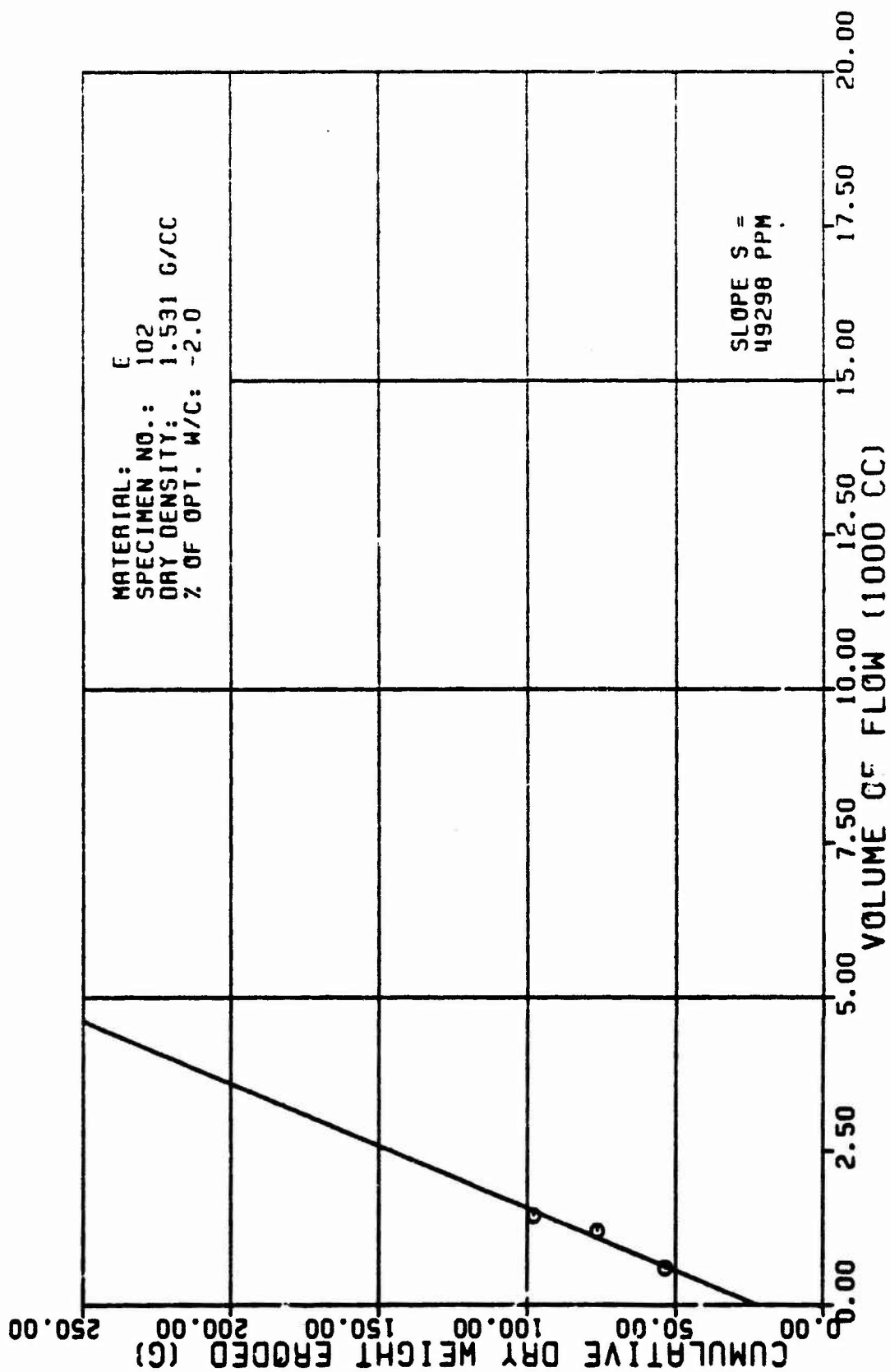


Figure A22c

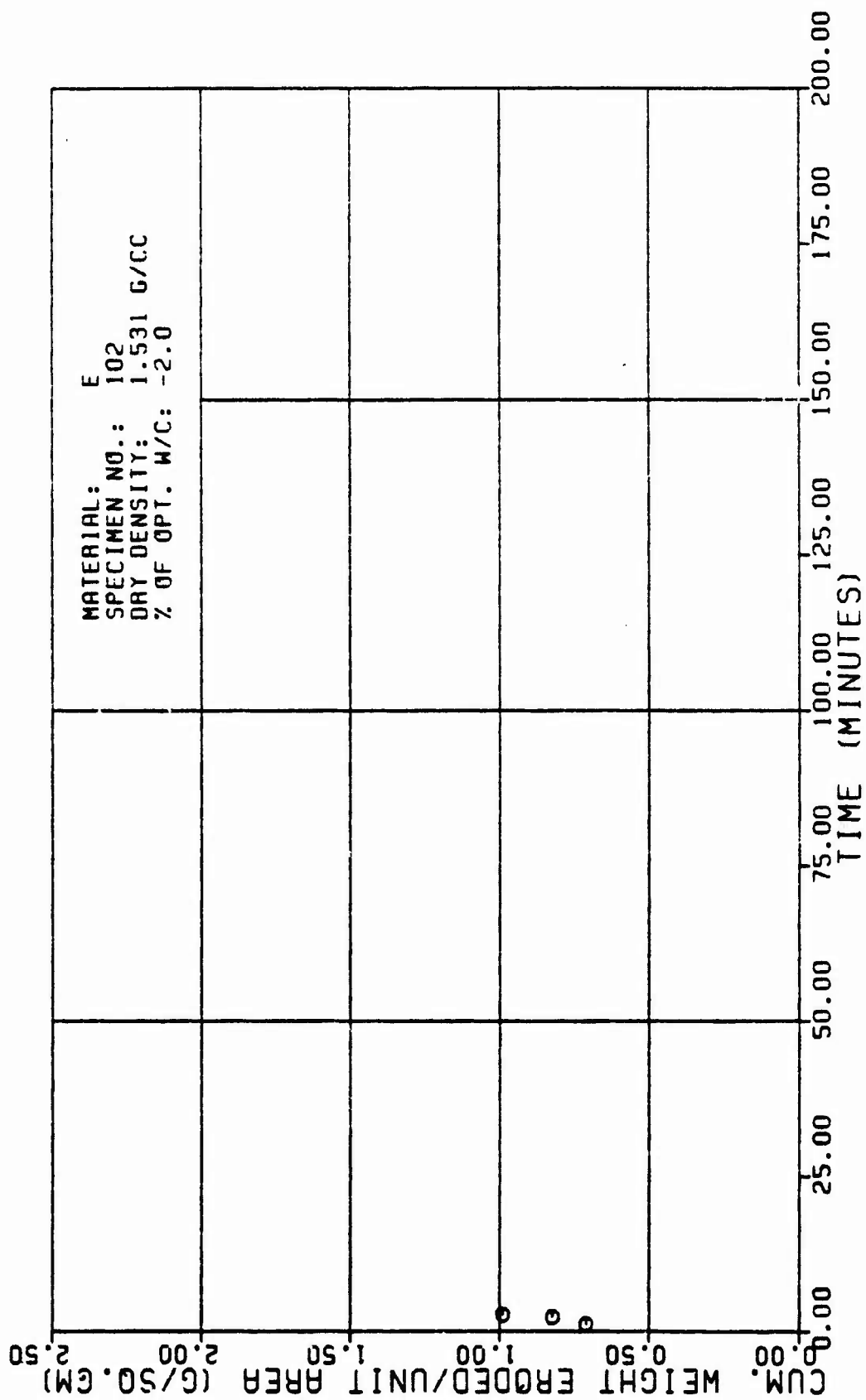


Figure A22d

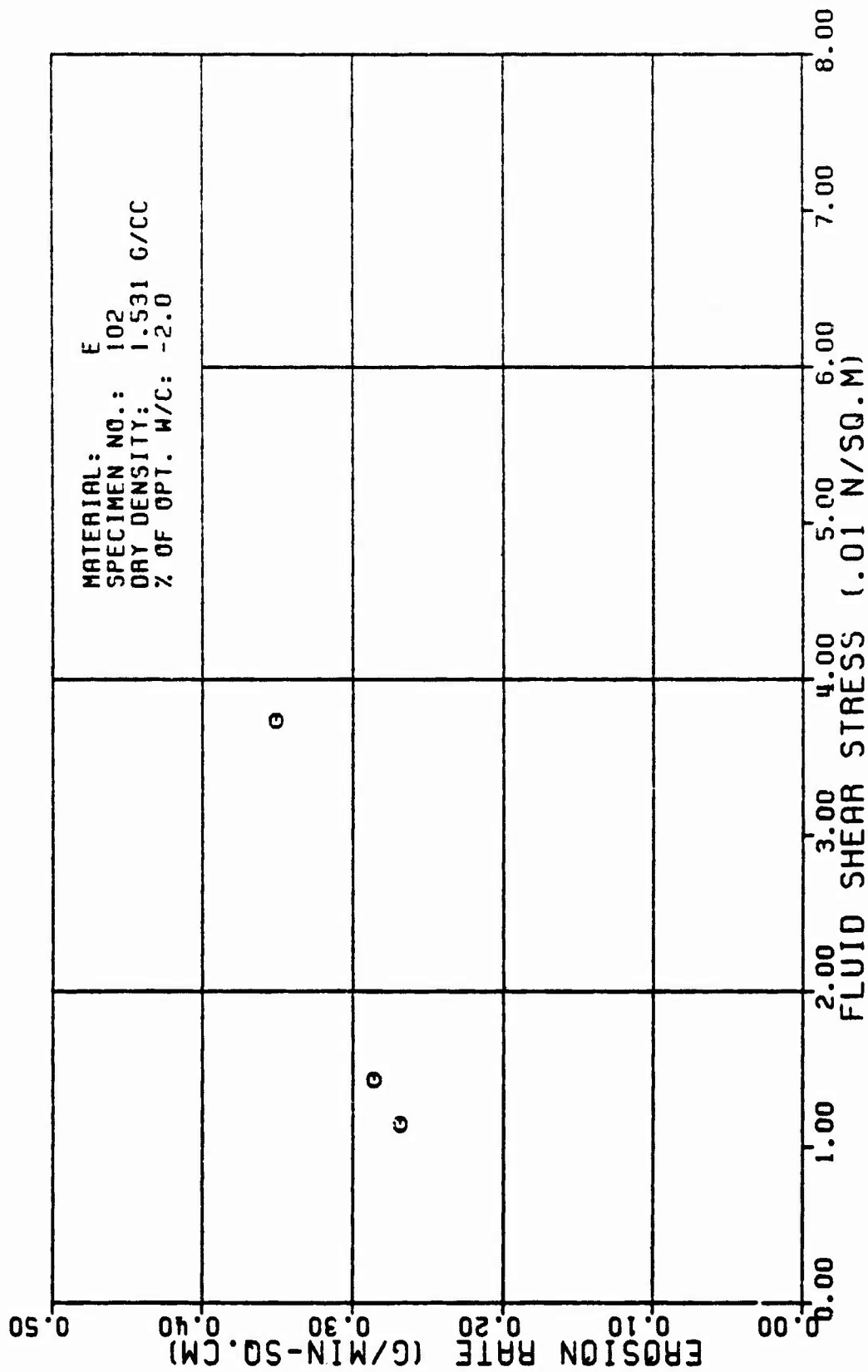


Figure A22e

TABLE A23

TEST RESULTS FOR TRIAXIAL EROSION TEST

MATERIAL TYPE:		E		103		SANCHEZ & ASSIAN		AVERAGE FLOW RATE (Q):		545. CC/MIN	
SPECIMEN NUMBER :		TESTED BY:		3 24 82		RATE OF WEIGHT EROSION (P):		22.8 G/MIN			
DATE TESTED:		SPECIMEN DRY DENSITY:		1.522 G/CC		DENSITY OF ERODING FLUID:		1.000 G/CC			
X OF OPTIMUM WATER CONTENT:		-1.8 PERCENT		2.32 CM		VISCOSITY OF ERODING FLUID:		0.001 N*SEC/SQ.M			
INITIAL SLOT WIDTH:		INITIAL SLOT THICKNESS:		0.23 CM		CONFINING PRESSURE:		98.10 KN/SQ.M			
ERODED LENGTH:		11.50 CM		HEAD OF WATER:		13.00 M					
				HYDRAULIC GRADIENT:		1.0 M/M					

VOLUME OF FLOW (1000 CC)	TIME (MIN)	CUM. WEIGHT ERODED (G)	CROSS SECTION AREA (SQ.CM)	VELOCITY OF FLOW (CM/MIN)	ERODED SURFACE AREA (SQ.CM)	CUM. WEIGHT ERODED PER AREA (G/SQ.CM)	EROSION RATE (GRAMS/ (MIN * SQ.CM))	FLUID SHEAR STRESS (N/SQ.M)	REYNOLDS NUMBER		
0.6	1.00	30.2	1.9	200.	72.	0.42	0.31	0.048		579.	
1.2	2.20	56.5	3.3	165.	86.	0.66	0.26	0.019		485.	
2.0	3.65	87.0	5.1	106.	104.	0.83	0.21	0.009		401.	

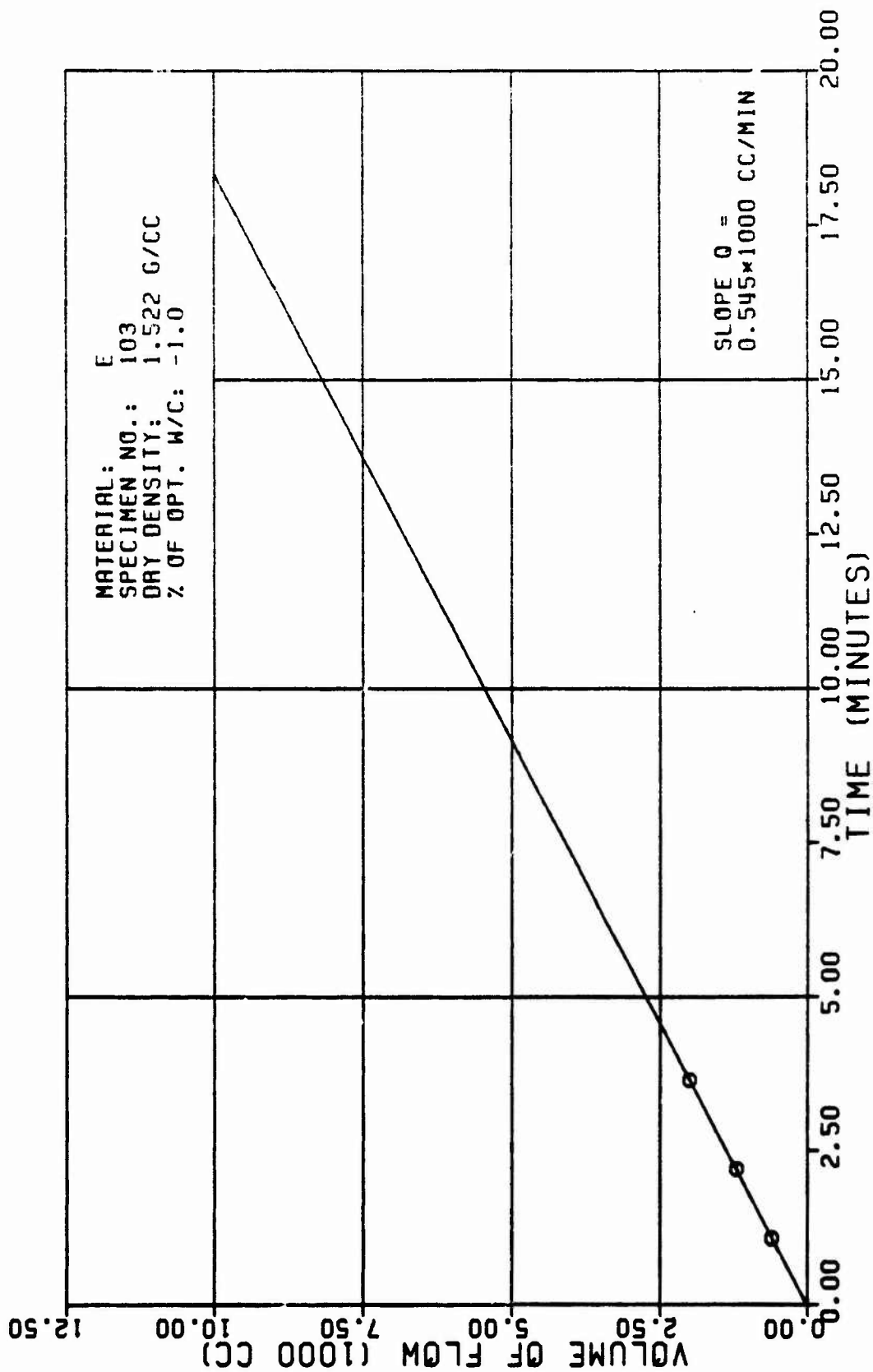


Figure A23a

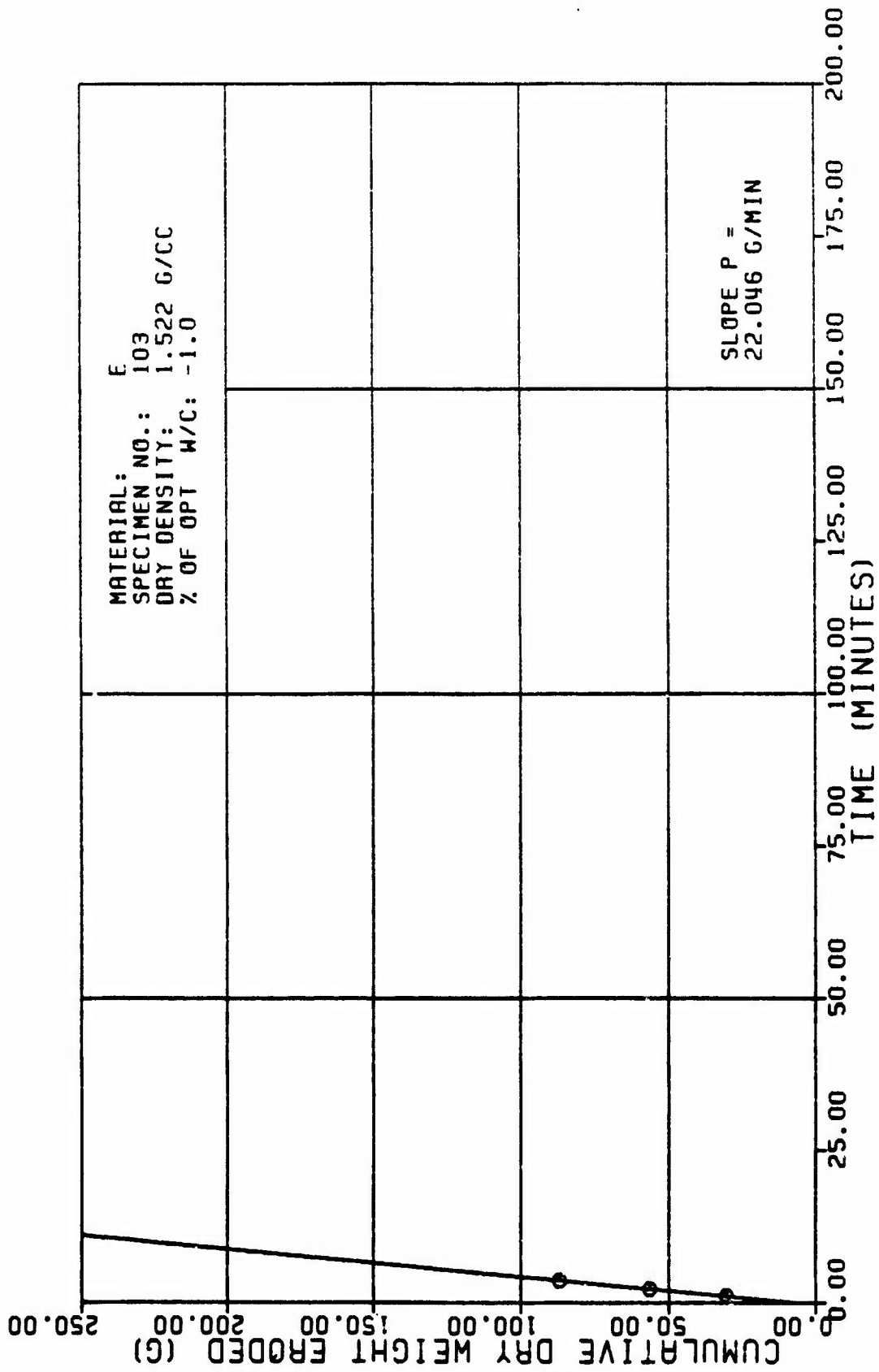


Figure A23b

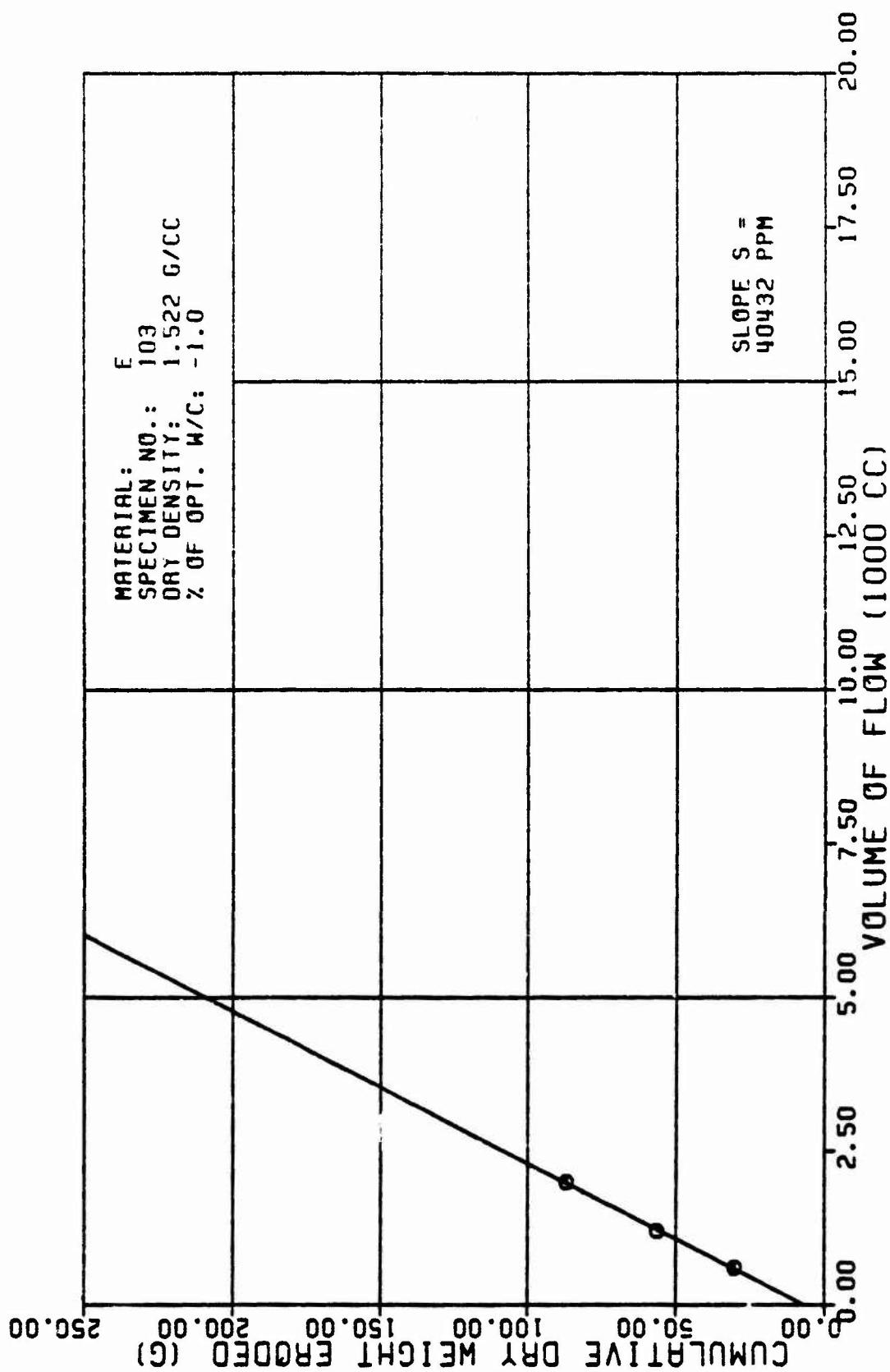


Figure A23c

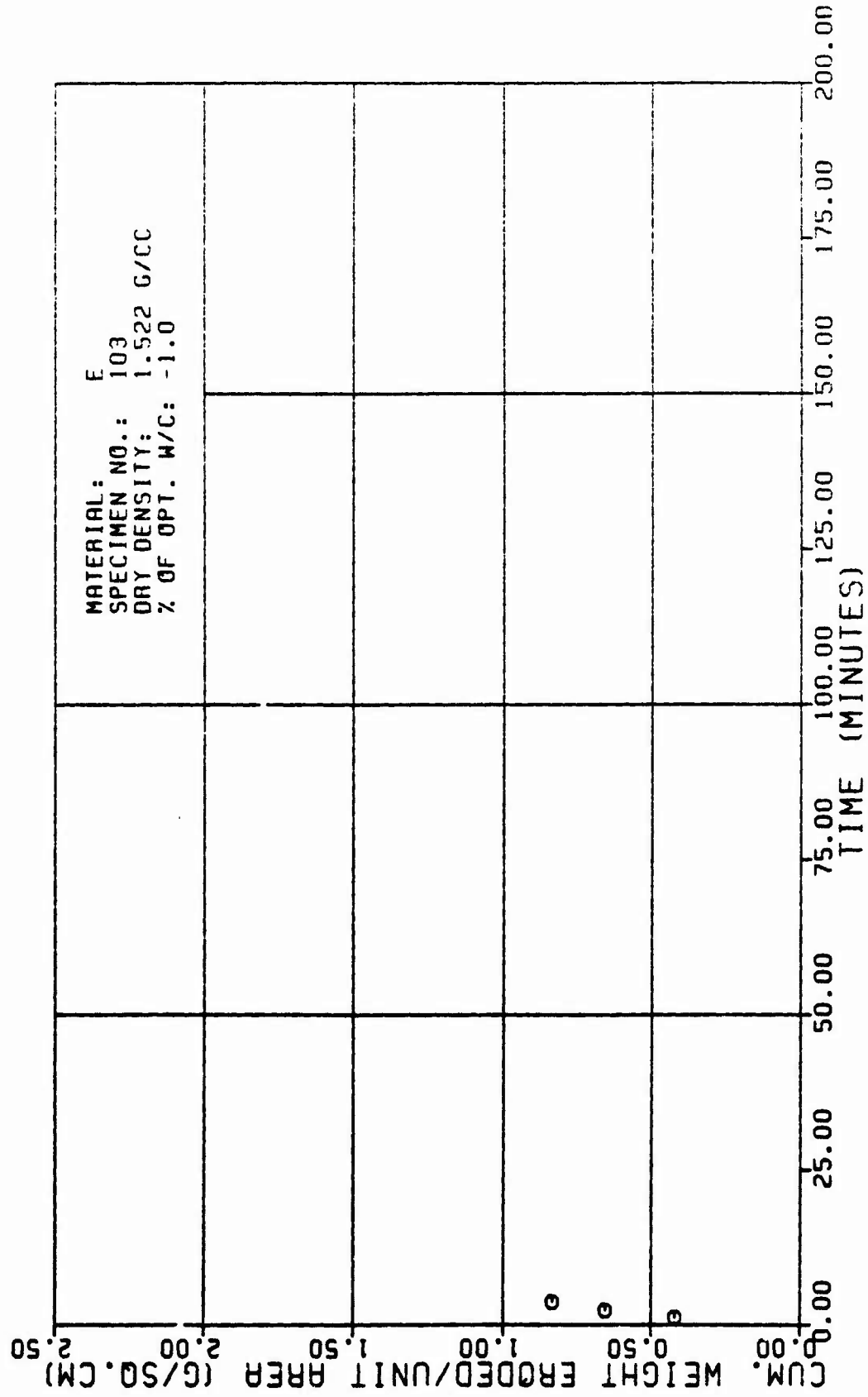


Figure A23d

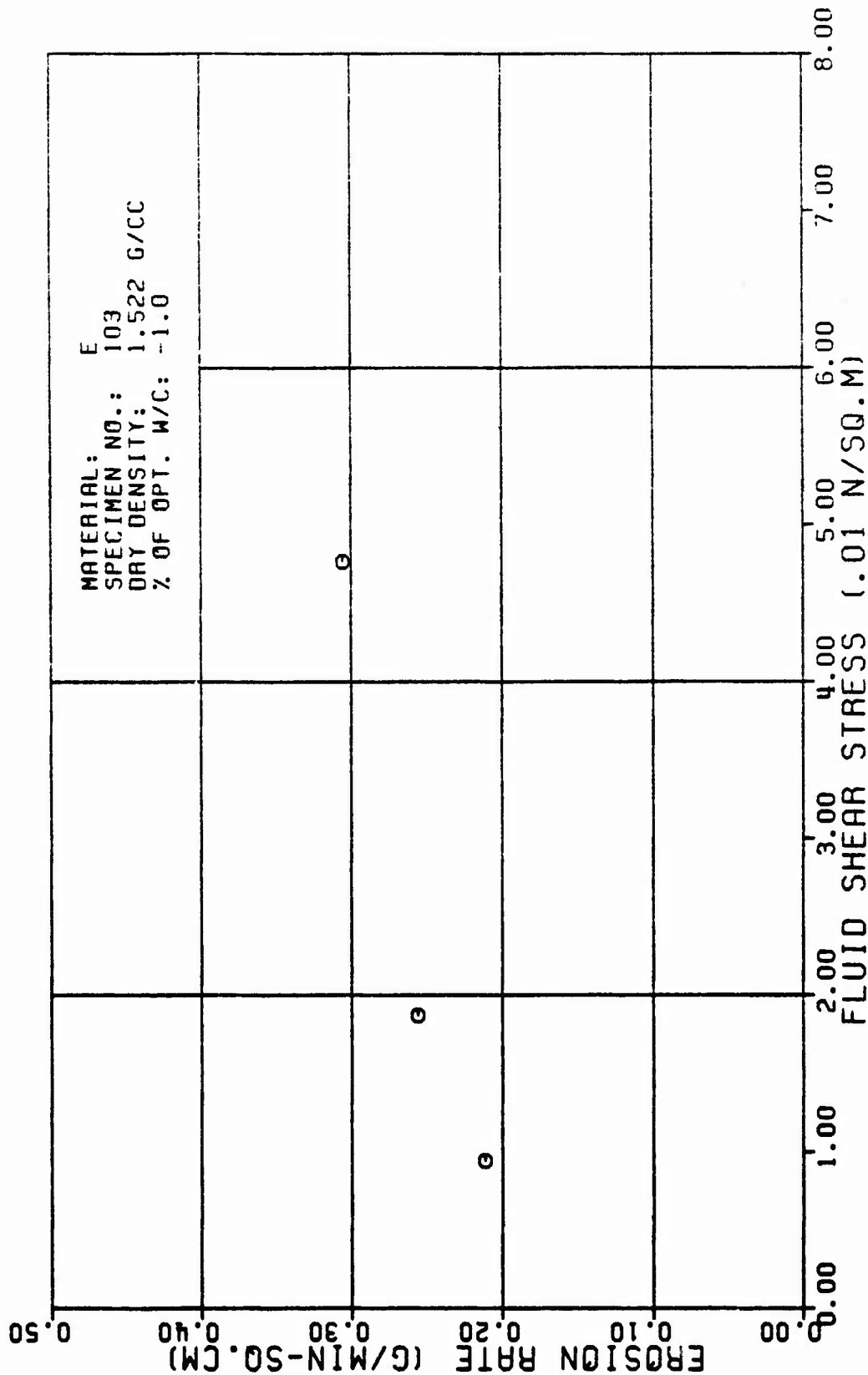


Figure A23e

TABLE A24

TEST RESULTS FOR TRIAXIAL EROSION TEST

MATERIAL TYPE: SPECIMEN NUMBER : TESTED BY:		E 104 SANCHEZ & ASSIAN		AVERAGE FLOW RATE (Q): 499. CC/MIN					
DATE TESTED:		3 24 82		RATE OF WEIGHT EROSION (P): 9.9 G/MIN					
SPECIMEN DRY DENSITY:		1.530 G/CC		DENSITY OF ERODING FLUID: 1.000 G/CC					
X OF OPTIMUM WATER CONTENT:		2.0 PERCENT		VISCOSITY OF ERODING FLUID: 0.001 M*SEC/SQ.M					
INITIAL SLOT WIDTH:		2.32 CM		CONFINING PRESSURE: 98.10 KN/SQ.M					
INITIAL SLOT THICKNESS:		0.23 CM		HEAD OF WATER: 1.3 00 M					
ERODED LENGTH:		11.50 CM		HYDRAULIC GRADIENT: 10. M/M					
<hr/>									
VOLUME OF FLOW (1000 CC)	TIME (MIN)	CUM. WEIGHT ERODED (G)	CROSS SECTION AREA (SQ.CM)	VELOCITY OF FLOW (CM/MIN)	ERODED SURFACE AREA (SQ.CM)	CUM. WEIGHT ERODED PER AREA (G/SQ.CM)	EROSION RATE (GRAMS/ (MIN * SQ.CM))	FLUID SHEAR STRESS (N/SQ.M)	REYNOLDS NUMBER
0.6	1.12	20.3	1.2	429.	65.	0.31	0.15	0.104	589.
1.2	2.10	32.0	1.0	284.	71.	0.46	0.14	0.050	540.
1.0	3.51	44.9	2.5	199.	70.	0.57	0.13	0.027	409.
2.4	4.59	56.9	3.1	160.	84.	0.68	0.12	0.019	454.
3.4	6.77	76.9	4.3	115.	96.	0.80	0.10	0.011	397.
4.4	0.64	95.4	5.4	93.	107.	0.89	0.09	0.008	358.

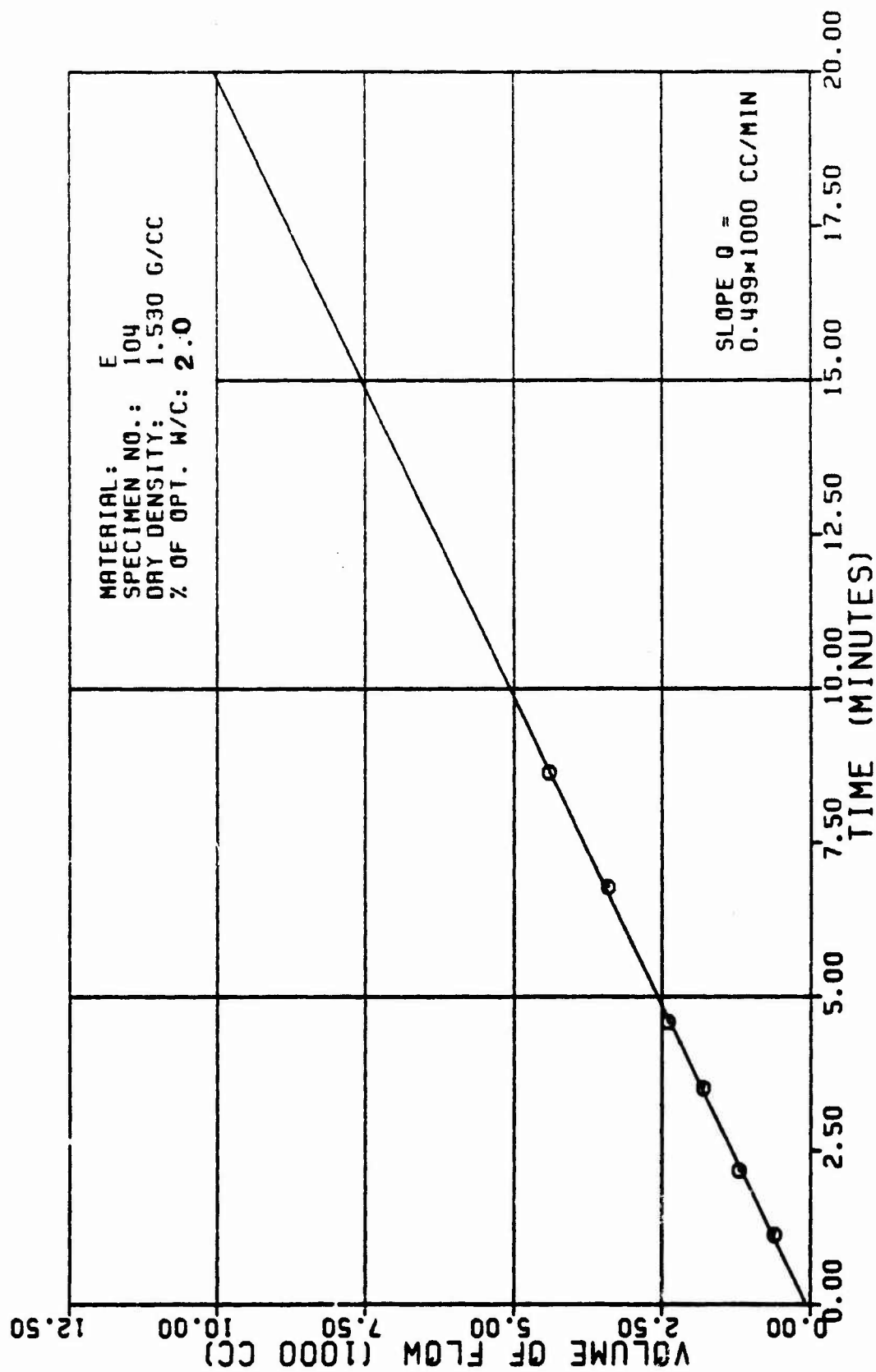


Figure A24a

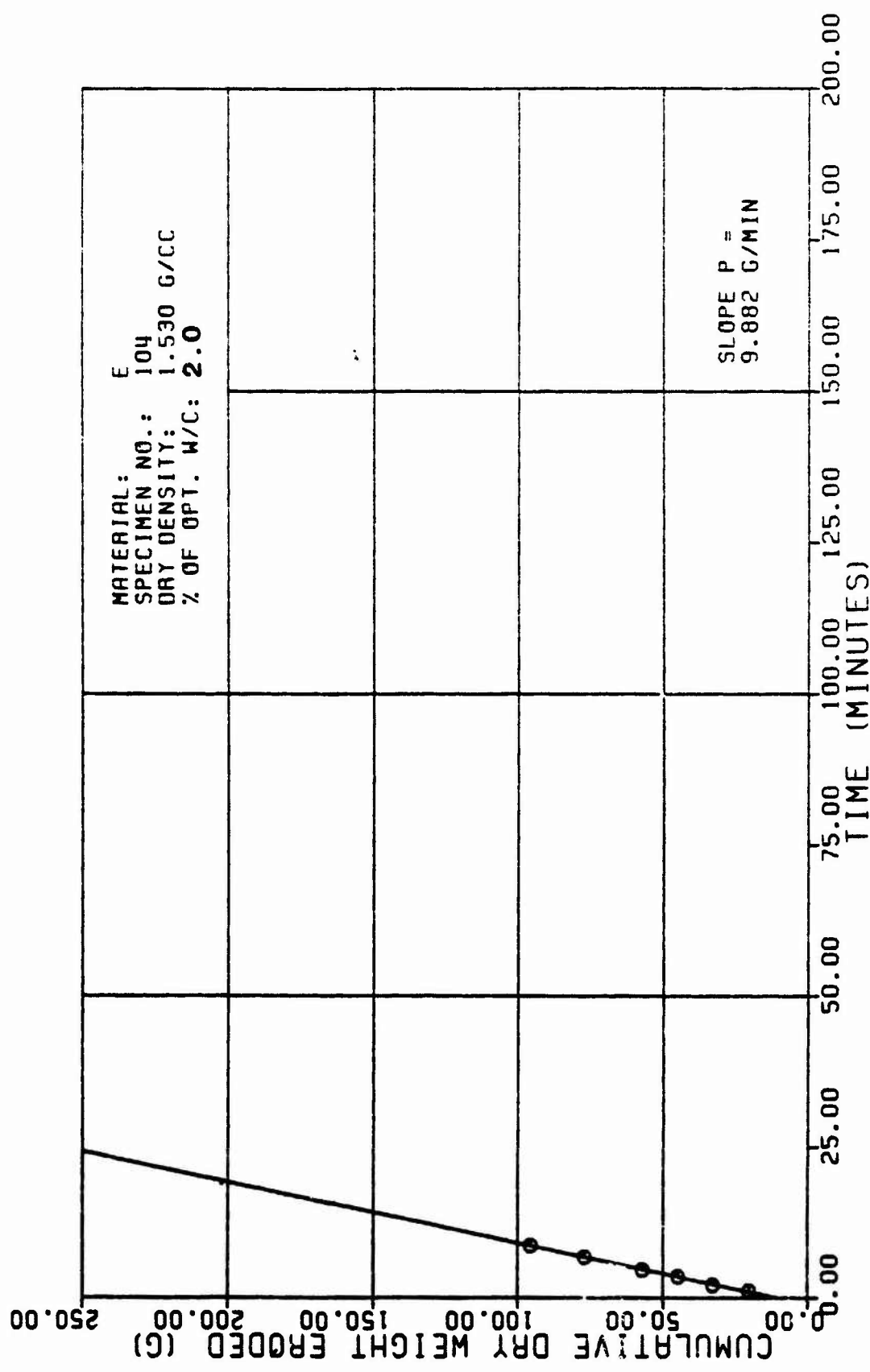


Figure A24b

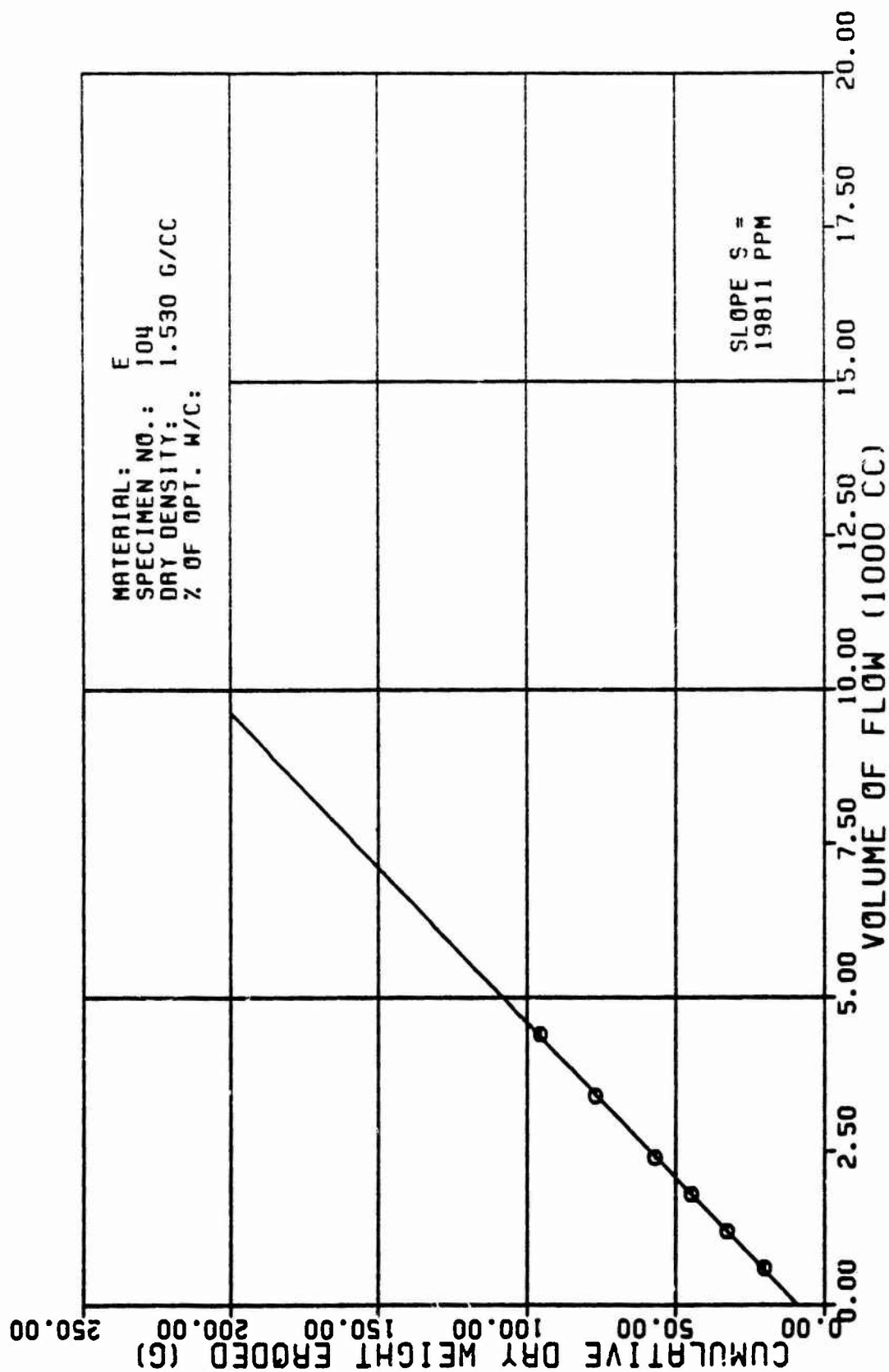


Figure A24c

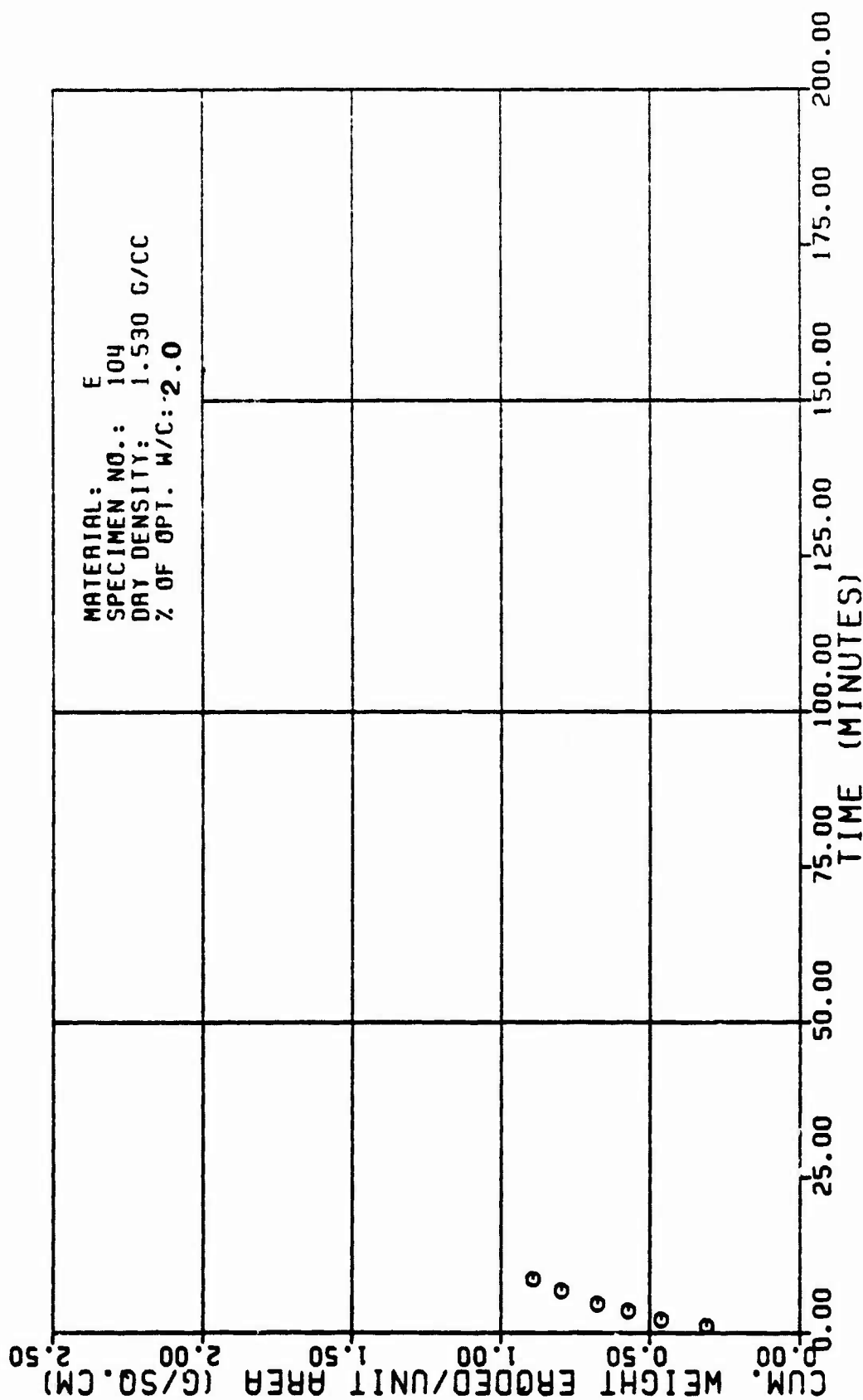


Figure A24d

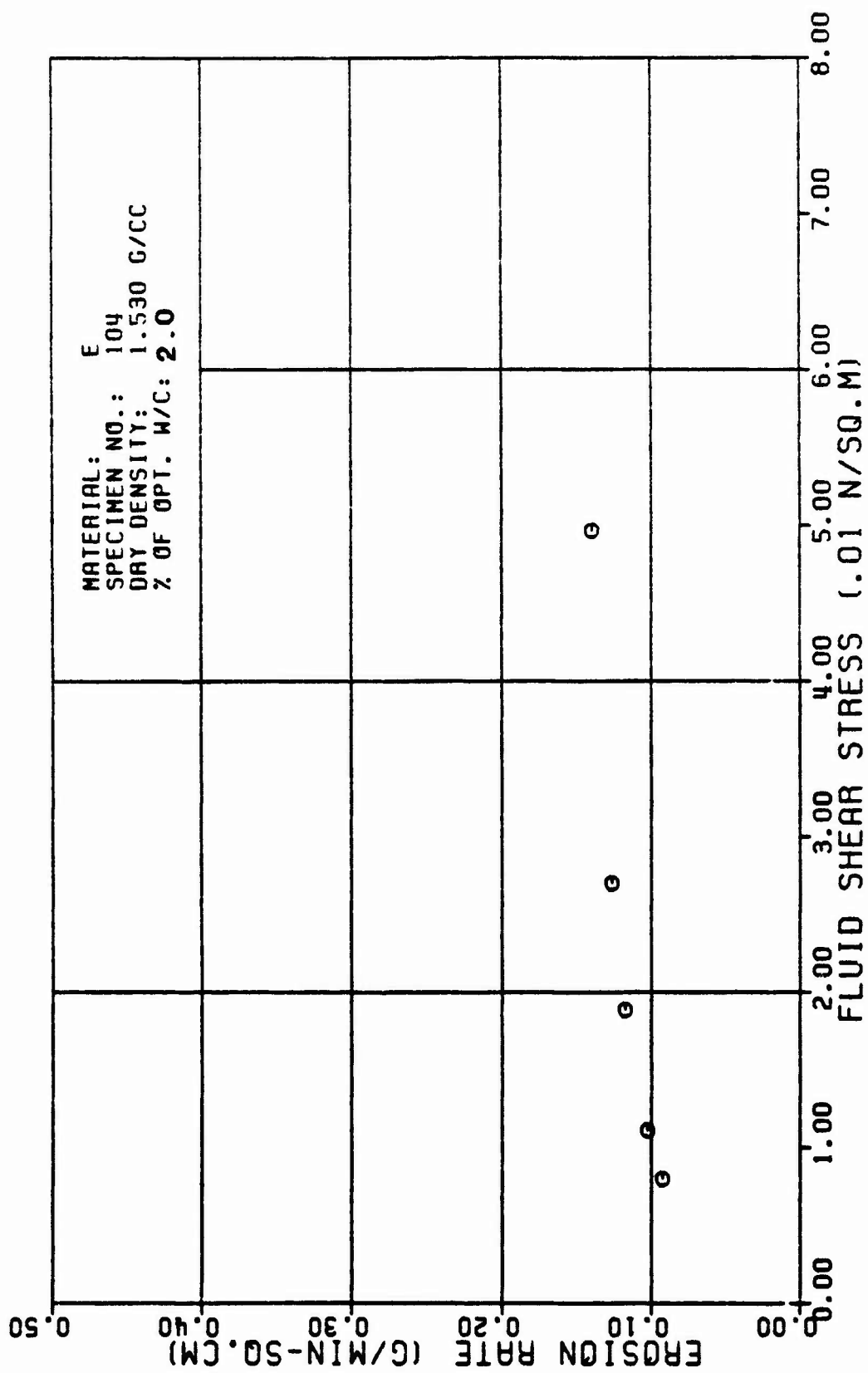


Figure A24e

TEST RESULTS FOR TRIAXIAL EROSION TEST

MATERIAL TYPE: E	SPECIMEN NUMBER : I8S	SANCHEZ & ASSIAN
TESTED BY:	DATE TESTED:	3 24 82
SPECIMEN DRY DENSITY:	1.599 G/CC	AVERAGE FLOW RATE (Q): 433. CC/MIN
% OF OPTIMUM WATER CONTENT:	8.8 PERCENT	RATE OF WEIGHT EROSION (P): 11.8 G/MIN
INITIAL SLOT WIDTH:	2.32 CM	DENSITY OF ERODING FLUID: 1.000 G/CC
INITIAL SLOT THICKNESS:	8.23 CM	VISCOSITY OF ERODING FLUID: 8.881 N*SEC/SO.M
ERODED LENGTH:	11.68 CM	CONFINING PRESSURE: 98.18 KN/SO.M
		HEAD OF WATER: 13.88 M
		HYDRAULIC GRADIENT: 18. M/M

VOLUME OF FLOW (LBS/CC)	TIME (MIN)	CUM. WEIGHT ERODED (G)
0.5	1.89	18.6
1.0	2.29	37.3
1.5	3.35	55.7
2.0	4.51	66.7
2.5	5.75	72.8
		CROSS SECTION AREA (SQ.CM)
		1.2
		2.8
		2.7
		3.4
		4.2
		VELOCITY OF FLOW (CM/MIN)
		353.
		218.
		163.
		128.
		184.
		ERODED SURFACE AREA (SQ.CH)
		66.
		74.
		88.
		88.
		96.
		CUM. WEIGHT ERODED PER AREA (G/SO.CH)
		8.28
		8.51
		8.69
		8.76
		8.75
		EROSION RATE (GRAMS/ (MIN * SO.CH))
		8.18
		8.16
		8.15
		8.13
		8.12
		FLUID SHEAR STRESS (N/SO.M)
		8.882
		8.835
		8.821
		8.814
		8.818
		REYNOLDS NUMBER
		587.
		454.
		416.
		382.
		358.

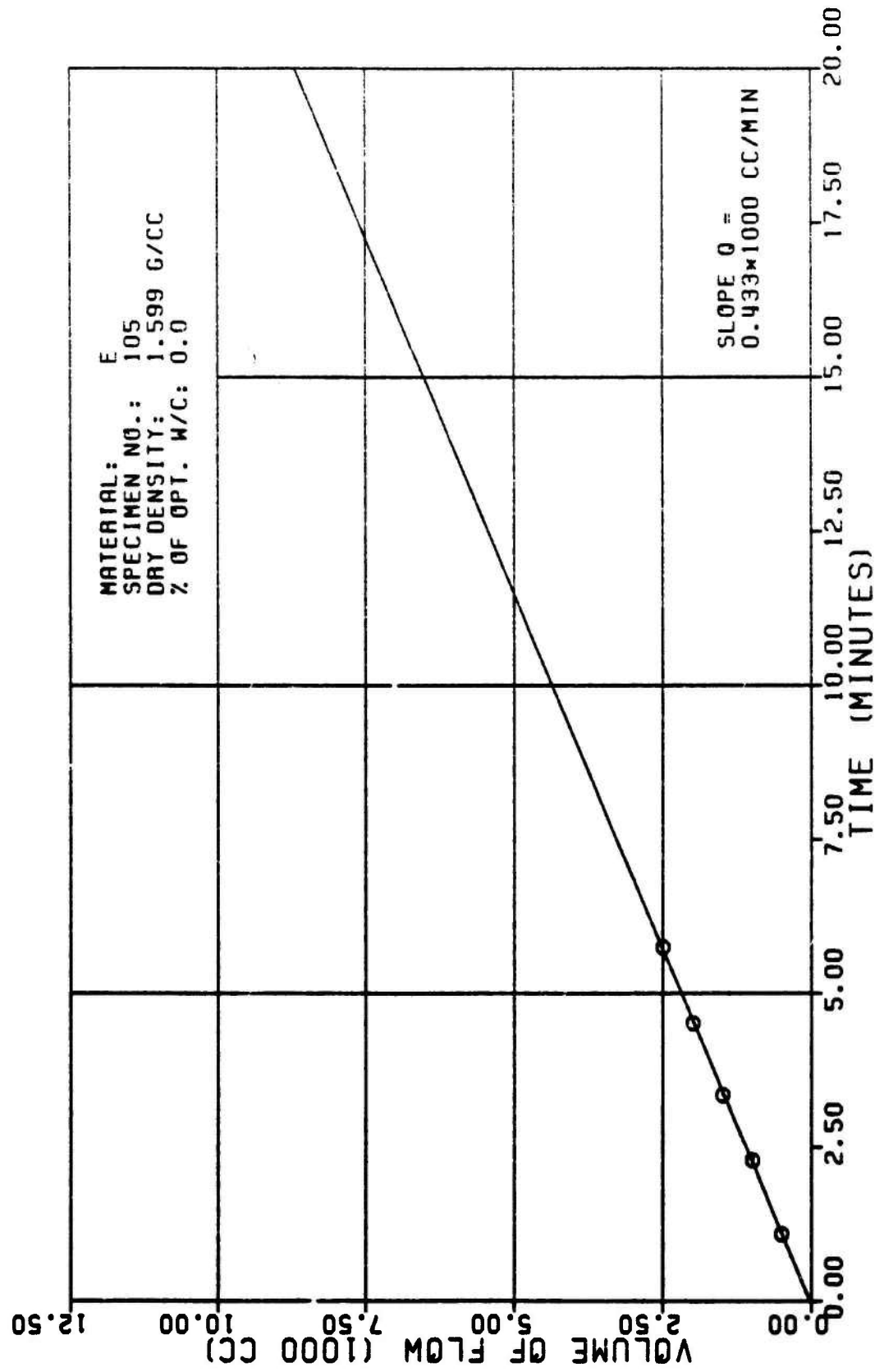


Figure A25a

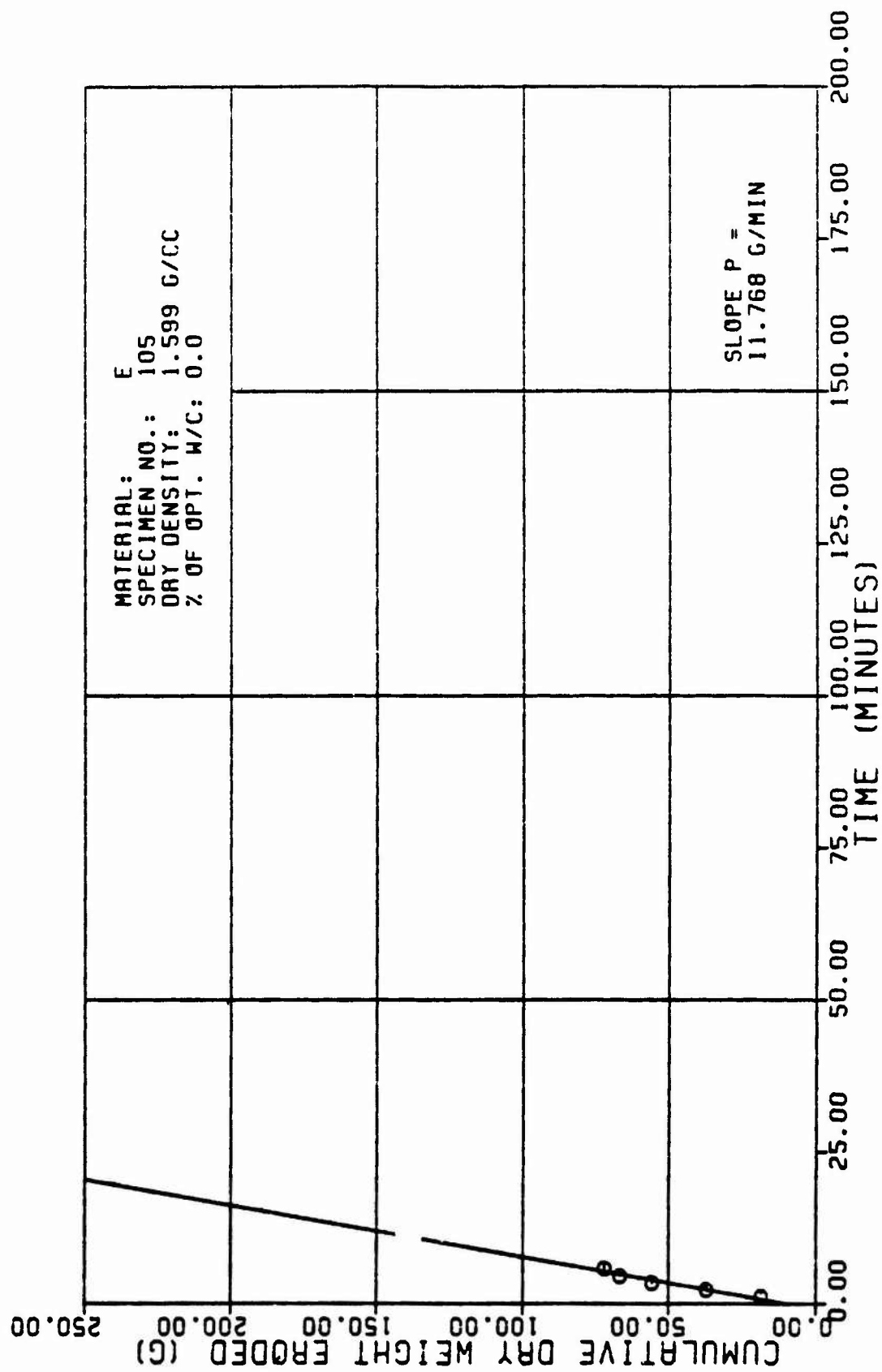


Figure A25b

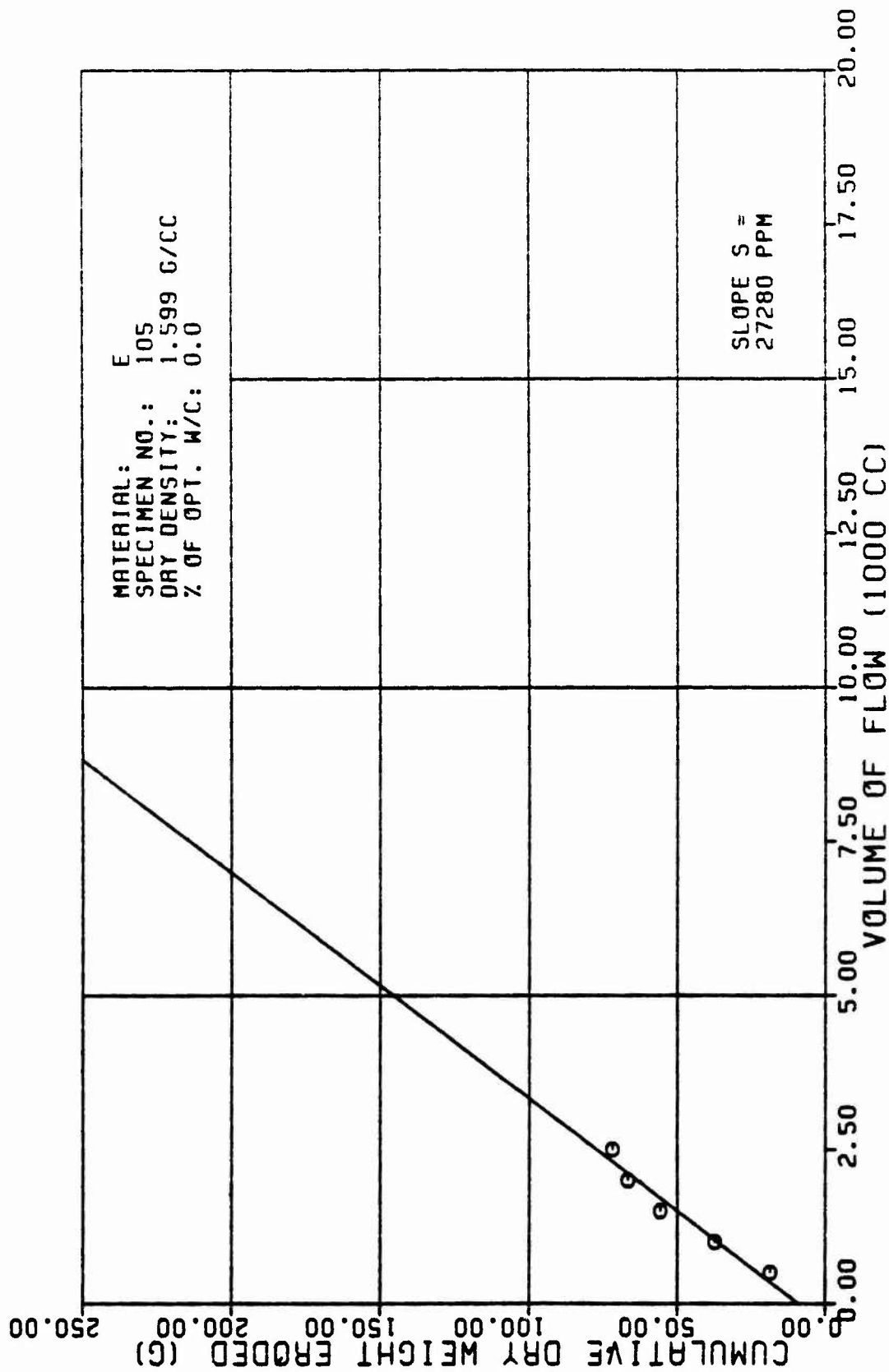


Figure A25c

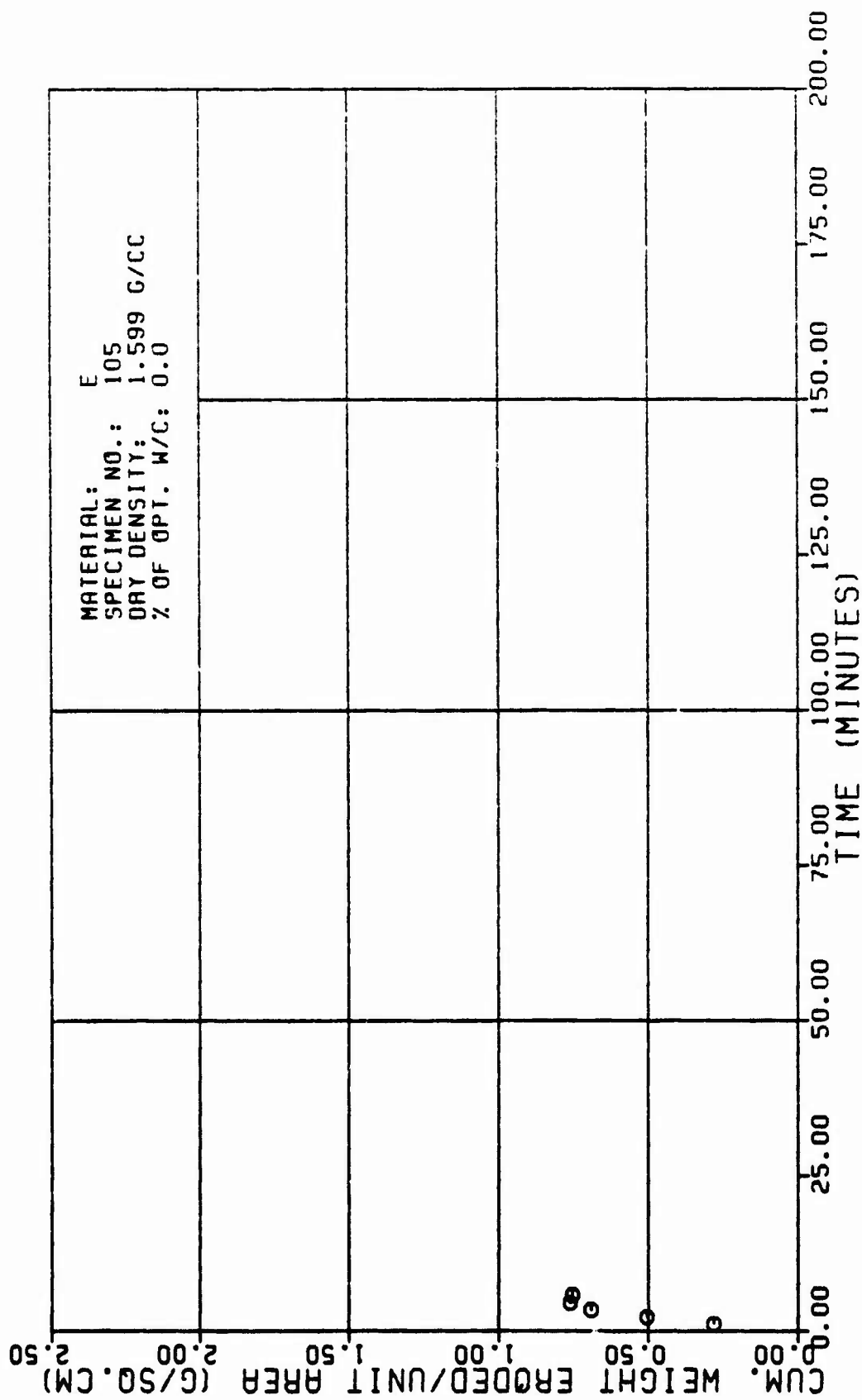


Figure A25d

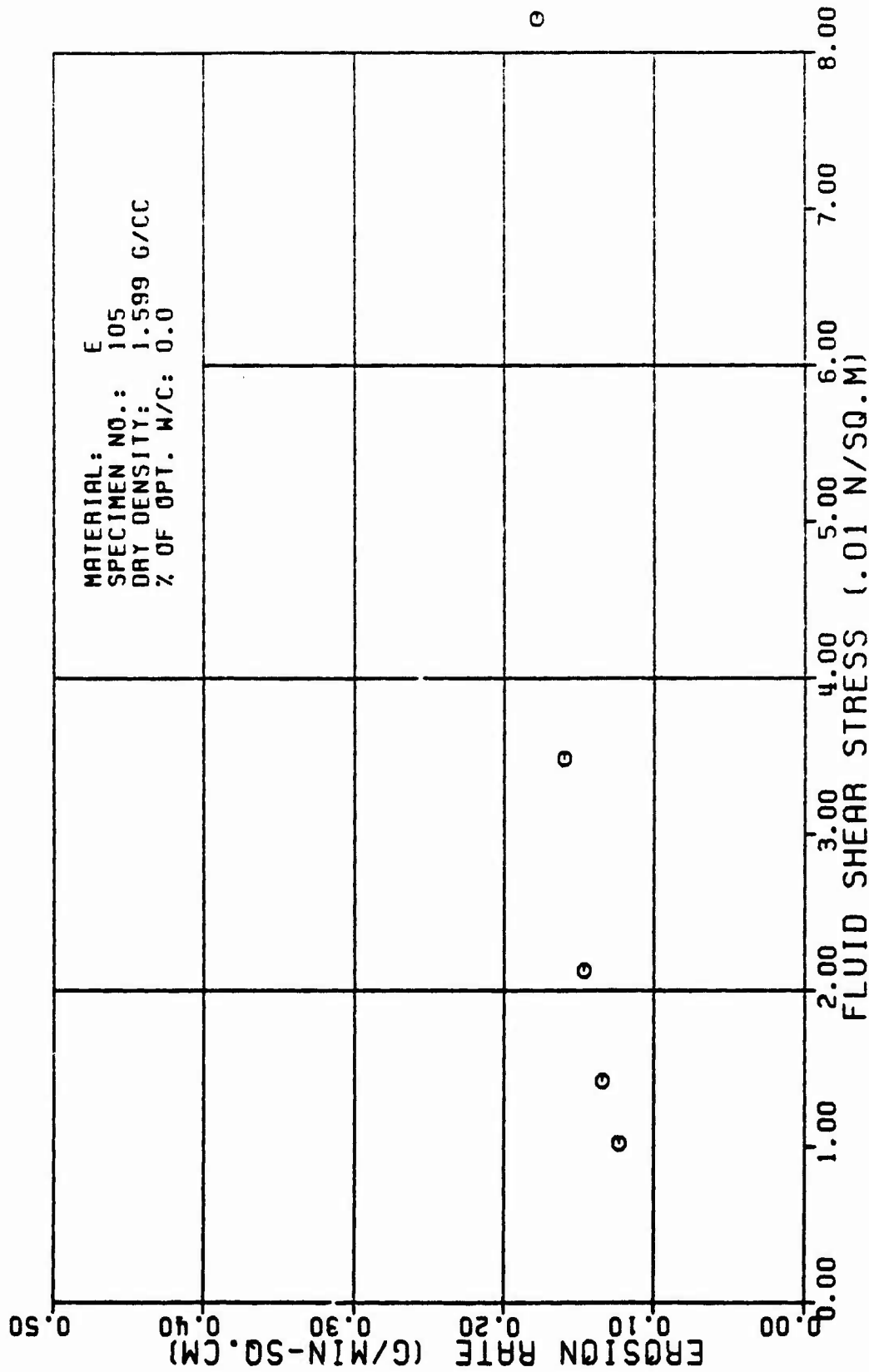


Figure A25e

TABLE A26

TEST RESULTS FOR TRIAXIAL EROSION TEST

MATERIAL TYPE: SPECIMEN NUMBER : TESTED BY:		E 106 SANCHEZ & ASSIAN		3 24 82		AVERAGE FLOW RATE (Q): RATE OF WEIGHT EROSION (P):		459. CC/MIN 11.9 G/MIN	
SPECIMEN DRY DENSITY:		1.536 G/CC		2.5 PERCENT		DENSITY OF ERODING FLUID:		1.000 G/CC	
X OF OPTIMUM WATER CONTENT:		2.32 CM		5.23 CM		VISCOSITY OF ERODING FLUID:		0.001 N*SEC/SQ.M	
INITIAL SLOT WIDTH:		11.20 CM		CONFIRMING PRESSURE:		HEAD OF WATER:		98.10 KN/SQ.M 13.00 M	
INITIAL SLOT THICKNESS:		HYDRAULIC GRADIENT:		10. M/M					
ERODED LENGTH:									
VOLUME OF FLOW (1000 CC)	TIME (MIN)	CUM. WEIGHT ERODED (G)	CROSS SECTION AREA (SQ.CM)	VELOCITY OF FLOW (CM/MIN)	ERODED SURFACE AREA (SQ.CM)	CUM. WEIGHT ERODED PER AREA (G/SQ.CM)	EROSION RATE (GRAMS/ (MIN * SQ.CM))	FLUID SHEAR STRESS (N/SQ.M)	REYNOLDS NUMBER
0.5	1.07	21.7	1.3	361.	64.	0.34	0.18	0.001	533.
1.0	2.10	38.4	2.0	225.	72.	0.54	0.17	0.035	478.
1.5	3.29	51.4	2.0	164.	79.	0.65	0.16	0.021	433.
2.0	4.47	67.5	3.6	127.	87.	0.70	0.14	0.014	394.
2.5	5.57	77.4	4.4	105.	94.	0.82	0.13	0.010	363.
3.0	6.65	89.4	5.1	90.	101.	0.88	0.12	0.008	338.
3.5	7.49	99.5	5.7	80.	107.	0.93	0.11	0.007	320.

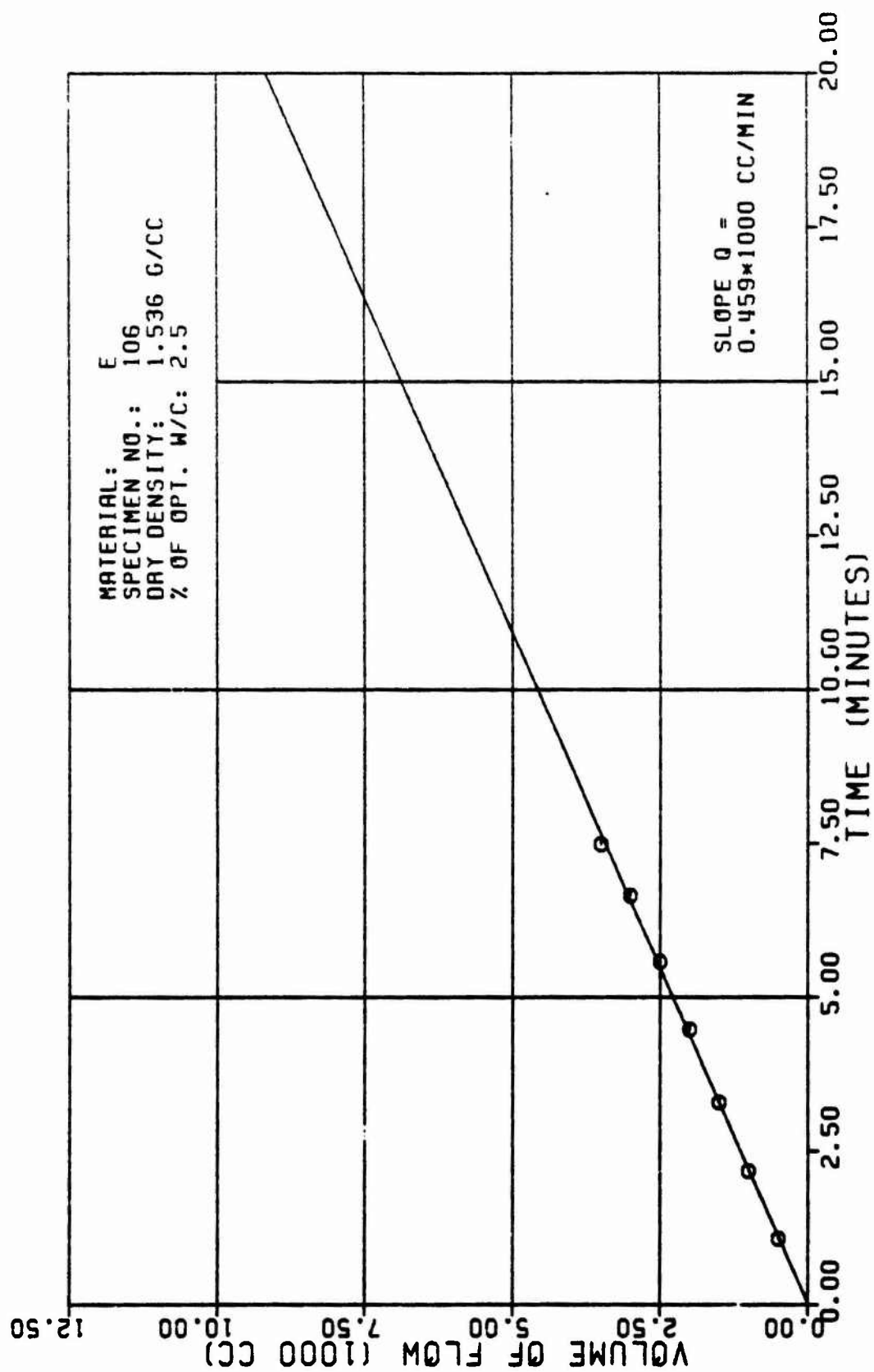


Figure A26a

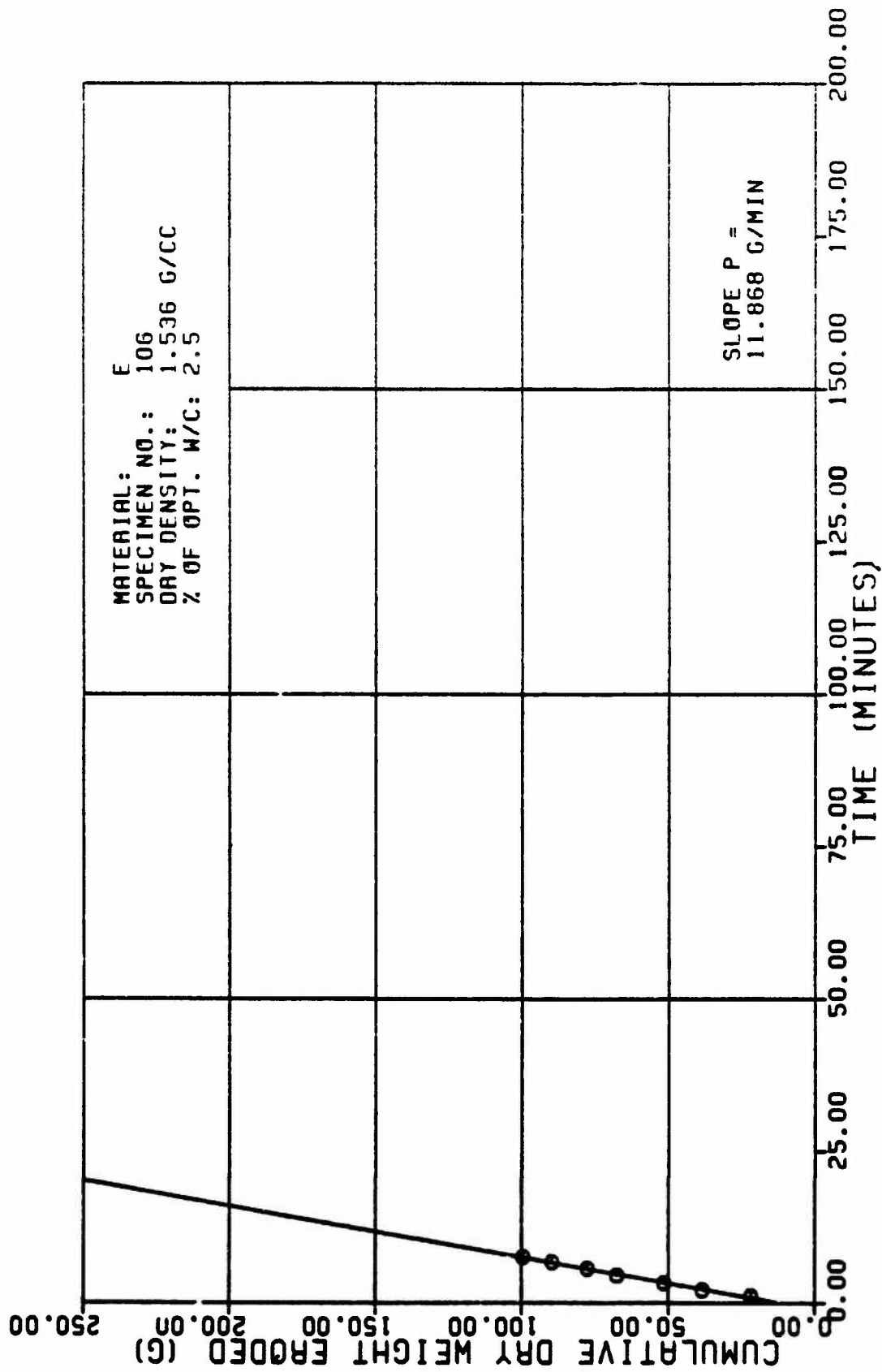


Figure A26b

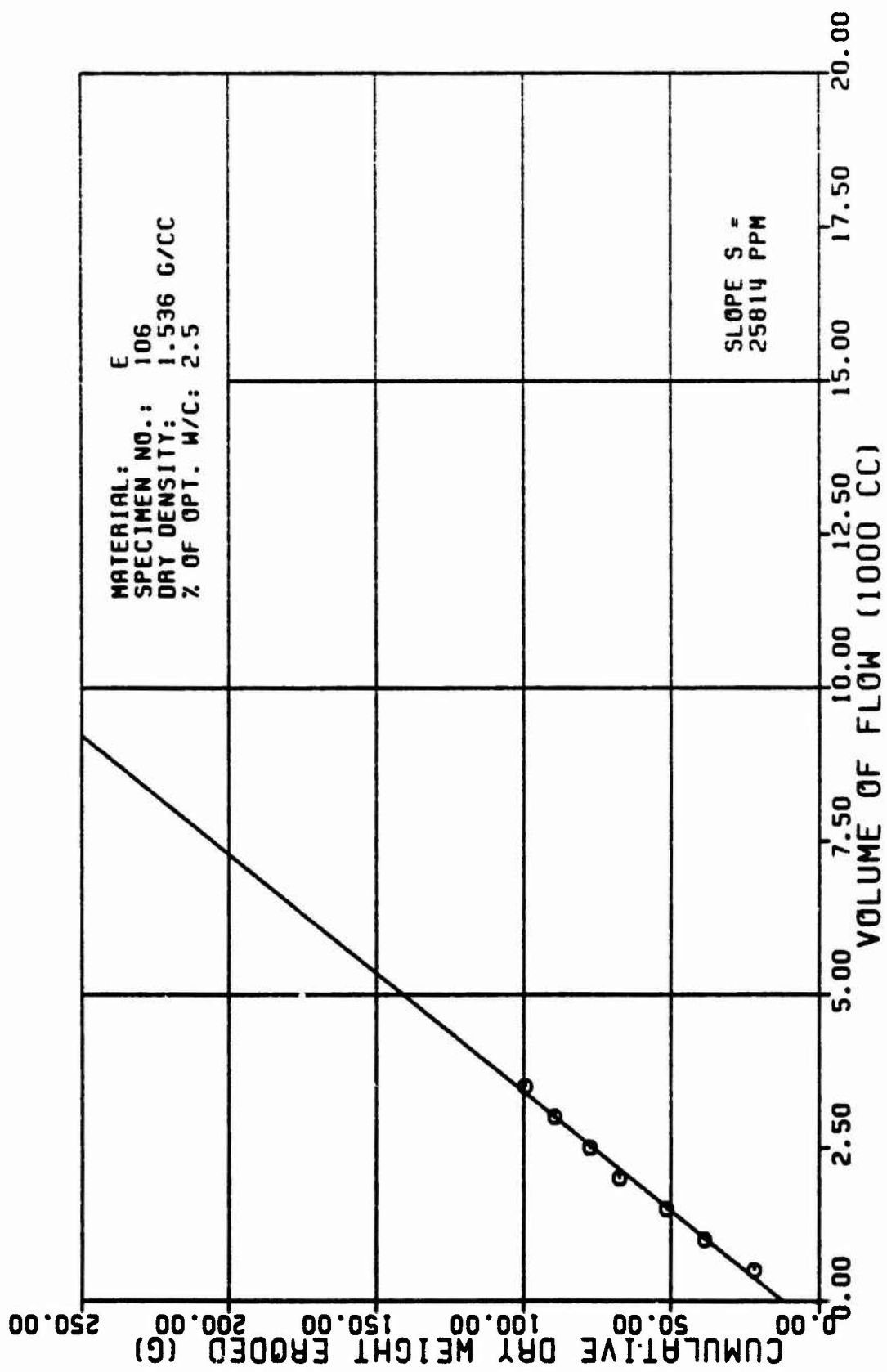


Figure A26c

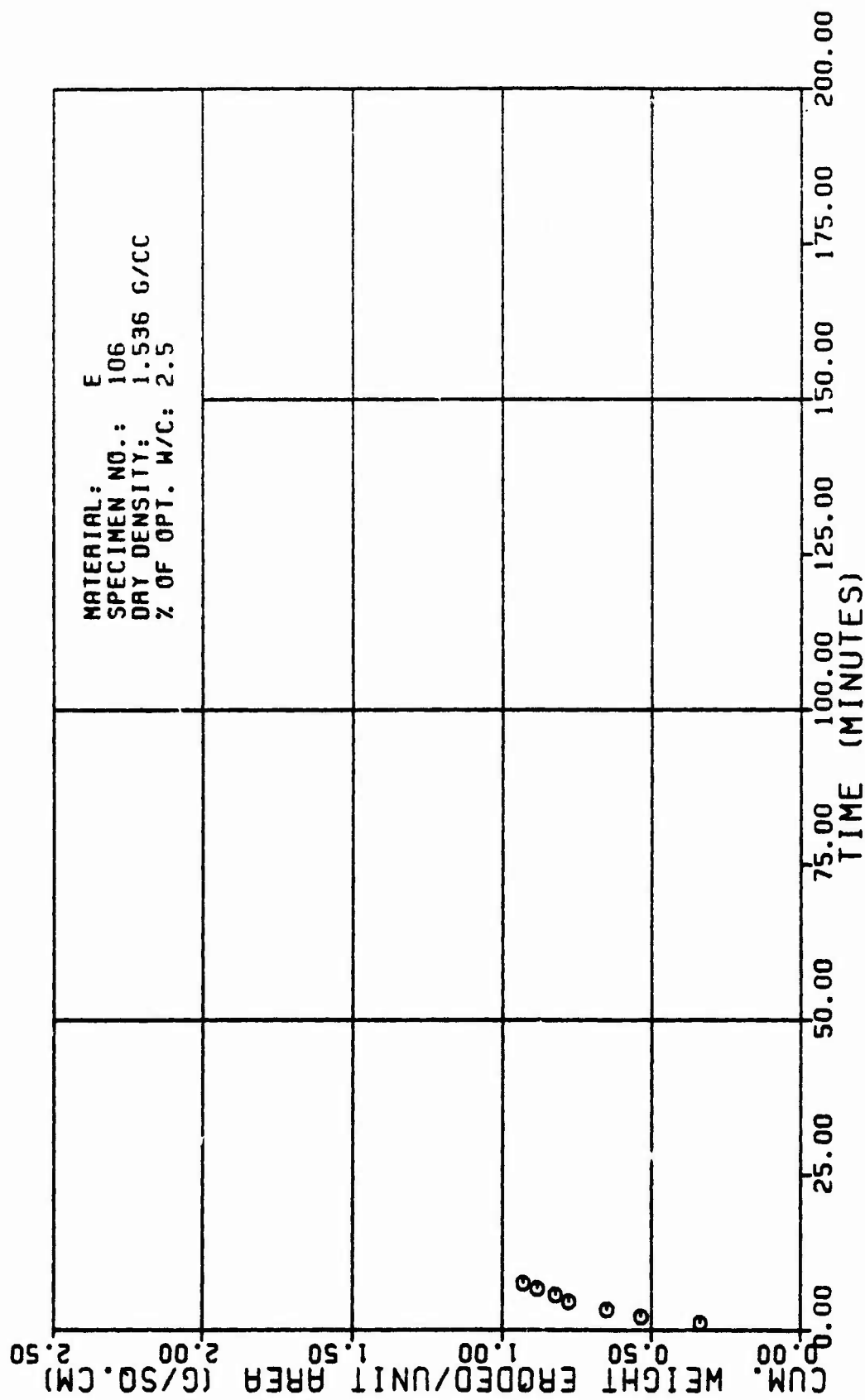


Figure A26d

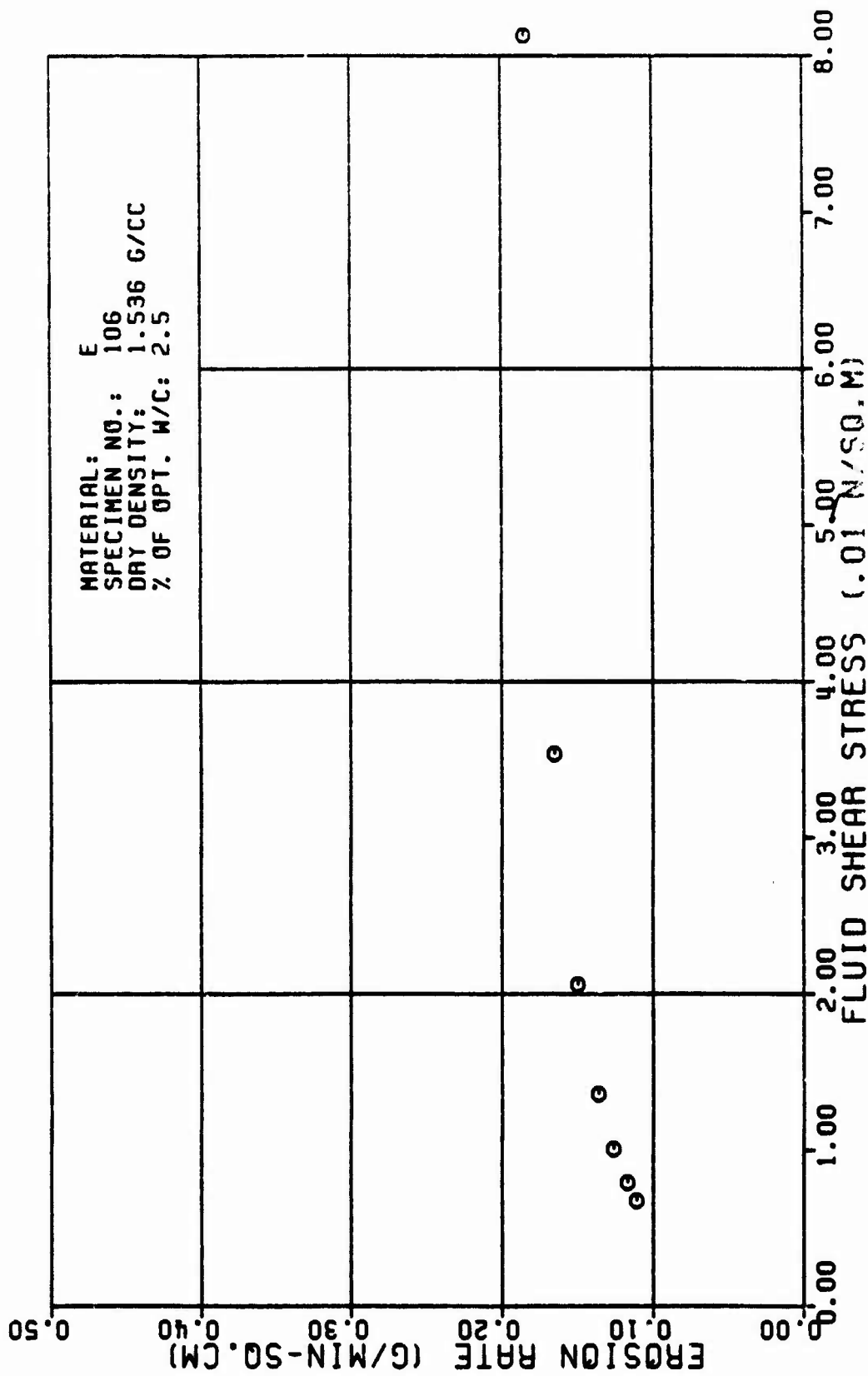


Figure A26e

TABLE A27

TEST RESULTS FOR TRIAXIAL EROSION TEST

MATERIAL TYPE: SPECIMEN NUMBER :		E 187		SANCHEZ & ASSIAN		AVERAGE FLOW RATE (Q):		555. CC/MIN	
TESTED BY:		4 15 82		1.547 G/CC		RATE OF WEIGHT EROSION (P):		11.1 G/MIN	
DATE TESTED:		8.8 PERCENT		2.32 CM		DENSITY OF ERODING FLUID:		1.000 G/CC	
SPECIMEN DRY DENSITY:		8.23 CM		11.48 CM		VISCOSITY OF ERODING FLUID:		8.881 M*SEC/SQ.M	
% OF OPTIMUM WATER CONTENT:		INITIAL SLOT WIDTH:		INITIAL SLOT THICKNESS:		CONFINING PRESSURE:		98.18 KN/SQ.M	
INITIAL SLOT WIDTH:		INITIAL SLOT THICKNESS:		ERODED LENGTH:		HEAD OF WATER:		13.88 M	
% OF OPTIMUM WATER CONTENT:		INITIAL SLOT WIDTH:		INITIAL SLOT THICKNESS:		HYDRAULIC GRADIENT:		18. M/M	
VOLUME OF FLOW (1000 CC)	TIME (MIN)	CUM. WEIGHT ERODED (G)	CROSS SECTION AREA (SQ.CM)	VELOCITY OF FLOW (CM/MIN)	ERODED SURFACE AREA (SQ.CM)	CUM. WEIGHT ERODED PER AREA (G/SQ.CM)	EROSION RATE (GRAMS/ (MIN * SQ.CM))	FLUID SHEAR STRESS (N/SQ.M)	REYNOLDS NUMBER
0.5	0.06	14.8	1.1	528.	53.	8.22	8.18	8.137	678.
1.0	1.77	21.5	1.7	342.	69.	8.31	8.16	8.863	622.
1.5	2.46	26.7	2.1	271.	73.	8.36	8.15	8.842	586.
2.0	3.43	33.2	2.7	289.	79.	8.42	8.14	8.827	541.
2.5	4.28	39.1	3.2	176.	85.	8.46	8.13	8.828	587.
3.0	5.88	47.7	3.7	153.	89.	8.53	8.12	8.816	482.
3.5	6.17	72.4	4.4	128.	96.	8.75	8.12	8.812	445.
4.0	7.85	81.9	5.8	113.	102.	8.88	8.11	8.818	422.
4.5	7.86	88.4	5.6	183.	107.	8.93	8.18	8.889	482.

TABLE FOR SPECIMEN NUMBER: E187 (CONTINUES)

VOLUME OF FLOW (1000 CC)	TIME (MIN)	CUM. WEIGHT ERODED (G)	CROSS SECTION AREA (SQ. CM)	VELOCITY OF FLOW (CM/MIN)	ERODED SURFACE AREA (SQ. CM)	CUM. WEIGHT ERODED PER AREA (G/SQ. CM)	EROSION RATE (GRAMS/ MIN. * SQ. CM)	FLUID SHEAR STRESS (N/SQ. M)	REYNOLDS NUMBER
5.8	0.74	98.6	6.1	93.	112.	8.05	8.18	8.888	382.
5.1	0.94	99.9	6.2	91.	114.	8.08	8.18	8.887	378.

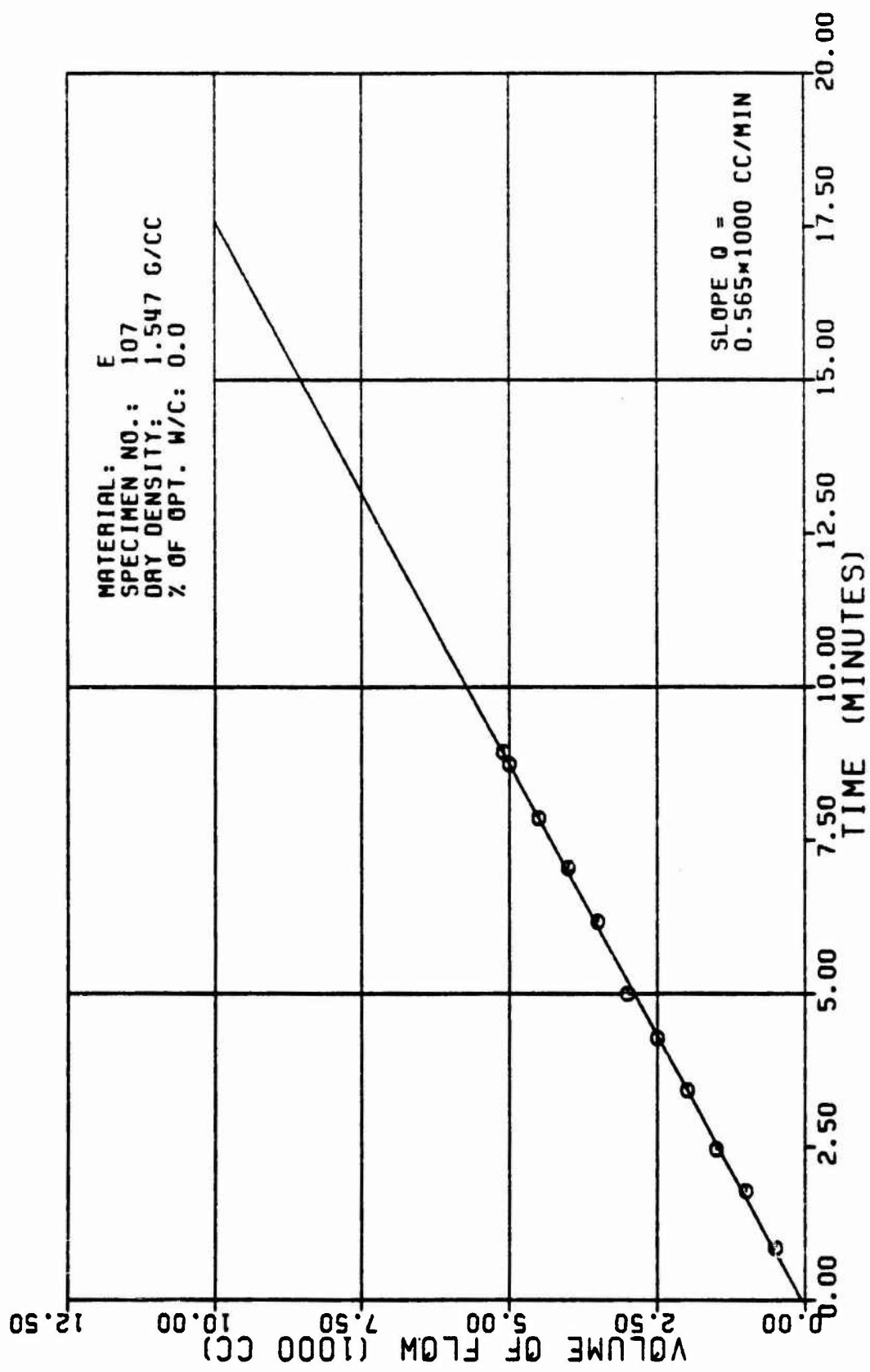


Figure A27a

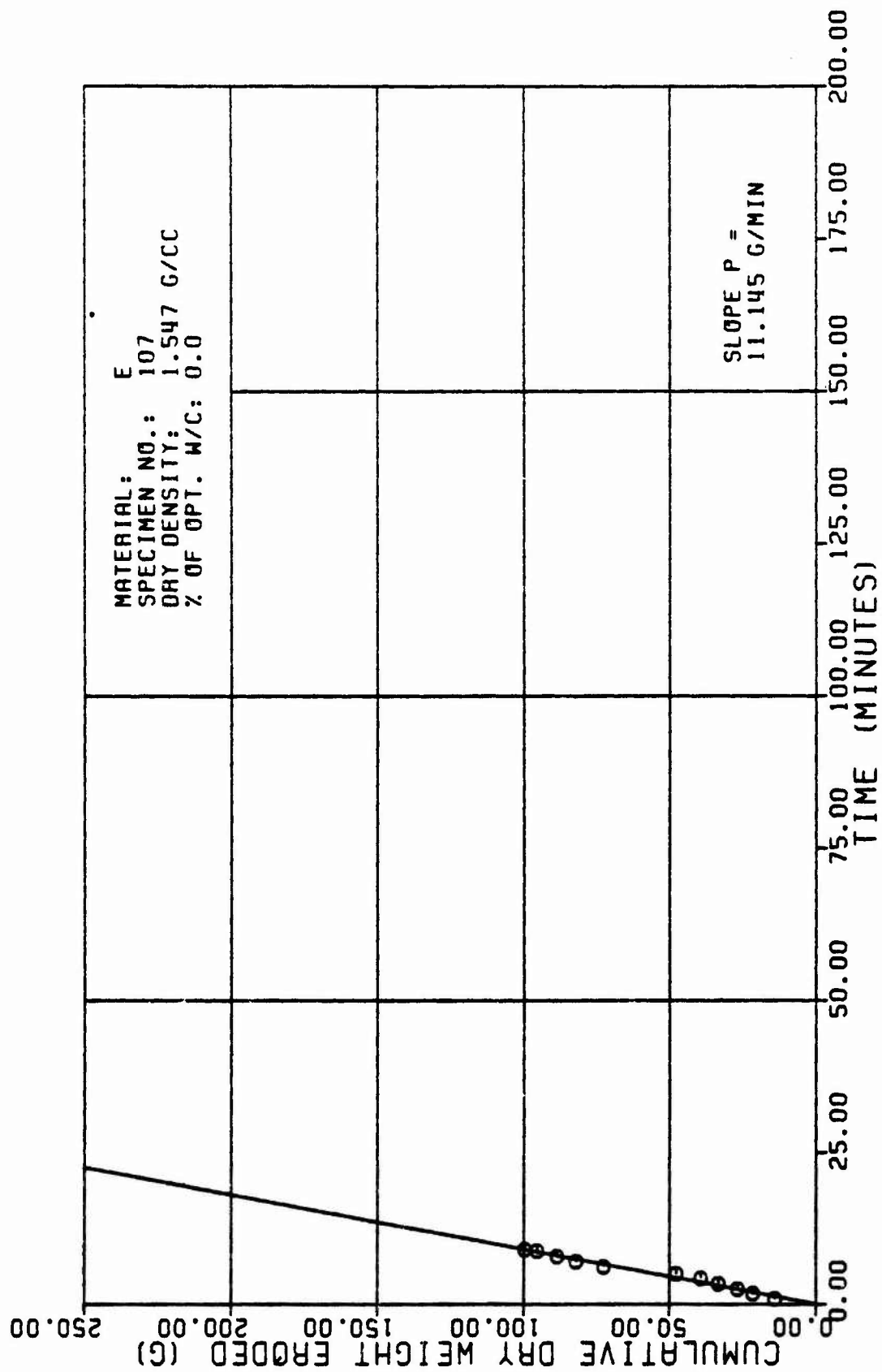


Figure A27b

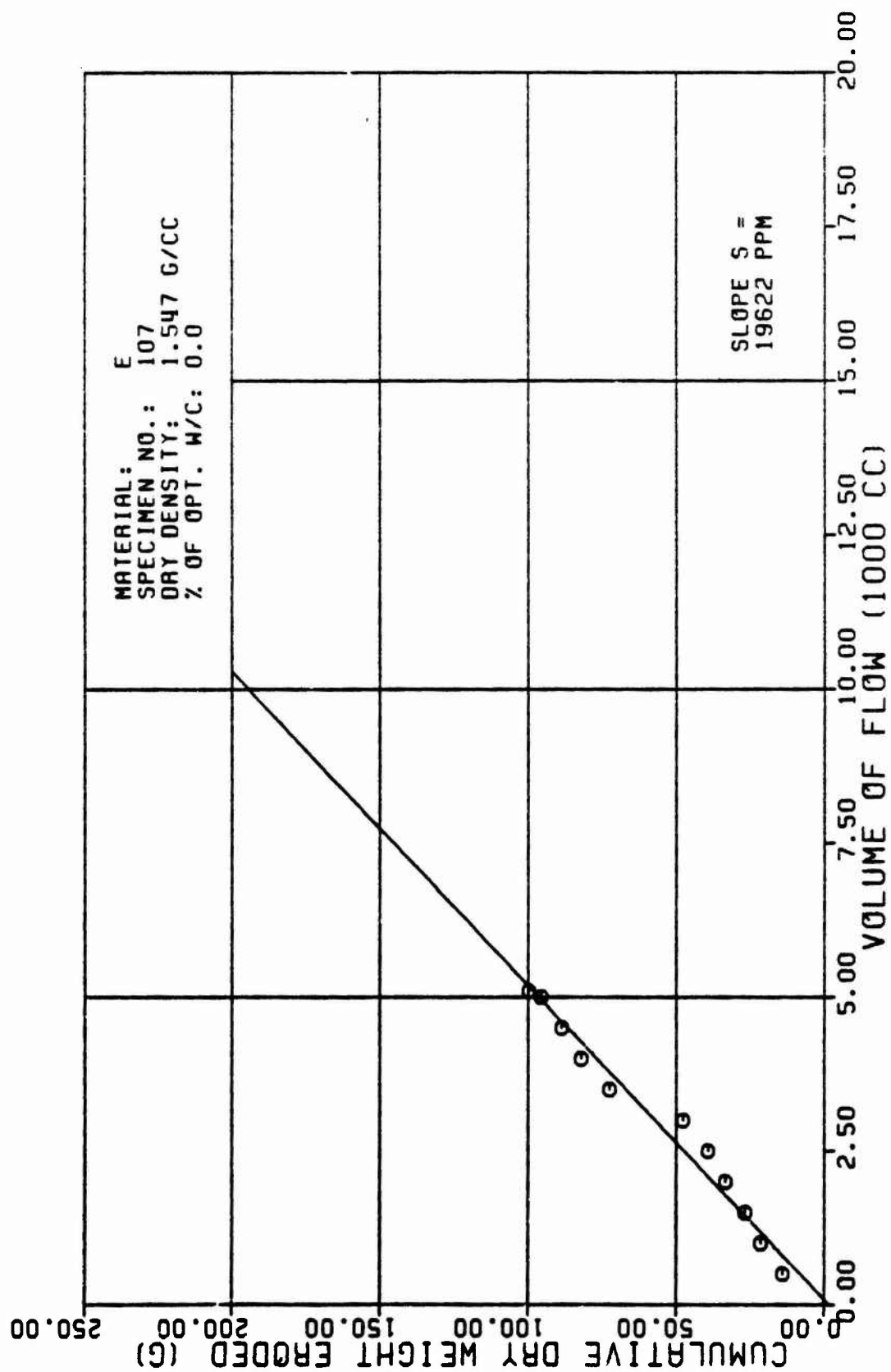


Figure A27c

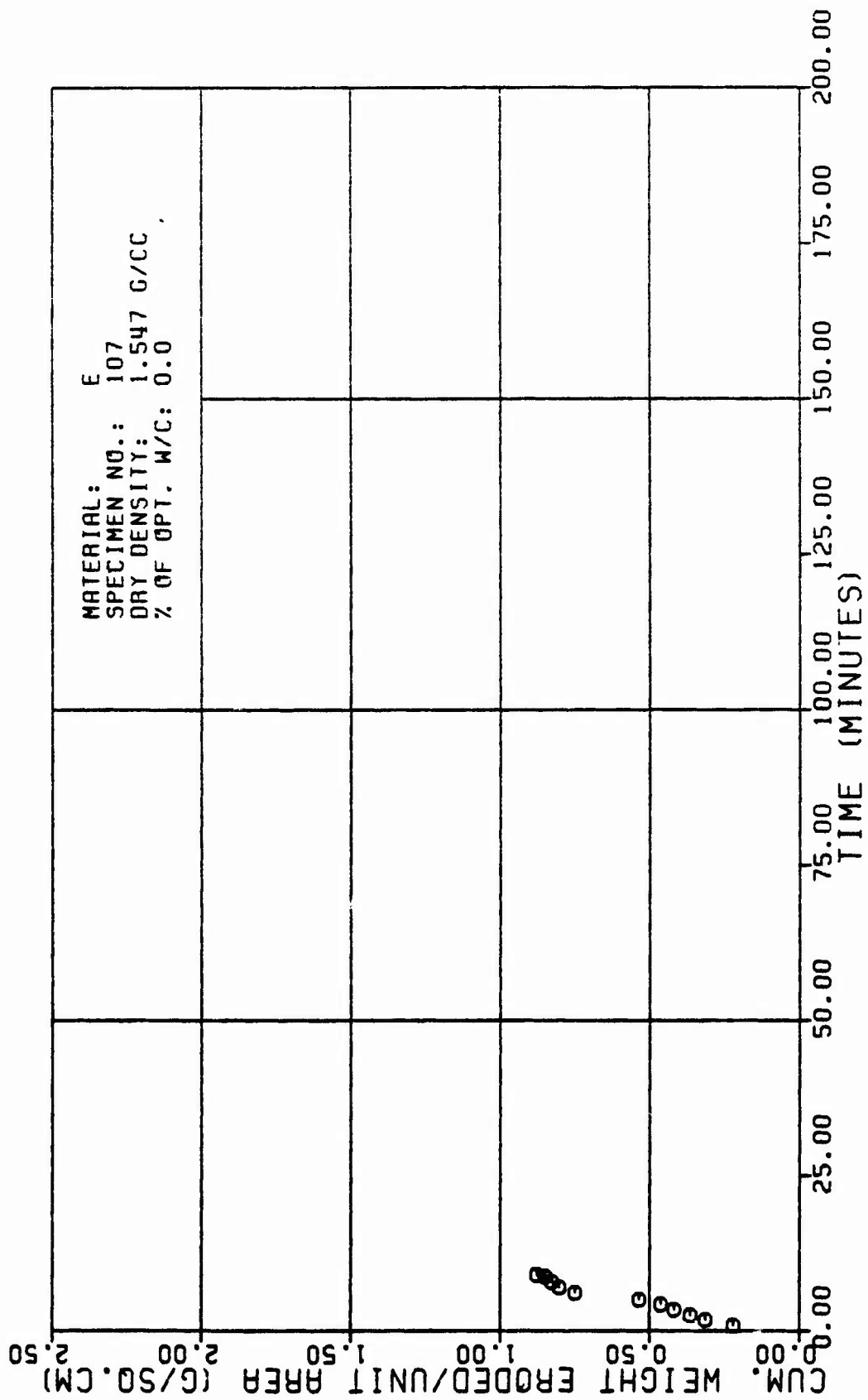


Figure A27d

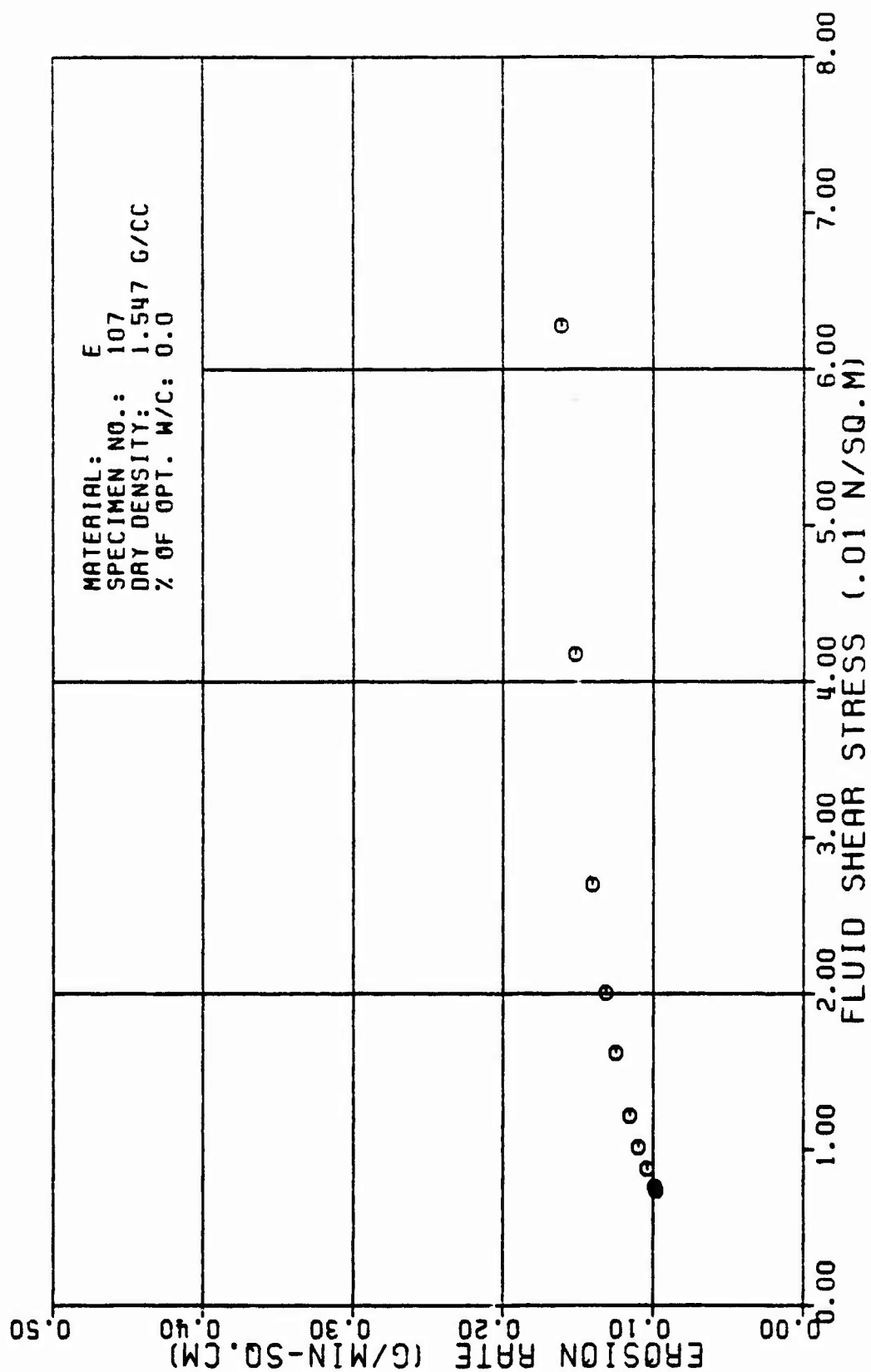


Figure A27e

TABLE A28

TEST RESULTS FOR TRIAXIAL EROSION TEST

MATERIAL TYPE: SPECIMEN NUMBER : TESTED BY:		E 788 SANCHEZ & ASSIAN		AVERAGE FLOW RATE (Q):		561. CC/MIN			
DATE TESTED:		4 15 82		RATE OF WEIGHT EROSION (P):		8.4 G/MIN			
SPECIMEN DRY DENSITY:		1.536 G/CC		DENSITY OF ERODING FLUID:		1.888 G/CC			
% OF OPTIMUM WATER CONTENT:		8.8 PERCENT		VISCOSITY OF ERODING FLUID:		8.881 M*SEC/SQ.M			
INITIAL SLOT WIDTH:		2.32 CM		CONFINING PRESSURE:		98.18 KN/SQ.M			
INITIAL SLOT THICKNESS:		8.23 CM		HEAD OF WATER:		13.88 M			
ERODED LENGTH:		11.48 CM		HYDRAULIC GRADIENT:		18. M/M			

VOLUME OF FLOW (1888 CC)	TIME (MIN)	CUM. WEIGHT ERODED (G)	CROSS SECTION AREA (SQ.CM)	VELOCITY OF FLOW (CM/MIN)	ERODED SURFACE AREA (SQ.CM)	CUM. WEIGHT ERODED PER AREA (G/SQ.CM)	EROSION RATE (GRAMS/ MIN * SQ.CM)	FLUID SHEAR STRESS (N/SQ.M)	REYNOLDS NUMBER
8.5	8.97	21.4	1.8	563.	63.	8.34	8.13	8.155	681.
1.8	1.89	32.2	1.4	391.	67.	8.48	8.12	8.888	637.
1.5	2.77	48.8	1.9	382.	71.	8.56	8.12	8.851	688.
2.8	3.71	48.6	2.3	243.	76.	8.62	8.11	8.835	565.
2.6	4.65	52.8	2.8	284.	88.	8.65	8.18	8.826	534.
3.8	5.58	59.4	3.2	175.	84.	8.78	8.18	8.828	586.
3.5	6.48	67.7	3.6	155.	89.	8.76	8.89	8.817	482.
4.8	7.81	76.5	3.9	145.	91.	8.84	8.89	8.815	469.

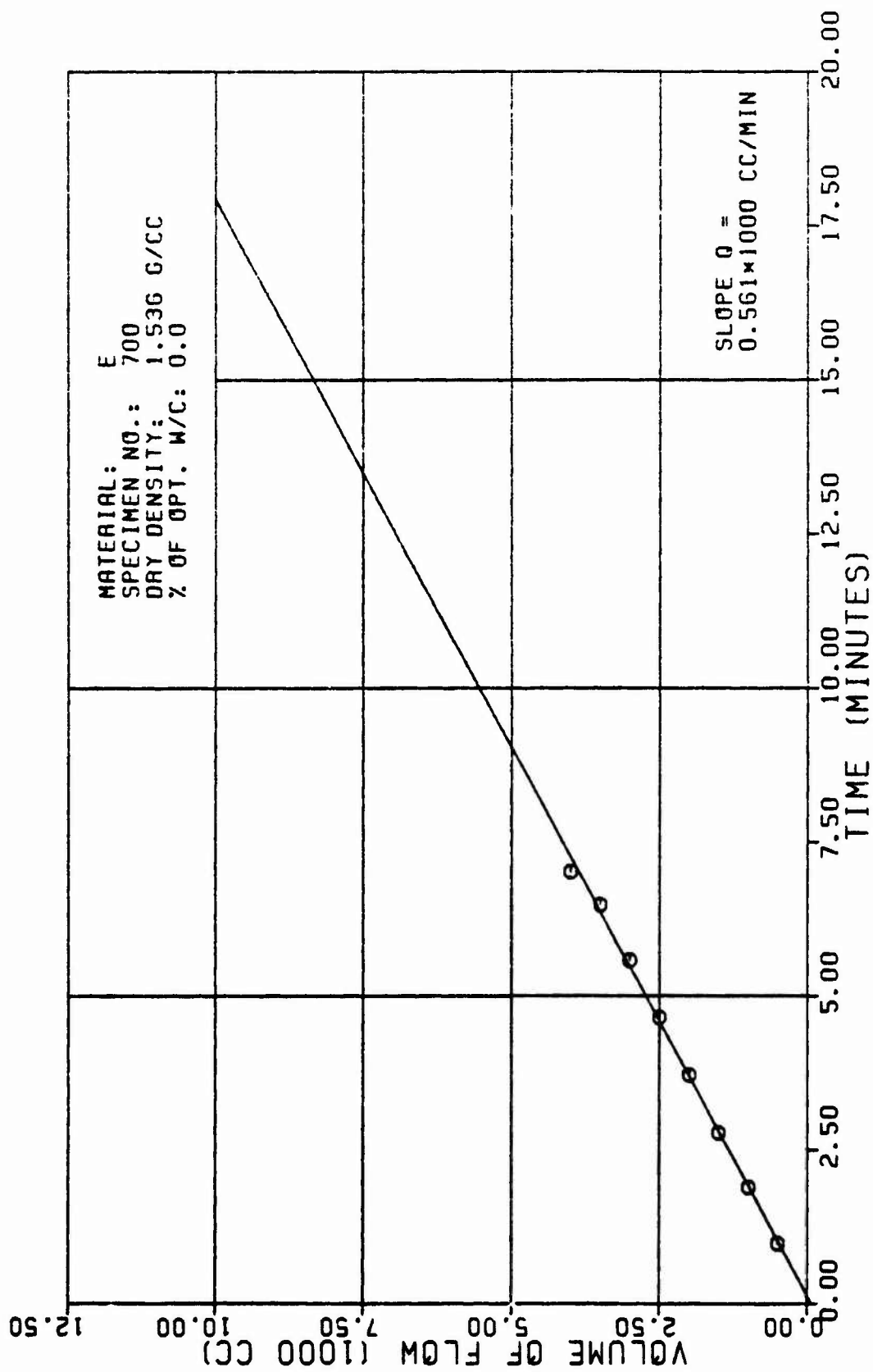


Figure A28a

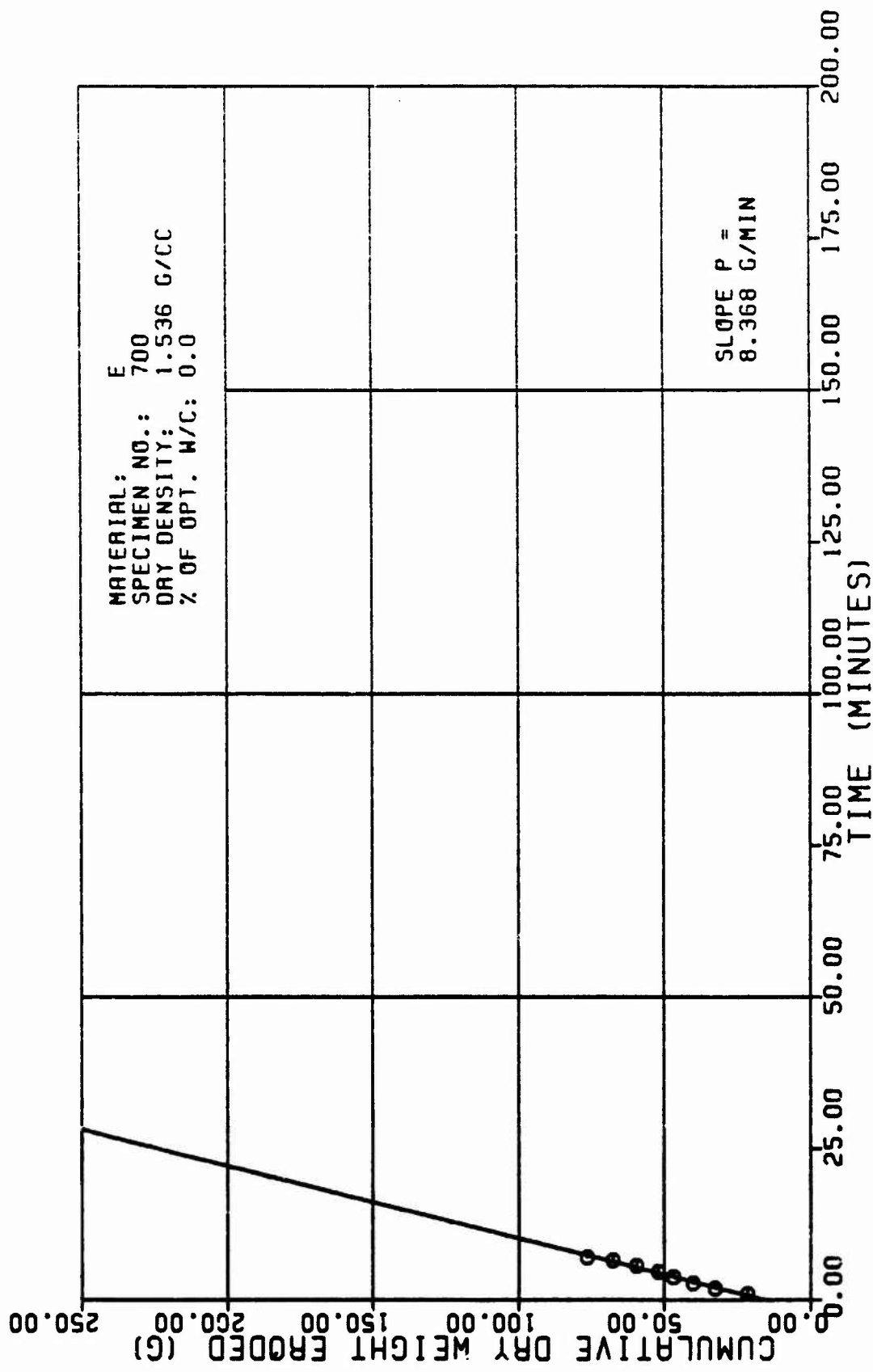


Figure A28b

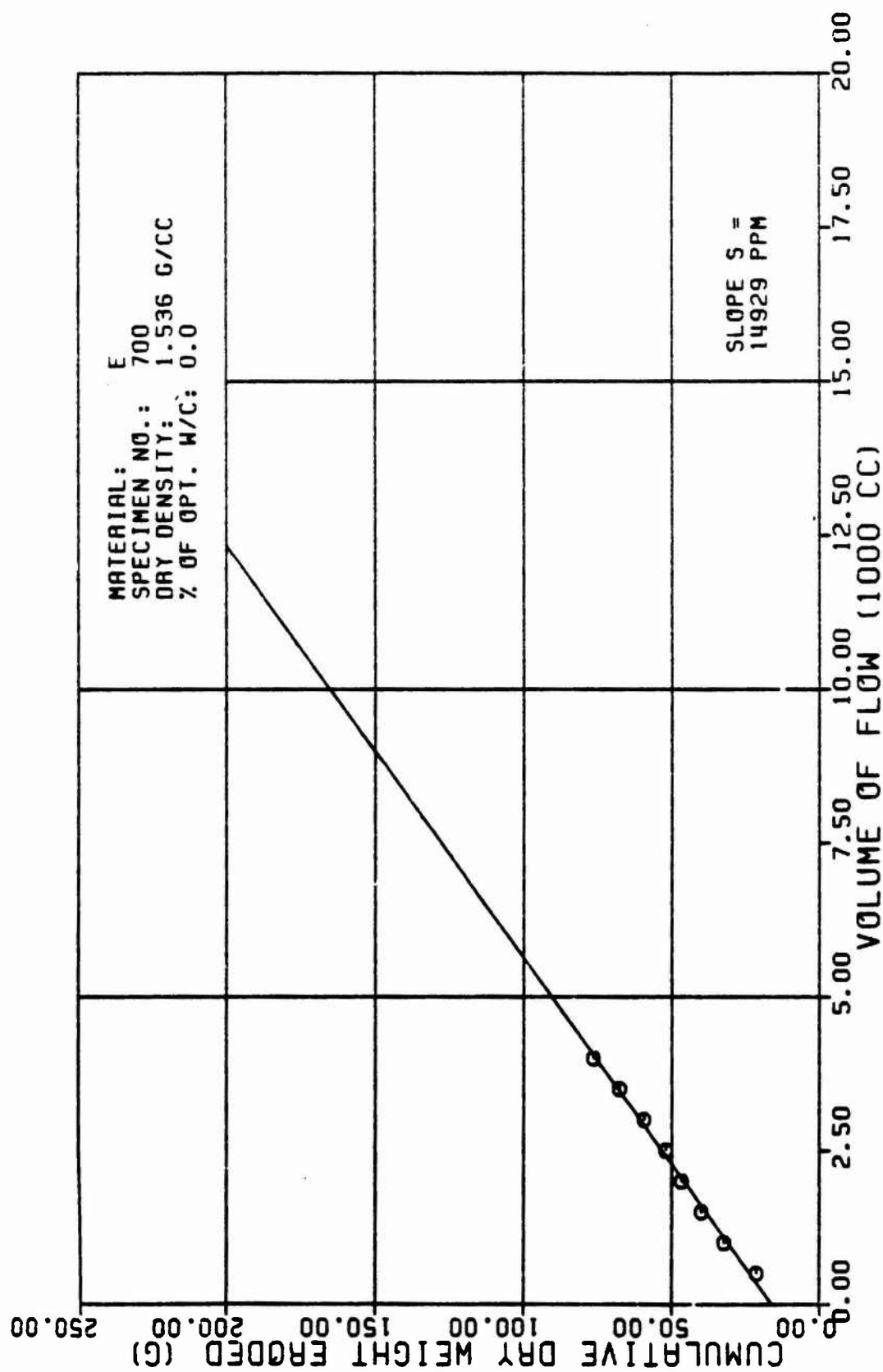


Figure A28c

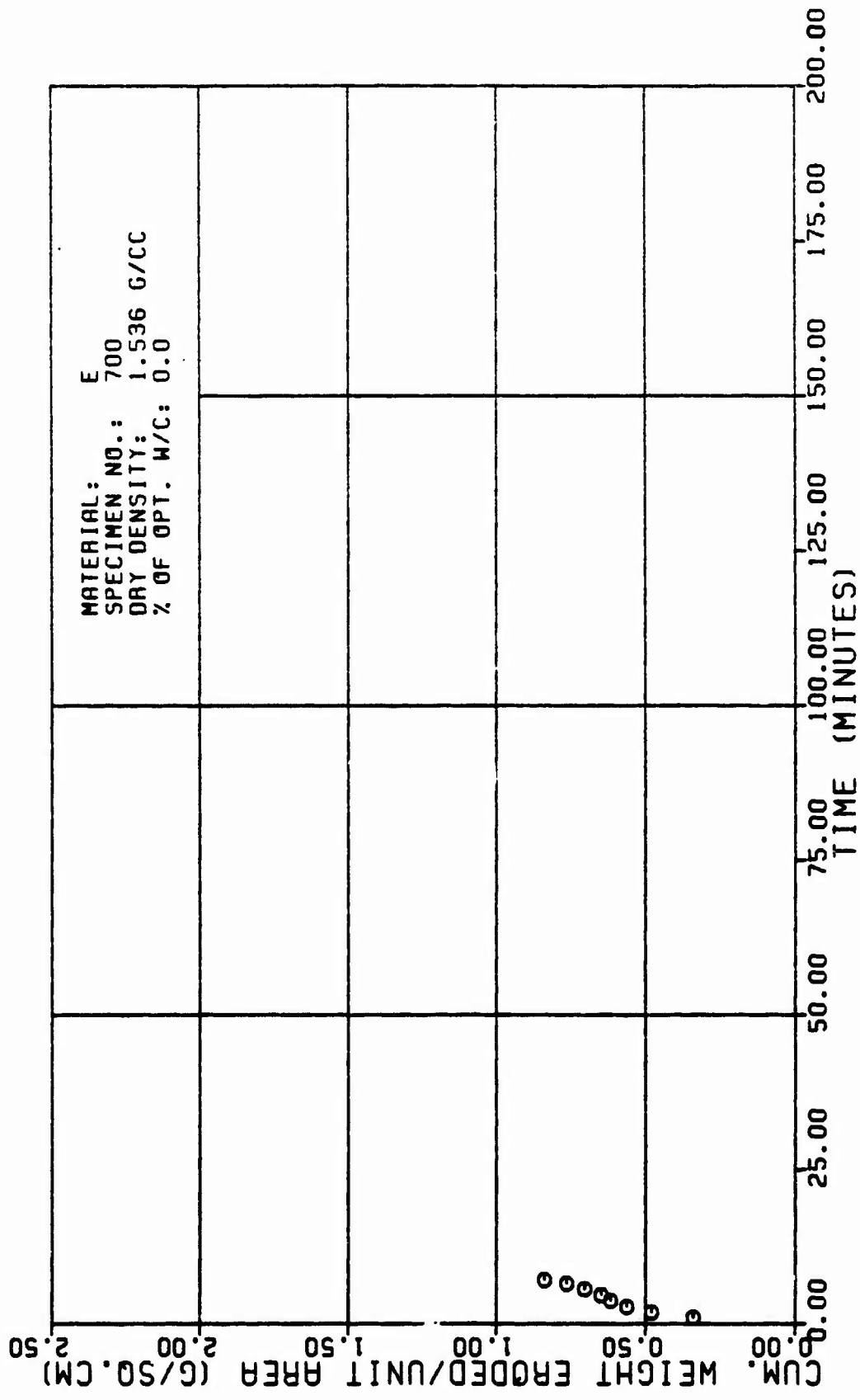


Figure A28d

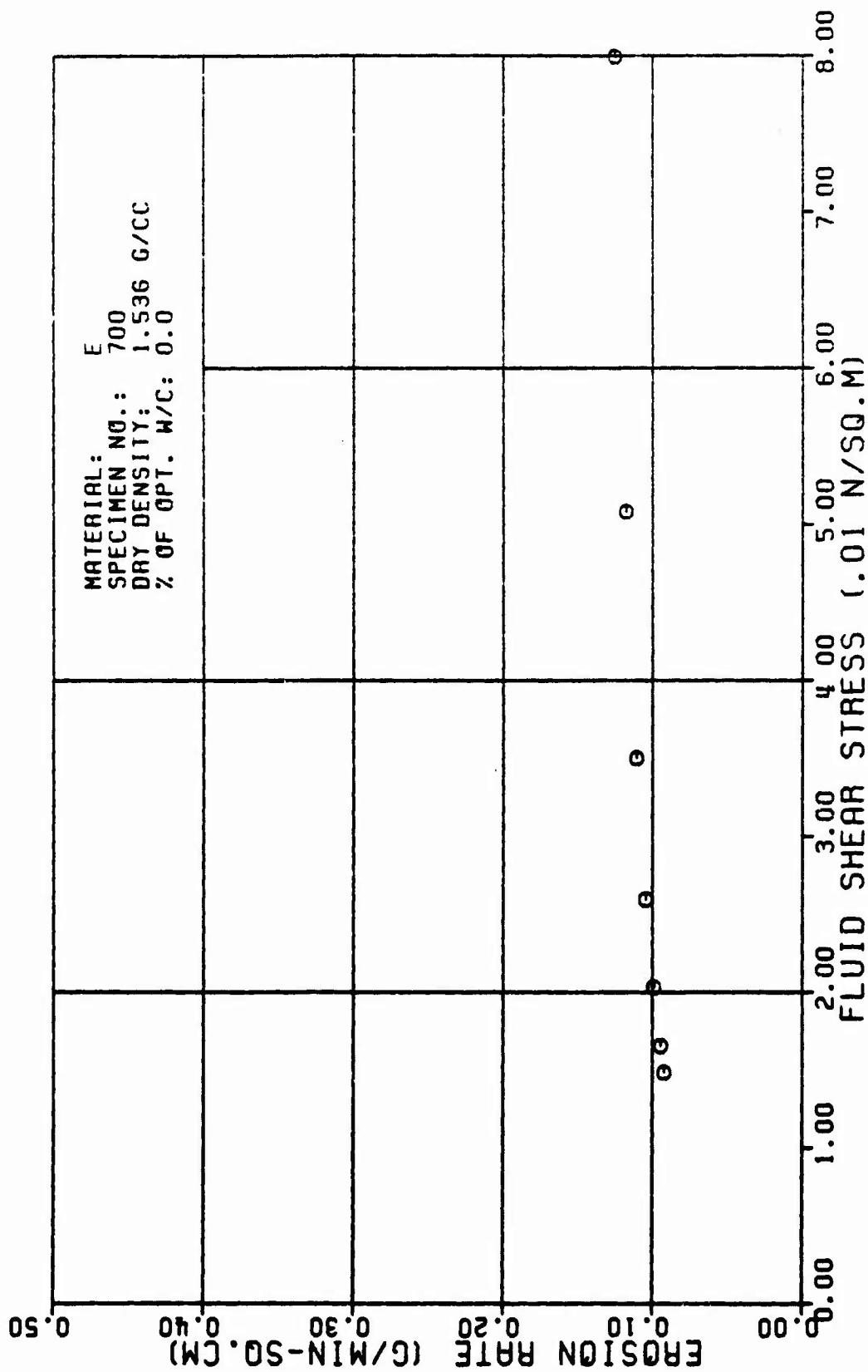


Figure A28e

TABLE A29

TEST RESULTS FOR TRIAXIAL EROSION TEST

MATERIAL TYPE: SPECIMEN NUMBER : TESTED BY:		7/1 SANCHEZ & ASSIAN		622. CC/MIN 0.2 G/MIN					
DATE TESTED:		4 10 82		1.000 G/CC 0.001 N*SEC/SQ.M					
SPECIMEN DRY DENSITY:		1.041 G/CC		98.10 KN/SQ.M					
% OF OPTIMUM WATER CONTENT:		2.0 PERCENT		13.00 M					
INITIAL SLOT WIDTH:		2.32 CM		10. M/M					
INITIAL SLOT THICKNESS:		0.23 CM							
ERODED LENGTH:		11.40 CM							
AVERAGE FLOW RATE (Q):									
RATE OF WEIGHT EROSION (P):									
DENSITY OF ERODING FLUID:									
VISCOSITY OF ERODING FLUID:									
CONFINING PRESSURE:									
HEAD OF WATER:									
HYDRAULIC GRADIENT:									
VOLUME OF FLOW (1000 CC)	TIME (MIN)	CUM. WEIGHT ERODED (G)	CROSS SECTION AREA (SQ.CM)	VELOCITY OF FLOW (CM/MIN)	ERODED SURFACE AREA (SQ.CM)	CUM. WEIGHT ERODED PER AREA (G/SQ.CM)	EROSION RATE (GRAMS/ (MIN * SQ.CM))	FLUID SHEAR STRESS (N/SQ.M)	REYNOLDS NUMBER
0.0	0.92	19.0	1.0	644.	62.	0.32	0.13	0.103	700.
1.0	1.00	33.4	1.4	444.	67.	0.50	0.12	0.093	709.
1.0	2.76	40.7	1.0	300.	71.	0.57	0.12	0.050	667.
2.0	3.09	40.0	2.3	275.	75.	0.65	0.11	0.040	629.
2.5	4.00	05.1	2.7	232.	79.	0.71	0.10	0.030	596.
3.0	0.30	63.7	3.0	206.	83.	0.77	0.10	0.025	572.
3.5	6.10	70.2	3.4	101.	87.	0.01	0.10	0.020	546.
4.0	0.00	75.0	3.0	105.	90.	0.03	0.09	0.017	526.
4.0	7.04	00.3	4.1	101.	93.	0.06	0.09	0.015	506.

TABLE FOR SPECIMEN NUMBER: E781 (CONTINUES)

VOLUME OF FLOW (1000 CC)	TIME (MIN)	CUM. WEIGHT ERODED (G)	CROSS SECTION AREA (SQ. CM)	VELOCITY OF FLOW (CM/MIN)	ERODED SURFACE AREA (SQ. CM)	CUM. WEIGHT ERODED PER AREA (G/SQ. CM)	EROSION RATE (GRAMS/ MIN * SQ. CM)	FLUID SHEAR STRESS (N/SQ. M)	REYNOLDS NUMBER
5.5	8.48	85.3	4.5	139.	97.	5.88	5.89	5.513	488.
5.5	9.24	91.3	4.9	128.	181.	5.91	5.88	5.512	459.
6.5	9.68	94.9	5.5	123.	182.	5.93	5.88	5.511	462.

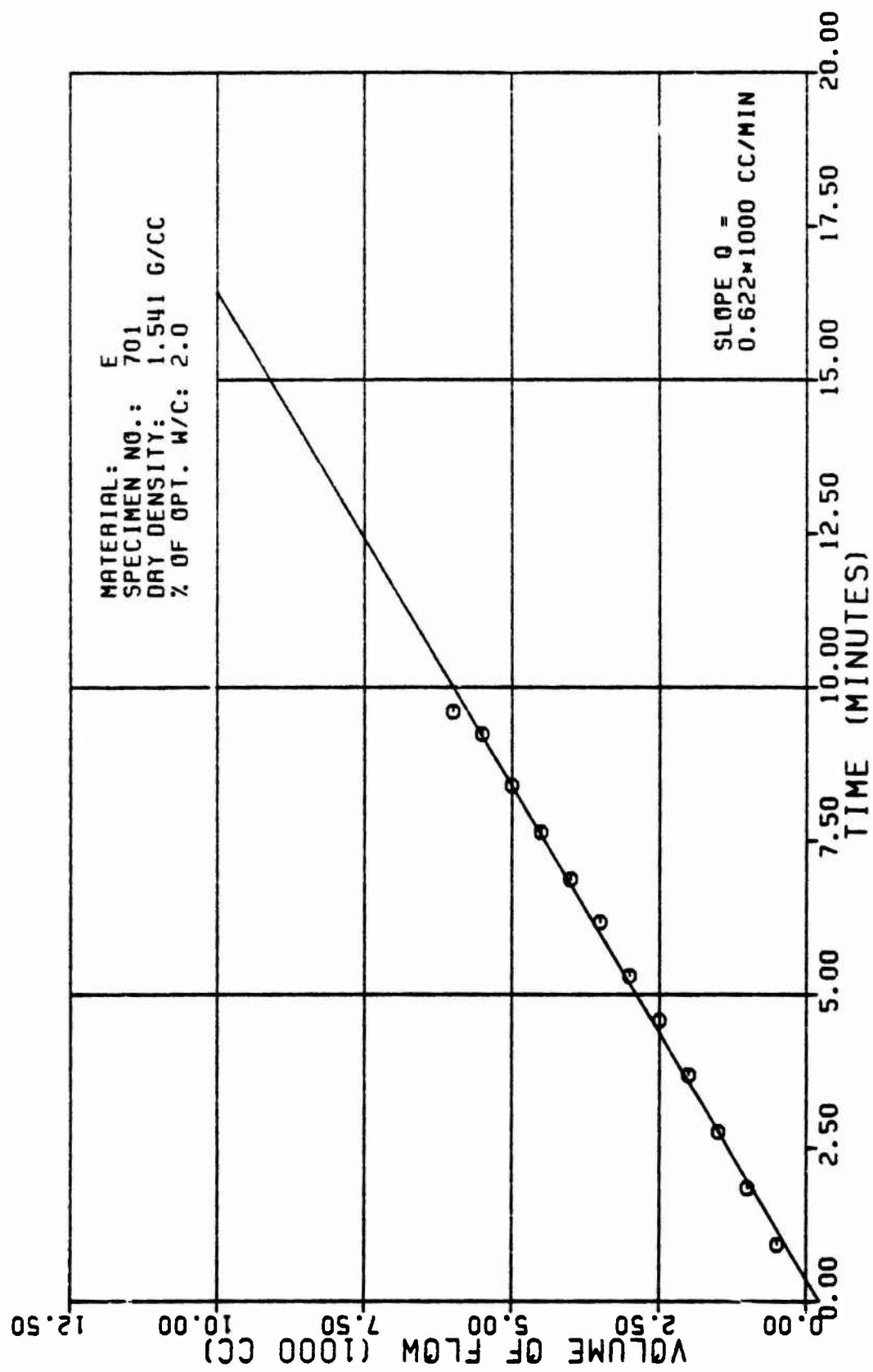


Figure A29a

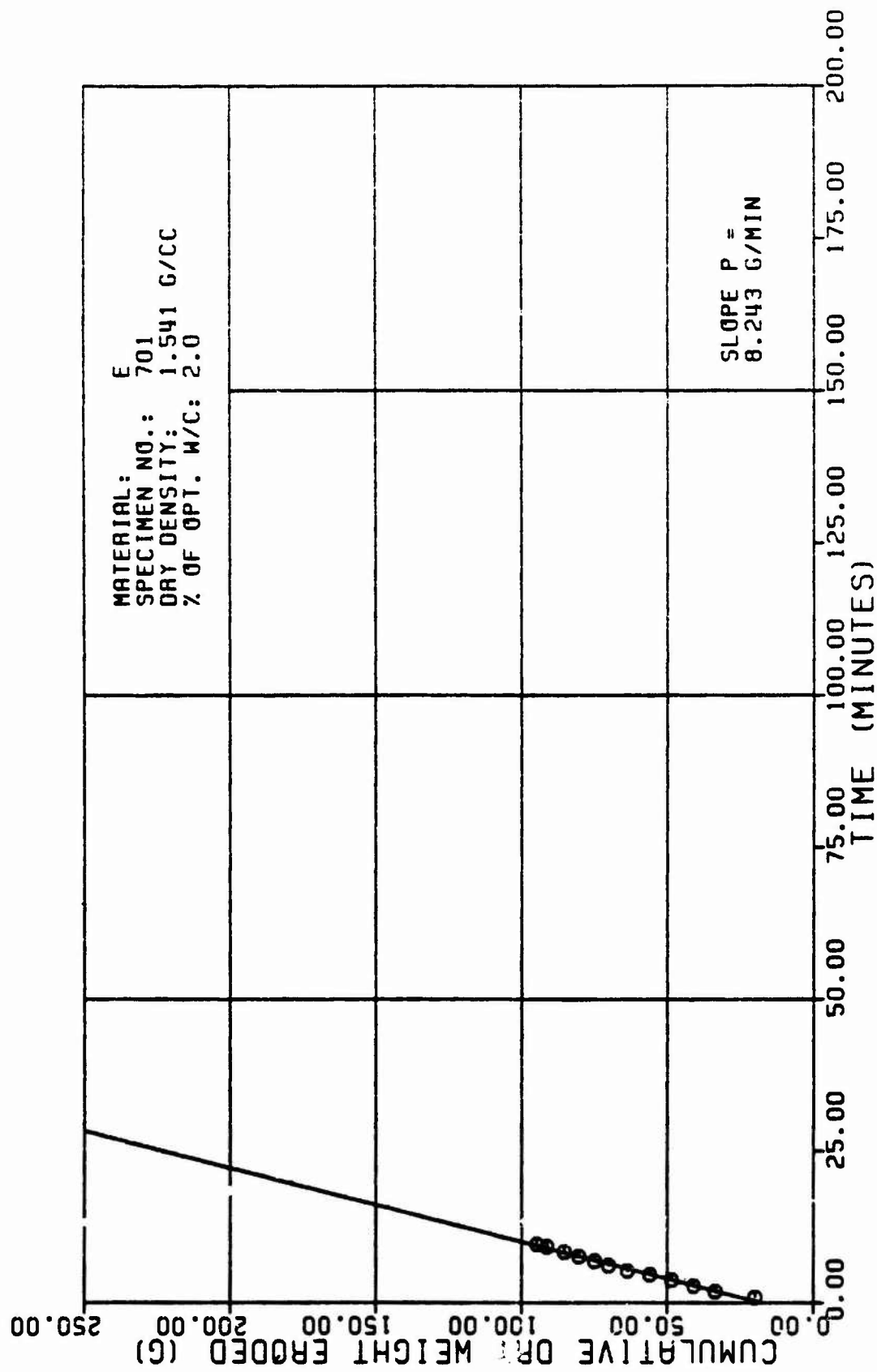


Figure A29b

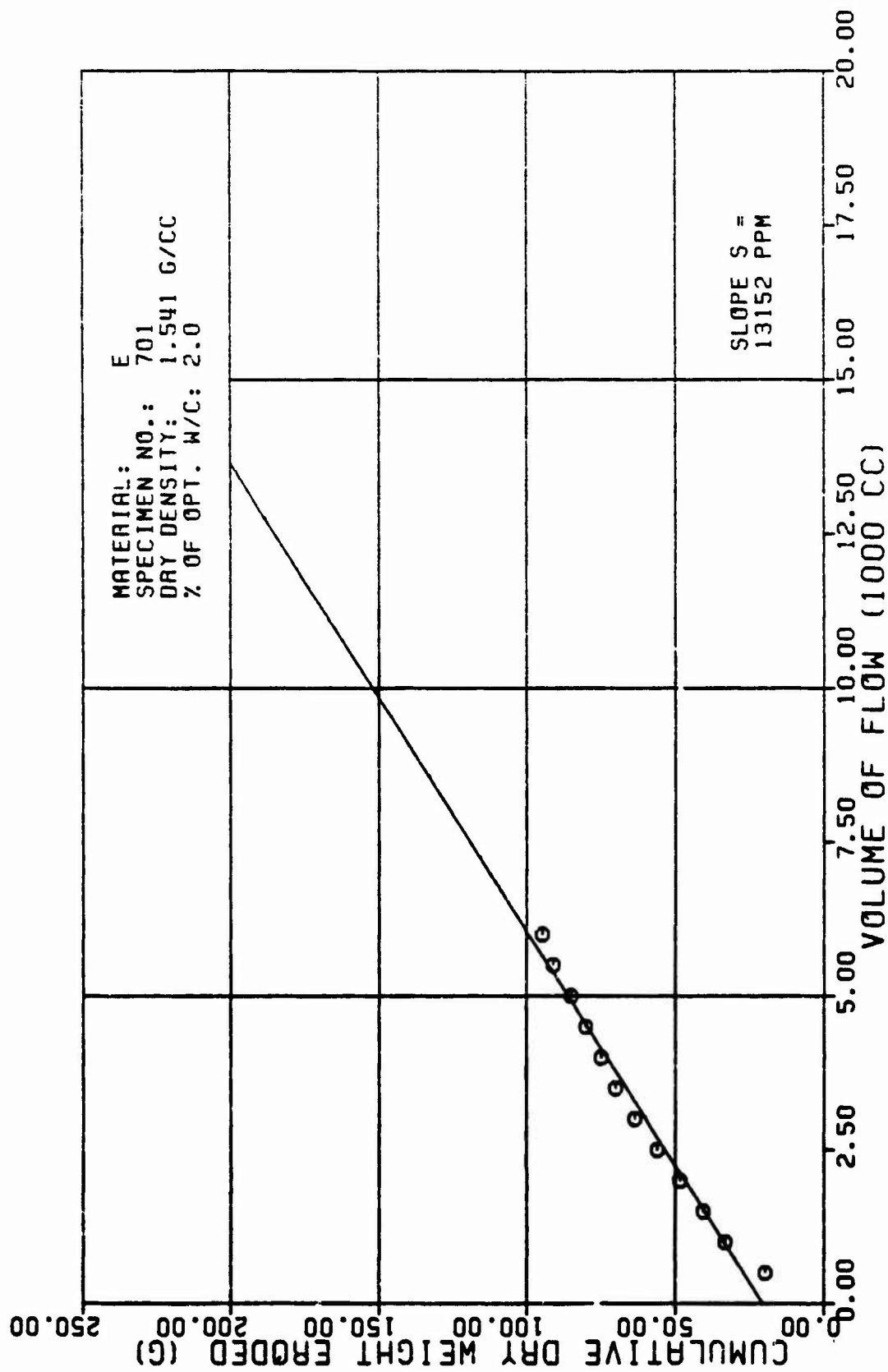


Figure A29c

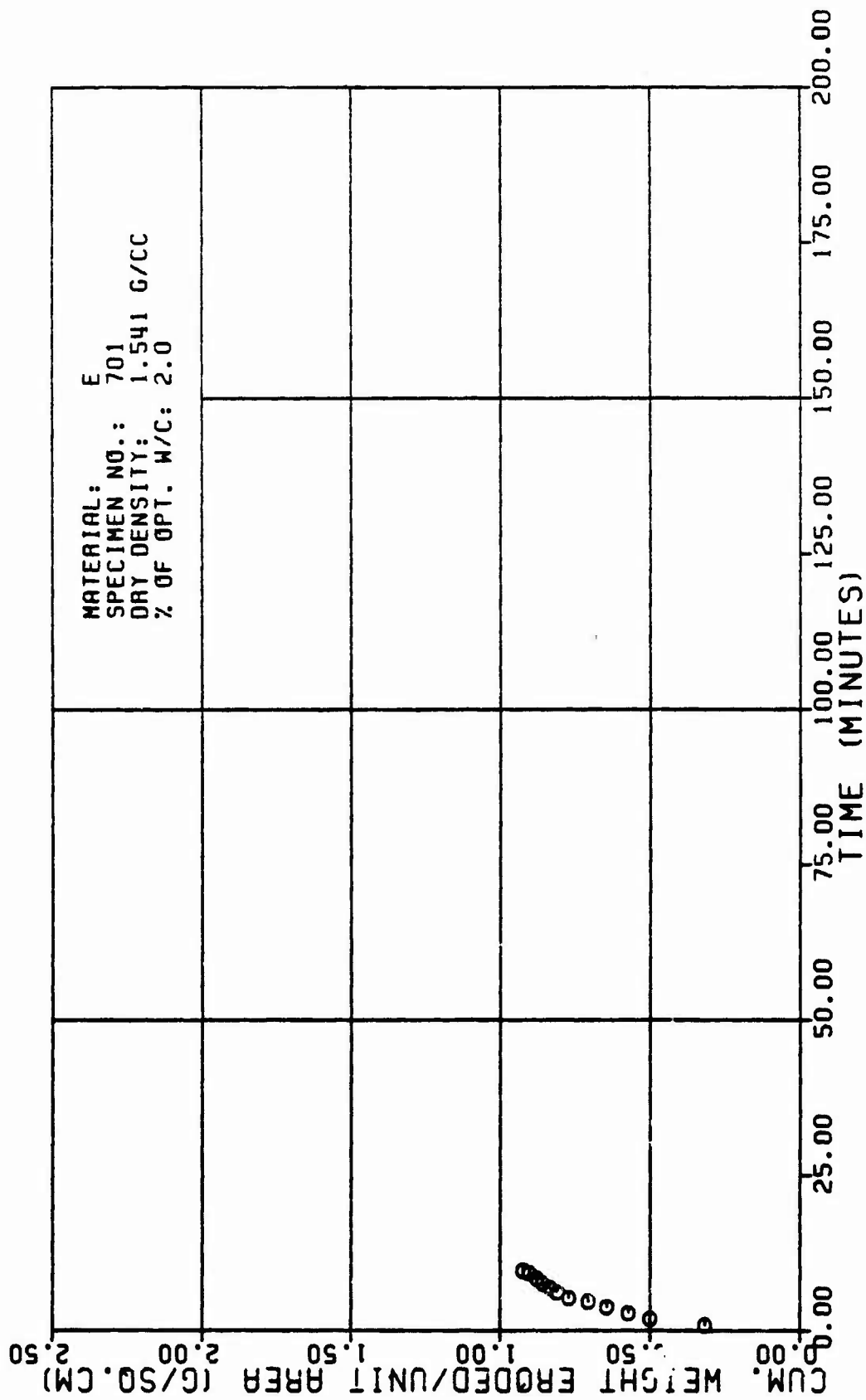


Figure A29d

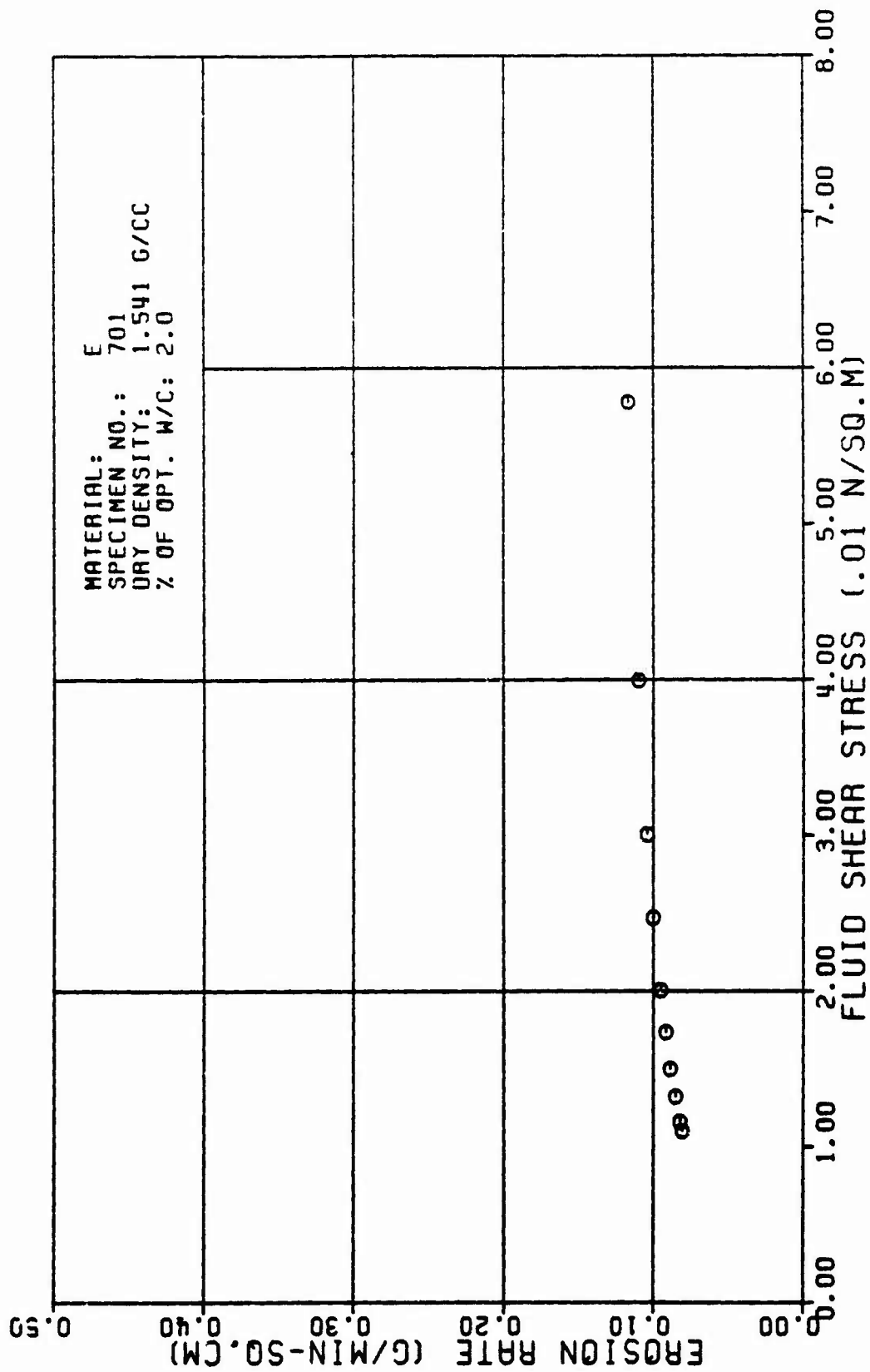


Figure A29e

APPENDIX B

SUMMARY OF TEST RESULTS GIVEN IN APPENDIX A

TABLE B1

SPECIMENS TESTED TO OBSERVE THE EFFECT OF WATER CONTENT
ON EROSION *

Specimen Number	Rate of Weight Erosion (g/min) P	Initial Specimen Dry Mass (g) W_i	Percent Erosion/Time e (%/min)	Max. Erosion Rate i_{Max} (g/cm ² - min)	% from Optimum w/c (%)	% of Max. Dry Density (%)
B110	0.5	995	0.05	0.01	+2.0	95
B111	1.0	1004	0.10	0.02	0.0	95
B113	2.5	998	0.25	0.04	-2.0	95
B117	1.2	1002	0.12	0.03	+3.0	95
B119	1.1	1002	0.11	0.02	+3.0	95
B120	1.7	998	0.17	0.03	+4.0	95
B121	0.5	989	0.05	0.01	+1.5	95
D170	13.9	1014	1.37	0.16	-0.5	95
D171	18.8	1013	1.86	0.25	+1.0	95
D173	36.6	1015	3.60	0.36	-3.0	95
D175	11.0	1018	1.08	0.18	-1.0	95

**SPECIMENS TESTED TO OBSERVE THE EFFECT OF WATER CONTENT
ON EROSION**

[illegible]

TABLE B 2
SPECIMENS TESTED TO OBSERVE THE EFFECT OF DENSITY
ON EROSION

Specimen Number	Rate of Weight Erosion (g/min) <i>P</i>	Initial Specimen Dry Mass (g) <i>w_i</i>	Percent Erosion/Time <i>a</i> (%/min)	Max. Erosion Rate <i>i</i> _{Max} (g/cm ² - min)	% from Optimum w/c (%)	% of Max. Dry Density (%)
B111	1.0	1004	0.10	0.02	0.0	95
B114	0.8	1042	0.08	0.01	0.0	98
B123	3.2	946	0.33	0.05	0.0	90
D170	13.9	1014	1.37	0.16	-0.5	95
D172	14.2	1035	1.37	0.19	-0.5	98
E105	11.8	969	1.22	0.18	0.0	99
E107	11.1	935	1.19	0.18	0.0	95

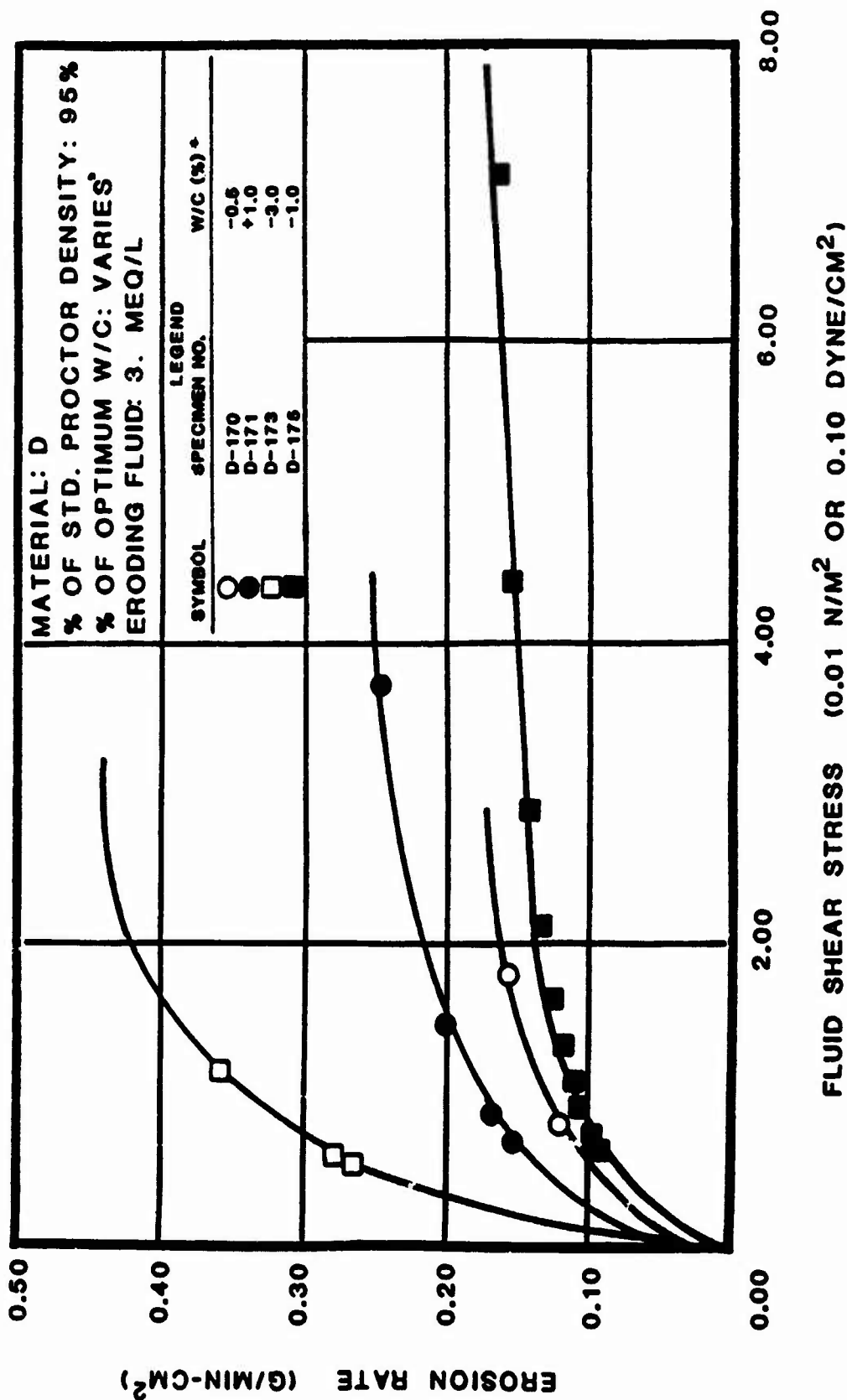


Fig. B2 Summary curve showing the effect of deviation from optimum molding water content on the erosion rate as a function of fluid shear stress for slightly clayey silt specimens (Material D).

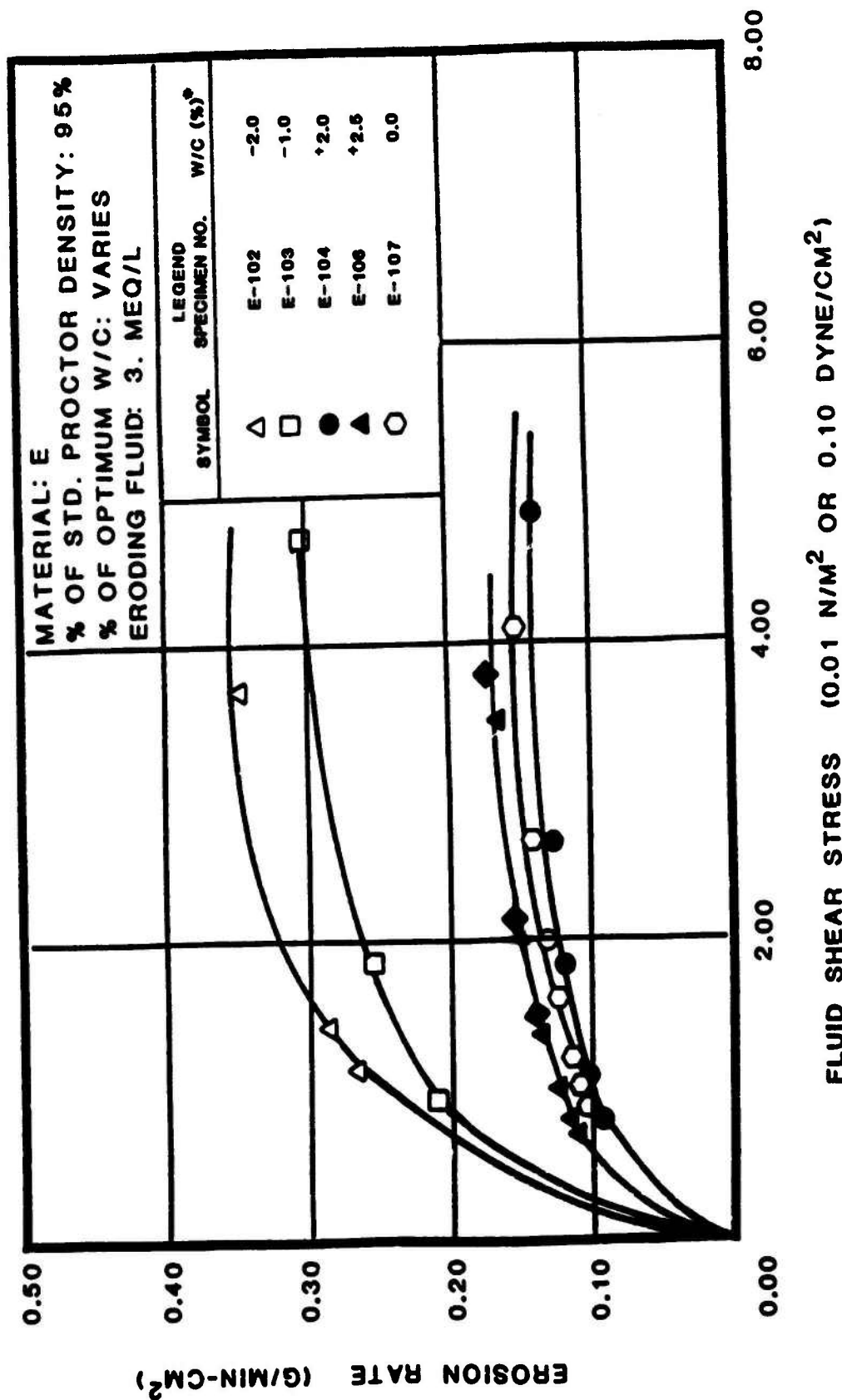


Fig. B3 Summary curve showing the effect of deviation from optimum molding water content on the erosion rate as a function of fluid shear stress for slightly clayey silt specimens (Material E).

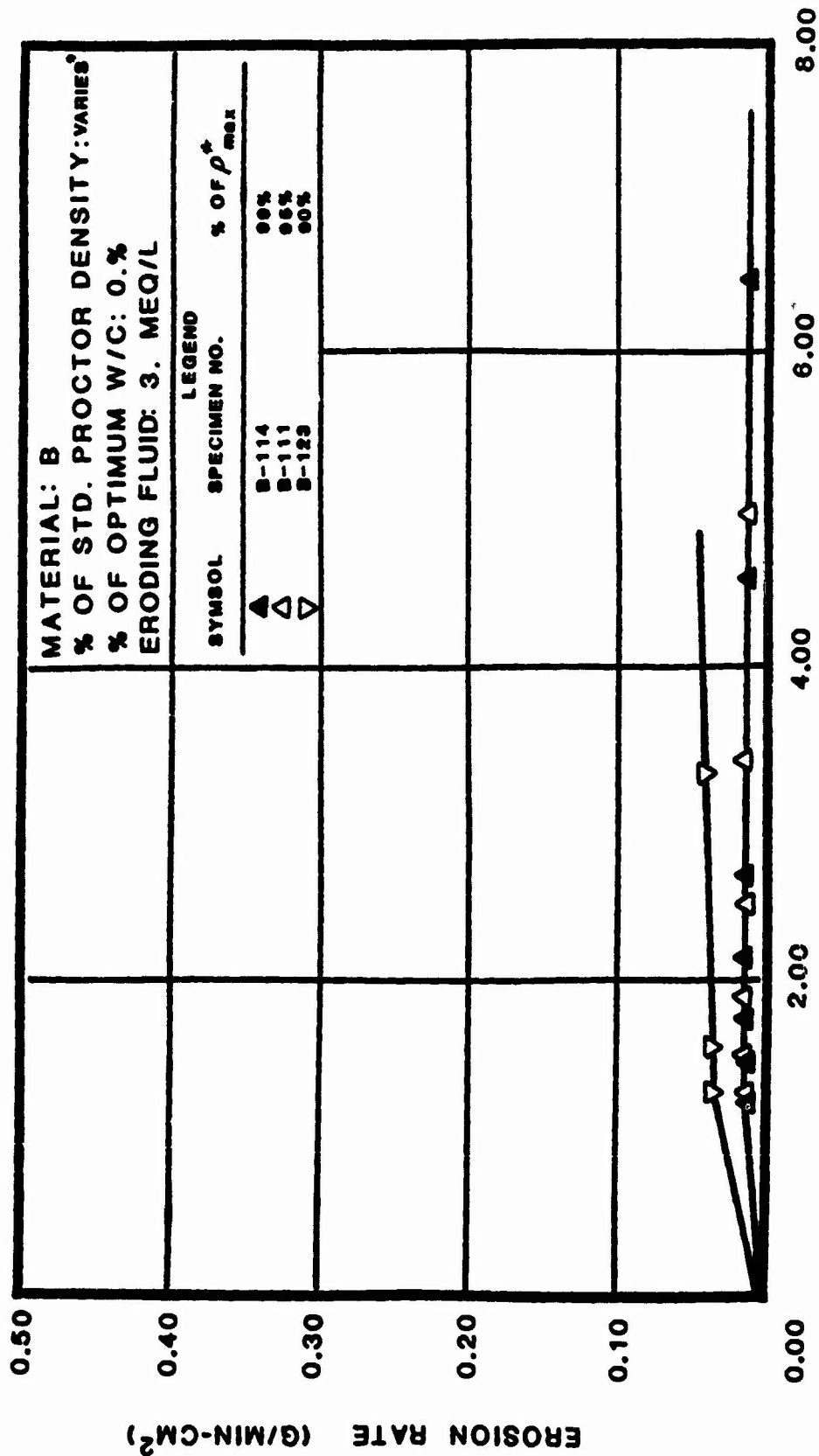


Fig. B4 Summary curve showing the effect of percent of standard Proctor dry density on the erosion rate as a function of fluid shear stress for slightly silty clay specimens (Material B).

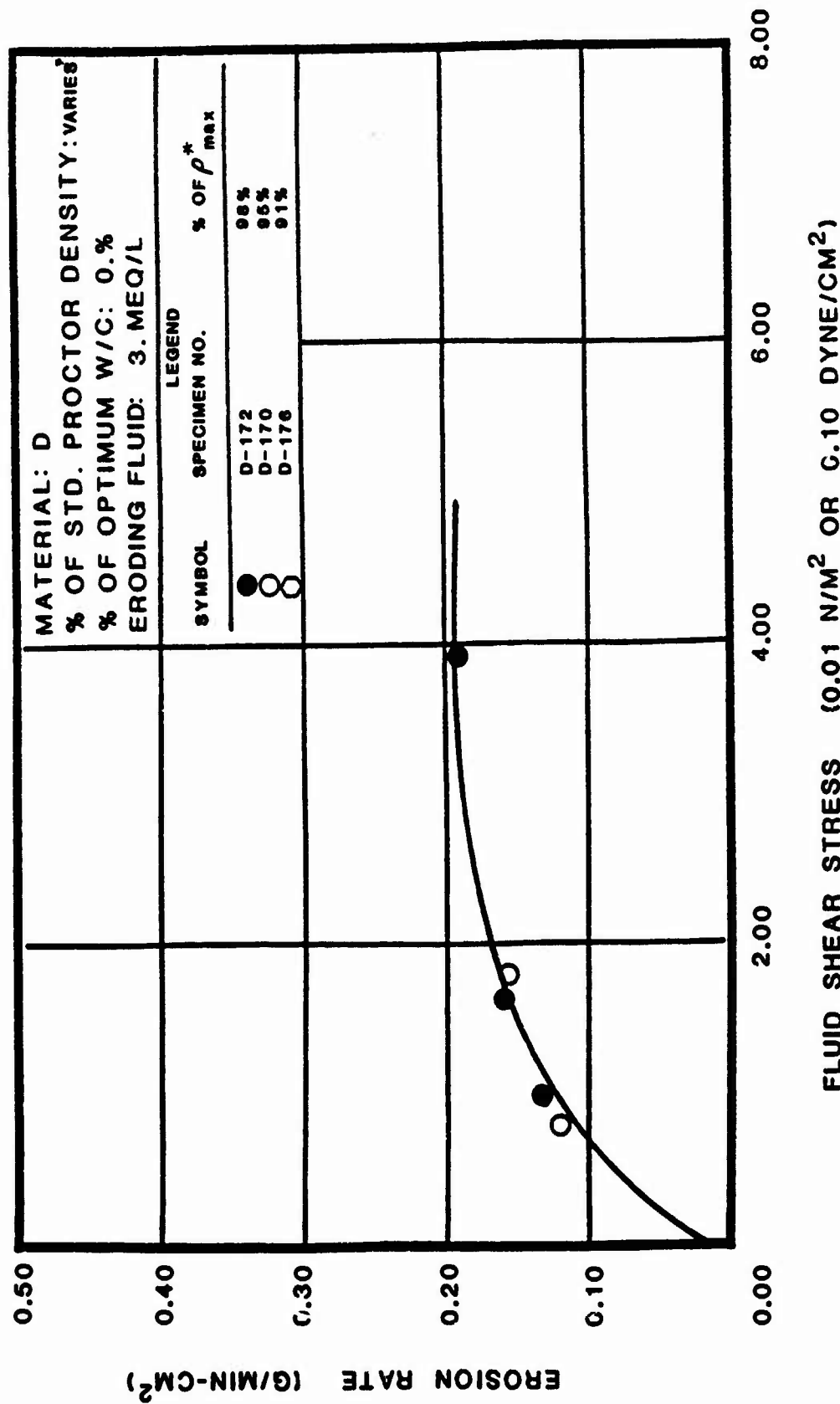


Fig. B5 Summary curve showing the effect of percent of standard Proctor dry density on the erosion rate as a function of fluid shear stress for slightly clayey silt specimens (Material D).

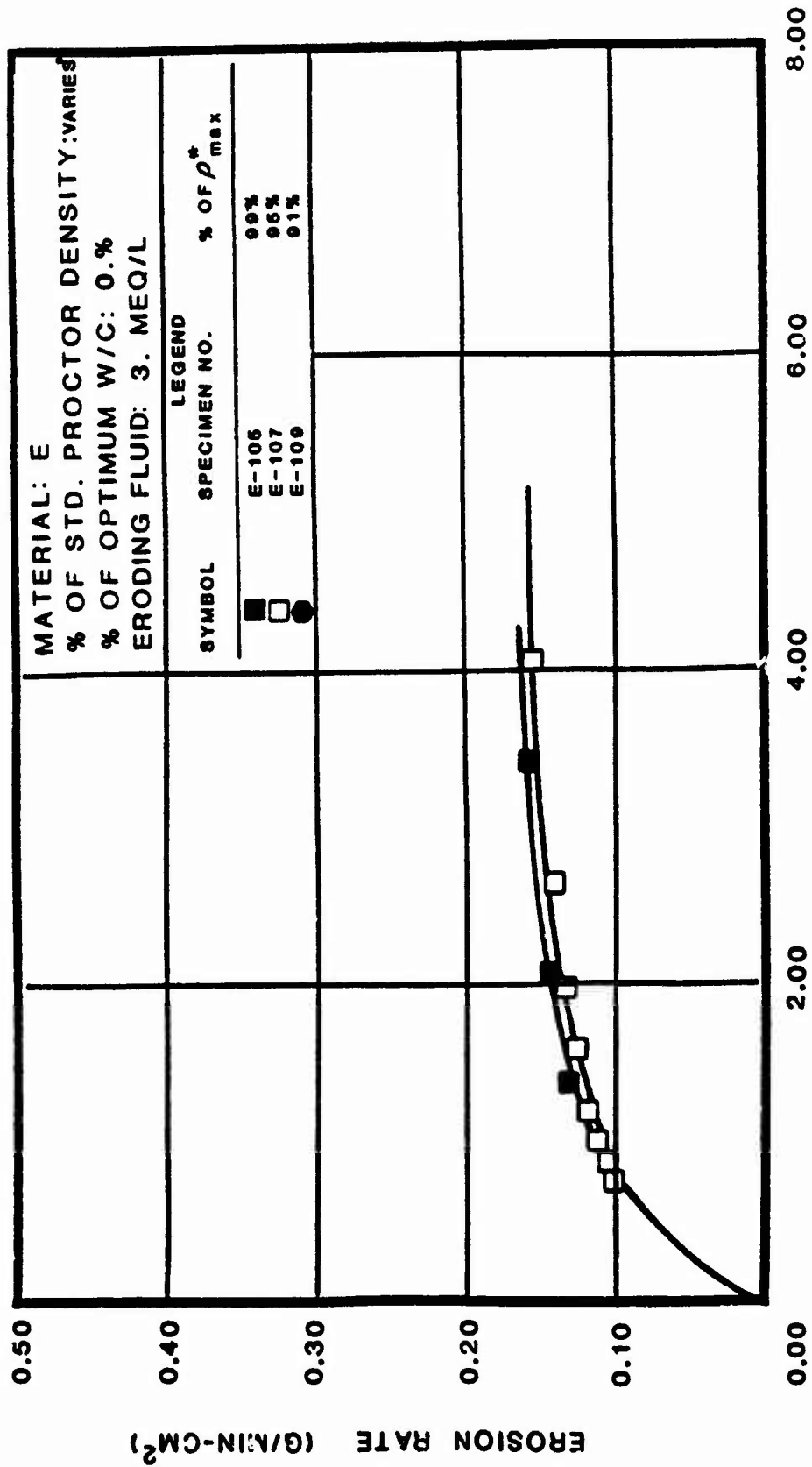


Fig. B6 Summary curve showing the effect of percent of standard Proctor dry density on the erosion rate as a function of fluid shear stress for slightly clayey silt specimens (Material E).

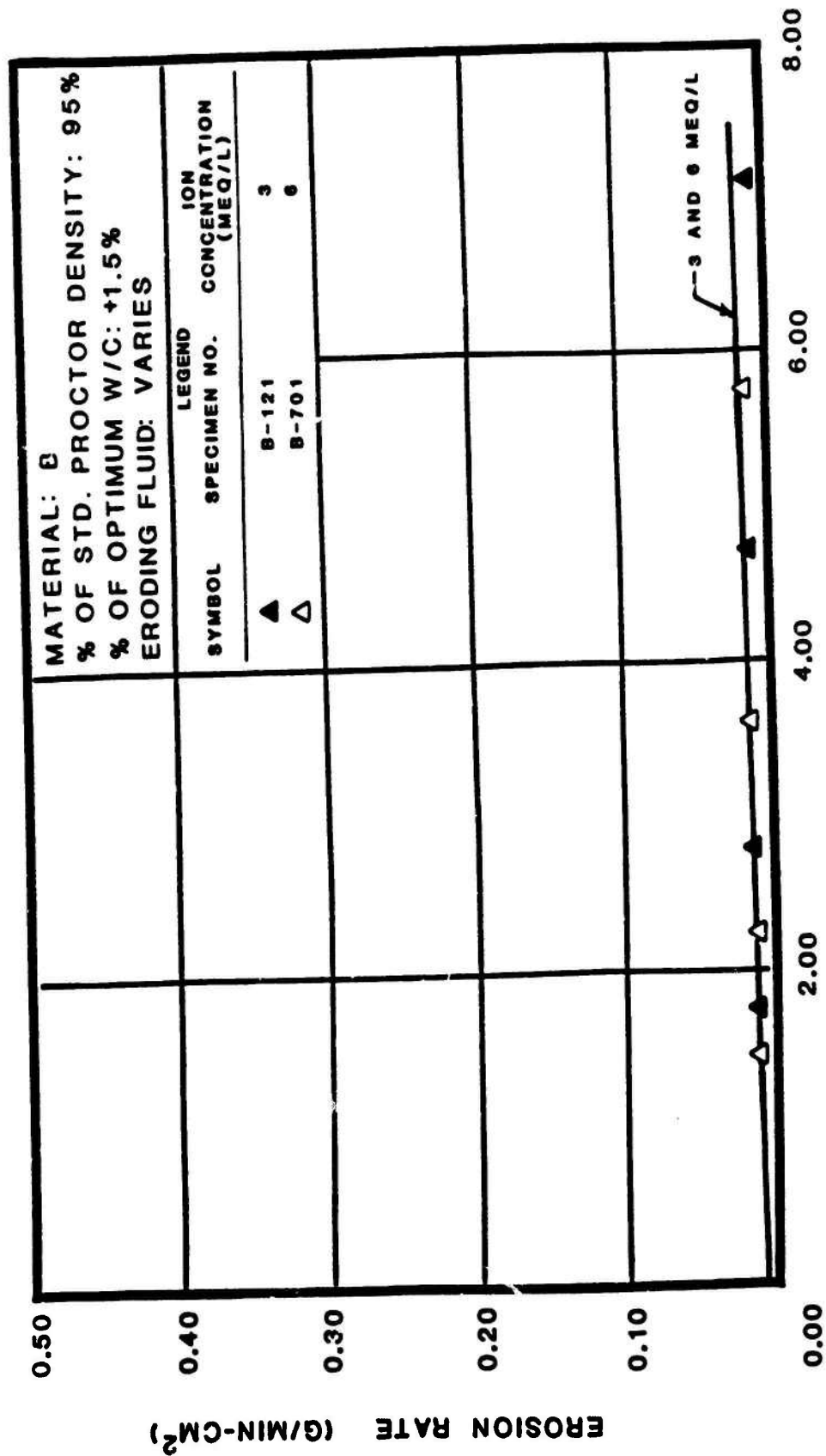
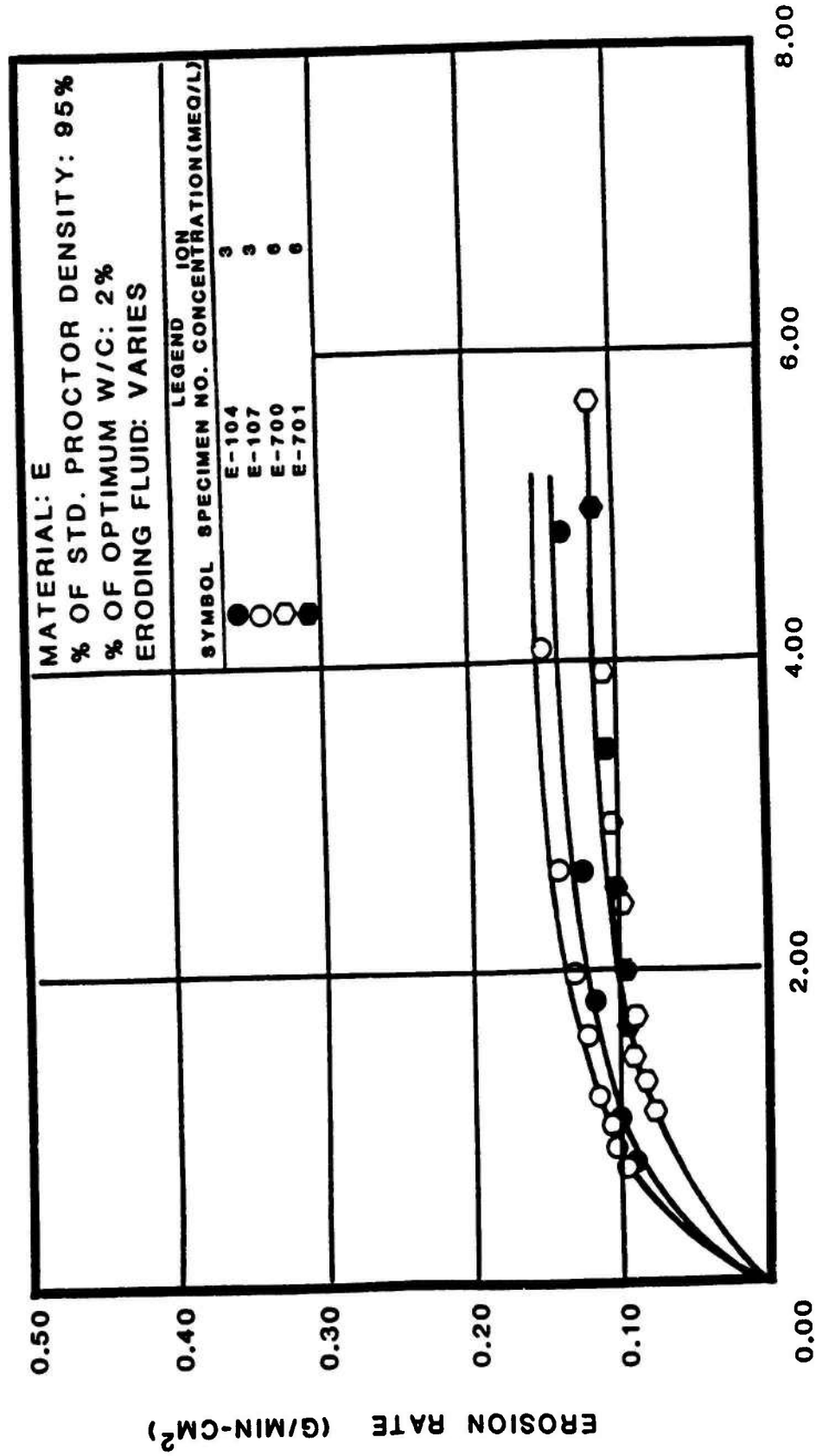


Fig. B7 Summary curve showing the effect of ion concentration of eroding fluid on the erosion rate as a function of shear stress for slightly silty clay specimens (Material B).



FLUID SHEAR STRESS (0.01 N/M² OR 0.10 DYNE/CM²)

Fig. B8 Summary curve showing the effect of ion concentration of eroding fluid on the erosion rate (\dot{e}) as a function of fluid shear stress for slightly clayey silt specimens (Material E).

APPENDIX C

PROCEDURE FOR OBTAINING SOIL
PORE WATER EXTRACTS

APPENDIX C: PROCEDURE FOR OBTAINING SOIL WATER EXTRACTS

This appendix describes the procedure recommended by Sherard (1972) and extensively described by Richards (1954) for obtaining soil-water extracts. These extracts are used to determine the amount of metallic cations (sodium, calcium, magnesium and potassium) present in the soil, expressed in milliequivalents per liter. These ionic concentrations may be used to determine the relative activity of sodium ions in exchange reactions with soil.

A high activity of sodium cations relative to the other ions in the porewater has been found to correlate to the incidence of erosion damage in many embankment dams. One widely used relationship to quantify this activity is the Sodium Adsorption Ratio (SAR), defined as:

$$SAR = \frac{Na}{\sqrt{0.5 (Ca + Mg)}} \quad (1)$$

The SAR may be plotted versus the total cation concentration of the eroding fluid to possibly predict the erosion failure of a dam embankment. To obtain the soil-water extracts required to compute the SAR, the following procedure is recommended:

1. Distilled water is added to a 250 gram soil sample and mixed with a spatula until the consistency of the soil paste is about the same as at the liquid limit. The mixing process may be facilitated if the soil is first allowed to air dry and then passed through a U.S. Standard No. 70 (2mm) sieve.

2. The soil paste is allowed to sit for a few hours in order to allow equilibrium to occur between the salts in the pore water and the salts on the cation complex.

3. After allowing the paste to sit for a few hours, the paste should be checked to see that free water does not collect on the soil surface. If the paste is too wet, dry soil may be added. The paste should not stiffen or lose its gloss. If the paste is too dry, it may be remixed with additional water. The consistency of the paste should be about the same as at the liquid limit.

4. The soil paste is transferred to a vacuum filter funnel system, as shown in Figure C1. Vacuum is applied and a small quantity (10 to 25 milliliters) of soil-water extract is collected in a bottle or test tube. The collection process is stopped when air begins to pass through the filter.

5. The amount of metallic cations is determined by chemical analysis. A detailed description of the procedures available for determining pore water chemistry and other properties of the soils may be found in texts edited by Richards (1954) and Black (1965).

References

1. Black, C.A., Ed. (1965), Method of Soil Analysis, Chemical and Microbiological Properties, American Society of Agronomy, Inc., Madison, Wisconsin.

2. Richards, L.A., Ed. (1954), Diagnosis and Improvement of Saline and Alkali Soils, Agriculture Handbook No.60, U.S. Department of Agriculture, Washington, D.C.

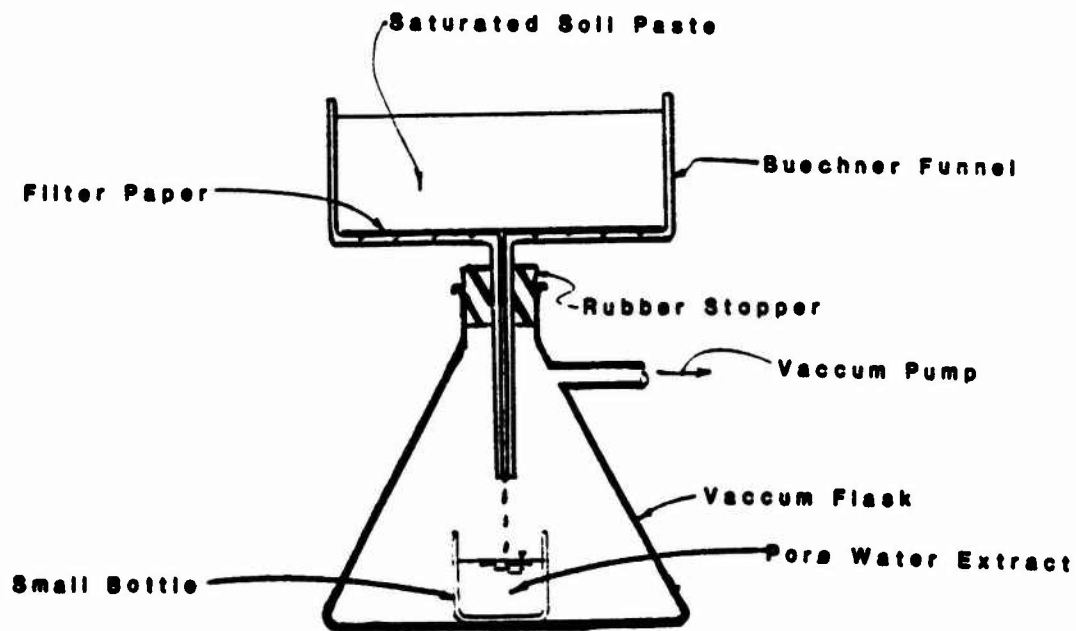


Fig. C1 Details of apparatus used to obtain soil pore water extracts for chemical analysis (from Sherard et.al., 1972)

APPENDIX D

NUMERICAL ANALYSIS OF THE EFFECT OF ASSUMED FLOW
CHANNEL SHAPE ON TRIAXIAL EROSION TEST RESULTS

APPENDIX D: NUMERICAL ANALYSIS OF THE EFFECT OF ASSUMED FLOW
CHANNEL SHAPE ON TRIAXIAL EROSION TEST RESULTS

Studies were performed to evaluate the effect of flow channel shape on parameters calculated for the triaxial erosion test. As discussed in the report, test results were computed assuming the flow channel shape was rectangular during a test. This rectangular channel was assumed to have a constant width; only the thickness varied with time to account for the soil volume being eroded. Possibly more accurate assumptions could also have been made by assuming the flow channel eroded as an ellipse with either a constant width or with both width and thickness varying with time. Therefore comparison calculations were performed by assuming these differently shaped flow channels. Flow channel size parameters compared were: width (w), thickness (d), hydraulic diameter (D_h), and erosional surface area ($A_s(t)$). The effects of the flow channel shape assumption on the erosion rate and fluid shear stress were also compared.

Method of Study

Erosion test values calculated for the two different elliptical shape flow channels were compared to test values calculated for the constant width rectangular shape flow channel on the basis of equal cross-sectional areas, $A_x(t)$. This was done because the area of any cross-section is independent of cross-sectional shape.

The constant width solutions were selected based on observation of the eroded flow channels after a test. These observations indicated

that the increase in crack width was much smaller than the increase in crack thickness. The variable width solution attempted to model this by using an empirical function to generate values of the small increase in crack width during an erosion test.

Constant Width Rectangular Shape Flow Channel: The solution for the constant width rectangular shape flow channel is described in PART IV of this report. The expressions for the channel thickness d and the channel area $A_s(t)$ as functions of time were:

$$d(t) = A_x(t)/w \quad (D1)$$

and

$$A_s(t) = l_e * 2 * (A_x(t) / w + w) \quad (D2)$$

where:

l_e = eroded length of specimen, in cm,

$d(t)$ = crack thickness at time = t , in cm,

w = original crack width at time = 0, in cm.

$A_s(t)$ = crack surface area at time = t , in sq. cm

$A_x(t)$ = crack cross-sectional area at time = t , in sq. cm.

Constant Width Elliptical Shape Flow Channel: The constant width ellipse solution was based on mensuration formulae which were used to obtain values of d and $A_s(t)$ as functions of w and $A_x(t)$. These mensuration formulae were:

$$d(t) = (4/\pi) * A_x(t)/w \quad (D3)$$

and

$$A_s(t) = l_e * (\pi/2) * (w+d) * (64 - 3*Z^4) / (64 - 16*Z^2) \quad (D4)$$

where:

$$Z = [w - d(t)] / [w + d(t)]$$

Variable Width Elliptical Shape Flow Channel: This solution utilized basically the same mensuration formulae as above, but required an additional function to generate values of w and d as the cross-sectional area $A_x(t)$ varied with time. For our computations, we empirically derived a function based on observed behavior of erosion channels such that:

$$\Delta w = [\Delta A_x(t) / \Delta t] * \Delta d * \text{RATE} \quad (D5)$$

where:

Δw = incremental change in crack width in cm,

Δd = incremental change in crack thickness in cm,

$\Delta A_x / \Delta t$ = change in cross-sectional area with time, cm^2/min ,

and

RATE = constant, min/cm^2 .

[The value of $\Delta A_x(t)/\Delta t$ was equal to P (the slope of the cumulative weight eroded vs. time curve) divided by ρ (the specimen dry density) and l_e (the eroded length of the specimen).]

Equation D5, with a suitable choice for the value of RATE, could fit a wide range of crack dimensions measured at the end of an erosion test. This equation was incrementally solved by using consecutive values of $A_x(t)$ and by starting with initial values of w and d at time = 0. Once these incremental values were known, the elliptical mensuration formulae could be used to compute flow channel size parameters.

The RATE parameter was used to evaluate the time history of the the shape of the flow channel based on measurements of flow channel dimensions at the end of a triaxial erosion test. Therefore values for RATE necessary to match the the test results were calculated analytically using measured test end values of d , w , time (or $A_x(t)$) and $\Delta A_x / \Delta t$.

An example of this tabulation is given in Table D1. Tables D2 through D4 present the measured test end crack dimensions and best fit values of RATE for most of the specimens tested.

Results of Study

Constant Width Ellipse: A numerical comparison of erosion test values calculated using the constant width ellipse solution and the constant width rectangle solution is presented in Tables D5 through D7 for each of the materials studied. The analysis indicated that for all of the materials, the constant width ellipse crack size parameters vary from the rectangular by less than $\pm 15\%$. It should also be noted that the ratio of the results between solutions were about the same for all of the materials studied.

Figure D1 shows graphically the effect of the assumed flow channel shape on values of erosion rate, \dot{e} , versus fluid shear stress, τ . Erosion rate values for the constant width ellipse solution were consistently higher than the values for rectangular solution of the materials tested. Plots of erosion rate versus fluid shear stress for Material B were not sensitive to the choice of assumed flow channel shape because the measured erosion rates were small.

Erosion test values for the highly erosive Material E were more sensitive to the choice of assumed flow channel shape for the less erosive materials. The slopes of the constant width ellipse solution were significantly greater than the slopes of the rectangular solution for this material. Calculated erosion values for the two solutions diverged moderately with increasing values of fluid shear stresses.

Calculated erosion values for the two solutions for the moderately erosive Material D were generally parallel except at low fluid shear

stresses. At low shear stress the slope of the constant width ellipse solution was slightly greater than the slope of the rectangular solution.

Variable Width Ellipse: The numerical comparison of the variable width ellipse solution to the constant width rectangle solution is presented in Tables D8 through D10 for each of the materials studied. The variable width ellipse solution also varied from the rectangle solution by less than $\pm 15\%$ for all of the materials tested.

Figure D1 presents graphical comparisons of the effect of assumed flow channel shape on values of erosion rate, \dot{e} , versus fluid shear stress, τ . For each of the tested materials the variable width ellipse solution resulted in curves higher than, but generally parallel to, the curves for the rectangle solution. Further, it may be seen in Figure D1 that the shapes of the curves for the two solutions are quite similar.

Conclusions

The results of the numerical analyses indicated that the simple constant width rectangular solution was reasonable. Another encouraging finding is that erosion values calculated using the possibly most accurate shape assumption of a variable width ellipse may be related to the constant width rectangle by using a simple constant.

An alternative test method that would avoid all of these shape assumptions would be to start the erosion test with a circular flow channel shape. Such tests were actually performed by making flow channels in specimens by drilling with a small (0.7 cm diameter) auger bit. Ob-

servations indicated that the resulting flow channel eroded circularly. The mathematics for calculating the change in size of an eroding circular flow channel are very simple and no flow channel shape assumptions are required. Also, since the aspect ratio of the circular channel does not vary, computation of fluid wall shear stress as a function of aspect ratio is simplified. Additional study is required to see if erosion parameters measured using a circular flow channel compare favorably with values measured using a rectangular flow channel.

THE CHANGE IN CRACK AREA PER UNIT TIME ($\Delta A/\Delta T$) IS 0.56 SQ. CM/MIN
 RATE IS EQUAL TO 0.74 MIN/SQ. CM

TIME AT FAILURE MIN	CRACK CROSS SECT. AREA AT FAILURE AXI SQ. CM	CRACK WIDTH AT FAILURE W CM	CRACK THICK. AT FAILURE D CM
0.00	0.53	2.32	0.29
1.00	1.09	2.44	0.57
2.00	1.65	2.56	0.82
3.00	2.21	2.66	1.06
4.00	2.77	2.76	1.28
5.00	3.33	2.85	1.49
6.00	3.89	2.94	1.69
7.00	4.45	3.02	1.88
8.00	5.01	3.10	2.06
9.00	5.57	3.17	2.24
10.00	6.13	3.24	2.41
11.00	<u>6.69</u>	<u>3.31</u>	<u>2.57</u> *
12.00	7.25	3.38	2.73
13.00	7.81	3.45	2.89
14.00	8.37	3.51	3.04
15.00	8.93	3.57	3.18
16.00	9.49	3.63	3.33

* Values for Specimen D-175

Table D1. Example Tabulation for Determining the Value of RATE.

TABLE OF EROSION
CHANNEL DIMENSIONS

MATERIAL: B

SPECIMEN NO.	CHANGE IN CRACK AREA PER UNIT TIME SQ. CM/MIN	CRACK WIDTH AT FAILURE W CM	CRACK THICK. AT FAILURE D CM	TIME AT FAILURE MIN	MEASURED AREA AT FAILURE SQ. CM	CALCULATED AREA AT FAILURE SQ. CM	RATE MIN/SQ. CM
B-110	0.03	3.5	.8	100.00	2.2	3.5	16.38
B-111	0.05	3.0	1.0	59.00	2.4	3.5	9.71
B-112	0.14	3.5	2.0	41.00	5.5	6.2	4.74
B-113	0.13	3.5	1.7	33.00	4.7	4.8	5.12
B-114	0.04	3.5	1.4	81.00	3.8	3.7	20.0
B-115	0.06	2.4	1.0	46.43	1.9	3.3	8.05
B-117	0.06	3.1	1.0	33.00	2.4	2.5	12.85
B-119	0.06	3.5	1.0	58.80	2.7	4.0	7.85
B-120	0.09	3.0	1.0	66.50	2.4	6.5	*
B-121	0.03	3.0	0.8	98.25	1.9	3.4	*
B-701	0.04	3.0	1.0	91.36	2.4	4.1	12.21

* MEASURED AND CALCULATED AREAS DO NOT AGREE. POSSIBLE CAUSE IS THAT SPECIMENS IMPOLOED AT FAILURE.

Table D-2. Tabulation of Test End Dimensions for Material B Specimens.

TABLE OF EROSION
CHANNEL DIMENSIONS

MATERIAL: D

SPECIMEN NO.	CHANGE IN CRACK AREA PER UNIT TIME DAX/DT SQ.CM/MIN	CRACK WIDTH AT FAILURE W CM	CRACK THICK. AT FAILURE D CM	TIME AT FAILURE T MIN	MEASURED AREA AT FAILURE SQ.CM	CALCULATED AREA AT FAILURE AXT SQ.CM	RATE MIN/SQ.CM
D-175	0.56	3.5	2.8	11.0	7.7	6.7	0.7

MEASUREMENTS FOR SPECIMEN NOS D-170 THROUGH D-173 ARE NOT AVAILABLE.

Table D-3. Tabulation of Test End Dimensions for Material D Specimens.

TABLE OF EROSION
CHANNEL DIMENSIONS

MATERIAL: E

SPECIMEN NO.	CHANGE IN CRACK AREA PER UNIT TIME DAX/DI SQ. CM/MIN	CRACK WIDTH AT FAILURE W CM	CRACK THICK. AT FAILURE D CM	TIME AT FAILURE T MIN	MEASURED AREA AT FAILURE SQ. CM	CALCULATED AREA AT FAILURE AXT SQ. CM	RATE MIN/SQ. CM
E-101	1.18	2.5	2.5	6.50	4.9	8.1	0.27
E-102	1.49	3.1	1.9	2.65	4.6	4.4	0.45
E-103	1.26	2.0	0.5	3.65	0.8	5.1	*
E-104	0.56	3.0	2.5	8.64	5.9	5.3	0.49
E-105	0.64	2.0	0.7	5.75	1.1	4.2	*
E-106	0.69	2.0	2.0	7.49	3.1	5.8	0.38
E-107	0.62	3.0	1.5	8.94	3.5	5.9	0.42
E-108	0.71	3.0	1.4	4.14	3.3	3.4	0.72
E-700	0.48	2.9	1.8	7.01	4.1	3.9	0.45
E-701	0.47	2.0	1.5	9.60	2.4	5.0	*

* MEASURED AND CALCULATED AREAS DO NOT AGREE. POSSIBLE CAUSE IS THAT SPECIMENS IMPOLODED AT FAILURE.

Table D-4. Tabulation of Test End Dimensions for Material E Specimens.

RESULTS OF ANALYSIS
TO COMPARE PARAMETERS OF ASSUMED SHAPES

SPECIMEN B117
CONSTANT WIDTH ELLIPSE

RATE OF WEIGHT EROSION : 1.20 G/MIN SOIL DRY DENSITY : 1.645 G/CC ERODED LENGTH : 11.50 CM

CRACK CROSS SECT. AREA	RECTANGULAR SHAPE CRACK PARAMETERS				ELLIPTICAL SHAPE CRACK PARAMETERS				RATIO OF RECTANGULAR TO ELLIPTICAL PARAMETERS			
	THICK	WIDTH	HYDRO DIA	ERODED SURFACE AREA	THICK	WIDTH	HYDRO DIA	ERODED SURFACE AREA	D/D	W/W	DI/DI	ASI/AST
AXI SQ. CM	D CM	W CM	DI CM	ASI SQ. CM	D CM	W CM	DI CM	ASI SQ. CM				
0.9	0.4	2.3	0.7	62.7	0.5	2.3	0.8	56.6	0.79	1.00	0.90	1.11
1.3	0.6	2.3	0.9	66.5	0.7	2.3	1.0	58.9	0.79	1.00	0.89	1.13
1.8	0.8	2.3	1.2	71.1	1.0	2.3	1.3	62.1	0.79	1.00	0.87	1.14
2.2	0.9	2.3	1.3	74.9	1.2	2.3	1.5	65.1	0.79	1.00	0.87	1.15
2.3	1.0	2.3	1.4	76.1	1.3	2.3	1.6	66.1	0.79	1.00	0.87	1.15
2.5	1.1	2.3	1.5	77.8	1.4	2.3	1.7	67.5	0.79	1.00	0.87	1.15
2.6	1.1	2.3	1.5	79.5	1.4	2.3	1.8	68.9	0.79	1.00	0.87	1.15

Table D-5. Tabulation of Numerical Comparison Between Constant Width Ellipse and Constant Width Rectangle Solutions for Specimen B-117.

RESULTS OF ANALYSIS
TO COMPARE PARAMETERS OF ASSUMED SHAPES

SPECIMEN D175
CONSTANT WIDTH ELLIPSE

RATE OF WEIGHT EROSION : 11.00 G/MIN SOIL DRY DENSITY : 1.688 G/CC ERODED LENGTH : 11.60 CM

CRACK CROSS SECT. AREA	RECTANGULAR SHAPE CRACK PARAMETERS				ELLIPTICAL SHAPE CRACK PARAMETERS				RATIO OF RECTANGULAR TO ELLIPTICAL PARAMETERS			
	THICK	WIDTH	HYDRO DIA	ERODED SURFACE AREA SQ. CM	THICK	WIDTH	HYDRO DIA	ERODED SURFACE AREA SQ. CM	U/O	W/W	OH/DH	AST/AST
AXT SQ. CM	U CM	W CM	DII CM	AST SQ. CM	D CM	W CM	DII CM	AST SQ. CM				
1.0	0.4	2.3	0.7	63.9	0.6	2.3	0.8	57.5	0.79	1.00	0.90	1.11
1.5	0.6	2.3	1.0	68.7	0.8	2.3	1.1	60.5	0.79	1.00	0.88	1.14
2.0	0.8	2.3	1.2	73.4	1.1	2.3	1.4	63.9	0.79	1.00	0.87	1.15
2.5	1.1	2.3	1.5	78.8	1.4	2.3	1.7	68.3	0.79	1.00	0.87	1.15
3.0	1.3	2.3	1.7	83.9	1.6	2.3	1.9	72.8	0.79	1.00	0.87	1.15
3.5	1.5	2.3	1.8	89.2	1.9	2.3	2.1	77.8	0.79	1.00	0.87	1.15
4.0	1.7	2.3	2.0	94.1	2.2	2.3	2.3	82.6	0.79	1.00	0.88	1.14
4.6	2.0	2.3	2.1	99.7	2.5	2.3	2.4	88.2	0.79	1.00	0.88	1.13
5.1	2.2	2.3	2.3	105.0	2.8	2.3	2.5	93.7	0.79	1.00	0.89	1.12
6.0	2.6	2.3	2.4	113.8	3.3	2.3	2.7	103.0	0.79	1.00	0.91	1.10
6.6	2.8	2.3	2.6	119.7	3.6	2.3	2.8	109.5	0.79	1.00	0.91	1.09

Table D-6. Tabulation of Numerical Comparison Between Constant Width Ellipse
and Constant Width Rectangle Solutions for Specimen D-175.

RESULTS OF ANALYSIS
ID COMPARE PARAMETERS OF ASSUMED SHAPES

SPECIMEN E102
CONSTANT WIDTH ELLIPSE

RATE OF WEIGHT EROSION : 26.50 G/MIN			SOIL DRY DENSITY : 1.531 G/CC			ERODED LENGTH : 11.60 CM						
CRACK CROSS SCT. AREA	RECTANGULAR SHAPE CRACK PARAMETERS			ELLIPTICAL SHAPE CRACK PARAMETERS			RATIO OF RECTANGULAR TO ELLIPTICAL PARAMETERS					
	THICK	WIDTH	HYDRO DIA	ERODED SURFACE AREA	THICK	WIDTH	HYDRO DIA	ERODED SURFACE AREA	D/D	W/W	DH/DH	AST/AST
	D CM	W CM	DH CM	AST SQ. CM	D CM	W CM	DH CM	AST SQ. CM				
2.2	0.9	2.3	1.3	75.6	1.2	2.3	1.5	65.7	0.79	1.00	0.87	1.15
3.9	1.7	2.3	1.9	92.7	2.1	2.3	2.2	81.2	0.79	1.00	0.88	1.14
4.5	1.9	2.3	2.1	98.7	2.5	2.3	2.4	87.2	0.79	1.00	0.88	1.13

Table D-7. Tabulation of Numerical Comparison Between Constant Width Ellipse and Constant Width Rectangle Solutions For Specimen E-102.

RESULTS OF ANALYSIS
TO COMPARE PARAMETERS OF ASSUMED SHAPES

SPECIMEN B117
VARIABLE WIDTH ELLIPSE
RATE EQUAL TO 12.65 MIN/CM**2

RATE OF WEIGHT EROSION : 1.20 G/MIN SOIL DRY DENSITY : 1.645 G/CC ERODED LENGTH : 11.50 CM

CRACK CROSS SECT. AREA	RECTANGULAR SHAPE CRACK PARAMETERS				ELLIPTICAL SHAPE CRACK PARAMETERS				RATIO OF RECTANGULAR TO ELLIPTICAL PARAMETERS			
	THICK	WIDTH	HYDRO DIA	ERODED SURFACE AREA	THICK	WIDTH	HYDRO DIA	ERODED SURFACE AREA	D/D	W/W	DH/DH	AST/AST
AXI SQ. CM	D CM	W CM	INI CM	AST SQ. CM	D CM	W CM	INI CM	AST SQ. CM				
0.9	0.4	2.3	0.7	62.7	0.5	2.3	0.8	56.6	0.79	1.00	0.90	1.11
1.3	0.6	2.3	0.9	66.5	0.7	2.5	1.0	62.3	0.85	0.93	0.94	1.07
1.6	0.8	2.3	1.2	71.1	0.9	2.6	1.2	67.2	0.89	0.88	0.95	1.06
2.2	0.9	2.3	1.3	74.9	1.0	2.8	1.4	72.1	0.94	0.83	0.96	1.04
2.3	1.0	2.3	1.4	76.1	1.0	2.9	1.4	74.6	0.98	0.80	0.98	1.02
2.5	1.1	2.3	1.5	77.8	1.1	2.9	1.5	75.8	0.98	0.80	0.97	1.03
2.6	1.1	2.3	1.5	79.5	1.1	3.0	1.6	77.7	1.00	0.78	0.98	1.02

Table D-8. Tabulation of Numerical Comparison Between Variable Width Ellipse and Constant Width Rectangle Solutions For Specimen B-117.

RESULTS OF ANALYSIS
TO COMPARE PARAMETERS OF ASSUMED SHAPES

SPECIMEN D175
VARIABLE WIDTH ELLIPSE
RATE EQUAL TO 0.70 MIN/CM**2

KATE OF WEIGHT EROSION : 11.00 G/MIN SOIL DRY DENSITY : 1.688 G/CC ERODED LENGTH : 11.60 CM

CRACK CROSS SECT. AREA	RECTANGULAR SHAPE CRACK PARAMETERS				ELLIPITICAL SHAPE CRACK PARAMETERS				RATIO OF RECTANGULAR TO ELLIPITICAL PARAMETERS			
	THICK	WIDTH	HYDRO DIA	THICKED SURFACE AREA	THICK	WIDTH	HYDRO DIA	ERODED SURFACE AREA	D/D	W/W	DI/DI	AS/AS
AXI SQ. CM	D CM	W CM	DI CM	AS SQ. CM	D CM	W CM	DI CM	AS SQ. CM				
1.0	0.4	2.3	0.7	63.9	0.6	2.3	0.8	57.5	0.79	1.00	0.90	1.11
1.5	0.6	2.3	1.0	68.7	0.8	2.4	1.1	62.3	0.82	0.96	0.91	1.10
2.0	0.8	2.3	1.2	73.4	1.0	2.5	1.4	66.9	0.85	0.92	0.91	1.10
2.5	1.1	2.3	1.5	78.8	1.2	2.6	1.6	71.8	0.88	0.89	0.91	1.10
3.0	1.3	2.3	1.7	83.9	1.4	2.7	1.8	76.7	0.91	0.86	0.91	1.09
3.5	1.5	2.3	1.8	89.2	1.6	2.8	2.0	81.4	0.94	0.84	0.91	1.10
4.0	1.7	2.3	2.0	94.1	1.8	2.8	2.2	85.8	0.96	0.82	0.91	1.10
4.6	2.0	2.3	2.1	99.7	2.0	2.9	2.4	90.4	0.99	0.80	0.91	1.10
5.1	2.2	2.3	2.3	105.0	2.2	3.0	2.5	94.8	1.01	0.77	0.90	1.11
6.0	2.6	2.3	2.4	113.8	2.5	3.1	2.7	101.5	1.04	0.76	0.89	1.12
6.6	2.8	2.3	2.6	119.7	2.6	3.2	2.9	106.3	1.08	0.73	0.89	1.13

Table D-9. Tabulation of Numerical Comparison Between Variable Width Ellipse and Constant Width Rectangle Solutions For Specimen D-175.

RESULTS OF ANALYSIS
10 COMPARE PARAMETERS OF ASSUMED SHAPES

SPECIMEN E102
VARIABLE WIDTH ELLIPSE
RATE EQUAL TO 0.45 MIN/CM**2

RATE OF WEIGHT EROSION : 26.50 G/MIN SOIL DRY DENSITY : 1.531 G/CC ERODED LENGTH : 11.60 CM

CRACK CROSS SECT. AREA	RECTANGULAR SHAPE CRACK PARAMETERS				ELLIPTICAL SHAPE CRACK PARAMETERS				RATIO OF RECTANGULAR TO ELLIPTICAL PARAMETERS			
	THICK	WIDTH	HYDRO DIA	ERODED SURFACE AREA	THICK	WIDTH	HYDRO DIA	ERODED SURFACE AREA	U/D	W/W	DIH/DII	AST/AST
AXI SQ. CM	D CM	W CM	DIH CM	AST SQ. CM	D CM	W CM	DIH CM	AST SQ. CM				
2.2	0.9	2.3	1.3	75.6	1.2	2.3	1.5	65.7	0.79	1.00	0.87	1.15
3.9	1.7	2.3	1.9	92.7	1.7	2.9	2.1	85.7	0.99	0.79	0.92	1.08
4.5	1.9	2.3	2.1	98.7	1.8	3.3	2.2	93.4	1.10	0.71	0.95	1.06

Table D-10. Tabulation of Numerical Comparisons Between Variable Width Ellipse
and Constant Width Rectangle Solutions For Specimen E-102.

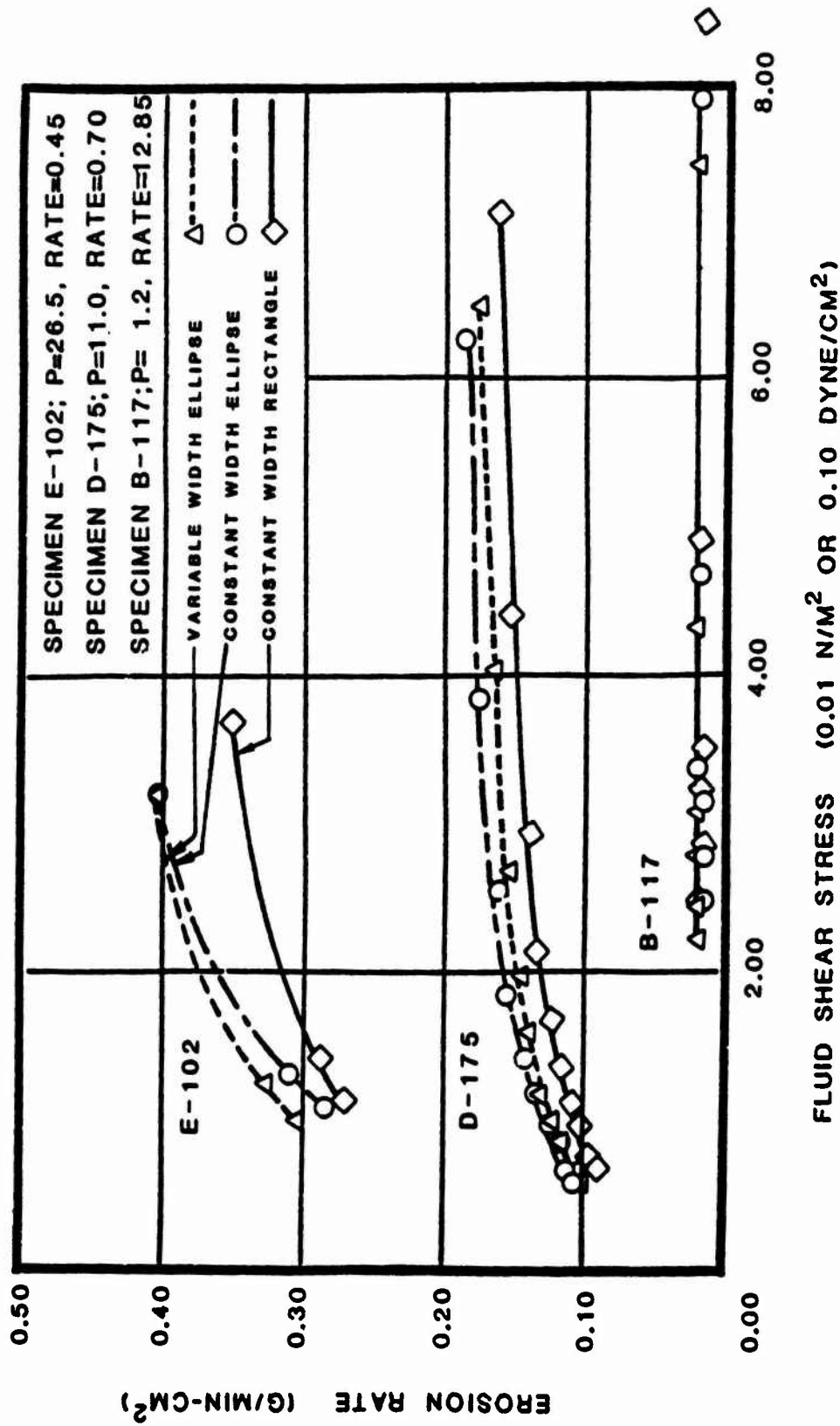


Fig. D1. Effect of Erosion Channel Shape Assumption on Erosion Rate vs. Fluid Shear Stress for Highly Erosive to Erosion-Resistant Materials.

APPENDIX E

EXPERIMENTAL STUDY OF TRIAXIAL EROSION TEST
HYDRAULIC BEHAVIOR

APPENDIX E: EXPERIMENTAL STUDY OF TRIAXIAL EROSION TEST

HYDRAULIC BEHAVIOR

A series of hydraulic experiments was performed to observe flow through a model of the erosional flow channel. These experiments were performed to investigate the validity of the assumption of laminar flow occurring in the triaxial erosion test. Additionally some experiments were performed to possibly optimize the hydraulic design of the top and bottom platens presently used in the triaxial erosion test.

Experimental Apparatus

A clear rectangular plexiglas channel was constructed to model the erosional flow channel. The model channel dimensions were 11.5 cm long, by 2.9 cm wide, by 1.2 cm thick. These dimensions approximately correspond to the values of l_e , w and d used for the tests performed in this report. The model channel thickness could be varied by placing plexiglas inserts 0.5 cm thick into the channel. Gradients of approximately 10, 35, 50 and 100 m/m were applied to each of the three model channel configurations possible: 0.2 cm, 0.7 cm and 1.2 cm thick by 2.9 cm wide.

The resulting flow regime was observed by mixing light reflective polyethylene beads with the water flowing through the model channel. The average diameter of the beads was between 0.03 and 0.05 cm. The beads had a specific gravity of slightly greater than 1. Observations were recorded by sketching and by photography.

Flows were channeled through the plexiglas model with either the same top and bottom platens used for the triaxial erosion test or with alternative platens. The platens were sealed to the model channel using modeling clay. Figure E1 shows a photograph of the experimental apparatus during use.

To see the effect of entrance and exit geometry on the flow regime, a platen with a gradual transition conical flow entrance (0.8 cm expanding out to 2.2 cm in diameter over a length of 1.2 cm) was substituted for either of the top or bottom platens. Figure E2 shows details of the conical flow entrance platen. An "infinitely large" exit was also studied by discharging the flow from the model channel directly into a large beaker. This was done for both the original top platen and the conical flow entrance top platen.

Experimental Observations, Triaxial Erosion Test Model

Crack Thickness = 0.2 cm (This thickness is analogous to the specimen flow channel thickness at the start of the erosion test). Flows were observed to be quite linear and regular at all applied gradients. Some small vortices, about 1 cm in diameter, were noticed along the edges of the model channel just below the injecting flow nozzle.

Crack Thickness = 0.7 cm (This approximately corresponds to $A_x(t) = 2.0 \text{ cm}^2$). Two vortices were observed: one large (1.5 cm wide by 3 cm long) well-defined vortex occurred just below one corner of the injecting flow nozzle, and a smaller (1 cm wide by 2 cm long) poorly formed vortex occurred below and to the other side of the model channel

opposite to the first vortex. This asymmetric arrangement became more and more symmetrical as applied gradients were increased. Random flow patterns with a length of about 2 cm occurred just below the vortices. The vortex fields took place over about 25% of the area of the model channel.

Crack Thickness = 1.2 cm (This approximately corresponds to $A_x(t)$ = 3.5 cm²). An intense vortex field filled the top 1/4 of the model channel. At gradients below 35, the flow in the rest of the model channel was about equally divided between an upper random non-linear flow region and a lower linear flow region. As gradients were increased, the vortex field in the top of the model channel became more intense, but did not change appreciably in extent; the random flow zone increased in length with a corresponding decrease in the linear flow zone. At a gradient of about 100, the linear flow zone disappeared entirely.

The observation of the intense vortex field at the top of the model channel corresponded with test observations that most erosion test specimens failed at a locally severely eroded area generally within the top 1/5 of the specimen. The intense vortex field may have caused increased erosion due to locally increased flow velocities in this region.

Saturation of Flow Channel Another experimental observation was that air pockets tended to form in the plexiglas model of the flow channel. Such air pockets could prevent the eroding fluid from acting on the erosional surface area of a specimen. An effective solution to this problem was to pre-fill the model channel with fluid immediately before a flow test. This was done by 1) holding the end of the outflow line

above the level of the top of the plexiglas model, 2) by filling the outflow line with fluid, and 3) by allowing the trapped air to escape from the disconnected inflow line. It is recommended that the triaxial erosion testing procedure used in this study be slightly modified to include pre-filling the flow channel with the eroding fluid immediately before an erosion test.

Experimental Observations, Optimization Models

Gradual Transition Conical Flow Entrance Platen Replacing the triaxial erosion test top platen and its injecting flow nozzle with a platen with a gradual transition conical flow entrance had a marked effect on suppressing the onset of flow separation and minimized the formation of vortices. This was probably because the abrupt transition between the injecting flow nozzle and the model channel was eliminated. However it should also be noted that removing the 3.5 cm long injecting flow nozzle increased the effective length of the model channel from 11.5 cm to 15 cm. This increase in length may have also tended to suppress the flow separation.

The observed flow using the conical flow entrance was linear for crack thicknesses of 0.2 and 0.7 cm at gradients between 10 and 100. Some small, 1 cm in diameter, vortices formed just below the conical flow entrance at a crack thickness of 0.7 cm. Higher gradients had little effect on this flow regime.

For a crack thickness of 1.2 cm, two vortices (3 cm long by 1 cm wide) symmetrically flanked the center line of the model channel just

beyond the conical flow entrance. A random flow area of about 3 cm long was present below the vortices, followed by linear flow throughout the rest of the model channel. Higher gradients had little effect on this regime.

Alternative Discharge Methods: The triaxial erosion test bottom platen with a 0.4 cm diameter discharge was replaced either by 1) the conical flow platen or by 2) discharging directly into a large beaker. Little visible effect on the flow regime was noticed using these different discharge methods. However, it was noticed that coarser particles had a tendency to lodge on the flat area of the triaxial erosion test bottom platen. This did not occur for the alternative bottom platen as this dead area did not exist (see Fig. E2). To prevent the lodging of particles and possible erosion channel sealing, the design of the discharge through the bottom platen may be modified in the future.

Numerical Analysis of Hydraulic Behavior

The plexiglas model, using the triaxial erosion test top and bottom platens, revealed that flow separation increased as the thickness of the model channel increased. This flow separation would tend to increase the wall shear stresses due to locally increased flow velocities. An explicit derivation for the exact amount of increase is not possible at present. However, an estimate of this increase in wall shear stress was obtained by using an equation for duct entrance effects on wall shear (Olson, 1980). The results of this analysis indicated that laminar fluid wall shear could be increased up to about 30% due to flow separation.

In our analysis of the assumed fully developed laminar flow through the triaxial erosion test flow channel, the wall shear stress, τ , varied with the aspect ratio of the flow channel (Olson, 1980). Thus the wall shear stress, τ , was equal to $10.6 V\mu/D_h$ at the start of the erosion test when the aspect ratio was 1/10, and decreased to a value of $8 V\mu/D_h$ when the flow channel eroded to an approximately circular shape. The average value of wall shear stress τ was thus equal to $9.3 V\mu/D_h$. Therefore our test values for τ were increased by 30% to account for the flow separation observed in the plexiglas model of the triaxial erosion test flow channel. This correction results in the wall shear stress τ being equal to $12 V\mu/D_h$. This last value was used in the computation of wall shear stresses reported in the text.

Conclusions

Observations indicated that as the flow channel erodes, flow separation occurs at the abrupt transition between the top platen injecting flow nozzle and the flow channel. The experiments indicated that upper bound solutions for wall shear stresses due to the assumed fully developed laminar flow are more valid than solutions based on average conditions. To reflect this, wall shear stresses were increased by 30% over average values to obtain the results presented in this report.

Some experiments were also conducted to investigate the triaxial erosion test apparatus hydraulics so that flow separation effects would be lessened. These experiments indicated that by changing the top platen having an abrupt flow nozzle to a top platen with a gradual transition conical flow entrance, a marked suppression of flow separation resulted.

However, increasing the size or changing the geometry of the flow discharge through the bottom platen had little visible effect on flow separation.

To improve the accuracy of the hydraulic analysis for the fluid wall shear stresses, further study is needed to optimize the configuration of the entrance to the flow channel. The goal of this optimization would be to lessen the flow separation occurring in the present entrance configuration. Another goal would be to prevent flow from occurring between the specimen and its membrane. The present top platen and injecting flow nozzle do prevent flow from occurring between the specimen and its membrane, but could better control flow separation in the transition between the flow entrance and the flow channel.

It is recommended, as previously discussed, that the triaxial erosion testing procedure be slightly modified to include pre-filling the flow channel with the eroding fluid immediately before an erosion test.

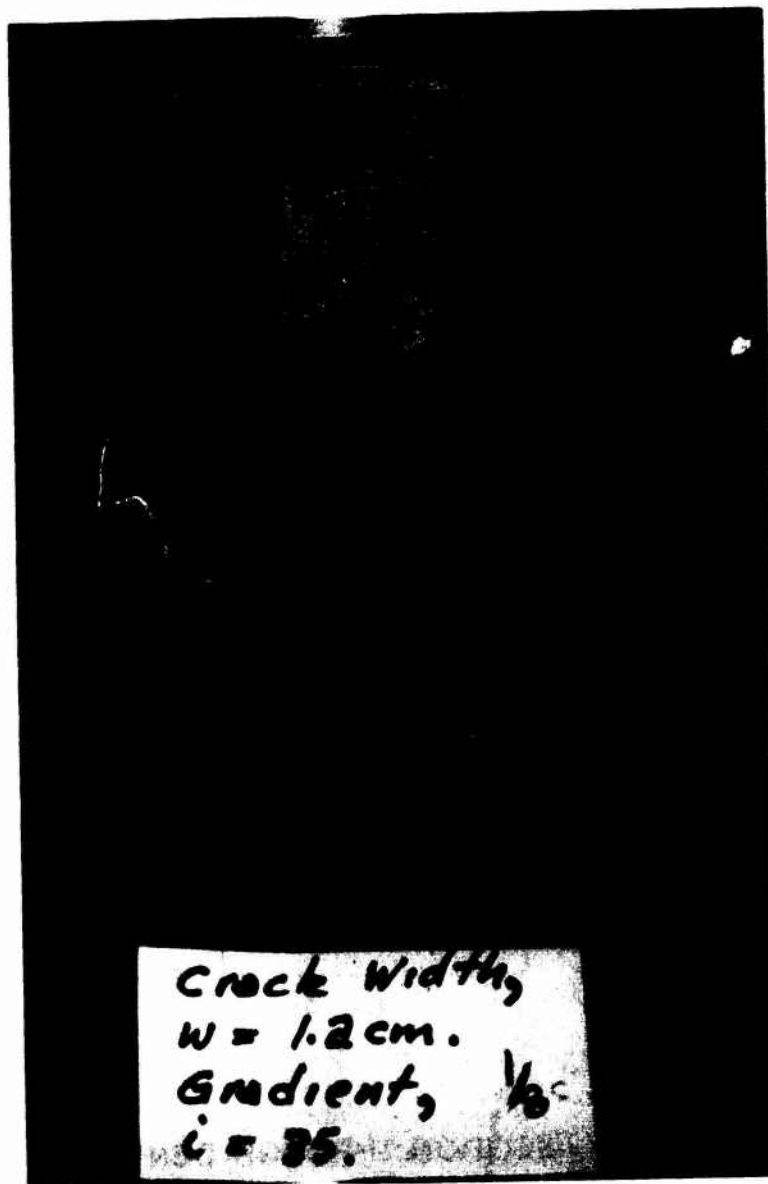
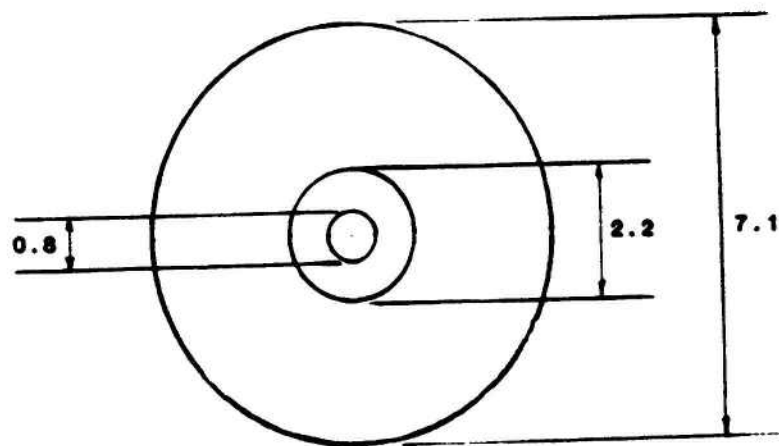
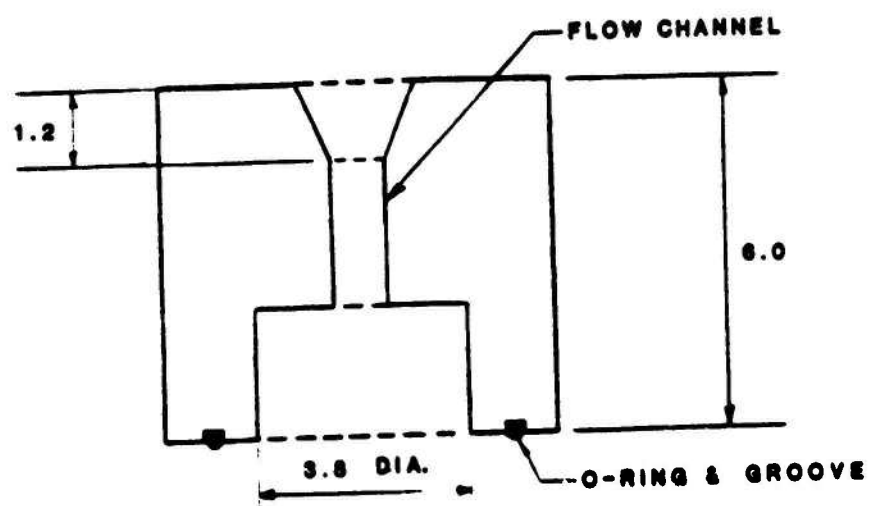


Fig. E1 Experimental Apparatus Used to Investigate Triaxial Erosion Test Hydraulic Behavior.



PLAN



SECTION THROUGH CENTER

SCALE 1:126 CENTIMETERS.

Fig. E2 Plan and Section of Platen with Gradual Transition Conical Flow Channel.

APPENDIX F
ESTIMATES OF FIELD EROSION RATES
FOR THE TETON DAM FAILURE AND
POSSIBLE DESIGN APPLICATIONS

APPENDIX F: ESTIMATES
OF FIELD EROSION RATES
FOR THE TETON DAM FAILURE AND POSSIBLE
DESIGN APPLICATIONS

Background

Based on field observations during the failure of the Teton Dam, calculations presented in this Appendix were made to obtain estimates of the erosion rate which may have occurred while an erosion channel was enlarging during the dam failure. These estimates were compared to values of the maximum erosion rate obtained using the Triaxial Erosion Test to observe if laboratory data corresponded with field observations. The following paragraphs summarize key erosion events presented in a report on the failure of the Teton Dam on the morning of June 5, 1976 (U.S. Department of the Interior, 1977).

Earliest Time at which Significant Erosion may have begun:

Testimony, presented on page F-37 of the aforementioned report, established that no serious leaks or seepage were observed during a routine inspection at 9:00 p.m. on June 4, 1976. Therefore, the earliest time at which significant erosion could have begun would be subsequent to 9:00 p.m. on June 4, 1976 (Page 35).

Latest Time at which Significant Erosion may have begun: The first leak was observed at about 7:45 a.m., on June 5, 1976. This leak occurred along the right abutment at El.5045 (in feet) near the toe of the dam (Page 36).

Observations and Dimension of the Path for a Second Leak: A second leak was observed between 10:00 a.m. and 10:30 a.m. at El.5195, approximately 46 meters (150 ft) above the first leak at El.5045. By 10:40 a.m., an eyewitness observed that the leak had developed into an erosion tunnel, about 1.8 meters (6 feet) in diameter, extending into the embankment

(Page 36). Unfortunately, that was the only quantitative description of the erosion channel provided in the report. Moreover, available photographs of the eroding dam for different times do not provide a useful scale that could be used to quantify the dimensions of the erosion channel.

Progression of the Erosion Channel: Seed and his co-workers (U.S. Department of the Interior, 1976 Appendix D) described the progression of flow and the development of the erosion channel through the Teton dam embankment. This progression is illustrated in Figures F1 and F2. They concluded that flow first occurred along the base of the dam, resulting in the first leak observed at El. 5045 ft. This flow path later shortened and allowed water to flow out of the embankment at El. 5195, resulting in a second leak. This second leak enlarged, into the 1.8 meter (6 ft) in diameter erosion channel described above, by 10:40 a.m. on June 5, 1976.

It may be noted that the maximum reservoir level on the eve of the failure was given at El. 5300 ft. Thus the head of water above the erosion channel at El. 5195 ft. was approximately 32 m (105 ft).

Calculations to Estimate Erosion Rates from Field Observations:

Computations were performed to obtain estimates of the erosion rate from the information given above. These computations used the two procedures:

- 1) A procedure similar to the one outlined in the text of this report using assumptions for the weight of material eroded, estimates of the duration of erosion, and assumptions for the erosional surface area; 2) A procedure outlined by Perry (1982) using a crack recession parameter, δ , defined as the maximum erosion rate \dot{e}_{\max} divided by the dry density of the core material. This recession parameter, δ , simply describes

the linear enlargement of an erosion channel. Details for using these two procedures to calculate the quantity of material eroded from the Teton Dam are outlined below.

Calculation of the Erosion Rate as Outlined in this Report (Method A):

This procedure requires knowledge of the volume of material eroded from the core, the weight of this volume, the time for this erosion to occur, and the erosional surface area. For these computations it was assumed that 1) the length of the erosion channel was 90 meters measured along the base of the core as shown in Fig. F2d, 2) the shape of the erosion channel was circular with a diameter of 1.8 meters, and 3) the duration of erosion ranged from a maximum time of 820 minutes (9:00 p.m. on June 4 to 10:40 a.m. on June 5, 1976) to a minimum time of 175 minutes (7:45 a.m. to 10:40 a.m. on June 5, 1976).

Volume of Material Eroded from the Core by 10:40 a.m.

$$V_c = A_c L_c = 229 \text{ m}^3$$

where:

V_c = Volume of material eroded from the core at 10:40 a.m.;

A_c = Cross-sectional area of erosion tunnel observed at 10:40 a.m. (equal to $\frac{\pi (1.8)^2}{4}$ or 2.54 sq. meters);

L_c = Approximate length of the core from upstream to downstream at El.5195 (equal to 90 meters).

Weight of Core Material Lost by 10:40 a.m.

$$W_c = \rho_c V_c = 362 \text{ Mg}$$

where:

W_c = Total weight of core material lost by 10:40 a.m.;

ρ = Mean dry density obtained for the core material (zone 1) during construction (equal to $1.583 \frac{\text{Mg}}{\text{m}^3}$);

V_c = Volume of material eroded from the core by 10:40 (equal to 225 m^3).

Estimate of Rate of Weight Erosion Until 10:40 a.m.

$$\frac{W_c}{T_{\max}} \leq P \leq \frac{W_c}{T_{\min}}$$

or

$$0.43 \leq P \leq 1.98 \frac{\text{Mg}}{\text{min}}$$

where:

P = Rate of weight erosion;

W_c = Total weight of core material lost (equal to 356 Mg);

T_{\max} = Elapsed time between 9:00 p.m., on June 4, and 10:40 a.m., on June 5, 1976 (equal to 840 minutes);

T_{\min} = Elapsed time between 7:45 a.m. and 10:40 a.m., June 5, 1976 (equal to 175 minutes).

Erosion Rate at 10:40 a.m.

$$\frac{P_{\min}}{A_{sc}} \leq \dot{\epsilon}_c \leq \frac{P_{\max}}{A_{sc}}$$

or

$$0.08 \leq \dot{\epsilon}_c \leq 0.39 \text{ g/cm}^2\text{-min}$$

where:

$\dot{\epsilon}_c$ = Estimate of erosion rate at 10:40 a.m. ($\text{g/cm}^2\text{-min}$);

P_{\min} = Minimum estimated rate of weight erosion (0.43 Mg/min);

P_{\max} = Maximum estimated rate of weight erosion (1.98 Mg/min);

A_{sc} = Erosional surface area extending for 90 meters through the core and with a diameter of 1.8 meters at 10:40 a.m. (equal to $5.1 \times 10^6 \text{ cm}^2$).

It is interesting to note that this calculated range of erosion rate values (0.08 to 0.39 g/cm²-min) is nearly identical to maximum erosion rate values obtained from Laboratory Triaxial Erosion Tests performed on Teton Dam specimens (Material E). These measured laboratory erosion rates ranged between 0.13 and 0.35 g/cm²-min.

Calculation of Erosion Rate as Outlined by Perry (1982) (Method B):

The maximum erosion rate values obtained from Laboratory Triaxial Erosion Tests presented in this report may be used to compute the recession of the wall of a crack due to erosion using the following expression

(Perry 1982):

$$\delta = \frac{\dot{\epsilon}_{\max}}{\rho} (47.24 \frac{\text{ft/day}}{\text{cm/min}}) \quad (\text{F1})$$

where:

δ = recession of wall of crack due to erosion, ft/day;

$\dot{\epsilon}_{\max}$ = maximum erosion rate, g/cm²-min; and

ρ = dry density of soil, g/cm³.

This relationship between the crack recession rate, δ , and the maximum erosion rate, $\dot{\epsilon}_{\max}$, is plotted in Figure F3 for various values of dry density. The recession rate calculated using Equation F1 may represent an upper bound for erosion for a dam having a downstream filter because it does not take into account accretion of eroded material at the interface between the cracked core and the downstream filter. On the other hand, this recession rate may represent a lower bound for erosion of a crack that is enlarging due to both wall erosion and the collapse of the embankment into the erosion channel. Thus, unless corrections are applied for filters and the rate of embankment collapse, Equation F1 will accurately model stable crack growth due to wall erosion in an embankment unprotected by a downstream filter.

Reviewing the design drawings and the field performance during the failure, it is clear that the Teton Dam embankment was not adequately protected by a downstream filter. Further, from laboratory tests and from observations made during the failure of the dam, it is clear that the core material collapsed into the erosion channel. Thus, Equation F1 will appear to give a lower bound for values of the recession of the wall of a crack in the Teton Dam.

Example Calculation of Maximum Erosion Rate

The two methods presented above may be used to back calculate the erosion rate that took place during the Teton Dam failure.

First, the recession rate, δ , may be computed for the Teton Dam assuming that the crack enlarged from a negligible thickness and only in the vertical direction. Further, it is reasonable to assume based on failure observations that the crack had a constant width of 1.8 meters (6 ft) and that it increased only in thickness from 0 meters to 1.8 meters (0 ft. to 6 ft.) during failure. This implies that the crack eroded as a constant width rectangle. This is a logical assumption if the crack was very wide compared to its thickness. The time for recession of the crack ranged from a maximum of 0.57 days (820 min) to a minimum of 0.12 days (175 min). Thus the recession rate, δ , ranged from 3.2 m/day (10.35 ft/day) to 15 m/day (50 ft/day).

Second, it is necessary to know the average dry density, ρ , of the eroding dam material. From field tests it is known that the average dry density of the core material (zone 1) was 1.583 Mg/m³.

Range of Estimated Maximum Erosion Rates: Using these values of the recession rate and the core material dry density, a range of values of the maximum erosion rate, \dot{e}_{\max} , can be read off from Figure F3 (Method B). The resulting values for the maximum erosion rate is from 0.36 to 1.7 g/cm²-min which is about 5 times greater than the range of values computed using the data and procedures developed in this report (Method A). This wide spread between calculated values using Method B and the values computed using Method A may be due to the effect of the implicit assumption made for the values obtained using Method B that the erosion channel enlarges only in one direction. Thus, Method B should be applied to estimate the erosion rates in dams where the crack enlarges such that the height and width of the crack remain approximately the same as in the case of circular erosion channel.

Design Use

These computations indicate that values for the maximum erosion rate as measured in the Triaxial Erosion Test are reasonable and may be used in design. However, the procedure for estimating the erosion rate of a eroding dam outlined in this Appendix requires that a variation of crack shape with time must be assumed. Method A, outlined in this Appendix, will be most useful for a wide variety of crack shapes. Method B, however, will be most useful if a crack is assumed (or measured) to be enlarging faster in one direction relative to it's other direction. An example of such a case is a long crack at the interface between the core and bedrock, or a long crack between compaction lifts. For such crack geometries, the recession rate analysis (Method B) will simplify computations and should result in reasonable values for estimated crack enlargement with time.

Recommendations

The authors believe that analyses of the rate of dam core erosion could become more credible if better eyewitness reports of embankment dam core erosion are provided in the literature. As a minimum these reports should include information on: 1) Fluid flow rate values; 2) An estimate of the flow channel shape or span length; 3) The weight of solids being eroded as a function of time; and 4) Estimates of the enlargement of the erosion channel with time.

References

1. Perry, E.B. (1982), Private Communication.
2. U.S. Department of the Interior (1976), "Failure of Teton Dam," Independent Panel to Review Cause of Teton Dam Failure, Denver, Colorado, December.
3. U.S. Department of the Interior (1977), "Failure of Teton Dam: A Report of Findings," Teton Dam Failure Review Group, Denver, Colorado, April.

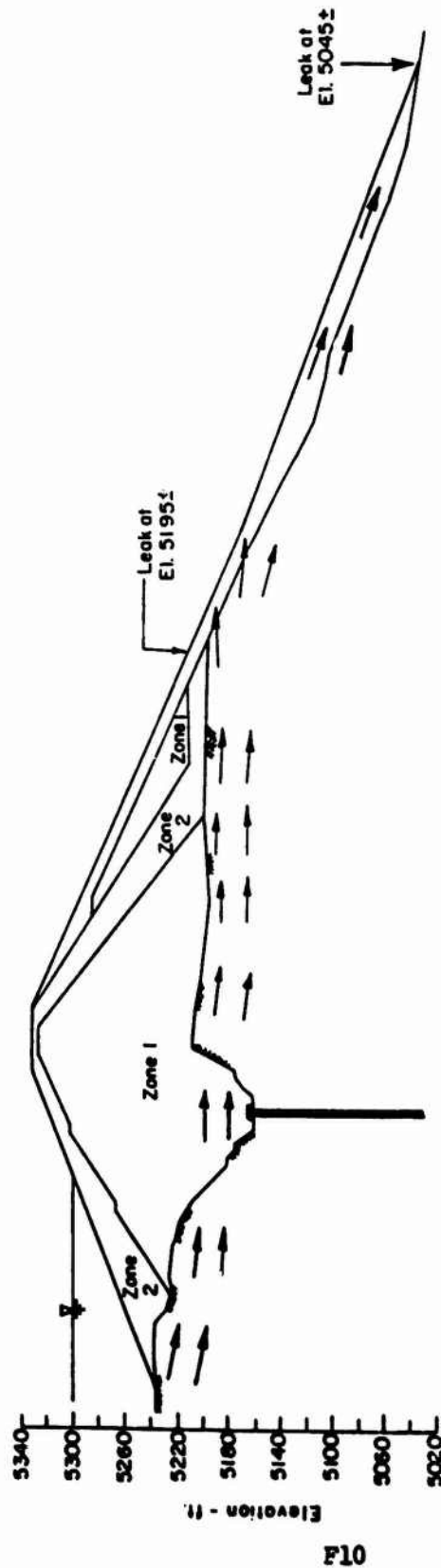


Fig. F1 Probable path of water flow through the Teton Dam embankment during early stages of leakage (from U.S. Department of the Interior, 1976).

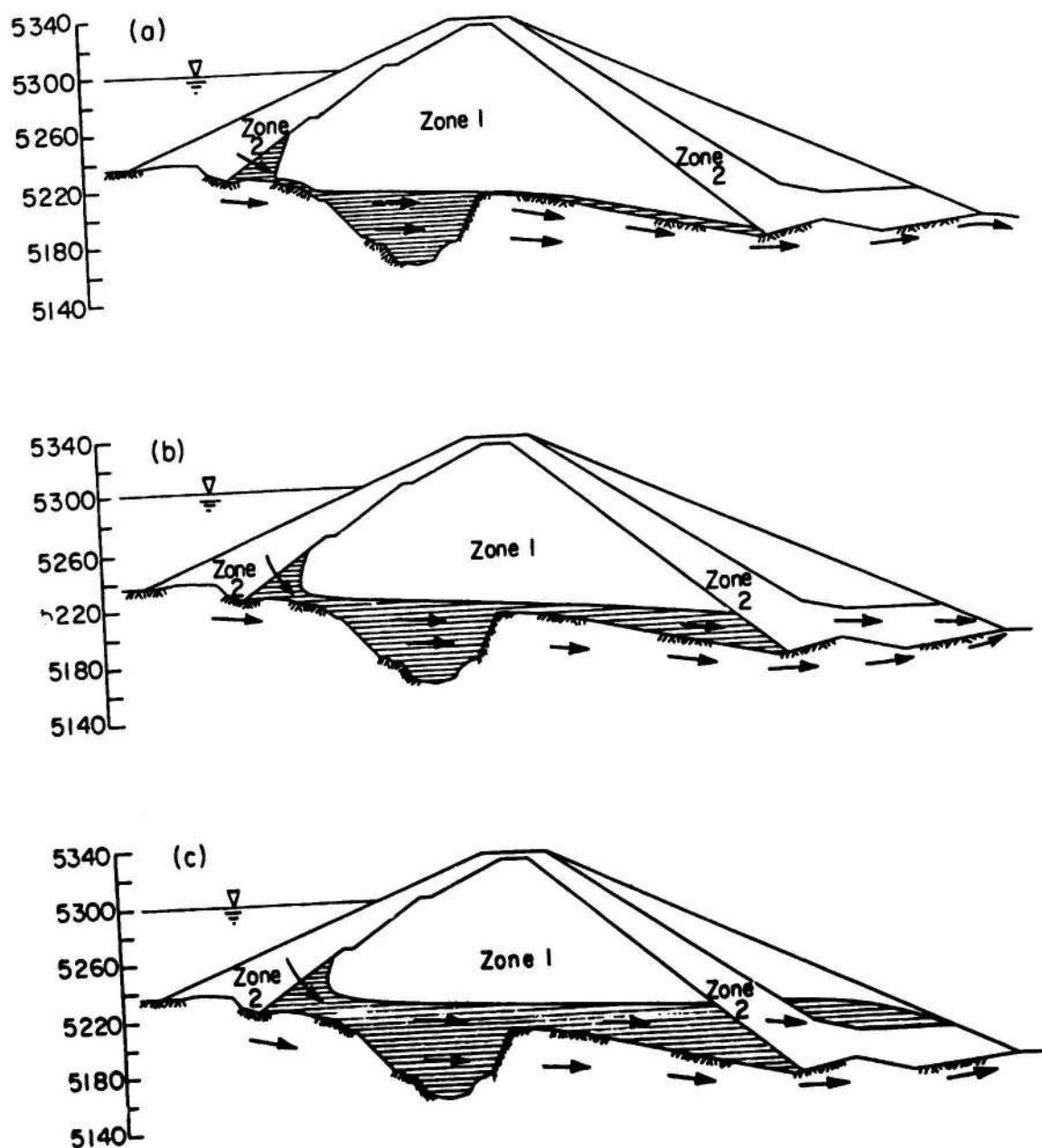


Fig. F2 Conceptual mechanism for the progression of the erosion channel through the Teton Dam embankment (from U.S. Department of the Interior, 1976).

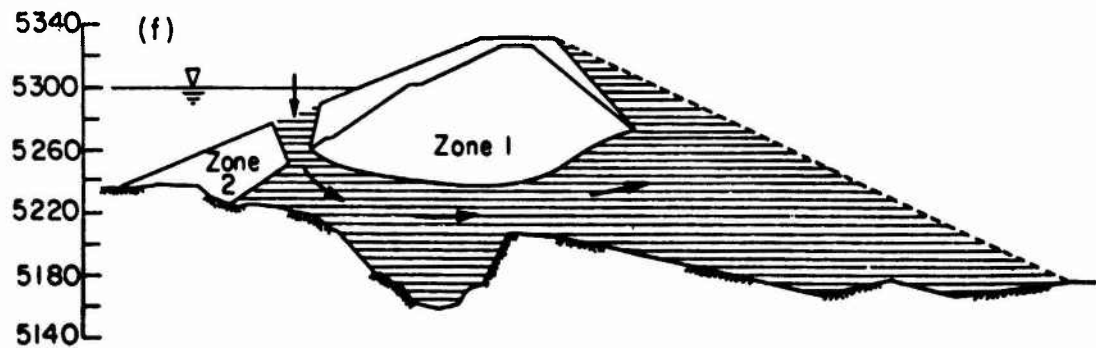
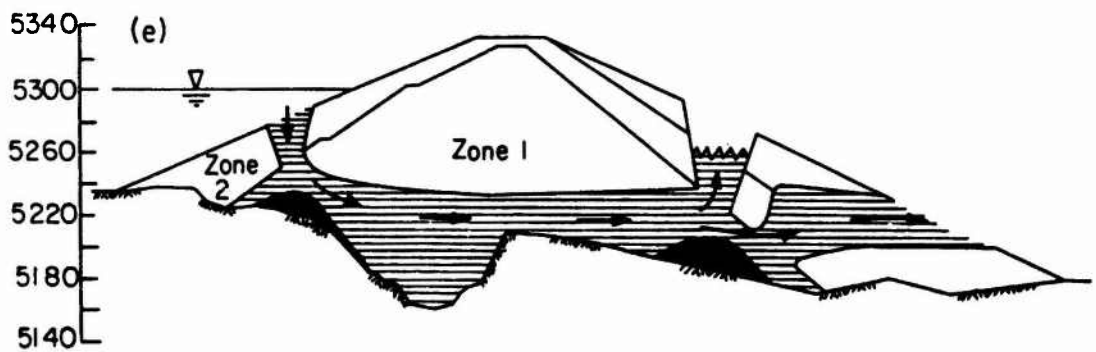
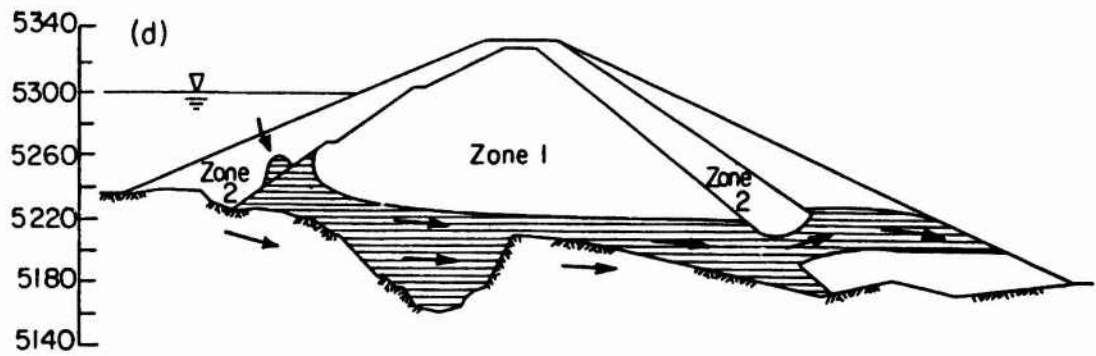


Fig. F2 (continued) Conceptual Mechanism for the progression of the erosion channel through the Teton Dam embankment (from U.S. Department of the Interior, 1976).

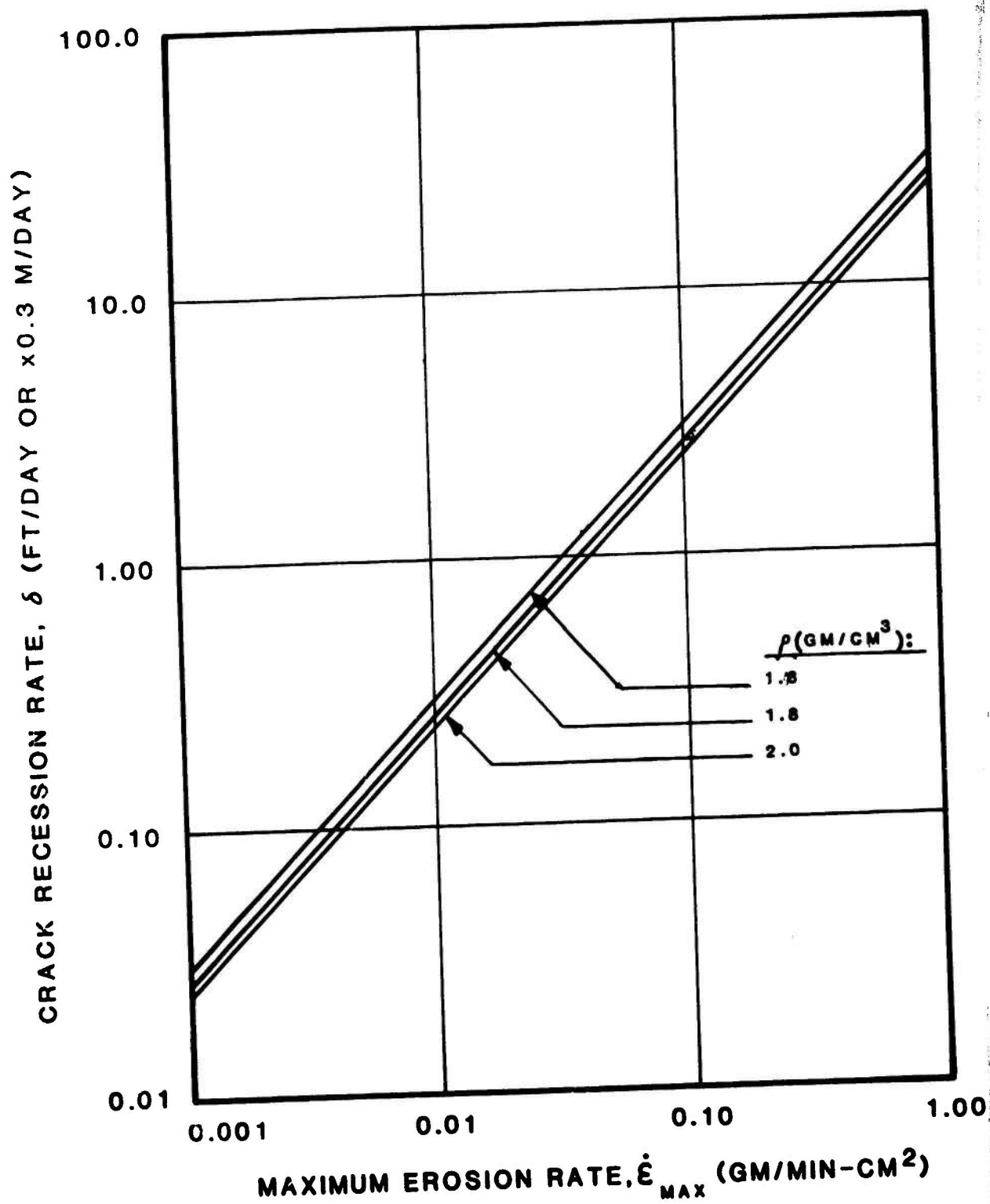


Fig. F3 Plot of crack Recession Rate, δ , versus Maximum Erosion Rate, $\dot{\epsilon}_{\max}$, (from Perry, 1982).

APPENDIX G: NOTATION

<u>SYMBOL</u>	<u>DESCRIPTION</u>	<u>UNITS</u>
$A_s(t)$	Eroded surface area as a function of time	cm^2
$A_s(0)$	Eroded surface area at time equal zero	cm^2
$A_x(t)$	Cross sectional area of crack in specimen as a function of time	cm^2
$A_x(0)$	Cross sectional area of crack in specimen at time equal zero	cm^2
D_h	Hydraulic diameter	cm
d	Thickness of crack- forming blade (crack thickness)	cm
h	Head of water applied to the top of the sample	m
h_b	Head of water applied at the end of outflow line (equal to zero in these tests)	m
i	Hydraulic gradient	m/m
L	Initial length of the specimen	cm
l_e	Eroded (crack) length	cm
P	Rate of weight erosion	g/min
Q	Flow rate	cm^3/min
Re	Reynold's number	-
S	Ratio of solids eroded to volume of flow collected at any time t (Parts per million)	mg/liter (ppm)

<u>SYMBOL</u>	<u>DESCRIPTION</u>	<u>UNITS</u>
T	Elapsed time	minutes
t	time	minutes
W_i	Dry weight of specimen at start of test	grams
W_f	Dry weight of specimen after erosion test	grams
w	Width of slot-forming blade (crack)	cm
α	Percent erosion per unit time	%/min
$\dot{\epsilon}$	Erosion rate	$\text{g}/(\text{cm}^2\text{-min})$
μ	Viscosity of Water	$\frac{\text{N-Sec}}{\text{m}^2}$
ρ	Dry density of specimen	g/cm^3
σ_{3c}	Triaxial Cell Pressure	KN/m^2
τ	Fluid Shear Stress	N/m^2
ψ	Flow parameter	-

In accordance with letter from DAEN-RDC, DAEN-ASI dated 22 July 1977, Subject: Facsimile Catalog Cards for Laboratory Technical Publications, a facsimile catalog card in Library of Congress MARC format is reproduced below.

Sanchez, Roberto L.

Evaluation of the erosion potential of embankment core materials using the laboratory triaxial erosion test procedure / by Roberto L. Sanchez, Andrew I. Strutynsky, Marshall L. Silver (Marshall L. Silver, Civil Engineer, Highland Park, Ill.). -- Vicksburg, Miss. : U.S. Army Engineer Waterways Experiment Station ; Springfield, Va. ; available from NTIS, 1983.

335 p. in various pagings : ill. ; 27 cm. -- (Technical report ; GL-83-4)

Cover title.

"April 1983."

Final report.

"Prepared for Office, Chief of Engineers, U.S. Army under Purchase Order No. DACW 39-80-M-4050; CWIS Work Unit 31618."

"Monitored by Geotechnical Laboratory, U.S. Army Engineer Waterways Experiment Station."

Bibliography: p. 47-51.

Sanchez, Roberto L.

Evaluation of the erosion potential of embankment : ... 1983.
(Card 2)

I. Earth dams. 2. Embankments. 3. Erosion.
4. Soils--Testing. I. Strutynsky, Andrew I. II. Silver, Marshall L. III. United States. Army. Corps of Engineers. Office of the Chief of Engineers. IV. U.S. Army Engineer Waterways Experiment Station. Geotechnical Laboratory. V. Title VI. Series: Technical report (U.S. Army Engineer Waterways Experiment Station) ; GL-83-4.
TA7.W34 no.GL-83-4